Analysis and Discretization of Time-Domain Impedance Boundary Conditions in Aeroacoustics

Florian Monteghetti

THÈSE

En vue de l'obtention du

Doctorat de l'Université de Toulouse

Délivré par : *l'Institut Supérieur de l'Aéronautique et de l'Espace (ISAE-SUPAERO)*

Spécialité : *Mathématiques Appliquées*

Présentée et soutenue le 16/10/2018 **par :**

Florian MONTEGHETTI

Analysis and Discretization of Time-Domain Impedance Boundary Conditions in Aeroacoustics

---

JURY

Patrick JOLY	Rapporteur
Gwénaël GABARD	Rapporteur
Bruno LOMBARD	Président, Examinateur
Julien DIAZ	Examinateur
Jean-Pierre RAYMOND	Examinateur
Sjoerd RIENSTRA	Examinateur
Denis MATIGNON	Directeur de thèse
Estelle PIOT	Codirectrice de thèse

École doctorale :
EDAA (ED467)
Unité de Recherche :
ONERA/DMPE
Date :
30 Octobre 2018 (version validée par le jury)

Dissertation submitted for the degree of

Doctor at the University of Toulouse

Awarded by: *l'Institut Supérieur de l'Aéronautique et de l'Espace (ISAE-SUPAERO)*

Specialty: *Applied Mathematics*

Defended on October 16, 2018 by:

Florian MONTEGHETTI

Analysis and Discretization of Time-Domain Impedance Boundary Conditions in Aeroacoustics

---

Date:

October 30, 2018 (version approved by the committee)

To cite this dissertation:

> Florian Monteghetti. Analysis and Discretization of Time-Domain Impedance Boundary Conditions in Aeroacoustics. ISAE-SUPAERO, Université de Toulouse, 2018.

BibTeX entry:

```
@phdthesis{monteghetti2018dissertation,
author={Monteghetti, Florian},
title={Analysis and Discretization of Time-Domain Impedance
   Boundary Conditions in Aeroacoustics},
school={ISAE-SUPAERO, Universit\'{e} de Toulouse},
year={2018},
address={Toulouse, France}
}
```

Analysis and Discretization of Time-Domain Impedance Boundary Conditions in Aeroacoustics

by

Florian Monteghetti

PhD dissertation defended on
October 16, 2018.
ISAE-SUPAERO, Université de Toulouse, France.

Abstract

In computational aeroacoustics, time-domain impedance boundary conditions (TDIBCs) can be employed to model a locally reacting sound absorbing material. They enable to compute the effect of a material on the sound field after a homogenization distance and have proven effective in noise level predictions. The broad objective of this work is to study the physical, mathematical, and computational aspects of TDIBCs, starting from the physical literature.

The first part of this dissertation defines admissibility conditions for nonlinear TDIBCs under the impedance, admittance, and scattering formulations. It then shows that linear physical models, whose Laplace transforms are irrational, admit in the time domain a time-delayed oscillatory-diffusive representation and gives its physical interpretation. This analysis enables to derive the discrete TDIBC best suited to a particular physical model, by contrast with a one-size-fits-all approach, and suggests elementary ways of computing the poles and weights. The proposed time-local formulation consists in composing a set of ordinary differential equations with a transport equation.

The main contribution of the second part is the proof of the asymptotic stability of the multidimensional wave equation coupled with various classes of admissible TDIBCs, whose Laplace transforms are positive-real functions. The method of proof consists in formulating an abstract Cauchy problem on an extended state space using a realization of the impedance, be it finite or infinite-dimensional. The asymptotic stability of the corresponding strongly continuous semigroup of contractions is then obtained by verifying the sufficient spectral conditions of the Arendt-Batty-Lyubich-Vũ theorem.

The third and last part of the dissertation tackles the discretization of the linearized Euler equations with TDIBCs. It demonstrates the computational advantage of using the scattering operator over the impedance and admittance operators, even for nonlinear TDIBCs. This is achieved by a systematic semi-discrete energy analysis of the weak enforcement of a generic nonlinear TDIBC in a discontinuous Galerkin finite element method. In particular, the analysis highlights that the sole definition of a discrete model is not enough to fully define a TDIBC. To support the analysis, an elementary physical nonlinear scattering operator is derived and its computational properties are investigated in an impedance tube. Then, the derivation of time-delayed broadband TDIBCs from physical reflection coefficient models is carried out for single degree of freedom acoustical liners. A high-order discretization of the derived time-local formulation, which consists in composing a set of ordinary differential equations with a transport equation, is applied to two flow ducts.

Keywords: Time-domain impedance boundary condition, Acoustic boundary condition, Time-delay systems, Fractional kernels, Completely monotone kernels, Oscillatory-diffusive representation, Irrational transfer functions, Positive-real functions, Wave equation, Asymptotic stability, Memory damping, Discontinuous Galerkin, Linearized Euler equations, Duct aeroacoustics.

Contents

List of Figures

List of Tables

Acronyms

ABLV	Arendt-Batty-Lyubich-Vũ
a.e.	almost everywhere
BVP	Boundary Value Problem
CAA	Computational Aeroacoustics
CRK	Continuous Runge-Kutta
CT	Ceramic Tubular
DoF	Degree of Freedom
DG	Discontinuous Galerkin
GFIT	Grazing Flow Impedance Tube
GIT	Grazing Incidence Tube
IBC	Impedance Boundary Condition
IBVP	Initial Boundary Value Problem
IVP	Initial Value Problem (also Cauchy problem)
LTI	Linear Continuous Time-Invariant
MP	Micro-Perforated
NASA	National Aeronautics and Space Administration
OD	Oscillatory-Diffusive
ODE	Ordinary Differential Equation
PDE	Partial Differential Equation
PPHW	Plane Progressive Harmonic Wave
SDOF	Single Degree of Freedom
SPL	Sound Pressure Level
DDOF	Double Degree of Freedom
TDIBC	Time-Domain Impedance Boundary Condition

Notation

Greek letters

β	reflection coefficient, defined as (1.15) in the Laplace domain
Γ	gamma function (Abramowitz and Stegun 1970, § 6)
γ	ratio of specific heat ($\simeq 1.4$ for air)
δ	Dirac distribution (A.1)
κ	thermal diffusivity $\left(\mathrm{m}^2 \cdot \mathrm{s}^{-1}\right)$
μ	dynamic viscosity $(\mathrm{Pa} \cdot \mathrm{s})$
μ_f	diffusive weight associated with the function f, defined as (2.17)
μ_α	diffusive weight, defined as (2.11) for $\alpha \in (0, 1)$
ν	kinematic viscosity $\left(\mathrm{m}^2 \cdot \mathrm{s}^{-1}\right)$
ρ_0	base flow density
$\rho(\mathcal{A})$	resolvent set of the operator $\mathcal{A}$ (Yosida 1980, § VIII.1)
σ	porosity (1.22)
$\sigma(\mathcal{A})$	spectrum of the operator $\mathcal{A}$ (Yosida 1980, § VIII.1)
$\sigma_p(\mathcal{A})$	point spectrum of $\mathcal{A}$
$\sigma_r(\mathcal{A})$	residual spectrum of $\mathcal{A}$
$\sigma_c(\mathcal{A})$	continuous spectrum of $\mathcal{A}$
φ	function defined as (2.6)
Ω	open set in $\mathbb{R}^d$
Ω_T	spacetime open set $(0, T) \times \Omega$
ω	angular frequency $\left(\mathrm{rad} \cdot \mathrm{s}^{-1}\right)$

Roman letters

Arg	principal value of the argument, in $(-\pi, \pi]$
arg	argument, in $\mathbb{R}$
$\mathcal{B}$	scattering operator (1.14)
CFL	CFL number (5.28)
$\mathbb{C}$	field of complex numbers
$\mathbb{C}_c^+$	open right half-plane $\mathbb{C}_c^+ \coloneqq \{s \in \mathbb{C} \mid \Re(s) > c\}$
$\overline{\mathbb{C}_c^+}$	closed right half-plane $\overline{\mathbb{C}_c^+} = \{s \in \mathbb{C} \mid \Re(s) \geq c\}$
$\mathcal{C}$	space of continuous functions
$\mathcal{C}^k$	space of functions with k continuous derivatives
$\mathcal{C}^\infty$	space of infinitely smooth functions
$\mathcal{C}_0^\infty$	space of infinitely smooth and compactly supported functions
card	cardinal of a set

c_0	speed of sound
$\operatorname{div} \boldsymbol{f}$	divergence of a vector, $\operatorname{div} \boldsymbol{f} \coloneqq \sum_i \partial_i f_i$
$\mathcal{D}(\mathbb{R})$	$\coloneqq \mathcal{C}_0^\infty(\mathbb{R})$, space of infinitely smooth and compactly supported functions of a real variable
$\mathcal{D}(\mathcal{A})$	domain of the operator $\mathcal{A}$
$\mathcal{D}'(\mathbb{R})$	space of distributions of a real variable
$\mathcal{D}_+(\mathbb{R})$	space of causal distributions of a real variable
e_x	first-order causal kernel (2.3)
$\mathcal{E}(\mathbb{R})$	$\coloneqq \mathcal{C}^\infty(\mathbb{R})$, space of infinitely smooth functions of a real variable
$\mathcal{E}'(\mathbb{R})$	space of compactly supported distributions
$\mathcal{F}$	Fourier transform, see Section A.2
$\mathcal{F}_h^i$	set of interior faces, see Section 5.2
$\mathcal{F}_h^b$	set of boundary faces, see Section 5.2
H	Heaviside or step function (1 over $(0, \infty)$, null elsewhere)
$H^1(\Omega)$	Sobolev space
$H_0^1(\Omega)$	Sobolev space $\{f \in H^1(\Omega) \mid f = 0 \text{ on } \partial\Omega\}$
$H^{-1}(\Omega)$	topological dual of $H^1(\Omega)$
I_n	modified Bessel function of the first kind of order n
$\mathbb{I}_d$	identity matrix of size $d \times d$
$\mathcal{I}$	identity operator
j	unit imaginary number $\mathrm{j}^2 = -1$
J_n	Bessel function of the first kind of order n
$\ker(\mathcal{A})$	kernel of the operator $\mathcal{A}$
k_ν	$\coloneqq \sqrt{s/\nu}$, wavenumber associated with viscous diffusion (m^{-1})
k_κ	$\coloneqq \sqrt{s/\kappa}$, wavenumber associated with thermal diffusion (m^{-1})
$L^1_{\mathrm{loc}}(\Omega)$	space of locally integrable functions
$L^2(\Omega)$	space of square integrable functions
$\mathcal{L}$	Laplace transform, see Section A.2
$\mathcal{L}(H)$	space of continuous linear operators on H
M_0	$\coloneqq \lvert\boldsymbol{u_0}\rvert / c_0$, base flow Mach number
$\mathbb{N}$	$\coloneqq [\![0, \infty[\![$, set of nonnegative integers
$\mathcal{O}$	big O notation
Pr	$\coloneqq \nu/\kappa$, Prandtl number
p	pressure (Pa)
pf	Hadamard finite part (Zemanian 1965, § 2.5)
pv	Cauchy principal value (Zemanian 1965, § 2.5) (Schwartz 1966, § I.2.2)
$\tilde{p}$	$\coloneqq p/z_0$ $(\mathrm{m} \cdot \mathrm{s}^{-1})$
$\mathbb{P}_d^k$	space of polynomials of $d <$variables and total degree at most k
$\mathbb{Q}$	field of rational numbers
Res	complex residue defined as (2.15)
$R(\mathcal{A})$	range of the operator $\mathcal{A}$
$R(\cdot, \mathcal{A})$	resolvent operator of $\mathcal{A}$, defined as (4.25)
$\mathbb{R}$	field of real numbers
s	Laplace variable in $\mathbb{C}$ (if applicable, $\mathrm{rad} \cdot \mathrm{s}^{-1}$)
supp	support (closed set)
s^α	principal branch of the power function (2.14) with $\alpha \in \mathbb{R}$
$\mathcal{S}'(\mathbb{R})$	space of tempered distributions of a real variable
t	time variable (s)
$\mathcal{T}_h$	mesh

$\boldsymbol{u}$	velocity $(\mathrm{m} \cdot \mathrm{s}^{-1})$
$\boldsymbol{u_0}$	base flow velocity $(\mathrm{m} \cdot \mathrm{s}^{-1})$
$\boldsymbol{v}$	state vector, defined as (3.12) with the LEEs
$\boldsymbol{x}$	space variable (m)
X'	topological dual of X
y	admittance kernel (1.10) $(\mathrm{kg}^{-1} \cdot \mathrm{m}^2 \cdot \mathrm{s}^1)$
Y_1	Heaviside function (1 over $(0, \infty)$, null elsewhere)
Y_α	fractional kernel (1.6) for $\alpha > 0$
$\mathcal{Y}$	admittance operator (1.9)
z	impedance kernel, see Section 1.1 $(\mathrm{kg} \cdot \mathrm{m}^{-2} \cdot \mathrm{s}^{-1})$
z_c	characteristic impedance $(\mathrm{kg} \cdot \mathrm{m}^{-2} \cdot \mathrm{s}^{-1})$
z_0	characteristic impedance of air $(\mathrm{kg} \cdot \mathrm{m}^{-2} \cdot \mathrm{s}^{-1})$
$\mathbb{Z}$	set of integers
$\mathcal{Z}$	impedance operator, see Section 1.1

Miscellaneous

$\mathbf{0_d}$	null vector of length d
0_d	null matrix of size $d \times d$
$\mathbb{1}_X$	characteristic function of X (1 over X, 0 elsewhere)
$A^\perp$	set orthogonal to A
$\Im(s)$	imaginary part of $s \in \mathbb{C}$
$\Re(s)$	real part of $s \in \mathbb{C}$
$\overline{s}$	complex conjugate
$\overline{\Omega}$	closure of Ω
$\mathring{\Omega}$	interior of Ω
$\partial\Omega$	boundary of Ω
X^*	$\coloneqq X \backslash \{0\}$
$\hat{z}$	Laplace transform
$\langle a, b \rangle$	duality bracket, see Appendix A
(a, b)	scalar product
(a, b)	open interval
$[a, b]$	closed interval
$[\![a, b]\!]$	ordered set of integer in $[a, b]$
$\langle \cdot \rangle_S$	spatial average over a surface S
$\{\boldsymbol{v}\}$	face average (5.8)
$[\![\boldsymbol{v}]\!]$	face jump (5.9)
$\| \cdot \|_X$	norm on X
$\| \cdot \|$	norm, absolute value, Lebesgue measure of a set
∇	nabla symbol, $\nabla f \coloneqq [\partial_i f]_{i \in [\![1,d]\!]}$
$\in$	element of
$\notin$	not element of
$\cap$	intersection
$\cup$	union
$\subset$	subset
$\coloneqq$	equal, by definition
$\propto$	proportional to
$\otimes$	tensor product of vectors, satisfies $(a \otimes b) \cdot c = (b \cdot c)a$ with $a, b, c \in \mathbb{R}^d$

$\circ$	composition
$\star$	convolution, see Section A.1

Introduction

This dissertation focuses on the analysis and discretization of a class of boundary conditions encountered in aeroacoustics, an area of fluid mechanics concerned with the generation, propagation, and absorption of sound waves in a moving medium (Lighthill 1952; Rienstra and Hirschberg 2016; Tam 2012). Specifically, the boundary conditions studied herein are known as impedance boundary conditions (IBCs) or also time-domain impedance boundary conditions (TDIBCs), to emphasize the contrast with IBCs used in conjunction with time-harmonic (also frequency-domain) partial differential equations (PDEs). This introduction is split into three parts. After a short overview of IBCs and their applications, the scope and contributions of the study are given. Lastly, an outline of the dissertation is provided.

Impedance boundary condition

Due to the growth in air traffic during the last decades, the regulation on aircraft environmental impact has become increasingly stringent, and bodies such as ACARE set high goals for future noise reductions. At the certification level, the European Aviation Safety Agency issues noise level requirements, but even an already certified airliner can see its commercial viability threatened by the demands of individual airports. From the point of view of an aircraft or engine manufacturer, it is of paramount importance to deal with these operational threats as well as to improve future designs. To reduce the noise emitted by an aircraft, one practical solution consists in mounting *passive* sound absorbing materials, commonly known as acoustical liners. Figure 1 illustrates the use of a Micro-perforated (MP) liner in the inlet of a jet engine.

Given the cost of testing, a lot of effort is being put into improving the reliability of computational aeroacoustics (CAA) (Tam 2012) to enable better noise level predictions. An accurate computation of the acoustic field inside a liner is costly by contemporary computing standard, and is thus the realm of specific studies that focus on the material in isolation, see e.g. (Zhang and Bodony 2016). Practical computations of sound absorption are typically done by modeling the material through a boundary condition, namely an IBC as defined below.

Let p (resp. $\boldsymbol{u}$) denote the acoustic pressure (resp. velocity) perturbation field, defined on an open bounded set Ω with a Lipschitz boundary $\partial\Omega$. A linear IBC links the acoustic pressure and velocity through a continuous linear time-invariant single-input single-output operator

$$p(t,\boldsymbol{x}) = \left[z(\cdot,\boldsymbol{x}) \star \boldsymbol{u}(\cdot,\boldsymbol{x}) \cdot \boldsymbol{n}\right](t) \quad (\boldsymbol{x} \in \partial\Omega), \tag{1}$$

where $\boldsymbol{n}$ is the outward unit normal on $\partial\Omega$, $\star$ denotes the time-domain convolution, and $z(\cdot,x) \in \mathcal{D}'_+(\mathbb{R}) \cap \mathcal{S}'(\mathbb{R})$ is a causal and tempered kernel known as the *impedance kernel*. A Dirichlet boundary condition ("pressure-release" wall) is recovered for $z = 0$ while "$z = \infty$" yields a Neumann boundary condition (hard wall).

Provided that the impedance kernel z is suitable, the IBC enables to compute the effect of a material on the sound field after a homogenization distance, see e.g. (Laurens et al. 2014) for a study of the homogenization problem for a perforated plate in acoustics. The effectiveness of this

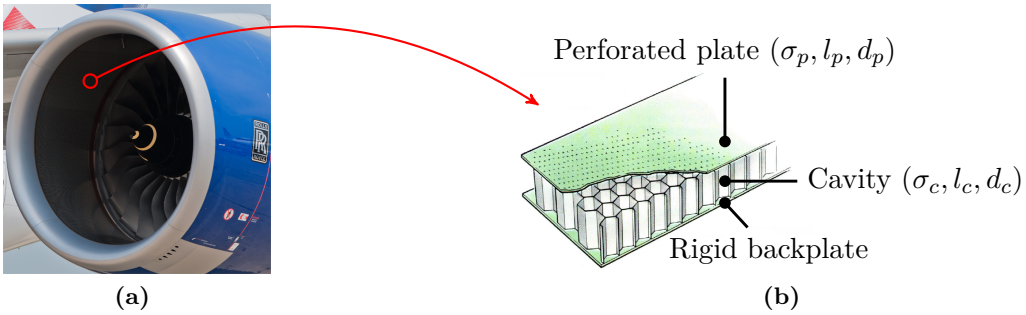

Figure 1. Application of a sound absorbing material to reduce the noise emitted by a jet engine. (a) Inlet duct of a Trent 900 (A380). The black area is the lined part of the duct. By Julian Herzog, used under CC BY 4.0 (`https://creativecommons.org/licenses/by/4.0/deed.en`). Cropped from original. (b) MP liner. Adapted from (Rolls-Royce plc 1996, Fig. 19-6).

modeling and the advent of acoustically treated jet engines has led to IBCs becoming a staple part of aeroacoustics (Hubbard 1991, Chaps. 13–14) (Tam 2012). Early works focused on the prediction of sound absorption in a duct with flow: Cremer (Cremer 1953) derived an approximation of the optimal impedance and Pridmore-Brown (Pridmore-Brown 1958) established his celebrated equation, widely used to compute duct modes. The identification of unstable surface modes by Tester (Tester 1973c) lead to a wealth of investigations focused on the hydrodynamic stability of a base flow with an IBC (Khamis and Brambley 2017). Inverse methodologies have been developed to identify the IBC and provide an alternative to more intrusive measurement techniques (Jones et al. 2005). In all of these studies, the IBC is linear and the Cauchy problem is formulated in the frequency domain. Although less popular than their time-harmonic counterparts, TDIBCs have been used in wave propagation problems including duct aeroacoustics (Bin et al. 2009; Liu et al. 2014; Özyörük et al. 1998; Zhong et al. 2016), room acoustics (Botteldooren 1995), as well as outdoor sound propagation (Cotté and Blanc-Benon 2009). Richter *et al.* (Richter 2010; Richter et al. 2011) and Troian *et al.* (Troian et al. 2017) identified an IBC in the time domain. Gabard & Brambley (Gabard and Brambley 2014) used a time-domain formulation to investigate the (in)stability of the Ingard-Myers boundary condition.

For a wide range of materials, accurate models for z can be derived from first principles under the following three hypotheses (Morse and Ingard 1968, § 6.3) (Kinsler and Frey 1962, Chap. 10): the material is locally reacting, i.e. the tangential component $\boldsymbol{u}_\parallel$ does not propagate (which is verified for materials based on the Helmholtz resonator such as MP liners); the incident sound pressure level (SPL) is low enough so that the material behaves linearly; there is no base flow (i.e. this is the purely acoustical case). For instance, the high-frequency approximation of an acoustic impedance model for a MP liner without losses in the cavity reads

$$\frac{\hat{z}_{\text{phys}}}{z_0}(s) = \frac{3l_p}{\sigma_p c_0 \left(d_p/2\right)^2}\nu + \frac{2l_p}{\sigma_p c_0 \, d_p/2}\sqrt{\nu}\sqrt{s} + \frac{l_p}{\sigma_p c_0}s + \frac{1}{\sigma_c}\coth\left(\frac{l_c}{c_0}s\right) \quad (\Re(s) > 0)\,,$$

where $\hat{z}$ is the Laplace transform of the kernel z (an analytic function defined on the open right half-plane), z_0 the characteristic impedance of air, ν the kinematic viscosity, c_0 the speed of sound, σ_p (resp. σ_c) the porosity of the perforation (resp. cavity), and (l_p, d_p) (resp. (l_c, d_c)) are the length and diameter of the perforation (resp. cavity). In the expression of the physical model $\hat{z}_{\text{phys}}$, a non-null viscosity ν induces both a constant and a fractional term $\sqrt{s}$, the latter yielding a long-memory kernel. Additionally, this model exhibit a time-delay

$$\tau = \frac{2l_c}{c_0}$$

due to a wave reflection in the cavity, which can be seen by rewriting the hyperbolic cotangent term as

$$\coth\left(\frac{l_c}{c_0}s\right) = 1 + e^{-\tau s}\hat{h}(s),\ \hat{h}(s) = \frac{2}{1-e^{-\tau s}}.$$

The rather strong hypotheses behind the derivation of impedance models mentioned above can be loosened to an extent, thus widening the practical applicability of IBCs. Partly empirical corrections have been developed to model the effect of both high incident SPLs and grazing base flows, at least separately: these effects are significant in most aeroacoustical applications. However, it must be borne in mind that there is only so much an IBC can do: a material that exhibits a significant tangential propagation, such as some porous media, cannot be accurately described with an IBC that only uses the normal component $\boldsymbol{u}\cdot\boldsymbol{n}$, as defined above and considered herein.

Remark (Time-harmonic formulation). Provided that (1) is used with a PDE linear with respect to time, it can equivalently be formulated in the Laplace domain as

$$\hat{p}(s,x) = \hat{z}(s,x)\widehat{\boldsymbol{u}}(s,x)\cdot\boldsymbol{n} \quad (x\in\partial\Omega,\ \Re(s)>0), \tag{2}$$

where $s = \mathrm{j}\omega$ yields the Fourier transform (only formally, since the solution $\boldsymbol{u}$ may not be tempered). As long as the problem is linear, (1) and (2) are equivalent formulations. The use of a TDIBC may merely be more convenient than a time-harmonic one, for instance when a broadband source is considered. However, it is indispensable when the harmonic problem *cannot* be formulated, such as in the presence of time-dependent domains, moving sources, or nonlinearities. Mathematically, nonlinearities can arise from the IBC or PDE. Physically, nonlinear IBCs are relevant when high incident SPLs are considered and nonlinear PDEs are of particular interest when hydrodynamic phenomena cannot be neglected, such as close to a supersonic fan tip where shocks occur (Astley et al. 2011, § 5.3) or for flow control, see (Scalo et al. 2015) and (Olivetti et al. 2015) for numerical investigations of the interaction between a turbulent boundary layer and an impedance wall.

Remark (IBCs in electromagnetics). Although this work solely focuses on aeroacoustics, let us briefly highlight that similar boundary conditions are encountered in electromagnetics, under the name of surface IBCs (SIBCs) (Yuferev and Ida 2010). Let $\boldsymbol{E}$ (resp. $\boldsymbol{H}$) be the electric (resp. magnetic) field on $\Omega\subset\mathbb{R}^3$. A linear SIBC links the tangential components of $\boldsymbol{E}$ and $\boldsymbol{H}$ through

$$\boldsymbol{E}_\parallel(t,\boldsymbol{x}) = \Big[z(\cdot,\boldsymbol{x})\star\boldsymbol{H}_\parallel(\cdot,\boldsymbol{x})\times\boldsymbol{n}\Big](t) \quad (\boldsymbol{x}\in\partial\Omega),$$

where $\boldsymbol{n}$ is the outward unit normal on $\partial\Omega$ and the subscript "$\parallel$" denotes the tangential component. Physically, z models a time-invariant non-perfect conducting material that behaves linearly. The case of a perfect conductor is recovered for $z=0$ (negligible penetration depth). The models encountered for z are similar to that from acoustics. For instance, the earliest impedance model, known as the Leontovich or first-order model, is given by (Yuferev and Ida 2010, Eq. 1.20) (Beggs et al. 1992, Eq. 9)

$$\hat{z}(s) = \sqrt{\frac{\mu}{\sigma}s} = \frac{\sqrt{2\mathrm{j}}}{\sigma\delta_{\text{skin}}},$$

where σ and μ are the conductivity and magnetic permeability of the conducting material, respectively. The quantity $\delta_{\text{skin}} = \sqrt{\frac{2}{\omega\mu\sigma}}$ is known as the skin depth.

Remark (IBCs in combustion). IBCs also have applications in combustion, where they are used to truncate a part of the combustion chamber or model injectors for instance (Douasbin et al. 2018; Jaensch et al. 2016; Tudisco et al. 2017).

Remark (IBCs with the wave equation). If p solves the wave equation, the IBC (1) reads

$$\partial_t p = -\frac{c_0}{z_0}\, z \star \partial_n p,$$

where $\partial_n p$ denotes the normal derivative, c_0 the propagation speed, and z_0 the characteristic impedance. Hence, a hard (resp. pressure-release) wall corresponds to a Neumann (resp. Dirichlet) boundary condition on p. In mathematical control, IBCs are commonly used to stabilize the wave equation since they modify the underlying semigroup generator and can yield asymptotic or even exponential stability: both finite-dimensional (Abbas and Nicaise 2015) and infinite-dimensional IBCs have been studied, involving for example a fractional derivative (Grabowski 2013) and a time delay (Wang et al. 2011). In these studies, the IBC (related to the Dirichlet to Neumann map) is usually written as

$$\partial_n p = -\frac{z_0}{c_0}\, y \star \partial_t p,$$

where y is the admittance kernel. See (Sauter and Schanz 2017) for a numerical treatment using convolution quadrature.

Scope and contributions

This dissertation focuses on the analysis and discretization of TDIBCs that model locally reacting sound absorbing materials such as the one depicted in Figure 1. Non locally reacting media or application of IBCs to combustion chambers is out of the scope of the present work. The starting point of this work was the finding that IBCs had been studied separately, under various forms, by physical, computational, and mathematical communities, without much connections. The broad objective is to consider all three aspects in a unified fashion, by starting from the physical literature. The present manuscript, which is a continuation of the master thesis (Monteghetti 2015), contributes to answering the following questions.

(a) What is the mathematical structure of physical impedance models? Part I.

(b) How does the IBC (1) affect well-posedness and stability? Part II.

(c) How to discretize an IBC? Part III.

(d) What about nonlinear absorption mechanisms? Chapter 1 and Part III.

The summary of this dissertation will be provided as answers to the above questions. A detailed outline of the dissertation is provided below.

Outline

This dissertation is split into three parts that contribute to answering the questions highlighted above.

—— Part I Physical impedance models in the time domain

This part gathers the definition and analysis of impedance models. Since the sole focus is on impedance models, the PDE satisfied by p and $\boldsymbol{u}$ in Ω need not be defined.

Chapter 4 Stability of the wave equation with impedance boundary conditions 87

This chapter focus on the no flow case, i.e. the multidimensional wave equation, and proves asymptotic stability with a wide range of admissible IBCs. A common method of proof, inspired by (Matignon and Prieur 2014), is employed that consists in formulating an abstract Cauchy problem on an extended state space using a realization of each impedance operator, be it finite or infinite-dimensional; asymptotic stability is then obtained with the Arendt-Batty-Lyubich-Vũ (ABLV) theorem, although a less general alternative based on the invariance principle is also discussed. In spite of the apparent unity of the approach, no single, unified proof is known to the author: this leads to the formulation of a conjecture at the end of this dissertation.

This chapter is drawn from (Monteghetti et al. 2018a) and has been partly communicated in (Monteghetti et al. 2017b).

—— Part III Discretization of impedance boundary conditions

This part deals with the discretization of the LEEs coupled with IBCs, for application in duct aeroacoustics.

This whole part is drawn from (Monteghetti et al. 2018b) and has been partly communicated in (Monteghetti et al. 2017b).

Chapter 5 Weak enforcement of impedance boundary conditions 123

This chapter analyzes the weak enforcement of an admissible IBC within a discontinuous Galerkin (DG) discretization of the LEEs, employing the numerical flux formalism to ease the transition to other methods popular in fluid mechanics. For the analysis the IBC is only assumed admissible and need not be given by one of the models analyzed in Chapter 2, so that both chapters are independent. The first two sections provide reminders: Section 5.1 summarizes the needed facts on the LEEs from Chapter 3, while Section 5.2 recalls the DG discretization of the LEEs as well as some standard estimates. The analysis given in Section 5.3 shows the computational interest of a numerical flux based on the scattering operator $\mathcal{B}$ over fluxes based on the impedance or admittance operators. These results will be further discussed in the numerical applications of Chapter 6.

Chapter 6 Numerical validation and application to duct aeroacoustics 145

This chapter gathers numerical applications of TDIBCs in aeroacoustics, with a focus on acoustical liners. Section 6.1 recalls the derivation of discrete models from the analysis of physical impedance models of liners presented in Section 2.4, leading to a time-local formulation that consists in composing a set of ODEs with a transport equation. The OD representation is discretized using an adaptation of the optimization method given in Section 2.2 while the transport equation is discretized with a high order DG method. Applications are then shown in the last two sections. Section 6.2 deals with the impedance tube whose analytical solution is known even for nonlinear impedance. In particular, it validates the analysis of Chapter 5 by investigating the computational properties of a nonlinear algebraic scattering operator. Section 6.3 presents an application to two flow ducts documented in the literature.

—— Appendices

Appendix A Convolution, Fourier and Laplace transforms 177

This appendix discusses the links between Fourier and Laplace transforms and its implications for the formulation of admissibility conditions.

This appendix is an extension of (Monteghetti et al. 2018b, App. A).

Reader's guide

Although there is a logical progression between the chapters, they are written to be mostly self-contained. The table below summarizes the parts of the dissertation relevant for each topic.

Topic	Relevant chapters
Design of TDIBCs	Part I, Chapter 5, and Sections 6.1–6.2
PDE	Section 1.1 and Part II
Numerical application to duct aeroacoustics	Section 1.1 and Chapter 6

Part I

Physical impedance models in the time domain

Chapter 1

Basics of impedance models

Contents

This chapter covers the mathematical and physical basics of impedance models. It introduces notations, definitions, and properties that are used throughout the dissertation. Section 1.1 presents three formulations of a nonlinear IBC and defines admissibility conditions using system theory. Section 1.2 recalls the physical assumptions behind IBCs and gathers physical models. It first lists some relevant and well-known *acoustical* models derived in the frequency domain from first principles. Then, it discusses the modeling of base flow and nonlinear effects, the latter due to high incident SPLs. Section 1.3 summarizes existing numerical models, known in both time and frequency domains by design.

1.1 Admissibility of impedance operators

In this section we discuss three formulations of IBCs, each relying on a different operator: the impedance operator $\mathcal{Z}$ (convolution kernel z in the linear case); the admittance operator $\mathcal{Y}$ (convolution kernel y in the linear case); the scattering operator $\mathcal{B}$ (convolution kernel β in the linear case, known as the reflection coefficient). The main purpose of the section, apart from introducing notations used in later chapters, is to introduce admissibility conditions for the operators $\mathcal{Z}$, $\mathcal{Y}$, and $\mathcal{B}$, as well as for the kernels z, y, and β.

1.1.1 Impedance formulation

We begin this section with the impedance formulation. This formulation naturally arises when modeling material made from connections of components in series, for example the single degree of freedom liners covered in Section 1.2.2.

If p (resp. $\boldsymbol{u}$) denotes the acoustic perturbation of pressure (resp. velocity), defined on an open bounded set Ω with a Lipschitz boundary $\partial\Omega$, an IBC can be generally written as

$$p(t,\boldsymbol{x}) = \mathcal{Z}[\boldsymbol{x}, \boldsymbol{u}(\cdot,\boldsymbol{x})\cdot\boldsymbol{n}(\boldsymbol{x})](t) \quad ((t,\boldsymbol{x}) \in (0,\infty)\times\partial\Omega), \tag{1.1}$$

where $\boldsymbol{n}$ is the outward unit normal (it points towards the material) and $\mathcal{Z}$ is a scalar-valued operator, known as the impedance operator. In the expression (1.1) the space and time variables are explicitly written to emphasize that the operator $\mathcal{Z}(\boldsymbol{x},\cdot)$, which may depend on space, applies to a function of time only, not space. For the sake of clarity, the space variable is omitted so that (1.1) is more concisely written

$$p(t) = \mathcal{Z}(\boldsymbol{u}\cdot\boldsymbol{n})(t) \quad t\in(0,\infty),$$

where it is implicitly understood that $\mathcal{Z}$, which may depend on $\boldsymbol{x}$, is applied to the function of time $t\mapsto\boldsymbol{u}(t,\boldsymbol{x})\cdot\boldsymbol{n}$. Examples of impedance operators $\mathcal{Z}$ are given throughout the chapter.

In this chapter, we seek to define conditions on $\mathcal{Z}$ so that it models a passive system; these kind of conditions are known in the acoustical literature as admissibility conditions (Rienstra 2006). To do so, we adopt a system theory viewpoint whereby the function of time $\boldsymbol{u}\cdot\boldsymbol{n}$ is an input, the function of time p is an output, and $\mathcal{Z}$ is a single-input single-ouput operator. In particular, this implies that we do not need to detail the PDE solved by p and $\boldsymbol{u}$ at this stage.

By system theory, we here mean the theory of passive linear systems that has been formalized in the 1950s and 1960s, often motivated by the study of electrical circuits. This section relies on the two introductory works (Zemanian 1965, Chap. 10) and (Beltrami and Wohlers 1966, § 3.5), which use the theory of distributions. Background material and references on harmonic analysis and distribution theory have been gathered in Appendix A.

Herein, to define the admissibility of a nonlinear impedance operator $\mathcal{Z}$ we use the three fundamental properties defined in these works, namely causality, reality, and passivity. This is formalized below.

Definition 1.1 (Admissibility conditions)**.** Let $\mathcal{Z} : \mathcal{E}'(\mathbb{R}) \to \mathcal{D}'(\mathbb{R})$ be a continuous operator. It is said to be an *admissible* impedance operator if it enjoys the following properties:

(i) (Causality) If u is causal, i.e. $u \in \mathcal{D}'_+(\mathbb{R})$, then $\mathcal{Z}(u)$ exists and is causal, i.e. $\mathcal{Z}(u) \in \mathcal{D}'_+(\mathbb{R})$.

(ii) (Reality) Real-valued inputs are mapped to real-valued outputs.

(iii) (Passivity) For every smooth and compactly supported input $u \in \mathcal{C}_0^\infty(\mathbb{R})$ and for every time instant $t > 0$,

$$\Re\left(\int_{-\infty}^{t} \overline{\mathcal{Z}(u)(\tau)}u(\tau)\,\mathrm{d}\tau\right) \geq 0, \tag{1.2}$$

where the overline denotes the complex conjugate.

Physically, the left-hand side of (1.2) is the energy supplied to the system over $(-\infty, t)$. For example, if u (resp. $\mathcal{Z}(u)$) has dimension $\mathrm{m}\cdot\mathrm{s}^{-1}$ (resp. $\mathrm{N}\cdot\mathrm{m}^{-2}$), then $\mathcal{Z}(u)u$ has dimension $\mathrm{W}\cdot\mathrm{m}^{-2}$, so that

$$I(t) = \int_{-\infty}^{t} \mathcal{Z}(u)(\tau)u(\tau)\,\mathrm{d}\tau$$

is an energy per unit surface. The passivity condition (1.2), which applies to every passive system encountered in physics, means that the system does not produce energy (Zemanian 1965, p. 301) (Lozano et al. 2000, p. 12).

Remark 1.2. The relevance of the passivity condition (1.2) can also be understood by considering the decay of acoustic energy in a smooth bounded open set $\Omega \subset \mathbb{R}^d$ ($d \in \mathbb{N}^*$). Formally, if the smooth functions $\tilde{p}$ and $\boldsymbol{u}$ satisfy

$$\partial_t \tilde{p} = -c_0 \nabla \cdot \boldsymbol{u},\ \partial_t \boldsymbol{u} = -c_0 \nabla \tilde{p},$$

then we have

$$\frac{1}{2}\frac{\mathrm{d}}{\mathrm{d}t}\left[\int_\Omega |\tilde{p}(t,\boldsymbol{x})|^2 \,\mathrm{d}\boldsymbol{x} + \int_\Omega |\boldsymbol{u}(t,\boldsymbol{x})|^2 \,\mathrm{d}\boldsymbol{x}\right] = -c_0 \int_{\partial\Omega} \tilde{p}\, \boldsymbol{u}\cdot\boldsymbol{n} \,\mathrm{d}\boldsymbol{x}.$$

The intuitive fact that passive impedance operators can yield energy decay will be at the heart of Parts II and III. However, this will not be developed further in this chapter, which focuses on the impedance operator in isolation.

Remark 1.3 (Passivity and reality). In some references, the definition of passivity includes reality, see e.g. (Beltrami and Wohlers 1966, § 3.5). In this dissertation, we separate the two conditions, which is in line with the acoustical literature (Rienstra 2006). Note that if $\mathcal{Z}$ satisfies the reality condition (ii) and the input u is real-valued, then the real part "$\Re$" and overline used in the inequality (1.2) are superfluous, since all the involved quantities are real-valued.

The admissibility of linear operators enjoys simpler characterizations. A standard result of distribution theory, recalled in Proposition A.4, gives that if $\mathcal{Z}$ is linear, continuous, and time-invariant (LTI) then it is a convolution operator. In this case, the IBC (1.1) reduces to

$$p(t) = [z \star \boldsymbol{u}\cdot\boldsymbol{n}](t), \tag{1.3}$$

where $z \in \mathcal{D}'(\mathbb{R})$ is the impedance kernel and "$\star$" denotes the time-domain convolution of distributions. (See Appendix A for a reminder on the convolution product.)

Remark 1.4 (Passivity and causality). If $\mathcal{Z}$ is LTI, then it is interesting to note that Definition 1.1 could be restricted to reality and passivity. Indeed, for real LTI systems, passivity *implies* causality (Zemanian 1965, Lemma. 10.3) (Beltrami and Wohlers 1966, Note 8). A consequence of this result is that a real anticausal LTI system cannot be passive: intuitively, for such a system the energy supplied over $(-\infty, t)$ can be made arbitrarily negative by modifying the input u in the future.

If the impedance kernel is causal and has a finite exponential growth, i.e. $z \in \mathcal{D}'_+(\mathbb{R})$ and $e^{-\sigma t} z \in \mathcal{S}'(\mathbb{R})$ for $\sigma > \sigma_0$, then the LTI IBC (1.3) can also be formulated in the Laplace domain as

$$\hat{p}(s,\boldsymbol{x}) = \hat{z}(s)\hat{\boldsymbol{u}}(s)\cdot\boldsymbol{n} \quad (\Re(s) > \sigma_0), \tag{1.4}$$

where $\hat{f}$ denotes the Laplace transform of f. In this dissertation, the Laplace transform is an analytic function on some open right half-plane

$$\mathbb{C}^+_{\sigma_0} \coloneqq \{s \in \mathbb{C} \,|\, \Re(s) > \sigma_0\}.$$

The definition of the Laplace transform is recalled in Appendix A.

Remark 1.5 (Laplace or Fourier?). Formally, $s = \mathrm{j}\omega$ yields the Fourier transform but such a mere formal substitution is error-prone, especially when dealing with admissibility conditions. The difficulty arises from the fact that the Fourier transform is in general a tempered distribution, by contrast with the Laplace transform which is an analytic function of an open right half-plane: a discussion on this topic is provided in Appendix A. The Laplace transform is also useful to derive time-domain representations of physical impedance models, as is done in Chapter 2.

Remark 1.6. The real (resp. imaginary) part of $\hat{z}$ is known as the *resistance* (resp. *reactance*).

In this dissertation, when there is no risk of confusion, the term "impedance" can designate the single-input single-output operator $\mathcal{Z}$, the convolution kernel z, or its Laplace transform $\hat{z}$. As already mentioned, each of these quantities can have a spatial dependency (i.e. $\mathcal{Z}(\boldsymbol{x},\cdot)$, $z(\boldsymbol{x},t)$, or $\hat{z}(\boldsymbol{x},s)$), although it is not explicitly written for the sake of clarity.

A key fact in practice is that the admissibility of an LTI impedance can be readily verified using its Laplace transform $\hat{z}$, as summarized in Proposition 1.8 below.

Definition 1.7 (Positive-real function)**.** Let

$$\mathbb{C}_0^+ \coloneqq \{s \in \mathbb{C} \,|\, \Re(s) > 0\}$$

be the open right half-plane. A function $f : \mathbb{C}_0^+ \to \mathbb{C}$ is *positive-real* if

(i) f is analytic in $\mathbb{C}_0^+$,

(ii) $f(s) \in \mathbb{R}$ for $s \in (0, \infty)$,

(iii) $\Re[f(s)] \geq 0$ for $\Re(s) > 0$.

Proposition 1.8. *If a LTI impedance operator $\mathcal{Z} : \mathcal{E}'(\mathbb{R}) \to \mathcal{D}'(\mathbb{R})$ is admissible, then*

(i) *$\mathcal{Z}(u) = z \star u$ with $z \coloneqq \mathcal{Z}(\delta) \in \mathcal{D}'_+(\mathbb{R}) \cap \mathcal{S}'(\mathbb{R})$,*

(ii) *The Laplace transform $\hat{z}$ is a positive-real function.*

Conversely, if f is a positive-real function, then $z \coloneqq \mathcal{L}^{-1}(f) \in \mathcal{D}'_+(\mathbb{R}) \cap \mathcal{S}'(\mathbb{R})$ and $u \mapsto z \star u$ is an admissible LTI impedance operator.

Proof. ($\Rightarrow$) Since $\mathcal{Z}$ is LTI and maps $\mathcal{D}'_+(\mathbb{R})$ to $\mathcal{D}'_+(\mathbb{R})$, it is a convolution operator with causal kernel, i.e. $\mathcal{Z}(u) = z \star u$ with $z \coloneqq \mathcal{Z}(\delta) \in \mathcal{D}'_+(\mathbb{R})$ (Beltrami and Wohlers 1966, p. 28). Moreover, since $\mathcal{Z}$ is real and passive, the Laplace transform $\hat{z}$ is a positive-real function (Beltrami and Wohlers 1966, Thm. 3.15) (Zemanian 1965, Thm. 10.4-1). This implies that, for any $\omega \in \mathbb{R}$, the limit

$$\lim_{\sigma \to 0} \hat{z}\,(\sigma + \mathrm{j}\omega) \tag{1.5}$$

is defined in $\mathcal{S}'(\mathbb{R})$ (Beltrami and Wohlers 1966, Thm. 3.17), so that by inverse Fourier transform z belongs to $\mathcal{S}'(\mathbb{R})$.

($\Leftarrow$) Since f is a positive-real function, its growth at infinity is at most polynomial:

$$|\hat{z}(s)| \leq C(a)P(|s|) \quad (\Re(s) \geq a > 0)\,,$$

where P is a second degree polynomial. This results follows from the integral representation of positive-real functions (Beltrami and Wohlers 1966, Eq. 3.21). Then, by inversion of the Laplace transform, $z \coloneqq \mathcal{L}^{-1}(f)$ is well-defined and belongs to $\mathcal{D}'_+(\mathbb{R})$. The conclusion follows from the fact that the limit (1.5) is defined in $\mathcal{S}'(\mathbb{R})$. □

To illustrate Proposition 1.8, let us give some practical examples of admissible impedance models that are encountered in Section 1.2.2.

The most elementary example is the proportional-integral-derivative kernel, defined as

$$\begin{cases} z_{\mathrm{PID}}(t) = a_{-1}\, H(t) + a_0 \delta(t) + a_1\, \delta'(t) \\ \hat{z}_{\mathrm{PID}}(s) = a_{-1}\, \frac{1}{s} + a_0 + a_1\, s, \end{cases}$$

where H is the Heaviside function, δ the Dirac distribution, and δ' is the derivative in the sense of distributions.

The fractional kernel of order $\alpha > 0$ is

$$Y_\alpha(t) \coloneqq \frac{H(t)}{\Gamma(\alpha)t^{1-\alpha}},\ \hat{Y}_\alpha(s) = \frac{1}{s^\alpha}, \tag{1.6}$$

and its distributional derivative for $\alpha \in (0,1)$ is

$$z(t) = Y_\alpha \star \delta' = \mathrm{pf}\left(\frac{H(t)}{\Gamma(\alpha-1)t^{2-\alpha}}\right),\ \hat{z}(s) = s^{1-\alpha},$$

where pf denotes Hadamard finite part (Zemanian 1965, § 2.5).

The time-delayed kernel

$$z(t) = a\delta(t) + b\delta(t-\tau),\ \hat{z}(s) = a + be^{-s\tau}$$

is admissible if $a \geq b \geq 0$ and $\tau \geq 0$.

However, the following kernels are *not* admissible:

$$z(t) = \frac{1}{\sqrt{\mathrm{j}}}\mathrm{pf}\left(\frac{H(t)}{\Gamma(-\frac{1}{2})t^{\frac{3}{2}}}\right),\ \hat{z}(s) = \sqrt{\frac{s}{\mathrm{j}}}, \tag{1.7}$$

which fails the reality condition;

$$\hat{z}(s) = a + be^{-s\tau}$$

with $a < b$ and $\tau \geq 0$, which is not passive;

$$z(t) = \delta(t+\tau),\ \hat{z}(s) = e^{s\tau},$$

with $\tau \geq 0$, which is not causal;

$$z(t) = e^t H(t),\ \hat{z}(s) = (s-1)^{-1},$$

which is not passive ($\hat{z}(s)$ is not analytic in $\mathbb{C}_0^+$ since it admits 1 as a pole).

The remainder of this section gives a similar treatment to the two other formulations of the IBC (1.1), namely the admittance and scattering formulations.

1.1.2 Admittance formulation

The admittance formulation is

$$\boldsymbol{u}(t) \cdot \boldsymbol{n} = \mathcal{Y}[p](t), \tag{1.8}$$

where $\mathcal{Y}$ is the admittance operator. When defined, the link between (1.1) and (1.8) is provided by

$$\mathcal{Y} \circ \mathcal{Z} = \mathcal{I}, \tag{1.9}$$

where $\mathcal{I}$ denotes the identity operator. Using the fact that the inverse of a positive-real function is a positive-real function, one simply obtains that if $\mathcal{Z}$ is LTI and admissible, then the admittance operator $\mathcal{Y}$ exists, is unique, and is also LTI and admissible with

$$y \star z = \delta,\ \hat{y}(s)\hat{z}(s) = 1, \tag{1.10}$$

where y is the admittance kernel. In this case, the IBC (1.8) reduces to

$$\boldsymbol{u}(t) \cdot \boldsymbol{n} = [y \star p](t). \tag{1.11}$$

The admissibility conditions on $\mathcal{Y}$ are strictly identical to that of $\mathcal{Z}$, so that Proposition 1.8 with "admittance" substituted for "impedance" holds true.

Remark 1.9. The real (resp. imaginary) part of $\hat{y}$ is known as the *conductance* (resp. *susceptance*).

In the LTI case, the admissibility of the impedance operator implies that of the admittance operator: if $\mathcal{Z}$ is an admissible LTI impedance operator, then $\mathcal{Y}$ is an admissible LTI admittance operator. This follows from the fact that the inverse of a positive-real function is a positive-real function, see the lemma below.

Lemma 1.10. *Let $f : \mathbb{C}_0^+ \to \mathbb{C}$ be a positive-real function. Then:*

(i) *f has no zeros in $\mathbb{C}_0^+$.*

(ii) *$1/f$ is a positive-real function.*

Proof. For the particular case where f is a rational function, this result is mentioned in (Ioannou and Tao 1987). We propose here an elementary proof. (i) By assumption, $\Re(f(s)) \geq 0$ for any $s \in \mathbb{C}_0^+$, so that

$$\forall (s_0, s_1) \in \mathbb{C}_0^+ \times \mathbb{C}_0^+,\ |\arg(f(s_0)) - \arg(f(s_1))| \leq \left(\frac{\pi}{2} - \left(-\frac{\pi}{2}\right)\right) = \pi.$$

Since f is analytic in $\mathbb{C}_0^+$, it follows from the argument principle (Gamelin 2001, § VIII.1) that

$$N_f \leq \frac{1}{2\pi}\pi = \frac{1}{2}$$

where N_f is the number of zeros of f in any open subset of $\mathbb{C}_0^+$. Since $N_f \in \mathbb{N}$, we deduce $N_f = 0$. (ii) Since f is analytic and has no zeros in $\mathbb{C}_0^+$, $1/f$ is analytic in $\mathbb{C}_0^+$. Moreover, by assumption on f, $1/f(s) \in \mathbb{R}$ for $s \in (0, \infty)$. The conclusion follows from the identity $\Re\left(\frac{1}{f(s)}\right) = \frac{\Re(f(s))}{|f(s)|^2}$. □

1.1.3 Scattering formulation

The third and last considered formulation of the IBC (1.1) is the so-called scattering formulation

$$\tilde{p}(t) - \boldsymbol{u}(t) \cdot \boldsymbol{n} = \mathcal{B}[\tilde{p} + \boldsymbol{u} \cdot \boldsymbol{n}](t), \tag{1.12}$$

where $\mathcal{B}$ is the scattering operator and

$$\tilde{p} \coloneqq \frac{p}{z_0}$$

with $z_0 > 0$ is dimensionally homogeneous to $\boldsymbol{u}$. The scattering formulation is ubiquitous in system theory, see (Lozano et al. 2000, § 2.8) (Staffans 2002) and references therein. It has an elementary physical interpretation that justifies its name: the incident wave $\tilde{p} + \boldsymbol{u} \cdot \boldsymbol{n}$ is reflected back as $\tilde{p} - \boldsymbol{u} \cdot \boldsymbol{n}$. (See for instance the characteristics of the linearized Euler equations (3.1).)

The admissibility conditions given in Definition 1.1 can be readily written under their scattering variant: the causality and reality properties are identical, while the passivity condition (1.2) can be rewritten using the elementary algebraic identity

$$4\tilde{p}u = (\tilde{p} + u)^2 - (\tilde{p} - u)^2.$$

This leads to the definition below.

Definition 1.11 (Admissibility conditions)**.** Let $\mathcal{B} : \mathcal{E}'(\mathbb{R}) \to \mathcal{D}'(\mathbb{R})$ be a continuous operator. It is said to be an *admissible* scattering operator if it enjoys the following properties:

(i) (Causality) If $u \in \mathcal{D}'_+(\mathbb{R})$, then $\mathcal{B}(u)$ exists and belongs to $\mathcal{D}'_+(\mathbb{R})$.

(ii) (Reality) Real-valued inputs are mapped to real-valued outputs.

(iii) (Passivity) For every $v \in \mathcal{C}_0^\infty(\mathbb{R})$ and $t > 0$,

$$\int_{-\infty}^{t} |\mathcal{B}(v)(\tau)|^2 \,\mathrm{d}\tau \leq \int_{-\infty}^{t} |v(\tau)|^2 \,\mathrm{d}\tau. \tag{1.13}$$

The passivity condition written under the form (1.13) implies that $\mathcal{B}$, as a map from $L^2(\mathbb{R})$ to $L^2(\mathbb{R})$, is a contraction. From this fact, the reader may guess the potential computational benefits of $\mathcal{B}$ over $\mathcal{Z}$ and $\mathcal{Y}$: an elementary numerical example is provided in Chapter 6.

When possible, the scattering operator $\mathcal{B}$ can be deduced from the (nonlinear) impedance operator $\mathcal{Z}$ through

$$\mathcal{B} \coloneqq \left(\frac{\mathcal{Z}}{z_0} - \mathcal{I}\right) \circ \left(\frac{\mathcal{Z}}{z_0} + \mathcal{I}\right)^{-1} = \mathcal{I} - 2\left(\frac{\mathcal{Z}}{z_0} + \mathcal{I}\right)^{-1}. \tag{1.14}$$

An example of physical nonlinear scattering operator derived using this expression is given in Chapter 2. If $\mathcal{Z}$ is LTI and admissible, then $\mathcal{B}$ exists, is unique, and is an admissible LTI scattering operator with kernel β so that the IBC (1.12) reads

$$\tilde{p}(t) - \boldsymbol{u}(t) \cdot \boldsymbol{n} = \beta \star [\tilde{p} + \boldsymbol{u} \cdot \boldsymbol{n}](t).$$

The Laplace transform of β is given by

$$\hat{\beta}(s) = \frac{\frac{\hat{z}(s)}{z_0} - 1}{\frac{\hat{z}(s)}{z_0} + 1} = 1 - \frac{2}{\frac{\hat{z}(s)}{z_0} + 1} \quad (\Re(s) > 0). \tag{1.15}$$

Intuitively, $z = \infty$, $y = 0$, and $\mathcal{B} = \mathcal{I}$ ($\beta = \delta$) yield a hard wall while $z = 0$, $y = \infty$, and $\mathcal{B} = -\mathcal{I}$ (kernel $\beta = -\delta$) yield a pressure-release wall.

Remark 1.12. The Laplace transform $\hat{\beta}$ is known as the *reflection coefficient* in the acoustical literature.

Similarly to the impedance and admittance cases, the admissibility of an LTI scattering operator can be conveniently characterized using the Laplace transform of its kernel, namely the reflection coefficient $\hat{\beta}$. The result, given in Proposition 1.14, is identical to that of Proposition 1.8 with "bounded-real" substituted for "positive-real".

Definition 1.13 (Bounded-real function)**.** A function $g : \mathbb{C}_0^+ \to \mathbb{C}$ is *bounded-real* if g is analytic in $\mathbb{C}_0^+$, $g(s) \in \mathbb{R}$ for $s \in (0, \infty)$, and $|g(s)| \leq 1$ for $\Re(s) > 0$.

Proposition 1.14. *If a LTI scattering operator $\mathcal{B} : \mathcal{E}'(\mathbb{R}) \to \mathcal{D}'(\mathbb{R})$ is admissible, then*

(i) *$\mathcal{B}(v) = \beta \star v$ with $\beta \coloneqq \mathcal{B}(\delta) \in \mathcal{D}'_+(\mathbb{R}) \cap \mathcal{S}'(\mathbb{R})$,*

(ii) *The Laplace transform $\hat{\beta}$ is a bounded-real function.*

Conversely, if g is a bounded-real function, then $\beta \coloneqq \mathcal{L}^{-1}(g) \in \mathcal{D}'_+(\mathbb{R}) \cap \mathcal{S}'(\mathbb{R})$ and $v \mapsto \beta \star v$ is an admissible LTI scattering operator.

Proof. The proof is similar to that of Proposition 1.8.
($\Rightarrow$) Since $\mathcal{B}$ is LTI and maps $\mathcal{D}'_+(\mathbb{R})$ to $\mathcal{D}'_+(\mathbb{R})$, it is a convolution operator with a causal kernel β. Moreover, since $\mathcal{B}$ is real and passive in the sense of (1.13), the Laplace transform $\hat{\beta}$ is a bounded-real function (Beltrami and Wohlers 1966, Thm. 3.18). The conclusion follows from the fact that, since $\hat{\beta}$ is a bounded holomorphic function, its boundary value on $\mathrm{j}\mathbb{R}$ belongs to $L^\infty(\mathbb{R})$.

($\Leftarrow$) Since g is analytic in $\mathbb{C}_0^+$ and bounded, inversion of the Laplace transform gives $\beta \in \mathcal{D}'_+(\mathbb{R})$. The conclusion follows from the same arguments than ($\Rightarrow$). □

Material	Illustration	Impedance model expression
CT liner	Figure 1.4	(1.24) with (1.17) or (1.25)
SDOF liner	Figure 1.6	(1.29) with (1.19,1.25) and, if needed, the additive nonlinear term (1.32)
DDOF liner	Figure 1.7	(1.30) with (1.16,1.19,1.25) and, if needed, the additive nonlinear term (1.32)

Table 1.1. Summary of the sound absorbing material impedance models given in Section 1.2.

An intuitive understanding of Proposition 1.14 can be obtained by noting that the map

$$\left|\begin{array}{l} \mathbb{C}_0^+ \to \{s \in \mathbb{C} \,|\, |s| < 1\} \\ s \mapsto \dfrac{s-1}{s+1} \end{array}\right.$$

is conformal, i.e. analytic, one-to-one, and onto (Gamelin 2001, § XI.1). See also the following proposition.

Proposition 1.15 ((Lozano et al. 2000, Thm. 2.9))**.** *Let $f, g : \mathbb{C}_0^+ \to \mathbb{C}$. If g is bounded real and $g \neq 1$ in $\mathbb{C}_0^+$, then $\frac{1+g}{1-g}$ is positive-real. If h is positive-real, then $\frac{h-1}{1+h}$ is bounded real.*

1.2 Physical impedance models

The purpose of this section is to introduce physical aspects of IBCs. Section 1.2.1 recalls the definition of a locally reacting surface and two basic impedance models. Section 1.2.2 builds upon these generalities to derive the standard linear models for single and double degree of freedom liners. The modeling of nonlinearities and grazing flow is discussed in Section 1.2.3.

We warn the reader that this section, by contrast with the previous one, contains mostly physical considerations. The reader only interested in the expressions of physical models can consult Table 1.1 and skip to Section 1.3.

1.2.1 Generalities

Locally reacting surface

As mentioned in the introduction and Section 1.1, IBCs are meant to model locally reacting surfaces. To define this concept, let us consider the case of a plane progressive harmonic wave (PPHW) reaching a surface Σ that materializes a discontinuous separation between two media having different acoustic properties. Figure 1.1a depicts the case where the transmitted wave has a wavenumber k_t with a non-null tangential component (i.e. a non-null angle θ_t). By definition, a locally reacting surface is obtained when $\theta_t = 0$. (See (Kinsler and Frey 1962, § 6.7) for a physical discussion.)

Definition 1.16 (Locally reacting surface)**.** A *locally reacting* (also *normally reacting*) surface is a surface that refracts waves such that the transmitted waves propagate only in the normal direction (i.e. only at right angle to the surface), as depicted in Figure 1.1b. Such a surface can be modeled using an IBC, introduced in Section 1.1.

Physically, an IBC models the effect of a locally reacting absorbing material on the sound field after a homogenization distance, see (Laurens et al. 2014) and (Popie 2016) for theoretical studies on perforated plates.

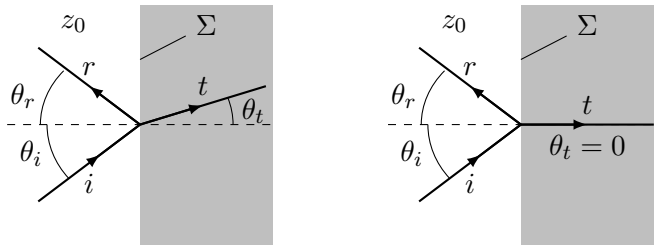

(a) Non-locally reacting surface. **(b)** Locally reacting surface.

Figure 1.1. Oblique incidence of a PPHW on a surface Σ that separates two media. The three depicted wavenumbers are associated with the incident (i), transmitted (t) and reflected (r) waves.

Remark 1.17 (Resonant frequencies). For a normally incident PPHW of angular frequency ω, the power absorption coefficient is given by (Kinsler and Frey 1962, Eq. 6.17)

$$\alpha_t = z_1 \frac{4\Re[\hat{z}(\mathrm{j}\omega)]}{|z_1 + \hat{z}(\mathrm{j}\omega)|^2}.$$

From this expression, we deduce that for an impedance $\hat{z}$ to be optimal at ω, i.e. to absorb the most energy, it is necessary that $\Im[\hat{z}(\mathrm{j}\omega)] = 0$. Frequencies at which the reactance is null (resp. maximal) are called *resonant* (resp. *anti-resonant*) frequencies. Note, however, that when higher-order modes are considered the reactance of the optimal impedance is not null in general (Cremer 1953; Tester 1973b).

Remark 1.18 (Experimental measurement). Reviews of experimental techniques can be found in (Primus 2012, § 1.3) and (Richter 2010, § 1.3). In acoustics, the impedance of an absorbing material can easily be deduced from two measurements of acoustic pressure in a device known as an impedance or Kundt tube. However, in the presence of flow, impedance measurement is a much more involved process; the existing methods can be split into two categories:

- Direct methods, where the impedance is deduced from local measurements, typically of acoustic velocity and pressure around or inside the material. These methods are also used with data coming from direct numerical simulations.
- Inverse methods, where the impedance is identified based on acoustic velocity and pressure measurements.

The remainder of this section focuses on recalling basic linear impedance models in preparation for the derivations of Section 1.2.2.

Basic impedance models: impedance tube

Let us consider the impedance tube depicted in Figure 1.2 that consists in a cavity of cross-section S_c and length l_c filled with a medium of characteristic impedance z_c. Its impedance, with respect to the surface S_c, is given by

$$\hat{z}_{|S_c} = \frac{\langle \hat{p} \rangle_{S_c}}{\langle \hat{\boldsymbol{u}} \cdot \boldsymbol{n} \rangle_{S_c}},$$

where $\langle \cdot \rangle_S$ denotes the spatial average over S and $\boldsymbol{n}$ is the *inward* unit normal (i.e. it points towards the tube).

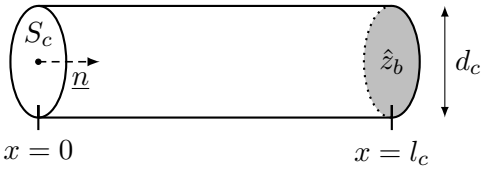

Figure 1.2. Cylindrical impedance tube of length l_c, diameter d_c, cross-section S_c, backing impedance $\hat{z}_b$, and characteristic impedance z_c.

The simplest way of assessing this impedance is to model the cavity as a monodimensional waveguide $(0, l_c)$ with propagation wavenumber k_c. In the Laplace domain, this reads

$$(\mathrm{j}k_c(s))^2\,\hat{p}(x,s) = \partial_x^2\hat{p}(x,s),\ \mathrm{j}k_c(s)\,\hat{u}(x,s) = -\frac{1}{z_c}\partial_x\hat{p}(s,x) \quad (x \in (0,l_c))\,.$$

With this modeling, the backing impedance $\hat{z}_b$ and tube impedance $\hat{z}_{|S_c}$ are given by

$$\hat{z}_b(s) = \frac{\hat{p}(s,x=l_c)}{\hat{u}(s,x=l_c)},\ \hat{z}_{|S_c} = \frac{\hat{p}(s,x=0)}{\hat{u}(s,x=0)}.$$

This leads to the standard formula

$$\hat{z}_{|S_c} = \hat{z}_{\mathrm{tube}}(k_c l_c, z_c, \hat{z}_b),$$

with (Kinsler and Frey 1962, Eq. 8.35) (Kuttruff 2007, Eq. 8.10) (Mechel 2008, Eq. C.2.12) (Allard and Atalla 2009, Eq. 2.16)

$$\hat{z}_{\mathrm{tube}}(k_c l_c, z_c, \hat{z}_b) \coloneqq z_c\frac{\hat{z}_b\cos(k_c l_c) + \mathrm{j}z_c\sin(k_c l_c)}{z_c\cos(k_c l_c) + \mathrm{j}\hat{z}_b\sin(k_c l_c)} = z_c\frac{\hat{z}_b\cosh(\mathrm{j}k_c l_c) + z_c\sinh(\mathrm{j}k_c l_c)}{z_c\cosh(\mathrm{j}k_c l_c) + \hat{z}_b\sinh(\mathrm{j}k_c l_c)}. \tag{1.16}$$

If the cavity is rigidly backed, i.e. if $\hat{z}_b = \infty$, then this impedance reduces to

$$\hat{z}_{|S_c} = -\mathrm{j}z_c\cot(k_c l_c) = z_c\coth(\mathrm{j}k_c l_c).$$

Following Proposition 1.8, the wavenumber k_c must be chosen so that the impedance is a positive-real function. A model for the wavenumber k_c suitable for liners is covered in Section 1.2.2. The simplest particular case is that of a lossless air-filled cavity (i.e. wave equation on $(0, l_c)$), which yields

$$\mathrm{j}k_c = \frac{s}{c_0} \tag{1.17}$$

so that the cavity impedance is a positive-real function given by

$$\hat{z}_{|S_c} = z_c\coth\left(\frac{sl_c}{c_0}\right) \underset{0}{=} \frac{c_0 l_c}{s} + \mathcal{O}\left(\left|\frac{sl_c}{c_0}\right|\right),$$

where

$$\mathrm{He} \coloneqq \left|\frac{sl_c}{c_0}\right|$$

is known as the Helmholtz number.

Remark 1.19. The derivation of (1.16) assumes that only plane waves propagate in the impedance tube, i.e. that the considered frequencies are below the cut-off frequency. For a cylindrical tube of diameter d_c, the cut-off frequency is given by (Rienstra and Hirschberg 2016, § 7.2)

$$f_{\text{cut-off}} = \frac{c_0}{2\pi}\frac{1.8412}{d_c/2},$$

so that this is not a practical restriction when modeling micro-perforations: a diameter of 9.5 mm gives a cut-off frequency of 21 kHz for instance.

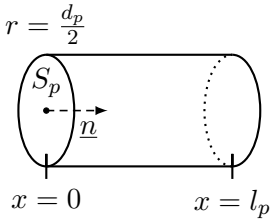

Figure 1.3. Cylindrical perforation of length l_p, diameter d_p, and cross-section S_p.

Basic impedance models: perforation impedance

The second basic component of an acoustical liner is its perforation. Figure 1.3 presents a schematic of a cylindrical perforation of length l_p, diameter d_p, and cross-section S_p. We recall below the model introduced in (Crandall 1926, App. A); a detailed derivation can be found in (Monteghetti 2015, App. C). The model relies on the following three hypotheses.

- The perforation is an infinite axisymmetric cylinder of diameter d_p.
- The pressure gradient is longitudinal, i.e. $\nabla p \propto \boldsymbol{e_x}$, and independent of the radial coordinate r.
- The flow obeys the Stokes equation

$$\rho_0 \partial_t u(r,x,t) = -\partial_x p(x,t) + \rho_0 \nu \Delta u(r,x,t), \tag{1.18}$$

  with a no-slip boundary condition at $r = {}^{d_p}/_2$.

Applying the Laplace transform to (1.18), solving the resulting PDE in (r,x), and taking a cross-section average leads to

$$\langle \hat{u} \rangle_{S_p}(x) = -\frac{1}{\rho_0 s}\left[1 - \Phi\left(k_\nu {}^{d_p}/_2\right)\right] \frac{\mathrm{d}\hat{p}}{\mathrm{d}x}(x),$$

where

$$\Phi(s) \coloneqq \frac{2}{s}\frac{I_1}{I_0}(s)$$

with I_n the *modified* Bessel function of the first kind of order n and

$$k_\nu \coloneqq \sqrt{\frac{s}{\nu}}$$

is the wavenumber associated with viscous diffusion. Since the incompressibility hypothesis implies that $\langle \hat{u} \rangle_{S_p}$ is independent of x, the perforation impedance is given by

$$\frac{\hat{p}(0) - \hat{p}(l_p)}{\langle \hat{u} \rangle_{S_p}} = \hat{z}_{\mathrm{perf}}(l_p, d_p)$$

where

$$\hat{z}_{\mathrm{perf}}(l_p,d_p) \coloneqq \rho_0 l_p s \left[1 - \Phi\left(k_\nu {}^{d_p}/_2\right)\right]^{-1} \tag{1.19}$$

$$\underset{+\infty}{=} 3\frac{\rho_0 l_p \nu}{\left({}^{d_p}/_2\right)^2} + 2\frac{\rho_0 l_p \sqrt{\nu}}{{}^{d_p}/_2}\sqrt{s} + \rho_0 l_p s + \mathcal{O}\left[\frac{1}{\left|k_\nu {}^{d_p}/_2\right|}\right] \tag{1.20}$$

$$\underset{0}{=} 8\frac{\rho_0 l_p \nu}{\left({}^{d_p}/_2\right)^2} + \frac{4}{3}\rho_0 l_p s + \mathcal{O}\left[\left|k_\nu {}^{d_p}/_2\right|^4\right]. \tag{1.21}$$

The nondimensional number

$$\mathrm{St} \coloneqq |k_\nu {}^{d_p}\!/_2|$$

is known as the Stokes number and is proportional to the ratio of the diameter d_p to the acoustic boundary layer thickness. The provided low and high frequency approximations are positive-real functions when the physical coefficients are nonnegative; it can be verified numerically that the same is true about the full model (1.19), but no proof is given herein.

Remark 1.20. If the perforation is not a cylinder but a slit of width d_p, the expression of $\hat{z}_{\mathrm{perf}}$ is still (1.19) but with $\Phi(s) \coloneqq {}^{\tanh(s)}\!/_s$ (Allard and Atalla 2009, Chap. 4).

Remark 1.21. The use of the Stokes equation in the derivation of the perforation impedance (1.19) assumes incompressibility; the quantity k_ν has the dimension of a wavenumber but is not associated with a propagation phenomenon, by contrast with k_c in (1.16). Incompressibility is physically satisfied provided that the minimum wavelength of the considered acoustic field is large compared to the dimensions of the cylinder, which reads $\mathrm{He} \ll 1$ or equivalently

$$f \ll \frac{c_0}{2\pi \max(l_p, d_p)}.$$

This is not a practical limitation with a micro-perforation: for $d_p = 0.3\,\mathrm{mm}$ and $l_p = 0.8\,\mathrm{mm}$, we get $f \ll 68\,\mathrm{kHz}$.

Impedance corrections

The two basic impedance models covered above discard finite length effects, which can be attributed to one of the following phenomena.

- (Radiation.) At a discontinuity, sound waves are radiated and diffracted.
- (Viscosity.) Although viscosity is present in the Crandall model (1.19), it does not account for all viscous effects such as the ones at the entrance of the perforation.
- (Interaction.) The cavity or the perforation modeled above is not alone in an infinite space, but rather one among many others on a surface.

In the acoustical literature, the common way to account for these effects is to use impedance corrections. Corrections applicable to the two introduced models can be found in (Melling 1973, § 2), (Malmary 2000, Chaps. 1–2), and (Monteghetti 2015, § 3.3). These corrections typically consists in modifying the length involved in the model, i.e. l_c or l_p. Since they do not change the mathematical nature of the impedance model in the time domain, we do not recall them here.

Remark 1.22 (Non admissible corrections). In the acoustical literature, one commonly encounters the viscous correction term $\hat{z}_{\mathrm{visc}}(\mathrm{j}\omega) = \sqrt{\omega}$, which was introduced in (Ingard 1953). This correction is not admissible in isolation, since the corresponding kernel z_{visc} is complex-valued, see (1.7). More generally, non positive-real correction terms can arise from truncated Taylor expansions. Consider for example the radiation correction term (Guess 1975, Eq. 11), which reads $\hat{z}_{\mathrm{rad}}(\mathrm{j}\omega) = z_0 \frac{d_p^2}{8c_0^2}\omega^2 + \mathrm{j} z_0 \frac{4d_p}{3\pi c_0}\omega$.

Surface impedance

When manipulating impedance models, it is of paramount importance to keep track of the surface with which they have been computed: this is the reason for using the subscript "$|S$"

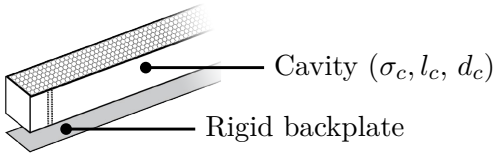

Figure 1.4. CT liner. (Adapted from (Jones et al. 2005, Fig. 3a).)

above. The mass conservation identity $S_0 \langle \hat{\boldsymbol{u}} \cdot \boldsymbol{n} \rangle_{S_0} = S_1 \langle \hat{\boldsymbol{u}} \cdot \boldsymbol{n} \rangle_{S_1}$ implies

$$\hat{z}_{|S_0} = \frac{S_0}{S_1} \hat{z}_{|S_1} = \frac{\sigma_0}{\sigma_1} \hat{z}_{|S_1},$$

where σ_i is the porosity of the surface S_i, defined as

$$\sigma_i \coloneqq \frac{S_i}{S_{\text{total}}}, \tag{1.22}$$

where S_{total} is the total surface. In particular, the surface impedance $\hat{z}$, which is the one used in the IBC (1.3), can be deduced from a given model $\hat{z}_{|S}$ using

$$\hat{z} = \hat{z}_{|S_{\text{total}}} = \frac{1}{\sigma} \hat{z}_{|S}. \tag{1.23}$$

1.2.2 Acoustical models for liners

Building upon the basic model introduced in Section 1.2.1, models for three kinds of liners are considered herein.

Ceramic tubular (CT) liner

CT liners, described in (Jones et al. 2005) and depicted in Figure 1.4, essentially consist in a set of long and narrow cavities. Their impedance operators stay linear for a wide range of incident SPLs, which make them valuable materials for code validation. They are mostly used for academic experiments.

The surface impedance is directly deduced from (1.16), namely

$$\hat{z}_{\text{CT}} = \frac{z_c}{\sigma_c} \coth(\mathrm{j} k_c l_c), \tag{1.24}$$

where σ_c is the porosity, l_c the cavity length, and k_c the propagation wavenumber. Assuming the cavities to be cylindrical with diameter d_c, a suitable wavenumber is (Bruneau 2006, § 3.7)

$$\mathrm{j} k_c(s) = \frac{s}{c_0} \left[\frac{1 + (\gamma - 1)\, \Phi\left(k_\kappa {}^{d_c}/_2\right)}{1 - \Phi\left(k_\nu {}^{d_c}/_2\right)} \right]^{1/2} \tag{1.25}$$

$$\underset{+\infty}{=} \frac{s}{c_0} \left[1 + \frac{\sqrt{\nu}}{{}^{d_c}/_2} \left(\frac{\gamma - 1}{\sqrt{\text{Pr}}} + 1 \right) \frac{1}{\sqrt{s}} \right] + \mathcal{O}[1] \tag{1.26}$$

$$\underset{0}{=} \frac{s}{c_0} \left[\frac{2\sqrt{2}\sqrt{\gamma\nu}}{{}^{d_c}/_2} \frac{1}{\sqrt{s}} \right] + \mathcal{O}\left[\left| k_\nu {}^{d_c}/_2 \right|^3 \right], \tag{1.27}$$

where γ denotes the ratio of specific heat, κ the thermal diffusivity, k_κ the wavenumber associated with thermal diffusion

$$k_\kappa \coloneqq \sqrt{\frac{s}{\kappa}} = k_\nu \sqrt{\text{Pr}},$$

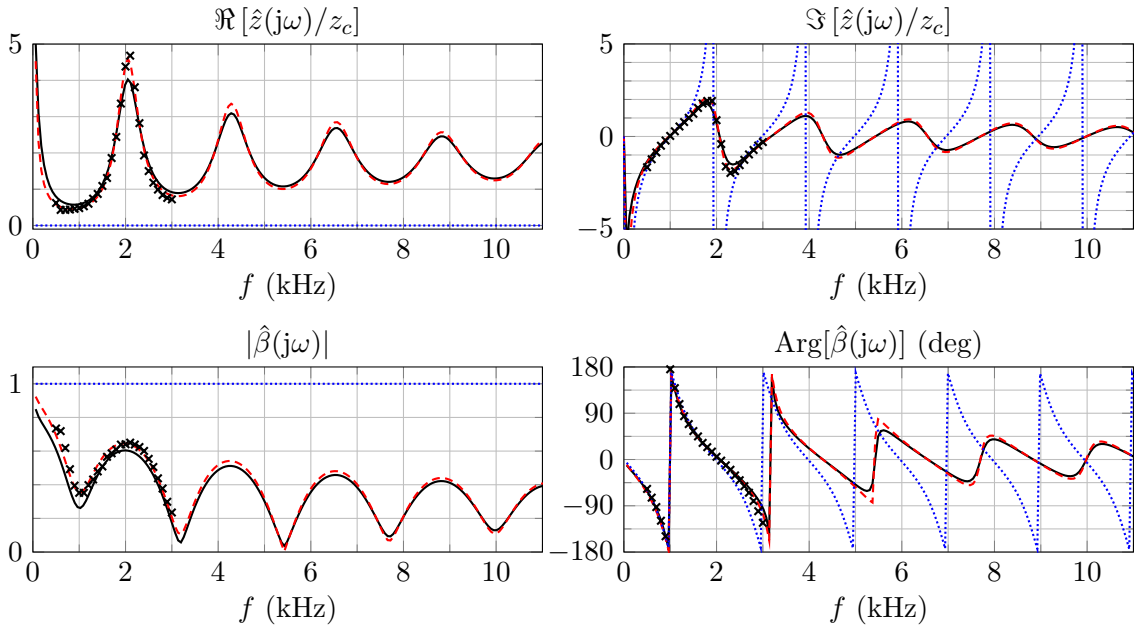

Figure 1.5. Impedance model (1.24) for the CT57 liner. (×) CT57 liner at 130 dB (Jones et al. 2005). Dimensions: $\sigma_c = 57\,\%$, $d_c = 0.6\,\mathrm{mm}$, and $l_c = 85.6\,\mathrm{mm}$. (——) Bruneau wavenumber (1.25) using the corrected length $l_c = 0.84 \times 85.6\,\mathrm{mm}$ and diameter $d_c = 0.8 \times 0.6\,\mathrm{mm}$. (- - - -) High-frequency approximation of the Bruneau wavenumber (1.26) using the same corrected values. (·····) Lossless wavenumber (1.17) using the uncorrected length $l_c = 85.6\,\mathrm{mm}$.

and Pr the Prandtl number. The provided low and high frequency approximations lead to a positive-real impedance model when the physical coefficients are nonnegative; it can be verified numerically that the same is true about the full model (1.24,1.25), but no proof is given herein.

The impedance model (1.24) with the three wavenumbers (1.17), (1.25), and (1.26) is plotted in Figure 1.5 against experimental impedance measurements for the CT57 liner available in (Jones et al. 2005). The wave number (1.17) is insufficient to fit the experimental data, as it does not model viscous and thermal dissipation in the cavity, leading to a null resistance (resp. reflection coefficient with modulus one) shown in the top left (resp. bottom left) graph. The two other wavenumbers give a satisfactory fit, provided that the cavity length and diameter are corrected. In particular, the resistance peak at 2 kHz, the first anti-resonant frequency, is well-captured. Additional experimental data is needed to assess the validity of the model at higher frequencies, where a damping of the resistance peaks is predicted.

Remark 1.23. In the lossless case (1.17,1.24) the resonant angular frequencies ω_n and associated wavelengths λ_n are given by

$$\omega_n = 2\pi f_n = \pi\,(2n+1)\,\frac{c_0}{2l_c},\ \lambda_n = \frac{4}{2n+1}l_c \quad (n \in \mathbb{Z}), \tag{1.28}$$

so that the CT liner is a quarter-wavelength resonator.

Single degree of freedom (SDOF) liner

SDOF liners are the acoustical treatment commonly mounted in the inlet of jet engines. They are based on the principle of the Helmholtz resonator and consist in a honeycomb structure covered by a perforated plate, see Figure 1.6. Intuitively, the cavities set the resonant frequency while the perforations set the viscous dissipation. As perforating a plate with sub-millimeter holes is a

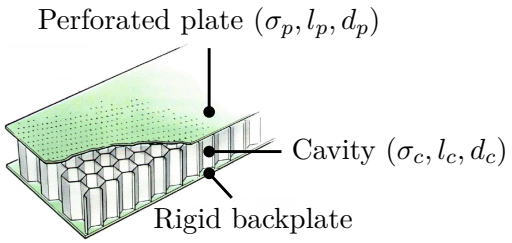

Figure 1.6. SDOF liner. (Adapted from (Rolls-Royce plc 1996, Fig. 19-6).)

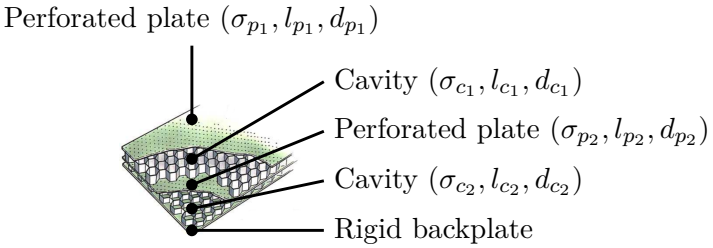

Figure 1.7. DDOF liner. (Adapted from (Rolls-Royce plc 1996, Fig. 19-6).)

technical challenge, it is common to distinguish between perforated and micro-perforated plates, which have sub-millimeter perforations. The absorption properties of micro-perforated plates are less dependent upon the incident SPL and Mach number than their non micro-perforated counterparts.

An impedance model can be built from the two models covered in Section 1.2.1. Namely,

$$\begin{aligned}\hat{z}_{\mathrm{SDOF}|S_p} = \frac{\langle \hat{p}(0)\rangle_{S_p}}{\langle \hat{u}(0)\rangle_{S_p}} &\simeq \frac{\langle \hat{p}(0)\rangle_{S_p} - \langle \hat{p}(l_p)\rangle_{S_p}}{\langle \hat{u}(0)\rangle_{S_p}} + \frac{\langle \hat{p}(l_p)\rangle_{S_p}}{\langle \hat{u}(l_p)\rangle_{S_p}} \\ &= \hat{z}_{\mathrm{perf}}(l_p, d_p) + \frac{S_p}{S_c} z_c \coth(\mathrm{j}k_c l_c),\end{aligned}$$

so that the corresponding surface impedance is

$$\hat{z}_{\mathrm{SDOF}} = \frac{1}{\sigma_p}\hat{z}_{\mathrm{perf}}(l_p, d_p) + \frac{z_c}{\sigma_c}\coth(\mathrm{j}k_c l_c). \tag{1.29}$$

In practice, the porosity of the honeycomb structure is close to unity, i.e. $\sigma_c \simeq 1$. Provided that the wavenumber k_c is chosen so that the cavity impedance is a positive-real function, the admissibility of (1.29) follows from the fact that the sum of two positive-real functions is a positive-real function.

Remark 1.24. In the SDOF liner, the perforation and cavity are connected in series. In the derivation above, we have assumed that $\langle u\rangle_{S_p}$ is conserved across the perforation so that the impedance $\hat{z}_{\mathrm{SDOF}}$ is the sum of of the perforation and cavity impedance kernels.

Double degree of freedom (DDOF) liner

As depicted in Figure 1.7, a DDOF liner is simply made from the superposition of two SDOF liners. Accordingly, the impedance model is derived along the same lines. Starting at $x = 0$ and using a perforation impedance yields

$$\hat{z}_{|S_{p_1}} = \hat{z}_{\mathrm{perf}}(l_{p_1}, d_{p_1}) + \frac{\langle \hat{p}(l_{p_1})\rangle_{S_{p_1}}}{\langle \hat{u}(l_{p_1})\rangle_{S_{p_1}}} = \hat{z}_{\mathrm{perf}}(l_{p_1}, d_{p_1}) + \frac{\sigma_{p_1}}{\sigma_{c_1}}\frac{\langle \hat{p}(l_{p_1})\rangle_{S_{c_1}}}{\langle \hat{u}(l_{p_1})\rangle_{S_{c_1}}}.$$

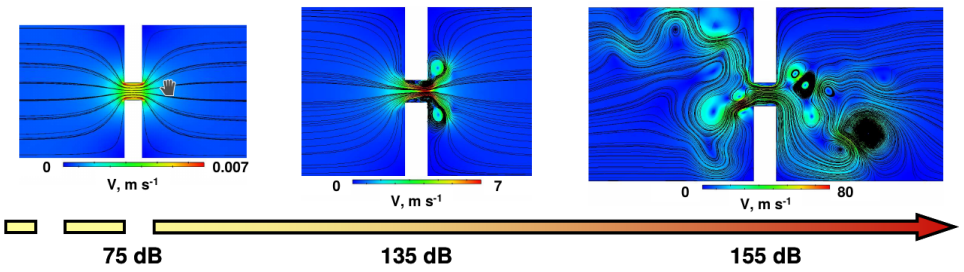

Figure 1.8. Acoustic field with increasing incident sound pressure. Direct numerical simulation of a 2D rectangular acoustic resonator. From (Roche 2011, Fig. 4.1).

The impedance ratio at $x = l_{p_1}$ is then computed using (1.16), leading to the surface impedance

$$\hat{z}_{\mathrm{DDOF}} = \frac{1}{\sigma_{p_1}} \hat{z}_{\mathrm{perf}}(l_{p_1}, d_{p_1}) + \frac{1}{\sigma_{c_1}} \hat{z}_{\mathrm{tube}}(k_{c_1} l_{c_1}, z_{c_1}, \hat{z}_{2|S_{c_1}}), \tag{1.30}$$

where

$$\hat{z}_{2|S_{c_1}} = \frac{\sigma_{c_1}}{\sigma_{p_2}} \hat{z}_{2|S_{p_2}} = \frac{\sigma_{c_1}}{\sigma_{p_2}} \left[\hat{z}_{\mathrm{perf}}(l_{p_2}, d_{p_2}) + z_{c_2} \frac{\sigma_{p_2}}{\sigma_{c_2}} \coth(\mathrm{j} k_{c_2} l_{c_2}) \right].$$

The admissibility of this model is obtained similarly to that of the SDOF model.

1.2.3 Grazing flow and nonlinearities

The models considered in Section 1.2.2 belong to the realm of linear acoustics. In particular, they assume that the propagation medium is quiescent and the incident SPL is low. Models covering grazing flow and high incident SPLs are covered below.

Nonlinear absorption mechanism

SDOF liners exhibit the following nonlinear absorption mechanism: as the amplitude of the incident sound wave increases past a given threshold, the acoustic boundary layer within the perforation separates, which induces vortices (Melling 1973). This purely acoustic phenomenon, known in the literature as *vortex shedding*, can be visualized in Figure 1.8. The associated sound absorption mechanism is, first, conversion of acoustic energy into rotational energy, and second, the dissipation of this rotational energy.

A simple model of the corresponding contribution to the impedance operator can been derived following (Cummings and Eversman 1983). Consider a perforated plate of porosity σ_p with perforations of length l_p, as depicted in Figure 1.3. At a given time t, the boundary layer separation in the perforation is modeled as a reduction of the effective cross-section, which is S_p at $x = 0$, but only

$$S_{\mathrm{vc}} = C_{\mathrm{vc}} S_p \leq S_p$$

at $x = l_p$ (*vena contracta*). Assuming the flow to be steady, incompressible, inviscid, and irrotational, Bernoulli's equation yields

$$p(x = l_p) - p(x = 0) + \frac{\rho_0}{2} \left(\langle u \rangle_{S_{\mathrm{vc}}}^2 - \langle u \rangle_{S_p}^2 \right) = 0.$$

Using the mass conservation identity

$$\langle u \rangle_{S_{\mathrm{tot}}} = \sigma_p \langle u \rangle_{S_p} = \sigma_p C_{\mathrm{vc}} \langle u \rangle_{S_{\mathrm{vc}}},$$

we get the pressure drop

$$p(x=0) - p(x=l_p) = \frac{\rho_0}{2}\left(\frac{1}{\sigma_p^2 C_{\mathrm{vc}}^2} - \frac{1}{\sigma_p^2}\right)\langle u\rangle_{S_{\mathrm{tot}}}^2,$$

so that the corresponding (surface) impedance operator is

$$\mathcal{Z}(\boldsymbol{u}\cdot\boldsymbol{n}) = \rho_0 C_{\mathrm{nl}}(\boldsymbol{u}\cdot\boldsymbol{n})^2,\ C_{\mathrm{nl}} \coloneqq \frac{1-C_{\mathrm{vc}}^2}{2\sigma_p^2 C_{\mathrm{vc}}^2}. \tag{1.31}$$

However, the impedance (1.31) does not account for the fact that the position of the vena contracta depends upon the flow direction: if $\langle u\rangle_{S_p} > 0$ (resp. < 0) then the vena contracta is located at $x = l_p$ (resp. $x = 0$). Including this phenomenon leads to (Cummings 1986, Eq. 1)

$$\mathcal{Z}(\boldsymbol{u}\cdot\boldsymbol{n}) = \rho_0 C_{\mathrm{nl}}|\boldsymbol{u}\cdot\boldsymbol{n}|\boldsymbol{u}\cdot\boldsymbol{n}. \tag{1.32}$$

The operator (1.32) is to be used as an additive correction to the surface impedance models covered in Section 1.2.2.

The assumption of irrotationality has been removed in (Meissner 1999, 2000), where the same model is derived. Based on these studies, a simplified frequency domain model is proposed in (Hersh et al. 2003) for engineering design purposes. Evidence for the relevance of (1.32) has been provided both theoretically in (Rienstra and Singh 2018), with an asymptotic study of the Helmholtz resonator, and numerically in (Zhang and Bodony 2016) where the contraction coefficient C_{vc} is computed using numerical simulations.

Note that, since we are dealing with a nonlinear phenomenon, the impedance operator is naturally derived in the time domain. Here, it is straightforward to check the admissibility conditions given in Definition 1.1. The impedance (1.31) satisfies the reality and causality conditions, but is *not* passive. The impedance (1.32), which accounts for the change of position of the vena contracta, is admissible. By contrast with linear models, expressing the admittance and scattering operators from a given nonlinear impedance model is more intricate, see Chapter 2 for examples.

Remark 1.25. In (Tudisco et al. 2017), a nonlinear model is used to model injectors of a combustion chamber in a LES simulation. The corresponding scattering operator is $\mathcal{B}(v)(t) = \chi_a(v)(t-\tau)$ where $\tau > 0$ is a time delay and χ_a is an algebraic function of the incoming characteristic (Tudisco et al. 2017, Eq. 2.15).

Grazing flow effect

For the CT and SDOF liners introduced in Section 1.2.2, the measured or identified impedance z exhibits a dependency on the base flow (Jones et al. 2005). This dependency typically impairs the liner performance and innovative material designs seek to reduce it.

The experimental study (Kirby and Cummings 1998), among many others, investigated the effect of a grazing flow on a perforated plate backed by an air cavity. The grazing flow is found to induce an increase in resistance and a decrease in mass reactance. The following experimental correlation between the impedance and the wall friction velocity u_* is proposed (Kirby and Cummings 1998, Eqs. 12-13):

$$\frac{\theta_f c_0}{fd} = \left(26.16\left(\frac{t}{d}\right)^{-0.169} - 20\right)\frac{u_*}{fd} - 4.055$$

with

$$\frac{\delta}{\delta_0} = \begin{cases} 1 & \frac{u_*}{ft} \le 0.18\frac{d}{t} \\ (1+0.6\frac{t}{d})e^{-\left(\frac{u_*}{ft}-0.18\frac{d}{t}\right)\left(1.8+\frac{t}{d}\right)} - 0.6\frac{t}{d} & \frac{u_*}{ft} > 0.18\frac{d}{t}, \end{cases}$$

where the experimental impedance is written as

$$\frac{\hat{z}_{\exp}(\mathrm{j}\omega)}{\rho_0 c_0} = \underbrace{\frac{t}{cd}\sqrt{16\pi\nu l} + \mathrm{j}kt}_{\text{no-flow impedance}} + \overbrace{\theta_f + \mathrm{j}k\delta}^{\text{correction}},$$

where $k = \omega/c_0$, $\delta_0 = 0.85d$ the mass end correction without flow, f is the frequency, t (resp. d) the perforation length (resp. diameter), and l is the effective orifice length defined as $l := \frac{\Im[\hat{z}_{\exp}(\mathrm{j}\omega)]}{\omega\rho_0}$. The physical phenomena that arise from interaction of a liner with a grazing flow can be studied using direct numerical simulations, see e.g. (Zhang and Bodony 2016).

Since this experimental correlation does not yield a positive-real function, it cannot be used as is in the time domain. Hence, for this dissertation, the key takeaway from (Kirby and Cummings 1998) is that the effect of a grazing flow can be *empirically* modeled as an additional parametric dependence, which preserves the locally reacting nature of the IBC. This strategy is followed for the numerical applications presented in Chapter 6.

Remark 1.26 (IBCs with grazing flow). The empirical formulas given above are an attempt to model the dependency of the impedance kernel z upon a grazing flow. This dependency should not be confused with the one found in the Ingard-Myers boundary condition (Ingard 1959; Myers 1980). Let us clarify that comment. In the literature two strategies are used to model the effect of a grazing flow at the impedance wall:

1. The first one, used in this dissertation, consists in using a viscous base flow $\boldsymbol{u_0}$ with a locally reacting IBC (1.1). Numerically, this can be a costly approach since the boundary layer of $\boldsymbol{u_0}$ must be well-discretized.

2. The second one consists in using a uniform "plug" flow with an Ingard-Myers type boundary condition, originally derived for plane boundaries in (Ingard 1959) using continuum mechanics arguments and extended to curved boundaries in (Myers 1980). This boundary condition has been shown to lead to an infinite absolute instability in (Brambley 2009) and (Joubert 2010). Other works have shown that asymptotic analysis enables to understand the corresponding assumption on the base flow: (Eversman and Beckemeyer 1972) and (Tester 1973a, § 2) showed that the standard Ingard-Myers boundary condition can be obtained from a linear-then-constant base flow in the limit of a vanishing boundary layer thickness; (Brambley 2011, §V) and (Khamis and Brambley 2016) derived corrections using a hyperbolic velocity profile, which is the one that we will use in the numerical applications of Section 6.3. These corrections have been shown to accurately recover the modes obtained by solving the boundary layer (i.e. the approach (1)).

Impedance identification has been carried out using both approaches, see (Jones et al. 2005; Primus et al. 2013). Regardless of the chosen formulation for the IBC, for many sound absorbing materials the identified or measured impedance values do exhibit a dependency on the base flow.

1.3 Numerical impedance models

The purpose of this section is to summarize the state of the art in numerical impedance models. Before proceeding, we introduce the following terminological precision, used throughout the dissertation. A *discrete* TDIBC consists of three components.

1. The discrete impedance model, i.e. the finite-dimensional operator (in the sense of system theory (Brockett 1970; Curtain and Zwart 1995)) that one wishes to apply at the boundary.

2. The numerical algorithm used to evaluate the said operator; in the case of linear continuous time-invariant operators (i.e. of linear TDIBCs) this amounts to computing a time-domain convolution.

Practically these first two elements go hand in hand since the expression of the convolution kernel dictates how the convolution can be efficiently computed.

3. The (semi-)discrete formulation, i.e. how the TDIBC is enforced at the (semi-)discrete level. In other words, this is the coupling method with the PDE.

As shown in Chapter 5, the third and last component of a discrete TDIBC should not be overlooked. In this state of the art, we focus on the first two aspects (the third one is not always detailed, so that it is difficult to make comparisons).

Early rational models In the earliest works, numerical impedance models were comprised of a *single* polynomial or rational fraction, which yields in the time domain an ODE between the acoustic pressure and normal velocity. This ODE is then approximated using finite-differences. A second-degree polynomial

$$\hat{z}_{\mathrm{num}}(s) = a_1 s - a_2 s^2, \tag{1.33}$$

was used in (S. Davis 1991) to model an open pipe. Note that if $a_2 \neq 0$ this model is not positive-real (although $\Re(\hat{z}_{\mathrm{num}}(\mathrm{j}\omega)) \geq 0$ for all $\omega \in \mathbb{R}$ when $a_2 \geq 0$). Tam and Auriault (Tam and Auriault 1996) (Tam 2012, Chap. 10) considered a proportional-integral-derivative model

$$\hat{z}_{\mathrm{num}}(s) = \frac{a_{-1}}{s} + a_0 + a_1 s, \tag{1.34}$$

which they called a three-parameter model. This model is positive-real when the three coefficients are nonnegative. Inspired by the progress made in the computational electromagnetics community, Özyörük *et al.* followed a heuristic approach to propose an admissible rational fraction of degree 4 (Özyörük et al. 1998, Eq. 15)

$$\hat{z}_{\mathrm{num}}(s) = r_1 + \frac{r_2 - r_1}{1 + r_3 s} + \frac{r_4 s}{1 + \left(\frac{s}{r_6}\right)^2 + r_5 s} + r_7 s.$$

Since it can match the behavior of a CT liner until the second resonance, it has been hailed as the first "broadband" model. This contrasts with the models (1.33,1.34) that are usually tuned at a single frequency. This model has been widely used in aeroacoustics, see e.g. (Escouflaire 2014); the practical challenge lies in finding the suitable weights r_i for the physical model at hand, since this numerical model is not positive-real for all values of r_i.

Multipole models After the work of Özyörük *et al.*, the need for a generic, efficient, broadband TDIBC has led to the introduction of a new family of models, known as multipole. They consist of a discrete sum of elementary first or second-order systems such as

$$\hat{z}_{\mathrm{num}}(s) = \sum_{k=1}^{N} \frac{a_k}{s - s_k}.$$

The number N of systems, as well as their respective gains a_k and poles s_k, are degrees of freedom (DoF) of the TDIBC, which translates as a considerable versatility. Moreover, admissibility conditions are straightforwardly verified, which is not the case for rational fractions expressed with polynomials (especially of higher degree). Typically, the gains and poles are chosen so that

the model can be written as a sum of positive-real functions (with real or complex conjugate poles). The drawback is that they lead to N elementary convolutions, e.g. for a causal input u

$$z \star u(t) = \sum_{k=1}^{N} a_k \left(e^{s_k \cdot} H \star u\right)(t) = \sum_{k=1}^{N} a_k \int_0^t e^{s_k \tau} u(t-\tau)\,\mathrm{d}\tau, \tag{1.35}$$

where H is the Heaviside or step function. First introduced in the acoustical literature in (Fung and Ju 2001), they have been used in a wealth of studies, to the point that they can by now be considered a de facto standard. These studies can be roughly split into two categories, based on the algorithms they use to compute the convolutions in (1.35).

1. A recurrent computation of the convolution, using properties of the convolution kernel, have been employed by many authors (Cotté and Blanc-Benon 2009; Fung and Ju 2001; X. Y. Li et al. 2012; Ostashev et al. 2007; Reymen et al. 2006). In the acoustical literature, this strategy is often named the "recursive" convolution technique and traced back to the computational electromagnetic work (Luebbers et al. 1990).

2. A computation of the N convolutions through ODEs. The first acoustical work using this technique, to the best of the author's knowledge, is (Bin et al. 2009). A comprehensive study (Dragna et al. 2015) showed the benefit of this method, named the auxiliary differential equations method, over "recursive" convolution techniques. In the fluid mechanics literature, this computational technique is also known as a "canonical form implementation" (Liu et al. 2014; Zhong et al. 2016) or a "state-space model" (Jaensch et al. 2016).

EHR model In all the works quoted above, the discrete impedance model is chosen based of its ease of implementation, without providing connection with physical models (this connection is studied in Chapter 2). As an alternative, Rienstra introduced the extended Helmholtz resonator (EHR) model (Rienstra 2006)

$$\hat{z}(s) = a_0 + a_1 s + a_2 \coth\left(b_0 + b_1 s\right), \tag{1.36}$$

which is positive-real when the coefficients are nonnegative. The physical meaning of each of the parameter, see e.g. (1.29), makes fitting against experimental data easier than with purely numerical models. The model (1.36) is however continuous and several discretization methods have been proposed, see e.g. (Chevaugeon et al. 2006; Richter et al. 2011).

Liner discretization In (Sbardella et al. 2001), the nonlinear model

$$\mathcal{Z}(\boldsymbol{u}\cdot\boldsymbol{n}) = z_{\mathrm{cav}} \star \boldsymbol{u}\cdot\boldsymbol{n} + a_1 |\boldsymbol{u}\cdot\boldsymbol{n}| \boldsymbol{u}\cdot\boldsymbol{n}$$

with the linear part given by

$$\hat{z}_{\mathrm{cav}}(s) = a_0 + z_0 \coth\left(\frac{s l_c}{c_0}\right)$$

is implemented as a discretized SDOF liner, i.e. the convolution $z_{\mathrm{cav}} \star \boldsymbol{u}\cdot\boldsymbol{n}$ is computed by solving the monodimensional Euler equations in the cavity using finite differences. This approach has been extended to the EHR model (1.36) in (Pascal et al. 2015). This model is admissible when the coefficients are nonnegative.

Chapter 2

Realization of irrational transfer functions

Contents

The objective of this chapter is to derive time-local realizations of classes of irrational transfer functions that include the physical models introduced in Section 1.2, for use in Chapters 4, 5, and 6. The derived realizations result from the combination of two components: first, a realization of the oscillatory-diffusive (OD) representation through ODEs, covered in both continuous and discrete forms in Sections 2.1 and 2.2; second, a hyperbolic realization of the time delay through a monodimensional transport equation, recalled in Section 2.3. Application to physical models is carried out in Section 2.4.

Terminology In this chapter, by "transfer function" we mean a Laplace transform $s \mapsto \hat{h}(s)$ or an analytic function f that is the Laplace transform of some causal kernel, i.e. $f = \hat{h}$. The impedance models covered in Chapter 1 are examples of transfer functions. The name of this chapter follows a standard terminology, see e.g. (Hélie and Matignon 2006b).

2.1 Oscillatory-diffusive representation

This section lays out a theory of the oscillatory-diffusive representation of a convolution kernel, rooted in complex analysis. After a standard reminder on the diffusive representation in Section 2.1.1, oscillatory-diffusive representations are covered in Section 2.1.2 where original representation theorems are given, tailored to our purposes. The realization of oscillatory-diffusive

representations is presented in Section 2.1.3. Lastly, Section 2.1.4 gathers basic examples that illustrate the application of the representation theorems derived in Section 2.1.2; these examples, some of them original to the best of the author's knowledge, are chosen for their relevance to the analysis of physical models that will be carried out in Section 2.4.

2.1.1 Introduction to the diffusive representation

This section is an introduction to the diffusive representation that draws from standard references. It purpose is to introduce definitions and notations used in later sections.

Diffusive representation

The first synthetic presentation of diffusive representations can be found in (Montseny 1998), see also the book (Montseny 2005).

Definition 2.1. A kernel $h \in \mathcal{C}^\infty((0,\infty))$ is said to be *diffusive* if there is a causal distribution $\mu \in \mathcal{D}'_+(\mathbb{R})$, with $e^{-\sigma\cdot}\mu \in \mathcal{S}'(\mathbb{R})$ for any $\sigma > 0$, such that

$$h(t) = \mathcal{L}(\mu)(t) \quad (t > 0). \tag{2.1}$$

From the property of the Laplace transform, the growth at infinity of a diffusive kernel h is at most polynomial, see Appendix A.

Remark 2.2 (Terminology). In this dissertation, we use the following terminology: the *diffusive representation* of h is the identity (2.1), while the distribution μ is called the *diffusive weight*. This slightly differs from (Montseny 1998) where μ is called the diffusive representation of h.

Let $h \in \mathcal{C}^\infty((0,\infty))$ be a diffusive kernel and let μ denotes its diffusive weight. To better understand Definition 2.1, let us assume that the diffusive weight is locally integrable i.e. $\mu \in L^1_{\mathrm{loc}}([0,\infty)$. Then, the diffusive representation (2.1) reduces to

$$h(t) = \int_0^\infty e^{-\xi t} H(t)\, \mu(\xi)\, \mathrm{d}\xi \quad (t \in \mathbb{R}), \tag{2.2}$$

where the sign of $\mu(\xi)$ is indefinite in general. The representation (2.2) can be understood as a "diagonalization" of h, whereby h is expressed using only a family of causal decaying exponential kernels. In this work, they are denoted

$$e_x(t) \coloneqq e^{-xt} H(t),\ \widehat{e_x}(s) = \frac{1}{s+x} \quad (x \in \mathbb{C},\ t \in \mathbb{R},\ s \in \mathbb{C}^+_x). \tag{2.3}$$

In the automatic control terminology, the convolution operator $u \mapsto e_\xi \star u$ is known as a first-order system.

Let us further assume that $h \in L^1_{\mathrm{loc}}([0,\infty))$. Then, h is Laplace-transformable and the diffusive representation (2.2) can also be written

$$\hat{h}(s) = \int_0^\infty \frac{1}{s+\xi} \mu(\xi)\, \mathrm{d}\xi \quad (\Re(s) > 0). \tag{2.4}$$

A third manner to write the diffusive representation is the following. For an input $u \in L^1_{\mathrm{loc}}([0,\infty))$, Fubini's theorem yields

$$h \star u(t) = \int_0^\infty \varphi(t,\xi)\, \mu(\xi)\, \mathrm{d}\xi, \tag{2.5}$$

where the function φ is defined as

$$\varphi(t,z) \coloneqq e_z \star u(t) = \int_0^t e_z(\tau) u(t-\tau)\,\mathrm{d}\tau \quad (t \in \mathbb{R},\ z \in \mathbb{C}). \tag{2.6}$$

For $\xi \in (0,\infty)$, $\varphi(\cdot,\xi)$ is known as a *diffusive variable*. Written as (2.5) the diffusive representation means that the computation of $h \star u$ is reduced to the computation of $e_\xi \star u$ for $\xi \in \operatorname{supp}\mu$. The interest of (2.5) lies in the fact that the diffusive variables can be computed using a first-order ODE, since φ is the solution of

$$\begin{cases} \partial_t \varphi(t,z) = -z\varphi(t,z) + u(t) & (t>0,\ z\in\mathbb{C}) \\ \varphi(t,0) = 0, \end{cases} \tag{2.7}$$

which can be seen from

$$e_z' = -z e_z + \delta. \tag{2.8}$$

The identities (2.5,2.7) constitute a time-local representation of the hereditary operator $u \mapsto h \star u$ and are called the *diffusive realization* of h, where "realization" is used in the sense of system theory (Brockett 1970, § 17) (Curtain and Zwart 1995, § 1.2). Numerically, the diffusive realization enables to compute $h \star u$ using standard time-integration schemes, provided that the integral in ξ is suitably discretized. Theoretically, the diffusive realization can be given a meaning as a well-posed linear system (Matignon and Zwart in revision); in Section 4.5, we define a functional framework tailored to the study of the stability of the wave equation with an IBC.

Remark 2.3. As defined in (2.1), the diffusive representation can be a series. To illustrate this, let us consider two sequences $\tilde{\mu}_k$ and $\xi_k \geq 0$ such that $|\tilde{\mu}_k| \underset{k\to\infty}{=} \mathcal{O}(k^{-1})$ and $\xi_k \underset{k\to\infty}{=} \mathcal{O}(k)$. From (Gasquet and Witomski 1999, Prop. 31.1.9), the diffusive weight $\mu = \sum_{k\in\mathbb{N}} \tilde{\mu}_k \delta_{\xi_k}$ is convergent in $\mathcal{S}'(\mathbb{R})$. From Proposition A.18, the series $\sum_{k\in\mathbb{Z}} \tilde{\mu}_k e_{\xi_k}$ is convergent in $\mathcal{S}'(\mathbb{R})$ and yields the diffusive kernel h given by

$$h = \sum_{k\in\mathbb{N}} \tilde{\mu}_k e_{\xi_k},\ \hat{h}(s) = \sum_{k\in\mathbb{N}} \frac{\tilde{\mu}_k}{s+\xi_k}.$$

The distinctive feature of the diffusive representation is that the poles, here given by $-\xi_k$ with $k \in \mathbb{N}$, belong to $(-\infty, 0]$.

Remark 2.4. The quantity μ is known under other names such as *spectral function* (Garrappa et al. 2016) or *relaxation spectrum* (Mainardi 1997).

Remark 2.5 (Parabolic realization). The adjective "diffusive" used in Definition 2.1 can be justified by noting that the realization (2.5,2.7) can be *formally* written using the heat equation as (Montseny 1998, Cor. 3.8)

$$\begin{cases} \partial_t \phi(t,x) = \partial_x^2 \phi(t,x) + u(t) \otimes \delta(x) & (t>0,\ x\in\mathbb{R}) \\ h \star u(t) = 2\pi \displaystyle\int_{-\infty}^{\infty} \phi(t,x)\, \mathcal{F}^{-1}\left[\mu(k^2)\,|k|\right](x)\mathrm{d}x, \end{cases} \tag{2.9}$$

where $\otimes$ is the product of distributions. (To make (2.9) meaningful, the observation integral should be interpreted as a suitable duality bracket.) This suggests the terminology of *parabolic realization* for (2.5,2.7). Physically, diffusive kernels model non-propagating diffusion phenomena; they arise for instance in acoustics, see Section 2.4 and (Hélie and Matignon 2006a), viscoelasticity (Desch and Miller 1988; Mainardi 1997; Staffans 1994), and electromagnetics (Garrappa et al. 2016).

Example 2.6 (Fractional kernel)**.** The archetypal diffusive kernel is the fractional kernel Y_α given by (1.6). For $\alpha \in (0,1)$, it admits the diffusive representation (Hélie and Matignon 2006b; Montseny 1998)

$$Y_\alpha(t) = \int_0^\infty e^{-\xi t} H(t)\, \mu_\alpha(\xi)\, \mathrm{d}\xi \tag{2.10}$$

with

$$\mu_\alpha(\xi) \coloneqq \frac{\sin(\alpha\pi)}{\pi} \times \frac{1}{\xi^\alpha} \mathbb{1}_{(0,\infty)}(\xi), \tag{2.11}$$

which can be derived using the integral expression of the Gamma function combined with Euler's reflection formula. The convolution operator $u \mapsto Y_\alpha \star u$ is known as the Riemann-Liouville fractional integral of order α, see e.g. (Samko et al. 1993, § 2.3) (Matignon 2009). Provided that the diffusive representation is suitably discretized, it constitutes a time-local alternative to, for instance, fractional linear multistep methods (Lubich 1986) or methods based on the Grünwald-Letnikov approximation (Scherer et al. 2011). Methods based on discrete diffusive representations are also known as "non-classical" methods (Birk and Song 2010; Diethelm 2008). Note that the long memory of the fractional derivative, induced by $Y_\alpha \underset{t\to\infty}{=} \mathcal{O}\left(t^{\alpha-1}\right)$, is reflected into the infinite dimension of the diffusive realization, induced by $\operatorname{supp}\mu = [0,\infty)$. By contrast, the kernel $h = e_\xi$ has a diffusive weight supported in $\{\xi\}$ only.

In this work we will be faced with the following problem: given an analytic function $s \mapsto f(s)$, coming for example from a physical impedance model, under what conditions does it admit a diffusive representation? A non constructive answer is provided by the theory of completely monotone functions recalled below, namely through Theorems 2.12 and 2.13. Constructive representation theorems will be derived in Section 2.1.2 using complex calculus.

Completely monotone functions

The following definition comes from (Widder 1946, Def. IV.2c).

Definition 2.7. A function $h \in \mathcal{C}^\infty((0,\infty))$ is said to be *completely monotone* in the open interval $(0,\infty)$ if

$$\forall t > 0,\ \forall k \in \mathbb{N},\ (-1)^k h^{(k)}(t) \geq 0.$$

For example, $t \mapsto t^{-p}$ with $p \in \mathbb{N}^*$ is completely monotone. This class of functions can be characterized by the following result, found in (Gripenberg et al. 1990, Thm. 5.2.5).

Theorem 2.8 (Bernstein's theorem)**.** *A function $h : (0,\infty) \to [0,\infty)$ is completely monotone on $(0,\infty)$ if and only if*

$$h(t) = \int_0^\infty e^{-\xi t} \mathrm{d}\nu(\xi), \tag{2.12}$$

where ν is a positive Radon measure on $[0,\infty)$.

An immediate consequence of Bernstein's theorem is that if $h \in \mathcal{C}^\infty((0,\infty))$ is a diffusive kernel with diffusive representation μ, then it is completely monotone in $(0,\infty)$ if and only if $\mu = T_\nu$ where ν is a *positive* Radon measure on $[0,\infty)$ and T_ν is the distribution induced by the measure ν. For instance, the fractional kernel Y_α with $\alpha \in (0,1)$ is completely monotone and admits the representation (2.12) with

$$\mathrm{d}\nu_\alpha(\xi) \coloneqq \mu_\alpha(\xi)\, \mathrm{d}\xi,$$

where $\mathrm{d}\xi$ is the Lebesgue measure.

Remark 2.9. For the definition of Radon measures, see (Folland 1999, Chap. 7) for a measure theory point of view and (Bony 2001, § 4.4.6) for a distribution theory point of view. Bernstein's theorem can also be written using the Riemann-Stieltjes integral, in which case ν denotes a function of bounded variation (in particular ν is bounded and can be assumed non-decreasing), see (Widder 1946, Thm. IV.12b).

Bernstein's theorem asserts that all the information about h is contained in the measure ν. Since it is common to know the measure ν in closed form but not h, it is therefore useful to be able to deduce properties of h knowing ν. A simple example is that h is defined at 0 if and only if

$$\int_0^\infty \mathrm{d}\nu(\xi) = \nu([0,\infty)) < \infty.$$

The most important properties for our purposes are the two following integrability conditions (Gripenberg et al. 1990, Thm. 5.2.5).

Proposition 2.10 (Integrability conditions)**.** *Let $h \in \mathcal{C}^\infty((0,\infty))$ be completely monotone on $(0,\infty)$. Then,*

$$h \in L^1_{\mathrm{loc}}([0,\infty)) \iff \int_0^\infty \frac{1}{1+\xi}\mathrm{d}\nu(\xi) < \infty$$
$$h \in L^1([0,\infty)) \iff \nu(\{0\}) = 0 \quad \textit{and} \quad \int_0^\infty \frac{1}{\xi}\mathrm{d}\nu(\xi) < \infty.$$

Remark 2.11. The condition "$\nu(\{0\}) = 0$" must not omitted: consider the discrete measure $\nu = \delta$ for instance.

Let h be a completely monotone kernel on $(0,\infty)$. If $h \in L^1_{\mathrm{loc}}([0,\infty)$, then it is Laplace-transformable and its Laplace transform is given by

$$\hat{h}(s) = \int_0^\infty \frac{1}{s+\xi}\mathrm{d}\nu(\xi) \quad (\Re(s) > 0), \tag{2.13}$$

which is the frequency-domain counterpart of the representation (2.12). The results below will show that $\hat{h}$ is a positive-real function.

The Laplace transform of completely monotone kernels can be characterized using the two following theorems. However, note that both theorems are not constructive in the sense that they do not give the expression of the measure ν; constructive results will be given in Section 2.1.2.

Theorem 2.12. *Let $h \in \mathcal{C}^\infty((0,\infty)) \cap L^1_{\mathrm{loc}}([0,\infty))$ be a completely monotone function in $(0,\infty)$. Then, $f := \hat{h}$ satisfies the following properties.*

(i) *f has an analytic extension to $\mathbb{C}\backslash(-\infty, 0]$.*

(ii) *$f(s) \in \mathbb{R}$ for $s \in (0,\infty)$.*

(iii) *$\lim_{\substack{s\to\infty \\ s\in\mathbb{R}}} f(s) = 0$.*

(iv) *$\Im(f(s)) \leq 0$ for $\Im(s) > 0$.*

Conversely, a function f that satisfies (i)–(iv) can be written as $f = \hat{h}$ where $h \in \mathcal{C}^\infty((0,\infty)) \cap L^1_{\mathrm{loc}}([0,\infty))$ is a completely monotone function in $(0,\infty)$, so that f is given by (2.13).

Proof. See (Gripenberg et al. 1990, Thm 5.2.6). The proof uses the map $s \mapsto \mathrm{j}^{(1+s)}/_{(1-s)}$ from the unit disk onto upper half-plane and a representation result for positive harmonic function in the open unit disk. □

The case where $f(\infty) \neq 0$ is covered by the following result (Gripenberg et al. 1990, Cor 5.2.7).

Theorem 2.13. *Let $f : \mathbb{C}_0^+ \to \mathbb{C}$ be an analytic function. If*

(i) *f has an analytic extension to $\mathbb{C}\backslash(-\infty, 0]$,*

(ii) *$f(s) \in [0, \infty)$ for $s \in (0, \infty)$,*

(iii) *$\limsup_{\substack{s\to\infty \\ s\in\mathbb{R}}} |f(s)| < \infty$,*

(iv) *$\Im(f(s)) \leq 0$ for $\Im(s) > 0$,*
then $f_\infty \coloneqq \lim_{\substack{s\to\infty \\ s\in\mathbb{R}}} f(s)$ exists and

$$f(s) - f_\infty = \hat{h},$$

where $h \in \mathcal{C}^\infty((0,\infty)) \cap L^1_{\mathrm{loc}}([0,\infty))$ is a completely monotone function in $(0,\infty)$.

2.1.2 Oscillatory-diffusive representation

The purpose of this section is to derive sufficient conditions for an analytic function $f : \mathbb{C}_0^+ \to \mathbb{C}$ to admit the representation

$$f(s) = \sum_k \frac{c_k}{s - s_k} + \int_0^\infty \frac{\mu(\xi)}{s + \xi}\,\mathrm{d}\xi \quad (\Re(s) > 0),$$

which we call in this dissertation the *oscillatory-diffusive* (OD) representation. The integral term is the *diffusive part* of f, a terminology already justified in Remark 2.5. The series is the *oscillatory part* of f. This terminology can be justified by the fact that when f satisfies $f(s) \in (0, \infty)$ for $s \in (0, \infty)$ (for example when f is positive-real), the poles s_k belong to $\mathbb{C}\backslash\mathbb{R}$ and go by conjugate pairs so that the series consists of terms like

$$\frac{c_k}{s - s_k} + \frac{\overline{c_k}}{s - \overline{s_k}} = \frac{2\Re(c_k)s - 2\Re(c_k\overline{s_k})}{s^2 - 2\Re(s_k)s + |s_k|^2},$$

which is the transfer function of a monodimensional oscillator, damped if $\Re(s_k) < 0$. By definition, a convolution kernel h whose Laplace transform $\hat{h}$ admits an OD representation is called an OD kernel.

If h is an OD kernel, then it admits a time-local realization, which will be written down in Section 2.1.3. The application of the results obtained in this section will be illustrated in Section 2.1.4 where basic examples are considered, chosen for their relevance to the model analysis that will be carried out in Section 2.4. Let us also note that the distinction between the oscillatory and diffusive parts is computationally relevant, as will be seen when discussing the discretization of OD representations later in this chapter, namely in Section 2.2.

The proposed representation theorems are derived by inverting the Laplace transform using a Bromwich contour, accounting for the presence of both poles and cuts, see (Duffy 2004) for a wealth of examples. In the context of diffusive representations, this approach has been followed in (Casenave and Montseny 2010) and (Héleschewitz 2000; Hélie and Matignon 2006a,b). Herein, we are interested in deriving sufficient conditions that are general enough to cover the physical models of interest, so that the presented theorems are tailored to our needs.

The proofs are mostly elementary and rely on standard facts of complex analysis, see (Gamelin 2001), and distribution theory, see the references in Appendix A. Let us recall the

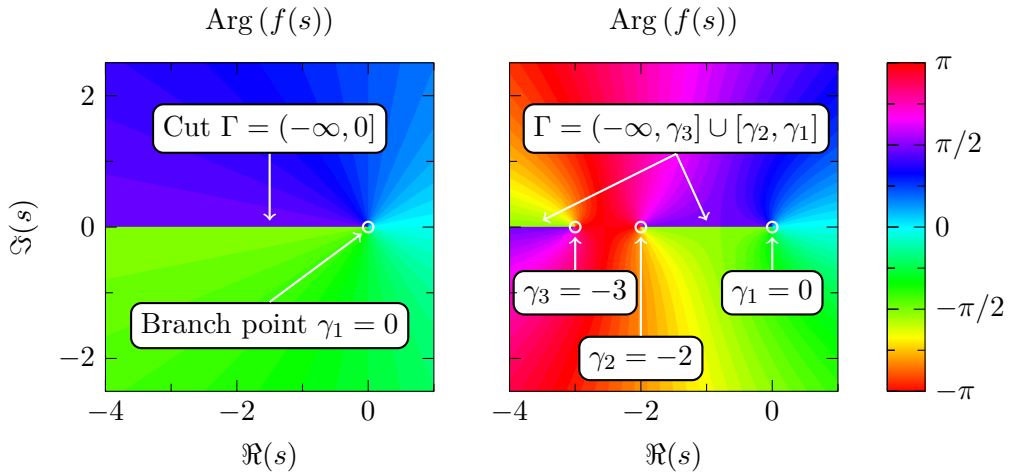

Figure 2.1. Plot of the principal value of the argument for two multivalued functions, which shows a jump across the cut Γ. (Left) $f(s) = \sqrt{s}$ where $\sqrt{\cdot}$ is the principal branch of the square root defined in Example 2.14. (Right) $f(s) = \sqrt{s}\sqrt{s+2}\sqrt{s+3}$.

terminology related to multivalued functions. A complex-valued function f is *multivalued* if there are complex numbers s such that $f(s)$ can have at least two different values. Typically, f can be viewed as an analytic function from a Riemann surface R to $\mathbb{C}$, where R is obtained by "suitably" joining at least two *sheets* $S_i \subset \mathbb{C}$. The restriction of f to each sheet defines a uniquely valued analytic function known as a *branch* of f. The definition of the sheets is usually not unique. In this chapter, we will only manipulate the principal branch of power functions, recalled in the example below; see also (Gamelin 2001, § 4& 7) for a detailed exposition.

Example 2.14 (Principal branch of power functions)**.** The square root $s \mapsto \sqrt{s}$ is multivalued since $\sqrt{|s|}e^{\mathrm{j}\frac{\arg(s)}{2}}$ is not invariant by, for instance, 2π rotations around 0. In fact, for any $s \in \mathbb{C}$ two values are possible. A conventional choice is two define the two sheets as identical "cut" versions of the complex plane, namely

$$S_1 = S_2 \coloneqq \mathbb{C}\backslash(-\infty, 0],$$

where the semi-infinite line $(-\infty, 0]$ is known as the *cut* and 0 and ∞ are said to be the *branch point*s. The two corresponding branches f_i are defined over S_i as

$$f_1(s) \coloneqq \sqrt{|s|}e^{\mathrm{j}\frac{\mathrm{Arg}(s)}{2}}, \; f_2(s) \coloneqq -f_1(s),$$

where $\mathrm{Arg}(s) \in (-\pi, \pi]$ is the principal value of $\arg(s)$. The branch f_1 is called the *principal branch* of $\sqrt{\cdot}$ and it satisfies $\Re(f_1(s)) \geq 0$. It is analytic on S_1, but exhibits a jump across the cut, i.e.

$$\forall \xi > 0, \; f_1(\xi e^{-\mathrm{j}\pi}) - f_i(\xi e^{+\mathrm{j}\pi}) = -\mathrm{j}\sqrt{\xi} - \left(+\mathrm{j}\sqrt{\xi}\right) = -2\mathrm{j}\sqrt{\xi}.$$

This jump is illustrated in the left plot of Figure 2.1, which shows that $\mathrm{Arg}\, f_1$ jumps from $+\pi/2$ over the cut to $-\pi/2$ under the cut. With a univalued function the jump would be 0 or 2π. Using f_1 more intricate multivalued functions can be built, see for example the right plot of Figure 2.1 where the plotted function has a cut that consists of two disjoint segments.

More generally, the function $f(s) = s^\alpha$ with $\alpha \in \mathbb{R}$ is multivalued with q branches if $\alpha = p/q$ with $p \in \mathbb{Z}$ and $q \in \mathbb{N}^*$, and with an infinite number of branches if $\alpha \in \mathbb{R}\backslash\mathbb{Q}$. Its principal branch is defined by

$$f_1(s) \coloneqq |s|^\alpha e^{\mathrm{j}\alpha\,\mathrm{Arg}(s)}. \tag{2.14}$$

In this dissertation, s^α always denotes the principal branch (2.14).

(a) $n = 4$. **(b)** $n = 3$.

Figure 2.2. Examples of diffusive cuts using the notation of Definition 2.15.

In this work we restrict ourselves to cuts that are included in $(-\infty, 0]$. This is captured by the definition below, which is illustrated in Figure 2.2. This definition is a convenient way of shortening the statement of the representation theorems to come.

Definition 2.15. A set $\Gamma \subset (-\infty, 0]$ is said to be a *diffusive cut* if there is a finite and decreasing sequence of $n \in \mathbb{N}$ distinct points $\gamma_i \leq 0$ such that

$$\Gamma = \begin{cases} \bigcup\limits_{i \in [\![1,p]\!]} [\gamma_{2i-1}, \gamma_{2i}] & (n = 2p) \\ \left(\bigcup\limits_{i \in [\![1,p]\!]} [\gamma_{2i-1}, \gamma_{2i}] \right) \cup [\gamma_n, -\infty) & (n = 2p+1). \end{cases}$$

The points γ_i are called the *endpoints* of Γ.

Before stating the first of the three representation theorems given in this section, let us briefly recall the definition of a complex residue, which we shall use repeatedly in this chapter. Let f be analytic in the punctured disc $\{0 < |s - s_0| < r\}$ with $r > 0$. We define the *residue* of f at s_0 by

$$\operatorname{Res}(f, s_0) \coloneqq \lim_{\epsilon \to 0} \frac{1}{2\mathrm{j}\pi} \oint_{|s-s_0|=\epsilon} f(s)\mathrm{d}s = \lim_{\epsilon \to 0} \frac{\epsilon}{2\pi} \int_{-\pi}^{+\pi} f(s_0 + \epsilon e^{\mathrm{j}\theta}) e^{\mathrm{j}\theta} \mathrm{d}\theta. \tag{2.15}$$

This limit exists, is finite, and is equal to the coefficient a_{-1} of the Laurent series of f at s_0, see for instance (Gamelin 2001, Chap. VII). However, since this work is mainly concerned with analytic functions f that have cuts in the complex plane, it will prove convenient to extend the above definition of $\operatorname{Res}(f, s_0)$ to the class of functions f such that: (i) f is analytic in $\{0 < |s - s_0| < r\} \backslash \Gamma$ with $r > 0$ and Γ closed straight segment; (ii) for $0 < \epsilon < r$, each circle integral $\oint_{|s-s_0|=\epsilon} f(s)\mathrm{d}s$ exists and is finite; (iii) the limit $\epsilon \to 0$ in (2.15) exists and is finite.

The archetypal example of such a function is the principal branch of the square root defined in Example 2.14, denoted $\sqrt{\cdot}$ and with branch point $\gamma_1 = 0$. For any $r > 0$, this function is analytic in $\{0 < |s| < r\} \backslash \Gamma$ with $\Gamma = [-r, 0]$. Since $\sqrt{\cdot}$ has a continuous upper and lower limit on Γ, each circle integral $\oint_{|s|=\epsilon} \sqrt{s}\mathrm{d}s$ exists and is finite. Then, an elementary computation shows that the residue of $s \mapsto \sqrt{s}$ at 0 exists and is given by

$$\operatorname{Res}\left(\sqrt{s}, 0\right) = \lim_{\epsilon \to 0} \frac{\epsilon}{2\pi} \int_{-\pi}^{+\pi} \sqrt{\epsilon e^{\mathrm{j}\theta}} e^{\mathrm{j}\theta} \mathrm{d}\theta = 0.$$

Similarly the residue of $s \mapsto 1/\sqrt{s}$ at 0 exists and is given by

$$\operatorname{Res}\left(\frac{1}{\sqrt{s}}, 0\right) = \lim_{\epsilon \to 0} \frac{\epsilon}{2\pi} \int_{-\pi}^{+\pi} \frac{e^{\mathrm{j}\theta}}{\sqrt{\epsilon e^{\mathrm{j}\theta}}} \mathrm{d}\theta = 0.$$

The first of the three representation theorems of this section is given below.

Theorem 2.16. *Let $\Gamma \subset (-\infty, 0]$ be a diffusive cut with n endpoints γ_k. Let $f : \mathbb{C}\backslash\Gamma \to \mathbb{C}$ be a meromorphic function with poles s_k. If*

(i) *f decays uniformly at infinity, i.e.*

$$\sup_{|s|=R} |f(s)| \underset{R\to\infty}{\longrightarrow} 0, \tag{2.16}$$

(ii) *at every endpoint γ_k, the residue $\mathrm{Res}(f, \gamma_k)$ is finite and satisfies*

$$\mathrm{Res}\left(f(s)e^{st}, \gamma_k\right) = \mathrm{Res}(f, \gamma_k)e^{\gamma_k t} \quad (t > 0),$$

(iii) *f has no singularity in the interior of Γ and is such that the diffusive weight*

$$\mu(\xi) \coloneqq \frac{1}{2\mathrm{j}\pi}\left[f(\xi e^{-\mathrm{j}\pi}) - f(\xi e^{+\mathrm{j}\pi})\right] \tag{2.17}$$

satisfies the integrability condition

$$\int_0^\infty \frac{|\mu(\xi)|}{1+\xi}\mathrm{d}\xi < \infty, \tag{2.18}$$

(iv) *the poles s_k are stable, i.e. $\Re(s_k) \leq 0$, simple, and satisfy the growth condition*

$$\frac{|\mathrm{Res}(f, s_k)|}{|s_k|^2} \underset{k\to\pm\infty}{=} \mathcal{O}\left(\frac{1}{k^2}\right) \quad \textit{and} \quad \lim_{K\to\infty} \sum_{k\in[\![-K,K]\!]} \frac{\mathrm{Res}(f, s_k)}{s_k} < \infty, \tag{2.19}$$

then $f = \hat{h}$ with $h \in \mathcal{S}'(\mathbb{R}) \cap \mathcal{D}'_+(\mathbb{R})$ given by

$$h(t) = \sum_{k\in[\![1,n]\!]} \mathrm{Res}(f, \gamma_k)e_{-\gamma_k}(t) + \sum_{k\in\mathbb{Z}} \mathrm{Res}(f, s_k)e_{-s_k}(t) + \int_0^\infty e_\xi(t)\mu(\xi)\,\mathrm{d}\xi \qquad (t \in \mathbb{R}) \tag{2.20}$$

$$\hat{h}(s) = \sum_{k\in[\![1,n]\!]} \frac{\mathrm{Res}(f, \gamma_k)}{s-\gamma_k} + \sum_{k\in\mathbb{Z}} \frac{\mathrm{Res}(f, s_k)}{s-s_k} + \int_0^\infty \frac{\mu(\xi)}{s+\xi}\,\mathrm{d}\xi \qquad (\Re(s) > 0). \tag{2.21}$$

Before giving the proof, let us discuss both the usefulness and meaning of this result through the following remarks.

Remark 2.17 (Notation of diffusive weights). In the above theorem, the diffusive weight μ is defined with f, through (2.17). In this dissertation, when there is a risk of ambiguity we will use a subscript to denote the function with which the diffusive weight is defined, e.g. "μ_f" or "$\mu_{\hat{h}}$". This notation will mostly be useful in Sections 2.1.4 and 2.4.

Remark 2.18 (Decay condition). When the meromorphic function f has poles, the decay condition (2.16) is to be understood in the following sense: there is a positive and increasing sequence $(R_n)_n$ such that $\sup_{|s|=R_n} |f(s)| \underset{n\to\infty}{\longrightarrow} 0$. This is possible since the poles of a meromorphic function are isolated. This abuse of notation is convenient when working with meromorphic functions and we shall use it repeatedly in the remaining of this chapter.

Remark 2.19. The right-hand side of the OD representation (2.21) can be computed numerically, which is useful to check the validity of an OD representation. Computing the diffusive weight μ is as cheap and accurate as evaluating f since it is given by (2.17). Computing the poles s_k requires a nonlinear solver, but this is not a major difficulty in practice. The most expensive quantities are the residues (2.15) and the diffusive part $\int_0^\infty \frac{\mu(\xi)}{s+\xi}\,\mathrm{d}\xi$, since they require a numerical quadrature with possibly many nodes.

Before proving this result, let us comment each of the four requirements of Theorem 2.16.

1. The decay condition (i) is failed by functions such as $s \mapsto s^k$ with $k \geq 0$ or $s \mapsto e^{\tau s}$ with $\tau \in \mathbb{R}$. However a function that fails (i) might still enjoy an OD representation. In Section 2.1.4 we will cover examples where f fails (i) but $s \mapsto {}^{f(s)}/_{s}$ satisfies the four conditions of Theorem 2.16, thus enabling to represent f.

2. Condition (ii) prevents f from being too singular at γ_k, which in practice is often a branch point of f. (The condition is obviously satisfied if γ_k is a simple pole of f.) For example, if $\gamma_1 = 0$ condition (ii) is failed by $s \mapsto s^{-\alpha}$ with $\alpha > 1$.

3. The diffusive weight μ, given by (2.17), is proportional to the jump of f across Γ, so that if f is univalued at $-\xi$ then $\mu(\xi) = 0$; this implies that the support of μ is restricted to the cut, i.e.

$$\operatorname{supp} \mu = -\Gamma.$$

   Hence the smoothness requirement on f implies that μ can only be singular at the endpoints γ_k. The integrability condition (2.18) then implies that any singularity of μ must remain integrable: from Proposition 2.10, the diffusive part of h belongs to $L^1_{\text{loc}}([0,\infty))$. This integrability condition (2.18) is known as the "well-posedness condition" in (Hélie and Matignon 2006a,b) and (Matignon and Zwart in revision). Note that the proposed proof shows that it is enough to require convergence of the improper integral, i.e.

$$\lim_{\substack{\epsilon \to 0 \\ R \to \infty}} \int_\epsilon^R \frac{\mu(\xi)}{1+\xi} \mathrm{d}\xi \quad \text{exists and is finite.} \tag{2.22}$$

   However, in most of the examples encountered in practice (2.18) is verified.

4. Lastly, condition (iv) restricts the growth of the residues compared to that of the poles. Of the four conditions, it is the most difficult one to verify in practice since a closed-form expression of the poles may not be available. However, it is lax enough so that it can be reasonably expected to be satisfied in practice. Although poles of higher order can be included in the representation without difficulty, we herein restrict ourselves to simple poles since they are computationally simpler and will prove sufficient for the applications of interest in this dissertation.

Proof. Let $\sigma > 0$ and $R > 0$. For $t \in \mathbb{R}$ we define

$$h_R(t) \coloneqq \frac{1}{2\mathrm{j}\pi} \int_{\sigma-\mathrm{j}R}^{\sigma+\mathrm{j}R} f(s) e^{st} \mathrm{d}s = \frac{e^{+\sigma t}}{2\pi} \overline{\mathcal{F}}[f(\sigma + \mathrm{j}\cdot)\mathbb{1}_{(-R,R)}](t). \tag{2.23}$$

The proof consists in computing $h_R(t)$ by using the residue theorem on a Bromwich contour and taking the limit $R \to \infty$ to show that $h_R \to h$ in $\mathcal{S}'(\mathbb{R})$ and $h \in \mathcal{D}'_+(\mathbb{R})$. The proof is inspired from (Schwartz 1966, § VI.4) for the existence of the limit and (Duffy 2004) for the definition of the Bromwhich contour. Let us first consider the case $t < 0$. Since f is analytic in $\mathbb{C}_0^+$ the residue theorem (Gamelin 2001, § VII.1) on the contour depicted in Figure 2.3(a) gives

$$|h_R(t)| = \left| \frac{1}{2\mathrm{j}\pi} \int_{\substack{|s-\sigma|=R \\ \Re(s)\geq\sigma}} f(s) e^{st} \mathrm{d}s \right| \leq C \sup_{\substack{|s-\sigma|=R \\ \Re(s)\geq\sigma}} |f(s)|,$$

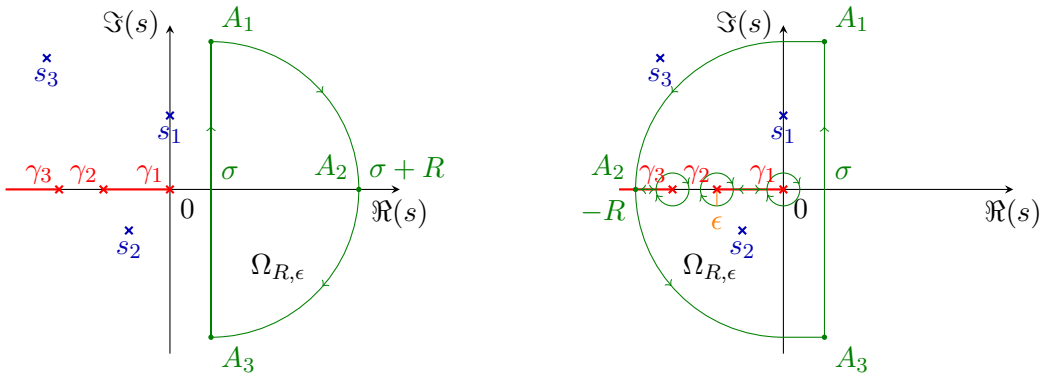

(a) Contour for $t < 0$. **(b)** Contour for $t > 0$.

Figure 2.3. Integration contours used in the proof of Theorem 2.16.

where we have used Jordan's lemma (Gamelin 2001, § VII.7). This estimates shows that for $t < 0$, $h_R(t) \to 0$ as $R \to \infty$.

The case $t > 0$ requires a more sophisticated contour depicted in Figure 2.3(b) where $R > 0$ (resp. $\epsilon > 0$) are chosen sufficiently large (resp. small). This contour is included in $\{|s| = R\}$, contains the straight line from $\sigma - \mathrm{j}R$ to $\sigma + \mathrm{j}R$, circles each endpoint γ_k with radius ϵ, and does not pass through any pole s_k, which is possible since the singularities of f in $\mathbb{C}\backslash\Gamma$ are isolated. This contour defines the piecewise smooth boundary of an open bounded connected set $\Omega_{R,\epsilon}$.

Since the function $s \mapsto f(s)e^{st}$ is meromorphic on $\Omega_{R,\epsilon}$ without singularities on $\partial\Omega_{R,\epsilon}$, the residue theorem yields

$$\frac{1}{2\mathrm{j}\pi}\oint_{\partial\Omega_{R,\epsilon}} f(s)e^{st}\mathrm{d}s = \sum_{k\in[\![1,N_{R,\epsilon}]\!]} \mathrm{Res}(f,s_k)e^{s_k t},$$

where we denote by $N_{R,\epsilon}$ the number of simple poles s_k in $\Omega_{R,\epsilon}$. By splitting the boundary integral on $\partial\Omega_{R,\epsilon}$ we get the identity

$$\begin{aligned} h_R(t) = &\sum_{k\in[\![1,N_{R,\epsilon}]\!]} \mathrm{Res}(f,s_k)e^{s_k t} + \int_0^R \mu(\xi)e^{-\xi t}\mathrm{d}\xi \\ &- \frac{1}{2\mathrm{j}\pi}\left[\int_{A_1A_2A_3} f(s)e^{st}\mathrm{d}s - \sum_{k\in[\![1,M_{R,\epsilon}]\!]} \oint_{|s-\gamma_k|=\epsilon} f(s)e^{st}\mathrm{d}s\right], \end{aligned} \tag{2.24}$$

where $M_{R,\epsilon}$ denotes the number of endpoints γ_k circled by $\Omega_{R,\epsilon}$. We will now prove that the right-hand side of (2.24), null for $t < 0$, admits a limit in $\mathcal{S}'(\mathbb{R})$ for $\epsilon \to 0$ and $R \to \infty$.

The line integral over $A_1A_2A_3$ can be estimated using Jordan's lemma as

$$\begin{aligned} \left|\int_{A_1A_2A_3} f(s)e^{st}\mathrm{d}s\right| &= \left|\int_{\substack{|s|=R\\ \Re(s)\le 0}} f(s)e^{st}\mathrm{d}s + \int_{\sigma+\mathrm{j}R}^{\mathrm{j}R} f(s)e^{st}\mathrm{d}s + \int_{-\mathrm{j}R}^{\sigma-\mathrm{j}R} f(s)e^{st}\mathrm{d}s\right| \\ &\le \pi \sup_{|s|=R} |f(s)| + 2\sigma e^{\sigma t} \sup_{R\le|s|\le\sqrt{\sigma^2+R^2}} |f(s)|, \end{aligned} \tag{2.25}$$

where we assume that R and σ are chosen so that there are no poles s_k in the annulus $R \le |s| \le \sqrt{R^2+\sigma^2}$. The estimate (2.25) shows that the line integral vanishes as $R \to \infty$. Next,

each circle integral around the endpoint γ_k converges towards the corresponding residue, i.e.

$$\oint_{|s-\gamma_k|=\epsilon} f(s)e^{st}\mathrm{d}s \underset{\epsilon\to 0}{\longrightarrow} 2\mathrm{j}\pi \operatorname{Res}(f(s)e^{\gamma_k t}, \gamma_k),$$

which is defined and finite by assumption; the series $\sum_{k\in[\![1,M_{R,\epsilon}]\!]}$ converges since there are only a finite number of endpoints. The convergence of $\sum_{k\in[\![1,N_{R,\epsilon}]\!]} \operatorname{Res}(f,s_k)e^{s_k t}H(t)$ for $R\to\infty$ in $\mathcal{S}'(\mathbb{R})\cap\mathcal{D}'_+(\mathbb{R})$ follows directly from Proposition A.18. Lastly, the convergence of $\int_0^R \mu(\xi)e^{-\xi t}\mathrm{d}\xi$ as $R\to\infty$ follows from the estimate $e^{-\xi t}H(t)\le(1+t\xi)^{-1}$. In conclusion, $h_R\to h$ in $\mathcal{S}'(\mathbb{R})$ and $h\in\mathcal{D}'_+(\mathbb{R})$. The continuity of the Fourier transform in $\mathcal{S}'(\mathbb{R})$ implies

$$e^{-\sigma t}h(t)=\frac{1}{2\pi}\overline{\mathcal{F}}[f(\sigma+\mathrm{j}\cdot)](t),$$

so that taking the Fourier transform in $\mathcal{S}'(\mathbb{R})$ yields

$$\forall\omega\in\mathbb{R},\ \mathcal{F}[e^{-\sigma\cdot}h](\omega)=f(\sigma+\mathrm{j}\omega),$$

which can be written $f(s)=\hat{h}(s)$ by definition of the Laplace transform. □

In practice, it often happens that the behavior of f at the endpoints γ_k is such that the corresponding residues vanish. In this case, the endpoints γ_k do not contribute to the OD representation. This is captured in the corollary below, whose condition (ii) is that found in (Casenave and Montseny 2010).

Corollary 2.20. *Let $\Gamma\subset(-\infty,0]$ be a diffusive cut with n endpoints γ_k. Let $f:\mathbb{C}\backslash\Gamma\to\mathbb{C}$ be a meromorphic function with poles s_k. Assume that the following conditions are satisfied:*

(i) *Identical to Theorem 2.16(i).*

(ii) *At every endpoint γ_k,*

$$\sup_{|s-\gamma_k|=\epsilon}|\epsilon f(s)|\underset{\epsilon\to 0}{\longrightarrow}0. \tag{2.26}$$

(iii) *Identical to Theorem 2.16(iii).*

(iv) *Identical to Theorem 2.16(iv).*

Then $f=\hat{h}$ with $h\in\mathcal{S}'(\mathbb{R})\cap\mathcal{D}'_+(\mathbb{R})$ given by

$$h(t)=\sum_{k\in\mathbb{Z}}\operatorname{Res}(f,s_k)e_{-s_k}(t)+\int_0^\infty e_\xi(t)\mu(\xi)\,\mathrm{d}\xi\qquad(t\in\mathbb{R}) \tag{2.27}$$

$$\hat{h}(s)=\sum_{k\in\mathbb{Z}}\operatorname{Res}(f,s_k)\frac{1}{s-s_k}+\int_0^\infty\frac{1}{s+\xi}\mu(\xi)\,\mathrm{d}\xi\quad(\Re(s)>0). \tag{2.28}$$

Proof. Identically to the proof of Theorem 2.16, the identity (2.24) is derived. The only difference is that the circle integrals around the endpoints γ_k are handled with

$$\left|\sum_{k\in[\![1,M_{R,\epsilon}]\!]}\oint_{|s-\gamma_k|=\epsilon}f(s)e^{st}\mathrm{d}s\right|\le 2\pi e^{\epsilon t}\sum_{k\in[\![1,n]\!]}e^{\Re(\gamma_k)t}\sup_{|s-\gamma_k|=\epsilon}|\epsilon f(s)|\underset{\epsilon\to0}{\longrightarrow}0,$$

so that they do not contribute to the representations (2.27,2.28). □

In the two results above, μ is assumed to be smooth in the interior of its support. The case where f has a simple pole on the cut is handled by the following result, which is similar to Theorem 2.16 except for the presence of a principal value.

Theorem 2.21. *Let $\Gamma \subset (-\infty, 0]$ be a diffusive cut with n endpoints γ_k. Let $f : \mathbb{C}\backslash\Gamma \to \mathbb{C}$ be a meromorphic function, with poles $s_k \in \mathbb{C}\backslash\Gamma$, which satisfies the conditions (i), (ii) and (iv) of Corollary 2.20. If*

(i) *f has a finite number of simple poles λ_k in the interior of Γ,*

(ii) *there is a neighborhood V of $\{|\lambda_1|, \cdots, |\lambda_L|\}$ in $(0, \infty)$ such that the diffusive weight (2.17) satisfies the integrability condition*

$$\int_{(0,\infty)\backslash V} \frac{|\mu(\xi)|}{1+\xi} \mathrm{d}\xi < \infty,$$

then $f = \hat{h}$ with $h \in \mathcal{S}'(\mathbb{R}) \cap \mathcal{D}'_+(\mathbb{R})$ given by

$$h(t) = \sum_{k\in\mathbb{Z}} \mathrm{Res}(f, s_k) e_{-s_k}(t) + \sum_{k\in[\![1,L]\!]} \mathrm{Res}(f, \lambda_k) e_{-\lambda_k}(t) + \mathrm{pv} \int_0^\infty e_\xi(t)\mu(\xi)\,\mathrm{d}\xi \qquad (t \in \mathbb{R})$$

$$\hat{h}(s) = \sum_{k\in\mathbb{Z}} \mathrm{Res}(f, s_k) \frac{1}{s - s_k} + \sum_{k\in[\![1,L]\!]} \mathrm{Res}(f, \lambda_k) \frac{1}{s-\lambda_k} + \mathrm{pv} \int_0^\infty \frac{1}{s+\xi}\mu(\xi)\,\mathrm{d}\xi \quad (\Re(s) > 0),$$

where pv *denotes the Cauchy principal value.*

Remark 2.22. In a neighborhood of λ_k, say $\{|s - \lambda_k| < \epsilon\}$, the function f can be expressed as $f(s) = \frac{A}{s-\lambda_k} g(s) + b(s)$, where g and b are analytic in the two half-disks $\{|s - \lambda_k| < \epsilon, \Im(s) \geq 0\}$ and $\{|s - \lambda_k| < \epsilon, \Im(s) \leq 0\}$. This implies that the residue at λ_k is given by

$$\mathrm{Res}(f, \lambda_k) \coloneqq \lim_{\epsilon\to 0} \frac{1}{2\mathrm{j}\pi} \oint_{|s-\lambda_k|=\epsilon} f(s)\mathrm{d}s = A\frac{g(|\lambda_k|e^{+\mathrm{j}\pi}) + g(|\lambda_k|e^{-\mathrm{j}\pi})}{2}, \tag{2.29}$$

which reduces to the standard expression $Ag(-\lambda_k)$ if g is not multivalued.

Proof. The proof is similar to that of Theorem 2.16 and Corollary 2.20 so that we only detail the differences. Let $\sigma > 0$ and $R > 0$. Define $h_R(t)$ for $t \in \mathbb{R}$ as (2.23). To compute h_R, we consider integration contours identical to the ones depicted in Figure 2.3 with the additional constraint that they circle not only the endpoints γ_k but also each of the L simple poles $\lambda_k \in \mathring{\Gamma}$. For $t < 0$, $h_R(t) \xrightarrow[R\to\infty]{} 0$. For $t > 0$, the residue theorem gives

$$\begin{aligned} h_R(t) = &\sum_{k\in[\![1,N_{R,\epsilon}]\!]} \mathrm{Res}(f, s_k)e^{s_k t} - \frac{1}{2\mathrm{j}\pi}\Big[\int_{A_1A_2A_3} f(s)e^{st}\mathrm{d}s - \sum_{k\in[\![1,M_{R,\epsilon}]\!]} \oint_{|s-\gamma_k|=\epsilon} f(s)e^{st}\mathrm{d}s\Big] \\ &+ \frac{1}{2\mathrm{j}\pi} \sum_{k\in[\![1,L_{R,\epsilon}]\!]} \oint_{|s-\lambda_k|=\epsilon} f(s)e^{st}\mathrm{d}s + \int_{(0,R)\cap\overline{\Omega_{R,\epsilon}}} \mu(\xi)e^{-\xi t}\mathrm{d}\xi, \end{aligned}$$

where $L_{R,\epsilon}$ denotes the number of simple poles λ_k in the contour. Let us focus on the only differences with (2.24), namely the two terms on the second line of the right-hand side. First, from Remark 2.22, the limit $\lim_{\epsilon\to 0} \frac{1}{2\mathrm{j}\pi} \oint_{|s-\lambda_k|=\epsilon} f(s)e^{st}\mathrm{d}s$ is finite with limit $\mathrm{Res}(f, \lambda_k)e^{\lambda_k t}$. Second, since μ has at most a simple pole at λ_k and $\xi \mapsto e^{-\xi t}$ is smooth on $(0, \infty)$, the limit $\lim_{\epsilon\to 0} \int_{(0,R)\cap\overline{\Omega_{R,\epsilon}}} \mu(\xi)e^{-\xi t}\mathrm{d}\xi$ exists in the sense of the principal value, see (Zemanian 1965, § 2.5) (Schwartz 1966, § I.2.2). □

All the results above assume in particular that f has uniform decay at infinity, i.e. that f obeys the uniform decay condition (2.16). This hypothesis is typically verified for models that arise from diffusion phenomena. On the other hand, physical phenomena that are lossless or without diffusion usually yield periodic functions, which are covered by the (last) theorem below. The main change compared to Theorem 2.16 is the absence of cut and the fact that the uniform decay condition is on a vertical line rather than a disk, to accommodate the periodic nature of f.

Theorem 2.23. *Let $f : \mathbb{C} \to \mathbb{C}$ be a meromorphic function with poles s_k and period $\mathrm{j}T$, $T > 0$. Assume that the following conditions are satisfied:*

(i) *f decays uniformly at infinity, i.e.*

$$\sup_{\Re(s)=R} |f(s)| \underset{R\to\infty}{\longrightarrow} 0.$$

(ii) *Identical to Theorem 2.16(iv).*

Then $f = \hat{h}$ with $h \in \mathcal{S}'(\mathbb{R}) \cap \mathcal{D}'_+(\mathbb{R})$ given by

$$h(t) = \sum_{k\in\mathbb{Z}} \mathrm{Res}(f, s_k) e_{-s_k}(t) \quad (t \in \mathbb{R}),\ \hat{h}(s) = \sum_{k\in\mathbb{Z}} \mathrm{Res}(f, s_k) \frac{1}{s - s_k} \quad (\Re(s) > 0).$$

Proof. The proof follows the same lines as that of Theorem 2.16 but with a square integration contour suited to the vertical periodicity of f. Intuitively, one consequence of this change of contour is that we cannot use Jordan's lemma anymore; however, we can use the oscillatory nature of the integrand at infinity to conclude (in spirit, this is close to the Riemann-Lebesgue lemma). Let $\sigma > 0$, $R > 0$, and h_R defined as (2.23).

For $t < 0$ we consider the square contour depicted in Figure 2.4(a), which does not pass through any pole of f. Since f is analytic in $\mathbb{C}_0^+$, the residue theorem gives

$$h_R(t) = \frac{1}{2\mathrm{j}\pi} \int_{\sigma+R-\mathrm{j}R}^{\sigma+R+\mathrm{j}R} f(s) e^{st} \mathrm{d}s + \frac{1}{2\mathrm{j}\pi} \left(\int_{\sigma}^{\sigma+R} \left[f(x - \mathrm{j}R) e^{-\mathrm{j}Rt} - f(x + \mathrm{j}R) e^{\mathrm{j}Rt} \right] e^{xt} \mathrm{d}x \right).$$

The fact that $h_R(t) \to 0$ as $R \to \infty$ is deduced from the following two estimates. The first integral is estimated with

$$\left| \int_{\sigma+R-\mathrm{j}R}^{\sigma+R+\mathrm{j}R} f(s) e^{st} \mathrm{d}s \right| \leq 2R e^{(\sigma+R)t} \sup_{\Re(s)=\sigma+R} |f(s)| \underset{R\to\infty}{\to} 0.$$

For the second integral, we take $R = \frac{pT}{2}$. (Without loss of generality, we can still assume that the contour does not pass trough any pole of f, otherwise we can shift the contour vertically.) The second integral is estimated with

$$\begin{aligned} \left| \frac{1}{2\mathrm{j}\pi} \int_{\sigma}^{\sigma+R} \left[f(x - \mathrm{j}R) e^{-\mathrm{j}Rt} - f(x + \mathrm{j}R) e^{\mathrm{j}Rt} \right] e^{xt} \mathrm{d}x \right| &= \left| \frac{\sin(Rt)}{\pi} \int_{\sigma}^{\sigma+R} f(x + \mathrm{j}R) e^{xt} \mathrm{d}x \right| \\ &\leq \frac{|\sin(Rt)|}{\pi t} \left(e^{\sigma t} - e^{(\sigma+R)t} \right) \sup_{0\leq\Re(s-\sigma)\leq R} |f(s)| \underset{p\to\infty}{\to} 0. \end{aligned}$$

The case $t > 0$ is similar with the contour depicted in Figure 2.4(b). The residue theorem yields

$$\begin{aligned} h_R(t) = &\sum_{k\in[\![1,N_{R,\epsilon}]\!]} \mathrm{Res}(f, s_k) e^{s_k t} + \frac{1}{2\mathrm{j}\pi} \int_{-R-\mathrm{j}R}^{-R+\mathrm{j}R} f(s) e^{st} \mathrm{d}s \\ &+ \frac{1}{2\mathrm{j}\pi} \int_{-R}^{\sigma} \left[f(x + \mathrm{j}R) e^{(x+\mathrm{j}R)t} - f(x - \mathrm{j}R) e^{(x-\mathrm{j}R)t} \right] \mathrm{d}x, \end{aligned} \tag{2.30}$$

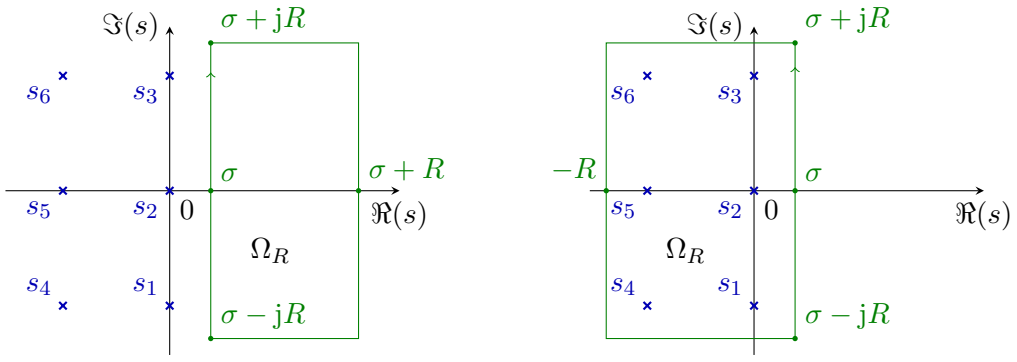

(a) Contour for $t < 0$. **(b)** Contour for $t > 0$.

Figure 2.4. Integration contours used in the proof of Theorem 2.23.

where we denote by $N_{R,\epsilon}$ the number of poles s_k within the contour. We will now prove that the right-hand side of (2.30), null for $t < 0$, admits a limit in $\mathcal{S}'(\mathbb{R})$ for $\epsilon \to 0$ and $R \to \infty$. Identically to Theorem 2.16, the convergence of $\sum_{k\in[\![1,N_{R,\epsilon}]\!]} \mathrm{Res}(f, s_k)e^{s_k t}H(t)$ for $R \to \infty$ in $\mathcal{S}'(\mathbb{R}) \cap \mathcal{D}'_+(\mathbb{R})$ follows from Proposition A.18. The two remaining integrals vanish thanks to the uniform decay of f. The first one is estimated with

$$\left| \int_{-R-\mathrm{j}R}^{-R+\mathrm{j}R} f(s)e^{st}\mathrm{d}s \right| \leq 2Re^{-Rt} \sup_{\Re(s)=-R} |f(s)| \xrightarrow[R\to\infty]{} 0.$$

For the second one we set $R = pT$ to use the vertical periodicity of f:

$$\left| \frac{1}{2\mathrm{j}\pi} \int_{-R}^{\sigma} \left[f(x + \mathrm{j}R)e^{(x+\mathrm{j}R)t} - f(x - \mathrm{j}R)e^{(x-\mathrm{j}R)t} \right] \mathrm{d}x \right|$$
$$\leq \frac{|\sin(Rt)|}{\pi t} \left| e^{\sigma t} - e^{-Rt} \right| \sup_{-R\leq\Re(s)\leq\sigma} |f(s)| \underset{p\to\infty}{\to} 0.$$

□

Remark 2.24 (Poles and cuts representation). The representation theorems given in this section can be extended to the case where the cut Γ is not included in $(-\infty, 0]$ but is a piecewise smooth complex path, with no loops. This leads to a more general *poles and cuts representation*, following the terminology of (Hélie and Matignon 2006a,b). For example, the kernel J_0, where J_0 denotes the zeroth-order Bessel function of the first kind, does not admit an OD representation (2.27) but admits a poles and cuts representation, see (Matignon 1998, § 3.3). When different cuts are mathematically possible, a "physical cut" can be identified using a limiting process, see (Mignot et al. 2009).

2.1.3 Standard and extended realizations

Identically to diffusive kernels, covered in Section 2.1.1, OD kernels enjoy a time-local realization. Let h be an OD kernel that admits, say, the representation (2.27). The corresponding realization is

$$h \star u(t) = \sum_{k\in\mathbb{Z}} \mathrm{Res}(\hat{h}, s_k)\varphi(t, -s_k) + \int_0^{\infty} \varphi(t, \xi)\, \mu_{\hat{h}}(\xi)\, \mathrm{d}\xi, \tag{2.31}$$

where the function φ has been defined in (2.6). The interest of (2.31) is that $\varphi(\cdot, -s_k)$ and $\varphi(\cdot, \xi)$ can be computed using the first-order ODE (2.7). The identities (2.7,2.31) are known as the *oscillatory-diffusive realization* of h.

In practice, as we will see in Sections 2.1.4 and 2.4, it can happen that a function $\hat{h}$ fails the decay condition (2.16) but $\hat{g}(s) \coloneqq \hat{h}(s)/s$ satisfies the conditions of, say, Corollary 2.20, so that $\hat{g}$ admits a standard OD representation (2.28), which reads

$$\hat{g}(s) = \sum_{k\in\mathbb{Z}} \mathrm{Res}(\hat{g}, s_k)\frac{1}{s-s_k} + \int_0^\infty \frac{1}{s+\xi}\mu_{\hat{g}}(\xi)\,\mathrm{d}\xi \quad (\Re(s) > 0),$$

where s_k is a pole of $\hat{g}$ and $\mu_{\hat{g}}$ is the diffusive weight associated with $\hat{g}$. The representation of $\hat{h}$ can then be deduced from that of $\hat{g}$

$$h(t) = \sum_{k\in\mathbb{Z}} \mathrm{Res}(\hat{g}, s_k)\left(s_k e_{-s_k}(t) + \delta(t)\right) + \int_0^\infty \left(-\xi e_\xi(t) + \delta(t)\right)\mu_{\hat{g}}(\xi)\,\mathrm{d}\xi \qquad (t \in \mathbb{R}) \tag{2.32}$$

$$\hat{h}(s) = \sum_{k\in\mathbb{Z}} \mathrm{Res}(\hat{g}, s_k)\frac{s}{s-s_k} + \int_0^\infty \frac{s}{s+\xi}\mu_{\hat{g}}(\xi)\,\mathrm{d}\xi \qquad (\Re(s) > 0), \tag{2.33}$$

where we have used (2.8) to obtain (2.32). The corresponding realization is

$$h \star u(t) = \sum_{k\in\mathbb{Z}} \mathrm{Res}(\hat{g}, s_k)\left(s_k\varphi(t, -s_k) + u(t)\right) + \int_0^\infty \left(-\xi\varphi(t,\xi) + u(t)\right)\mu_{\hat{g}}(\xi)\,\mathrm{d}\xi. \tag{2.34}$$

Borrowing the terminology employed in (Montseny 1998), we will say that the OD representations (2.32,2.33) and the OD realization (2.7,2.34) are *extended by* differentiation, or simply *extended.*

To conclude this presentation of realizations, let us highlight the following fact that is seldom mentioned in the literature, despite its computational interest: it may happen that an extended OD kernel also admits a standard OD representation. To illustrate this, assume that h admits the OD representation extended by differentiation (2.33). If the residues and diffusive weight decay sufficiently fast, namely

$$\sum_{k\in\mathbb{Z}} \mathrm{Res}(\hat{g}, s_k) < \infty \quad \text{and} \quad \int_0^\infty \mu_{\hat{g}}(\xi)\,\mathrm{d}\xi < \infty, \tag{2.35}$$

then the extended representation (2.33) can be rewritten as

$$\hat{h}(s) = \sum_{k\in\mathbb{Z}} \mathrm{Res}(\hat{g}, s_k) + \int_0^\infty \mu_{\hat{g}}(\xi)\,\mathrm{d}\xi + \sum_{k\in\mathbb{Z}} \mathrm{Res}(\hat{g}, s_k)s_k\frac{1}{s-s_k} + \int_0^\infty \frac{1}{s+\xi}\left(-\xi\mu_{\hat{g}}(\xi)\right)\,\mathrm{d}\xi,$$

which consists of a constant and a standard OD representation. As a rule of thumb, the conditions (2.35) are likely to be verified for kernels that satisfy $\hat{h}(s) \underset{|s|\to\infty}{=} \mathcal{O}(1)$, but will fail when $\hat{h}(s) \underset{|s|\to\infty}{=} \mathcal{O}(|s|^\alpha)$ with $\alpha > 0$. Both cases will be encountered in the examples of Section 2.1.4 as well as the in the application of Section 2.4.

Remark 2.25 (Regularization of extended OD realization). Let $h = g'$ be a kernel that admits an extended OD representation given by (2.32), obtained as we have seen above by differentiating the OD representation of g. This differentiation incurs a loss of regularity on the kernel, so that (2.34) may only be defined in $\mathcal{D}'_+(\mathbb{R})$; for instance, $h \star u(0)$ may not be finite. Let us clarify this statement. For a smooth input $u \in \mathcal{C}^\infty_0(\mathbb{R})$ and $z \in \mathbb{C}^*$, let us define $\tilde{\varphi}(\cdot, z)$ as the solution of

$$\begin{cases} \partial_t\tilde{\varphi}(t,z) = -z\tilde{\varphi}(t,z) + u(t) \quad (t > 0,\ z \in \mathbb{C}^*) \\ \tilde{\varphi}(t,0) = \dfrac{u(0)}{z}, \end{cases}$$

which differs from (2.7) through the initial condition at $t = 0$. By using the identity $\tilde{\varphi}(t, z) = \varphi(t, z) + \frac{u(0)}{z} e_z(t)$, we can rewrite (2.34) as the sum of two terms, namely

$$h \star u(t) = u(0) \left[\sum_{k \in \mathbb{Z}} \operatorname{Res}(\hat{g}, s_k) e_{-s_k}(t) + \int_0^\infty e_\xi(t) \mu_{\hat{g}}(\xi) \, \mathrm{d}\xi \right] + \langle T(t), u \rangle \,, \tag{2.36}$$

where the distribution T is defined by

$$\langle T(t), u \rangle \coloneqq \sum_{k \in \mathbb{Z}} \operatorname{Res}(\hat{g}, s_k) \left(s_k \tilde{\varphi}(t, -s_k) + u(t) \right) + \int_0^\infty \left(-\xi \tilde{\varphi}(t, \xi) + u(t) \right) \mu_{\hat{g}}(\xi) \, \mathrm{d}\xi$$

and is null at $t = 0$. If the conditions (2.35) are not satisfied, then the operator $u \mapsto \langle T, u \rangle$ can be interpreted as a regularization of the convolution operator $u \mapsto h \star u$. This regularization is useful to deal with input signals such that $u(0) \neq 0$ and is well-known in the context of fractional calculus, see Remark 2.27 below for references. Another expression of $\langle T, u \rangle$ is given in Remark A.3.

2.1.4 Basic examples

The purpose of this section is to gather examples to illustrate the application of the representation theorems derived in Section 2.1.2. Only examples representative of the functions that arise in physical modeling have been chosen. As such, this section is preparatory to Section 2.4, where physical impedance models are analyzed. Note that some known representations, such as that given by Lemmas 2.26 and 2.34 for example, have been recalled and discussed when it is illustrative to do so, for example when it helps highlighting pitfalls. However, to the best of the author's knowledge, the representations presented in Lemmas 2.30, 2.35, and 2.40 are original.

We recall that in this dissertation the power function $s \mapsto s^\alpha$ with $\alpha \in \mathbb{R}$ is the principal branch, defined in Example 2.14 as (2.14).

Diffusive kernels

As already mentioned in Example 2.6, the fractional kernel Y_α with $\alpha \in (0, 1)$ is diffusive. Since it is a simple yet illustrative example, we recall the derivation of the diffusive representations of both Y_α and its (distributional) derivative Y_α' below.

Lemma 2.26. *Let $\alpha \in (0, 1)$. The function $s \mapsto s^{-\alpha}$ has the diffusive representation*

$$s^{-\alpha} = \int_0^\infty \frac{1}{s + \xi} \, \mu_\alpha(\xi) \, \mathrm{d}\xi \quad (s \in \mathbb{C} \backslash (-\infty, 0]),$$

where μ_α is given by (2.11). As a consequence, $s \mapsto s^\alpha$ has the (extended) diffusive representation

$$s^\alpha = \int_0^\infty \frac{s}{s + \xi} \, \mu_{1-\alpha}(\xi) \, \mathrm{d}\xi \quad (s \in \mathbb{C} \backslash (-\infty, 0]).$$

Proof. Let $\alpha \in (0, 1)$ and $f(s) = s^{-\alpha}$. Let us check each of the four conditions of Corollary 2.20. By choosing the cut as $\Gamma \coloneqq (-\infty, 0]$, f is an analytic function in $\mathbb{C} \backslash \Gamma$. The uniform decay condition (2.16) is easily verified. The only branch point is $\gamma_1 = 0$ and condition (2.26) is satisfied. The diffusive weight can be explicitly computed using (2.17), which leads to, for $\xi \in (0, \infty)$

$$\mu(\xi) \coloneqq \frac{1}{2\mathrm{j}\pi} \left[f(\xi e^{-\mathrm{j}\pi}) - f(\xi e^{+\mathrm{j}\pi}) \right] = \frac{1}{2\mathrm{j}\pi \xi^\alpha} \left[e^{\alpha \mathrm{j}\pi} - e^{-\alpha \mathrm{j}\pi} \right] = \mu_\alpha(\xi).$$

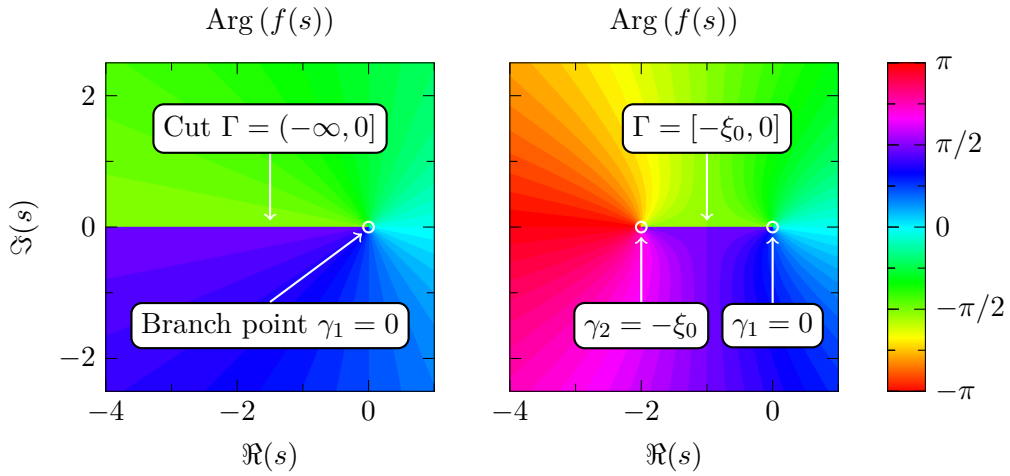

Figure 2.5. Plot of the principal value of the argument for two multivalued functions, which shows a jump across the cut Γ. (Left) $f(s) = \frac{1}{\sqrt{s}}$ where $\sqrt{\cdot}$ is the principal branch of the square root defined in Example 2.14. (Right) $f(s) = \frac{1}{\sqrt{s}\sqrt{s+\xi_0}}$ with $\xi_0 = 2$.

Condition (iii) is satisfied since f has no singularity in the interior of Γ, which is $\mathring{\Gamma} = (-\infty, 0)$, and μ satisfies the integrability condition (2.18). Since f has no poles, condition (iv) is automatically verified.

The kernel $f(s) = s^\alpha$ with $\alpha \in (0,1)$ fails (2.16) as well as (2.18). However, since $g(s) = \frac{f(s)}{s} = s^{\alpha-1}$ satisfies all the conditions of Corollary 2.20, we deduce the diffusive representation of f from that of g. □

Remark 2.27. For $\alpha \in (0,1)$, note that we *cannot* write s^α as

$$s^\alpha = \int_0^\infty \mu_{1-\alpha}(\xi)\,\mathrm{d}\xi + \int_0^\infty \frac{1}{s+\xi}\left[-\xi\mu_{1-\alpha}(\xi)\right]\,\mathrm{d}\xi$$

since $\int_0^\infty \mu_{1-\alpha}(\xi)\,\mathrm{d}\xi = +\infty$. In other words, $\hat{h}(s) = s^\alpha$ fails condition (2.35) with $\mu_g(\xi) = \mu_{1-\alpha}(\xi)$ discussed in Section 2.1.3. This implies that the corresponding realization cannot be reduced to the addition of a constant to a standard OD realization (2.31): it must be an extended realization of the form (2.34). Following Remark 2.25, the operator $u \mapsto h \star u$, known as the Riemann-Liouville fractional derivative of order α (Samko et al. 1993, § 2.3), is not finite at $t = 0$ if $u(0) \neq 0$. Its regularization T, known as the Caputo fractional derivative of order α, is finite at $t = 0$ even if $t \neq 0$ (Caputo 1976) (Podlubny 1999, § 2.4.1). See also (Matignon 2009), (Lombard and Matignon 2016), and (Monteghetti et al. 2017a, App. B).

Using Lemma 2.26, we can represent a function such as

$$f(s) = \frac{1}{s} + s^{-\beta} + 1 + s^\alpha + s \quad (\beta \in (0,1),\ \alpha \in (0,1),\ s \in \mathbb{C}\backslash(-\infty, 0]).$$

The inverse of a fractional polynomial can be represented similarly, see the lemma below.

Lemma 2.28. *The function*

$$f(s) = \frac{1}{a_0 + a_{1/2}\sqrt{s} + a_1 s} = \frac{1}{P(\sqrt{s})} \quad (\Re(s) > 0),$$

where $a_0 \geq 0$, $a_1 \geq 0$, $a_{1/2} > 0$, *and*

$$P(\sigma) \coloneqq a_0 + a_{1/2}\sigma + a_1\sigma^2$$

admits the diffusive representation

$$f(s) = \int_0^\infty \frac{1}{s+\xi}\mu(\xi)\,\mathrm{d}\xi,\ \mu(\xi) = \frac{1}{\pi}\frac{a_{1/2}\sqrt{\xi}}{a_0^2 + \left(a_{1/2}^2 - 2a_0a_1\right)\xi + a_1^2\xi^2}\mathbb{1}_{(0,\infty)}(\xi).$$

Proof. The (diffusive) cut is $\Gamma = (-\infty, 0]$ with branch point $\gamma_1 = 0$. Let us verify the conditions of Corollary 2.20. The uniform decay condition (i) is satisfied. At the only branch point $\gamma_1 = 0$, condition (ii) holds true. Condition (iii) can be verified by explicitly computing the diffusive weight using (2.17) for $\xi \in (0, \infty)$, which yields

$$\mu(\xi) = \frac{1}{2\mathrm{j}\pi}\left[\frac{1}{P(-\mathrm{j}\sqrt{\xi})} - \frac{1}{P(+\mathrm{j}\sqrt{\xi})}\right] = \frac{1}{\pi}\frac{\Im\left[P(+\mathrm{j}\sqrt{\xi})\right]}{\left|P(+\mathrm{j}\sqrt{\xi})\right|^2}.$$

The lemma below shows that f has no poles, so that condition (iv) is satisfied. In conclusion, f admits the OD representation (2.28).

Lemma 2.29. *Let $a_0, a_1 \geq 0$ and $a_{1/2} > 0$. The only possible zero of $s \mapsto a_0 + a_{1/2}\sqrt{s} + a_1 s$ is 0.*

Proof. If $a_1 = 0$, the result follows directly from $\Re(\sqrt{s}) \geq 0$. Let us now assume that $a_1 > 0$. The roots of P are then given by $\zeta_\pm = \frac{a_{1/2}}{2a_1}\left(-1 \pm \sqrt{1 - \frac{4a_1a_0}{a_{1/2}^2}}\right)$, so that the only possible zero of $s \mapsto a_0 + a_{1/2}\sqrt{s} + a_1 s$ would be ζ_+^2. The conclusion follows from the equivalence $\Re(\zeta_+) \geq 0 \Leftrightarrow a_0a_1 = 0$. □

□

Let us conclude this series of diffusive kernels with the example below, which will be useful when analyzing physical impedance models in Section 2.4. An extended representation of this function has been given in (Hélie and Matignon 2006b); here we derive a standard representation.

Lemma 2.30. *The function*

$$f(s) = e^{-\epsilon\sqrt{s}} \quad (s \in \mathbb{C}\backslash(-\infty, 0])$$

with $\epsilon > 0$ admits the representation

$$f(s) = 2 + \int_0^\infty \frac{1}{s+\xi}\mu(\xi)\mathrm{d}\xi,\ \mu(\xi) = -\frac{\sin(\epsilon\sqrt{\xi})}{\pi}\mathbb{1}_{(0,\infty)}(\xi).$$

Proof. The (diffusive) cut is $\Gamma = (-\infty, 0]$ with branch point $\gamma_1 = 0$. f fails the decay condition (2.16). The function $g(s) = \frac{f(s)}{s}$ fails the condition (ii) of Corollary 2.20, since $g(s) \underset{s\to 0}{=} \mathcal{O}\left(|s|^{-1}\right)$, but satisfies all the conditions of Theorem 2.16. Since $\mathrm{Res}(g, 0) = f(0)$, g admits the OD representation

$$g(s) = \frac{1}{s} + \int_0^\infty \frac{1}{s+\xi}\mu_g(\xi)\mathrm{d}\xi,$$

with diffusive weight

$$\mu_g(\xi) \coloneqq \frac{1}{2\mathrm{j}\pi}\left[g(\xi e^{-\mathrm{j}\pi}) - g(\xi e^{+\mathrm{j}\pi})\right] = \frac{1}{2\mathrm{j}\pi}\frac{1}{\xi}\left[e^{+\epsilon\mathrm{j}\sqrt{\xi}} - e^{-\epsilon\mathrm{j}\sqrt{\xi}}\right] = \frac{\sin(\epsilon\sqrt{\xi})}{\pi\xi},$$

from which we deduce the following representation of f

$$\begin{aligned} f(s) &= 1 + \int_0^\infty \frac{s+\xi-\xi}{s+\xi}\mu_g(\xi)\mathrm{d}\xi \\ &= 1 + \int_0^\infty \mu_g(\xi)\mathrm{d}\xi + \int_0^\infty \frac{1}{s+\xi}\left[-\xi\mu_g(\xi)\right]\mathrm{d}\xi, \end{aligned}$$

which is the claimed representation using $\int_0^\infty \mu_g(\xi)\mathrm{d}\xi = \frac{2}{\pi}\int_0^\infty \frac{\sin(x)}{x}\mathrm{d}x = 1$. □

Remark 2.31. In the proof of Lemma 2.30, the representation of f has been obtained from that of $g(s) = f(s)/s$ using the fact that the diffusive weight of g has a convergent improper integral on $(0, \infty)$, i.e. that it satisfies condition (2.35) discussed in Section 2.1.3. The representation of f is therefore reduced to a constant added to a standard OD representation (2.28) whose diffusive weight μ fails the integrability condition (2.18) but satisfies (2.22). This contrasts with $s \mapsto s^\alpha$ with $\alpha \in (0, 1)$ where the OD representation was necessarily extended, see Remark 2.27.

Bounded branch cut

In the examples covered so far, there is only one branch point γ_1 and the cut is $(-\infty, 0]$. Let us consider an example where the cut is bounded.

Lemma 2.32. *The function*

$$f(s) = \frac{1}{\sqrt{s}\sqrt{s+\xi_0}} \quad (s \in \mathbb{C}\backslash[-\xi_0, 0]),$$

with $\xi_0 > 0$ *admits the diffusive representation*

$$f(s) = \int_0^{\xi_0} \frac{1}{s+\xi}\mu(\xi)\,\mathrm{d}\xi,\ \mu(\xi) = \frac{\mu_{1/2}(\xi)}{\sqrt{\xi_0 - \xi}}\mathbb{1}_{(0,\xi_0)}(\xi).$$

Proof. The (diffusive) cut is defined as $\Gamma = [-\xi_0, 0]$ with two branch points $\gamma_1 = 0$ and $\gamma_2 = -\xi_0$. The conditions (i), (ii), and (iv) of Corollary 2.20 are satisfied. To verify condition (iii), we compute the diffusive weight using (2.17). For $\xi > a$, $\mu(\xi) = 0$ since f is continuous there. For $\xi \in (0, \xi_0)$, there is a jump across the cut given by

$$\mu(\xi) = \frac{1}{2\mathrm{j}\pi}\left[\frac{1}{\sqrt{\xi e^{-\mathrm{j}\pi}}\sqrt{\xi_0 - \xi}} - \frac{1}{\sqrt{\xi e^{+\mathrm{j}\pi}}\sqrt{\xi_0 - \xi}}\right] = \frac{\mu_{1/2}(\xi)}{\sqrt{\xi_0 - \xi}}.$$

□

This kind of function arise in e.g. the modeling of semi-infinite ground layers (Dragna and Blanc-Benon 2014). Note that the boundedness of the cut Γ implies the boundedness of the support of μ, see Figure 2.5 for an illustration and a comparison with the fractional kernel $Y_{1/2}$.

Simple pole on branch cut

To illustrate the application of Theorem 2.21, let us consider a case where there is a simple pole on the cut. This representation can be found in (Héleschewitz 2000, § 4.3.2), (Casenave and Montseny 2010, Tab. 1), and (Montseny 2005, Tab. 2).

Lemma 2.33. *The function*

$$f(s) = \frac{1}{s^\alpha(s+s_0)} \quad (s \in \mathbb{C}\backslash(-\infty, 0]),$$

with $s_0 > 0$ *and* $\alpha \in (0, 1)$ *admits the OD representation*

$$f(s) = \frac{\cos(\alpha\pi)}{s_0^\alpha}\frac{1}{s+s_0} + \mathrm{pv}\int_0^\infty \frac{1}{s+\xi}\mu(\xi)\,\mathrm{d}\xi,\ \mu(\xi) = \frac{\mu_\alpha(\xi)}{s_0 - \xi}.$$

Proof. The conditions (i), (ii), and (iv) of Corollary 2.20 are satisfied, but (iii) fails since the diffusive weight μ has a simple pole at $\xi = s_0$, which belongs to $\mathring{\Gamma} = (-\infty, 0)$ (note that condition (ii) would fail for $s_0 = 0$). Hence we resort to Theorem 2.21 to obtain that f admits the OD representation

$$f(s) = \operatorname{Res}(f, -s_0)\frac{1}{s+s_0} + \operatorname{pv}\int_0^\infty \frac{1}{s+\xi}\mu(\xi)\,\mathrm{d}\xi.$$

Using (2.29) with $A = 1$ and $g(s) = s^{-\alpha}$, we get $\operatorname{Res}(f, -s_0) = \frac{\cos(\alpha\pi)}{s_0^\alpha}$. □

The expression of the Cauchy principal value can be further explicited. For any $\zeta \in (0, s_0)$ we have

$$\begin{aligned}\operatorname{pv}\int_0^\infty \frac{1}{s+\xi}\mu(\xi)\,\mathrm{d}\xi = \int_0^{s_0-\zeta} \frac{1}{s_0-\xi}\frac{\mu_\alpha(\xi)}{s+\xi}\,\mathrm{d}\xi + \int_{s_0+\zeta}^\infty \frac{1}{s_0-\xi}\frac{\mu_\alpha(\xi)}{s+\xi}\,\mathrm{d}\xi \\ + \int_{s_0-\zeta}^{s_0+\zeta} \frac{\frac{\mu_\alpha(\xi)}{s+\xi} - \frac{\mu_\alpha(s_0)}{s+s_0}}{s_0-\xi}\,\mathrm{d}\xi + \frac{\mu_\alpha(s_0)}{s+s_0}\underbrace{\operatorname{pv}\int_{s_0-\zeta}^{s_0+\zeta} \frac{1}{s_0-\xi}\,\mathrm{d}\xi}_{:=0}.\end{aligned}$$

The first three integrals of the right-hand side have a continuous integrand, so that $\operatorname{pv}\int = \int$. The only singular term left cancels by property of the principal value, since the integrand is odd and the integration interval is symmetric around the singularity s_0 (Schwartz 1966, § I.2.2).

Oscillatory kernels

Let us consider two examples of purely oscillatory kernels (i.e. OD kernels that do not have a diffusive part) that arise from physical models that do not include dissipation phenomena. The first function models a lossless brass and has been studied in (Matignon 1994, Chap. 5) while the second one is obtained from an inviscid cavity impedance model, which will be covered in Section 2.4.

Lemma 2.34. *The function*

$$f(s) = \frac{e^{-s}}{1-\rho e^{-2bs}} \quad (s \in \mathbb{C}),$$

with $\rho \in \mathbb{R}^*$ and $2b > 1$ admits the oscillatory representation

$$f(s) = \frac{1}{2b}\sum_{k\in\mathbb{Z}} \frac{e^{-s_k}}{s-s_k},$$

where the poles are given by

$$\forall k \in \mathbb{Z},\ \begin{cases} bs_k = \ln\sqrt{\rho} + \mathrm{j}k\pi & (\rho > 0) \\ bs_k = \ln\sqrt{|\rho|} + \mathrm{j}\dfrac{\pi}{2} + \mathrm{j}k\pi & (\rho < 0). \end{cases} \tag{2.37}$$

Proof. The function f is meromorphic and periodic when b is rational. Its poles and residues are given by (2.37) and

$$\operatorname{Res}(f, s_k) = \frac{e^{-s_k}}{\frac{\mathrm{d}}{\mathrm{d}s}\left[1-\rho e^{-2bs}\right]_{s_k}} = \frac{e^{-s_k}}{2b\rho e^{-2bs_k}} = \frac{e^{-s_k}}{2b} \quad (k \in \mathbb{Z}),$$

where we have used L'Hôpital rule to compute the residue since s_k is a simple pole. If b is rational, then both conditions (i) and (ii) of Theorem 2.23 are satisfied so that f admits a purely oscillatory representation (2.28). This representation still holds true for the case where b is irrational, using the density of $\mathbb{Q}$ in $\mathbb{R}$ and continuity with respect to b. (It can also be obtained directly using a series expansion, without assumption on b.) □

In the above lemma, note that both exponential terms e^{-s} and e^{-2bs} are necessary to obtain the uniform decay condition at infinity. When the e^{-s} term is absent, which occurs in practice, the oscillatory representation exhibits a constant term, see the lemma below.

Lemma 2.35. *The function*

$$f(s) = \frac{1}{1-\rho e^{-2bs}} \quad (s \in \mathbb{C}),$$

with $b > 0$ and $\rho \in \mathbb{R}^*$ admits the oscillatory representation

$$f(s) = \frac{1}{2} + \frac{1}{2b} \sum_{k\in\mathbb{Z}} \frac{1}{s - s_k},$$

where the poles s_k are given by (2.37).

Proof. The absence a damping term in the numerator implies that the decay condition (2.16) fails, which prevents the direct application of Corollary 2.20. Let us consider instead

$$g(s) = \frac{f(s)}{s},$$

which satisfies the decay condition, so that, provided that the poles and residues of g satisfy condition (iv), g admits the OD representation (2.28) from Corollary 2.20. The expression of the poles of g depends on the value of $\rho \in \mathbb{R}^*$. Let us denote s_k the quantity (2.37). To compute the representation of g, we must distinguish the cases $\rho \neq 1$ and $\rho = 1$.

Let us first consider the case $\rho \neq 1$. Then g has only simple poles given by $(s_k)_{k\in\mathbb{Z}}$ and 0, so that the representation of g is obtained from a direct application of Corollary 2.20:

$$g(s) = \operatorname{Res}(g(s), 0)\frac{1}{s} + \sum_{k\in\mathbb{Z}} \operatorname{Res}(g(s), s_k)\frac{1}{s - s_k} \quad (\rho \neq 1)$$

with residues given by

$$\operatorname{Res}(g, 0) = \frac{1}{1-\rho} \quad (\rho \neq 1), \quad \operatorname{Res}(g, s_k) = \frac{1}{s_k \frac{\mathrm{d}}{\mathrm{d}s}\left[1 - \rho e^{-2bs}\right]_{s=s_k}} = \frac{1}{2bs_k} \quad (s_k \neq 0).$$

The corresponding representation of f exhibits a constant term C:

$$f(s) = C + \frac{1}{2b} \sum_{k\in\mathbb{Z}} \frac{1}{s - s_k}, \; C = \frac{1}{1-\rho} + \frac{1}{2b} \sum_{k\in\mathbb{Z}} \frac{1}{s_k} \quad (\rho \neq 1).$$

If $\rho = 1$, then g has $s_0 = 0$ as a *double* pole and $(s_k)_{k\in\mathbb{Z}^*}$ as simple poles. The representation of g reads, for $t \in \mathbb{R}$,

$$\mathcal{L}^{-1}[g](t) = \operatorname{Res}\left(g(s)e^{st}, 0\right) H(t) + \sum_{k\in\mathbb{Z}^*} \operatorname{Res}(g(s), s_k)\, e^{s_k t} H(t) \quad (\rho = 1).$$

A computation of the residue gives

$$\operatorname{Res}\left(g(s)e^{st}, 0\right) = \frac{1}{2} + \frac{1}{2b}t \quad (\rho = 1),$$

so that we get

$$g(s) = \frac{1}{2s} + \frac{1}{2bs^2} + \frac{1}{2b} \sum_{k\in\mathbb{Z}^*} \frac{1}{s_k} \frac{1}{s - s_k} \quad (\rho = 1),$$

and

$$f(s) = C + \frac{1}{2b}\frac{1}{s} + \frac{1}{2b}\sum_{k\in\mathbb{Z}^*}\frac{1}{s-s_k} = C + \frac{1}{2b}\sum_{k\in\mathbb{Z}}\frac{1}{s-s_k} \quad (\rho = 1),$$

where the constant C has a slightly different expression, namely

$$C = \frac{1}{2} + \frac{1}{2b}\sum_{k\in\mathbb{Z}^*}\frac{1}{s_k} \quad (\rho = 1).$$

The computation of C is tedious but elementary. If $\rho = 1$, then $bs_k = \mathrm{j}k\pi$ so that the sum $\sum_{k\in\mathbb{Z}^*}\frac{1}{bs_k}$ is null. If $\rho = -1$, then $bs_k = \mathrm{j}(2k+1)\pi/2$ so that the sum $\sum_{k\in\mathbb{Z}}\frac{1}{bs_k}$ is null. If $\rho \notin \{-1, 0, 1\}$, we have

$$\sum_{k\in\mathbb{Z}}\frac{1}{bs_k} = -\frac{1+\rho}{1-\rho},$$

which can be proven using the following identities ($a \neq 0$)

$$\sum_{k=1}^{\infty}\frac{1}{a^2+k^2} = -\frac{1}{2a^2} + \frac{\pi}{2a}\coth(\pi a), \sum_{k=0}^{\infty}\frac{1}{a^2+(2k+1)^2} = \frac{\pi}{2a}\left[\coth(\pi a) - \frac{1}{2}\coth\left(\frac{\pi a}{2}\right)\right].$$

□

Remark 2.36. In the time domain, the representation of f is $\mathcal{L}^{-1}(f) = \frac{1}{2}\delta + \frac{1}{2b}\sum_k e_{-s_k}$. This is a purely oscillatory representation with an added Dirac distribution. The presence of δ could have been expected since $f(s) \underset{s\to+\infty}{=} \mathcal{O}(1)$.

Oscillatory-diffusive kernels

Let us now consider a kernel with both a diffusive and an oscillatory part. The two functions considered below arise in the modeling of cavities with viscous and thermal losses, as we shall see in Section 2.4.

Lemma 2.37. *Let f denotes the function*

$$f(s) = \frac{e^{-2\epsilon\sqrt{s}}}{1-\rho e^{-2(\epsilon\sqrt{s}+bs)}} \quad (s \in \mathbb{C}\backslash(-\infty, 0]),$$

with $b, \epsilon > 0$ and $\rho \in \mathbb{R}^*$. (If $\epsilon = 0$ see Lemma 2.35.) It admits the OD representation

$$f(s) = \sum_{k\in\mathcal{K}}\frac{e^{-2\epsilon\sqrt{s_k}}}{2b + \frac{\epsilon}{\sqrt{s_k}}}\frac{1}{s-s_k} + \int_0^{\infty}\frac{1}{s+\xi}\mu(\xi)\,\mathrm{d}\xi,$$

where the poles s_k are the non-null solutions of

$$\forall k \in \mathcal{K}, \begin{cases} bs_k + \epsilon\sqrt{s_k} - \ln\sqrt{\rho} - \mathrm{j}k\pi = 0 & (\rho > 0) \\ bs_k + \epsilon\sqrt{s_k} - \ln\sqrt{|\rho|} + \mathrm{j}\dfrac{\pi}{2} + \mathrm{j}k\pi = 0 & (\rho < 0), \end{cases} \tag{2.38}$$

and the diffusive weight is given by

$$\mu(\xi) = \frac{1}{\pi}\frac{\sin(2\epsilon\sqrt{\xi})}{1 - 2\rho e^{2b\xi}\cos(2\epsilon\sqrt{\xi}) + \rho^2 e^{4b\xi}}\mathbb{1}_{(0,\infty)}(\xi). \tag{2.39}$$

(There may not be a non-null solution of (2.38) for a given $k \in \mathbb{Z}$ so that $\mathcal{K}$ may be strictly embedded in $\mathbb{Z}$.)

Proof. The diffusive cut is $\Gamma = (-\infty, 0]$ with single branch point $\gamma_1 = 0$. Let us show that f satisfies the four conditions of Corollary 2.20. Conditions (i) and (ii) are satisfied, even when $\rho = 1$. To verify condition (iii), let us compute the diffusive weight using (2.17), which gives for $\xi \in (0, \infty)$

$$\mu(\xi) = \frac{1}{2\mathrm{j}\pi}\left[\frac{e^{-2\epsilon\left(-\mathrm{j}\sqrt{\xi}\right)}}{1-\rho e^{-2(-\mathrm{j}\epsilon\sqrt{\xi}-b\xi)}} - \frac{e^{-\mathrm{j}2\epsilon\sqrt{\xi}}}{1-\rho e^{-2(\mathrm{j}\epsilon\sqrt{\xi}-b\xi)}}\right] = \frac{1}{\pi}\Im\left(\frac{e^{\mathrm{j}2\epsilon\sqrt{\xi}}}{1-\rho e^{2b\xi}e^{2\mathrm{j}\epsilon\sqrt{\xi}}}\right),$$

which is smooth on $(0, \infty)$ from the lemma below. Moreover, it satisfies the integrability condition since $\mu(\xi) \underset{\xi\to\infty}{=} \mathcal{O}\left(e^{-4b\xi}\right)$ and

$$\mu(\xi) \underset{\xi\to 0}{=} \frac{1}{\pi}\frac{\mathcal{O}(\sqrt{\xi})}{(1-\rho)^2 + \mathcal{O}(\xi)},$$

so that condition (iii) is satisfied. The poles of f satisfy $e^{2(\epsilon\sqrt{s_k}+bs_k)} = \rho$ with associated residues

$$\mathrm{Res}(f, s_k) = \frac{e^{-2\epsilon\sqrt{s_k}}}{\frac{\mathrm{d}}{\mathrm{d}s}\left[1-\rho e^{-2(\epsilon\sqrt{s}+bs)}\right]_{s=s_k}} = \frac{e^{-2\epsilon\sqrt{s_k}}}{2b + \frac{\epsilon}{\sqrt{s_k}}},$$

from which we verify condition (iv).

Lemma 2.38. *Let $b, \epsilon > 0$ and $\rho \in \mathbb{R}^*$. The diffusive weight μ has no singularity in $(0, \infty)$.*

Proof. The diffusive weight can be written, for $\xi \in (0, \infty)$,

$$\mu(\xi) = \frac{1}{\pi}\frac{\sin(2\epsilon\sqrt{\xi})}{\left(1-\rho e^{2b\xi}\cos(2\epsilon\sqrt{\xi})\right)^2 + \rho^2 e^{4b\xi}\sin(2\epsilon\sqrt{\xi})^2},$$

so that a singularity $\xi_* \geq 0$ must satisfy

$$\cos(2\epsilon\sqrt{\xi_*}) = 1, \quad \sin(2\epsilon\sqrt{\xi_*}) = 0, \quad e^{2b\xi_*} = \frac{1}{|\rho|}.$$

If $|\rho| > 1$ there is no such ξ_*. If $\rho = \pm 1$ then $\xi_* = 0 \notin (0, \infty)$. If $|\rho| < 1$, then $\xi_* \in (0, \infty)$ and the behavior of μ around ξ_* is given by

$$\begin{aligned}\mu(\xi) = \frac{1}{\pi}\frac{\sin(2\epsilon\sqrt{\xi})}{1-2\rho e^{2b\xi}\cos(2\epsilon\sqrt{\xi}) + \rho^2 e^{4b\xi}} &\underset{\xi\to\xi_*}{=} \frac{1}{\pi}\frac{\mathcal{O}\left(|\xi-\xi_*|\right)}{1-2\left(1+\mathcal{O}\left(|\xi-\xi_*|\right)\right)+\left(1+\mathcal{O}\left(|\xi-\xi_*|\right)\right)} \\ &\underset{\xi\to\xi_*}{=} \frac{1}{\pi}\frac{\mathcal{O}\left(|\xi-\xi_*|\right)}{\mathcal{O}\left(|\xi-\xi_*|\right)},\end{aligned}$$

so that ξ_* is not a singularity of μ. □

□

Let us briefly recall that the poles s_k can be computed using the change of variable $\sigma := \sqrt{s}$, see e.g. (Matignon 1994), so that (2.38) reduces to

$$P_k(\sigma_k) = 0, \ \Re(\sigma_k) \geq 0,$$

where P_k is a second-degree polynomial. A plot of the poles, which go by conjugate pairs since $f(s) \in (0, \infty)$ for $s \in (0, \infty)$, is given in the left plot of Figure 2.6 for several values of the parameters ϵ and ρ. The parameter ϵ, physically linked to dissipation phenomena, controls the

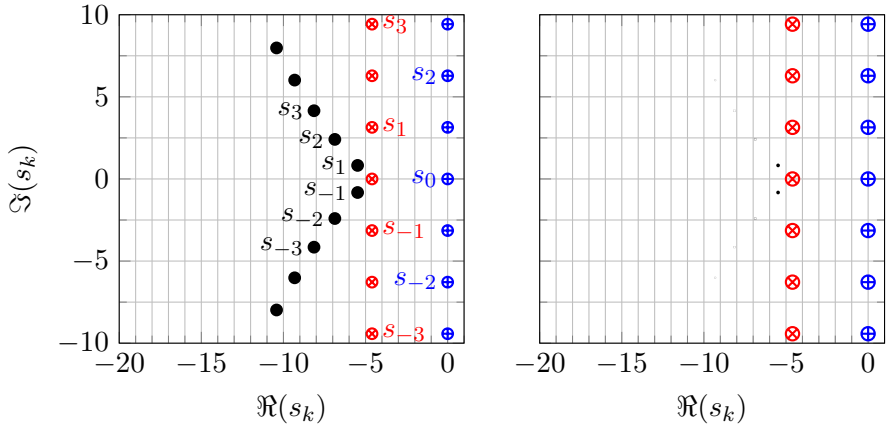

Figure 2.6. Plot of poles defined in Lemmas 2.35 and 2.37, for $b = 1$. (Left) (⊕) $\epsilon = 0$, $\rho = 1$. (⊗) $\epsilon = 0$, $\rho = 10^{-4}$. (●) $\epsilon = 5$, $\rho = 10^{-4}$. (Right) Same poles as left plot, but the marker size is proportional to the residue $\operatorname{Res}(f, s_k)$.

frequency-dependent losses. Specifically, if $\epsilon > 0$, then the higher $\Im(s_k)$ (i.e. the higher the pole frequency), the lower $\Re(s_k)$ (i.e. the higher the pole attenuation); by contrast, when $\epsilon = 0$ every pole has the same real part. The parameter ρ controls the frequency-independent losses (for $\epsilon > 0$ it shifts all the poles horizontally for instance). In the right plot of Figure 2.6, the exact same poles are plotted but with a marker size proportional to the corresponding residue, thus illustrating the exponential decay of the residues when $\epsilon > 0$. Another illustration is proposed in Figure 2.7 where the principal argument of f is plotted, showing both the poles and the cut.

Remark 2.39. A similar function arise in the study of the Lokshin equation, namely

$$f(s) = \frac{e^{-\epsilon\sqrt{s}}}{1 - \rho e^{-2(\epsilon\sqrt{s}+bs)}} \quad (s \in \mathbb{C}\backslash(-\infty, 0]),$$

see (Matignon 1994, Chap. 6) and (Héleschewitz 2000, Chap. 9).

The lemma below can be seen as a variation on Lemma 2.35 with an added cut. Again, the lack of exponential damping in the numerator implies a constant term in the OD representation; both the poles s_k and the diffusive weight μ contribute to this constant.

Lemma 2.40. *Let f denotes the function*

$$f(s) = \frac{1}{1 - \rho e^{-2(\epsilon\sqrt{s}+bs)}} \quad (s \in \mathbb{C}\backslash(-\infty, 0]),$$

with $b, \epsilon > 0$ and $\rho \in \mathbb{R}\backslash\{0, 1\}$. (If $\epsilon = 0$ see Lemma 2.35.) It admits the OD representation

$$f(s) = C + \sum_{k\in\mathcal{K}} \frac{1}{2b + \frac{\epsilon}{\sqrt{s_k}}} \frac{1}{s - s_k} + \int_0^\infty \frac{1}{s + \xi} \mu(\xi)\, \mathrm{d}\xi,$$

where the constant is given by

$$C = \frac{1}{1-\rho} + \sum_{k\in\mathcal{K}} \frac{1}{s_k} \frac{1}{2b + \frac{\epsilon}{\sqrt{s_k}}} - \left(\int_0^\infty \frac{\mu(\xi)}{\xi}\, \mathrm{d}\xi \right) \underset{\epsilon \ll 1}{\simeq} \frac{1}{1-\rho} + \sum_{k\in\mathcal{K}} \frac{1}{2bs_k}.$$

The poles s_k are the solutions of (2.38), which are non-null. The diffusive weight is

$$\mu(\xi) = \frac{1}{\pi} \frac{\rho e^{2b\xi} \sin(2\epsilon\sqrt{\xi})}{1 - 2\rho e^{2b\xi} \cos(2\epsilon\sqrt{\xi}) + \rho^2 e^{4b\xi}} \mathbb{1}_{(0,\infty)}(\xi).$$

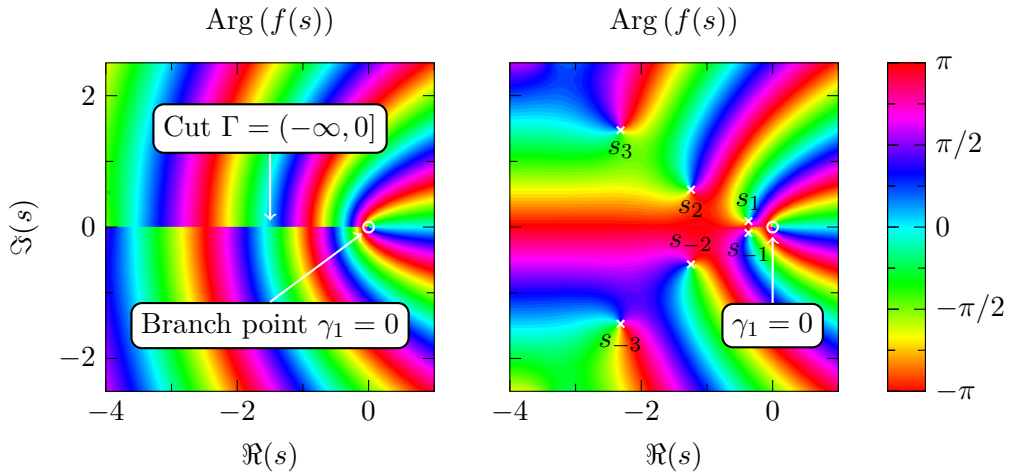

Figure 2.7. Plot of the principal value of the argument for two multivalued functions, which shows a jump across the branch cut Γ and the presence of poles. Function defined in Lemma 2.37 with $b = 1$. (Left) $\epsilon = 5$, $\rho = 10^{-4}$. All the poles s_k are outside the plotted area. (Right) $\epsilon = 5$, $\rho = 1$.

Proof. The fact that $\epsilon > 0$ implies that $\gamma_1 = 0$ is a branch point, with $\Gamma = (-\infty, 0]$ branch cut. Corollary 2.20 cannot be applied since the decay condition (i) fails in the right half-plane. Hence we consider instead

$$g(s) = \frac{f(s)}{s},$$

which satisfies (i) but fails (ii) since, for instance, $g(s) \underset{s\to 0}{=} \frac{1}{1-\rho}\mathcal{O}\left(\frac{1}{|s|}\right)$ for $\rho \neq 1$. To obtain a representation, we resort to applying Theorem 2.16 on g. The condition (ii) is satisfied since the residue $\mathrm{Res}(g(s)e^{st}, \gamma_1)$ with $t \in \mathbb{R}$ is finite and given by

$$\mathrm{Res}(g(s)e^{st}, \gamma_1) = \lim_{r\to 0} \frac{1}{2\pi} \int_{-\pi}^{+\pi} f(re^{\mathrm{j}\theta}) e^{tre^{\mathrm{j}\theta}} \mathrm{d}\theta = f(0) = \frac{1}{1-\rho}.$$

(Note that if $\rho = 1$, then $g(s) \underset{s\to 0}{=} \frac{1}{2\epsilon}\mathcal{O}\left(|s|^{-3/2}\right)$ so that this residue is not finite.) To check the condition (iii), we compute the diffusive weight using (2.17), which yields for $\xi \in (0, \infty)$

$$\begin{aligned}\mu_g(\xi) &= \frac{1}{2\mathrm{j}\pi}\left[g(\xi e^{-\mathrm{j}\pi}) - g(\xi e^{+\mathrm{j}\pi})\right] = -\frac{1}{\pi}\frac{1}{\xi}\Im\left[\frac{1}{1-\rho e^{2(\mathrm{j}\epsilon\sqrt{\xi}+b\xi)}}\right] \\ &= -\frac{1}{\pi\xi}\frac{\rho e^{2b\xi}\sin(2\epsilon\sqrt{\xi})}{1-2\rho e^{2b\xi}\cos(2\epsilon\sqrt{\xi})+\rho^2 e^{4b\xi}},\end{aligned}$$

which is smooth on $(0, \infty)$, see Lemma 2.38, and is integrable on $(0, \infty)$. Hence, (iii) is satisfied. The poles s_k are the solutions of (2.38), which are non-null since $\epsilon > 0$. As $s_k \neq 0$, the poles are simple and the associated residues are given by

$$\mathrm{Res}(g, s_k) = \frac{1}{s_k}\frac{1}{\frac{\mathrm{d}}{\mathrm{d}s}\left[1-\rho e^{-2(\epsilon\sqrt{s}+bs)}\right]_{s=s_k}} = \frac{1}{s_k}\frac{1}{2b+\frac{\epsilon}{\sqrt{s_k}}},$$

and condition (iv) is satisfied. Therefore, we have the following OD representation for g:

$$g(s) = \frac{\mathrm{Res}(g,0)}{s} + \sum_{k\in\mathcal{K}} \mathrm{Res}(g, s_k)\frac{1}{s-s_k} + \int_0^\infty \frac{1}{s+\xi}\mu_g(\xi)\,\mathrm{d}\xi,$$

from which we deduce

$$f(s) = \left[\mathrm{Res}(g,0) + \sum_{k\in\mathcal{K}} \mathrm{Res}(g,s_k) + \int_0^\infty \mu_g(\xi)\,\mathrm{d}\xi\right] + \sum_{k\in\mathcal{K}} \mathrm{Res}(g,s_k)\frac{s_k}{s-s_k} + \int_0^\infty \frac{1}{s+\xi}(-\xi\mu_g(\xi))\,\mathrm{d}\xi,$$

which is the claimed identity, by defining $\mu(\xi) \coloneqq -\xi\mu_g(\xi)$. □

2.2 Discretization of oscillatory-diffusive representations

Let h be a given OD kernel that enjoys the representation (2.20). This section focuses on the computation of a numerical approximation of h denoted h_{num} and given by

$$h_{\mathrm{num}}(t) = \sum_{n=1}^{N_s} r_n e_{-\tilde{s}_n}(t) + \sum_{n=1}^{N_\xi} \mu_n e_{\xi_n}(t) \qquad (t\in\mathbb{R}) \tag{2.40}$$

$$\hat{h}_{\mathrm{num}}(s) = \sum_{n=1}^{N_s} \frac{r_n}{s-\tilde{s}_n} + \sum_{n=1}^{N_\xi} \frac{\mu_n}{s+\xi_n} \qquad (\Re(s)>0)\,, \tag{2.41}$$

where r_n, μ_n are the discrete weights and $\tilde{s}_n, \xi_n$ are the discrete poles. The expression of h_{num} given above contains two sums instead of just one: intuitively, we expect each sum to approximate one half of the OD representation of h, i.e.

$$\sum_{n=1}^{N_s} \frac{r_n}{s-\tilde{s}_n} \simeq \sum_{k\in[\![1,n]\!]} \frac{\mathrm{Res}(\hat{h},\gamma_k)}{s-\gamma_k} + \sum_{k\in\mathbb{Z}} \frac{\mathrm{Res}(\hat{h},s_k)}{s-s_k},\ \sum_{n=1}^{N_\xi} \frac{\mu_n}{s+\xi_n} \simeq \int_0^\infty \frac{\mu_{\hat{h}}(\xi)}{s+\xi}\,\mathrm{d}\xi.$$

We are interested in methods that yield parsimonious approximations, i.e. for which N_s and N_ξ are as small as possible. This section is split into two parts, each one covering one family of discretization methods for (2.20).

1. Section 2.2.1 deals with methods that rely on an optimization. It presents a standard method that relies on a linear least squares optimization, which will be used in the time-domain application of Chapter 6.

2. Section 2.2.2 is focused on methods based on known quadrature rules. It defines a method, proposed in (Monteghetti et al. 2018d), which is well-suited for diffusive kernels whose diffusive weight is "well-behaved".

2.2.1 Optimization-based discretization

Optimization-based methods have enjoyed a wide range of applications, notably in wave propagation problems. A method based on a linear least squares optimization, where the pole distribution is chosen a priori has been introduced in (Garcia and Bernussou 1998) for the identification of a lead acid battery impedance model using time-domain measurements, and further refined in (Hélie and Matignon 2006b) with application to a wide range of diffusive kernels. A method based on a nonlinear least squares method has been introduced in (Lombard and Matignon 2016).

Here, we describe a method based on a linear least squares optimization that will prove useful in the time-domain application of Chapter 6. Since we are interested in approximating models

that arise from physics, we assume that the OD kernel h introduced above satisfies the reality condition, i.e. $h(t) \in \mathbb{R}$, so that the poles s_n of $\hat{h}$ go by conjugate pairs, see e.g. Figure 2.6. In light of this remark, we rewrite the discrete model $\hat{h}_{\text{num}}$ given by (2.41) under a form that separates real poles from complex conjugate ones, namely

$$\hat{h}_{\text{num}}(s) = \sum_{n \in \mathcal{N}_r} \frac{r_n}{s - \tilde{s}_n} + \sum_{n \in \mathcal{N}_p} \frac{r_n}{s - \tilde{s}_n} + \frac{\overline{r_n}}{s - \overline{\tilde{s}_n}} + \sum_{n=1}^{N_\xi} \frac{\mu_n}{s + \xi_n}, \tag{2.42}$$

where the set of indices $\mathcal{N}_r$ (real poles) and $\mathcal{N}_p$ (complex conjugate poles) are formally defined as

$$\mathcal{N}_r \coloneqq \{n \in [\![1, N_s]\!] \,|\, \tilde{s}_n \in \mathbb{R}\}\,,\ \mathcal{N}_r \coloneqq \{n \in [\![1, N_s]\!] \,|\, \Im(\tilde{s}_n) > 0\}\,,$$

so that

$$N_s = N_r + 2N_p,\ N_r \coloneqq \operatorname{card} \mathcal{N}_r,\ N_p \coloneqq \operatorname{card} \mathcal{N}_p.$$

Note that the reality condition $h_{\text{num}}(t) \in \mathbb{R}$ also constrains the weights, so that $\mu_n \in \mathbb{R}$ and

$$n \in \mathcal{N}_r \Rightarrow r_n \in \mathbb{R}.$$

We wish to compute the discrete poles and weights by minimizing

$$\sum_{k=1}^{K} |\hat{h}(\mathrm{j}\omega_k) - \hat{h}_{\text{num}}(\mathrm{j}\omega_k)|^2, \tag{2.43}$$

where the K angular frequencies ω_k are given. The main challenge of such an optimization is that $\hat{h}_{\text{num}}$ is nonlinear with respect to its poles ξ_n and $\tilde{s}_n$, which furthermore can have a wide variation since typically $\xi \in \operatorname{supp} \mu_{\hat{h}} = (0, \infty)$ and $|s_n| \xrightarrow[\to\infty]{} \infty$. The principle of the method described below is to circumvent this difficulty by either *choosing* the poles following a suitable heuristic or *computing* them from the knowledge of $\hat{h}$.

1. The desired number of poles in each category is chosen, namely N_r (number of real poles), N_p (number of complex conjugate poles), N_ξ (number of diffusive poles).

2. Each category of poles is computed as follows.

   (a) The N_ξ diffusive poles are logarithmically spaced in $[\xi_{\min}, \xi_{\max}] \subset \operatorname{supp} \mu_{\hat{h}}$, where $\xi_{\min}$ (resp. $\xi_{\max}$) is the lower (resp. upper) bound of the angular frequencies of interest.

   (b) The $N_r + N_p$ poles $\tilde{s}_n$ are defined using the first poles and branch points of $\hat{h}$, i.e.

   $$\tilde{s}_n \coloneqq s_n \text{ or } \tilde{s}_n \coloneqq \gamma_n \quad (n \in \mathcal{N}_r \cup \mathcal{N}_p)\,.$$

   The poles s_n of $\hat{h}$ are obtained either by numerical computations or using an analytical expression such as (2.37). The computational gain stems from the fact that computing the poles of $\hat{h}$ is typically a relatively cheap and accurate process. The branch points γ_n are known by definition of $\hat{h}$. Note that, as shown in Section 2.1.2, they need not be accounted for if condition (2.26) holds. Note also that, although $\tilde{s}_n \in \mathbb{R}$ when $n \in \mathcal{N}_r$, these real poles are treated separately from the diffusive poles μ_n.

3. The computation of the discrete weights r_n and μ_n is then done with a minimization of (2.43), which is a *linear* least squares minimization problem. The cost function is defined as

   $$J(x) \coloneqq \|Cx - d\|_2, \tag{2.44}$$

with the matrix C and the column vectors x and d defined as

$$x^\intercal \coloneqq \left[\begin{array}{ccc} [\Re(r_n)]_{n\in\mathcal{N}_r\cup\mathcal{N}_p} & [\Im(r_n)]_{n\in\mathcal{N}_p} & [\mu_n]_{n\in[\![1,N_\xi]\!]} \end{array} \right] \in \mathbb{R}^{1\times(N_r+2N_p+N_\xi)}$$

$$Cx \coloneqq \left[\begin{array}{c} \left[\Re\left(\hat{h}_{\mathrm{num}}(\mathrm{j}\omega_k)\right)\right]_{k\in[\![1,K]\!]} \\ \left[\Im\left(\hat{h}_{\mathrm{num}}(\mathrm{j}\omega_k)\right)\right]_{k\in[\![1,K]\!]} \end{array} \right]_k \in \mathbb{R}^{2K\times 1},\ d \coloneqq \left[\begin{array}{c} \left[\Re\left(\hat{h}(\mathrm{j}\omega_k)\right)\right]_{k\in[\![1,K]\!]} \\ \left[\Im\left(\hat{h}(\mathrm{j}\omega_k)\right)\right]_{k\in[\![1,K]\!]} \end{array} \right]_k \in \mathbb{R}^{2K\times 1},$$

where the K angular frequencies ω_k are logarithmically spaced in $[\xi_{\min}, \xi_{\max}]$.

By choosing K to be large, i.e.

$$K \gg N_r + 2N_p + N_\xi,$$

the optimization problem of step 3 is overdetermined and can be directly solved by a pseudo-inverse at a computational cost that is typically negligible on a contemporary computer. Note that the cost function J is defined in such a way that the reality of x is enforced.

This three-step method is particularly suited for time-domain simulations, where $\xi_{\max}$ is naturally known from e.g. the minimum acceptable time step or the maximum frequency of interest. The practical choice of the lower bound $\xi_{\min}$, which governs the long-time behavior of h_{num}, can be trickier: for a given $\xi_{\max}$ and number of poles there is usually an optimal range for $\xi_{\min}$, so that $\xi_{\min}$ must not be chosen too small. For the kernels considered in this dissertation, a logarithmic spacing of the diffusive poles ξ_n have proven to yield a satisfactory result, better than, say, a linear spacing.

Remark 2.41 (Alternative step 3). An alternative to step 3 is to compute the discrete weight r_n with

$$r_n \coloneqq \mathrm{Res}\left(\hat{h}, \tilde{s}_n\right),$$

so that the optimization is then only done on μ_n. The residue can be computed either with an analytical formula or by numerically evaluating the integral (2.15). This is particularly effective when the residues have a fast decay (physically, when dissipation phenomena are significant in the model, see e.g. Lemma 2.37).

The application of this method to the fractional kernel $Y_{1/2}$, whose diffusive representation is given by (2.10), is illustrated in Figure 2.8 in both time and frequency domains. The frequency-domain plot in logarithmic axes shows that with eight variables the method yields a seven-decade approximation. The frequency-domain plot with linear axes shows that the diffusive poles are concentrated close to 0, where μ_α varies the most. A linear spacing of the diffusive poles in $[\xi_{\min}, \xi_{\max}]$ leads to a poorer approximation, see Figure 2.9. An additional illustration of the above method will be given in Section 2.4, where a physical model is discretized. Many additional examples can be found in (Hélie and Matignon 2006b).

Remark 2.42 (Enhancements). The presented optimization method can be improved on the two following aspects. First, although the reality of x is enforced, its sign is indefinite. When discretizing an OD kernel whose diffusive weight is nonnegative, one might want the discrete weights μ_n to be nonnegative as well. This can be done by using, instead of the pseudo-inverse, a nonnegative least squares algorithm such as (Lawson and Hanson 1974, (23.10)), implemented in MATLAB® `lsqnonneg`. The drawback of such iterative methods is that convergence may be difficult for some triplets $(\xi_{\min}, \xi_{\max}, N_\xi)$. This is not considered further in this dissertation.

Second, a *nonlinear* optimization can also be considered to refine the values computed through the linear least squares minimization. This can be done with a general algorithm like the vector fitting algorithm (Gustavsen and Semlyen 1999) or the more specific method proposed in (Lombard and Matignon 2016). In the numerical application of Chapter 6, we will use a nonlinear least squares minimization to account for experimental data.

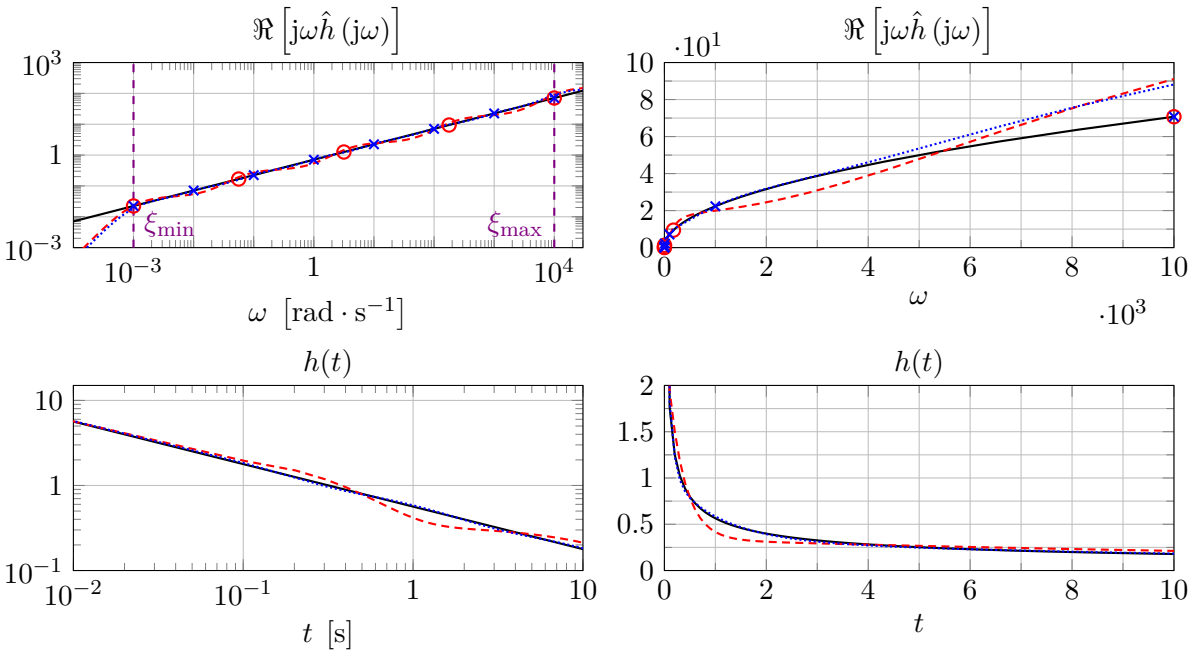

Figure 2.8. Application of the optimization method presented in Section 2.2.1. (——) Exact kernel $h = Y_{1/2}$, $\hat{h}(s) = 1/\sqrt{s}$. (----,○) Discrete kernel h_{num} obtained with $N_\xi = 5$ logarithmically spaced diffusive poles in $[\xi_{\min}, \xi_{\max}]$ with $\xi_{\min} = 10^{-3}$ and $\xi_{\max} = 10^4$. (·····,×) h_{num} with $N_\xi = 8$.

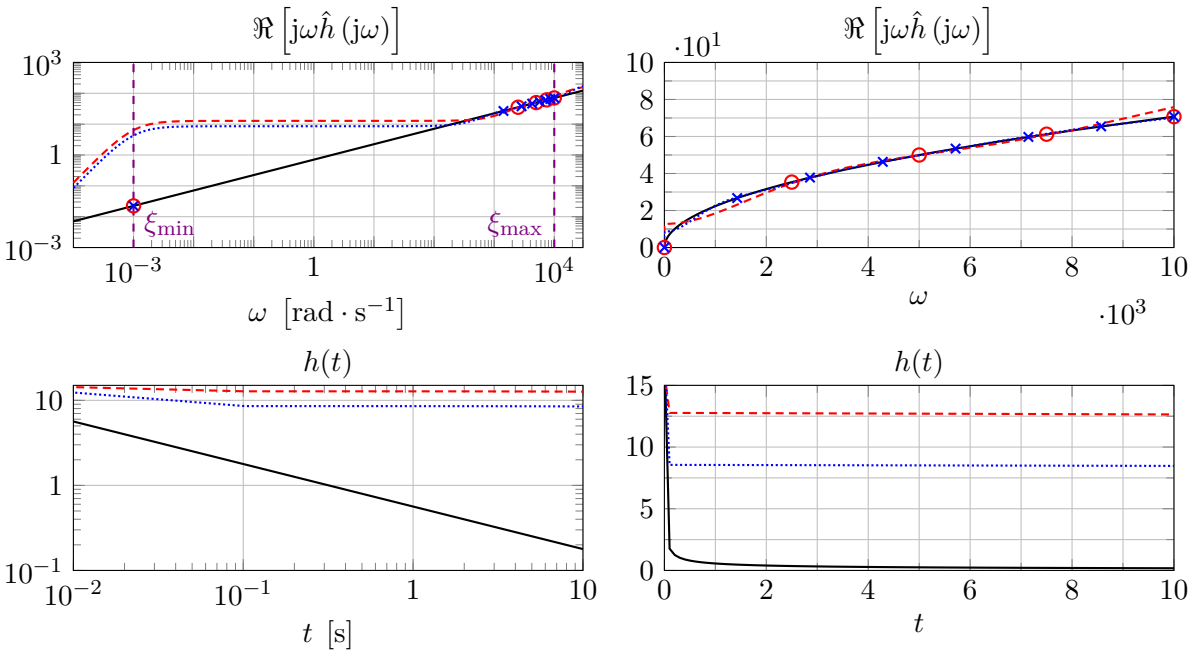

Figure 2.9. Application of the optimization method presented in Section 2.2.1. (——) Exact kernel $h = Y_{1/2}$, $\hat{h}(s) = 1/\sqrt{s}$. (----,○) Discrete kernel h_{num} obtained with $N_\xi = 5$ linearly spaced diffusive poles in $[\xi_{\min}, \xi_{\max}]$ with $\xi_{\min} = 10^{-3}$ and $\xi_{\max} = 10^4$. (·····,×) h_{num} with $N_\xi = 8$. (The optimization is done on $\|\mathrm{j}\omega(\hat{h}(\mathrm{j}\omega) - \hat{h}_{\text{num}}(\mathrm{j}\omega))\|_2$.)

Remark 2.43. Note that any optimization-based discretization cannot be reliably used to check whether a given kernel h is OD. Following Remark 2.19, verifications of this kind are better done by discretizing the right-hand side of (2.21) as accurately as possible regardless of the cost.

2.2.2 Quadrature-based discretization

Quadrature-based methods are an alternative way to discretize the diffusive part of (2.20) by relying on a quadrature rule instead of an optimization. Since these methods are solely focused on the diffusive part, we redefine the kernel h and its approximation h_{num} as

$$h(t) = \int_0^\infty e_\xi(t)\mu(\xi)\,\mathrm{d}\xi \simeq h_{\mathrm{num}}(t) = \sum_{n=1}^{N_\xi} \mu_n e_\xi(t) \quad (t \in \mathbb{R}), \tag{2.45}$$

where μ is smooth on $(0,\infty)$ (the case where $\operatorname{supp}\mu$ is bounded is similar). As already highlighted above, we are here exclusively interested in methods that lead to parsimonious approximations. (Expensive approximations of the diffusive integral are mainly of interest to verify whether a given kernel h is OD.) In principle, the advantage of a quadrature-based method over an optimization-based one is the presence of only one discretization parameter N_ξ, thus making it easier to compute h_{num} at the desired accuracy provided that $h_{\mathrm{num}}(t) \xrightarrow[N_\xi\to\infty]{} h(t)$. The challenge lies in finding a rule suited for the diffusive weight at hand. This section is drawn from (Monteghetti et al. 2018d).

In (Haddar et al. 2010), which deals with a fractional monodimensional wave equation, the diffusive integral is split into two parts, namely a local and a historical one: while the former is approximated ad hoc, a Gauss-Legendre quadrature rule is employed for the later, see (J.-R. Li 2010) for an analysis. Another approach consists in directly using a quadrature rule, without any split. To get back to a finite interval, one can either truncate the semi-infinite integration domain (Baranowski 2017) or use a change of variable (Birk and Song 2010; Diethelm 2008; Yuan and Agrawal 2002). In (Baranowski 2017), Gauss-Legendre and Curtis-Clenshaw quadrature rules are used on a truncated domain. A method proposed in (Yuan and Agrawal 2002), based on a Gauss-Laguerre quadrature rule with a change of variable, has been widely investigated and led to the definitions of methods based instead on the Gauss-Jacobi quadrature rule (Birk and Song 2010; Diethelm 2008), see (Birk and Song 2010) for a comparison that favor (Birk and Song 2010, Eq. 23).

Let us now describe in more details how h can be discretized using a quadrature rule. We assume that the diffusive weight μ is smooth and monotone on $(0,\infty)$ with a power-law singularity at $\xi = 0$, i.e.

$$\mu(\xi) \underset{\xi\to 0}{=} \mathcal{O}\left(\frac{1}{\xi^\alpha}\right), \tag{2.46}$$

with $\alpha \in (0,1)$. An example of such kernel is the fractional kernel Y_α. Following classical works on numerical quadrature (P. Davis and Rabinowitz 1984, Chap. 3) (Atkinson 1989, § 5.6), the following two methods could be envisaged to deal with a singular integral like (2.45).

1. Consider μ as a weight function and define either a new set of Gauss nodes (if possible) or a new product quadrature rule with equidistant nodes (Atkinson 1989, § 5.6).

2. Recover a continuous integrand using a change of variables. For example, for this integral, MATLAB® `integral` function uses the change of variable $\xi = \left(\frac{v}{1-v}\right)^2$, see (Shampine 2008, § 4.2).

To simplify the implementation, we choose the second method, i.e. we seek a suitable change of variables $\Psi : (-1,1) \to (0,\infty)$ ($\Psi(-1) = 0$, $\Psi(1) = \infty$), so that the right-hand side of the identity

$$h(t) = \int_{-1}^{1} \mu\left(\Psi(v)\right) e^{-\Psi(v)t} \frac{\mathrm{d}\Psi}{\mathrm{d}v}(v)\,\mathrm{d}v \tag{2.47}$$

can be accurately discretized using the Gauss-Legendre quadrature rule (v_n, w_n), thus yielding

$$\xi_n \coloneqq \Psi(v_n),\ \mu_n \coloneqq w_n \frac{\mathrm{d}\Psi}{\mathrm{d}v}(v_n)\,\mu(\xi_n). \tag{2.48}$$

Given the singularity condition (2.46), a natural choice is (P. Davis and Rabinowitz 1984, § 3.1) (Atkinson 1989, § 5.6)

$$\Psi_\beta(v) \coloneqq \left(\frac{1+v}{1-v}\right)^{\frac{1}{\beta}},\ \beta > 0. \tag{2.49}$$

This change of variables results from the composition of $v \mapsto \frac{1+v}{1-v}$, which maps $(-1,1)$ to $(0,\infty)$, and the power law $v \mapsto v^{\frac{1}{\beta}}$. Using Ψ_β, the representation (2.47) reads

$$h(t) = \frac{2}{\beta} \int_{-1}^{1} e^{-t\left(\frac{1+v}{1-v}\right)^{\frac{1}{\beta}}} (1-v)^{-1-\frac{1}{\beta}} (1+v)^{\frac{1}{\beta}-1} \mu\left(\left(\frac{1+v}{1-v}\right)^{\frac{1}{\beta}}\right) \mathrm{d}v, \tag{2.50}$$

which leads to the definition of the $Q_{\beta,N}$ discretization method given below.

Definition 2.44. The $Q_{\beta,N}$ discretization of (2.45) is

$$\xi_n \coloneqq \left(\frac{1+v_n}{1-v_n}\right)^{\frac{1}{\beta}},\ \mu_n \coloneqq w_n \frac{2}{\beta} (1+v_n)^{\frac{1}{\beta}-1} (1-v_n)^{-1-\frac{1}{\beta}} \mu\left(\xi_n\right), \tag{2.51}$$

where (v_n, w_n) is the Gauss-Legendre quadrature rule.

Intuitively, one may expect the best value for β to be dependent on properties of the diffusive weight μ, such as the value of α in (2.46). Based on a convergence study of the quadrature rule for the fractional kernel Y_α, the two following values of β stand out.

1. If $\alpha \in (0,1) \cap \mathbb{Q}$ such that $\alpha = \frac{n_0}{n_1}$ with $n_i \in \mathbb{N}^*$, then

$$\beta_1 \coloneqq \frac{1}{n_1} \tag{2.52}$$

   yields a spectrally convergent approximation. This value is also suited for $\alpha \in (0,1) \cap (\mathbb{R} \setminus \mathbb{Q})$ with $\alpha \simeq \frac{n_0}{n_1}$.

2. A larger value of β, namely

$$\beta_2 \coloneqq \min(\alpha, 1-\alpha), \tag{2.53}$$

   yields a convergent but not spectrally convergent approximation. Numerical results show that β_2 can be preferable to β_1 for moderate values of N.

In practice, both values are satisfactory, but since the largest diffusive pole grows as

$$\xi_{\max} \underset{N_\xi \to \infty}{=} \mathcal{O}\left(N_\xi^{\frac{2}{\beta}}\right),$$

for time-domain applications the largest value of the two, namely β_2, is to be favored.

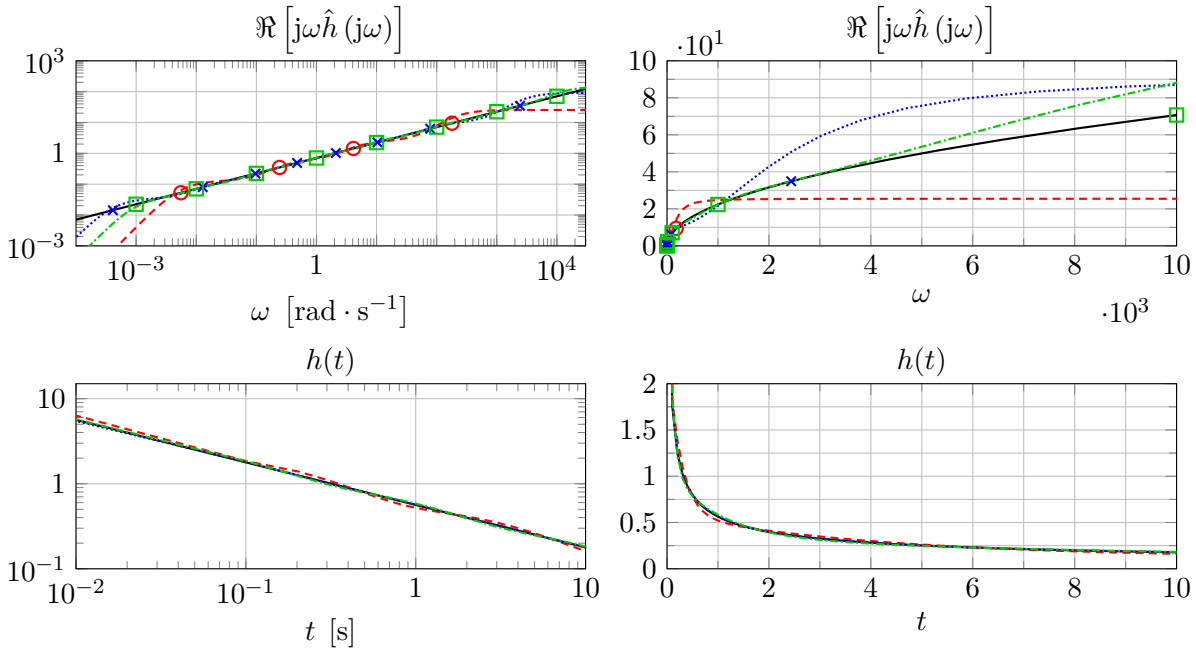

Figure 2.10. Application of the quadrature rule of Definition 2.44. (——) Exact kernel $h = Y_{1/2}$, $\hat{h}(s) = 1/\sqrt{s}$. (----,○) Discrete kernel h_{num} obtained with $N_\xi = 4$ and $\beta = \beta_2$, giving $\xi_{\min} = 5.6 \times 10^{-3}$ and $\xi_{\max} = 180$. (·····,×) h_{num} with $N_\xi = 8$ and $\beta = \beta_2$ ($\xi_{\min} = 4.1 \times 10^{-4}$, $\xi_{\max} = 2.4 \times 10^3$). (-·-·-,□) h_{num} obtained with the optimization method defined in Section 2.2.1 with $N_\xi = 8$ logarithmically spaced diffusive poles in $[\xi_{\min}, \xi_{\max}]$ with $\xi_{\min} = 10^{-3}$ and $\xi_{\max} = 10^4$. (Already plotted in Figure 2.8.)

A numerical application to the fractional kernel Y_α is shown in Figure 2.10 for $N_\xi = 4$, giving $\xi_{\max} = 180$, and $N_\xi = 8$, giving $\xi_{\max} = 2.4 \times 10^3$. For comparison, the plot also shows a kernel obtained with the optimization method for $N = 8$, $\xi_{\min} = 10^{-3}$, and $\xi_{\max} = 10^4$, already plotted in Figure 2.8. The two top graphs illustrate for $N = 8$ the difference between a logarithmic pole distribution and that given by (2.51). The optimized kernel yields the most accurate approximation, as one would expect since it has the highest $\xi_{\max}$. However, modifying the value of $\xi_{\min}$, from 10^{-3} to 10^{-5} for instance, would alter its accuracy so that the quadrature method has the advantage of being easier to use in practice. As a rule, as far as accuracy is concerned, the optimization method has the upper hand for moderate values of N_ξ, provided that the triplet $(\xi_{\min}, \xi_{\max}, N_\xi)$ is well-chosen. These remarks do not constitute a comparison between the two discretization methods: further details, including convergence rates in both time and frequency domains are available in (Monteghetti et al. 2018d). In this dissertation, we will restrict ourselves to the optimization method.

2.3 Hyperbolic realization of time delays

The purpose of this short section is to recall the realization of time delays and present its application to the realization of irrational transfer functions, in preparation for Section 2.4.

Let $\tau_i > 0$ and $a_i \in \mathbb{C}$. The time-delay kernel

$$\hat{h}(s) = \sum_{i \in [\![1,n]\!]} a_i e^{-\tau_i s} \quad (\Re(s) > 0)\,, \quad h(t) = \sum_{i \in [\![1,n]\!]} a_i \delta\left(t - \tau_i\right)$$

is causal and tempered. The corresponding convolution operator $u \mapsto h \star u$ is given by

$$h \star u(t) = \sum_{i \in [\![1,n]\!]} a_i u\left(t - \tau_i\right).$$

Since $\hat{h}$ fails the decay conditions of Theorems 2.16 and 2.23, an OD representation of h cannot be derived by inverting its Laplace transform. In fact, an infinite-dimensional realization of h can be obtained using a monodimensional transport equation as follows

$$\begin{cases} \partial_t \psi(t,\theta) = c_\tau \partial_\theta \psi(t,\theta) \quad (t > 0,\ \theta \in (-l_\tau, 0)) \\ \psi(t,0) = u(t),\ \psi(0,\theta) = 0 \\ h \star u(t) = \sum\limits_{i \in [\![1,n]\!]} a_i \psi(t, -c_\tau \tau_i), \end{cases} \tag{2.54}$$

where

$$l_\tau = c_\tau \max_i \tau_i > 0.$$

The intuitive interpretation of (2.54) is that *delaying* a quantity is formally identical to *transporting* that quantity. This realization has been well-studied, see (Curtain and Zwart 1995, § 2.4), (Engel and Nagel 2000, § VI.6), (Richard 2003), and (Michiels and Niculescu 2014, Chap. 2). Since the transport equation is hyperbolic, the function $\psi(t,\cdot)$ is called the *hyperbolic state* or *variable* and (2.54) is called the *hyperbolic realization* of h. Our motivation for using this realization is both theoretical and numerical, as it will be used in Chapter 4 to study the stability of the wave equation and in Chapter 6 to delay a quantity in a time-local fashion.

What is important for our purposes is that the hyperbolic realization (2.54) enables to obtain realizations of a wider range of kernels than that covered in Section 2.1. To illustrate this, let us consider the kernel

$$\hat{g}(s) = 1 + e^{-\tau s}\hat{h}(s) \quad (\Re(s) > 0)\,,\ g(t) = \delta(t) + h(t-\tau) \quad (t \in \mathbb{R})\,,$$

where h is an OD kernel that satisfies the conditions of Corollary 2.20 and $\tau > 0$ is a time delay. Using the OD realization of h given by (2.31), the convolution writes

$$\begin{aligned} g \star u(t) &= u(t) + h \star u(t-\tau) \\ &= u(t) + \sum_{k \in \mathbb{Z}} \operatorname{Res}(\hat{h}, s_k) \varphi(t-\tau, -s_k) + \int_0^\infty \varphi(t-\tau, \xi)\, \mu_{\hat{h}}(\xi)\, \mathrm{d}\xi, \end{aligned} \tag{2.55}$$

where φ follows the ODE (2.7). The identity (2.55) implies that $g \star u$ can be computed through a set of delayed ODEs. A (time-local) realization of g can be obtained by composing the hyperbolic realization of $s \mapsto e^{-s\tau}$ with the OD realization of h given by (2.31), which yields

$$g \star u(t) = u(t) + \sum_{k \in \mathbb{Z}} \operatorname{Res}(\hat{h}, s_k) \psi(t, -s_k, -c_\tau \tau) + \int_0^\infty \psi(t, \xi, -c_\tau \tau)\, \mu_{\hat{h}}(\xi)\, \mathrm{d}\xi,$$

where the hyperbolic variable follows

$$\begin{cases} \partial_t \psi(t,z,\theta) = c_\tau \partial_\theta \psi(t,z,\theta) \quad (t > 0,\ \theta \in (-l_\tau, 0),\ z \in \mathbb{C}) \\ \psi(t,z,0) = \varphi(t,z),\ \psi(0,z,\theta) = 0. \end{cases} \tag{2.56}$$

An intuitive summary of the classes of kernels that we have encountered so far in this chapter is provided in Table 2.1. To close this section, let us consider a kernel that models a cavity with dissipation, which will arise in the application of Section 2.4.

Physical phenomenon		Kernel $\hat{h}$	Time-domain realization	
Dissipation without propagation	Without oscillations	Diffusive kernel $\int_0^\infty \frac{\mu(\xi)}{s+\xi}\mathrm{d}\xi$	ODE φ	Heat equation, Parabolic
	With oscillations	Oscillatory kernel $\sum_{k\in\mathbb{Z}} \frac{\mathrm{Res}(\hat{h},s_k)}{s-s_k}$		Oscillator
Propagation without dissipation		$e^{-s\tau}$, $\tau>0$	PDE ψ	Transport equation, Hyperbolic

Table 2.1. Intuitive summary of the classes of kernels covered.

Lemma 2.45. *Let us consider the positive-real function*

$$f(s) = \coth(a + \epsilon\sqrt{s} + bs) \quad (s \in \mathbb{C}\backslash(-\infty, 0]),$$

with $a, \epsilon \geq 0$ and $b > 0$. Let $\tau = 2b$ and $\rho = e^{-2a}$. If $\epsilon = 0$, f admits the representation

$$f(s) = 1 + \rho e^{-\tau s} + \frac{\rho}{b} e^{-\tau s} \sum_{k\in\mathbb{Z}} \frac{1}{s - s_k},$$

where the poles s_k are given by (2.37). If $\epsilon > 0$, f admits the representation

$$f(s) = 1 + 2\rho e^{-\tau s} \left(\sum_{k\in\mathcal{K}} \frac{e^{-2\epsilon\sqrt{s_k}}}{2b + \frac{\epsilon}{\sqrt{s_k}}} \frac{1}{s - s_k} + \int_0^\infty \frac{1}{s+\xi} \mu(\xi)\, \mathrm{d}\xi \right),$$

where the poles s_k are the non-null solutions of (2.38) and the diffusive weight is given by (2.39).

Proof. The function f satisfies $f(s) \underset{s\to+\infty}{=} \mathcal{O}(1)$ so that Theorem 2.16 cannot be applied directly. To build a representation of f, we use the identity

$$\coth(s) = 1 + 2\frac{e^{-2s}}{1 - e^{-2s}}, \tag{2.57}$$

which leads to

$$f(s) = 1 + 2\rho e^{-2bs} g(s),\ g(s) = \frac{e^{-2\epsilon\sqrt{s}}}{1 - \rho e^{-2(\epsilon\sqrt{s}+bs)}},\ \rho = e^{-2a} \in (0, 1].$$

If $\epsilon = 0$, the representation of g is given by Lemma 2.35. If $\epsilon > 0$, the representation of g is given by Lemma 2.37. □

2.4 Application to physical impedance models

The purpose of this section is to derive time-local realizations of the physical impedance models introduced in Section 1.2.2, using the results of the previous sections.

2.4.1 Linear models

We cover below the CT and SDOF liner models under their impedance, admittance, and reflection coefficient formulations. Although this section is restricted to liner models, models that cover some porous media and ground layers have been covered in (Monteghetti et al. 2016a).

CT liner

The model (1.24) with wavenumber (1.26) reads

$$\frac{\hat{z}_{\mathrm{CT}}(s)}{z_c} = \frac{1}{\sigma_c} \coth\left(b_0 + b_{1/2}\sqrt{s} + b_1 s\right), \tag{2.58}$$

where $b_1 > 0$, $b_0, b_{1/2} \geq 0$, and $\sigma_c \in (0, 1]$. The representation of this kernel can be obtained using the identity (2.57), which leads to

$$\begin{cases} \dfrac{\hat{z}_{\mathrm{CT}}(s)}{z_c} = \dfrac{1}{\sigma_c} + e^{-\tau s}\hat{h}(s) \\ \dfrac{z_{\mathrm{CT}}(t)}{z_c} = \dfrac{1}{\sigma_c}\delta(t) + h(t-\tau), \end{cases} \tag{2.59}$$

where

$$\tau = 2b_1$$

is a time delay and

$$\hat{h}(s) = \frac{2e^{-2b_0}}{\sigma_c}\frac{e^{-2b_{1/2}\sqrt{s}}}{R(s)},\ R(s) = 1 - e^{-2b_0}e^{-2\left(b_{1/2}\sqrt{s}+b_1 s\right)}. \tag{2.60}$$

The kernel h is OD with representation given in Lemma 2.35 (resp. Lemma 2.37) if $b_{1/2} = 0$ (resp. $b_{1/2} > 0$). Note the physical interpretation of the time delay τ: the model (1.26) gives $b_1 = {}^{l_c}/_{c_0}$ where l_c is the cavity length and c_0 the propagation speed, so that τ is the back and forth traveling time. Let us now assume that $b_{1/2} > 0$, so that Lemma 2.37 gives

$$\frac{\hat{z}_{\mathrm{CT}}(s)}{z_c} = \frac{1}{\sigma_c} + e^{-\tau s}\left[\sum_{k\in\mathbb{Z}} \frac{\mathrm{Res}(\hat{h}, s_k)}{s - s_k} + \int_0^\infty \frac{1}{s+\xi}\mu_{\hat{h}}(\xi)\,\mathrm{d}\xi\right], \tag{2.61}$$

where the poles s_k are the non-null solutions of $R(s_k) = 0$. The corresponding realization is similar to the one covered in Section 2.3. First, the realization (2.31) of the OD representation leads to

$$z_{\mathrm{CT}} \star u(t) = \frac{1}{\sigma_c}u(t) + \sum_{k\in\mathbb{Z}} \mathrm{Res}(\hat{h}, s_k)\varphi(t-\tau, -s_k) + \int_0^\infty \varphi(t-\tau, \xi)\,\mu_{\hat{h}}(\xi)\,\mathrm{d}\xi,$$

where φ follows the ODE (2.7). The sought (time-local) realization is then obtained using the hyperbolic realization of the time delay:

$$z_{\mathrm{CT}} \star u(t) = \frac{1}{\sigma_c}u(t) + \sum_{k\in\mathbb{Z}} \mathrm{Res}(\hat{h}, s_k)\psi(t, -s_k, -c_\tau\tau) + \int_0^\infty \psi(t, \xi, -c_\tau\tau)\,\mu_{\hat{h}}(\xi)\,\mathrm{d}\xi, \tag{2.62}$$

where the hyperbolic variable ψ follows the transport equation (2.56).

The representation of the physical model given by (2.61) naturally suggests the following discrete impedance model

$$\frac{\hat{z}_{\mathrm{num}}(s)}{z_c} = \frac{1}{\sigma_c} + e^{-\tau s}\left[\sum_{n=1}^{N_s} \frac{r_n}{s - s_n} + \sum_{n=1}^{N_\xi} \frac{\mu_n}{s + \xi_n}\right], \tag{2.63}$$

which is a "multipole" model, following the terminology of Section 1.3. The following remarks can be made.

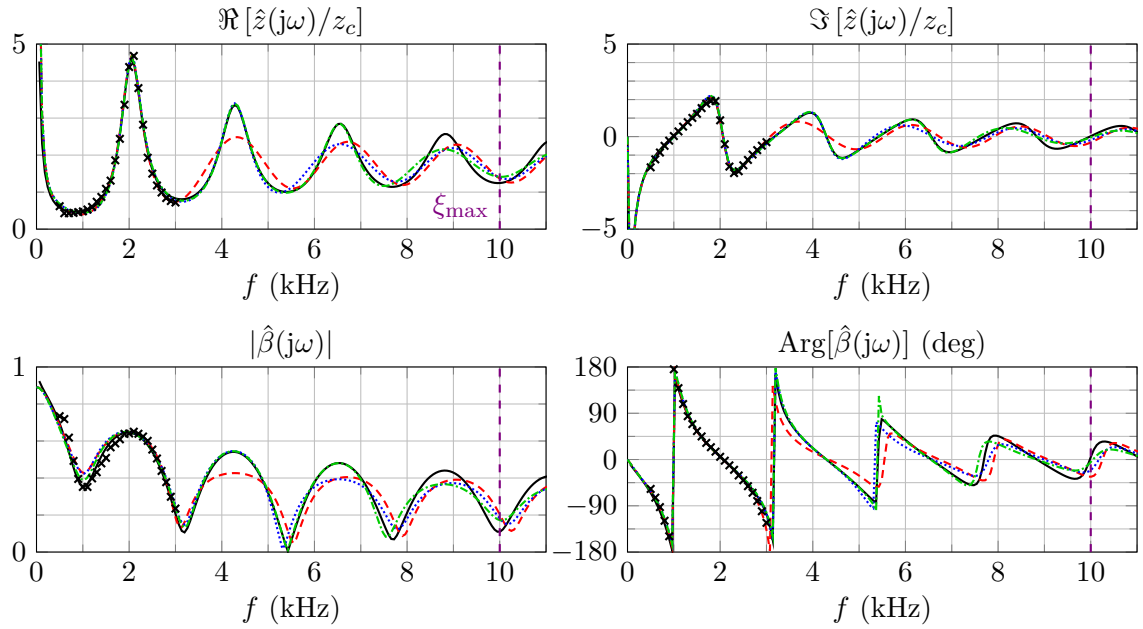

Figure 2.11. Broadband approximation of $\hat{z}_{\mathrm{CT}}$. (×) CT57 liner at 130 dB (Jones et al. 2005). (——) Physical model $\hat{z}_{\mathrm{CT}}$ given by (1.24,1.26) with $\sigma_c = 57\,\%$, $d_c = 0.8 \times 0.6\,\mathrm{mm}$, and $l_c = 0.84 \times 85.6\,\mathrm{mm}$ leading to $b_0 = 0$, $b_{1/2} = 5.0 \times 10^{-3}$, and $b_1 = 2.11 \times 10^{-4}$. (- - - -) Discrete model $\hat{z}_{\mathrm{num}}$ with $N_\xi = 2$ diffusive poles at 50 Hz and 10 kHz and $N_s = 2$ oscillatory poles (1 pair). (·····) $\hat{z}_{\mathrm{num}}$ with $N_\xi = 2$ and $N_s = 4$ (2 pairs). (-·-·-) $\hat{z}_{\mathrm{num}}$ with $N_\xi = 2$ and $N_s = 8$ (3 pairs).

- The discrete model (2.63) has been derived from (2.58), which is a high/low-frequency approximation of the physical model (1.24,1.25). This sheds a light on the meaning and applicability of multipole models, which so far were only postulated in the literature. The physical interpretation of the components of $\hat{z}_{\mathrm{num}}$, namely the delay and the oscillatory and diffusive parts, can be done with Table 2.1.

- The practical interest of this derivation is that it gives a simple way of computing the poles and the weights in (2.63) using the methods given in Section 2.2. When these methods are used, the poles and weights are directly obtained from a discretization of the physical model (2.58) with b_0, $b_{1/2}$, and b_1 given by e.g. (1.26).

- A different physical model is likely to lead to a different discrete model. This contrasts with a one-size-fits-all approach, where one numerical model is postulated and applied regardless of the material considered.

A comparison between $\hat{z}_{\mathrm{num}}$ and $\hat{z}_{\mathrm{CT}}$ for the CT57 liner is proposed in Figure 2.11, where $\hat{z}_{\mathrm{num}}$ is computed using the linear least squares method presented in Section 2.2.1. The diffusive part of $\hat{z}_{\mathrm{CT}}$ is well-approximated with only two diffusive poles, one at 50 Hz and one at 10 kHz. The only difference between the three plotted discrete models is the number of oscillatory poles s_n: 2, 4, and 6. The graph shows that the n-th pair of oscillatory poles enables to model the n-th anti-resonance. Therefore, the presented model analysis has enabled us to compute a broadband approximation of $\hat{z}_{\mathrm{CT}}$ with only a linear least squares optimization. Here, following Remark 2.41, we compute the discrete weights r_n by numerically evaluating the residues using (2.15), so that only μ_1 and μ_2 are obtained through an optimization: the oscillatory and diffusive parts are thus discretized differently.

Remark 2.46 (Delay discretization). It is of paramount importance to note that the plots of $\hat{z}_{\text{num}}$ given in Figure 2.11 assume that the time delay is perfectly discretized in the frequency range of interest. When the time delay is discretized, the factor $e^{-s\tau}$ in (2.63) is replaced with $\hat{h}_{\tau,\text{num}}$, which is a property of the chosen delay discretization method.

Remark 2.47. From now on, to avoid repetitions, we only write the representation in the Laplace domain. The admittance of the CT liner model (2.58) is given by

$$z_c\hat{y}_{\text{CT}} = \sigma_c \tanh\left(b_0 + b_{1/2}\sqrt{s} + b_1 s\right).$$

By using the identity (2.57) we get a representation similar to (2.59), namely

$$z_c\hat{y}_{\text{CT}}(s) = \hat{h}_1(s) + e^{-\tau s}\hat{h}_2(s), \tag{2.64}$$

where $\tau = 2b_1$ and the OD kernels are given by

$$\hat{h}_1(s) = \frac{1}{R(s)},\ \hat{h}_2(s) = -e^{-2b_0}\frac{e^{-2b_{1/2}\sqrt{s}}}{R(s)},\ R(s) = \frac{1}{\sigma_c} + \frac{1}{\sigma_c}e^{-2\left(b_0+b_{1/2}\sqrt{s}+b_1 s\right)}. \tag{2.65}$$

The representation of $\hat{h}_1$ is given in Lemma 2.35 (resp. 2.40) if $b_{1/2} = 0$ (resp. b_0, $b_{1/2} > 0$). The representation of $\hat{h}_2$ is given in Lemma 2.35 (resp. 2.37) if $b_{1/2} = 0$ (resp. $b_{1/2} > 0$). Note that $\hat{h}_1$ and $\hat{h}_2$ have the same denominator R, so that they share the same poles. However, their residues and diffusive weights are different.

The last formulation we consider is the reflection coefficient $\hat{\beta}_{\text{CT}}$, for which we will derive two representations. The first one is obtained using the identity

$$\hat{\beta}_{\text{CT}}(s) = \frac{\frac{\hat{z}_{\text{CT}}(s)}{z_c} - 1}{\frac{\hat{z}_{\text{CT}}(s)}{z_c} + 1},$$

which leads to

$$\begin{aligned}\hat{\beta}_{\text{CT}}(s) &= \frac{1 + 2\frac{e^{-2\left(b_0+b_{1/2}\sqrt{s}+b_1 s\right)}}{1-e^{-2\left(b_0+b_{1/2}\sqrt{s}+b_1 s\right)}} - \sigma_c}{1 + 2\frac{e^{-2\left(b_0+b_{1/2}\sqrt{s}+b_1 s\right)}}{1-e^{-2\left(b_0+b_{1/2}\sqrt{s}+b_1 s\right)}} + \sigma_c} \\ &= \hat{h}_1(s) + e^{-\tau s}\hat{h}_2(s),\end{aligned} \tag{2.66}$$

where $\tau = 2b_1$ and the OD kernels similar to that obtained with the admittance:

$$\hat{h}_1(s) = \frac{\frac{1-\sigma_c}{1+\sigma_c}}{R(s)},\ \hat{h}_2(s) = e^{-2b_0}\frac{e^{-2b_{1/2}\sqrt{s}}}{R(s)},\ R(s) = 1 + \frac{1-\sigma_c}{1+\sigma_c}e^{-2\left(b_0+b_{1/2}\sqrt{s}+b_1 s\right)}. \tag{2.67}$$

Assume $\sigma_c \neq 1$. The representation of $\hat{h}_1$ is given in Lemma 2.35 (resp. Lemma 2.40) if $b_{1/2} = 0$ (resp. b_0, $b_{1/2} > 0$), while the representation of $\hat{h}_2$ is given in Lemma 2.35 (resp. Lemma 2.37) if $b_{1/2} = 0$ (resp. $b_{1/2} > 0$). If $\sigma_c = 1$, then $\hat{h}_1 = 0$ and the representation of $\hat{h}_2$ is provided by Lemma 2.30 if $b_{1/2} > 0$ (otherwise $\hat{h}_2 = e^{-2b_0}$). The second representation relies on

$$\hat{\beta}_{\text{CT}}(s) = 1 - 2\frac{1}{\frac{\hat{z}_{\text{CT}}(s)}{z_c} + 1},$$

which leads to

$$\hat{\beta}_{\mathrm{CT}}(s) = 1 - 2\frac{1}{1+\frac{1}{\sigma_c}\left(1+2\frac{e^{-2\left(b_0+b_{1/2}\sqrt{s}+b_1 s\right)}}{1-e^{-2\left(b_0+b_{1/2}\sqrt{s}+b_1 s\right)}}\right)} = 1 - 2\frac{1-e^{-2\left(b_0+b_{1/2}\sqrt{s}+b_1 s\right)}}{1+\frac{1}{\sigma_c}+\left(\frac{1}{\sigma_c}-1\right)e^{-2\left(b_0+b_{1/2}\sqrt{s}+b_1 s\right)}}$$
$$= 1 + \hat{h}_1(s) + e^{-\tau s}\hat{h}_2(s), \tag{2.68}$$

where $\tau = 2b_1$ and the OD kernels are given by

$$\hat{h}_1(s) = -\frac{2}{R(s)},\ \hat{h}_2(s) = 2e^{-2b_0}\frac{e^{-2b_{1/2}\sqrt{s}}}{R(s)},\ R(s) = 1+\frac{1}{\sigma_c}+\left(\frac{1}{\sigma_c}-1\right)e^{-2\left(b_0+b_{1/2}\sqrt{s}+b_1 s\right)}, \tag{2.69}$$

and their representations are obtained similarly to the previous ones. The main difference is that, when $\sigma_c = 1$ we do not have $\hat{h}_1 = 0$ but $1 + \hat{h}_1 = 0$. The differences between the two representations (2.66,2.67) and (2.68,2.69) are insignificant enough that they can be considered equivalent. However, the differences between them grow significantly when considering the SDOF liner model, covered below.

Remark 2.48 (Erratum). The representation of $\hat{z}_4$ given in (Monteghetti et al. 2016a, Eq. 93) is only valid for $a_{0,}\, a_\alpha > 0$: if $a_\alpha = 0$, then a constant term must be added, as discussed in this chapter. Let us detail this statement, using the notations of the paper. The function $\hat{h}_4$ is similar to (2.60) with $\sqrt{s}$ replaced by s^α, $\alpha \in (0,1)$. If $a_\alpha > 0$, then $\hat{h}_4$ satisfies the conditions of Corollary 2.20, so that (2.28) is (Monteghetti et al. 2016a, Eq. 93). If $a_\alpha = 0$ and $a_0 > 0$, then $\hat{h}_4$ fails the decay condition (2.16) but $s \mapsto \hat{h}_4(s)/s$ satisfies the conditions of Theorem 2.16 with $\gamma_1 = 0$, so that the representation of $\hat{h}_4$ must be changed accordingly, as in Lemma 2.40. Specifically, Theorem 2.16 yields

$$\frac{\hat{h}_4}{s}(s) = \frac{\mathrm{Res}\left(\frac{\hat{h}_4}{s},0\right)}{s} + \sum_k \frac{\mathrm{Res}\left(\frac{\hat{h}_4}{s},s_k\right)}{s-s_k} + \int_0^\infty \frac{\mu_{\frac{\hat{h}_4}{s}}(\xi)}{s+\xi}\,\mathrm{d}\xi,$$

where the diffusive weight is given by

$$\mu_{\frac{\hat{h}_4}{s}}(\xi) = -\frac{1}{\xi}\mu_{\hat{h}_4}(\xi) = -\frac{1}{\xi}\mu_4^\alpha(\xi)$$

and $(s_k)_k$ is the sequence of poles of $\hat{h}_4$ (which are non-null by definition of $\hat{h}_4$, since $\Upsilon \in (0,1)$). The representation of $\hat{h}_4$ is therefore

$$\hat{h}_4(s) = C + \sum_k \frac{\mathrm{Res}(\hat{h}_4,s_k)}{s-s_k} + \int_0^\infty \frac{1}{s+\xi}\mu_4^\alpha(\xi)\,\mathrm{d}\xi,$$

where the added constant is given by

$$C = \hat{h}_4(0) + \sum_k \frac{\mathrm{Res}(\hat{h}_4,s_k)}{s_k} - \int_0^\infty \frac{1}{\xi}\mu_4^\alpha(\xi)\,\mathrm{d}\xi.$$

SDOF liner

The impedance (1.29) with perforation model (1.20) and wavenumber (1.26) writes

$$\frac{\hat{z}_{\mathrm{SDOF}}(s)}{z_c} = a_0 + a_{1/2}\sqrt{s} + a_1 s + \frac{1}{\sigma_c}\coth(b_0 + b_{1/2}\sqrt{s} + b_1 s), \tag{2.70}$$

where $a_0, a_{1/2}, a_1, b_0, b_{1/2} \geq 0$, $b_1 > 0$, and $\sigma_c \in (0, 1]$. The representation is

$$\frac{\hat{z}_{\mathrm{SDOF}}(s)}{z_c} = a_0 + a_{1/2}\hat{h}_1(s) + a_1 s + e^{-\tau s}\hat{h}_2(s),$$

where $\hat{h}_1(s) = \sqrt{s}$, whose (extended) diffusive representation has been given in Section 2.1.4, and $\hat{h}_2$ is given by (2.60). For the sake of conciseness, in the next identities we use the polynomial

$$P(\sigma) = a_0 + a_{1/2}\sigma + a_1\sigma^2.$$

The admittance is given by

$$\begin{aligned} z_c\hat{y}_{\mathrm{SDOF}}(s) &= \frac{1}{P(\sqrt{s}) + \frac{1}{\sigma_c}\coth(b_0 + b_{1/2}\sqrt{s} + b_1 s)} \\ &= \hat{h}_1(s) + e^{-\tau s}\hat{h}_2(s), \end{aligned}$$

where $\tau = 2b_1$ and the OD kernels are given by

$$\hat{h}_1(s) = \frac{1}{R(s)},\ \hat{h}_2(s) = -e^{-2b_0}\frac{e^{-2b_{1/2}\sqrt{s}}}{R(s)},\ R(s) = \frac{1}{\sigma_c} + P(\sqrt{s}) + \left(\frac{1}{\sigma_c} - P(\sqrt{s})\right)e^{-2\left(b_0 + b_{1/2}\sqrt{s} + b_1 s\right)}. \tag{2.71}$$

The representations of these two kernels are as follows. Assume first that both $a_{1/2}$ and a_1 are null. In this case, (2.71) is similar to (2.65) so that, if $\sigma_c a_0 \neq 1$, the representation of $\hat{h}_1$ is given in Lemma 2.35 (resp. 2.40) if $b_{1/2} = 0$ (resp. b_0, $b_{1/2} > 0$ or a_0, $b_{1/2} > 0$), while the representation of $\hat{h}_2$ is given in Lemma 2.35 (resp. 2.37) if $b_{1/2} = 0$ (resp. $b_{1/2} > 0$). On the other hand, if $\sigma_c a_0 = 1$, then $R(s) = 2/\sigma_c$ so that $\hat{h}_1$ is constant while the representation of $\hat{h}_2$ is given by Lemma 2.30.

Assume now that $a_{1/2} \neq 0$ or $a_1 \neq 0$, which is likely in practice. This implies that $P(\infty) = \infty$, thus ensuring that both $\hat{h}_1$ and $\hat{h}_2$ satisfy the decay condition at infinity (2.16). Both $\hat{h}_1$ and $\hat{h}_2$ have the OD representation (2.21) given by Theorem 2.16.

Finally, let us consider the reflection coefficient, using the two approaches discussed when analyzing the CT liner model above. The first approach reads

$$\begin{aligned} \hat{\beta}_{\mathrm{SDOF}}(s) =& \frac{\frac{\hat{z}_{\mathrm{SDOF}}(s)}{z_c} - 1}{\frac{\hat{z}_{\mathrm{SDOF}}(s)}{z_c} + 1} = \frac{P(\sqrt{s}) - 1 + \frac{1}{\sigma_c}\coth(b_0 + b_{1/2}\sqrt{s} + b_1 s)}{1 + P(\sqrt{s}) + \frac{1}{\sigma_c}\coth(b_0 + b_{1/2}\sqrt{s} + b_1 s)} \\ =& \frac{\frac{1-\sigma_c}{1+\sigma_c} + \frac{\sigma_c}{1+\sigma_c}P(\sqrt{s})}{1 + \frac{\sigma_c}{1+\sigma_c}P(\sqrt{s}) + \left(\frac{1-\sigma_c}{1+\sigma_c} - \frac{\sigma_c}{1+\sigma_c}P(\sqrt{s})\right)e^{-2\left(b_0 + b_{1/2}\sqrt{s} + b_1 s\right)}} \\ &+ \frac{\left(1 - \frac{\sigma_c}{1+\sigma_c}P(\sqrt{s})\right)e^{-2\left(b_0 + b_{1/2}\sqrt{s} + b_1 s\right)}}{1 + \frac{\sigma_c}{1+\sigma_c}P(\sqrt{s}) + \left(\frac{1-\sigma_c}{1+\sigma_c} - \frac{\sigma_c}{1+\sigma_c}P(\sqrt{s})\right)e^{-2\left(b_0 + b_{1/2}\sqrt{s} + b_1 s\right)}}. \end{aligned}$$

It leads to expressions with polynomials in both numerator and denominator, so that no decay at infinity is achieved in general. Here, this approach is not convenient to build a representation of $\hat{\beta}_{\mathrm{SDOF}}$. By contrast the second approach directly yields an easier representation, namely

$$\begin{aligned} \hat{\beta}_{\mathrm{SDOF}}(s) &= 1 - 2\frac{1}{1 + \frac{\hat{z}_{\mathrm{SDOF}}(s)}{z_c}} = 1 - 2\frac{1}{1 + P(\sqrt{s}) + \frac{1}{\sigma_c}\coth(b_0 + b_{1/2}\sqrt{s} + b_1 s)} \\ &= 1 + \hat{h}_1(s) + e^{-\tau s}\hat{h}_2(s), \end{aligned}$$

where the OD kernels are given by

$$\begin{aligned}&\hat{h}_1(s) = -\frac{2}{R(s)},\ \hat{h}_2(s) = 2e^{-2b_0}\frac{e^{-2b_{1/2}\sqrt{s}}}{R(s)}\\&R(s) = 1 + \frac{1}{\sigma_c} + P(\sqrt{s}) + \left(\frac{1}{\sigma_c} - 1 - P(\sqrt{s})\right)e^{-2\left(b_0 + b_{1/2}\sqrt{s} + b_1 s\right)},\end{aligned} \tag{2.72}$$

which is similar to (2.71). For the sake of completeness, let us distinguish all cases.

- If $a_{1/2} \neq 0$ or $a_1 \neq 0$, then both $\hat{h}_1$ and $\hat{h}_2$ have the OD representation (2.21) given by Theorem 2.16.
- Assume now that both $a_{1/2}$ and a_1 are null. In this case, (2.72) is similar to (2.69).
  - If $a_0 \neq \frac{1}{\sigma_c} - 1$, then the representation of $\hat{h}_1$ is given in Lemma 2.35 (resp. Lemma 2.40) if $b_{1/2} = 0$ (resp. $b_{1/2} > 0$), while the representation of $\hat{h}_2$ is given in Lemma 2.35 (resp. Lemma 2.37) if $b_{1/2} = 0$ (resp. $b_{1/2} > 0$).
  - If $a_0 = \frac{1}{\sigma_c} - 1$, then $R(s) = \frac{2}{\sigma_c}$ and $\hat{h}_1(s) = -\sigma_c$ is a constant and the representation of $\hat{h}_2$ is provided by Lemma 2.30 if $b_{1/2} > 0$ (otherwise $\hat{h}_2 = e^{-2b_0}\sigma_c$).

DDOF liner

The analysis of the DDOF, not used in the numerical application of Chapter 6, is proposed in Appendix B.

2.4.2 Nonlinear model

The purpose of this section is to consider the realization of an impedance model that includes the nonlinear term (19) recalled in Chapter 1. The computation of the impedance, admittance, and scattering operators is discussed first on a simple example, thus illustrating the definitions proposed in Section 3, then in the general case.

Algebraic model

Let us start with the following elementary example

$$\frac{\mathcal{Z}}{z_0}(u) = a_0 u + \frac{C_{\mathrm{nl}}}{c_0}|u|u, \tag{2.73}$$

where $a_0, C_{\mathrm{nl}} \geq 0$. Since $\mathcal{Z}$ is algebraic, we can analytically compute the corresponding admittance and scattering operators. The admittance operator is known implicitly as the solution of

$$p = \mathcal{Z}\left(\mathcal{Y}(p)\right) \quad (p \in \mathbb{R}).$$

Hence, using Lemma 2.50 below, we get

$$\mathcal{Y}(p) = \frac{2p}{z_0 a_0 + \sqrt{z_0^2 a_0^2 + 4\frac{z_0 C_{\mathrm{nl}}}{c_0}|p|}}. \tag{2.74}$$

Note that if $C_{\rm nl} = 0$ in (2.74) it reduces to $p = z_0 a_0 \mathcal{Y}(p)$. The scattering operator can be computed in the same fashion. Using the definition (1.14) we have

$$\begin{aligned}\mathcal{B}(v) &= \left(\frac{\mathcal{Z}}{z_0} - \mathcal{I}\right) \circ \left(\frac{\mathcal{Z}}{z_0} + \mathcal{I}\right)^{-1}(v) \\ &= (a_0 - 1)\left(\frac{\mathcal{Z}}{z_0} + \mathcal{I}\right)^{-1}(v) + \frac{C_{\rm nl}}{c_0}\left|\left(\frac{\mathcal{Z}}{z_0} + \mathcal{I}\right)^{-1}(v)\right|\left(\frac{\mathcal{Z}}{z_0} + \mathcal{I}\right)^{-1}(v),\end{aligned}$$

so that by using Lemma 2.50 to express $\left(\frac{\mathcal{Z}}{z_0} + \mathcal{I}\right)^{-1}(v)$ we obtain

$$\mathcal{B}(v) = \beta_0 \frac{2v}{1 + \sqrt{1 + 4\frac{C_{\rm nl}}{c_0(a_0+1)^2}|v|}} + \frac{C_{\rm nl}}{c_0\,(a_0+1)^2} \frac{4|v|v}{\left(1 + \sqrt{1 + 4\frac{C_{\rm nl}}{c_0(a_0+1)^2}|v|}\right)^2}, \tag{2.75}$$

where β_0 is the reflection coefficient associated with a_0, namely

$$\beta_0 = \frac{a_0 - 1}{a_0 + 1}.$$

Note that if $C_{\rm nl} = 0$ in (2.75) we recover $\mathcal{B}(v) = \beta_0 v$. The nonlinear admittance operator (2.74) satisfies the passivity condition (1.2) with $\mathcal{Z}$ replaced by $\mathcal{Y}$. Similarly, the nonlinear scattering operator (2.75) is passive since it satisfies (1.13), see Lemma 2.51. The expressions of $\mathcal{Z}$, $\mathcal{Y}$, and $\mathcal{B}$ above are used in Chapter 6 to illustrate the computational interest of using a nonlinear scattering operator.

Remark 2.49. Since the operators $\left(\frac{\mathcal{Z}}{z_0} - \mathcal{I}\right)$ and $\left(\frac{\mathcal{Z}}{z_0} + \mathcal{I}\right)^{-1}$ commute, we could also have found an expression of $\mathcal{B}(v)$ by solving

$$\frac{\mathcal{Z}}{z_0}(\mathcal{B}(v)) + \mathcal{B}(v) = \frac{\mathcal{Z}}{z_0}(v) - v,$$

but this yields a less appealing formula.

Lemma 2.50. *The inverse of the non-null nonlinear function*

$$f(x) = ax + b|x|x \quad (x \in \mathbb{R}),$$

with $a, b \geq 0$ *is given by*

$$f^{-1}(y) = \frac{2y}{a + \sqrt{a^2 + 4b|y|}}.$$

Proof. Let $x \in \mathbb{R}$ and $y = f(x)$. We seek to solve

$$\begin{cases} bx^2 + ax - y = 0 & (x > 0,\ y > 0) \\ -bx^2 + ax - y = 0 & (x < 0,\ y < 0). \end{cases}$$

Using Vieta's formula to avoid a singularity at $b = 0$, the solutions are

$$\begin{cases} x_\pm = \dfrac{2y}{a \pm \sqrt{a^2 + 4by}} & (x > 0,\ y > 0) \\ x_\pm = \dfrac{2y}{a \pm \sqrt{a^2 - 4by}} & (x < 0,\ y < 0), \end{cases}$$

which yields the claimed expression. □

Lemma 2.51. *Let $\mathcal{B} : \mathbb{R} \to \mathbb{R}$ be defined as (2.75) with $C_{\mathrm{nl}}, c_0, a_0 \geq 0$. Then,*

$$\mathcal{B}(v) \leq v \quad (v \in \mathbb{R}).$$

Proof. It suffices to rewrite $\mathcal{B}$ as

$$\mathcal{B}(v) = \left[\frac{2\beta_0 \left(1 + \Phi(v)\right) + \frac{4C_{\mathrm{nl}}}{c_0(a_0+1)^2}|v|}{2\left(1 + \Phi(v)\right) + \frac{4C_{\mathrm{nl}}}{c_0(a_0+1)^2}|v|} \right] \times v,$$

where

$$\Phi(v) \coloneqq \sqrt{1 + \frac{4C_{\mathrm{nl}}}{c_0 \left(a_0 + 1\right)^2}|v|}.$$

□

General model

Let us now discuss the computation of the admittance and scattering operators when $\mathcal{Z}$ is a generic nonlinear operator. For example, $\mathcal{Z}$ could be

$$\frac{\mathcal{Z}}{z_0}(u) = \frac{1}{z_0} z_l \star u + \frac{C_{\mathrm{nl}}}{c_0}|u|u, \tag{2.76}$$

where z_l is an admissible impedance kernel, such as z_{SDOF} or z_{CT} covered in 2.4.1. Since $z_l \star u$ can be a delayed integro-differential operator, the admittance and scattering operators cannot be expressed analytically in general, by contrast with the algebraic model (2.73). The computation of the admittance operator $\mathcal{Y}$ requires the inversion of $\mathcal{Z}$, which writes

$$\begin{cases} \mathcal{Z}\left(w(t)\right) = p(t) \quad (t > 0) \\ \mathcal{Y}(p) = w, \end{cases} \tag{2.77}$$

with suitable initial conditions depending on the nature of $\mathcal{Z}$. For example, if $\mathcal{Z}$ is given by (2.76) with $z_l = a_0\delta + a_1\delta'$, we get

$$\begin{cases} a_1 \dot{w}(t) = -\left(a_0 + \dfrac{z_0 C_{\mathrm{nl}}}{c_0}|w(t)|\right) w(t) + p(t) \quad (t > 0), \quad w(0) = 0 \\ w(0) = 0, \end{cases}$$

which is a nonlinear ODE, possibly stiff.

The computation of the scattering operator can be done in the two following ways. The first method relies on the identity

$$\mathcal{B}(v) = v - 2\left(\frac{\mathcal{Z}}{z_0} + \mathcal{I}\right)^{-1}(v),$$

which implies that $\mathcal{B}(v)$ can be computed by inverting $\frac{\mathcal{Z}}{z_0} + \mathcal{I}$:

$$\begin{cases} \dfrac{\mathcal{Z}}{z_0}\left(w(t)\right) + w(t) = v(t) \quad (t > 0) \\ \mathcal{B}(v) = v - 2w. \end{cases} \tag{2.78}$$

The difficulty is that, similarly to (2.77), (2.78) may be a stiff ODE. The second way of computing $\mathcal{B}(v)$ is by solving

$$\begin{cases} \dfrac{\mathcal{Z}}{z_0}\left(w\right)(t) + w(t) = \dfrac{\mathcal{Z}}{z_0}(v)(t) - v(t) \quad (t > 0) \\ \mathcal{B}(v) = w, \end{cases} \tag{2.79}$$

which comes from the identity

$$\left(\frac{\mathcal{Z}}{z_0} + \mathcal{I}\right) \circ \mathcal{B} = \frac{\mathcal{Z}}{z_0} - \mathcal{I}.$$

The interest of (2.79) is that it may be less stiff than (2.78). However, none of the expressions (2.77,2.78,2.79) are further considered in this dissertation: as will be stated in the conclusion, this constitutes a perspective of this study.

Part II

Well-posedness and stability with impedance boundary conditions

Chapter 3

Boundary conditions for the linearized Euler equations

Contents

The objective of this chapter is to define boundary conditions suitable for the LEEs. To discuss well-posedness it relies on the theory of Friedrichs systems, whose concise formalism will prove handy in the energy analysis of Chapter 5. The contribution of this chapter is the application of recent results of the theory of Friedrichs systems to the LEEs. Section 3.1 recalls the LEEs and a proof of well-posedness in free space that relies on an a priori energy estimate. The initial boundary value problem (IBVP) is covered in Section 3.2, where a literature review shows that existing proofs of well-posedness also crucially depend on a priori energy estimates, so that boundary conditions are required to be maximal positive, maximal dissipative, or Friedrichs-admissible. The definition of such boundary conditions for the LEEs is investigated in Section 3.3, which naturally leads to the definition of IBCs. Proving well-posedness of the LEEs with IBCs is discussed in Section 3.4.

Motivation The problem that motivates this whole chapter comes from the numerical application of Section 6.3. It consists in establishing the well-posedness of the LEEs (3.1) in finite time, namely on $\Omega_T = (0,T) \times \Omega$ with $\Omega \subset \mathbb{R}^d$, $d = 2$, and $T > 0$. The domain of interest is the rectangle $\Omega = (0, L_1) \times (0, L_2)$ with a boundary $\partial\Omega$ split into three disjoint parts, namely Γ_{in}, Γ_{out}, and Γ_z:

$$\Gamma_{\text{in}} = \{x_1 = 0\} \cap \overline{\Omega},\ \Gamma_{\text{out}} = \{x_1 = L_1\} \cap \overline{\Omega},\ \Gamma_z = \partial\Omega \backslash \Gamma_{\text{in}} \cup \Gamma_{\text{out}}.$$

To each part of the boundary is associated a different boundary condition: inflow on Γ_{in}, outflow on Γ_{out}, and finally an IBC on Γ_z. The subsonic base flow has only one component: $\boldsymbol{u_0} = u_0 \boldsymbol{e_1}$

with $u_0 \in W^{1,\infty}(\Omega)$ that vanishes on Γ_z and is positive on both Γ_{in} and Γ_{out}. The well-posedness of this problem is discussed in the last section of this chapter, namely Section 3.4, using the notations and concepts introduced in the previous sections.

3.1 Linearized Euler equations in free space

In this work the hydrodynamic field is split between a steady base flow and an unsteady acoustic perturbation. The perturbations of pressure p, velocity $\boldsymbol{u}$, and density ρ are governed by the homentropic linearized Euler equations (LEEs), defined on $(0,T)\times\Omega$ with $\Omega \subset \mathbb{R}^d$ an open set and $T > 0$,

$$\begin{cases} \partial_t p + (\boldsymbol{u_0}\cdot\nabla)p + z_0 c_0 \nabla\cdot\boldsymbol{u} + \gamma p \nabla\cdot\boldsymbol{u_0} = 0 \\ \partial_t \boldsymbol{u} + (\boldsymbol{u_0}\cdot\nabla)\boldsymbol{u} + z_0^{-1} c_0 \nabla p + (\boldsymbol{u}\cdot\nabla)\boldsymbol{u_0} + z_0^{-1} c_0^{-1} p(\boldsymbol{u_0}\cdot\nabla)\boldsymbol{u_0} = 0 \\ p = c_0^2 \rho. \end{cases} \tag{3.1}$$

The specific heat ratio is denoted $\gamma > 1$. Quantities related to the base flow are designated by the subscript "0": $\boldsymbol{u_0}$ is the base flow velocity, ρ_0 the base flow density, c_0 the speed of sound, and $z_0 \coloneqq \rho_0 c_0$ the characteristic impedance of the propagation medium. All quantities are dimensional. Column vectors are denoted in bold and the symbol $(\boldsymbol{u}\cdot\nabla)$ denotes the convective derivative defined as

$$(\boldsymbol{u}\cdot\nabla)f \coloneqq \sum_{i=1}^{d} u_i \partial_i f$$

and

$$(\boldsymbol{u}\cdot\nabla)\boldsymbol{f} \coloneqq \nabla\boldsymbol{f}\cdot\boldsymbol{u} = \left[\sum_{j=1}^{d} u_j \partial_j f_i\right]_{i\in[\![1,d]\!]}$$

when applied to scalar-valued and vector-valued functions, respectively. The LEEs (3.1) entail hypotheses on both the base flow and the perturbations. The base flow is an ideal gas such that $c_0^2 = \gamma r T_0 = \gamma p_0/\rho_0$ and solves the steady Navier-Stokes equations. The perturbations are "small", inviscid, and homentropic. The rather strong homentropicity assumption enables to replace the energy equation by the algebraic relation $p = c_0^2\rho$ and implies that c_0 must be constant in Ω. As a result, the LEEs (3.1) do not include an entropy mode, but only hydrodynamic and acoustic ones. In spite of its simplicity, this model is commonly used in duct aeroacoustics, see Chapter 6. For the detailed derivation of the LEEs and additional physical insights, the reader is referred to (Richter 2010, Chap. 2) and references therein.

A key feature of the LEEs (3.1) is that they can be written as a symmetric hyperbolic system, which is useful to establish well-posedness in free space as well as to define admissible boundary conditions, see Section 3.2. Generalities on symmetric hyperbolic systems are introduced in Section 3.1.1 and applied to the LEEs in Section 3.1.2.

3.1.1 Well-posedness of symmetric hyperbolic IVPs

Definition 3.1 (Friedrichs operator (Friedrichs 1958) (Rauch 1985) (Ern et al. 2007, § 5.1) (Antonić and Burazin 2010))**.** Let $\Omega \subset \mathbb{R}^d$ be an open set. Let the first-order operator $\mathcal{A} : L^2(\Omega) \to \mathcal{D}(\Omega)'$ be defined by

$$\mathcal{A}\boldsymbol{v} \coloneqq \sum_{i=1}^{d} A_i \partial_i \boldsymbol{v} + B\boldsymbol{v}, \tag{3.2}$$

where $A_i, B : \Omega \to \mathbb{R}^{m\times m}$ are two real-valued matrix fields over Ω such that $A_i \in W^{1,\infty}(\Omega)^{m\times m}$ and $B \in L^\infty(\Omega)^{m\times m}$. The operator $\mathcal{A}$ is said to be a *Friedrichs* (also *symmetric positive*)

operator if $A_i = A_i^\intercal$ a.e. on Ω, and there is $\mu_0 > 0$ such that $B + B^\intercal - \sum_i \partial_i A_i \geq \mu_0 \mathbb{I}_m$ a.e. on Ω.

For spacetime operators, the following definition is relevant.

Definition 3.2 (Symmetric hyperbolic operator (Benzoni-Gavage and Serre 2007, Def. 1.2))**.** Let $\Omega \subset \mathbb{R}^d$ be an open set and define $\Omega_T \coloneqq (0,T) \times \Omega$ for $T > 0$. Let the first-order operator $\mathcal{L} : L^2(\Omega_T) \to \mathcal{D}(\Omega_T)'$ be defined by

$$\mathcal{L}\boldsymbol{v} \coloneqq \partial_t \boldsymbol{v} + \sum_{i=1}^{d} A_i \partial_i \boldsymbol{v} + B\boldsymbol{v}, \tag{3.3}$$

where $A_i, B : \Omega \to \mathbb{R}^{m\times m}$ are two real-valued matrix fields over Ω_T such that $A_i \in W^{1,\infty}(\Omega_T)^{m\times m}$ and $B \in L^\infty(\Omega_T)^{m\times m}$. The operator $\mathcal{L}$ is said to be *symmetric hyperbolic* if $A_i = A_i^\intercal$ a.e. on Ω_T.

Throughout this chapter, $\mathcal{A}$ denotes a spatial operator given by (3.2) and $\mathcal{L}$ denotes a spacetime operator given by (3.3).

Remark 3.3. The *graph space* of $\mathcal{A}$ is defined as

$$H^1_{\mathcal{A}}(\Omega) \coloneqq \{\boldsymbol{v} \in L^2(\Omega) \mid \mathcal{A}\boldsymbol{v} \in L^2(\Omega)\},$$

and is equipped with the usual scalar product $(\cdot,\cdot)_{H^1_{\mathcal{A}}}$ and graph norm $\|\cdot\|_{H^1_{\mathcal{A}}}$ (Antonić and Burazin 2009). This definition includes familiar spaces like $H^1 \coloneqq H^1_\nabla$, H^1_{div} and H^1_{rot}.

Remark 3.4. If $\mathcal{A}$ is a Friedrichs operator, then $\mathcal{L}$ is both a symmetric hyperbolic and Friedrichs operator. However, in general, a Friedrichs operator is not symmetric hyperbolic. Examples include the heat equation (Antonić et al. 2013), and the Tricomi equation, an equation of mixed type (elliptic-hyperbolic) with links to the modeling of transonic flow (Friedrichs 1958).

Remark 3.5. The name of Friedrichs is linked to the study of both symmetric hyperbolic and symmetric positive systems (Friedrichs 1954, 1958). His investigation of the (I)BVP for symmetric positive systems was motivated by the study of the Tricomi equation.

Remark 3.6 ((Jensen 2005, § 2.1)). Beware that a Friedrichs operator $\mathcal{A}$ is not necessarily symmetric. In fact, if $B + B^\intercal = \sum_{i=1}^d \partial_i A_i$, then $(\mathcal{A}\boldsymbol{v}, \boldsymbol{w})_{L^2(\Omega)} = -(\boldsymbol{v}, \mathcal{A}\boldsymbol{w})_{L^2(\Omega)}$ for $\boldsymbol{v},\boldsymbol{w} \in \mathcal{C}_0^\infty(\Omega)$.

The *characteristic matrix* of the spacetime operator $\mathcal{L}$ is formally defined as the following matrix-valued field (Benzoni-Gavage and Serre 2007, Chap. 9)

$$A(t,\boldsymbol{x},\boldsymbol{n}) \coloneqq \sum_{i=1}^{d} n_i A_i(t,\boldsymbol{x}), \tag{3.4}$$

where $\boldsymbol{n} \in \mathbb{S}^{d-1}$. The hyperbolic nature of $\mathcal{L}$ is fully defined by the properties of $A(\boldsymbol{n})$, without consideration for its zeroth-order term B. The zeroth-order term, if defined by a sufficiently smooth matrix B, cannot influence strong well-posedness, i.e. well-posedness in $\mathcal{C}([0,T];X)$ where X is a Banach space, which is the sole concern of this chapter. (Note, however, that B can influence weaker well-posedness, such as $\mathcal{S} \to \mathcal{S}'$, see (Benzoni-Gavage and Serre 2007, Chap. 1) for a presentation of the link between hyperbolicity and well-posedness of the free space constant coefficient Cauchy problem.) The characteristic matrix is also of primary importance for the study of the initial boundary value problem, see Section 3.2.

Remark 3.7. A constant-coefficient symmetric hyperbolic operator $\mathcal{L}$ is *hyperbolic* in the sense that its characteristic matrix $A(\boldsymbol{n}) \coloneqq \sum_{i=1}^d n_i A_i$ is uniformly diagonalizable for $\boldsymbol{n} \in \mathbb{S}^{d-1}$ (Benzoni-Gavage and Serre 2007, Thm. 1.4).

The interest of the introduced formulation lies in its suitability for the study of the following Cauchy problem

$$\partial_t \boldsymbol{v} + \mathcal{A}\boldsymbol{v} = \boldsymbol{f} \quad \text{on } \Omega_T, \tag{3.5}$$

where the spatial operator $\mathcal{A}$ is defined by (3.2). We distinguish between the initial value problem (IVP), obtained for $\Omega = \mathbb{R}^d$, and the initial boundary value problem (IBVP), obtained when Ω is an open bounded set strictly included in $\mathbb{R}^d$. Note that the IBVP (3.5) can also be seen as the boundary value problem (BVP)

$$\mathcal{L}\boldsymbol{v} = \boldsymbol{f} \quad \text{on } \Omega_T, \tag{3.6}$$

with $\mathcal{L}$ defined by (3.3).

Remark 3.8. If $\mathcal{L}$ is a symmetric hyperbolic operator, then there is $\lambda > 0$ such that $\mathcal{A} + \lambda\mathcal{I}$ is a Friedrichs operator. This is useful to recast the Cauchy problem (3.5) as $\partial_t\tilde{\boldsymbol{v}} + (\mathcal{A}+\lambda\mathcal{I})\tilde{\boldsymbol{v}} = e^{-\lambda t}\boldsymbol{f}$ by defining $\tilde{\boldsymbol{v}} \coloneqq e^{-\lambda t}\boldsymbol{v}$. (Burazin and Erceg 2016)

Proofs of well-posedness for symmetric hyperbolic systems in both free and bounded space crucially hinge on the derivation of a priori energy estimates, which are also useful in numerical analysis, see Chapter 5. Let us assume that Ω is a bounded Lipschitz open set and that A_i and B are smooth. An integration by parts with $\boldsymbol{v} \in \mathcal{C}^1(\overline{\Omega})$ yields, using the symmetry of each matrix A_i,

$$(\mathcal{A}\boldsymbol{v}, \boldsymbol{v})_{L^2(\Omega)} = \frac{1}{2}(C\boldsymbol{v}, \boldsymbol{v})_{L^2(\Omega)} + \frac{1}{2}(A(\boldsymbol{n})\boldsymbol{v}, \boldsymbol{v})_{L^2(\partial\Omega)}, \tag{3.7}$$

where the symmetric matrix C is

$$C \coloneqq B + B^\intercal - \sum_{i=1}^{d} \partial_i A_i. \tag{3.8}$$

This identity enables to derive a so-called continuous energy balance that expresses the evolution of energy in the domain Ω

$$\begin{aligned} \frac{1}{2}\frac{\mathrm{d}}{\mathrm{d}t}\|\boldsymbol{v}(t)\|^2_{L^2(\Omega)} &= -(\mathcal{A}\boldsymbol{v}, \boldsymbol{v})_{L^2(\Omega)} + (\boldsymbol{f}, \boldsymbol{v})_{L^2(\Omega)} \\ &= -\frac{1}{2}(C\boldsymbol{v}, \boldsymbol{v})_{L^2(\Omega)} - \frac{1}{2}(A(\boldsymbol{n})\boldsymbol{v}, \boldsymbol{v})_{L^2(\partial\Omega)} + (\boldsymbol{f}, \boldsymbol{v})_{L^2(\Omega)}, \end{aligned} \tag{3.9}$$

where

$$\|\boldsymbol{v}(t)\|^2_{L^2(\Omega)} \coloneqq \int_\Omega |\boldsymbol{v}(t,\boldsymbol{x})|^2 \,\mathrm{d}\boldsymbol{x} = \int_\Omega |\tilde{p}(t,\boldsymbol{x})|^2 \,\mathrm{d}\boldsymbol{x} + \int_\Omega |\boldsymbol{u}(t,\boldsymbol{x})|^2 \,\mathrm{d}\boldsymbol{x}. \tag{3.10}$$

The continuous energy balance (3.9) can be formalized as the following a priori estimate.

Proposition 3.9 (A priori energy estimate)**.** *Let $\Omega = \mathbb{R}^d$. Assume $\mathcal{L}$ is a symmetric hyperbolic operator such that A_i and B belong to $\mathcal{C}^\infty(\Omega_T)$. There is $\kappa_0 \geq 0$ such that for every $T > 0$, $\kappa \geq \kappa_0$, and $\boldsymbol{v} \in \mathcal{C}([0,T]; H^1(\Omega)) \cap \mathcal{C}^1([0,T]; L^2(\Omega))$, the following a priori estimate holds*

$$\max_{\tau\in[0,T]} e^{-\frac{\kappa}{2}\tau}\|\boldsymbol{v}(\tau)\|_{L^2(\Omega)} \leq \|\boldsymbol{v}(0)\|_{L^2(\Omega)} + 2\int_0^T e^{-\frac{\kappa}{2}\tau}\|\mathcal{L}\boldsymbol{v}(\tau)\|_{L^2(\Omega)}\mathrm{d}\tau. \tag{3.11}$$

Proof. Let $\boldsymbol{v} \in \mathcal{C}^1([0,T]; \mathcal{C}^\infty_0(\Omega))$, $T > 0$, and define $\boldsymbol{f} \coloneqq \mathcal{L}\boldsymbol{v}$. For any $\kappa \geq 0$, the following continuous energy balance holds

$$\frac{\mathrm{d}}{\mathrm{d}t}\left(e^{-\kappa t}\|\boldsymbol{v}(t)\|^2_{L^2(\Omega)}\right) = -e^{-\kappa t}((C + \kappa\mathbb{I}_{n+1})\boldsymbol{v}, \boldsymbol{v})_{L^2(\Omega)} + 2e^{-\kappa t}(\boldsymbol{f}, \boldsymbol{v})_{L^2(\Omega)}.$$

Let $\kappa_0 = \min_{x\in\Omega} \lambda_{\min}(C)$, where $\lambda_{\min}(C)$ is the minimum eigenvalue of C, so that $C+\kappa\mathbb{I}_{n+1} \geq 0$. For $\kappa \geq \kappa_0$,

$$\frac{\mathrm{d}}{\mathrm{d}t}\left(e^{-\kappa t}\|\boldsymbol{v}(t)\|^2_{L^2(\Omega)}\right) \leq 2e^{-\kappa t}(\boldsymbol{f},\boldsymbol{v})_{L^2(\Omega)},$$

and integrating over $(0,t)$ with $0 \leq t \leq T$ gives

$$e^{-\kappa t}\|\boldsymbol{v}(t)\|^2_{L^2(\Omega)} \leq \|\boldsymbol{v}(0)\|^2_{L^2(\Omega)} + 2\int_0^t e^{-\kappa\tau}\|\boldsymbol{f}(\tau)\|_{L^2(\Omega)}\|\boldsymbol{v}(\tau)\|_{L^2(\Omega)}\mathrm{d}\tau,$$

using the Cauchy–Schwarz inequality in $L^2(\Omega)$. Following for instance (Alinhac 2009, § 6.1), we deduce

$$\begin{aligned}\max_{\tau\in[0,T]} e^{-\kappa\tau}\|\boldsymbol{v}(\tau)\|^2_{L^2(\Omega)} &\leq \|\boldsymbol{v}(0)\|^2_{L^2(\Omega)} + 2\int_0^T e^{-\kappa\tau}\|\boldsymbol{f}(\tau)\|_{L^2(\Omega)}\|\boldsymbol{v}(\tau)\|_{L^2(\Omega)}\mathrm{d}\tau \\ &\leq \|\boldsymbol{v}(0)\|^2_{L^2(\Omega)} + 2\max_{\tau\in[0,T]} e^{-\frac{\kappa}{2}\tau}\|\boldsymbol{v}(\tau)\|_{L^2(\Omega)}\int_0^T e^{-\frac{\kappa}{2}\tau}\|\boldsymbol{f}(\tau)\|_{L^2(\Omega)}\mathrm{d}\tau,\end{aligned}$$

from which the claimed estimate follows, after a density argument. □

The strong well-posedness of the IVP is given by the following result.

Theorem 3.10 (Free-space well-posedness)**.** *Let $\Omega = \mathbb{R}^d$. Assume $\mathcal{L}$ is a symmetric hyperbolic operator with $A_i, B \in \mathcal{C}^\infty(\Omega_T)$. For every $T > 0$, $f \in L^2(\Omega_T)$, and $\boldsymbol{v}_0 \in L^2(\Omega)$, there is a unique $\boldsymbol{v} \in \mathcal{C}([0,T];L^2(\Omega))$ solving (3.6) with $\boldsymbol{v}(t=0) = \boldsymbol{v}_0$. Additionally, there is $C > 0$ such that*

$$\max_{\tau\in[0,T]} \|\boldsymbol{v}(\tau)\|^2_{L^2(\Omega)} \leq C\left(\|\boldsymbol{v}_0\|^2_{L^2(\Omega)} + \int_0^T \|\boldsymbol{f}(\tau)\|^2_{L^2(\Omega)}\,\mathrm{d}\tau\right).$$

Proof (Sketch). A stronger version of this result, in $H^s(\mathbb{R}^n)$, is proven in (Benzoni-Gavage and Serre 2007, Thm. 2.6). The first step of the proof is to extend the a priori estimate (3.9) to $\boldsymbol{v} \in \mathcal{C}([0,T];H^{s+1}(\Omega)) \cap \mathcal{C}^1([0,T];H^s(\Omega))$ for any $s \in \mathbb{R}$, which can be done using pseudo-differential calculus (Benzoni-Gavage and Serre 2007, Thm. 2.1). Let $s \in \mathbb{R}$. Uniqueness in $\mathcal{C}([0,T];H^s(\Omega))$ follows directly from the a priori estimate. Existence in $\mathcal{C}([0,T];H^{s-1})$ relies on the integration by parts formula: $\forall\varphi,\psi \in \mathcal{C}^\infty_0([0,T]\times\Omega)$,

$$(\varphi,\tilde{\mathcal{L}}\psi)_{L^2((0,T)\times\Omega)} = (\mathcal{L}\varphi,\psi)_{L^2((0,T)\times\Omega)} - (\varphi(T),\psi(T))_{L^2(\Omega)} + (\varphi(0),\psi(0))_{L^2(\Omega)},$$

where the formal adjoint operator $\tilde{\mathcal{L}}$ is defined as $\tilde{\mathcal{L}}\boldsymbol{v} \coloneqq -\partial_t\boldsymbol{v} - A_i^\intercal\partial_i\boldsymbol{v} + (B^\intercal - \partial_i A_i)\,\boldsymbol{v}$. By using the a priori estimate on $\|\psi(t)\|_{H^{-s}(\Omega)}$, it can be shown that the linear form

$$\tilde{\mathcal{L}}\psi \mapsto \langle\boldsymbol{f},\psi\rangle_{L^2(0,T;H^s),L^2(0,T;H^{-s})} + \langle\boldsymbol{v}_0,\psi(0)\rangle_{H^s(\Omega),H^{-s}(\Omega)}$$

is both uniquely defined and bounded over $\tilde{\mathcal{L}}(\mathcal{C}^\infty_0([0,T]\times\Omega) \cap \{\psi \,|\, \psi(T) = 0\})$, so that it can be extended to a bounded linear form on $L^2(0,T;H^s(\Omega))$ by Hahn-Banach. The Riesz representation theorem and distribution arguments yield a weak solution $\boldsymbol{v}$ in $\mathcal{C}([0,T];H^{s-1})$. A weak=strong argument, relying again on the a priori estimate in H^s, shows that the solution is actually in $\mathcal{C}([0,T];H^s)$. □

3.1.2 Application to the linearized Euler equations

To recast the LEEs into a symmetric hyperbolic system, it suffices to define the perturbation (column) vector as

$$\boldsymbol{v} \coloneqq \begin{pmatrix} \boldsymbol{u} \\ \tilde{p} \end{pmatrix} \in \mathbb{R}^{d+1}, \tag{3.12}$$

which is homogeneous to a velocity. Using this state vector, the LEEs (3.1) read (3.5) where the characteristic matrix is given by

$$A(\boldsymbol{n}) = \begin{pmatrix} (\boldsymbol{u_0}\cdot\boldsymbol{n})\mathbb{I}_d & c_0\boldsymbol{n} \\ c_0\boldsymbol{n}^\intercal & \boldsymbol{u_0}\cdot\boldsymbol{n} \end{pmatrix} \tag{3.13}$$

and

$$B = \begin{pmatrix} \nabla\boldsymbol{u_0} & \frac{1}{c_0}\nabla\boldsymbol{u_0}\cdot\boldsymbol{u_0} \\ \boldsymbol{0_n}^\intercal & \gamma\nabla\cdot\boldsymbol{u_0} \end{pmatrix}, \tag{3.14}$$

where $\mathbb{I}_d$ denotes the $d\times d$ identity matrix. The symmetric amplification matrix (3.8) reads

$$C = \begin{pmatrix} \nabla\boldsymbol{u_0} + \nabla^\intercal\boldsymbol{u_0} - (\nabla\cdot\boldsymbol{u_0})\mathbb{I}_n & \frac{1}{c_0}\nabla\boldsymbol{u_0}\cdot\boldsymbol{u_0} \\ \frac{1}{c_0}\boldsymbol{u_0}\cdot\nabla^\intercal\boldsymbol{u_0} & (2\gamma-1)\nabla\cdot\boldsymbol{u_0} \end{pmatrix}.$$

The right-hand side of the energy balance (3.9) is

$$(C(\boldsymbol{u_0})\boldsymbol{v},\boldsymbol{v})_{\mathbb{R}^{n+1}} = (\nabla\cdot\boldsymbol{u_0})\left[(2\gamma-1)\tilde{p}^2 - |\boldsymbol{u}|^2\right] + 2\boldsymbol{u}\cdot\nabla\boldsymbol{u_0}\cdot\left(\boldsymbol{u} + \frac{1}{c_0}\tilde{p}\,\boldsymbol{u_0}\right) \tag{3.15}$$

$$(A(\boldsymbol{n})\boldsymbol{v},\boldsymbol{v})_{\mathbb{R}^{n+1}} = (\boldsymbol{u_0}\cdot\boldsymbol{n})\left[\tilde{p}^2 + |\boldsymbol{u}|^2\right] + 2c_0\,\tilde{p}(\boldsymbol{u}\cdot\boldsymbol{n}). \tag{3.16}$$

These expressions will be useful for the definition of boundary conditions in Section 3.3. Since the operator $\mathcal{L}$ thus defined is a symmetric hyperbolic operator, Theorem 3.10 gives free-space well-posedness for a smooth base flow $\boldsymbol{u_0} \in W^{1,\infty}(\Omega_T)\cap\mathcal{C}^\infty(\Omega_T)$. If the base flow is steady, Proposition 3.9 naturally suggests the following stability condition

$$\min_{x\in\Omega}\lambda_{\min}(C) \geq 0,$$

where $\lambda_{\min}(C)$ is the minimum eigenvalue of C: this turns out to be a stringent condition on the base flow $\boldsymbol{u_0}$ that is typically not satisfied in applications. For example, it holds for a constant flow but fails for a Poiseuille flow. More relevant stability conditions can be obtained not by energy analysis but by normal mode analysis, also known in the literature as a Briggs-Bers or Kreiss analysis, see e.g. (Brambley 2009; Joubert 2010).

This section ends on Proposition 3.11 below, which gives the spectrum of the characteristic matrix. It implies that the symmetric hyperbolic operator $\mathcal{L}$ obtained from the LEEs (3.1) using the state (3.12) is also constantly hyperbolic (Benzoni-Gavage and Serre 2007, Def. 1.2) (it is however *not* strictly hyperbolic since $\boldsymbol{u_0}\cdot\boldsymbol{n}$ is not a simple eigenvalue).

Proposition 3.11. *Assume $c_0 \neq 0$ and $\boldsymbol{n} \neq \boldsymbol{0}$. The real symmetric matrix (3.13) can be diagonalized as*

$$A(\boldsymbol{n}) = P(\boldsymbol{n})\Lambda(\boldsymbol{n})P(\boldsymbol{n})^{-1},$$

with

$$\Lambda(\boldsymbol{n}) \coloneqq \operatorname{diag}(\boldsymbol{u_0}\cdot\boldsymbol{n} + c_0, \boldsymbol{u_0}\cdot\boldsymbol{n} - c_0, \boldsymbol{u_0}\cdot\boldsymbol{n}, \cdots, \boldsymbol{u_0}\cdot\boldsymbol{n})$$

and change of basis matrix P given by

$$P(\boldsymbol{n}) \coloneqq \begin{bmatrix} 1/\sqrt{2}\,\boldsymbol{n} & -1/\sqrt{2}\,\boldsymbol{n} & \boldsymbol{t}_1 & \cdots & \boldsymbol{t}_{d-1} \\ 1/\sqrt{2} & 1/\sqrt{2} & 0 & \cdots & 0 \end{bmatrix} \tag{3.17}$$

with $(\boldsymbol{t}_i)_{i\in[\![1,d-1]\!]}$ an orthonormal basis of the hyperplane of $\mathbb{R}^d$ defined by $\{\boldsymbol{t}\in\mathbb{R}^d \mid \boldsymbol{t}\cdot\boldsymbol{n}=0\}$. In particular, the multiplicity of each eigenvalue of $A(\boldsymbol{n})$ remains constant for any $\boldsymbol{n}\in\mathbb{S}^{d-1}$. Moreover, if $|\boldsymbol{n}|=1$, the matrix $P(\boldsymbol{n})$ is orthogonal, i.e. $P(\boldsymbol{n})^\intercal P(\boldsymbol{n}) = \mathbb{I}_{d+1}$.

Remark 3.12. The positive and negative parts of the characteristic matrix $A(\boldsymbol{n})$ are defined as

$$A(\boldsymbol{n})^\oplus \coloneqq P(\boldsymbol{n})\Lambda(\boldsymbol{n})^\oplus P(\boldsymbol{n})^{-1} \quad \text{and} \quad A(\boldsymbol{n})^\ominus \coloneqq P(\boldsymbol{n})\Lambda(\boldsymbol{n})^\ominus P(\boldsymbol{n})^{-1},$$

where $\Lambda(\boldsymbol{n})^\oplus \coloneqq \max(\Lambda(\boldsymbol{n}),0)$ and $\Lambda(\boldsymbol{n})^\ominus \coloneqq -\min(\Lambda(\boldsymbol{n}),0)$ (component-wise) so that

$$A(\boldsymbol{n}) = A(\boldsymbol{n})^\oplus - A(\boldsymbol{n})^\ominus.$$

These quantities are useful to build approximate nonreflecting boundary conditions for numerical simulations, see Example 3.17 and Chapter 6. Assuming $|\boldsymbol{n}|=1$ so that $P(\boldsymbol{n})$ is orthogonal, we have

$$\begin{aligned} A(\boldsymbol{n})^\oplus = {} & \frac{(\boldsymbol{u_0}\cdot\boldsymbol{n}+c_0)^\oplus}{2}\begin{bmatrix} \boldsymbol{n}\otimes\boldsymbol{n} & \boldsymbol{n} \\ \boldsymbol{n}^\intercal & 1 \end{bmatrix} + \frac{(\boldsymbol{u_0}\cdot\boldsymbol{n}-c_0)^\oplus}{2}\begin{bmatrix} \boldsymbol{n}\otimes\boldsymbol{n} & -\boldsymbol{n} \\ -\boldsymbol{n}^\intercal & 1 \end{bmatrix} \\ & + (\boldsymbol{u_0}\cdot\boldsymbol{n})^\oplus \begin{bmatrix} \sum_{i=1}^{d-1}\boldsymbol{t}_i\otimes\boldsymbol{t}_i & \boldsymbol{0_d} \\ \boldsymbol{0_d}^\intercal & 0 \end{bmatrix}, \end{aligned}$$

where the matrix $\sum_{i=1}^{d-1}\boldsymbol{t}_i\otimes\boldsymbol{t}_i$ satisfies

$$\mathbb{I}_d = \boldsymbol{n}\otimes\boldsymbol{n} + \sum_{i=1}^{d-1}\boldsymbol{t}_i\otimes\boldsymbol{t}_i.$$

The corresponding decomposition of $\boldsymbol{u}$,

$$\boldsymbol{u} = (\boldsymbol{n}\otimes\boldsymbol{n})\cdot\boldsymbol{u} + \left(\sum_{i=1}^{d-1}\boldsymbol{t}_i\otimes\boldsymbol{t}_i\right)\cdot\boldsymbol{u} = (\boldsymbol{u}\cdot\boldsymbol{n})\boldsymbol{n} + \boldsymbol{u}_t,$$

enables to write $A(\boldsymbol{n})^\oplus\boldsymbol{v}$ as

$$\begin{aligned} A(\boldsymbol{n})^\oplus\boldsymbol{v} = {} & \frac{(\boldsymbol{u_0}\cdot\boldsymbol{n}+c_0)^\oplus}{2}\begin{bmatrix} (\boldsymbol{u}\cdot\boldsymbol{n})\boldsymbol{n}+\tilde{p}\boldsymbol{n} \\ \boldsymbol{u}\cdot\boldsymbol{n}+\tilde{p} \end{bmatrix} + \frac{(\boldsymbol{u_0}\cdot\boldsymbol{n}-c_0)^\oplus}{2}\begin{bmatrix} (\boldsymbol{u}\cdot\boldsymbol{n})\boldsymbol{n}-\tilde{p}\boldsymbol{n} \\ -\boldsymbol{u}\cdot\boldsymbol{n}+\tilde{p} \end{bmatrix} \\ & + (\boldsymbol{u_0}\cdot\boldsymbol{n})^\oplus\begin{bmatrix} \boldsymbol{u}_t \\ 0 \end{bmatrix}. \end{aligned}$$

The expressions of $A(\boldsymbol{n})^\ominus$ and $A(\boldsymbol{n})^\ominus\boldsymbol{v}$ is obtained by substituting "$\ominus$" for "$\oplus$" in the above expressions. If $\boldsymbol{n}$ is the outward unit normal, $\dim\ker A(\boldsymbol{n})^\ominus$ is the number of *outgoing* characteristics, i.e. the number of *nonnegative* eigenvalues of $A(\boldsymbol{n})$. *Incoming* characteristics are associated with the *negative* eigenvalues of $A(\boldsymbol{n})$.

Remark 3.13. The same conclusions hold for the matrix associated with the spacetime operator $\mathcal{L}$

$$L(t,\boldsymbol{x},n_t,\boldsymbol{n}) = n_t\mathbb{I}_{d+1} + \sum_{i=1}^{d} n_i A_i(t,\boldsymbol{x}),$$

where $(n_t,\boldsymbol{n})\in\mathbb{S}^d$, by substituting $\boldsymbol{u_0}\cdot\boldsymbol{n}$ by "$n_t+\boldsymbol{u_0}\cdot\boldsymbol{n}$".

Proof. The result follows from an elementary computation of the spectrum. Let $\boldsymbol{v}$ be such that $A(\boldsymbol{n})\boldsymbol{v} = \lambda\boldsymbol{v}$, i.e.

$$((\boldsymbol{u_0}\cdot\boldsymbol{n}) - \lambda)\,\boldsymbol{u} + c_0\tilde{p}\,\boldsymbol{n} = 0,\ c_0\boldsymbol{u}\cdot\boldsymbol{n} + ((\boldsymbol{u_0}\cdot\boldsymbol{n}) - \lambda)\,\tilde{p} = 0.$$

We distinguish two cases (acoustic and hydrodynamic modes).

($\lambda = \boldsymbol{u_0}\cdot\boldsymbol{n}$) Then $\tilde{p}\,\boldsymbol{n} = 0$ and $\boldsymbol{u}\cdot\boldsymbol{n} = 0$ and the corresponding eigenspace is $(d-1)$-dimensional.

($\lambda \neq \boldsymbol{u_0}\cdot\boldsymbol{n}$) Injecting the expression of $\tilde{p}$ from the second line into the first one yields

$$\boldsymbol{u} = \left(\frac{c_0}{(\boldsymbol{u_0}\cdot\boldsymbol{n}) - \lambda}\right)^2 (\boldsymbol{u}\cdot\boldsymbol{n})\boldsymbol{n},\ \tilde{p} = -\frac{c_0}{(\boldsymbol{u_0}\cdot\boldsymbol{n}) - \lambda}\boldsymbol{u}\cdot\boldsymbol{n},$$

from which we deduce that $\boldsymbol{u} \propto \boldsymbol{n}$, and λ is an eigenvalue iff $\boldsymbol{u}\cdot\boldsymbol{n} \neq 0$. There are now only two cases to distinguish to get the last two one-dimensional eigenspaces.

- ($\lambda = \boldsymbol{u_0}\cdot\boldsymbol{n} - c_0$) Then $\tilde{p} = -\boldsymbol{u}\cdot\boldsymbol{n}$ and $\boldsymbol{u} = -\tilde{p}\boldsymbol{n}$.
- ($\lambda = \boldsymbol{u_0}\cdot\boldsymbol{n} + c_0$) Then $\tilde{p} = \boldsymbol{u}\cdot\boldsymbol{n}$ and $\boldsymbol{u} = \tilde{p}\boldsymbol{n}$.

Let us denote by $\boldsymbol{\psi_j}$ the columns of the change of basis matrix (3.17), i.e. $P = [\boldsymbol{\psi_1}\cdots\boldsymbol{\psi_{n+1}}]$. If $|\boldsymbol{n}| = 1$, it is straightforward to see that, by construction, $P^\intercal P = [(\boldsymbol{\psi_i}, \boldsymbol{\psi_j})]_{i,j} = \mathbb{I}_{d+1}$. □

3.2 Literature review on Friedrichs BVPs and IBVPs

This section reviews available results on the well-posedness of the BVP and IBVP for Friedrichs systems with an emphasis on the formulation of boundary conditions, in preparation for Sections 3.3 and 3.4. Well-posedness of the IBVP (3.5) also relies on the derivation of a priori energy estimates, but it presents significant additional difficulties compared to the free space case covered in Section 3.1, let us mention three that are encountered with the LEEs (as with many other problems arising from fluid mechanics): lack of smoothness of $\partial\Omega$ (results on Lipschitz domains are scarce); boundary of varying multiplicity (i.e. $\dim\ker A(\boldsymbol{n})$ varies along some components of $\partial\Omega$); characteristic boundary (i.e. $\dim\ker A(\boldsymbol{n}) \neq 0$ on parts of $\partial\Omega$). (Note that the three aforementioned difficulties are amplified should the hyperbolic system at hand be not symmetric nor symmetrizable: in such cases, the well-posedness theory relies on proving the existence of so-called symmetrizers (Benzoni-Gavage and Serre 2007, Chap. 9).)

An important question is the definition of a class of "admissible" boundary conditions, to which various answers have been provided. As a preparation for the literature review, let us intuitively introduce what an "admissible" boundary condition could look like, staying in the energy approach initiated in Section 3.1. The first constraint is obtained by generalizing Proposition 3.9 to a bounded set Ω.

Proposition 3.14 (A priori energy estimate)**.** *Let $\Omega \subset \mathbb{R}^d$ be a bounded Lipschitz open set. Assume $\mathcal{L}$ is a symmetric hyperbolic operator such that A_i and B belong to $\mathcal{C}^\infty(\Omega_T)$. If for every $T > 0$ and $\boldsymbol{v} \in \mathcal{C}([0,T]; H^1(\Omega))$*

$$\int_0^T (A(\boldsymbol{n})\boldsymbol{v}, \boldsymbol{v})_{L^2(\partial\Omega)}\mathrm{d}\tau \geq 0, \tag{3.18}$$

then there is $\kappa_0 \geq 0$ such that for every $T > 0$, $\kappa \geq \kappa_0$ and $\boldsymbol{v} \in \mathcal{C}([0,T]; H^1(\Omega)) \cap \mathcal{C}^1([0,T]; L^2(\Omega))$ the a priori estimate (3.11) holds.

Proof. Integrating the continuous energy balance (3.9) leads to

$$e^{-\kappa t}\|\boldsymbol{v}(t)\|^2_{L^2(\Omega)} \leq \|\boldsymbol{v}(0)\|^2_{L^2(\Omega)} + 2\int_0^t e^{-\kappa\tau}(\boldsymbol{f},\boldsymbol{v})_{L^2(\Omega)}\mathrm{d}\tau - \int_0^t e^{-\kappa\tau}(A(\boldsymbol{n})\boldsymbol{v},\boldsymbol{v})_{L^2(\partial\Omega)}\mathrm{d}\tau,$$

so that the conclusion is immediate in view of the proof of Proposition 3.9. □

Condition (3.18) is known as a *positivity*, *dissipativity*, or *passivity* condition. The second constraint is based on elementary considerations from the theory of characteristics: the number of scalar boundary conditions must equal the number of incoming characteristics (Benzoni-Gavage and Serre 2007, § 4.1.1). These two conditions loosely defines *maximal positive* boundary conditions, one of the cornerstones of the theory of Friedrichs systems. There are two variants of the theory that differ from their formulation of the boundary conditions. In the classical theory, boundary conditions are explicitly defined by relying on properties of traces in the graph space $H^1_{\mathcal{L}}(\Omega)$ (Antonić and Burazin 2009). By contrast, in the abstract theory, boundary conditions are implicitly defined through the definition of a subspace $V \subset H^1_{\mathcal{L}}(\Omega)$ in which the solution is sought (Ern et al. 2007).

3.2.1 Classical theory

In the classical theory, three classes of boundary conditions are prevalent: maximal positive, maximal dissipative, and Friedrichs-admissible. Each class is presented below, along with the corresponding well-posedness result. (See also the literature review (Jensen 2005, § 2.6).)

Maximal positive Rauch (Rauch 1985) considers the boundary condition (we omit t for clarity)

$$\boldsymbol{v}(\boldsymbol{x}) \in N(\boldsymbol{x}) \quad \text{a.e. in } \partial\Omega, \tag{3.19}$$

where $N(\boldsymbol{x}) \subset \mathbb{R}^m$ is a linear subspace and Ω is a bounded open set lying on one side of its $\mathcal{C}^1$ boundary. Condition (3.19) constrains $m - \dim N$ components of $\boldsymbol{v}$. Well-posedness in $\mathcal{C}([0,T];L^2(\Omega))$ of the IBVP (3.5) with $\mathcal{L}$ symmetric hyperbolic is shown under the assumptions that the boundary condition be *maximal positive*, i.e.

$$\begin{cases} \forall \boldsymbol{v} \in N, \quad (A(\boldsymbol{n})\boldsymbol{v},\boldsymbol{v})_{\mathbb{R}^m} \geq 0 \quad \text{for a.e. } x \in \partial\Omega \\ \dim N = \#\text{ of nonnegative eigenvalues of } A(\boldsymbol{n}) \text{ counting multiplicity} \\ \qquad (= \#\text{ of outgoing characteristics}) \\ \qquad (= \dim\ker A(\boldsymbol{n})^{\ominus}), \end{cases} \tag{3.20}$$

and that $\partial\Omega$ be of constant multiplicity, i.e. $\dim\ker A(\boldsymbol{n})$ remains constant on each component of $\partial\Omega$. Note that $\dim N$ (resp. $m - \dim N$) is the number of outgoing (resp. incoming) characteristics and $\ker A(\boldsymbol{n}) \subset N$. In a later work (Rauch 1994), the constant multiplicity hypothesis is loosened: $\dim\ker A(\boldsymbol{n})$ must be constant on the two components $\partial\Omega_1$ and $\partial\Omega_2$ of $\partial\Omega\backslash\Gamma$, where Γ is a $d-2$ dimensional $\mathcal{C}^1$ submanifold of $\partial\Omega$. Furthermore,

$$N(\boldsymbol{x}) = \begin{cases} N_{\text{small}} & \boldsymbol{x} \in \Omega_1 \\ N_{\text{big}} & \boldsymbol{x} \in \Omega_2 \end{cases} \quad \text{with} \quad N_{\text{small}} \subset N_{\text{big}}. \tag{3.21}$$

This requirement prevents the two boundary conditions, namely $\boldsymbol{v} \in N_{\text{small}}$ on $\partial\Omega_1$ and $\boldsymbol{v} \in N_{\text{big}}$ on $\partial\Omega_2$, from being unrelated. It has implication for the LEEs, see Section 3.3.

Remark 3.15. Merely imposing maximal positive boundary conditions (3.20) on each part of the boundary $\partial\Omega$ is not enough for well-posedness (Rauch 1994).

Remark 3.16. The definition (3.20) of maximal positive boundary condition is equivalent to (Antonić and Burazin 2010, Thm. 2)

$$\begin{cases} \forall \boldsymbol{v} \in N, \quad (A(\boldsymbol{n})\boldsymbol{v}, \boldsymbol{v})_{\mathbb{R}^m} \geq 0 & \text{for a.e. } x \in \partial\Omega \\ \forall \boldsymbol{v} \in (A(\boldsymbol{n})N)^{\perp}, \quad (A(\boldsymbol{n})\boldsymbol{v}, \boldsymbol{v})_{\mathbb{R}^m} \leq 0 & \text{for a.e. } x \in \partial\Omega. \end{cases} \tag{3.22}$$

Maximal dissipative Defining $N \coloneqq \ker R(\boldsymbol{n})$ in (3.19,3.20) with a rectangular real-valued matrix $R(\boldsymbol{x}, \boldsymbol{n}) \in \mathbb{R}^{p\times m}$ yields a *maximal dissipative* boundary condition (Benzoni-Gavage and Serre 2007, Def. 3.2). If $R(\boldsymbol{n})$ is full rank, then p is the number of incoming characteristics. In (Benzoni-Gavage and Serre 2007, Thm. 3.2) a strong well-posedness result is obtained by generating a C_0-semigroup of contractions in the constant-coefficient half-plane case.

Friedrichs-admissible In the original work of Friedrichs (Friedrichs 1958), the boundary condition is enforced with a real-valued matrix $M(\boldsymbol{x}, \boldsymbol{n}) \in \mathbb{R}^{m\times m}$ through $N \coloneqq \ker(A(\boldsymbol{n}) - M(\boldsymbol{n}))$. The matrix $M(\boldsymbol{n})$ is said to be *Friedrichs-admissible* if

$$\begin{cases} \forall \boldsymbol{v} \in \mathbb{R}^m, \quad (M(\boldsymbol{n})\boldsymbol{v}, \boldsymbol{v})_{\mathbb{R}^m} \geq 0 \quad \text{for a.e. } x \in \partial\Omega \\ \mathbb{R}^m = \ker(A(\boldsymbol{n}) - M(\boldsymbol{n})) + \ker(A(\boldsymbol{n}) + M(\boldsymbol{n})). \end{cases} \tag{3.23}$$

Well-posedness of the BVP $\mathcal{A}\boldsymbol{v} = \boldsymbol{f}$ is shown by Jensen (Jensen 2005, Thm. 39) under technical conditions. In particular, the application $v \mapsto (A(\boldsymbol{n}) - M(\boldsymbol{n}))v_{|\partial\Omega}$ must define a bounded operator from the graph space $H^1_{\mathcal{A}}$ to some appropriate trace space. However, by contrast with Rauch (Rauch 1994), the result theoretically applies to non-smooth domains.

Equivalence between the formulations (3.20) and (3.23) has been established in (Antonić and Burazin 2010). If $M(\boldsymbol{n})$ is Friedrichs-admissible, then $N \coloneqq \ker(A(\boldsymbol{n}) - M(\boldsymbol{n}))$ is maximal positive. Conversely if N is maximal positive, then there exists a Friedrichs-admissible $M(\boldsymbol{n})$ such that $N = \ker(A(\boldsymbol{n}) - M(\boldsymbol{n}))$, which can be built using (Ern et al. 2007, Thm. 4.3). Note that in practice one encounters non Friedrichs-admissible matrices $M(\boldsymbol{n})$ such that $N = \ker(A(\boldsymbol{n}) - M(\boldsymbol{n}))$ is maximal positive: see the example below and Section 3.3.

Example 3.17 (Nonreflecting boundary conditions)**.** With an hyperbolic law, an approximate nonreflecting boundary condition is naturally obtained by choosing $M(\boldsymbol{n}) \coloneqq A(\boldsymbol{n})^{\oplus}$ and $R(\boldsymbol{n}) \coloneqq A(\boldsymbol{n}) - M(\boldsymbol{n}) = -A(\boldsymbol{n})^{\ominus}$, which constrains only the incoming characteristics and is used in the numerical application presented in Chapter 6 at the inlet and outlet. From (3.20) it defines a maximal positive boundary condition. Even though the matrix $M(\boldsymbol{n})$ is *not* Friedrichs-admissible in general (consider the diagonal system $A(\boldsymbol{n}) = \operatorname{diag}(1, 0, -1)$), there exists a Friedrichs-admissible matrix $\check{M}(\boldsymbol{n})$ such that $\ker R(\boldsymbol{n}) = \ker(A(\boldsymbol{n}) - \check{M}(\boldsymbol{n}))$.

3.2.2 Abstract theory

In the abstract theory, the issue of formulating admissible boundary conditions is replaced by that of finding a space $V \subset H^1_{\mathcal{A}}$ for which the BVP

$$\mathcal{A}\boldsymbol{v} = \boldsymbol{f} \in L^2(\Omega) \tag{3.24}$$

is well-posed, where $\mathcal{A}$ is a Friedrichs operator given by (3.2). The theory has been introduced in (Ern et al. 2007) by Ern, Guermond, and Caplain who gave sufficient conditions on V that are abstract analogous of (3.22). Similarly to the equivalence between (3.22,3.23) in the classical

theory, these sufficient conditions have been proven in (Antonić and Burazin 2010, Cor. 3) to be equivalent to the existence of a *bounded* boundary operator $\mathcal{M} \in \mathcal{L}(H^1_{\mathcal{L}}, H^{1'}_{\mathcal{L}})$ such that

$$\begin{cases} \forall \boldsymbol{v} \in H^1_{\mathcal{L}}, \quad \langle \mathcal{M}\boldsymbol{v}, \boldsymbol{v} \rangle_{H^{1'}_{\mathcal{L}}, H^1_{\mathcal{L}}} \geq 0 \\ H^1_{\mathcal{L}} = \ker(\mathcal{D} - \mathcal{M}) + \ker(\mathcal{D} + \mathcal{M}), \end{cases} \tag{3.25}$$

where the boundary operator $\mathcal{D} \in \mathcal{L}(H^1_{\mathcal{L}}, H^{1'}_{\mathcal{L}})$ can be expressed using the boundary integral

$$\forall \boldsymbol{v}, \boldsymbol{w} \in \mathcal{C}^\infty_0(\mathbb{R}^d),\ \langle \mathcal{D}\boldsymbol{v}, \boldsymbol{w} \rangle_{H^{1'}_{\mathcal{L}}, H^1_{\mathcal{L}}} = \int_{\partial\Omega} (A(\boldsymbol{n})\boldsymbol{v}, \boldsymbol{w})_{\mathbb{R}^m} \,\mathrm{d}\boldsymbol{x}.$$

In that case the space V is $V \coloneqq \ker(\mathcal{D} - \mathcal{M})$ and the analogy between (3.23) and (3.25) is by design. The link between the classical (3.25) and abstract (3.23) conditions can be established by also defining the boundary operator $\mathcal{M}$ through a boundary integral

$$\forall \boldsymbol{v}, \boldsymbol{w} \in \mathcal{C}^\infty_0(\mathbb{R}^d),\ \langle \mathcal{M}\boldsymbol{v}, \boldsymbol{w} \rangle_{H^{1'}_{\mathcal{L}}, H^1_{\mathcal{L}}} = \int_{\partial\Omega} (M(\boldsymbol{n})\boldsymbol{v}, \boldsymbol{w})_{\mathbb{R}^m} \,\mathrm{d}\boldsymbol{x}, \tag{3.26}$$

where $M(\boldsymbol{n})$ is a matrix as encountered in the classical theory. Practically, the well-posedness of the BVP (3.24) in $\ker(\mathcal{D} - \mathcal{M})$ is then mostly reduced to assessing whether (3.26) obeys (3.25) and defines a *bounded* operator $\mathcal{L}(H^1_{\mathcal{L}}, H^{1'}_{\mathcal{L}})$. The boundedness of the matrix $M(\boldsymbol{n})$ is not enough, and sufficient conditions have been proposed and applied to hyperbolic and elliptic PDEs (Antonić and Burazin 2011, Thm. 4) (Antonić et al. 2013, Cor. 4). For later consideration in Section 3.4, let us recall one of them.

Theorem 3.18 ((Antonić et al. 2013, Cor. 4) with (Ern et al. 2007, Thm. 4.2))**.** *Let $\mathcal{A}$ be a Friedrichs operator given by (3.2). Assume that there is a Lipschitz function $P : \overline{\Omega} \to \mathbb{R}^{m\times m}$ satisfying $\exists R \in W^{1,\infty}(\Omega)$:*

$$\forall k \in [\![1, d]\!],\ A_k P = R A_k. \tag{3.27}$$

If $M(\boldsymbol{n}) \coloneqq A(\boldsymbol{n})(\mathbb{I}_m - 2P)$ satisfies (3.23), then for $V \coloneqq \ker(\mathcal{D} - \mathcal{M})$ the operator $\mathcal{A}$ is an isomorphism from $(V, \|\cdot\|_{H^1_{\mathcal{L}}})$ to $L^2(\Omega)$ and the BVP (3.24) is well posed in V.

However, Theorem 3.18 is not suited for the IBVP (3.6) with $\mathcal{L}$ given by (3.3), since then condition (3.27) in the time direction is $P = R$, which is often too restrictive. An alternative is to consider the IBVP as the evolution problem (3.5) and apply Theorem 3.18 to the spatial operator $\mathcal{A}$. Then, $\mathcal{A}$ generates a C_0-semigroup of contractions (Burazin and Erceg 2016). The applicability of this strategy to the LEEs is discussed in Section 3.4.

Remark 3.19 (Non maximal positive conditions). Although not considered herein, we mention that boundary conditions that are not maximal positive can still lead to well-posed problems. An alternative is provided by the Kreiss-Lopatinskiĭ conditions (Benzoni-Gavage and Serre 2007, Defs. 4.1-4.2) that, intuitively, require the absence of unstable normal modes (i.e. $e^{st}\boldsymbol{v}(\boldsymbol{x})$ with $\Re(s) > 0$). Such an analysis is known under various names: normal mode analysis, Kreiss analysis (Joubert 2010, Chaps. 5–6), or also Briggs-Bers analysis in the physical community (Brambley 2009). See (Benzoni-Gavage and Serre 2007, Chap. 14) for an application to the Euler equations.

3.3 Boundary conditions for the linearized Euler equations

This section investigates the definition of maximal positive (3.20) and Friedrichs-admissible (3.23) boundary conditions for the LEEs (3.1), whose characteristic matrix (3.13) satisfies (3.16)

and Proposition 3.11. Boundary conditions are sorted below by increasing number of incoming characteristics (i.e. of negative eigenvalues of $A(\boldsymbol{n})$). Following Example 3.17, the square matrix $R \coloneqq A(\boldsymbol{n})^{\ominus}$ always defines a maximal positive boundary condition, so this case is not covered further.

(Super)sonic outflow $\boldsymbol{u_0} \cdot \boldsymbol{n} \geq c_0$

There are $d+1$ outgoing characteristics, so that no boundary conditions need to be enforced. If $\boldsymbol{u_0} \cdot \boldsymbol{n} = c_0$ (resp. $\boldsymbol{u_0} \cdot \boldsymbol{n} > c_0$), the boundary is characteristic (resp. non characteristic) since $\dim\ker A(\boldsymbol{n}) = 1$ (resp. $\dim\ker A(\boldsymbol{n}) = 0$). Given the lower bound

$$(A(\boldsymbol{n})\boldsymbol{v}, \boldsymbol{v})_{\mathbb{R}^{d+1}} \geq c_0(\tilde{p} + \boldsymbol{u} \cdot \boldsymbol{n})^2,$$

the matrix $R \coloneqq 0_{d+1}$ defines a maximal positive boundary condition and $M(\boldsymbol{n}) \coloneqq A(\boldsymbol{n})$ is Friedrichs-admissible.

Impedance boundary $\boldsymbol{u_0} \cdot \boldsymbol{n} = 0$

There are d (resp. 1) outgoing (resp. incoming) characteristics and the boundary is characteristic since $\dim\ker A(\boldsymbol{n}) = d - 1$. A maximal positive boundary condition is naturally defined by $R \in \mathbb{R}^{d+1}$ with $\dim\ker R = d$. Without loss of generality let R be given by a non-null vector

$$R \coloneqq [\boldsymbol{r}^\intercal - z],$$

with $|\boldsymbol{r}| = 1$ and $z \geq 0$. Only the positivity condition of (3.20) needs to be checked. The boundary term (3.16) is

$$(A(\boldsymbol{n})\boldsymbol{v}, \boldsymbol{v})_{\mathbb{R}^{d+1}} = 2c_0\tilde{p}\boldsymbol{u} \cdot \boldsymbol{n},$$

so that the boundary condition $\boldsymbol{r} \cdot \boldsymbol{u} = z\tilde{p}$ is maximal positive if and only if

$$\begin{cases} z = 0,\ \boldsymbol{r} = \boldsymbol{n} & \text{(Hard wall)} \\ z \neq 0,\ \boldsymbol{r} = \boldsymbol{0}d & \text{(Presure-release wall)} \\ z > 0,\ \boldsymbol{r} = \boldsymbol{n}. & \text{(Impedance wall)} \end{cases}$$

By extension, this suggests defining the impedance boundary condition as $p = \mathcal{Z}(\boldsymbol{u} \cdot \boldsymbol{n})$ where $\mathcal{Z}$ is any passive operator. Discretization of such boundary conditions is considered in Chapters 5 and 6. Each of the three cases can be written in Friedrichs' formalism by defining

$$M_{\mathrm{HW}}(\boldsymbol{n}) \coloneqq c_0 \begin{bmatrix} \zeta\boldsymbol{n} \otimes \boldsymbol{n} & \boldsymbol{n} \\ -\boldsymbol{n}^\intercal & 0 \end{bmatrix}, M_{\mathrm{PR}}(\boldsymbol{n}) \coloneqq c_0 \begin{bmatrix} 0_d & -\boldsymbol{n} \\ \boldsymbol{n}^\intercal & \zeta \end{bmatrix}, M_{\mathrm{IW1}}(\boldsymbol{n}) \coloneqq c_0 \begin{bmatrix} z\boldsymbol{n} \otimes \boldsymbol{n} & \boldsymbol{0}_n \\ \boldsymbol{0}_n & \frac{1}{z} \end{bmatrix},$$
$$M_{\mathrm{IW2}}(\boldsymbol{n}) \coloneqq c_0 \begin{bmatrix} 0_d & \boldsymbol{n} \\ -\boldsymbol{n}^\intercal & \frac{2}{z} \end{bmatrix}, \quad M_{\mathrm{IW3}}(\boldsymbol{n}) \coloneqq c_0 \begin{bmatrix} 2z\boldsymbol{n} \otimes \boldsymbol{n} & -\boldsymbol{n} \\ \boldsymbol{n}^\intercal & 0 \end{bmatrix}.$$

where $\zeta \geq 0$ is a free parameter. All of these matrices $M(\boldsymbol{n})$ are Friedrichs-admissible, except $M_{\mathrm{IW1}}(\boldsymbol{n})$ that fails the second condition of (3.23). However, the corresponding matrix $R \coloneqq A(\boldsymbol{n}) - M(\boldsymbol{n})$ always defines a maximal positive boundary condition. Similar matrices $M(\boldsymbol{n})$ can be written for the admittance boundary condition (see Chapter 5 where the same formalism is used).

As recalled in Section 1.1, one drawback of the impedance (resp. admittance) formulation is that it does not include the hard (resp. pressure release) wall case, which is reflected in the

singularities of the matrices M_{IW} above. An alternative is to use the reflection coefficient β so that the IBC writes (1.12). The corresponding matrix in Friedrichs' formalism is

$$M_{\mathrm{IW4}}(\boldsymbol{n}) = c_0 \begin{bmatrix} (1+\beta)\boldsymbol{n}\otimes\boldsymbol{n} & \beta\boldsymbol{n} \\ -\beta\boldsymbol{n}^\intercal & 1-\beta \end{bmatrix}.$$

To the best of our knowledge, this matrix was first introduced in (Ventribout 2006, § 1.3.2) where it is shown to define a maximal positive boundary condition using (3.22). Since $|\beta| \leq 1$, $M_{\mathrm{IW4}}(\boldsymbol{n})$ is also Friedrichs-admissible; the second condition of (3.23) is obtained with

$$\begin{bmatrix} \boldsymbol{u} \\ \tilde{p} \end{bmatrix} = \frac{1}{2} \underbrace{\begin{bmatrix} \boldsymbol{u}_t + (\tilde{p} + \boldsymbol{u}\cdot\boldsymbol{n} - \beta(\tilde{p} + \boldsymbol{u}\cdot\boldsymbol{n}))\,\boldsymbol{n} \\ \tilde{p} + \boldsymbol{u}\cdot\boldsymbol{n} + \beta(\tilde{p} + \boldsymbol{u}\cdot\boldsymbol{n}) \end{bmatrix}}_{\in\ker(A(\boldsymbol{n}) - M_{\mathrm{IW4}}(\boldsymbol{n}))} + \frac{1}{2} \underbrace{\begin{bmatrix} \boldsymbol{u}_t - (\tilde{p} - \boldsymbol{u}\cdot\boldsymbol{n} - \beta(\tilde{p} + \boldsymbol{u}\cdot\boldsymbol{n}))\,\boldsymbol{n} \\ \tilde{p} - \boldsymbol{u}\cdot\boldsymbol{n} - \beta(\tilde{p} + \boldsymbol{u}\cdot\boldsymbol{n}) \end{bmatrix}}_{\in\ker(A(\boldsymbol{n}) + M_{\mathrm{IW4}}(\boldsymbol{n}))}.$$

In Chapter 5, the matrix M_{IW4} is obtained using an energy method and generalized to the scattering operator $\mathcal{B}$. The numerical applications of Chapter 6 rely on this formulation.

Subsonic outflow $0 < \boldsymbol{u_0}\cdot\boldsymbol{n} < c_0$

There are d (resp. 1) outgoing (resp. incoming) characteristics and the boundary is noncharacteristic. The boundary term (3.16) satisfies

$$(A(\boldsymbol{n})\boldsymbol{v}, \boldsymbol{v})_{\mathbb{R}^{d+1}} \geq 2c_0\,\tilde{p}(\boldsymbol{u}\cdot\boldsymbol{n}),$$

hence the maximal positive and Friedrichs-admissible boundary conditions covered in the impedance wall case apply directly.

Subsonic and sonic inflow $-c_0 \leq \boldsymbol{u_0}\cdot\boldsymbol{n} < 0$

There is 1 (resp. d) outgoing (resp. incoming) characteristic, with $\dim\ker A(\boldsymbol{n}) = 0$ (resp. $\dim\ker A(\boldsymbol{n}) = 1$) in the subsonic (resp. sonic) case. One incoming characteristic is associated with the eigenvalue $\boldsymbol{u_0}\cdot\boldsymbol{n} - c_0$, which in view of the impedance wall case suggests the scalar condition $\tilde{p} = z\boldsymbol{u}\cdot\boldsymbol{n}$. (This choice is necessary to verify the jump condition (3.21).) A set of $d-1$ additional independent scalar conditions is required, let us choose $\boldsymbol{u}_t = \zeta\tilde{p}\boldsymbol{n}$. This leads to defining a full rank matrix $R \in \mathbb{R}^{d\times(d+1)}$ such that

$$R\boldsymbol{v} \coloneqq \begin{bmatrix} \tilde{p} - z\boldsymbol{u}\cdot\boldsymbol{n} \\ \boldsymbol{u}_t - \zeta\tilde{p}\boldsymbol{n} \end{bmatrix}.$$

This matrix satisfies the maximality condition of (3.20) by design. Let us check the positivity condition. The boundary term (3.16) is, for any $\boldsymbol{v} \in \ker R$,

$$(A(\boldsymbol{n})\boldsymbol{v}, \boldsymbol{v})_{\mathbb{R}^{d+1}} = c_0 \left[-|\boldsymbol{M_0}\cdot\boldsymbol{n}|(1+\zeta^2)z^2 + 2\,z - |\boldsymbol{M_0}\cdot\boldsymbol{n}|\right](\boldsymbol{u}\cdot\boldsymbol{n})^2 = c_0 P(z)(\boldsymbol{u}\cdot\boldsymbol{n})^2.$$

The positivity condition requires that $z \geq 0$. Assuming $|\zeta|$ small enough, any value of z within the two real-valued roots of P leads to a maximal positive condition. In particular, if $\zeta = 0$, then $z = 1$ is admissible. Note that the non-homogeneous variant $\tilde{p} - \boldsymbol{u}\cdot\boldsymbol{n} = \phi_s$ and $\boldsymbol{u}_t = \boldsymbol{0}$, where ϕ_s is given function, is a source boundary condition.

If $z \neq 0$, the same condition can be enforced in Friedrichs' formalism by re-defining $R \coloneqq A(\boldsymbol{n}) - M(\boldsymbol{n})$ with

$$M(\boldsymbol{n}) \coloneqq c_0 \begin{bmatrix} (\boldsymbol{M_0}\cdot\boldsymbol{n} + (\boldsymbol{M_0}\cdot\boldsymbol{n})z\zeta + z)\boldsymbol{n}\otimes\boldsymbol{n} & \boldsymbol{0}_n \\ \boldsymbol{0}_n^\intercal & \frac{1}{z} + \boldsymbol{M_0}\cdot\boldsymbol{n} \end{bmatrix}.$$

Such R defines a maximal positive boundary condition if and only if

$$\zeta < 1,\ \frac{|\boldsymbol{M_0}\cdot\boldsymbol{n}|}{1-|\boldsymbol{M_0}\cdot\boldsymbol{n}|\zeta} \le z \le \frac{1}{|\boldsymbol{M_0}\cdot\boldsymbol{n}|}.$$

However, it is not clear whether $M(\boldsymbol{n})$ satisfies the second condition of (3.23).

Supersonic inflow $\boldsymbol{u_0}\cdot\boldsymbol{n} < -c_0$

There $d+1$ incoming characteristics so that the whole state $\boldsymbol{v}$ must be imposed. The matrix $R \coloneqq \mathbb{I}_{d+1}$ yields a maximal positive boundary condition. However, $M(\boldsymbol{n}) \coloneqq A(\boldsymbol{n}) - \mathbb{I}_{d+1}$ is not Friedrichs-admissible since it fails the second condition of (3.23).

3.4 Discussion of the LEEs IBVP well-posedness

This section discusses the applicability of the results presented in Section 3.2 to the well-posedness of the LEEs (3.1). The problem of interest, motivated by the numerical application of Chapter 6, is the IBVP (3.5,3.12,3.13,3.14) on $\Omega_T = (0,T)\times\Omega$ with $\Omega \subset \mathbb{R}^d$ and $d=2$. The domain Ω is rectangular with a boundary $\partial\Omega$ split into three disjoint parts

$$\Omega = (0,L_1)\times(0,L_2),\ \Gamma_{\text{in}} = \{x_1 = 0\}\cap\overline{\Omega},\ \Gamma_{\text{out}} = \{x_1 = L_1\}\cap\overline{\Omega},\ \Gamma_z = \partial\Omega\backslash\Gamma_{\text{in}}\cup\Gamma_{\text{out}}.$$

The subsonic base flow has only one component $\boldsymbol{u_0} = u_0\boldsymbol{e_1}$ with $u_0 = c_0M_0 \in W^{1,\infty}(\Omega)$ that vanishes on Γ_z and is positive on Γ_{in} and Γ_{out}. Note that the two noncharacteristic inflow and outflow boundaries are separated from each other by the characteristic boundary Γ_z. Following the discussion of Section 3.3, the following maximal positive boundary condition is considered

$$\boldsymbol{u}_t = \boldsymbol{0} \quad \text{a.e. on } \Gamma_{\text{in}},\ \tilde{p} = \mathcal{Z}(\boldsymbol{x}, \boldsymbol{u}\cdot\boldsymbol{n}) \quad \text{a.e. on } \partial\Omega, \tag{3.28}$$

where $\mathcal{Z}(\boldsymbol{x},\cdot)$ is a real-valued passive operator. In summary, this is an IBVP for a symmetric hyperbolic system with a partly characteristic connected boundary along which $\dim\ker A(\boldsymbol{n})$ varies: 0 on Γ_{in} and Γ_{out}, and $d-1$ on Γ_z. A Friedrichs system can be obtained following Remark 3.8. The case $\mathcal{Z} \propto \mathcal{I}$ is discussed first.

3.4.1 Proportional impedance boundary condition

Here, we consider a proportional impedance boundary condition

$$\mathcal{Z}(\boldsymbol{u}\cdot\boldsymbol{n}) = \begin{cases} z_{\text{in}}\boldsymbol{u}\cdot\boldsymbol{n} & (\boldsymbol{x}\in\Gamma_{\text{in}}) \\ z\boldsymbol{u}\cdot\boldsymbol{n} & (\boldsymbol{x}\in\Gamma_z) \\ z_{\text{out}}\boldsymbol{u}\cdot\boldsymbol{n} & (\boldsymbol{x}\in\Gamma_{\text{out}}), \end{cases}$$

which is the simplest of the memoryless impedance kernels. Although it is physically simplistic, it fits within both the classical and abstract theories presented in Section 3.2.

Classical theory

The boundary conditions (3.28) are maximal positive and verify the jump conditions (3.21) if and only if z_{in}, z, and z_{out} are equal. Therefore, the IBVP can fit into the framework of (Rauch 1994), provided that Ω is changed so that $\partial\Omega$ is of class $\mathcal{C}^1$. We refer to (Ventribout 2006, Chap. 1) for a discussion.

Abstract theory by the boundary operator approach

In view of Remark 3.8, the LEEs on Ω_T fit within the framework of the abstract Friedrichs theory. Following (Burazin and Erceg 2016), strong well-posedness of the evolution problem can be obtained from the Lumer-Phillips theorem if the abstract theory applies successfully to $\mathcal{A}$, i.e. if a subspace $V \subset H^1_{\mathcal{A}}$ can be found for which $\mathcal{A}$ is an isomorphism from $(V, \|\cdot\|_{H^1_{\mathcal{A}}})$ to $L^2(\Omega)$. To build V, we use the boundary operator approach of Theorem 3.18. This choice is motivated by the fact that this theorem applies to a transport equation over Ω, provided that the inflow and outflow boundaries are well-separated (Antonić et al. 2014), which is the case herein since $|\Gamma_z| > 0$. Applying Theorem 3.18 only requires elementary, but tedious, algebra. The matrices $P, R \in \mathbb{R}^{(d+1)\times(d+1)}$ are sought as

$$P = \begin{bmatrix} P_1 & \boldsymbol{P_2} \\ \boldsymbol{P_3}^\intercal & p_4 \end{bmatrix}, \; R = \begin{bmatrix} R_1 & \boldsymbol{R_2} \\ \boldsymbol{R_3}^\intercal & r_4 \end{bmatrix},$$

where $P_1, R_1 \in \mathbb{R}^{d\times d}$ and $p_4, r_4 \in \mathbb{R}$. The admissible matrices P and R are given by the lemma below.

Lemma 3.20. *Assume $\boldsymbol{u_0} \neq \boldsymbol{0}$ and $\boldsymbol{u_0} = u_0\boldsymbol{e}_1$, where $(\boldsymbol{e_k})_k$ is an orthonormal basis of $\mathbb{R}^d$. If $d = 2$, then the algebraic condition (3.27) is equivalent to*

$$P = \begin{bmatrix} \delta_1\mathbb{I}_d + \boldsymbol{e_1}\otimes\boldsymbol{\delta_2} & -M_0(\boldsymbol{\delta_2}\cdot\boldsymbol{e_2})\boldsymbol{e_2} + \frac{1}{M_0}\boldsymbol{\delta_2} \\ -M_0(\boldsymbol{\delta_2}\cdot\boldsymbol{e_2})\boldsymbol{e_2}^\intercal & \delta_1 \end{bmatrix}, \; R = \begin{bmatrix} \delta_1\mathbb{I}_d + \boldsymbol{\delta_2}\otimes\boldsymbol{e_1} & \boldsymbol{P_3} \\ \boldsymbol{P_2}^\intercal & \delta_1 \end{bmatrix}. \tag{3.29}$$

where $\delta_1 \in \mathbb{R}$ and $\boldsymbol{\delta_2} \in \mathbb{R}^2$ are free parameters. If $d > 2$, then the equivalence is obtained with

$$P = \begin{bmatrix} \delta_1\mathbb{I}_d + (\boldsymbol{\delta_2}\cdot\boldsymbol{e_1})\boldsymbol{e_1}\otimes\boldsymbol{e_1} & \frac{1}{M_0}(\boldsymbol{\delta_2}\cdot\boldsymbol{e_1})\boldsymbol{e_1} \\ \boldsymbol{0}_d^\intercal & \delta_1 \end{bmatrix}, \; R = \begin{bmatrix} P_1 & \boldsymbol{0_d} \\ \boldsymbol{P_2}^\intercal & \delta_1 \end{bmatrix},$$

where there is only two scalar parameters, δ_1 and $\boldsymbol{\delta_2}\cdot\boldsymbol{e_1}$.

In view of Lemma 3.20, let us investigate the relevance of Theorem 3.18 for the LEEs in the case $d = 2$. To obtain well-posedness P must be Lipschitz on $\overline{\Omega}$, in particular continuous on $\partial\Omega$. Since M_0 vanishes on Γ_z, this requires to impose $\boldsymbol{\delta_2} = M_0\tilde{\boldsymbol{\delta}}_{\boldsymbol{2}}$ with $\tilde{\boldsymbol{\delta}}_{\boldsymbol{2}} \in L^\infty(\Omega)$ so that

$$P = \begin{bmatrix} \delta_1\mathbb{I}_d + M_0\boldsymbol{e_1}\otimes\tilde{\boldsymbol{\delta}}_{\boldsymbol{2}} & -M_0^2(\tilde{\boldsymbol{\delta}}_{\boldsymbol{2}}\cdot\boldsymbol{e_2})\boldsymbol{e_2} + \tilde{\boldsymbol{\delta}}_{\boldsymbol{2}} \\ -M_0^2(\tilde{\boldsymbol{\delta}}_{\boldsymbol{2}}\cdot\boldsymbol{e_2})\boldsymbol{e_2}^\intercal & \delta_1 \end{bmatrix}.$$

The corresponding boundary conditions are given by $A(\boldsymbol{n}) = M(\boldsymbol{n})$ with $M(\boldsymbol{n}) = A(\boldsymbol{n})(\mathbb{I}_{d+1} - 2P)$. On Γ_z, $M_0 = 0$ so that

$$M(\boldsymbol{n}) = c_0\begin{bmatrix} 0_d & \tilde{\delta}_1\boldsymbol{n} \\ \tilde{\delta}_1\boldsymbol{n}^\intercal & -2\boldsymbol{n}\cdot\tilde{\boldsymbol{\delta}}_{\boldsymbol{2}} \end{bmatrix},$$

where we defined $\tilde{\delta}_1 = 1 - 2\delta_1$. This matrix $M(\boldsymbol{n})$ cannot define a maximal positive (3.20) boundary condition: positivity requires $\tilde{\delta}_1 = 0$ and $-2\boldsymbol{n}\cdot\tilde{\boldsymbol{\delta}}_{\boldsymbol{2}} \geq 0$, while maximality requires $\tilde{\delta}_1 = 1$ and $\boldsymbol{n}\cdot\tilde{\boldsymbol{\delta}}_{\boldsymbol{2}} \neq 0$. Therefore, Theorem 3.18 does *not* apply to the LEEs if $d = 2$, hence if $d \geq 2$ from Lemma 3.20.

However, this does not mean that the abstract theory cannot yield a well-posedness result for the LEEs. A positive result might be obtained by defining the space V and directly verifying the conditions (Ern et al. 2007, Thm. 3.1): this is done in (Burazin and Erceg 2016, § 3.3) for the wave equation and in (Antonić et al. 2013) for the heat equation. Moreover, the representation of a PDE as a Friedrichs system is not unique and different representations can enable different boundary conditions, see (Antonić et al. 2014) for an example on the wave equation. Therefore, it might also be fruitful to consider a different state than (3.12).

Proof of Lemma 3.20. The conditions (3.27) read

$$\begin{cases} \boldsymbol{R_2}\otimes\boldsymbol{e_k} &= \boldsymbol{e_k}\otimes\boldsymbol{P_3} - M_0(\boldsymbol{e_1}\cdot\boldsymbol{e_k})(R_1-P_1)\\ R_1\boldsymbol{e_k} &= p_4\boldsymbol{e_k} - M_0(\boldsymbol{e_1}\cdot\boldsymbol{e_k})(\boldsymbol{R_2}-\boldsymbol{P_2})\\ r_4\boldsymbol{e_k} &= P_1^\intercal\boldsymbol{e_k} - M_0(\boldsymbol{e_1}\cdot\boldsymbol{e_k})(\boldsymbol{R_3}-\boldsymbol{P_3})\\ \boldsymbol{R_3}\cdot\boldsymbol{e_k} &= \boldsymbol{P_2}\cdot\boldsymbol{e_k} - M_0(\boldsymbol{e_1}\cdot\boldsymbol{e_k})(r_4-p_4). \end{cases} \tag{3.30}$$

(Note that without any assumption on the base flow $\boldsymbol{u_0}$, (3.27) would lead to $P = R \propto \mathbb{I}_{d+1}$, hence $M(\boldsymbol{n}) \propto A(\boldsymbol{n})$.) The given expressions for P and R satisfy (3.30). To derive an expression for $\boldsymbol{P}$, we first cover the case ($d \geq 2$,$k \neq 1$) then the cases ($d = 2$,$k = 1$) and ($d > 2$,$k = 1$) separately, always proceeding by equivalence.

($d \geq 2$,$k \neq 1$) If $k \neq 1$, then $\boldsymbol{e_1}\cdot\boldsymbol{e_k} = 0$ and we have the equivalence

$$\forall k \in [\![1,d]\!],\ k\neq 1,\ \begin{cases} \boldsymbol{R_2}\otimes\boldsymbol{e_k} &= \boldsymbol{e_k}\otimes\boldsymbol{P_3}\\ R_1\boldsymbol{e_k} &= p_4\boldsymbol{e_k}\\ r_4\boldsymbol{e_k} &= P_1^\intercal\boldsymbol{e_k}\\ \boldsymbol{R_3}\cdot\boldsymbol{e_k} &= \boldsymbol{P_2}\cdot\boldsymbol{e_k} \end{cases} \Leftrightarrow \begin{cases} \boldsymbol{R_2} = \boldsymbol{P_3} = p_3\boldsymbol{e_2} & (\text{if } d=2)\\ \boldsymbol{R_2} = \boldsymbol{P_3} = \boldsymbol{0_d} & (\text{if } d>2)\\ R_1 = p_4\mathbb{I}_d + \boldsymbol{\delta_4}\otimes\boldsymbol{e_1}\\ r_4\mathbb{I}_d = P_1^\intercal + \boldsymbol{\delta_1}\otimes\boldsymbol{e_1}\\ \boldsymbol{R_3} = \boldsymbol{P_2} + \delta_2\boldsymbol{e_1}, \end{cases} \tag{3.31}$$

where the first equation requires to distinguish on the dimension d, since $\boldsymbol{R_2}\otimes\boldsymbol{e_k} = \boldsymbol{e_k}\otimes\boldsymbol{P_3}$ for every $k \neq 1$ is not equivalent to $\boldsymbol{R_2} = \boldsymbol{P_3} = \boldsymbol{0_d}$ if $d = 2$. The parameters p_4, r_4, and δ_i are seemingly free and will be constrained when considering the case $k = 1$ below. We now distinguish between $d = 2$ and $d > 2$, covering $d = 2$ first.

($d = 2$,$k = 1$) Using the expressions of R_1, $\boldsymbol{R_2}$, $\boldsymbol{R_3}$, and $\boldsymbol{P_3}$ given by (3.31), we obtain an equivalence between (3.30) and

$$\begin{cases} \boldsymbol{R_2} = \boldsymbol{P_3} = p_3\boldsymbol{e_2}\\ R_1 = p_4\mathbb{I}_d + \boldsymbol{\delta_4}\otimes\boldsymbol{e_1}\\ r_4\mathbb{I}_d = P_1^\intercal + \boldsymbol{\delta_1}\otimes\boldsymbol{e_1}\\ \boldsymbol{R_3} = \boldsymbol{P_2} + \delta_2\boldsymbol{e_1} \end{cases} \quad\text{and}\quad \begin{cases} P_1 = p_4\mathbb{I}_d + \boldsymbol{\delta_4}\otimes\boldsymbol{e_1} + \frac{p_3}{M_0}(\boldsymbol{e_2}\otimes\boldsymbol{e_1} - \boldsymbol{e_1}\otimes\boldsymbol{e_2})\\ \boldsymbol{P_2} = p_3\boldsymbol{e_2} + \frac{1}{M_0}\boldsymbol{\delta_4}\\ r_4\boldsymbol{e_1} = P_1^\intercal\boldsymbol{e_1} - M_0\boldsymbol{P_2} - M_0\delta_2\boldsymbol{e_1} + M_0p_3\boldsymbol{e_2}\\ r_4 = p_4 - \frac{1}{M_0}\delta_2. \end{cases}$$

The expression of P_1 gives

$$P_1^\intercal\boldsymbol{e_1} = p_4\boldsymbol{e_1} + (\boldsymbol{\delta_4}\cdot\boldsymbol{e_1})\boldsymbol{e_1} - \frac{p_3}{M_0}\boldsymbol{e_2}.$$

Replacing r_4, $P_1^\intercal\boldsymbol{e_1}$, and $\boldsymbol{P_2}$ by their expressions in the third equation of the second system yields the two scalar identities $(M_0 - \frac{1}{M_0})\delta_2 = 0$ and $p_3 = -M_0(\boldsymbol{\delta_4}\cdot\boldsymbol{e_2})$. The conditions (3.30) are then equivalent to

$$\begin{cases} \boldsymbol{R_2} = \boldsymbol{P_3} = -M_0(\boldsymbol{\delta_4}\cdot\boldsymbol{e_2})\boldsymbol{e_2}\\ R_1 = p_4\mathbb{I}_d + \boldsymbol{\delta_4}\otimes\boldsymbol{e_1}\\ r_4\mathbb{I}_d = P_1^\intercal + \boldsymbol{\delta_1}\otimes\boldsymbol{e_1}\\ \boldsymbol{R_3} = \boldsymbol{P_2} + \delta_2\boldsymbol{e_1} \end{cases} \quad\text{and}\quad \begin{cases} P_1 = p_4\mathbb{I}_d + \boldsymbol{e_1}\otimes\boldsymbol{\delta_4}\\ \boldsymbol{P_2} = -M_0(\boldsymbol{\delta_4}\cdot\boldsymbol{e_2})\boldsymbol{e_2} + \frac{1}{M_0}\boldsymbol{\delta_4}\\ (M_0 - \frac{1}{M_0})\delta_2 = 0\\ r_4 = p_4 - \frac{1}{M_0}\delta_2, \end{cases}$$

where we have used the identity $(\boldsymbol{\delta_4}\cdot\boldsymbol{e_1})\boldsymbol{e_1}\otimes\boldsymbol{e_1} + (\boldsymbol{\delta_4}\cdot\boldsymbol{e_2})\boldsymbol{e_1}\otimes\boldsymbol{e_2} = \boldsymbol{e_1}\otimes\boldsymbol{\delta_4}$. Combining the two expressions of P_1 shows that $\delta_2\mathbb{I}_d = -M_0\boldsymbol{e_1}\otimes(\boldsymbol{\delta_1}+\boldsymbol{\delta_4})$, hence $\boldsymbol{\delta_1} = -\boldsymbol{\delta_4}$ and $\delta_2 = 0$, yielding the claimed equivalence (with the change of notation $\boldsymbol{\delta_4}\to\boldsymbol{\delta_2}$ and $\delta_2\to\delta_1$).

($d > 2$,$k = 1$) When $d > 2$, there are less available DoF than in the case $d = 2$. Using the expressions of R_1, $\boldsymbol{R_2}$, $\boldsymbol{R_3}$, and $\boldsymbol{P_3}$ given by (3.31), we obtain an equivalence between (3.30) and

$$\begin{cases} \boldsymbol{R_2} = \boldsymbol{P_3} = \boldsymbol{0}_d \\ R_1 = P_1 \\ r_4 \mathbb{I}_d = P_1^\intercal + \boldsymbol{\delta_1} \otimes \boldsymbol{e_1} \\ \boldsymbol{R_3} = \boldsymbol{P_2} + \delta_2 \boldsymbol{e_1} \end{cases} \quad \text{and} \quad \begin{cases} P_1 = p_4 \mathbb{I}_d + \boldsymbol{\delta_4} \otimes \boldsymbol{e_1} \\ \boldsymbol{P_2} = \frac{1}{M_0}(P_1 \boldsymbol{e_1} - p_4 \boldsymbol{e_1}) \\ r_4 \boldsymbol{e_1} = P_1^\intercal \boldsymbol{e_1} - M_0 \boldsymbol{P_2} - M_0 \delta_2 \boldsymbol{e_1} \\ \delta_2 = -M_0(r_4 - p_4). \end{cases}$$

Replacing P_1 by its expression in the third equation of the first system yields $(r_4 - p_4)\mathbb{I}_d = \boldsymbol{e_1} \otimes \boldsymbol{\delta_4} + \boldsymbol{\delta_1} \otimes \boldsymbol{e_1}$, which gives $r_4 = p_4$ and $\boldsymbol{\delta_1} \otimes \boldsymbol{e_1} = -\boldsymbol{e_1} \otimes \boldsymbol{\delta_4}$, from which is deduced $\boldsymbol{\delta_4} = (\boldsymbol{\delta_4} \cdot \boldsymbol{e_1})\boldsymbol{e_1}$, $\boldsymbol{\delta_1} = -\boldsymbol{\delta_4}$, and $\delta_2 = 0$. Replacing $P_1^\intercal \boldsymbol{e_1}$ and $\boldsymbol{P_2}$ in the third equation of the second system yields $(\boldsymbol{\delta_4} \otimes \boldsymbol{e_1})\boldsymbol{e_1} = (\boldsymbol{\delta_4} \cdot \boldsymbol{e_1})\boldsymbol{e_1}$. The claimed equivalence follows. □

3.4.2 Positive-real impedance boundary condition

Chapter 1 has highlighted the physical relevance of an impedance boundary condition

$$\tilde{p} = z \star \boldsymbol{u} \cdot \boldsymbol{n},$$

where the Laplace transform of the convolution kernel $\hat{z}(s)$ is a positive-real function. This boundary condition does not fit in general in the classical theory discussed in Section 3.2. However, the passivity condition (1.2) naturally suggests using the abstract theory in Ω_T: consider the spacetime equivalent of (3.25,3.26) for instance. The next chapter deals with impedance boundary conditions under two simplifying assumptions, namely that the kernel z has a particular structure and that $\boldsymbol{u_0} = \boldsymbol{0}$.

Chapter 4

Asymptotic stability of the wave equation with admissible impedance boundary conditions

Contents

This chapter, which has been submitted to (Monteghetti et al. 2018a), proves the asymptotic stability of the multidimensional wave equation coupled with a wide range of admissible IBCs using a common method of proof that relies on the Arendt-Batty-Lyubich-Vũ (ABLV) theorem. Section 4.1 introduces the model considered and establishes a preliminary well-posedness result that is the cornerstone of the presented stability proofs. Section 4.2 recalls the ABLV theorem, sets up the energy space on the elementary example of the proportional IBC, and discusses the applicability of LaSalle's invariance principle. Admissible IBCs of increasing complexity are then covered in Sections 4.3–4.6. The extension of the derived asymptotic stability results to IBCs that contain a pure derivative term is carried out in Section 4.7.

Introduction

The broad focus of this chapter is the asymptotic stability of the wave equation with IBCs, also known in the mathematical literature as acoustic boundary conditions.

Herein, the impedance operator, related to the Neumann-to-Dirichlet map, is assumed to be continuous linear time-invariant, so that it reduces to a time-domain convolution. *Passive* convolution operators (Beltrami and Wohlers 1966, § 3.5), the kernels of which have a positive-real Laplace transform, find applications in physics in the modeling of locally reacting energy absorbing material, such as non perfect conductors in electromagnetism (Yuferev and Ida 2010) and liners in acoustics (Monteghetti et al. 2018b). As a result, IBCs are commonly used with Maxwell's equations (Hiptmair et al. 2014), the linearized Euler equations (Monteghetti et al. 2018b), or the wave equation (Sauter and Schanz 2017).

Two classes of convolution operators are well-known due to the ubiquity of the physical phenomena they model. Slowly decaying kernels, which yield so-called *long-memory* operators, arise from losses without propagation (due to e.g. viscosity or electrical/thermal resistance); they include fractional kernels. On the other hand, lossless propagation, encountered in acoustical cavity for instance, can be represented as a *time delay*. Both effects can be combined, so that time-delayed long-memory operators model a propagation with losses.

Stabilization of the wave equation by a boundary damping, as opposed to an internal damping, has been investigated in a wealth of works, most of which employing the equivalent admittance formulation (4.5), see Remark 4.2 for the terminology. Unless otherwise specified, the works quoted below deal with the multidimensional wave equation.

Early studies established exponential stability with a proportional admittance (Chen 1981; Komornik and Zuazua 1990; Lagnese 1983). A delay admittance is considered in (Nicaise and Pignotti 2006), where exponential stability is proven under a sufficient delay-independent stability condition that can be interpreted as a passivity condition of the admittance operator. The proof of well-posedness relies on the formulation of an evolution problem using an infinite-dimensional realization of the delay through a transport equation (see (Engel and Nagel 2000, § VI.6) (Curtain and Zwart 1995, § 2.4) and references therein) and stability is obtained using observability inequalities. The addition of a 2-dimensional realization to a delay admittance has been considered in (Peralta 2018), where both exponential and asymptotic stability results are shown under a passivity condition using the energy multiplier method. See also (Wang et al. 2011) for a monodimensional wave equation with a non-passive delay admittance, where it is shown that exponential stability can be achieved provided that the delay is a multiple of the domain back-and-forth traveling time.

A class of space-varying admittance with finite-dimensional realizations have received thorough scrutiny in (Abbas and Nicaise 2013) for the monodimensional case and (Abbas and Nicaise 2015) for the multidimensional case. In particular, asymptotic stability is shown using the ABLV theorem in an extended state space.

Admittance kernels defined by a Borel measure on $(0, \infty)$ have been considered in (Cornilleau and Nicaise 2009), where exponential stability is shown under an integrability condition on the measure (Cornilleau and Nicaise 2009, Eq. 7). This result covers both distributed and discrete time delays, as well as a class of integrable kernels. Other classes of integrable kernels have been studied in (Desch et al. 2010; C. Li et al. 2018; Peralta 2016). Integrable kernels coupled with a 2-dimensional realization are considered in (C. Li et al. 2018) using energy estimates. Kernels that are both completely monotone and integrable are considered in (Desch et al. 2010), which uses the ABLV theorem on an extended state space, and in (Peralta 2016) with an added time delay, which uses the energy method to prove exponential stability. The energy multiplier method is also used in (Alabau-Boussouira et al. 2009) to prove exponential stability for a class

of non-integrable singular kernels.

The works quoted so far do not cover fractional kernels, which are non-integrable, singular, and completely monotone. As shown in (Matignon and Prieur 2005), asymptotic stability results with fractional kernels can be obtained with the ABLV theorem by using their realization; two works that follow this methodology are (Matignon and Prieur 2014), which covers the monodimensional Webster-Lokshin equation with a rational IBC, and (Grabowski 2013), which covers a monodimensional wave equation with a fractional admittance.

The objective of this chapter is to prove the asymptotic stability of the multidimensional wave equation (4.2) coupled with a wide range of IBCs (4.3) chosen for their physical relevance. All the considered IBCs share a common property: the Laplace transform of their kernel is a positive-real function. A common method of proof, inspired by (Matignon and Prieur 2014), is employed that consists in formulating an abstract Cauchy problem on an extended state space (4.13) using a realization of each impedance operator, be it finite or infinite-dimensional; asymptotic stability is then obtained with the ABLV theorem, although a less general alternative based on the invariance principle is also discussed. In spite of the apparent unity of the approach, no single, unified proof is known to the author: this leads to the formulation of a conjecture at the end of this dissertation.

This chapter is organized as follows. Section 4.1 introduces the model considered, recalls some known facts about positive-real functions, and establishes a preliminary well-posedness result in the Laplace domain that is the cornerstone of the stability proofs. Section 4.2 formulates the ABLV theorem as Corollary 4.13, sets up the energy space on the elementary example of the proportional IBC, and discusses the applicability of the invariance principle. The applicability of Corollary 4.13 to positive-real IBCs of increasing complexity is then shown in the subsequent sections. Rational IBCs, whose realizations are finite-dimensional, are covered in Section 4.3 using the celebrated positive-real lemma. The remaining sections focus on IBCs with infinite-dimensional realizations that arise in physical applications. Delay IBCs are covered in Section 4.4, standard diffusive IBCs (e.g. fractional integral) are covered in Section 4.5, while extended diffusive IBCs (e.g. fractional derivative) are covered in Section 4.6. The extension of the obtained asymptotic stability results to IBCs that contain a pure derivative term is carried out in Section 4.7.

Notation

Vector-valued quantities are denoted in bold, e.g. $\boldsymbol{f}$. The canonical scalar product in $\mathbb{C}^d$, $d \in [\![1, \infty[\![$, is denoted by

$$(\boldsymbol{f}, \boldsymbol{g})_{\mathbb{C}^d} \coloneqq \sum_{i=1}^{d} f_i \overline{g_i},$$

where $\overline{g_i}$ is the complex conjugate. Throughout the chapter, scalar products are antilinear with respect to the second argument. Gradient and divergence are denoted by

$$\nabla f \coloneqq [\partial_i f]_{i \in [\![1,d]\!]}, \ \operatorname{div} \boldsymbol{f} \coloneqq \sum_{i=1}^{d} \partial_i f_i,$$

where ∂_i is the weak derivative with respect to the i-th coordinate. The scalar product (resp. norm) on a Hilbert space H is denoted by $(\cdot, \cdot)_H$ (resp. $\|\cdot\|_H$). The only exception is the space of square integrable functions $(L^2(\Omega))^d$, with $\Omega \subset \mathbb{R}^d$ open set, for which the space is omitted, i.e.

$$(\boldsymbol{f}, \boldsymbol{g}) \coloneqq \int_\Omega (\boldsymbol{f}(\boldsymbol{x}), \boldsymbol{g}(\boldsymbol{x}))_{\mathbb{C}^d} \, \mathrm{d}\boldsymbol{x}, \ \|\boldsymbol{f}\| \coloneqq \sqrt{(\boldsymbol{f}, \boldsymbol{f})}.$$

The scalar product on $(H^1(\Omega))^d$ is

$$(\boldsymbol{f},\boldsymbol{g})_{H^1(\Omega)} \coloneqq (\boldsymbol{f},\boldsymbol{g}) + (\nabla\boldsymbol{f},\nabla\boldsymbol{g}).$$

The topological dual of a Hilbert space H is denoted by H', and L^2 is used as a pivot space so that for instance

$$H^{\frac{1}{2}} \subset L^2 \simeq (L^2)' \subset H^{-\frac{1}{2}},$$

which leads to the following repeatedly used identity, for $p \in L^2$ and $\psi \in H^{\frac{1}{2}}$,

$$\langle p,\psi\rangle_{H^{-\frac{1}{2}},H^{\frac{1}{2}}} = \langle p,\psi\rangle_{(L^2)',L^2} = (p,\overline{\psi})_{L^2}, \tag{4.1}$$

where $\langle\cdot,\cdot\rangle$ denotes the duality bracket (linear in both arguments).

Remark 4.1. All the Hilbert spaces considered in this chapter are over $\mathbb{C}$.

Other commonly used notations are $\mathbb{R}^* \coloneqq \mathbb{R}\backslash\{0\}$, $\Re(s)$ (resp. $\Im(s)$) for the real (resp. imaginary) part of $s \in \mathbb{C}$, $A^\intercal$ for the transpose of a matrix A, $R(A)$ (resp. $\ker(A)$) for the range (resp. kernel) of A, $\mathcal{C}(\Omega)$ for the space of continuous functions, $\mathcal{C}_0^\infty(\Omega)$ for the space of infinitely smooth and compactly supported functions, $\mathcal{D}'(\Omega)$ for the space of distributions (dual of $\mathcal{C}_0^\infty(\Omega)$), $\mathcal{E}'(\Omega)$ for the space of compactly supported distributions, $\mathcal{L}(H)$ for the space of continuous linear operators over H, $\overline{\Omega}$ for the closure of Ω, $Y_1 : \mathbb{R} \to \{0,1\}$ for the Heaviside function (1 over $(0,\infty)$, null elsewhere), and δ for the Dirac distribution.

4.1 Model and preliminary results

Let $\Omega \subset \mathbb{R}^d$ be a bounded open set. The Cauchy problem considered in this chapter is the wave equation under one of its first-order form, namely

$$\partial_t \begin{pmatrix} \boldsymbol{u} \\ p \end{pmatrix} + \begin{pmatrix} \nabla p \\ \operatorname{div}\boldsymbol{u} \end{pmatrix} = \boldsymbol{0} \quad \text{on } \Omega, \tag{4.2}$$

where $\boldsymbol{u}(t,\boldsymbol{x}) \in \mathbb{C}^d$ and $p(t,\boldsymbol{x}) \in \mathbb{C}$. To (4.2) is associated the so-called *impedance boundary condition* (IBC), formally defined as a time-domain convolution between p and $\boldsymbol{u}\cdot\boldsymbol{n}$,

$$p = z \star \boldsymbol{u}\cdot\boldsymbol{n} \quad \text{a.e. on } \partial\Omega, \tag{4.3}$$

where $\boldsymbol{n}$ is the unit outward normal and z is the impedance kernel. In general, z is a causal distribution, i.e. $z \in \mathcal{D}'_+(\mathbb{R})$, so that the convolution is to be understood in the sense of distributions (Schwartz 1966, Chap. III) (Hörmander 1990, Chap. IV).

This chapter proves the asymptotic stability of strong solutions of the evolution problem (4.2,4.3) with an impedance kernel z whose positive-real Laplace transform is given by

$$\hat{z}(s) = (z_0 + z_\tau e^{-\tau s}) + z_1 s + \hat{Z}(s) + \hat{z}_{\text{diff},1}(s) + s\,\hat{z}_{\text{diff},2}(s) \quad (\Re(s) > 0), \tag{4.4}$$

where $\tau > 0$, $z_\tau \in \mathbb{R}$, $z_0 \geq |z_\tau|$, $z_1 > 0$, $\hat{Z}$ is a positive-real and strictly proper rational function, and $z_{\text{diff},1}$ as well as $z_{\text{diff},2}$ are both locally integrable completely monotone kernels. The motivation behind the definition of this kernel is physical as it models passive systems that arise in e.g. electromagnetics (Garrappa et al. 2016), viscoelasticity (Desch and Miller 1988; Mainardi 1997), and acoustics (Hélie and Matignon 2006a; Lombard and Matignon 2016; Monteghetti et al. 2016a). The proposed proof relies on the fact that the right-hand side of (4.4) is a sum of positive-real kernels that each admit a dissipative realization. Mathematically, each of them requires a specific treatment so that they are covered in separate sections, namely

Sections 4.3–4.7. As already mentioned in the introduction, the similarity between the proofs suggests a conjecture, which is given at the end of this dissertation.

The purpose of this section is to provide results that will prove useful in the later sections. It is organized as follows. Section 4.1.1 recalls some elementary facts of system theory to show that, in order to obtain a well-posed problem in L^2, the Laplace transform of the impedance kernel must be a *positive-real* function on the right half-plane. Then, a well-posedness result on the Laplace-transformed wave equation is shown in Section 4.1.2 for later use in the proofs of asymptotic stability. This well-posedness result relies on a lemma that is proven in Section 4.1.3.

Remark 4.2 (Terminology from Section 1.1). The boundary condition (4.3) can equivalently be written as

$$\boldsymbol{u} \cdot \boldsymbol{n} = y \star p \quad \text{a.e. on } \partial\Omega, \tag{4.5}$$

where y is known as the *admittance* kernel ($y \star z = \delta$, where δ is the Dirac distribution). This terminology can be justified, for example, by the acoustical application: an acoustic impedance is homogeneous to a pressure divided by a velocity. The asymptotic stability results obtained in this chapter still hold by replacing the impedance by the admittance (in particular, the statement "$z \neq 0$" becomes "$y \neq 0$"). The third way of formulating (4.3), not considered in this chapter, is the so-called *scattering* formulation (Beltrami and Wohlers 1966, p. 89) (Lozano et al. 2000, § 2.8)

$$p - \boldsymbol{u} \cdot \boldsymbol{n} = \beta \star (p + \boldsymbol{u} \cdot \boldsymbol{n}) \quad \text{a.e. on } \partial\Omega,$$

where β is known as the *reflection coefficient*. A Dirichlet boundary condition is recovered for $z = 0$ ($\beta = -\delta$) while a Neumann boundary condition is recovered for $y = 0$ ($\beta = +\delta$), so that the proportional IBC, obtained for $z = z_0\delta$ ($\beta = \frac{z_0-1}{z_0+1}\,\delta$), $z_0 \geq 0$, can be seen as an intermediate between the two.

Remark 4.3. The use of a convolution in (4.3) can be justified with the following classical result (Schwartz 1966, § III.3) (Beltrami and Wohlers 1966, Thm. 1.18): if $\mathcal{Z}$ is a linear time-invariant and continuous mapping from $\mathcal{E}'(\mathbb{R})$ into $\mathcal{D}'(\mathbb{R})$, then $\mathcal{Z}(u) = \mathcal{Z}(\delta) \star u$ for all $u \in \mathcal{E}'(\mathbb{R})$.

4.1.1 Some elementary facts from system theory

Assume that $(\boldsymbol{u}, p)$ is a strong solution, i.e. that it belongs to $\mathcal{C}([0,T]; (H^1(\Omega))^{d+1})$. The elementary a priori estimate

$$\|(\boldsymbol{u},p)(T)\|^2 = \|(\boldsymbol{u},p)(0)\|^2 - 2\,\Re\left[\int_0^T (p(\tau), \boldsymbol{u}(\tau)\cdot\boldsymbol{n})_{L^2(\partial\Omega)}\,\mathrm{d}\tau\right] \tag{4.6}$$

suggests that to obtain a contraction semigroup, the impedance kernel must satisfy a passivity condition, well-known in system theory. This justifies why we restrict ourselves to impedance kernels that are *admissible* in the sense of Definition 1.1. As recalled in Section 1.1, an important feature of admissible impedance kernels z is that their Laplace transforms $\hat{z}$ are *positive-real* functions, see Definition 1.7 and Proposition 1.8. Herein, the Laplace transform $\hat{z}$ is an analytic function on an open *right* half-plane, i.e.

$$\hat{z}(s) \coloneqq \int_0^\infty z(t) e^{-st}\,\mathrm{d}t \quad \left(s \in \mathbb{C}_c^+\right),$$

for some $c \geq 0$ with

$$\mathbb{C}_c^+ \coloneqq \{s \in \mathbb{C} \,|\, \Re(s) > c\},$$

see Appendix A for background and references when $z \in \mathcal{D}'_+(\mathbb{R})$.

4.1.2 A well-posedness result in the Laplace domain

The following result is used repeatedly in the next sections. We define

$$\overline{\mathbb{C}_0^+} \coloneqq \{s \in \mathbb{C} \,|\, \Re(s) \geq 0\}.$$

Proposition 4.4. *Let $\Omega \subset \mathbb{R}^d$ be a bounded open set with an infinitely smooth boundary. Let $z : \overline{\mathbb{C}_0^+}\backslash\{0\} \to \mathbb{C}_0^+$ be such that $z(s) \in \mathbb{R}$ for $s \in (0, \infty)$. For every $s \in \overline{\mathbb{C}_0^+}\backslash\{0\}$ and $l \in H^{-1}(\Omega)$ there exists a unique $p \in H^1(\Omega)$ such that*

$$\forall \psi \in H^1(\Omega),\ (\nabla p, \nabla \psi) + s^2(p, \psi) + \frac{s}{z(s)}(p, \psi)_{L^2(\partial\Omega)} = \overline{l(\psi)}. \tag{4.7}$$

Moreover, there is $C(s) > 0$ such that

$$\|p\|_{H^1(\Omega)} \leq C(s)\, \|l\|_{H^{-1}(\Omega)}.$$

Remark 4.5. Note that $s \mapsto z(s)$ need not be continuous, so that Proposition 4.4 can be used pointwise, i.e. for only some $s \in \overline{\mathbb{C}_0^+}\backslash\{0\}$.

Remark 4.6. For $s \in \mathbb{C}_0^+$, the result holds for Ω any bounded open set with a Lipschitz boundary: the smoothness hypothesis is only required for $s \in \mathrm{j}\mathbb{R}^*$, due to the use of Lemma 4.11.

Remark 4.7 (Intuition). Although the need for Proposition 4.4 will appear in the proofs of the next sections, let us give a *formal* motivation for Formulation (4.7). Assume that $(\boldsymbol{u}, p)$ is a smooth solution of (4.2,4.3). Then p solves the wave equation

$$\partial_t^2 p - \Delta p = 0 \quad \text{on } \Omega,$$

with the impedance boundary condition

$$\partial_t p = z \star \partial_t \boldsymbol{u} \cdot \boldsymbol{n} = z \star (-\nabla p) \cdot \boldsymbol{n} = -z \star \partial_n p \quad \text{on } \partial\Omega,$$

where $\partial_n p$ denotes the normal derivative of p and the causal kernel z is, say, tempered and locally integrable. An integration by parts with $\psi \in H^1(\Omega)$ reads

$$(\nabla p, \nabla \psi) + (\partial_t^2 p, \psi) - (\partial_n p, \psi)_{L^2(\partial\Omega)} = 0.$$

Formulation (4.7) then follows from the application of the Laplace transform in time, which gives $\widehat{z \star \partial_n p}(s) = \hat{z}(s)\partial_n \hat{p}(s)$ and $\widehat{\partial_t p}(s) = s\hat{p}(s)$ assuming that $p(t = 0) = 0$ on $\partial\Omega$.

Proof for $s \in (0, \infty)$. If $s \in (0, \infty)$ this is an immediate consequence of the Lax-Milgram lemma (Lax 2002, Thm. 6.6). Define the following bilinear form over $H^1(\Omega) \times H^1(\Omega)$:

$$\overline{a(p, \psi)} \coloneqq (\nabla p, \nabla \psi) + s^2(p, \psi) + \frac{s}{z(s)}(p, \psi)_{L^2(\partial\Omega)}.$$

Its boundedness follows from the continuity of the trace $H^1(\Omega) \to L^2(\partial\Omega)$ (see Section C.1). The fact that $z(s) > 0$ gives

$$|a(\psi, \psi)| \geq \min(1, s^2)\|\psi\|^2_{H^1(\Omega)},$$

which establishes the coercivity of a. □

Proof. Let $s \in \overline{\mathbb{C}_0^+}\backslash\{0\}$. The Lax-Milgram lemma does not apply since the sign of $\Re(\overline{s}z(s))$ is indefinite in general, but the Fredholm alternative is applicable. Using the Riesz-Fréchet representation theorem (Lax 2002, Thm. 6.4), (4.7) can be rewritten uniquely as

$$(\mathcal{I} - \mathcal{K}(s))p = L \quad \text{in } H^1(\Omega), \tag{4.8}$$

where $L \in H^1(\Omega)$ satisfies $\overline{l(\psi)} = (L, \psi)_{H^1(\Omega)}$ and the operator $\mathcal{K}(s) \in \mathcal{L}(H^1(\Omega))$ is given by

$$(\mathcal{K}(s)p, \psi)_{H^1(\Omega)} \coloneqq (1 - s^2)(p, \psi) - \frac{s}{z(s)}(p, \psi)_{L^2(\partial\Omega)}.$$

The interest of (4.8) lies in the fact that $\mathcal{K}(s)$ turns out to be a compact operator, see Lemma 4.8. The Fredholm alternative states that $\mathcal{I} - \mathcal{K}(s)$ is injective if and only if it is surjective (Brezis 2011, Thm. 6.6). Using Lemma 4.9 and the open mapping theorem (Yosida 1980, § II.5), we conclude that $\mathcal{I} - \mathcal{K}(s)$ is a bijection with continuous inverse, which yields the claimed well-posedness result. □

Lemma 4.8. *Let $s \in \overline{\mathbb{C}_0^+}\backslash\{0\}$. The operator $\mathcal{K}(s) \in \mathcal{L}(H^1(\Omega))$ is compact.*

Proof. Let $p, \psi \in H^1(\Omega)$. The Cauchy–Schwarz inequality and the continuity of the trace $H^1(\Omega) \to L^2(\partial\Omega)$ yield the existence of a constant $C > 0$ such that

$$\left|(\mathcal{K}(s)p, \psi)_{H^1(\Omega)}\right| \leq \left(\left|1 - s^2\right| \|p\| + C\left|\frac{s}{z(s)}\right| \|p\|_{L^2(\partial\Omega)}\right) \|\psi\|_{H^1(\Omega)},$$

from which we deduce

$$\|\mathcal{K}(s)p\|_{H^1(\Omega)} \leq \left|1 - s^2\right| \|p\| + C\left|\frac{s}{z(s)}\right| \|p\|_{L^2(\partial\Omega)}.$$

Let $\epsilon \in (0, 1)$. The continuous embedding $H^{\frac{1}{2}+\epsilon}(\Omega) \subset L^2(\Omega)$ and the continuity of the trace $H^{\frac{1}{2}+\epsilon}(\Omega) \to L^2(\partial\Omega)$, see Section C.1, yield

$$\|\mathcal{K}(s)p\|_{H^1(\Omega)} \leq \left(\left|1 - s^2\right| + C'\left|\frac{s}{z(s)}\right|\right) \|p\|_{H^{\epsilon+\frac{1}{2}}(\Omega)}.$$

The compactness of the embedding $H^1(\Omega) \subset H^{\frac{1}{2}+\epsilon}(\Omega)$, see Section C.1, enables to conclude. □

Lemma 4.9. *Let $s \in \overline{\mathbb{C}_0^+}\backslash\{0\}$. The operator $\mathcal{I} - \mathcal{K}(s)$ is injective.*

Proof. Assume that $\mathcal{I} - \mathcal{K}(s)$ is not injective. Then there exists $p \in H^1(\Omega)\backslash\{0\}$ such that $\mathcal{K}(s)p = p$, i.e. for any $\psi \in H^1(\Omega)$,

$$(\nabla p, \nabla\psi) + s^2(p, \psi) + \frac{s}{z(s)}(p, \psi)_{L^2(\partial\Omega)} = 0. \tag{4.9}$$

In particular, for $\psi = p$,

$$z(s)\|\nabla p\|^2 + s^2 z(s)\|p\|^2 + s\|p\|^2_{L^2(\partial\Omega)} = 0. \tag{4.10}$$

To derive a contradiction, we distinguish between $s \in \mathbb{C}_0^+$ and $s \in \mathrm{j}\mathbb{R}^*$.
($s \in \mathbb{C}_0^+$) This is a direct consequence of Lemma 4.10.
($s \in \mathrm{j}\mathbb{R}^*$) Let $s = \mathrm{j}\omega$ with $\omega \in \mathbb{R}^*$. Then (4.10) reads

$$\begin{cases} \Re(z(\mathrm{j}\omega))\left(\|\nabla p\|^2 - \omega^2\|p\|^2\right) = 0 \\ \Im(z(\mathrm{j}\omega))\left(\|\nabla p\|^2 - \omega^2\|p\|^2\right) + \omega\|p\|^2_{L^2(\partial\Omega)} = 0, \end{cases}$$

so that $p \in H^1_0(\Omega)$. Going back to the first identity (4.9), we therefore have

$$\forall \psi \in H^1(\Omega),\ (\nabla p, \nabla \psi) = \omega^2 (p, \psi).$$

The contradiction then follows from Lemma 4.11, written in its own section below. □

Lemma 4.10. *Let $(a_0, a_1, a_2) \in [0, \infty)^3$ and $z \in \mathbb{C}^+_0$. The polynomial $s \mapsto z a_2 s^2 + a_1 s + z a_0$ has no roots in $\mathbb{C}^+_0$.*

Proof. The only case that needs investigating is $a_i > 0$ for $i \in [\![0, 2]\!]$. Let us denote by $\sqrt{\cdot}$ the branch of the square root that has a nonnegative real part, with a cut on $(-\infty, 0]$ (i.e. $\sqrt{\cdot}$ is analytic over $\mathbb{C}\backslash(-\infty, 0]$). The roots are given by

$$s_\pm \coloneqq \frac{a_1 \overline{z}}{2 a_2 |z|^2} \left(-1 \pm \sqrt{1 - \gamma z^2} \right)$$

with $\gamma \coloneqq 4 \frac{a_0 a_2}{a_1^2} > 0$ so that

$$\Re(s_\pm) = \frac{a_1}{2 a_2 |z|^2} f_\pm(z) \quad \text{with} \quad f_\pm(z) \coloneqq \Re \left[\overline{z} \left(-1 \pm \sqrt{1 - \gamma z^2} \right) \right].$$

The function $f_\pm$ is continuous on $\mathbb{C}^+_0 \backslash [\gamma^{-1/2}, \infty)$ (but not analytic) and vanishes only on $\mathrm{j}\mathbb{R}$ (if $f_\pm(z) = 0$, then there is $\omega \in \mathbb{R}$ such that $2\omega z = \mathrm{j}\,(\omega^2 - \gamma |z|^4)$). The claim therefore follows from

$$f_\pm \left(\frac{1}{\sqrt{2\gamma}} \right) = \frac{-\sqrt{2} \pm 1}{2\sqrt{\gamma}} < 0.$$

□

4.1.3 A consequence of the Rellich identity

This lemma is used in the proof of Proposition 4.4; it requires the smoothness of $\partial\Omega$.

Lemma 4.11. *Let $\Omega \subset \mathbb{R}^d$ be a bounded open set with an infinitely smooth boundary. If $p \in H^1_0(\Omega)$ satisfies*

$$\forall \psi \in H^1(\Omega),\ (\nabla p, \nabla \psi) = \lambda (p, \psi) \tag{4.11}$$

for some $\lambda \in \mathbb{C}$, then $p \in \mathcal{C}(\overline{\Omega})$ and $p = 0$ in Ω.

Proof. Let $p \in H^1_0(\Omega)$ be such that (4.11) holds for some $\lambda \in \mathbb{C}$. In particular,

$$\forall \psi \in H^1_0(\Omega),\ (\nabla p, \nabla \psi) = \lambda (p, \psi),$$

so that p is either null a.e. in Ω or an eigenfunction of the Dirichlet Laplacian. In the latter case, since the boundary $\partial\Omega$ is of class $\mathcal{C}^\infty$, we have the regularity result $p \in \mathcal{C}^\infty(\overline{\Omega})$ (Gilbarg and Trudinger 2001, Thm. 8.13). An integration by parts then shows that, for $\psi \in H^1(\Omega)$,

$$(\partial_n p, \psi)_{L^2(\partial\Omega)} = (\Delta p + \lambda p, \psi) = 0,$$

so that $\partial_n p = 0$ in $\partial\Omega$. However since p is $\mathcal{C}^2(\overline{\Omega})$ and $\partial\Omega$ is smooth we have (Rellich 1940)

$$\|p\|^2 = \frac{\int_{\partial\Omega} (\partial_n p)^2 \partial_n (|\boldsymbol{x}|^2)\, \mathrm{d}\boldsymbol{x}}{4\lambda}, \tag{4.12}$$

which shows that $p = 0$ in Ω. (The spectrum of the Dirichlet Laplacian does not include 0 (Gilbarg and Trudinger 2001, § 8.12).) □

Remark 4.12. In the proof of Lemma 4.11, the use of the Rellich identity (4.12) can be avoided. Once $p \in \mathcal{C}^2(\overline{\Omega})$ is established, the fact that $p = 0$ in Ω can be deduced from (Willms and Gladwell 1994, Lem. 1) that requires Ω to be bounded, connected, with $\mathcal{C}^{2+\epsilon}$ boundary, $\epsilon > 0$. Moreover, although this is not the topic of the work, this method of proof could enable to loosen the regularity assumption on Ω.

4.2 Abstract framework for asymptotic stability

The purpose of this section is to present the strategy used in this chapter to establish asymptotic stability, as well as to demonstrate it on an elementary example, namely the proportional IBC (4.18).

4.2.1 Strategy

Let the causal distribution $z \in \mathcal{D}'_+(\mathbb{R})$ be an admissible impedance kernel. In order to prove the asymptotic stability of (4.2,4.3), we will use in the next sections the following strategy. We first rely on the knowledge of a realization of the impedance operator $u \mapsto z \star u$ to formulate an abstract Cauchy problem on a Hilbert space H,

$$\dot{X}(t) = \mathcal{A}X,\ X(0) = X_0 \in H, \tag{4.13}$$

where the extended state X accounts for the memory of the IBC. The scalar product $(\cdot,\cdot)_H$ is defined using a Lyapunov functional associated with the realization. Since, by design, the problem has the energy estimate $\|X(t)\|_H \leq \|X_0\|_H$, it is natural to use the Lumer-Phillips theorem to show that the unbounded operator

$$\mathcal{A} :\ \mathcal{D}(\mathcal{A}) \subset H \to H \tag{4.14}$$

generates a strongly continuous semigroup of contractions on H, denoted by $\mathcal{T}(t)$. For initial data in $\mathcal{D}(\mathcal{A})$, the function

$$t \mapsto \mathcal{T}(t)X_0 \tag{4.15}$$

provides the unique strong solution in $\mathcal{C}([0,\infty);\mathcal{D}(\mathcal{A})) \cap \mathcal{C}^1([0,\infty);H)$ of the evolution problem (4.13) (Pazy 1983, Thm. 1.3). For (less regular) initial data in H, the solution is milder, namely $\mathcal{C}([0,\infty);H)$.

In Sections 4.3–4.7, to prove the asymptotic stability of this solution, we rely upon the following result, where we denote by $\sigma(\mathcal{A})$ (resp. $\sigma_p(\mathcal{A})$) the spectrum (resp. point spectrum) of $\mathcal{A}$ (Yosida 1980, § VIII.1). This result is a corollary of the ABLV theorem, recalled in Theorem C.3.

Corollary 4.13. *Let H be a complex Hilbert space and $\mathcal{A}$ be defined as (4.14). If*

(i) *$\mathcal{A}$ is dissipative, i.e. $\Re(\mathcal{A}X, X)_H \leq 0$ for every $X \in \mathcal{D}(\mathcal{A})$,*

(ii) *$\mathcal{A}$ is injective,*

(iii) *$s\mathcal{I} - \mathcal{A}$ is bijective for $s \in (0,\infty) \cup \mathrm{j}\mathbb{R}^*$,*

then $\mathcal{A}$ is the infinitesimal generator of a strongly continuous semigroup of contractions $\mathcal{T}(t) \in \mathcal{L}(H)$ that is asymptotically stable, i.e.

$$\forall X_0 \in H,\ \|\mathcal{T}(t)X_0\|_H \underset{t\to\infty}{\longrightarrow} 0. \tag{4.16}$$

Proof. The Lumer-Phillips theorem, recalled in Theorem C.2, shows that $\mathcal{A}$ generates a strongly continuous semigroup of contractions $\mathcal{T}(t) \in \mathcal{L}(H)$. In particular $\mathcal{A}$ is closed, from the Hille-Yosida theorem (Pazy 1983, Thm. 3.1), so that the resolvent operator $(s\mathcal{I} - \mathcal{A})^{-1}$ is closed whenever it is defined. A direct application of the closed graph theorem (Yosida 1980, § II.6) then yields

$$\{s \in \mathbb{C} \mid s\mathcal{I} - \mathcal{A} \text{ is bijective}\} \subset \rho(\mathcal{A}),$$

where $\rho(\mathcal{A})$ denotes the resolvent set of $\mathcal{A}$ (Yosida 1980, § VIII.1). Hence $\mathrm{j}\mathbb{R}^* \subset \rho(\mathcal{A})$ and Theorem C.3 applies since $0 \notin \sigma_p(\mathcal{A})$. □

Remark 4.14. Condition (iii) of Corollary 4.13 could be loosened by only requiring that $s\mathcal{I} - \mathcal{A}$ be surjective for $s \in (0, \infty)$ and bijective for $s \in \mathrm{j}\mathbb{R}^*$. However, in the proofs presented in this chapter we always prove bijectivity for $s \in (0, \infty) \cup \mathrm{j}\mathbb{R}^*$.

4.2.2 Proportional impedance as an elementary example

Let us consider the simplest of all positive-real kernels, namely the so-called proportional impedance

$$\hat{z}(s) \coloneqq z_0 \tag{4.17}$$

with $z_0 > 0$, so that IBC (4.3) reads

$$p = z_0 \, \boldsymbol{u} \cdot \boldsymbol{n} \quad \text{a.e. on } \partial\Omega. \tag{4.18}$$

This case is elementary (it is known that exponential stability is achieved (Chen 1981; Komornik and Zuazua 1990; Lagnese 1983)), but it is covered here for the sake of clarity since it provides a blueprint for handling more advanced IBCs in Sections 4.3–4.7. In view of Proposition 4.4, in the remainder of this chapter, we make the following assumption on the set Ω.

Assumption 4.15. *The set $\Omega \subset \mathbb{R}^d$, $d \in [\![1, \infty[\![$, is an open bounded set with an infinitely smooth boundary $\partial\Omega$.*

Since the IBC (4.18) is memoryless, the state X classically reduces to

$$X \coloneqq (\boldsymbol{u}, p)$$

and does not include any additional variable. A direct application of the Lumer-Phillips theorem shows that well-posedness is achieved with the following setting

$$\begin{aligned} \breve{H} &\coloneqq (L^2(\Omega))^{d+1}, \ \breve{\mathcal{A}} X \coloneqq - \begin{pmatrix} \nabla p \\ \operatorname{div} \boldsymbol{u} \end{pmatrix}, \\ \mathcal{D}(\breve{\mathcal{A}}) &\coloneqq \left\{ (\boldsymbol{u}, p) \in H_{\operatorname{div}}(\Omega) \times H^1(\Omega) \;\middle|\; p = z_0 \boldsymbol{u} \cdot \boldsymbol{n} \text{ in } H^{-\frac{1}{2}}(\partial\Omega) \right\}, \end{aligned} \tag{4.19}$$

with

$$H_{\operatorname{div}}(\Omega) \coloneqq \left\{ \boldsymbol{u} \in L^2(\Omega)^d \mid \operatorname{div} \boldsymbol{u} \in L^2(\Omega) \right\}.$$

However, this setting is not suited for asymptotic stability, since $\breve{\mathcal{A}}$ is not injective. Indeed, the definition of $\breve{\mathcal{A}}$ in (4.19) shows that

$$H_{\operatorname{div} 0,0}(\Omega) \times \{0_{L^2(\Omega)}\} \subset \ker(\breve{\mathcal{A}}),$$

where $H_{\operatorname{div} 0,0}(\Omega)$ is defined by

$$H_{\operatorname{div} 0,0}(\Omega) \coloneqq \left\{ \boldsymbol{u} \in H_{\operatorname{div}}(\Omega) \;\middle|\; \operatorname{div} \boldsymbol{u} = 0, \ \boldsymbol{u} \cdot \boldsymbol{n} = 0 \text{ in } H^{-\frac{1}{2}}(\partial\Omega) \right\}.$$

In view of the orthogonal decomposition (C.2), recalled in the Section C.2, an injective evolution operator $\mathcal{A}$ can be obtained by adapting the definition of the state space, namely

$$\begin{aligned} H &\coloneqq \nabla H^1(\Omega) \times L^2(\Omega), \ \mathcal{A} X \coloneqq - \begin{pmatrix} \nabla p \\ \operatorname{div} \boldsymbol{u} \end{pmatrix}, \\ \mathcal{D}(\mathcal{A}) &\coloneqq \left\{ (\boldsymbol{u}, p) \in H \;\middle|\; \begin{array}{l} (\boldsymbol{u}, p) \in H_{\operatorname{div}}(\Omega) \times H^1(\Omega), \\ p = z_0 \boldsymbol{u} \cdot \boldsymbol{n} \text{ in } H^{-\frac{1}{2}}(\partial\Omega) \end{array} \right\}. \end{aligned} \tag{4.20}$$

Since $\nabla H^1(\Omega)$ is a closed subspace of $L^2(\Omega)^d$, H is a Hilbert space equipped with the usual L^2 scalar product, see Section C.2 for some background.

Remark 4.16. The exclusion of the solenoidal fields $\boldsymbol{u}$ that belong to $H_{\mathrm{div}\,0,0}(\Omega)$ from the domain of $\mathcal{A}$ can be physically justified by the fact that these fields are non-propagating.

To obtain the asymptotic stability of the solution of (4.13,4.20), we apply Corollary 4.13: each of the three lemmas below cover one condition, namely Lemma 4.17 condition (i), Lemma 4.18 condition (ii), and Lemma 4.19 condition (iii).

Lemma 4.17. *The operator $\mathcal{A}$ given by (4.20) is dissipative.*

Proof. Let $X \in \mathcal{D}(\mathcal{A})$. Green's formula (C.1) yields

$$\Re(\mathcal{A}X, X)_H = -\Re\left[\langle \boldsymbol{u}\cdot\boldsymbol{n}, \overline{p}\rangle_{H^{-\frac{1}{2}}(\partial\Omega), H^{\frac{1}{2}}(\partial\Omega)}\right].$$

The IBC (4.18), which implies in particular that $\boldsymbol{u}\cdot\boldsymbol{n} \in L^2(\partial\Omega)$, and (4.1) yield

$$\Re(\mathcal{A}X, X)_H = -\Re\left[(\boldsymbol{u}\cdot\boldsymbol{n}, p)_{L^2(\partial\Omega)}\right] = -z_0\|\boldsymbol{u}\cdot\boldsymbol{n}\|^2_{L^2(\partial\Omega)} \le 0,$$

so that $\mathcal{A}$ is dissipative. □

Lemma 4.18. *The operator $\mathcal{A}$ given by (4.20) is injective.*

Proof. Assume $X \in \mathcal{D}(\mathcal{A})$ satisfies $\mathcal{A}X = 0$. Then $\nabla p = \boldsymbol{0}$ and $\operatorname{div}\boldsymbol{u} = 0$ so that Green's formula (C.1) yields

$$\langle \boldsymbol{u}\cdot\boldsymbol{n}, \overline{p}\rangle_{H^{-\frac{1}{2}}(\partial\Omega), H^{\frac{1}{2}}(\partial\Omega)} = 0.$$

The IBC (4.18) implies $\boldsymbol{u}\cdot\boldsymbol{n} = p = 0$ in $H^{\frac{1}{2}}(\partial\Omega)$, so that $p = 0$ and $\boldsymbol{u} \in H_{\mathrm{div}\,0,0}(\Omega)$. Since $\boldsymbol{u} \in \nabla H^1(\Omega)$ by assumption, the orthogonal decomposition (C.2) implies that $\boldsymbol{u} = \boldsymbol{0}$, hence $X = 0$. □

Lemma 4.19. *Let $\mathcal{A}$ be given by (4.20). Then, $s\mathcal{I} - \mathcal{A}$ is bijective for $s \in (0,\infty) \cup \mathrm{j}\mathbb{R}^*$.*

Proof. Let $F \in H$ and $s \in (0,\infty)\cup\mathrm{j}\mathbb{R}^*$. We seek a *unique* $X \in \mathcal{D}(\mathcal{A})$ such that $(s\mathcal{I}-\mathcal{A})X = F$, i.e.

$$\begin{cases} s\boldsymbol{u} + \nabla p = \boldsymbol{f}_{\boldsymbol{u}} & \text{(a)} \\ sp + \operatorname{div}\boldsymbol{u} = f_p. & \text{(b)} \end{cases} \tag{4.21}$$

Let $\psi \in H^1(\Omega)$. Using Green's formula (C.1) on $(\boldsymbol{f}_{\boldsymbol{u}}, \nabla\psi) + s\,(f_p, \psi)$ yields

$$\begin{aligned} s(\boldsymbol{u}, \nabla\psi) + (\nabla p, \nabla\psi) + s\left[s(p,\psi) + \langle \boldsymbol{u}\cdot\boldsymbol{n}, \overline{\psi}\rangle_{H^{-\frac{1}{2}}(\partial\Omega), H^{\frac{1}{2}}(\partial\Omega)} - (\boldsymbol{u}, \nabla\psi)\right] \\ = (\boldsymbol{f}_{\boldsymbol{u}}, \nabla\psi) + s(f_p, \psi). \end{aligned}$$

In summary, $(s\mathcal{I}-\mathcal{A})X = F$ with $X \in \mathcal{D}(\mathcal{A})$ implies

$$(\nabla p, \nabla\psi) + s^2(p,\psi) + \frac{s}{z_0}(p,\psi)_{L^2(\partial\Omega)} = (\boldsymbol{f}_{\boldsymbol{u}}, \nabla\psi) + s(f_p, \psi). \tag{4.22}$$

Let us denote by p the unique solution of (4.22) in $H^1(\Omega)$, obtained by applying Proposition 4.4 with (4.17) and $\overline{l(\psi)} \coloneqq (\boldsymbol{f}_{\boldsymbol{u}}, \nabla\psi) + s(f_p, \psi)$.

Let us define $\boldsymbol{u}$ using (4.21a), i.e.

$$\boldsymbol{u} \coloneqq \frac{1}{s}(-\nabla p + \boldsymbol{f}_{\boldsymbol{u}}) \in \nabla H^1(\Omega).$$

Using the expression of $\boldsymbol{u}$, (4.22) can be rewritten as

$$(\boldsymbol{u}, \nabla\psi) = -(-sp + f_p, \psi) + \frac{1}{z_0}(p, \psi)_{L^2(\partial\Omega)}, \tag{4.23}$$

so that taking $\psi \in \mathcal{C}_0^\infty(\Omega)$ in (4.23) shows that $\boldsymbol{u} \in H_{\mathrm{div}}(\Omega)$ with (4.21b). Using the expression of $\operatorname{div}\boldsymbol{u}$, (4.23) becomes

$$(\boldsymbol{u}, \nabla\psi) + (\operatorname{div}\boldsymbol{u}, \psi) = \frac{1}{z_0}(p, \psi)_{L^2(\partial\Omega)}$$

and Green's formula (C.1) shows that the proportional IBC (4.18) holds.

In summary, we have found $\boldsymbol{u} \in H_{\mathrm{div}}(\Omega)$ and a *unique* $p \in H^1(\Omega)$ such that (4.21) holds with the proportional IBC (4.18) in $H^{-\frac{1}{2}}(\partial\Omega)$. Although $\boldsymbol{u}$ is not unique in $H_{\mathrm{div}}(\Omega)$, it is unique in $H_{\mathrm{div}}(\Omega) \cap \nabla H^1(\Omega)$ following (C.2). Hence there is a unique X that solves $(s\mathcal{I} - \mathcal{A})X = F$ in $\mathcal{D}(\mathcal{A})$. □

4.2.3 Application of LaSalle's invariance principle

The purpose of this section is to justify why, in this chapter, we rely on Corollary 4.13 rather than the invariance principle, commonly used with dynamical systems on Banach spaces.

Theorem 4.20 states the invariance principle for the case of interest herein, i.e. a linear Cauchy problem (4.13) for which the Lyapunov functional is $\frac{1}{2}\|\cdot\|_H^2$. (For further background, see (Luo et al. 2012, § 3.7) and (Cazenave and Haraux 1998, Chap. 9).)

Theorem 4.20 (Invariance principle)**.** *Let $\mathcal{A}$ be the infinitesimal generator of a strongly continuous semigroup of contractions $\mathcal{T}(t) \in \mathcal{L}(H)$ and $X_0 \in H$. If the orbit $\gamma(X_0) \coloneqq \bigcup_{t\geq 0} \mathcal{T}(t)X_0$ lies in a compact set of H, then $\mathcal{T}(t)X_0 \to M$ as $t \to \infty$, where M is the largest $\mathcal{T}$-invariant set in*

$$\{X \in \mathcal{D}(\mathcal{A}) \mid \Re[(\mathcal{A}X, X)_H] = 0\}. \tag{4.24}$$

Proof. The function $\Phi \coloneqq \frac{1}{2}\|\cdot\|_H^2$ is continuous on H and satisfies $\Phi(\mathcal{T}(t)X) \leq \Phi(X)$ for any $X \in H$ so that it is a Lyapunov functional. The invariance principle (Hale 1969, Thm. 1) then shows that $\mathcal{T}(t)X_0$ is attracted to the largest invariant set of

$$\left\{X \in H \;\middle|\; \lim_{t\to 0^+} t^{-1}(\Phi(\mathcal{T}(t)X) - \Phi(X)) = 0\right\}.$$

□

The following criterion can be used to prove precompactness of the orbits, where for $s \in \rho(\mathcal{A})$ we denote the resolvent operator by

$$R(s, \mathcal{A}) \coloneqq (s\mathcal{I} - \mathcal{A})^{-1}. \tag{4.25}$$

Theorem 4.21 ((Dafermos and Slemrod 1973, Thm. 3))**.** *Let $\mathcal{A}$ be the infinitesimal generator of a strongly continuous semigroup of contractions on H. If $R(s, \mathcal{A})$ is compact for some $s > 0$, then $\gamma(X_0)$ is precompact for any $X_0 \in H$.*

Let us now discuss the application of the invariance principle to (4.20), already covered in Section 4.2.2 using Corollary 4.13. They are two main steps.

The first step is to establish that the largest invariant subset of (4.24), given by

$$\mathcal{D}(\mathcal{A}) \cap \left(H_{\mathrm{div},0}(\Omega) \times H_0^1(\Omega)\right), \tag{4.26}$$

reduces to $\{0\}$. This amounts to showing that the only solution of (4.13) in (4.26) is null.

The second step is to prove the precompactness of the orbit $\gamma(X_0)$ for any X_0 in H. This is obvious if $d = 1$. If $d = 3$, the compactness of the embedding $\mathcal{D}(\mathcal{A}) \subset H$ can be proven using the following regularity result: if Ω is a bounded simply connected open set with Lipschitz boundary, (Costabel 1990, Thm. 2)

$$H_{\mathrm{curl}}(\Omega) \cap \left\{ \boldsymbol{u} \in H_{\mathrm{div}}(\Omega) \;\middle|\; \boldsymbol{u} \cdot \boldsymbol{n} \in L^2(\partial\Omega) \right\} \subset H^{\frac{1}{2}}(\Omega)^d$$

and $\nabla H^1(\Omega) \subset H_{\mathrm{curl}}(\Omega)$ (Girault and Raviart 1986, Thm. 2.9). (Note the stringent requirement that Ω be simply connected.) However, this step complicates further when IBCs with infinite-dimensional realizations are considered: in Sections 4.4–4.6, we will encounter IBCs that induce a lack of precompactness of the orbit, although the cause of this lack of precompactness differs as will be discussed in Remarks 4.36 and 4.48. These technical difficulties justify why we herein use Corollary 4.13 instead of the invariance principle.

4.3 Rational impedance

In this section, we consider the positive-real impedance given by

$$\hat{z}(s) \coloneqq z_0 + \hat{Z}(s), \tag{4.27}$$

with $z_0 \geq 0$ and $\hat{Z}$ a positive-real rational function, analytic in $\overline{\mathbb{C}_0^+}$, such that $\hat{Z}(\infty) = 0$. We further impose that

$$\hat{z}(0) \neq 0,$$

so that z_0 can be null iff $\hat{Z}(0) \neq 0$. The impedance (4.27) can be understood as arising from a rational approximation of a physical impedance model, as done in practical numerical simulations (Monteghetti et al. 2018b).

This section is organized as follows. Section 4.3.1 formulates a minimal realization of $\hat{z}$, namely (4.28), and obtains a Lyapunov functional using the positive-real lemma. This is then used in Section 4.3.2 to formulate the coupled system (4.32) and prove asymptotic stability using Corollary 4.13.

4.3.1 Positive-real lemma

Since $\hat{z}$ is a rational function such that

$$\hat{z}(\infty) = z_0$$

is finite and

$$\hat{z}(s) \in \mathbb{R} \quad (s \in (0, \infty)),$$

the corresponding linear time-invariant operator $u \mapsto z \star u$ admits a minimal finite-dimensional state-space realization (A, B, C, z_0)

$$\begin{cases} \dot{\boldsymbol{\varphi}} & = A\boldsymbol{\varphi} + Bu \\ z \star u & = C\boldsymbol{\varphi} + z_0 u, \end{cases} \tag{4.28}$$

where u is a causal input (i.e. $u(t) = 0$ for $t < 0$), $\boldsymbol{\varphi}(t) \in \mathbb{R}^m$ is the state vector, $A \in \mathbb{R}^{m \times m}$ is the state matrix, $B \in \mathbb{R}^{m \times 1}$ is the control matrix, $C \in \mathbb{R}^{1 \times m}$ is the observation matrix, and the feedthrough matrix is here the scalar z_0. For background on this result, see e.g. the textbook (Zhou et al. 1996, § 3.7). For $s \in \rho(A)$, the resolvent set of A, the impedance (4.27) can be re-expressed as

$$\hat{z}(s) = z_0 + CR(s, A)B, \tag{4.29}$$

where $R(s,A)$ denotes the resolvent

$$R(s,A) \coloneqq (s\mathbb{I}_m - A)^{-1}.$$

The minimality of the realization (4.28) means that m is the smallest possible integer for (4.29) to hold. For example, if $\hat{z}$ has only N simple poles then $m = N$.

To use (4.28) with the semigroup approach considered herein, it is imperative to exhibit an energy balance (equivalently, a Lyapunov functional). It is provided by the celebrated positive-real lemma, also known as the Kalman–Yakubovich–Popov lemma, recalled below under a form different than that given in (Matignon and Prieur 2014) and more suited to our purposes.

Theorem 4.22 (Positive-real lemma (Anderson 1967, Thm. 3))**.** *Let f be a rational function that is analytic on $\overline{\mathbb{C}_0^+}$ apart from simple poles on $\mathrm{j}\mathbb{R}$ and such that $f_\infty \coloneqq f(\infty)$ is finite. Let (A,B,C,f_∞) be a minimal realization of f (hence f is given by (4.29) with "f_∞" instead of "z_0"). Then, f is positive-real if and only if there exists a symmetric matrix $P > 0$ such that*

$$\begin{bmatrix} PA^\intercal + A^\intercal P & PB - C^\intercal \\ B^\intercal P - C & -2f_\infty \end{bmatrix} \leq 0.$$

Let $P \in \mathbb{R}^{m\times m}$ be the symmetric positive definite matrix obtained by applying Theorem 4.22 to (4.27) and let us define the induced scalar product and norm by

$$(\boldsymbol{f},\boldsymbol{g})_P \coloneqq (P\boldsymbol{f},\boldsymbol{g})_{\mathbb{C}^m},\ \|\boldsymbol{f}\|_P^2 \coloneqq (\boldsymbol{f},\boldsymbol{f})_P,$$

for any $\boldsymbol{f},\boldsymbol{g} \in \mathbb{C}^m$. If $\boldsymbol{\varphi}$ is a $\mathcal{C}^1$ solution of (4.28), an elementary computation shows the following equivalence:

$$\frac{\mathrm{d}}{\mathrm{d}t}\|\boldsymbol{\varphi}\|_P^2 \leq 2\Re\left[(u, z\star u)_{\mathbb{C}}\right] \tag{4.30}$$

$$\Updownarrow$$

$$((PA + A^\intercal P)\boldsymbol{\varphi},\boldsymbol{\varphi})_{\mathbb{C}^m} + ((PB - C^\intercal)u,\boldsymbol{\varphi})_{\mathbb{C}^m} + ((B^\intercal P - C)\boldsymbol{\varphi},u)_{\mathbb{C}} - 2\Re(z_0)|u|^2 \leq 0$$

$$\Updownarrow$$

$$2\Re\left[(A\boldsymbol{\varphi} + Bu,\boldsymbol{\varphi})_P - (u, z_0u + C\boldsymbol{\varphi})_{\mathbb{C}}\right] \leq 0. \tag{4.31}$$

In summary, thanks to the positive-real lemma, the realization (4.28) enjoys the energy balance (4.30).

In preparation for the analysis of Section 4.3.2, we define the Hilbert space

$$L^2_P(\partial\Omega;\mathbb{C}^m) \coloneqq \left\{\boldsymbol{\varphi} :\ \partial\Omega \to \mathbb{C}^m \text{ measurable } \middle|\ \int_{\partial\Omega} \|\boldsymbol{\varphi}\|_P^2\,\mathrm{d}\boldsymbol{x} < \infty\right\},$$

with scalar product

$$(\boldsymbol{\varphi},\boldsymbol{\psi})_{L^2_P(\partial\Omega;\mathbb{C}^m)} \coloneqq \int_{\partial\Omega} (\boldsymbol{\varphi},\boldsymbol{\psi})_P.$$

Since P is invertible, the two norms $\|\cdot\|_{L^2_P(\partial\Omega;\mathbb{C}^m)}$ and $\|\cdot\|_{L^2(\partial\Omega;\mathbb{C}^m)}$ are equivalent.

Remark 4.23. Let $m \geq 1$. In (Abbas and Nicaise 2013, 2015) asymptotic stability is shown with the admittance realization

$$\begin{cases} \dot{\boldsymbol{\varphi}} &= A\boldsymbol{\varphi} + Bu \\ y\star u &= (B,\boldsymbol{\varphi})_{\mathbb{C}^m}, \end{cases}$$

which is (4.28) with $z_0 = 0$ and $C = B^\intercal$. This realization is additionally space-varying as both A and B are Lipschitz continuous with

$$\Re\left[(A(\boldsymbol{x})\cdot,\cdot)_{P(\boldsymbol{x})}\right] \leq 0$$

where $\boldsymbol{x} \mapsto P(\boldsymbol{x})$ is Lipschitz continuous with $P(\boldsymbol{x})$ a Hermitian positive-definite matrix.

4.3.2 Asymptotic stability

Using the realization of the IBC obtained in Section 4.3.1, we now recast (4.2,4.3) into an abstract Cauchy problem (4.13), following the program set out in Section 4.2.1. The extended state space is defined as

$$H \coloneqq \nabla H^1(\Omega) \times L^2(\Omega) \times L^2_P(\partial\Omega;\mathbb{C}^m),$$
$$((\boldsymbol{u},p,\boldsymbol{\varphi}),(\boldsymbol{f_u},f_p,\boldsymbol{f_\varphi}))_H \coloneqq (\boldsymbol{u},\boldsymbol{f_u}) + (p,f_p) + \int_{\partial\Omega} (\boldsymbol{\varphi},\boldsymbol{f_\varphi})_P,$$

and the evolution operator (4.14) is defined by

$$\begin{aligned} \mathcal{D}(\mathcal{A}) \ni X \coloneqq \begin{pmatrix} \boldsymbol{u} \\ p \\ \boldsymbol{\varphi} \end{pmatrix} &\longmapsto \mathcal{A}X \coloneqq \begin{pmatrix} -\nabla p \\ -\operatorname{div}\boldsymbol{u} \\ A\boldsymbol{\varphi} + B\boldsymbol{u}\cdot\boldsymbol{n} \end{pmatrix}, \\ \mathcal{D}(\mathcal{A}) \coloneqq \left\{ (\boldsymbol{u},p,\boldsymbol{\varphi}) \in H \;\middle|\; \begin{array}{l} (\boldsymbol{u},p) \in H_{\mathrm{div}}(\Omega) \times H^1(\Omega), \\ p = z_0\boldsymbol{u}\cdot\boldsymbol{n} + C\boldsymbol{\varphi} \text{ in } H^{-\frac{1}{2}}(\partial\Omega) \end{array} \right\}. \end{aligned} \tag{4.32}$$

Remark 4.24. For the sake of clarity there is an abuse of notation in (4.32), since we do not differentiate between the state matrix $A \in \mathbb{R}^{m\times m}$ and the state operator

$$\begin{vmatrix} L^2_P(\partial\Omega;\mathbb{C}^m) \to L^2_P(\partial\Omega;\mathbb{C}^m) \\ \boldsymbol{\varphi} \mapsto (\boldsymbol{x} \mapsto A\boldsymbol{\varphi}(\boldsymbol{x})). \end{vmatrix}$$

We proceed similarly for B and C.

As in Section 4.2.2, we verify the conditions of Corollary 4.13 through three lemmas, namely Lemmas 4.25, 4.26, and 4.27 given below.

Lemma 4.25. *$\mathcal{A}$ given by (4.32) is dissipative.*

Proof. Let $X \in \mathcal{D}(\mathcal{A})$. In particular, the IBC implies that $\boldsymbol{u}\cdot\boldsymbol{n} \in L^2(\partial\Omega)$, see Remark 4.24. Green's formula (C.1) and the inequality (4.31) yield

$$\begin{aligned} \Re(\mathcal{A}X,X)_H &= \Re\left[(A\boldsymbol{\varphi} + B\boldsymbol{u}\cdot\boldsymbol{n},\boldsymbol{\varphi})_{L^2_P(\partial\Omega)} - \langle \boldsymbol{u}\cdot\boldsymbol{n},\overline{p}\rangle_{H^{-\frac{1}{2}}(\partial\Omega),H^{\frac{1}{2}}(\partial\Omega)} \right] \\ &= \Re\left[(A\boldsymbol{\varphi} + B\boldsymbol{u}\cdot\boldsymbol{n},\boldsymbol{\varphi})_{L^2_P(\partial\Omega)} - (\boldsymbol{u}\cdot\boldsymbol{n}, z_0\boldsymbol{u}\cdot\boldsymbol{n} + C\boldsymbol{\varphi})_{L^2(\partial\Omega)} \right] \le 0, \end{aligned}$$

where we have used (4.1). □

Lemma 4.26. *$\mathcal{A}$ given by (4.32) is injective.*

Proof. Assume $X \in \mathcal{D}(\mathcal{A})$ satisfies $\mathcal{A}X = 0$, i.e. $\nabla p = \boldsymbol{0}$, $\operatorname{div}\boldsymbol{u} = 0$, and

$$A\boldsymbol{\varphi} + B\boldsymbol{u}\cdot\boldsymbol{n} = 0 \quad \text{in } L^2_P(\partial\Omega). \tag{4.33}$$

Identically to the proportional case covered in Lemma 4.18, Green's formula (C.1) yields

$$\langle \boldsymbol{u}\cdot\boldsymbol{n},\overline{p}\rangle_{H^{-\frac{1}{2}}(\partial\Omega),H^{\frac{1}{2}}(\partial\Omega)} = 0,$$

and using (4.1) with the fact that $\boldsymbol{u}\cdot\boldsymbol{n} \in L^2(\partial\Omega)$ we get

$$(\boldsymbol{u}\cdot\boldsymbol{n}, z_0\boldsymbol{u}\cdot\boldsymbol{n} + C\boldsymbol{\varphi})_{L^2(\partial\Omega)} = 0. \tag{4.34}$$

Since by assumption $\ker A = \{0\}$ (i.e. $\hat{Z}$ does not have a pole at 0), the identity (4.33) has a unique solution $\boldsymbol{\varphi} = -A^{-1}B\boldsymbol{u}\cdot\boldsymbol{n}$ so that (4.34) reads

$$\hat{z}(0)(\boldsymbol{u}\cdot\boldsymbol{n}, \boldsymbol{u}\cdot\boldsymbol{n})_{L^2(\partial\Omega)} = 0,$$

where we have used (4.29). As $\hat{z}(0) \neq 0$ by assumption, we deduce that $\boldsymbol{u}$ belongs to $H_{\mathrm{div}\,0,0}(\Omega)$, $\boldsymbol{\varphi} = 0$ in $L^2_P(\partial\Omega)$, and $p = 0$ in $L^2(\partial\Omega)$. The nullity of $\boldsymbol{u}$ follows from $H_{\mathrm{div}\,0,0}(\Omega)\cap\nabla H^1(\Omega) = \{0\}$, see (C.2). □

Lemma 4.27. *$s\mathcal{I} - \mathcal{A}$, with $\mathcal{A}$ given by (4.32), is bijective for $s \in (0,\infty)\cup \mathrm{j}\mathbb{R}^*$.*

Proof. Let $F \in H$ and $s \in (0,\infty)\cup\mathrm{j}\mathbb{R}^*$. We seek a *unique* $X \in \mathcal{D}(\mathcal{A})$ such that $(s\mathcal{I}-\mathcal{A})X = F$, i.e.

$$\begin{cases} s\boldsymbol{u} + \nabla p = \boldsymbol{f_u} & \text{(a)} \\ sp + \operatorname{div}\boldsymbol{u} = f_p & \text{(b)} \\ s\boldsymbol{\varphi} - A\boldsymbol{\varphi} - B\boldsymbol{u}\cdot\boldsymbol{n} = \boldsymbol{f_\varphi}. & \text{(c)} \end{cases} \tag{4.35}$$

For later use, let us note that Equation (4.35c) and the IBC imply

$$\boldsymbol{\varphi} = R(s,A)(B\boldsymbol{u}\cdot\boldsymbol{n} + \boldsymbol{f_\varphi}) \qquad \text{in } L^2_P(\partial\Omega) \tag{4.36}$$

$$p = \hat{z}(s)\boldsymbol{u}\cdot\boldsymbol{n} + CR(s,A)\boldsymbol{f_\varphi} \quad \text{in } L^2(\partial\Omega). \tag{4.37}$$

Let $\psi \in H^1(\Omega)$. Similarly to what was done in the proof of Lemma 4.19, combining $(\boldsymbol{f_u}, \nabla\psi) + s(f_p,\psi)$ with (4.37) yields

$$\begin{aligned}(\nabla p, \nabla\psi) + s^2(p,\psi) + \frac{s}{\hat{z}(s)}(p,\psi)_{L^2(\partial\Omega)} = (\boldsymbol{f_u},\nabla\psi) + s(f_p,\psi) \\ + \frac{s}{\hat{z}(s)}(CR(s,A)\boldsymbol{f_\varphi},\psi)_{L^2(\partial\Omega)}.\end{aligned} \tag{4.38}$$

Proposition 4.4 shows that (4.38) has a unique solution $p \in H^1(\Omega)$. It remains to find suitable $\boldsymbol{u}$ and $\boldsymbol{\varphi}$ so that $(\boldsymbol{u}, p, \boldsymbol{\varphi}) \in \mathcal{D}(\mathcal{A})$. Let us *define* $\boldsymbol{u} \in \nabla H^1(\Omega)$ by (4.35a). Taking $\psi \in \mathcal{C}^\infty_0(\Omega)$ in (4.38) shows that $\boldsymbol{u} \in H_{\mathrm{div}}(\Omega)$ and that (4.35b) holds. Using the expressions of both $\boldsymbol{u}$ and $\operatorname{div}\boldsymbol{u}$, the weak formulation (4.38) can be rewritten as

$$(\boldsymbol{u},\nabla\psi) + (\operatorname{div}\boldsymbol{u},\psi) = \hat{z}(s)^{-1}(p,\psi)_{L^2(\partial\Omega)} - \hat{z}(s)^{-1}(CR(s,A)\boldsymbol{f_\varphi},\psi)_{L^2(\partial\Omega)}.$$

Green's formula (C.1) then yields

$$\langle \boldsymbol{u}\cdot\boldsymbol{n}, \overline{\psi}\rangle_{H^{-\frac{1}{2}}(\partial\Omega), H^{\frac{1}{2}}(\partial\Omega)} = \hat{z}(s)^{-1}(p,\psi)_{L^2(\partial\Omega)} - \hat{z}(s)^{-1}(CR(s,A)\boldsymbol{f_\varphi},\psi)_{L^2(\partial\Omega)},$$

which shows that p and $\boldsymbol{u}$ satisfy (4.37). Let us now *define* $\boldsymbol{\varphi}$ as (4.36); it belongs to $L^2_P(\partial\Omega)$ since $\boldsymbol{u}\cdot\boldsymbol{n} \in L^2(\partial\Omega)$ from (4.37). By rewriting (4.37) as

$$p = (\hat{z}(s) - CR(s,A)B)\boldsymbol{u}\cdot\boldsymbol{n} + CR(s,A)(B\boldsymbol{u}\cdot\boldsymbol{n} + \boldsymbol{f_\varphi}),$$

we obtain from (4.29) and (4.36) that the IBC holds, hence $(\boldsymbol{u}, p, \boldsymbol{\varphi}) \in \mathcal{D}(\mathcal{A})$. The uniqueness of p follows from Proposition 4.4, that of $\boldsymbol{u}$ from (C.2), and that of $\boldsymbol{\varphi}$ from the bijectivity of $s\mathbb{I} - A$. □

Remark 4.28 (Invariance principle). Since the realization of $\hat{z}$ is finite-dimensional, proving asymptotic stability using the invariance principle would lead to similar discussions than those presented at the end of Section 4.2.3. See (Matignon 2006) for the case $d = 1$.

4.4 Delay impedance

This section, as well as Sections 4.5 and 4.6, deals with IBCs that have an *infinite*-dimensional realization, which arise naturally in physical modeling (Monteghetti et al. 2016a). Let us first consider the time-delayed impedance

$$\hat{z}(s) \coloneqq z_0 + z_\tau e^{-\tau s}, \tag{4.39}$$

where $z_0, z_\tau, \tau \in \mathbb{R}$, so that the corresponding IBC (4.3) reads

$$p(t) = z_0 \boldsymbol{u}(t) \cdot \boldsymbol{n} + z_\tau \boldsymbol{u}(t-\tau) \cdot \boldsymbol{n} \quad \text{a.e. on } \partial\Omega,\ t > 0.$$

The function (4.39) is positive-real if and only if

$$z_0 \geq |z_\tau|,\ \tau \geq 0, \tag{4.40}$$

which is assumed in the following. From now on, in addition to (4.40), we further assume

$$\hat{z}(0) \neq 0,\ \tau \neq 0.$$

This section is organized similarly to Section 4.3: a realization of $\hat{z}$ is recalled in Section 4.4.1 and the stability of the coupled system is shown in Section 4.4.2.

Remark 4.29. In (Nicaise and Pignotti 2006), exponential (resp. asymptotic) stability is shown under the condition $z_0 > z_\tau > 0$ (resp. $z_0 \geq z_\tau > 0$) and $\tau > 0$.

4.4.1 Time-delay realization

Following a well-known device, time-delays can be realized using a transport equation on a bounded interval (Curtain and Zwart 1995, § 2.4) (Engel and Nagel 2000, § VI.6). Let u be a causal input. The linear time-invariant operator $u \mapsto z \star u$ can be realized as

$$z \star u(t) = z_0 u(t) + z_\tau \chi(t, -\tau) \quad (t > 0),$$

where the state $\chi \in H^1(-\tau, 0)$ with $t \geq 0$ follows the transport equation

$$\begin{cases} \partial_t \chi(t,\theta) = \partial_\theta \chi(t,\theta), & (\theta \in (-\tau, 0),\ t > 0)\,, \quad \text{(a)} \\ \chi(0,\theta) = 0, & (\theta \in (-\tau, 0))\,, \quad \text{(b)} \\ \chi(t,0) = u(t), & (t > 0)\,. \quad \text{(c)} \end{cases} \tag{4.41}$$

For $\chi \in \mathcal{C}^1([0,T]; H^1(-\tau,0))$ solution of (4.41a), we have the following energy balance

$$\begin{aligned} \frac{1}{2}\frac{\mathrm{d}}{\mathrm{d}t}\|\chi(t,\cdot)\|^2_{L^2(-\tau,0)} &= \Re(\partial_\theta \chi(t,\cdot), \chi(t,\cdot))_{L^2(-\tau,0)} \\ &= \frac{1}{2}\left[|\chi(t,0)|^2 - |\chi(t,-\tau)|^2\right], \end{aligned}$$

which we shall use in the proof of Lemma 4.32.

Remark 4.30 (Multiple delays). Note that a finite number of time-delays $\tau_i > 0$ can be accounted for by setting $\tau \coloneqq \max_i \tau_i$ and writing

$$z \star u(t) = z_0 u(t) + \sum_i z_{\tau_i} \chi(t, -\tau_i).$$

The corresponding impedance $\hat{z}(s) = z_0 + \sum_i z_{\tau_i} e^{-\tau_i s}$ is positive-real if $z_0 \geq \sum_i |z_{\tau_i}|$. No substantial change to the proofs of Section 4.4.2 is required to handle this more general case.

4.4.2 Asymptotic stability

The state space is defined as

$$\begin{aligned} H &\coloneqq \nabla H^1(\Omega) \times L^2(\Omega) \times L^2(\partial\Omega; L^2(-\tau, 0)), \\ ((\boldsymbol{u}, p, \chi), (\boldsymbol{f_u}, f_p, f_\chi))_H &\coloneqq (\boldsymbol{u}, \boldsymbol{f_u}) + (p, f_p) + k(\chi, f_\chi)_{L^2(\partial\Omega; L^2(-\tau,0))}, \end{aligned} \tag{4.42}$$

where $k \in (0, \infty)$ is a constant to be tuned to achieve dissipativity, see Lemma 4.32. The evolution operator is defined as

$$\begin{aligned} \mathcal{D}(\mathcal{A}) \ni X \coloneqq \begin{pmatrix} \boldsymbol{u} \\ p \\ \chi \end{pmatrix} &\longmapsto \mathcal{A}X \coloneqq \begin{pmatrix} -\nabla p \\ -\operatorname{div} \boldsymbol{u} \\ \partial_\theta \chi \end{pmatrix}, \\ \mathcal{D}(\mathcal{A}) \coloneqq \left\{ (\boldsymbol{u}, p, \chi) \in H \;\middle|\; \begin{array}{l} (\boldsymbol{u}, p) \in H_{\operatorname{div}}(\Omega) \times H^1(\Omega) \\ \chi \in L^2(\partial\Omega; H^1(-\tau, 0)) \\ p = z_0 \boldsymbol{u} \cdot \boldsymbol{n} + z_\tau \chi(\cdot, -\tau) \text{ in } H^{-\frac{1}{2}}(\partial\Omega) \\ \chi(\cdot, 0) = \boldsymbol{u} \cdot \boldsymbol{n} \text{ in } H^{-\frac{1}{2}}(\partial\Omega) \end{array} \right\}. \end{aligned} \tag{4.43}$$

We apply Corollary 4.13, see the Lemmas 4.32, 4.33, and 4.34 below. Lemma 4.32 shows that the seemingly free parameter k must be restricted for $\|\cdot\|_H$ to be a Lyapunov functional, as formally highlighted in (Monteghetti et al. 2017a).

Remark 4.31 (Bochner's integral). For the integrability of vector-valued functions, we follow the definitions and results presented in (Yosida 1980, § V.5). Let $\mathcal{B}$ be a Banach space. We have (Yosida 1980, Thm. V.5.1)

$$L^2(\partial\Omega; \mathcal{B}) = \left\{ f : \partial\Omega \to \mathcal{B} \text{ strongly measurable} \;\middle|\; \|f\|_{\mathcal{B}} \in L^2(\partial\Omega) \right\}.$$

In Sections 4.5 and 4.6, we repeatedly use the following result: if $A \in \mathcal{L}(\mathcal{B}_1, \mathcal{B}_2)$ and $u \in L^2(\partial\Omega; \mathcal{B}_1)$, then $Au \in L^2(\partial\Omega; \mathcal{B}_2)$.

Lemma 4.32. *The operator $\mathcal{A}$ given by (4.43) is dissipative if and only if*

$$k \in \left[z_0 - \sqrt{z_0^2 - z_\tau^2}, z_0 + \sqrt{z_0^2 - z_\tau^2} \right].$$

Proof. Let $X \in \mathcal{D}(\mathcal{A})$. In particular, $\boldsymbol{u} \cdot \boldsymbol{n} \in L^2(\partial\Omega)$ since $\chi(\cdot, 0) \in L^2(\partial\Omega)$. Using Green's formula (C.1)

$$\begin{aligned} \Re(\mathcal{A}X, X)_H &= -\Re\left[\langle \boldsymbol{u} \cdot \boldsymbol{n}, \overline{p} \rangle_{H^{-\frac{1}{2}}(\partial\Omega), H^{\frac{1}{2}}(\partial\Omega)} \right] + k \Re\left(\partial_\theta \chi, \chi \right)_{L^2(\partial\Omega; L^2(-\tau,0))} \\ &= -\Re\left[(\boldsymbol{u} \cdot \boldsymbol{n}, p)_{L^2(\partial\Omega)} \right] + \frac{k}{2} \|\chi(\cdot, 0)\|^2_{L^2(\partial\Omega)} - \frac{k}{2} \|\chi(\cdot, -\tau)\|^2_{L^2(\partial\Omega)}, \\ &= \left(\frac{k}{2} - z_0 \right) \|\chi(\cdot, 0)\|^2_{L^2(\partial\Omega)} - \frac{k}{2} \|\chi(\cdot, -\tau)\|^2_{L^2(\partial\Omega)} \\ &\quad - z_\tau \Re\left[(\chi(\cdot, 0), \chi(\cdot, -\tau))_{L^2(\partial\Omega)} \right], \end{aligned}$$

from which we deduce that $\mathcal{A}$ is dissipative if and only if the matrix

$$\begin{bmatrix} z_0 - \frac{k}{2} & \frac{z_\tau}{2} \\ \frac{z_\tau}{2} & \frac{k}{2} \end{bmatrix}$$

is positive semidefinite, i.e. if and only if its determinant and trace are nonnegative:

$$(2z_0 - k)k \geq z_\tau^2 \quad \text{and} \quad z_0 \geq 0.$$

The conclusion follows the expressions of the roots of $k \mapsto -k^2 + 2z_0 k - z_\tau^2$. □

Lemma 4.33. *The operator $\mathcal{A}$ given by (4.43) is injective.*

Proof. Assume $X \in \mathcal{D}(\mathcal{A})$ satisfies $\mathcal{A}X = 0$, i.e. $\nabla p = \mathbf{0}$, $\operatorname{div} \boldsymbol{u} = 0$, and

$$\partial_\theta \chi(\boldsymbol{x}, \theta) = 0 \quad \text{a.e. in } \partial\Omega \times (-\tau, 0). \tag{4.44}$$

Hence $\chi(\boldsymbol{x}, \cdot)$ is constant with

$$\chi(\cdot, 0) = \chi(\cdot, -\tau) = \boldsymbol{u} \cdot \boldsymbol{n} \quad \text{a.e. in } \partial\Omega. \tag{4.45}$$

Green's formula (C.1) yields

$$\langle \boldsymbol{u} \cdot \boldsymbol{n}, \overline{p} \rangle_{H^{-\frac{1}{2}}(\partial\Omega), H^{\frac{1}{2}}(\partial\Omega)} = 0,$$

and by combining with the IBC and (4.45)

$$\hat{z}(0) \|\boldsymbol{u} \cdot \boldsymbol{n}\|^2_{L^2(\partial\Omega)} = 0,$$

where we have used that $\boldsymbol{u} \cdot \boldsymbol{n} \in L^2(\partial\Omega)$ since $\chi(\cdot, 0) \in L^2(\partial\Omega)$. Since $\hat{z}(0) \neq 0$ we deduce that $\boldsymbol{u} \in H_{\operatorname{div} 0,0}(\Omega)$, hence $\boldsymbol{u} = \mathbf{0}$ from (C.2) and $\chi = 0$. The IBC gives $p = 0$ a.e. on $\partial\Omega$, hence $p = 0$ a.e. on Ω. □

Lemma 4.34. *Let $\mathcal{A}$ be given by (4.43). Then, $s\mathcal{I} - \mathcal{A}$ is bijective for $s \in (0, \infty) \cup \mathrm{j}\mathbb{R}^*$.*

Proof. Let $F \in H$ and $s \in (0, \infty) \cup \mathrm{j}\mathbb{R}^*$. We seek a *unique* $X \in \mathcal{D}(\mathcal{A})$ such that $(s\mathcal{I} - \mathcal{A})X = F$, i.e.

$$\begin{cases} s\boldsymbol{u} + \nabla p = \boldsymbol{f_u} & \text{(a)} \\ sp + \operatorname{div} \boldsymbol{u} = f_p & \text{(b)} \\ s\chi - \partial_\theta \chi = f_\chi. & \text{(c)} \end{cases} \tag{4.46}$$

Equation (4.46c) can be uniquely solved as

$$\chi(\cdot, \theta) = e^{s\theta} \boldsymbol{u} \cdot \boldsymbol{n} + R(s, \partial_\theta) f_\chi(\cdot, \theta), \tag{4.47}$$

where we formally denote (see Remark 4.35)

$$R(s, \partial_\theta) f_\chi(\boldsymbol{x}, \theta) \coloneqq \left[Y_1 e^{s\cdot} \star f_\chi(\boldsymbol{x}, \cdot) \right](\theta) = \int_0^\theta e^{s(\theta - \tilde{\theta})} f_\chi(\boldsymbol{x}, \tilde{\theta}) \, \mathrm{d}\tilde{\theta}.$$

The IBC can then be written as

$$p = \hat{z}(s) \boldsymbol{u} \cdot \boldsymbol{n} + z_\tau R(s, \partial_\theta) f_\chi(\cdot, -\tau) \quad \text{in } H^{-\frac{1}{2}}(\partial\Omega), \tag{4.48}$$

and this identity actually takes place in $L^2(\partial\Omega)$ since

$$\boldsymbol{x} \mapsto R(s, \partial_\theta) f_\chi(\boldsymbol{x}, -\tau) \in L^2(\partial\Omega).$$

Let $\psi \in H^1(\Omega)$. Combining $(\boldsymbol{f_u}, \nabla\psi) + s(f_p, \psi)$ with (4.48) yields

$$\begin{aligned} (\nabla p, \nabla\psi) + s^2(p, \psi) + \frac{s}{\hat{z}(s)}(p, \psi)_{L^2(\partial\Omega)} =& (\boldsymbol{f_u}, \nabla\psi) + s(f_p, \psi) \\ &+ \frac{s z_\tau}{\hat{z}(s)} (R(s, \partial_\theta) f_\chi(\cdot, -\tau), \psi)_{L^2(\partial\Omega)}. \end{aligned} \tag{4.49}$$

Let $p \in H^1(\Omega)$ be the unique solution of (4.49) obtained with Proposition 4.4. It remains to find suitable $\boldsymbol{u}$ and χ so that $(\boldsymbol{u}, p, \chi) \in \mathcal{D}(\mathcal{A})$. Let us *define* $\boldsymbol{u} \in \nabla H^1(\Omega)$ by (4.46a). Taking

$\psi \in \mathcal{C}_0^\infty(\Omega)$ in (4.49) shows that $\boldsymbol{u} \in H_{\mathrm{div}}(\Omega)$ with (4.46b). Using the expressions of $\boldsymbol{u}$ and $\operatorname{div} \boldsymbol{u}$, and Green's formula (C.1), the weak formulation (4.49) can be rewritten as

$$\langle \boldsymbol{u}\cdot\boldsymbol{n}, \overline{\psi}\rangle_{H^{-\frac{1}{2}}(\partial\Omega),H^{\frac{1}{2}}(\partial\Omega)} = \frac{1}{\hat{z}(s)}(p,\psi)_{L^2(\partial\Omega)} - \frac{z_\tau}{\hat{z}(s)}(R(s,\partial_\theta)f_\chi(\cdot,-\tau),\psi)_{L^2(\partial\Omega)}.$$

which shows that p and $\boldsymbol{u}$ satisfy (4.48). Let us now *define* χ in $L^2(\partial\Omega; H^1(-\tau,0))$ by (4.47). By rewriting (4.48) as

$$p = (\hat{z}(s) - z_\tau e^{-s\tau})\boldsymbol{u}\cdot\boldsymbol{n} + z_\tau\left(e^{-s\tau}\boldsymbol{u}\cdot\boldsymbol{n} + R(s,\partial_\theta)f_\chi(\cdot,-\tau)\right) \quad \text{in } H^{-\frac{1}{2}}(\partial\Omega),$$

we deduce thanks to (4.39) and (4.47) that the IBC holds, i.e. that $(\boldsymbol{u},p,\chi) \in \mathcal{D}(\mathcal{A})$. The uniqueness of p follows Proposition 4.4, that of $\boldsymbol{u}$ from (C.2), and that of χ from the fact that (4.46c) is uniquely solvable in $\mathcal{D}(\mathcal{A})$. □

Remark 4.35. In the proof, $R(s,\partial_\theta)$ is only a notation since ∂_θ (hence also its resolvent operator) cannot be defined separately from $\mathcal{A}$. Indeed, the definition of ∂_θ would be

$$\left|\begin{array}{l}\partial_\theta : \mathcal{D}(\partial_\theta) \subset L^2(\partial\Omega; L^2(-\tau,0)) \to L^2(\partial\Omega; L^2(-\tau,0)) \\ \qquad \chi \mapsto \partial_\theta \chi,\end{array}\right.$$

with domain

$$\mathcal{D}(\partial_\theta) = \left\{\chi \in L^2(\partial\Omega; H^1(-\tau,0)) \mid \chi(\cdot,0) = \boldsymbol{u}\cdot\boldsymbol{n}\right\}$$

that depends upon $\boldsymbol{u}$.

Remark 4.36 (Invariance principle). Since the realization of $\hat{z}$ is infinite dimensional, proving asymptotic stability using the invariance principle is more involved: the key technical difficulty is establishing precompactness of the orbits. Following the discussion presented in Section 4.2.3, the compactness of $R(s,\mathcal{A})$ could be established by proving that the embedding

$$L^2(\partial\Omega; H^1(-\tau,0)) \subset L^2(\partial\Omega; L^2(-\tau,0)) \tag{4.50}$$

is compact, which is not obvious to the author if $d \geq 2$.

4.5 Standard diffusive impedance

This section focuses on the class of so-called *standard diffusive* kernels (Montseny 1998), defined as

$$z(t) \coloneqq \int_0^\infty e^{-\xi t} Y_1(t)\,\mathrm{d}\mu(\xi), \tag{4.51}$$

where $t \in \mathbb{R}$ and μ is a positive Radon measure on $[0,\infty)$ that satisfies the following well-posedness condition

$$\int_0^\infty \frac{\mathrm{d}\mu(\xi)}{1+\xi} < \infty, \tag{4.52}$$

which guarantees that $z \in L^1_{\mathrm{loc}}([0,\infty))$ with Laplace transform

$$\hat{z}(s) = \int_0^\infty \frac{1}{s+\xi}\mathrm{d}\mu(\xi). \tag{4.53}$$

The estimate

$$\forall s \in \overline{\mathbb{C}_0^+}\backslash\{0\}, \quad \frac{1}{|s+\xi|} \leq \sqrt{2}\max\left[1,\frac{1}{|s|}\right]\frac{1}{1+\xi}, \tag{4.54}$$

which is used below, shows that $\hat{z}$ is defined on $\overline{\mathbb{C}_0^+}\backslash\{0\}$.

This class of (positive-real) kernels is physically linked to non-propagating lossy phenomena and arises in electromagnetics (Garrappa et al. 2016), viscoelasticity (Desch and Miller 1988; Mainardi 1997), and acoustics (Hélie and Matignon 2006a; Lombard and Matignon 2016; Monteghetti et al. 2016a). Formally, $\hat{z}$ admits the following realization

$$\begin{cases} \partial_t \varphi(t,\xi) = -\xi\varphi(t,\xi) + u(t),\ \varphi(0,\xi) = 0 \quad (\xi \in (0,\infty))\,, \\ z \star u(t) = \displaystyle\int_0^\infty \varphi(t,\xi)\,\mathrm{d}\mu(\xi). \end{cases} \tag{4.55}$$

The realization (4.55) can be given a meaning using the theory of well-posed linear systems (Matignon and Zwart in revision; Staffans 2005; Tucsnak and Weiss 2014; Weiss et al. 2001). However, in order to prove asymptotic stability, we need a framework to give a meaning to the *coupled* system (4.2,4.3,4.55), which, it turns out, can be done without defining a well-posed linear system out of (4.55).

Similarly to the previous sections, this section is divided into two parts. Section 4.5.1 defines the realization of (4.55) and establishes some of its properties. These properties are then used in Section 4.5.2 to prove the asymptotic stability of the coupled system.

Remark 4.37. The typical standard diffusive operator is the Riemann-Liouville fractional integral (Samko et al. 1993, § 2.3) (Matignon 2009)

$$\hat{z}(s) = \frac{1}{s^\alpha},\ \mathrm{d}\mu(\xi) = \mu_\alpha(\xi)\mathrm{d}\xi, \tag{4.56}$$

where $\alpha \in (0,1)$ and μ_α is given by (2.11).

Remark 4.38. The expression (4.51) arises naturally when inverting multivalued Laplace transforms, see (Duffy 2004, Chap. 4) for applications in partial differential equations. However, a standard diffusive kernel can also be defined as follows: a causal kernel z is said to be *standard diffusive* if it belongs to $L^1_{\mathrm{loc}}([0,\infty))$ and is completely monotone on $(0,\infty)$. By Bernstein's representation theorem (Gripenberg et al. 1990, Thm. 5.2.5), z is standard diffusive iff (4.51,4.52) hold. Additionally, a standard diffusive kernel z is integrable on $(0,\infty)$ iff

$$\mu(\{0\}) = 0 \quad \text{and} \quad \int_0^\infty \frac{1}{\xi}\mathrm{d}\mu(\xi) < \infty,$$

a property which will be referred to in Section 4.5.1. State spaces for the realization of classes of completely monotone kernels have been studied in (Desch and Miller 1988; Staffans 1994) and references therein.

4.5.1 Abstract realization

To give a meaning to (4.55) suited for our purpose, we define, for any $s \in \mathbb{R}$, the following Hilbert space

$$V_s \coloneqq \left\{ \varphi :\ (0,\infty) \to \mathbb{C} \text{ measurable} \;\middle|\; \int_0^\infty |\varphi(\xi)|^2 (1+\xi)^s\,\mathrm{d}\mu(\xi) < \infty \right\},$$

with scalar product

$$(\varphi,\psi)_{V_s} \coloneqq \int_0^\infty (\varphi(\xi),\psi(\xi))_{\mathbb{C}} (1+\xi)^s\,\mathrm{d}\mu(\xi),$$

so that the triplet (V_{-1}, V_0, V_1) satisfies the continuous embeddings

$$V_1 \subset V_0 \subset V_{-1}. \tag{4.57}$$

The space V_0 will be the energy space of the realization, see (4.67). Note that the spaces V_{-1} and V_1 defined above are different from those encountered when defining a well-posed linear system out of (4.55), see (Matignon and Zwart in revision). When $\mathrm{d}\mu$ is given by (4.56), the spaces V_0 and V_1 reduce to the spaces "H_α" and "V_α" defined in (Haddar and Matignon 2008, Chap. 2) and (Matignon and Prieur 2014, § 3.2).

On these spaces, we wish to define the unbounded state operator A, the control operator B, and the observation operator C so that

$$A : \mathcal{D}(A) \coloneqq V_1 \subset V_{-1} \to V_{-1},\ B \in \mathcal{L}(\mathbb{C}, V_{-1}),\ C \in \mathcal{L}(V_1, \mathbb{C}). \tag{4.58}$$

The state operator is defined as the following multiplication operator

$$A : \left| \begin{array}{l} \mathcal{D}(\mathcal{A}) \coloneqq V_1 \subset V_{-1} \to V_{-1} \\ \varphi \mapsto (\xi \mapsto -\xi\varphi(\xi)). \end{array} \right. \tag{4.59}$$

The control operator is simply

$$Bu \coloneqq \xi \mapsto 1 \times u, \tag{4.60}$$

and belongs to $\mathcal{L}(\mathbb{C}, V_{-1})$ thanks to condition (4.52) since, for $u \in \mathbb{C}$,

$$\|Bu\|_{V_{-1}} = \left[\int_0^\infty \frac{1}{1+\xi}\,\mathrm{d}\mu(\xi)\right]^{1/2} |u|.$$

The observation operator is

$$C\varphi \coloneqq \int_0^\infty \varphi(\xi)\,\mathrm{d}\mu(\xi),$$

and $C \in \mathcal{L}(V_1, \mathbb{C})$ thanks to (4.52) as, for $\varphi \in V_1$,

$$|C\varphi| \le \left[\int_0^\infty \frac{1}{1+\xi}\,\mathrm{d}\mu(\xi)\right]^{1/2} \|\varphi\|_{V_1}.$$

The next lemma gathers properties of the triplet (A, B, C) that are used in Section 4.5.2 to obtain asymptotic stability. Recall that if A is closed and $s \in \rho(A)$, then the resolvent operator $R(s, A)$ defined by (4.25) belongs to $\mathcal{L}(V_{-1}, V_1)$ (Kato 1995, § III.6.1).

Lemma 4.39. *The operator A defined by (4.59) is injective, generates a strongly continuous semigroup of contractions on V_{-1}, and satisfies $\overline{\mathbb{C}_0^+}\backslash\{0\} \subset \rho(A)$.*

Proof. The proof is split into three steps, (a), (b), and (c). (a) The injectivity of A follows directly from its definition. (b) Let us show that $(0,\infty) \cup \mathrm{j}\mathbb{R}^* \subset \rho(A)$. Let $f_\varphi \in V_{-1}$, $s \in (0,\infty) \cup \mathrm{j}\mathbb{R}^*$, and define

$$\varphi(\xi) \coloneqq \frac{1}{s+\xi} f_\varphi(\xi) \quad \text{a.e. on } (0,\infty). \tag{4.61}$$

Using the estimate (4.54), we have

$$\|\varphi\|_{V_1} \le \sqrt{2}\max\left[1, \frac{1}{|s|}\right] \|f_\varphi\|_{V_{-1}},$$

so that φ belongs to V_1 and $(s\mathcal{I} - A)\varphi = f_\varphi$ is well-posed. (c) For any $\varphi \in V_1$, we have $\Re\left[(A\varphi, \varphi)_{V_{-1}}\right] \le -\|\varphi\|_{V_0}^2$, so A is dissipative. By the Lumer-Phillips theorem, A generates a strongly continuous semigroup of contractions on V_{-1}, so that $\mathbb{C}_0^+ \subset \rho(A)$ (Pazy 1983, Cor. 3.6). □

Lemma 4.40. *The triplet of operators (A, B, C) defined above satisfies (4.58) as well as the following properties.*

(i) *(Stability) A is closed and injective with $\overline{\mathbb{C}_0^+}\backslash\{0\} \subset \rho(A)$.*

(ii) *(Regularity)*

(a) $A_{|V_1} \in \mathcal{L}(V_1, V_{-1})$, where the vertical line denotes the restriction.

(b) For any $s \in \overline{\mathbb{C}_0^+}\backslash\{0\}$,

$$AR(s, A)_{|V_0} \in \mathcal{L}(V_0, V_0). \tag{4.62}$$

(iii) *(Reality) For any $s \in (0, \infty)$,*

$$CR(s, A)B_{|\mathbb{R}} \in \mathcal{L}(\mathbb{R}, \mathbb{R}), \tag{4.63}$$

(iv) *(Passivity) For any $(\varphi, u) \in \mathcal{D}(A\&B)$,*

$$\Re\left[(A\varphi + Bu, \varphi)_{V_0} - (u, C\varphi)_{\mathbb{C}}\right] \leq 0, \tag{4.64}$$

where we define

$$\mathcal{D}(A\&B) \coloneqq \{(\varphi, u) \in V_1 \times \mathbb{C} \mid A\varphi + Bu \in V_0\}.$$

Proof. Let A, B, and C be defined as above. Each of the properties is proven below.

(i) This condition is satisfied from Lemma 4.39.

(iia) Let $\varphi \in V_1$. We have

$$\begin{aligned}\|A\varphi\|_{V_{-1}}^2 &= \int_0^\infty |\varphi(\xi)|^2 \frac{\xi^2}{1+\xi}\,\mathrm{d}\mu(\xi) \\ &\leq \int_0^\infty |\varphi(\xi)|^2 (1+\xi)\,\mathrm{d}\mu(\xi) = \|\varphi\|_{V_1}^2,\end{aligned}$$

using the inequality $\xi^2 \leq (1+\xi)^2$.

(iib) Let $f_\varphi \in V_0$ and $s \in \overline{\mathbb{C}_0^+}\backslash\{0\}$,

$$\|AR(s, A)f_\varphi\|_{V_0} = \left[\int_0^\infty \left|\frac{\xi}{s+\xi} f_\varphi\right|^2 \mathrm{d}\mu(\xi)\right]^{1/2} \leq \|f_\varphi\|_{V_0},$$

where we have used $\left|\frac{\xi}{s+\xi}\right| \leq \frac{\xi}{\Re(s)+\xi} \leq 1$.

(iii) Let $s \in (0, \infty)$ and $u \in \mathbb{R}$. The reality condition is fulfilled since

$$CR(s, A)Bu = u \int_0^\infty \frac{\mathrm{d}\mu(\xi)}{s+\xi}.$$

(iv) Let $(\varphi, u) \in \mathcal{D}(A\&B)$. We have

$$\Re\left[(A\varphi + Bu, \varphi)_{V_0} - (u, C\varphi)_{\mathbb{C}}\right] = -\Re\left[\int_0^\infty \xi |\varphi(\xi)|^2\,\mathrm{d}\mu(\xi)\right] \leq 0, \tag{4.65}$$

so that the passivity condition is satisfied.

□

Remark 4.41. The space $\mathcal{D}(A\&B)$ is nonempty. Indeed, it contains at least the following one dimensional subspace

$$\{(\varphi, u) \in V_1 \times \mathbb{C} \mid \varphi = R(s, A)Bu\}$$

for any $s \in \rho(A)$ (which is nonempty from Lemma 4.40(i)); this follows from

$$\begin{aligned} A\varphi + Bu =& AR(s, A)Bu + Bu \\ =& sR(s, A)Bu \in V_1. \end{aligned}$$

It also contains $\{(R(s, A)\varphi, 0) \mid \varphi \in V_0\}$.

For any $s \in \rho(A)$, we define

$$z \coloneqq s \mapsto CR(s, A)B, \tag{4.66}$$

which is analytic, from the analyticity of $R(\cdot, A)$ (Kato 1995, Thm. III.6.7). Additionally, we have $z(s) \in \mathbb{R}$ for $s \in (0, \infty)$ from (4.63), and $\Re(z(s)) \geq 0$ from the passivity condition (4.64) with $\varphi \coloneqq R(s, A)Bu \in \mathcal{D}(A\&B)$:

$$\Re(s)\|R(s, A)Bu\|_{V_0}^2 \leq \Re\left[(u, z(s)u)_{\mathbb{C}}\right].$$

Since $\mathbb{C}_0^+ \subset \rho(A)$, the function z defined by (4.66) is positive-real.

Remark 4.42 (Rational case). The matrices $A \in \mathbb{C}^{m\times m}$, $B \in \mathbb{C}^{m\times 1}$, and $C \in \mathbb{C}^{1\times m}$ considered in Section 4.3.1 verify the properties of Lemma 4.40 with the spaces V_{-1}, V_0, V_1, and $\mathcal{D}(A\&B)$ identified to $\mathbb{C}^m$. Condition (i) is satisfied iff $[0, \infty) \cup \mathrm{j}\mathbb{R} \subset \rho(A)$. Condition (ii) is satisfied. Condition (iii) is satisfied if (A, B, C) are real-valued matrices. Condition (iv) is (4.31) (in particular, it implies that $\mathbb{C}_0^+ \subset \rho(A)$).

4.5.2 Asymptotic stability

Let (A, B, C) be defined as in Section 4.5.1. We further assume that A, B, and C are non-null operators. The coupling between the wave equation (4.2) and the infinite-dimensional realization (A, B, C) can be formulated as the abstract Cauchy problem (4.13) using the following definitions. The extended state space is

$$\begin{aligned} H &\coloneqq \nabla H^1(\Omega) \times L^2(\Omega) \times L^2(\partial\Omega; V_0), \\ ((\boldsymbol{u}, p, \varphi), (\boldsymbol{f_u}, f_p, f_\varphi))_H &\coloneqq (\boldsymbol{u}, \boldsymbol{f_u}) + (p, f_p) + (\varphi, f_\varphi)_{L^2(\partial\Omega; V_0)}, \end{aligned} \tag{4.67}$$

and the evolution operator $\mathcal{A}$ is

$$\begin{aligned} \mathcal{D}(\mathcal{A}) \ni X \coloneqq \begin{pmatrix} \boldsymbol{u} \\ p \\ \varphi \end{pmatrix} &\longmapsto \mathcal{A}X \coloneqq \begin{pmatrix} -\nabla p \\ -\operatorname{div} \boldsymbol{u} \\ A\varphi + B\boldsymbol{u} \cdot \boldsymbol{n} \end{pmatrix}, \\ \mathcal{D}(\mathcal{A}) \coloneqq \left\{ (\boldsymbol{u}, p, \varphi) \in H \;\middle|\; \begin{array}{l} (\boldsymbol{u}, p, \varphi) \in H_{\mathrm{div}}(\Omega) \times H^1(\Omega) \times L^2(\partial\Omega; V_1) \\ (A\varphi + B\boldsymbol{u} \cdot \boldsymbol{n}) \in L^2(\partial\Omega; V_0) \\ p = C\varphi \text{ in } H^{\frac{1}{2}}(\partial\Omega) \end{array} \right\}. \end{aligned} \tag{4.68}$$

Remark 4.43. In the definition of $\mathcal{A}$, there is an abuse of notation similar to that employed in the rational case. Indeed, we still denote by A the following operator

$$\begin{vmatrix} L^2(\partial\Omega; V_1) \to L^2(\partial\Omega; V_{-1}) \\ \varphi \mapsto (\boldsymbol{x} \mapsto A\varphi(\boldsymbol{x}, \cdot)), \end{vmatrix}$$

which is well-defined from Lemma 4.40(iia) and Remark 4.31. A similar abuse of notation is employed for B and C.

Asymptotic stability is proven by applying Corollary 4.13 through Lemmas 4.45, 4.46, and 4.47 below. In order to clarify the proofs presented in Lemmas 4.45 and 4.46, we first prove a regularity property on $\boldsymbol{u}$ that follows from the definition of $\mathcal{D}(\mathcal{A})$.

Lemma 4.44 (Boundary regularity)**.** *If $X = (\boldsymbol{u}, p, \varphi) \in \mathcal{D}(\mathcal{A})$, then $\boldsymbol{u} \cdot \boldsymbol{n} \in L^2(\partial\Omega)$.*

Proof. Let $X \in \mathcal{D}(\mathcal{A})$. By definition of $\mathcal{D}(\mathcal{A})$, we have $\varphi \in L^2(\partial\Omega; V_1)$ so that $A\varphi \in L^2(\partial\Omega; V_{-1})$ from Lemma 4.40(iia) and Remark 4.31. From

$$B\boldsymbol{u} \cdot \boldsymbol{n} = \underbrace{A\varphi + B\boldsymbol{u} \cdot \boldsymbol{n}}_{\in L^2(\partial\Omega; V_0)} - \overbrace{A\varphi}^{\in L^2(\partial\Omega; V_{-1})},$$

we deduce that $B\boldsymbol{u} \cdot \boldsymbol{n} \in L^2(\partial\Omega; V_{-1})$. The conclusion then follows from the definition of B and condition (4.52). □

Lemma 4.45. *The operator $\mathcal{A}$ given by (4.68) is dissipative.*

Proof. Let $X \in \mathcal{D}(\mathcal{A})$. In particular, $\boldsymbol{u} \cdot \boldsymbol{n} \in L^2(\partial\Omega)$ from Lemma 4.44. Green's formula (C.1) and the inequality (4.64) yield

$$\begin{aligned} \Re(\mathcal{A}X, X)_H &= \Re\left[(A\varphi + B\boldsymbol{u} \cdot \boldsymbol{n}, \varphi)_{L^2(\partial\Omega; V_0)} - \langle \boldsymbol{u} \cdot \boldsymbol{n}, \overline{p} \rangle_{H^{-\frac{1}{2}}(\partial\Omega), H^{\frac{1}{2}}(\partial\Omega)}\right] \\ &= \Re\left[(A\varphi + B\boldsymbol{u} \cdot \boldsymbol{n}, \varphi)_{L^2(\partial\Omega; V_0)} - (\boldsymbol{u} \cdot \boldsymbol{n}, C\varphi)_{L^2(\partial\Omega)}\right] \leq 0, \end{aligned}$$

where we have used that $\boldsymbol{u} \cdot \boldsymbol{n} \in L^2(\partial\Omega)$. □

Lemma 4.46. *The operator $\mathcal{A}$ given by (4.68) is injective.*

Proof. Assume $X \in \mathcal{D}(\mathcal{A})$ satisfies $\mathcal{A}X = 0$. In particular $\nabla p = \boldsymbol{0}$ and $\operatorname{div} \boldsymbol{u} = 0$, so that Green's formula (C.1) yields

$$\langle \boldsymbol{u} \cdot \boldsymbol{n}, \overline{p} \rangle_{H^{-\frac{1}{2}}(\partial\Omega), H^{\frac{1}{2}}(\partial\Omega)} = 0,$$

and by combining with the IBC

$$(\boldsymbol{u} \cdot \boldsymbol{n}, C\varphi)_{L^2(\partial\Omega)} = 0, \tag{4.69}$$

where we have used that $\boldsymbol{u} \cdot \boldsymbol{n} \in L^2(\partial\Omega)$ from Lemma 4.44. The third equation that comes from $\mathcal{A}X = 0$ is

$$A\varphi(\boldsymbol{x}, \cdot) + B\boldsymbol{u}(\boldsymbol{x}) \cdot \boldsymbol{n}(\boldsymbol{x}) = 0 \quad \text{in } V_0 \text{ for a.e. } \boldsymbol{x} \in \partial\Omega. \tag{4.70}$$

We now prove that $X = 0$, the key step being solving (4.70). Since A is injective, (4.70) has at most one solution $\varphi \in L^2(\partial\Omega; V_1)$. Let us distinguish the possible cases.

- If $0 \in \rho(A)$, then $\varphi = R(0, A)B\boldsymbol{u} \cdot \boldsymbol{n} \in L^2(\partial\Omega; V_1)$ is the unique solution. Inserting in (4.69) and using (4.66) yields

  $$(\boldsymbol{u} \cdot \boldsymbol{n}, z(0)\boldsymbol{u} \cdot \boldsymbol{n})_{L^2(\partial\Omega)} = 0,$$

  from which we deduce that $\boldsymbol{u} \cdot \boldsymbol{n} = 0$ since $z(0)$ is non-null.

- If $0 \in \sigma_r(A) \cup \sigma_c(A)$, then either $\overline{R(A)} \neq V_{-1}$ (definition of the residual spectrum) or $\overline{R(A)} = V_{-1}$ but $R(A) \neq V_{-1}$ (definition of the continuous spectrum combined with the closed graph theorem, since A is closed). If $B\boldsymbol{u} \cdot \boldsymbol{n} \notin L^2(\partial\Omega; R(A))$, then the only solution is $\varphi = 0$ and $\boldsymbol{u} \cdot \boldsymbol{n} = 0$. If $B\boldsymbol{u} \cdot \boldsymbol{n} \in L^2(\partial\Omega; R(A))$, then $\varphi = -A^{-1}B\boldsymbol{u} \cdot \boldsymbol{n}$ is the unique solution, where $A^{-1} : R(A) \to V_1$ is an unbounded closed bijection. Inserting in (4.69) yields

  $$(\boldsymbol{u} \cdot \boldsymbol{n}, (-CA^{-1}B)\boldsymbol{u} \cdot \boldsymbol{n})_{L^2(\partial\Omega)} = 0.$$

  Since $(-CA^{-1}B) \in \mathcal{L}(\mathbb{C}, \mathbb{C})$ is a non-null operator, we deduce that $\boldsymbol{u} \cdot \boldsymbol{n} = 0$.

In summary, $\boldsymbol{u} \in H_{\mathrm{div}\,0,0}(\Omega)$, $\varphi = 0$ in $L^2(\partial\Omega; V_1)$, and $p = 0$ in $L^2(\partial\Omega)$. The nullity of p follows from $\nabla p = 0$. The nullity of $\boldsymbol{u}$ follows from $H_{\mathrm{div}\,0,0}(\Omega) \cap \nabla H^1(\Omega) = \{0\}$, see (C.2). □

Lemma 4.47. *Let $\mathcal{A}$ be given by (4.68). Then, $s\mathcal{I} - \mathcal{A}$ is bijective for $s \in (0,\infty) \cup \mathrm{j}\mathbb{R}^*$.*

Proof. Let $F \in H$ and $s \in (0,\infty) \cup \mathrm{j}\mathbb{R}^*$. We seek a *unique* $X \in \mathcal{D}(\mathcal{A})$ such that $(s\mathcal{I} - \mathcal{A})X = F$, i.e.

$$\begin{cases} s\boldsymbol{u} + \nabla p = \boldsymbol{f_u} & \text{(a)} \\ sp + \mathrm{div}\,\boldsymbol{u} = f_p & \text{(b)} \\ s\varphi - A\varphi - B\boldsymbol{u}\cdot\boldsymbol{n} = f_\varphi. & \text{(c)} \end{cases} \tag{4.71}$$

For later use, let us note that Equation (4.71c) and the IBC implies

$$\varphi = R(s,A)(B\boldsymbol{u}\cdot\boldsymbol{n} + f_\varphi) \qquad \text{in } L^2(\partial\Omega; V_1) \tag{4.72}$$

$$p = z(s)\boldsymbol{u}\cdot\boldsymbol{n} + CR(s,A)f_\varphi \quad \text{in } L^2(\partial\Omega). \tag{4.73}$$

Let $\psi \in H^1(\Omega)$. Combining $(\boldsymbol{f_u}, \nabla\psi) + s(f_p, \psi)$ with (4.73) yields

$$\begin{aligned}(\nabla p, \nabla\psi) + s^2(p,\psi) + \frac{s}{z(s)}(p,\psi)_{L^2(\partial\Omega)} = (\boldsymbol{f_u}, \nabla\psi) + s(f_p,\psi) \\ + \frac{s}{z(s)}(CR(s,A)f_\varphi, \psi)_{L^2(\partial\Omega)}.\end{aligned} \tag{4.74}$$

Note that since $CR(s,A) \in \mathcal{L}(V_{-1}, \mathbb{C})$, we have

$$\boldsymbol{x} \mapsto CR(s,A)f_\varphi(\boldsymbol{x}) \in L^2(\partial\Omega),$$

so that (4.74) is meaningful. Moreover, we have $\Re(z(s)) \geq 0$, and $z(s) \in (0,\infty)$ for $s \in (0,\infty)$. Therefore, we can apply Proposition 4.4, pointwise, for $s \in (0,\infty) \cup \mathrm{j}\mathbb{R}^*$.

Let us denote by p the unique solution of (4.74) in $H^1(\Omega)$, obtained from Proposition 4.4. It remains to find suitable $\boldsymbol{u}$ and φ, which is mostly similar to the rational case thanks to the hypothesis (4.62).

Let us *define* $\boldsymbol{u} \in \nabla H^1(\Omega)$ by (4.71a). Taking $\psi \in \mathcal{C}_0^\infty(\Omega)$ in (4.74) shows that $\boldsymbol{u} \in H_{\mathrm{div}}(\Omega)$ and (4.71b) holds. Using the expressions of $\boldsymbol{u}$ and $\mathrm{div}\,\boldsymbol{u}$, and Green's formula (C.1), the weak formulation (4.74) can be rewritten as

$$\langle \boldsymbol{u}\cdot\boldsymbol{n}, \overline{\psi}\rangle_{H^{-\frac{1}{2}}(\partial\Omega), H^{\frac{1}{2}}(\partial\Omega)} = z(s)^{-1}(p,\psi)_{L^2(\partial\Omega)} - z(s)^{-1}(CR(s,A)f_\varphi, \psi)_{L^2(\partial\Omega)},$$

which shows that p and $\boldsymbol{u}$ satisfy (4.73).

Let us now *define* φ with (4.72); it belongs to $L^2(\partial\Omega; V_1)$ since $\boldsymbol{u}\cdot\boldsymbol{n} \in L^2(\partial\Omega)$ from (4.73) and $f_\varphi \in L^2(\partial\Omega; V_0)$. By rewriting (4.73) as

$$p = (z(s) - CR(s,A)B)\boldsymbol{u}\cdot\boldsymbol{n} + CR(s,A)(B\boldsymbol{u}\cdot\boldsymbol{n} + f_\varphi),$$

we obtain from (4.66) and (4.72) that the IBC holds.

To obtain $(\boldsymbol{u}, p, \varphi) \in \mathcal{D}(\mathcal{A})$ it remains to show that $A\varphi + B\boldsymbol{u}\cdot\boldsymbol{n}$ belongs to $L^2(\partial\Omega; V_0)$. Using the definition of φ, we have

$$\begin{aligned} A\varphi + B\boldsymbol{u}\cdot\boldsymbol{n} &= AR(s,A)(B\boldsymbol{u}\cdot\boldsymbol{n} + f_\varphi) + B\boldsymbol{u}\cdot\boldsymbol{n} \\ &= (AR(s,A) + \mathcal{I})B\boldsymbol{u}\cdot\boldsymbol{n} + AR(s,A)f_\varphi \\ &= sR(s,A)B\boldsymbol{u}\cdot\boldsymbol{n} + AR(s,A)f_\varphi. \end{aligned}$$

Since $\boldsymbol{u}\cdot\boldsymbol{n}\in L^2(\partial\Omega)$ and $R(s,A)B\in\mathcal{L}(\mathbb{C},V_1)$, we have

$$sR(s,A)B\boldsymbol{u}\cdot\boldsymbol{n}\in L^2(\partial\Omega;V_1).$$

The hypothesis (4.62) implies that

$$AR(s,A)f_\varphi\in L^2(\partial\Omega;V_0),$$

hence that $(\boldsymbol{u},p,\varphi)\in\mathcal{D}(\mathcal{A})$.

The uniqueness of p follows from Proposition 4.4, that of $\boldsymbol{u}$ from (C.2), and that of φ from the bijectivity of $s\mathbb{I}-A$. □

Remark 4.48 (Invariance principle). As pointed out in (Matignon and Prieur 2014) in the context of the Webster-Lokshin equation, the lack of precompactness of the orbits prevents from using the invariance principle. This can be understood by noting that the embedding

$$L^2(\partial\Omega;V_1)\subset L^2(\partial\Omega;V_0) \tag{4.75}$$

is not compact since the embedding $V_1\subset V_0$ is not compact. This contrasts with the time-delay impedance (4.39) for which, although the embedding $H^1(-\tau,0)\subset L^2(-\tau,0)$ is compact, the compactness of the embedding (4.50) is doubtful. Theorem 4.21 does not apply since the continuous spectrum $\sigma_c(R(s,\mathcal{A}))$ can be nonempty.

Remark 4.49 ((Exponential stability)). If $\mathrm{d}\mu(\xi)=\tilde{\mu}(\xi)\,\mathrm{d}\xi$ with $\tilde{\mu}(\xi)>0$ over $(0,\epsilon)$ for some $\epsilon>0$, we have $(-\epsilon,0)\subset(\sigma(A)\backslash\sigma_p(A))$; in particular, $(-\epsilon,0)$ belongs to the spectrum of $\mathcal{A}$ by properties of the multiplication operator, see e.g. (Engel and Nagel 2000, § I.4.b) and (Matignon and Zwart in revision). Since 0 is an accumulation point of the spectrum of $\mathcal{A}$, the growth bound of $\mathcal{T}$ is nonnegative (Engel and Nagel 2000, Cor. II.1.13) and $\mathcal{T}$ cannot be exponentially stable.

Remark 4.50. The time-delay case does not fit into the framework proposed in Section 4.5.1, see Remark 4.35. This justifies why delay and standard diffusive IBCs are covered separately.

4.6 Extended diffusive impedance

In this section, we focus on a variant of the standard diffusive kernel, namely the so-called *extended diffusive* kernel given by

$$\hat{z}(s)\coloneqq\int_0^\infty\frac{s}{s+\xi}\mathrm{d}\mu(\xi), \tag{4.76}$$

where μ is a Radon measure that satisfies condition (4.52), already encountered in the standard case, and

$$\int_0^\infty\frac{1}{\xi}\mathrm{d}\mu(\xi)=\infty. \tag{4.77}$$

The additional condition (4.77) implies that $t\mapsto\int_0^\infty e^{-\xi t}\,\mathrm{d}\mu(\xi)$ is not integrable on $(0,\infty)$, see Remark 4.38.

From (4.55), we directly deduce that $\hat{z}$ *formally* admits the realization

$$\begin{cases}\partial_t\varphi(t,\xi)=-\xi\varphi(t,\xi)+u(t),\ \varphi(0,\xi)=0\quad(\xi\in(0,\infty))\,,\\ z\star u(t)=\displaystyle\int_0^\infty(-\xi\varphi(t,\xi)+u(t))\,\mathrm{d}\mu(\xi),\end{cases} \tag{4.78}$$

where u is a causal input. The separate treatment of the standard (4.53) and extended (4.76) cases is justified by the fact that physical models typically yield non-integrable kernels, i.e.

$$\int_0^\infty \mathrm{d}\mu(\xi) = +\infty, \tag{4.79}$$

which prevents from splitting the observation integral in (4.78): the observation and feedthrough operators are combined into $C\&D$. Although a functional setting for (4.78) has been obtained in (Monteghetti et al. 2017a, § B.3), we shall again follow the philosophy laid out in Section 4.5. Namely, Section 4.6.1 presents an abstract realization framework whose properties are given in Lemma 4.54, which slightly differs from the standard case, and Section 4.6.2 shows asymptotic stability of the coupled system (4.88).

Remark 4.51. Let $\alpha \in (0,1)$. The typical extended diffusive operator is the Riemman-Liouville fractional derivative (Podlubny 1999, § 2.3) (Matignon 2009), obtained for $\hat{z}(s) = s^{1-\alpha}$ and $\mathrm{d}\mu$ given by (4.56), which satisfies condition (4.77). For this measure $\mathrm{d}\mu$, choosing the initialization $\varphi(0,\xi) = {}^{u(0)}/_{\xi}$ in (4.78) yields the Caputo derivative (Lombard and Matignon 2016).

4.6.1 Abstract realization

To give meaning to the realization (4.78) we follow a similar philosophy to the standard case, namely the definition of a triplet of Hilbert spaces (V_{-1}, V_0, V_1) that satisfies the continuous embeddings (4.57) as well as a suitable triplet of operators (A, B, C).

The Hilbert spaces V_{-1}, V_0, and V_1 are defined as

$$\begin{aligned}
V_1 &\coloneqq \left\{ \varphi : (0,\infty) \to \mathbb{C} \text{ measurable} \;\middle|\; \int_0^\infty |\varphi(\xi)|^2 (1+\xi)\,\mathrm{d}\mu(\xi) < \infty \right\} \\
V_0 &\coloneqq \left\{ \varphi : (0,\infty) \to \mathbb{C} \text{ measurable} \;\middle|\; \int_0^\infty |\varphi(\xi)|^2 \xi\,\mathrm{d}\mu(\xi) < \infty \right\} \\
V_{-1} &\coloneqq \left\{ \varphi : (0,\infty) \to \mathbb{C} \text{ measurable} \;\middle|\; \int_0^\infty |\varphi(\xi)|^2 \frac{\xi}{1+\xi^2}\,\mathrm{d}\mu(\xi) < \infty \right\},
\end{aligned}$$

with scalar products

$$\begin{aligned}
(\varphi,\psi)_{V_1} &\coloneqq \int_0^\infty (\varphi(\xi),\psi(\xi))_{\mathbb{C}} (1+\xi)\,\mathrm{d}\mu(\xi) \\
(\varphi,\psi)_{V_0} &\coloneqq \int_0^\infty (\varphi(\xi),\psi(\xi))_{\mathbb{C}}\, \xi\,\mathrm{d}\mu(\xi) \\
(\varphi,\psi)_{V_{-1}} &\coloneqq \int_0^\infty (\varphi(\xi),\psi(\xi))_{\mathbb{C}} \frac{\xi}{1+\xi^2}\,\mathrm{d}\mu(\xi),
\end{aligned}$$

so that the continuous embeddings (4.57) are satisfied. Note the change of definition of the energy space V_0, which reflects the fact that the Lyapunov functional of (4.55) is different from that of (4.78): compare the energy balance (4.65) with (4.85). The change in the definition of V_{-1} is a consequence of this new definition of V_0. When $\mathrm{d}\mu$ is given by (4.56), the spaces V_0 and V_1 reduce to the spaces "$\tilde{H}_\alpha$" and "V_α" defined in (Haddar and Matignon 2008, Chap. 2) and (Matignon and Prieur 2014, § 3.2).

The operators A, B, and C satisfy (contrast with (4.58))

$$A : \mathcal{D}(A) \coloneqq V_0 \subset V_{-1} \to V_{-1},\ B \in \mathcal{L}(\mathbb{C}, V_{-1}),\ C \in \mathcal{L}(V_1, \mathbb{C}). \tag{4.80}$$

The state operator A is still the multiplication operator (4.59), but with domain V_0 instead of V_1. Let us check that this definition makes sense. For any $\varphi \in V_0$, we have

$$\|A\varphi\|_{V_{-1}} = \left[\int_0^\infty |\varphi(\xi)|^2 \frac{\xi^3}{1+\xi^2}\,\mathrm{d}\mu(\xi) \right]^{1/2} \leq \|\varphi\|_{V_0}. \tag{4.81}$$

The control operator B is defined as (4.60) and we have for any $u \in \mathbb{C}$

$$\|Bu\|_{V_{-1}} = \left[\int_0^\infty |u|^2 \frac{\xi}{1+\xi^2}\,\mathrm{d}\mu(\xi)\right]^{1/2} \leq \tilde{C}\left[\int_0^\infty \frac{1}{1+\xi}\,\mathrm{d}\mu(\xi)\right]^{1/2} |u|,$$

where the constant $\tilde{C} > 0$ is

$$\tilde{C} \coloneqq \left\|\frac{\xi(1+\xi)}{1+\xi^2}\right\|_{L^\infty(0,\infty)}.$$

The observation operator C is identical to the standard case. For use in Section 4.6.2, properties of (A, B, C) are gathered in Lemma 4.54 below.

Lemma 4.52. *The operator A generates a strongly continuous semigroup of contractions on V_{-1} and satisfies $\overline{\mathbb{C}_0^+}\backslash\{0\} \subset \rho(A)$.*

Proof. The proof is similar to that of Lemma 4.39. Let $s \in \overline{\mathbb{C}_0^+}\backslash\{0\}$ and $f_\varphi \in V_{-1}$. Let us define φ by (4.61). (a) We have

$$\begin{aligned}\|\varphi\|_{V_0} &= \left[\int_0^\infty \left|\frac{1}{s+\xi} f_\varphi\right|^2 \xi\,\mathrm{d}\mu(\xi)\right]^{1/2} \\ &\leq \sqrt{2}\max\left[1, \frac{1}{|s|}\right] \left\|\frac{1+\xi^2}{(1+\xi)^2}\right\|_{L^\infty(0,\infty)} \|f_\varphi\|_{V_{-1}},\end{aligned}$$

so that φ solves $(s\mathcal{I} - A)\varphi = f_\varphi$ in V_0. Since $s\mathcal{I} - A$ is injective, we deduce that $s \in \rho(A)$. (b) Let $\varphi \in V_0$. We have

$$(A\varphi, \varphi)_{V_{-1}} = -\int_0^\infty |\varphi(\xi)|^2 \frac{\xi^2}{1+\xi^2}\,\mathrm{d}\mu(\xi) \leq -\|\varphi\|_{V_0}^2,$$

so that A is dissipative. The conclusion follows from the Lumer-Phillips theorem. □

Lemma 4.53. *The operators A and B are injective. Moreover, if (4.77) holds, then $R(A) \cap R(B) = \{0\}$.*

Proof. The injectivity of A and B is immediate. Let $f_\varphi \in R(A) \cap R(B)$, so that there is $\varphi \in V_0$ and $u \in \mathbb{C}$ such that $A\varphi = Bu$, i.e. $-\xi\varphi(\xi) = u$ a.e. on $(0, \infty)$. The function φ belongs to V_0 if and only if

$$|u|^2 \int_0^\infty \frac{1}{\xi}\mathrm{d}\mu(\xi) < \infty.$$

So that, assuming (4.77), φ belongs to V_0 if and only if $u = 0$ a.e on $(0, \infty)$. □

Lemma 4.54. *The triplet of operators (A, B, C) defined above satisfies (4.80) as well as the following properties.*

(i) *(Stability) A is closed with $\overline{\mathbb{C}_0^+}\backslash\{0\} \subset \rho(A)$ and satisfies*

$$\forall(\varphi, u) \in \mathcal{D}(C\&D),\ A\varphi = Bu \Rightarrow (\varphi, u) = (0, 0), \tag{4.82}$$

where we define

$$\mathcal{D}(C\&D) \coloneqq \{(\varphi, u) \in V_0 \times \mathbb{C} \mid A\varphi + Bu \in V_1\}.$$

(ii) *(Regularity)*

(a) $A_{|V_0} \in \mathcal{L}(V_0, V_{-1})$.

(b) *For any* $s \in \overline{\mathbb{C}_0^+}\backslash\{0\}$,

$$AR(s,A)_{|V_0} \in \mathcal{L}(V_0, V_1),\ R(s,A)B \in \mathcal{L}(\mathbb{C}, V_1). \tag{4.83}$$

(iii) *(Reality) Identical to Lemma 4.40(iii).*

(iv) *(Passivity) For any* $(\varphi, u) \in \mathcal{D}(C\&D)$,

$$\Re\left[(A\varphi + Bu, \varphi)_{V_0} - (u, C(A\varphi + Bu))_{\mathbb{C}}\right] \leq 0. \tag{4.84}$$

Proof. Let (A, B, C) be as defined above. Each of the properties is proven below.

(i) Follows from Lemmas 4.52 and 4.53.

(iia) Follows from (4.81).

(iib) Let $s \in \overline{\mathbb{C}_0^+}\backslash\{0\}$, $f_\varphi \in V_0$, and $u \in \mathbb{C}$. We have

$$\begin{aligned}\|AR(s,A)f_\varphi\|_{V_1} &= \left[\int_0^\infty |f_\varphi(\xi)|^2 \frac{\xi^2(1+\xi)}{|s+\xi|^2}\,\mathrm{d}\mu(\xi)\right]^{1/2} \\ &\leq \sqrt{2}\max\left[1, \frac{1}{|s|}\right]\|f_\varphi\|_{V_0},\end{aligned}$$

and

$$\begin{aligned}\|R(s,A)Bu\|_{V_1} &= \left(\int_0^\infty \frac{1+\xi}{|s+\xi|^2}\,\mathrm{d}\mu(\xi)\right)^{1/2}|u| \\ &\leq \sqrt{2}\max\left[1, \frac{1}{|s|}\right]\left(\int_0^\infty \frac{1}{1+\xi}\,\mathrm{d}\mu(\xi)\right)^{1/2}|u|.\end{aligned}$$

(iii) Immediate.

(iv) Let $(\varphi, u) \in \mathcal{D}(C\&D)$. We have

$$\begin{aligned}&\Re\Big[(A\varphi+Bu, \varphi)_{V_0} - (u, C(A\varphi + Bu))_{\mathbb{C}}\Big] \\ &\quad= \Re\left[\int_0^\infty (-\xi\varphi(\xi) + u, \varphi(\xi))_{\mathbb{C}}\,\xi\,\mathrm{d}\mu(\xi) - \left(u, \int_0^\infty (-\xi\varphi(\xi) + u)\,\mathrm{d}\mu(\xi)\right)_{\mathbb{C}}\right] \\ &\quad= \Re\left[\int_0^\infty (-\xi\varphi(\xi) + u, \xi\varphi(\xi) - u)_{\mathbb{C}}\,\mathrm{d}\mu(\xi)\right] \\ &\quad= -\Re\left[\int_0^\infty |-\xi\varphi(\xi) + u|^2\,\mathrm{d}\mu(\xi)\right] \leq 0.\end{aligned} \tag{4.85}$$

□

The remarks made for the standard case hold identically (in particular, $\mathcal{D}(C\&D)$ is nonempty). For $s \in \rho(A)$ we define

$$z(s) \coloneqq s\,CR(s,A)B. \tag{4.86}$$

4.6.2 Asymptotic stability

Let (A, B, C) be the triplet of operators defined in Section 4.6.1, further assumed to be non-null. The abstract Cauchy problem (4.13) considered herein is the following. The state space is

$$\begin{aligned} H &\coloneqq \nabla H^1(\Omega) \times L^2(\Omega) \times L^2(\partial\Omega; V_0), \\ ((\boldsymbol{u}, p, \varphi), (\boldsymbol{f_u}, f_p, f_\varphi))_H &\coloneqq (\boldsymbol{u}, \boldsymbol{f_u}) + (p, f_p) + (\varphi, f_\varphi)_{L^2(\partial\Omega;V_0)}, \end{aligned} \tag{4.87}$$

and $\mathcal{A}$ is defined as

$$\begin{aligned} \mathcal{D}(\mathcal{A}) \ni X \coloneqq \begin{pmatrix} \boldsymbol{u} \\ p \\ \varphi \end{pmatrix} &\longmapsto \mathcal{A}X \coloneqq \begin{pmatrix} -\nabla p \\ -\operatorname{div} \boldsymbol{u} \\ A\varphi + B\boldsymbol{u} \cdot \boldsymbol{n} \end{pmatrix}, \\ \mathcal{D}(\mathcal{A}) \coloneqq \left\{ (\boldsymbol{u}, p, \varphi) \in H \;\middle|\; \begin{array}{l} (\boldsymbol{u}, p) \in H_{\operatorname{div}}(\Omega) \times H^1(\Omega) \\ (A\varphi + B\boldsymbol{u} \cdot \boldsymbol{n}) \in L^2(\partial\Omega; V_1) \\ p = C(A\varphi + B\boldsymbol{u} \cdot \boldsymbol{n}) \text{ in } H^{\frac{1}{2}}(\partial\Omega) \end{array} \right\}. \end{aligned} \tag{4.88}$$

The technicality here is that the operator $(\varphi, u) \mapsto C(A\varphi + Bu)$ is defined over $\mathcal{D}(C\&D)$, but CB is not defined in general: this is the abstract counterpart of (4.79). An immediate consequence of the definition of $\mathcal{D}(\mathcal{A})$ is given in the following lemma.

Lemma 4.55 (Boundary regularity)**.** *If $X = (\boldsymbol{u}, p, \varphi) \in \mathcal{D}(\mathcal{A})$, then $\boldsymbol{u} \cdot \boldsymbol{n} \in L^2(\partial\Omega)$.*

Proof. Let $X \in \mathcal{D}(\mathcal{A})$. By definition of $\mathcal{D}(\mathcal{A})$, we have $\varphi \in L^2(\partial\Omega; V_0)$ so that $A\varphi \in L^2(\partial\Omega; V_{-1})$ from Lemma 4.54(iia) and Remark 4.31. The proof is then identical to that of Lemma 4.44. □

The application of Corollary 4.13 is summarized in the lemmas below, namely Lemmas 4.56, 4.57, and 4.58. Due to the similarities with the standard case, the proofs are more concise and focus on the differences.

Lemma 4.56. *The operator $\mathcal{A}$ defined by (4.88) is dissipative.*

Proof. Let $X \in \mathcal{D}(\mathcal{A})$. In particular, $\boldsymbol{u} \cdot \boldsymbol{n} \in L^2(\partial\Omega)$ from Lemma 4.55. Green's formula (C.1) and (4.84) yield

$$\begin{aligned} \Re(\mathcal{A}X, X)_H = \Re\Big[&(A\varphi + B\boldsymbol{u} \cdot \boldsymbol{n}, \varphi)_{L^2(\partial\Omega;V_0)} \\ &- (\boldsymbol{u} \cdot \boldsymbol{n}, C(A\varphi + B\boldsymbol{u} \cdot \boldsymbol{n}))_{L^2(\partial\Omega)} \Big] \leq 0, \end{aligned}$$

using Lemma 4.54. □

The next proof is much simpler than in the standard case.

Lemma 4.57. *$\mathcal{A}$, given by (4.88), is injective.*

Proof. Assume $X \in \mathcal{D}(\mathcal{A})$ satisfies $\mathcal{A}X = 0$, hence $\nabla p = \boldsymbol{0}$ and $\operatorname{div} \boldsymbol{u} = 0$. Green's formula (C.1) and the IBC yield (contrast with (4.69))

$$(\boldsymbol{u} \cdot \boldsymbol{n}, C(\underbrace{A\varphi + B\boldsymbol{u} \cdot \boldsymbol{n}}_{=0}))_{L^2(\partial\Omega)} = 0,$$

where we have used that $\boldsymbol{u} \cdot \boldsymbol{n} \in L^2(\partial\Omega)$ from Lemma 4.55. The IBC gives $p = 0$ in $L^2(\Omega)$. Using (4.82), we deduce $\varphi = 0$ and $\boldsymbol{u} \cdot \boldsymbol{n} = 0$, hence $\boldsymbol{u} = 0$ from (C.2). □

Lemma 4.58. *$s\mathcal{I} - \mathcal{A}$, with $\mathcal{A}$ given by (4.88), is bijective for $s \in (0,\infty) \cup \mathrm{j}\mathbb{R}^*$.*

Proof. Let $F \in H$, $s \in (0,\infty) \cup \mathrm{j}\mathbb{R}^*$, and $\psi \in H^1(\Omega)$. We seek a *unique* $X \in \mathcal{D}(\mathcal{A})$ such that $(s\mathcal{I} - \mathcal{A})X = F$, i.e. (4.71), which implies

$$\begin{aligned}(\nabla p, \nabla\psi) + s^2(p,\psi) + \frac{s}{z(s)}(p,\psi)_{L^2(\partial\Omega)} =& (\boldsymbol{f_u}, \nabla\psi) + s(f_p,\psi) \\ &+ \frac{s}{z(s)}(CAR(s,A)f_\varphi,\psi)_{L^2(\partial\Omega)}.\end{aligned} \tag{4.89}$$

Note that, from hypothesis (4.83), the left-hand side defines an anti-linear form on $H^1(\Omega)$. Let us denote by p the unique solution of (4.89) obtained from a pointwise application of Proposition 4.4 (we rely here on (4.63)). It remains to find suitable $\boldsymbol{u}$ and φ, in a manner identical to the standard diffusive case.

Taking $\psi \in \mathcal{C}_0^\infty(\Omega)$ in (4.89) shows that $\boldsymbol{u} \in H_{\mathrm{div}}(\Omega)$ with (4.71b). Using the expressions of $\boldsymbol{u} \in \nabla H^1(\Omega)$ and $\operatorname{div}\boldsymbol{u}$, and Green's formula (C.1), the weak formulation (4.89) shows that p and $\boldsymbol{u}$ satisfy, in $L^2(\partial\Omega)$,

$$p = z(s)\boldsymbol{u}\cdot\boldsymbol{n} + CAR(s,A)f_\varphi. \tag{4.90}$$

Let us now *define* φ as

$$\varphi \coloneqq R(s,A)\left(B\boldsymbol{u}\cdot\boldsymbol{n} + f_\varphi\right) \in L^2(\partial\Omega; V_0).$$

Using the hypothesis (4.83), we obtain that

$$\begin{aligned}A\varphi + B\boldsymbol{u}\cdot\boldsymbol{n} &= AR(s,A)\left(B\boldsymbol{u}\cdot\boldsymbol{n} + f_\varphi\right) + B\boldsymbol{u}\cdot\boldsymbol{n} \\ &= sR(s,A)B\boldsymbol{u}\cdot\boldsymbol{n} + AR(s,A)f_\varphi\end{aligned}$$

belongs to $L^2(\partial\Omega; V_1)$. We show that the IBC holds by rewriting (4.90) as

$$\begin{aligned}p &= C(sR(s,A)B\boldsymbol{u}\cdot\boldsymbol{n} + AR(s,A)f_\varphi) \\ &= C(AR(s,A)B\boldsymbol{u}\cdot\boldsymbol{n} + B\boldsymbol{u}\cdot\boldsymbol{n} + AR(s,A)f_\varphi) \\ &= C(A\varphi + B\boldsymbol{u}\cdot\boldsymbol{n}),\end{aligned}$$

using (4.86). Thus $(\boldsymbol{u}, p, \varphi) \in \mathcal{D}(\mathcal{A})$. The uniqueness of p follows from Proposition 4.4, that of $\boldsymbol{u}$ from (C.2), and that of φ from $s \in \rho(A)$. □

4.7 Addition of a derivative term

By *derivative impedance* we mean

$$\hat{z}(s) = z_1 s,\ z_1 > 0,$$

for which the IBC (4.3) reduces to $p = z_1\partial_t\boldsymbol{u}\cdot\boldsymbol{n}$. The addition of such a derivative term to the IBCs covered so far (4.17,4.27,4.39,4.53,4.76) leaves unchanged the asymptotic stability results obtained with Corollary 4.13, it only makes the proofs more cumbersome as the state space becomes lengthier. This justifies a posteriori why this term has not been included in Sections 4.2–4.6.

Let us illustrate this fact by revisiting the delay impedance (4.4), covered in Section 4.4. Hence, let us consider the impedance

$$\hat{z}(s) \coloneqq z_1 s + z_0 + z_\tau e^{-\tau s},$$

where $z_1 > 0$ and (z_0, z_τ) are defined as in Section 4.4, so that $\hat{z}$ is positive-real. The inclusion of the derivative implies the presence of an additional variable in the extended state, i.e. the state space is (compare with (4.42))

$$\begin{aligned} H &\coloneqq \nabla H^1(\Omega) \times L^2(\Omega) \times L^2(\partial\Omega; L^2(-\tau, 0)) \times L^2(\partial\Omega), \\ ((\boldsymbol{u}, p, \chi, \eta), (\boldsymbol{f_u}, f_p, f_\chi, f_\eta))_H &\coloneqq (\boldsymbol{u}, \boldsymbol{f_u}) + (p, f_p) + k(\chi, f_\chi)_{L^2(\partial\Omega; L^2(-\tau,0))} \\ &\quad + z_1(\eta, f_\eta)_{L^2(\partial\Omega)}. \end{aligned}$$

The operator $\mathcal{A}$ becomes (compare with (4.43))

$$\mathcal{D}(\mathcal{A}) \ni X \coloneqq \begin{pmatrix} \boldsymbol{u} \\ p \\ \chi \\ \eta \end{pmatrix} \longmapsto \mathcal{A}X \coloneqq \begin{pmatrix} -\nabla p \\ -\operatorname{div} \boldsymbol{u} \\ \partial_\theta \chi \\ \frac{1}{z_1}\left[p - z_0 \boldsymbol{u}\cdot\boldsymbol{n} - z_\tau \chi(\cdot, -\tau)\right] \end{pmatrix},$$

$$\mathcal{D}(\mathcal{A}) \coloneqq \left\{ (\boldsymbol{u}, p, \chi, \eta) \in H \;\middle|\; \begin{array}{l} (\boldsymbol{u}, p, \chi) \in H_{\mathrm{div}}(\Omega) \times H^1(\Omega) \times L^2(\partial\Omega; H^1(-\tau, 0)) \\ \chi(\cdot, 0) = \boldsymbol{u}\cdot\boldsymbol{n} \text{ in } L^2(\partial\Omega) \\ \eta = \boldsymbol{u}\cdot\boldsymbol{n} \text{ in } L^2(\partial\Omega) \end{array} \right\}.$$

The application of Corollary 4.13 is identical to Section 4.4.2. For instance, for $X \in \mathcal{D}(\mathcal{A})$, we have

$$\begin{aligned} \Re(\mathcal{A}X, X)_H &= -\Re\left[(\boldsymbol{u}\cdot\boldsymbol{n}, p)_{L^2(\partial\Omega)}\right] + \Re\left[k(\partial_\theta\chi, \chi)_{L^2(\partial\Omega; L^2(-\tau,0))}\right] \\ &\quad + \Re\left[(p - z_0\boldsymbol{u}\cdot\boldsymbol{n} - z_\tau\chi(\cdot,-\tau), \eta)_{L^2(\partial\Omega)}\right] \\ &= -\Re\left[(\boldsymbol{u}\cdot\boldsymbol{n}, p)_{L^2(\partial\Omega)}\right] + \frac{k}{2}\Re\left[\|\boldsymbol{u}\cdot\boldsymbol{n}\|^2_{L^2(\partial\Omega)} - \|\chi(\cdot,-\tau)\|^2_{L^2(\partial\Omega)}\right] \\ &\quad + \Re\left[(p - z_0\boldsymbol{u}\cdot\boldsymbol{n} - z_\tau\chi(\cdot,-\tau), \boldsymbol{u}\cdot\boldsymbol{n})_{L^2(\partial\Omega)}\right] \\ &= \left(\frac{k}{2} - z_0\right)\|\boldsymbol{u}\cdot\boldsymbol{n}\|^2_{L^2(\partial\Omega)} - \frac{k}{2}\|\chi(\cdot,-\tau)\|^2_{L^2(\partial\Omega)} \\ &\quad - z_\tau\Re\left[(\chi(\cdot,-\tau), \boldsymbol{u}\cdot\boldsymbol{n})_{L^2(\partial\Omega)}\right], \end{aligned}$$

so that the expression of $\Re(\mathcal{A}X, X)_H$ is identical to that without a derivative term, see the proof of Lemma 4.32. The proof of the injectivity of $\mathcal{A}$ is also identical to that carried out in Lemma 4.33: the condition $\mathcal{A}X = 0$ yields $\chi(\cdot, 0) = \chi(\cdot, -\tau) = \boldsymbol{u}\cdot\boldsymbol{n} = \eta$ a.e. on $\partial\Omega$. Finally, the proof of Lemma 4.34 can also be followed almost identically to solve $(s\mathcal{I} - \mathcal{A})X = F$ with $F = (\boldsymbol{f_u}, f_p, f_\chi, f_\eta)$, the additional steps being straightforward; after defining uniquely p, $\boldsymbol{u}$, and χ, the only possibility for η is $\eta \coloneqq \boldsymbol{u}\cdot\boldsymbol{n}$, which belongs to $L^2(\partial\Omega)$, and $\eta = \chi(\cdot, 0)$ is deduced from (4.47).

Conclusion

This chapter has focused on the asymptotic stability of the wave equation coupled with positive-real IBCs drawn from physical applications, namely rational impedance in Section 4.3, time-delayed impedance in Section 4.4, standard diffusive impedance (e.g. fractional integral) in Section 4.5, and extended diffusive impedance (e.g. fractional derivative) in Section 4.6. Finally, the invariance of the derived asymptotic stability results under the addition of a derivative term in the impedance has been discussed in Section 4.7. The proofs crucially hinge upon the

knowledge of a dissipative realization of the IBC, since it employs the semigroup asymptotic stability result given in (Arendt and Batty 1988; Lyubich and Vũ 1988).

By combining these results, asymptotic stability is obtained for the impedance $\hat{z}$ introduced in Section 4.1 and given by (4.4). This suggests a perspective of this work, formulated as a conjecture in the conclusion of this dissertation.

Part III

Discretization of impedance boundary conditions

Chapter 5

Weak enforcement of impedance boundary conditions

Contents

This chapter, drawn from (Monteghetti et al. 2018b), deals with the third component of a TDIBC, i.e. its (semi-)discrete formulation following the terminology introduced in Section 1.3. Specifically, it analyzes the weak enforcement of an admissible IBC within a discontinuous Galerkin (DG) discretization of the LEEs, employing the numerical flux formalism to ease the transition to other methods popular in fluid mechanics. For the analysis the IBC is only assumed admissible and need not be given by one of the models analyzed in Chapter 2, so that both chapters are independent. The first two sections provide reminders: Section 5.1 summarizes the needed facts on the LEEs from Chapter 3, while Section 5.2 recalls the DG discretization of the LEEs as well as some standard estimates. The analysis given in Section 5.3 shows the computational interest of a numerical flux based on the scattering operator $\mathcal{B}$ (1.14), namely the so-called $\mathcal{B}$-flux (5.14,5.39), over fluxes based on the impedance and admittance, namely the $\mathcal{Z}$-flux (5.14,5.35) and the $\mathcal{Y}$-flux (5.14,5.37). These results will be further discussed in the numerical applications of Chapter 6.

State of the art

In the literature, there does not seem to be a consensus on whether a TDIBC should be based on the impedance z (Bin et al. 2009; Gabard and Brambley 2014; Olivetti et al. 2015; Özyörük et al. 1998; Rienstra 2006), the admittance y (Liu et al. 2014; Zhong et al. 2016), or the reflection coefficient β (Fung and Ju 2004; Jaensch et al. 2016; Scalo et al. 2015). This topic has been mentioned by Gabard & Brambley (Gabard and Brambley 2014) who warned that some instabilities reported in the literature may be due to an unsuitable implementation and showed the benefit of a characteristic-based implementation in their study, which is echoed in works

that focus on large eddy simulations and direct numerical simulations (Douasbin et al. 2018; Jaensch et al. 2016; Scalo et al. 2015; Tudisco et al. 2017).

The choice of one formulation over the other can be motivated by the impact of the TDIBC on the maximum admissible time step. Although this aspect is of secondary concern for stability studies, it is of crucial importance for large-scale applications like those that involve hydrodynamics or for inverse methods that need to explore the impedance parameter space. To the best of the author's knowledge, the only known result is that for a proportional impedance (i.e. $z(t) \propto \delta(t)$), using the reflection coefficient yields a CFL stability condition independent of the impedance coefficient (Delorme et al. 2005, § 3.3) (Ventribout 2006, 2.3).

The objective of this chapter is to establish the computational advantage of the reflection coefficient, or scattering operator for nonlinear TDIBCs, with the LEEs. This is achieved by a systematic investigation of the weak enforcement of a generic nonlinear TDIBC in a discontinuous Galerkin finite element method. The presented analysis will be supported in Section 6.2 by a numerical investigation into the computational properties of an elementary nonlinear scattering operator in an impedance tube.

5.1 Linearized Euler equations with IBCs

This chapter focuses on the discretization of the LEEs with IBCs, see Chapters 1 and 3. The purpose of this section is to summarize the facts needed for the next sections. In order to make this chapter as self-sufficient as possible some equations are copied verbatim from Chapter 3.

Linearized Euler equations

The LEEs are given by (3.1) and can be written as Friedrichs-symmetric system

$$\partial_t \boldsymbol{v}(t,\boldsymbol{x}) + \mathcal{A}\boldsymbol{v}(t,\boldsymbol{x}) = 0 \quad (t \in (0,\infty),\ \boldsymbol{x} \in \Omega), \tag{5.1}$$

where

$$\boldsymbol{v} \coloneqq \begin{pmatrix} \boldsymbol{u} \\ \tilde{p} \end{pmatrix} \in \mathbb{R}^{d+1}$$

is the perturbation vector homogeneous to a velocity, and the spatial operator $\mathcal{A}$ is defined as

$$\mathcal{A}\boldsymbol{v} \coloneqq A(\nabla)\boldsymbol{v} + B\boldsymbol{v}$$

with

$$A(\boldsymbol{n}) = \begin{pmatrix} (\boldsymbol{u_0}\cdot\boldsymbol{n})\mathbb{I}_d & c_0\boldsymbol{n} \\ c_0\boldsymbol{n}^\intercal & \boldsymbol{u_0}\cdot\boldsymbol{n} \end{pmatrix},\ B = \begin{pmatrix} \nabla\boldsymbol{u_0} & \frac{1}{c_0}\nabla\boldsymbol{u_0}\cdot\boldsymbol{u_0} \\ \boldsymbol{0_d}^\intercal & \gamma\nabla\cdot\boldsymbol{u_0} \end{pmatrix},$$

where $\mathbb{I}_d$ denotes the $d\times d$ identity matrix. From Proposition 3.11, the characteristic matrix $A(\boldsymbol{n})$ is symmetric, with eigenvalues $\boldsymbol{u_0}\cdot\boldsymbol{n}$ of multiplicity $(d-1)$ and $\boldsymbol{u_0}\cdot\boldsymbol{n}\pm c_0|\boldsymbol{n}|$ of multiplicity 2. (Due to the homentropicity assumption, the entropy mode is absent.) The absolute value $|A(\boldsymbol{n})|$, the positive part $A(\boldsymbol{n})^\oplus$, and the negative part $A(\boldsymbol{n})^\ominus$ are defined using the diagonal form of $A(\boldsymbol{n})$ through

$$|A(\boldsymbol{n})| \coloneqq P(\boldsymbol{n})\,|\Lambda(\boldsymbol{n})|\,P(\boldsymbol{n})^{-1},\ 2A(\boldsymbol{n})^\oplus \coloneqq |A(\boldsymbol{n})| + A(\boldsymbol{n}),\ 2A(\boldsymbol{n})^\ominus \coloneqq |A(\boldsymbol{n})| - A(\boldsymbol{n}),$$

where

$$|\Lambda(\boldsymbol{n})| \coloneqq \operatorname{diag}\left(\left[|\Lambda_i|\right]_{i\in[\![1,d+1]\!]}\right).$$

The symmetry of $A(\boldsymbol{n})$ implies, by definition, that the operator $\partial_t + A(\nabla)$ is a Friedrichs-symmetric operator; equivalently, (5.1) is a symmetric hyperbolic system. Using an integration by parts, this symmetry property yields

$$(\mathcal{A}\boldsymbol{v}, \boldsymbol{v})_{L^2(\Omega)} = \frac{1}{2}(C(\boldsymbol{u_0})\boldsymbol{v}, \boldsymbol{v})_{L^2(\Omega)} + \frac{1}{2}(A(\boldsymbol{n})\boldsymbol{v}, \boldsymbol{v})_{L^2(\partial\Omega)}, \tag{5.2}$$

where the symmetric amplification matrix $C(\boldsymbol{u_0})$ and the L^2 scalar products are given by

$$C(\boldsymbol{u_0}) = \begin{pmatrix} \nabla \boldsymbol{u_0} + \nabla^\intercal \boldsymbol{u_0} - (\nabla \cdot \boldsymbol{u_0})\mathbb{I}_d & \frac{1}{c_0}\nabla \boldsymbol{u_0} \cdot \boldsymbol{u_0} \\ \frac{1}{c_0}\boldsymbol{u_0} \cdot \nabla^\intercal \boldsymbol{u_0} & (2\gamma - 1)\nabla \cdot \boldsymbol{u_0} \end{pmatrix}$$

and

$$(\boldsymbol{v}, \boldsymbol{w})_{L^2(\Omega)} \coloneqq \int_\Omega (\boldsymbol{v}, \boldsymbol{w})_{\mathbb{R}^{d+1}} \,\mathrm{d}\boldsymbol{x},\ (\boldsymbol{v}, \boldsymbol{w})_{L^2(\partial\Omega)} \coloneqq \int_{\partial\Omega} (\boldsymbol{v}, \boldsymbol{w})_{\mathbb{R}^{d+1}} \,\mathrm{d}\boldsymbol{x}.$$

In this paper, the energy analysis is carried out with the standard acoustic energy defined as (Morse and Ingard 1968, § 6.2) (Kinsler and Frey 1962, § 5.6)

$$\|\boldsymbol{v}(t)\|^2_{L^2(\Omega)} \coloneqq (\boldsymbol{v}, \boldsymbol{v})_{L^2(\Omega)} = \int_\Omega |\tilde{p}(t, \boldsymbol{x})|^2 \,\mathrm{d}\boldsymbol{x} + \int_\Omega |\boldsymbol{u}(t, \boldsymbol{x})|^2 \,\mathrm{d}\boldsymbol{x}, \tag{5.3}$$

so that the continuous energy balance, which expresses the evolution of acoustic energy in the domain Ω, reads

$$\frac{1}{2}\frac{\mathrm{d}}{\mathrm{d}t}\|\boldsymbol{v}(t)\|^2_{L^2(\Omega)} = -(\mathcal{A}\boldsymbol{v}, \boldsymbol{v})_{L^2(\Omega)} = -\frac{1}{2}(C(\boldsymbol{u_0})\boldsymbol{v}, \boldsymbol{v})_{L^2(\Omega)} - \frac{1}{2}(A(\boldsymbol{n})\boldsymbol{v}, \boldsymbol{v})_{L^2(\partial\Omega)}, \tag{5.4}$$

where the right-hand side is given by

$$\begin{aligned} (C(\boldsymbol{u_0})\boldsymbol{v}, \boldsymbol{v})_{\mathbb{R}^{d+1}} &= (\nabla \cdot \boldsymbol{u_0}) \left[(2\gamma - 1)\tilde{p}^2 - |\boldsymbol{u}|^2\right] + 2\boldsymbol{u} \cdot \nabla \boldsymbol{u_0} \cdot (\boldsymbol{u} + \frac{1}{c_0}\tilde{p}\,\boldsymbol{u_0}) \\ (A(\boldsymbol{n})\boldsymbol{v}, \boldsymbol{v})_{\mathbb{R}^{d+1}} &= (\boldsymbol{u_0} \cdot \boldsymbol{n}) \left[\tilde{p}^2 + |\boldsymbol{u}|^2\right] + 2c_0\,\tilde{p}(\boldsymbol{u} \cdot \boldsymbol{n}). \end{aligned} \tag{5.5}$$

Impedance boundary condition

The IBC associated with the LEEs is formulated as in Section 1.1. The expression of the boundary term $(A(\boldsymbol{n})\boldsymbol{v}, \boldsymbol{v})_{\mathbb{R}^{d+1}}$ in the energy balance (5.4) suggests the following assumption.

Assumption 5.1. *The base flow $\boldsymbol{u_0}$ obeys (at least) a slip condition $\boldsymbol{u_0} \cdot \boldsymbol{n} = 0$ at the impedance boundary Γ_z.*

Thanks to this assumption, an admissible impedance yields

$$\int_0^t (A(\boldsymbol{n})\boldsymbol{v}, \boldsymbol{v})_{L^2(\Gamma_z)} \,\mathrm{d}\tau \geq 0 \quad (t > 0),$$

so that there is energy dissipation at the impedance boundary Γ_z. Therefore, in the absence of other boundary sources, the presence of an instability is linked to the spectrum of the amplification matrix $C(\boldsymbol{u_0})$. As covered in Chapter 3, this a priori energy estimate yields uniqueness of the solution and is the stepping stone to obtain well-posedness in e.g. $e^{-\kappa t}\mathcal{C}((0, \infty); H^1(\Omega)^{d+1})$ with κ finite. It also follows from the energy estimate that $\kappa \geq \min_{x\in\Omega} \lambda_{\min}(\boldsymbol{u_0})$, where $\lambda_{\min}(\boldsymbol{u_0})$ is the minimum eigenvalue of $C(\boldsymbol{u_0})$. A sufficient condition for stability is that $\min_{x\in\Omega} \lambda_{\min}(\boldsymbol{u_0}) \geq 0$, which is a stringent condition on the base flow $\boldsymbol{u_0}(\boldsymbol{x})$. This assumption is typically not satisfied in applications: it holds for a constant flow but fails for a Poiseuille flow for instance.

Remark 5.2. Although the mathematical analysis leads to assuming $\boldsymbol{u_0} \cdot \boldsymbol{n} = 0$, it is interesting to note that physically a no-slip condition $\boldsymbol{u_0} = 0$ is *required* at the impedance wall. Indeed, if $\boldsymbol{u_0} \neq 0$ the effect of the hydrodynamic boundary layer (refraction of sound waves (Pridmore-Brown 1958)) must be explicitly modeled, which leads to a non-locally reacting impedance, out of the scope of this paper. For example, the standard Ingard-Myers boundary condition reads $u_n = Y(p, \nabla p)$, and has been shown by Brambley using a Briggs-Bers analysis to prevent well-posedness, in the sense that there is no finite value for κ (Brambley 2009). A corrected impedance that accounts for both the acoustic and hydrodynamic boundary layers has been derived by Khamis & Brambley (Khamis and Brambley 2017). The computational interest of such non-local boundary conditions is that the boundary layer need not be discretized, see (Gabard and Brambley 2014) for a use in the time domain.

Remark 5.3. Choosing an aeroacoustic energy instead of the acoustic energy (5.3) used herein would not not modify the results obtained in this chapter, see Appendix D for details.

5.2 Discontinuous Galerkin discretization

This section recalls the DG discretization of the LEEs written as a Friedrichs system. Let $(\mathcal{T}_h)_h$ be a quasi-uniform sequence of meshes indexed by

$$h \coloneqq \max_{T \in \mathcal{T}_h} h_T,$$

where h_T denotes the diameter of the element $T \in \mathcal{T}_h$. For simplicity, each mesh $\mathcal{T}_h$ is assumed to be simplicial, geometrically conformal, and shape-regular, see See (Ern and Guermond 2004, Chap. 1) and (Di Pietro and Ern 2012, Chap. 1) for definitions of the mentioned properties (more specific citations will be given when proving estimates). In the DG finite element method, the approximation space is taken as

$$V_h \coloneqq \mathbb{P}_d^k(\mathcal{T}_h)^{d+1},$$

where $\mathbb{P}_d^k(\mathcal{T}_h)$ is the broken polynomial space defined as

$$\mathbb{P}_d^k(\mathcal{T}_h) \coloneqq \{v \in L^2(\Omega) \mid \forall T \in \mathcal{T}_h,\ v_{|T} \in \mathbb{P}_d^k(T)\}$$

with $\mathbb{P}_d^k$ denoting the space of polynomials of d variables and total degree at most k. The spatial domain Ω is assumed to be a polyhedron, so that it can be exactly covered by each mesh. The semi-discrete formulation of (5.1) reads: find $\boldsymbol{v}_h \in \mathcal{C}^1([0, \infty), V_h)$ such that

$$\partial_t \boldsymbol{v}_h + \mathcal{A}_h \boldsymbol{v}_h = 0, \tag{5.6}$$

where the spatial discretization is embodied by the finite-dimensional operator

$$\mathcal{A}_h : V_h \to V_h$$

defined by

$$\forall \boldsymbol{w}_h \in V_h,\ (\mathcal{A}_h \boldsymbol{v}_h, \boldsymbol{w}_h)_{L^2(\Omega)} \coloneqq \sum_{T \in \mathcal{T}_h} (\mathcal{A}\boldsymbol{v}_h, \boldsymbol{w}_h)_{L^2(T)} + ((A(\boldsymbol{n})\boldsymbol{v}_h)^* - A(\boldsymbol{n})\boldsymbol{v}_h, \boldsymbol{w}_h)_{L^2(\partial T)},$$

where the quantity $(A(\boldsymbol{n})\boldsymbol{v}_h)^*$ is the so-called numerical flux function, uniquely defined at each face. Intuitively, this definition can be viewed as resulting from two integration by parts. At an interior face $F \in \mathcal{F}_h^i$ we use the upwind flux

$$(A(\boldsymbol{n}_F)\boldsymbol{v})^* \coloneqq A(\boldsymbol{n}_F)^{\oplus} \boldsymbol{v}_{|T_1} - A(\boldsymbol{n}_F)^{\ominus} \boldsymbol{v}_{|T_2} = A(\boldsymbol{n}_F)\{\boldsymbol{v}\} + \frac{1}{2}|A(\boldsymbol{n}_F)|[\![\boldsymbol{v}]\!], \tag{5.7}$$

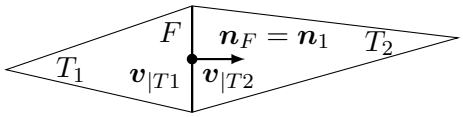

Figure 5.1. Notations for an interior face $F \in \mathcal{F}_h^i$.

where

$$\{\boldsymbol{v}\} \coloneqq \frac{1}{2}(\boldsymbol{v}_{|T_1} + \boldsymbol{v}_{|T_2}) \tag{5.8}$$

is the face average and

$$[\![\boldsymbol{v}]\!] \coloneqq \boldsymbol{v}_{|T_1} - \boldsymbol{v}_{|T_2} \tag{5.9}$$

is the face jump, see Figure 5.1 for the face-specific notations. This leads to

$$\begin{aligned}(\mathcal{A}_h \boldsymbol{v}_h, \boldsymbol{w}_h)_{L^2(\Omega)} = &\sum_{T\in\mathcal{T}_h} (\mathcal{A}\boldsymbol{v}_h, \boldsymbol{w}_h)_{L^2(T)} + ((A(\boldsymbol{n})\boldsymbol{v}_h)^* - A(\boldsymbol{n})\boldsymbol{v}_h, \boldsymbol{w}_h)_{L^2(\partial\Omega)} \\ &- \sum_{F\in\mathcal{F}_h^i} (A(\boldsymbol{n}_F)[\![\boldsymbol{v}_h]\!], \{\boldsymbol{w}_h\})_{L^2(F)} + \frac{1}{2}\sum_{F\in\mathcal{F}_h^i} (|A(\boldsymbol{n}_F)|[\![\boldsymbol{v}_h]\!], [\![\boldsymbol{w}_h]\!])_{L^2(F)}.\end{aligned} \tag{5.10}$$

At a boundary face $F \in \mathcal{F}_h^b$, the IBC is weakly enforced through a numerical flux introduced in Section 5.3.1 and analyzed in Sections 5.3.2 and 5.3.3.

The bilinear form (5.10) is standard and fits within the framework proposed by Ern & Guermond (Ern and Guermond 2006) for the DG discretization of Friedrichs systems, and notations have been kept as close as possible to that employed in this seminal work. The reader interested in an error analysis with the standard boundary condition "$A(\boldsymbol{n})\boldsymbol{v} = M(\boldsymbol{n})\boldsymbol{v}$" is referred to (Ern and Guermond 2006) and (Di Pietro and Ern 2012, Chaps. 3 & 7). The well-posedness of the semi-discrete formulation (5.6) follows from the Cauchy-Lipschitz-Picard theorem (Brezis 2011, Thm. 7.3) since it is a finite-dimensional ODE.

Using the identity (5.2) on each element T enables to get

$$(\mathcal{A}_h \boldsymbol{v}_h, \boldsymbol{v}_h)_{L^2(\Omega)} = \frac{1}{2}(C(\boldsymbol{u_0})\boldsymbol{v}_h, \boldsymbol{v}_h)_{L^2(\Omega)} + \frac{1}{2}|\boldsymbol{v}_h|^2_{\mathrm{upw}} + \Big((A(\boldsymbol{n})\boldsymbol{v}_h)^* - \frac{1}{2}A(\boldsymbol{n})\boldsymbol{v}_h, \boldsymbol{v}_h\Big)_{L^2(\partial\Omega)}, \tag{5.11}$$

where the upwind seminorm is defined as

$$|\boldsymbol{v}_h|^2_{\mathrm{upw}} \coloneqq \sum_{F\in\mathcal{F}_h^i} (|A(\boldsymbol{n}_F)|[\![\boldsymbol{v}_h]\!], [\![\boldsymbol{v}_h]\!])_{L^2(F)}.$$

This leads to the following semi-discrete energy balance

$$\begin{aligned}\frac{1}{2}\frac{\mathrm{d}}{\mathrm{d}t}\|\boldsymbol{v}_h\|^2_{L^2(\Omega)} &= -(\mathcal{A}_h\boldsymbol{v}_h, \boldsymbol{v}_h)_{L^2(\Omega)} \\ &= -\frac{1}{2}(C(\boldsymbol{u_0})\boldsymbol{v}_h, \boldsymbol{v}_h)_{L^2(\Omega)} - \frac{1}{2}|\boldsymbol{v}_h|^2_{\mathrm{upw}} \\ &\quad - \Big((A(\boldsymbol{n})\boldsymbol{v}_h)^* - \frac{1}{2}(A(\boldsymbol{n})\boldsymbol{v}_h), \boldsymbol{v}_h\Big)_{L^2(\partial\Omega)},\end{aligned} \tag{5.12}$$

which is to be contrasted with its continuous counterpart (5.4). The term $|\boldsymbol{v}_h|^2_{\mathrm{upw}}$ is the energy dissipation due to the use of an upwind flux (it would be null had a centered flux been used) while the boundary term $((A(\boldsymbol{n})\boldsymbol{v}_h)^* - \frac{1}{2}A(\boldsymbol{n})\boldsymbol{v}_h, \boldsymbol{v}_h)_{L^2(\partial\Omega)}$ includes the contribution of the weakly enforced IBC, studied below.

Discrete trace inequality

We end this section with a standard estimate, namely the discrete trace inequality, that will be used to derive CFL-type stability conditions in Section 5.3. The background material for the analysis can be found in (Di Pietro and Ern 2012), (Ern and Guermond 2004), and (Ern and Guermond 2006). As mentioned above, for simplicity each mesh $\mathcal{T}_h$ is assumed to be simplicial (Ern and Guermond 2004, Def. 1.53) (Di Pietro and Ern 2012, Def. 1.11), geometrically conformal (Ern and Guermond 2004, Def. 1.55) or "matching" (Di Pietro and Ern 2012, Def. 1.36), shape-regular (Ern and Guermond 2004, Def. 1.107) (Di Pietro and Ern 2012, Def. 1.38), and the mesh sequence $(\mathcal{T}_h)_h$ is assumed to be quasi-uniform (Ern and Guermond 2004, Def. 1.140) (Di Pietro and Ern 2012, § 3.1.2).

Lemma 5.4 (Discrete trace inequality)**.** *Let $(\mathcal{T}_h)_h$ be a quasi-uniform sequence of simplicial, geometrically conformal, and shape-regular meshes. For any dimension $d \in \mathbb{N}^*$ and degree $k \in \mathbb{N}^*$, there is a constant $C_{\mathrm{tr}} > 0$ such that $\forall h > 0$, $\forall T \in \mathcal{T}_h$, for any face F_T,*

$$\forall \boldsymbol{v}_h \in \mathbb{P}_d^k(\mathcal{T}_h)^{d+1},\ h^{1/2}\|\boldsymbol{v}_h\|_{L^2(F_T)} \le C_{\mathrm{tr}}\|\boldsymbol{v}_h\|_{L^2(T)}. \tag{5.13}$$

The constant C_{tr} only depends upon d, k, and the mesh regularity parameter

$$\rho_1 \coloneqq \inf_h \inf_{T\in\mathcal{T}_h} \frac{r_T}{h_T}$$

with r_T the radius of the largest ball inscribed in T.

Proof. Let $h > 0$ and $T \in \mathcal{T}_h$. Since $\mathcal{T}_h$ is a simplicial, geometrically conformal, and shape-regular mesh, we have (Di Pietro and Ern 2012, Eq. 1.39)

$$h_T^{1/2}\|\boldsymbol{v}_h\|_{L^2(F_T)} \le C_{\mathrm{tr,s}}\|\boldsymbol{v}_h\|_{L^2(T)},$$

where $C_{\mathrm{tr,s}}$ only depends upon ρ_1, d, and k. By definition, the quasi-uniformity of $\mathcal{T}_h$ gives a constant $C > 0$ such that $Ch \le \min_{T\in\mathcal{T}_h} h_T$. □

5.3 Numerical flux for impedance boundary conditions

This section, which is the contribution of the chapter, presents an analysis of the weak enforcement of an admissible IBC within a DG discretization of the LEEs. The numerical flux formalism is employed to ease the transition to other methods popular in fluid mechanics such as finite volume or spectral differences. In the presented analysis, the IBC need only be admissible in the sense given in in Section 1.1, so that we do not assume any particular impedance model. The analysis given here shows the computational interest of a numerical flux based on the scattering operator $\mathcal{B}$ (1.14), namely the so-called $\mathcal{B}$-flux (5.14,5.39), over fluxes based on the impedance and admittance, namely the $\mathcal{Z}$-flux (5.14,5.35) and the $\mathcal{Y}$-flux (5.14,5.37).

This section is organized as follows. Section 5.3.1 defines admissibility conditions for an impedance numerical flux, upon which the analyses of Sections 5.3.2 and 5.3.3 rely. Section 5.3.4 gathers technical proofs for the CFL-type stability conditions claimed in the previous sections.

5.3.1 Admissibility conditions for an impedance numerical flux

On a part of the boundary $\Gamma \coloneqq \partial\Omega$ denoted Γ_z, the IBC is weakly enforced through a centered flux

$$(A(\boldsymbol{n})\boldsymbol{v})^* \coloneqq \frac{1}{2}A(\boldsymbol{n})(\boldsymbol{v} + \boldsymbol{v}^g), \tag{5.14}$$

where $\boldsymbol{v}^g$ is the so-called ghost state that needs to be suitably defined as a function of $\boldsymbol{v}$ and $\mathcal{Z}$, $\mathcal{Y}$, or $\mathcal{B}$. A systematic derivation of the possible expressions for $A(\boldsymbol{n})\boldsymbol{v}^g$ is carried out in Section 5.3.3 with an energy analysis formalized through the so-called admissibility and continuity conditions defined below.

Remark 5.5. The ghost state $\boldsymbol{v}^g$ is a function known in closed-form and in this paper the numerical flux (5.14) is enforced without adding computational nodes outside of Ω: the terminology "ghost state" is chosen for its intuitive nature, and does not imply that "ghost nodes" or "ghost cells" are used whatsoever.

From now on we assume that the LEEs, when coupled with admissible IBCs, always admit a unique exact solution $\boldsymbol{v}$ in $e^{-\kappa t}\mathcal{C}((0,\infty);V)$ with κ finite and

$$V \coloneqq H^1(\Omega)^{d+1},$$

see Chapter 3 for a justification. However, to carry out the semi-discrete energy analysis presented in this section, the only property that we shall use is that if $\boldsymbol{v}$ is the exact solution, then $\boldsymbol{v}$ satisfies the IBC on Γ_z. By contrast, a function $\boldsymbol{v}_h$ in $\mathcal{C}^1([0,\infty),V_h)$ does not necessarily satisfy the IBC on Γ_z.

Before stating the admissibility conditions for an impedance numerical flux, let us recall that the spatial discretization is said to be *consistent* if for $\boldsymbol{v}(t) \in V$ the exact solution of (5.1) with the considered boundary conditions:

$$\forall \boldsymbol{w}_h \in V_h,\ (\mathcal{A}_h\boldsymbol{v},\boldsymbol{w}_h)_{L^2(\Omega)} = (\mathcal{A}\boldsymbol{v},\boldsymbol{w}_h)_{L^2(\Omega)}.$$

Definition 5.6 (Admissibility)**.** The impedance numerical flux (5.14), uniquely determined by the expression of $A(\boldsymbol{n})\boldsymbol{v}^g$, is said to be *admissible* if it is both consistent and passive.

- (Consistency) Let $\boldsymbol{v}(t) \in V$ be the exact solution (in particular, it does obey the IBC). The consistency condition reads $(A(\boldsymbol{n})\boldsymbol{v})^* = A(\boldsymbol{n})\boldsymbol{v}$ or equivalently

$$A(\boldsymbol{n})\boldsymbol{v}^g = A(\boldsymbol{n})\boldsymbol{v}. \tag{5.15}$$

- (Passivity) Let $\boldsymbol{v}_h(t) \in V_h$ (in particular, it does *not* obey the IBC). The passivity condition reads

$$\forall t>0,\ \int_0^t \Big((A(\boldsymbol{n})\boldsymbol{v}_h)^* - \frac{1}{2}A(\boldsymbol{n})\boldsymbol{v}_h,\boldsymbol{v}_h\Big)_{L^2(\Gamma_z)}\,\mathrm{d}\tau = \frac{1}{2}\int_0^t (A(\boldsymbol{n})\boldsymbol{v}_h^g,\boldsymbol{v}_h)_{L^2(\Gamma_z)}\,\mathrm{d}\tau \geq 0. \tag{5.16}$$

The passivity condition is to be understood in light of the semi-discrete energy balance (5.12), see Example 5.14 for a numerical illustration of its necessity. In addition to these two admissibility conditions, the two following continuity properties are also computationally desirable.

- (Hard-wall continuity) As "$\mathcal{Z}\to\infty$" (or "$\mathcal{Y}\to 0$", or "$\mathcal{B}\to\mathcal{I}$"), a hard wall ($\boldsymbol{u}\cdot\boldsymbol{n}=0$) is recovered without singularity, which can be written formally as

$$\lim_{\mathcal{Z}\to\infty} A(\boldsymbol{n})\boldsymbol{v}^g = M_{\mathrm{hw}}(\boldsymbol{n})\boldsymbol{v},\ M_{\mathrm{hw}}(\boldsymbol{n}) \coloneqq c_0\begin{bmatrix} 2\zeta\boldsymbol{n}\otimes\boldsymbol{n} & \boldsymbol{n} \\ -\boldsymbol{n}^\intercal & 0 \end{bmatrix} \tag{5.17}$$

  and ζ is an arbitrary non-negative parameter.

- (Pressure-release continuity) As "$\mathcal{Z}\to 0$" (or "$\mathcal{Y}\to\infty$", or "$\mathcal{B}\to -\mathcal{I}$"), a pressure-release boundary ($\tilde{p}=0$) is recovered without singularity, i.e.

$$\lim_{\mathcal{Z}\to 0} A(\boldsymbol{n})\boldsymbol{v}^g = M_{\mathrm{pr}}(\boldsymbol{n})\boldsymbol{v},\ M_{\mathrm{pr}}(\boldsymbol{n}) \coloneqq c_0\begin{bmatrix} 0_{d,d} & -\boldsymbol{n} \\ \boldsymbol{n}^\intercal & 2\zeta \end{bmatrix} \tag{5.18}$$

  and ζ is an arbitrary non-negative parameter.

It is straightforward to verify that $A(\boldsymbol{n})\boldsymbol{v}^g \coloneqq M_{\mathrm{hw/pr}}(\boldsymbol{n})\boldsymbol{v}$ respects the consistency (5.15) and passivity (5.16) conditions stated in Definition 5.6. The given expressions $M_{\mathrm{hw}}(\boldsymbol{n})$ and $M_{\mathrm{pr}}(\boldsymbol{n})$, or variations thereof, are common in the literature (Ern and Guermond 2006, § 5.3) (Di Pietro and Ern 2012, § 7.1.2) (Hesthaven and Warburton 2008, § 7.1). The ability to recover both the hard-wall and pressure-release cases is of particular interest when performing an inverse method on the IBC where the parameter space needs to be explored.

Remark 5.7. Note that at this stage no assumption is made regarding the time-domain discretization of the IBC: Definition 5.6 is purely semi-discrete.

The application of the energy analysis to generic nonlinear IBCs, which leads to the derivation of the $\mathcal{Z}$, $\mathcal{Y}$, and $\mathcal{B}$ fluxes, is done in Section 5.3.3. For the sake of clarity, the elementary case of a proportional impedance $\mathcal{Z}(\boldsymbol{u}\cdot\boldsymbol{n}) \propto \boldsymbol{u}\cdot\boldsymbol{n}$ is first fully worked out in Section 5.3.2. In spite of its simplicity, this example provides an intuitive understanding of the computational advantage of the scattering operator $\mathcal{B}$.

5.3.2 Weak enforcement of proportional impedance boundary conditions

This section focuses on the computational properties of numerical fluxes for the so-called proportional impedance

$$\frac{1}{z_0}z(t) = a_0\delta(t),\ a_0 > 0,$$

so that the corresponding IBC reads

$$\tilde{p} = a_0\boldsymbol{u}\cdot\boldsymbol{n}.$$

From Proposition 1.8 it is admissible. To weakly enforce the IBC (1.1) using the numerical flux (5.14), the ghost state $\boldsymbol{v}^g$ is sought as linearly dependent upon $\boldsymbol{v}$

$$\boldsymbol{v}^g \coloneqq \begin{bmatrix} \alpha_3\boldsymbol{n}\otimes\boldsymbol{n} & \alpha_4\boldsymbol{n} \\ \alpha_1\boldsymbol{n}^\intercal & \alpha_2 \end{bmatrix}\boldsymbol{v},\ A(\boldsymbol{n})\boldsymbol{v}^g = c_0\begin{bmatrix} \tilde{p}^g\boldsymbol{n} \\ \boldsymbol{u}^g\cdot\boldsymbol{n} \end{bmatrix} = M_0(\boldsymbol{n})\boldsymbol{v}, \tag{5.19}$$

where

$$M_0(\boldsymbol{n}) = c_0\begin{bmatrix} \alpha_1\boldsymbol{n}\otimes\boldsymbol{n} & \alpha_2\boldsymbol{n} \\ \alpha_3\boldsymbol{n}^\intercal & \alpha_4 \end{bmatrix}. \tag{5.20}$$

To obtain an admissible flux from this generic expression, two of the four DoF must be removed, as summarized in the proposition below.

Proposition 5.8. *The numerical flux function given by (5.14,5.19) is admissible if and only if*

$$\alpha_1 = (1-\alpha_2)a_0,\ \alpha_4 = \frac{1}{a_0}(1-\alpha_3),$$

with

$$\alpha_2 \le 1,\ \alpha_3 \le 1,\ (\alpha_2+\alpha_3)^2 \le 4(1-\alpha_2)(1-\alpha_3).$$

Proof. The proof is elementary and consists in using the admissibility conditions. (Consistency) Let $\boldsymbol{v} = [\boldsymbol{u}^\intercal, \tilde{p}]^\intercal$ be the exact solution. The consistency condition (5.15) reads

$$\begin{bmatrix} \alpha_1\boldsymbol{n}\otimes\boldsymbol{n} & (\alpha_2-1)\boldsymbol{n} \\ (\alpha_3-1)\boldsymbol{n}^\intercal & \alpha_4 \end{bmatrix}\boldsymbol{v} = 0.$$

The fact that $\boldsymbol{v}$ obeys the IBC $\tilde{p} = a_0\boldsymbol{u}\cdot\boldsymbol{n}$ readily leads to $\alpha_1 = (1-\alpha_2)a_0$ and $\alpha_4 = (1-\alpha_3)/a_0$, so that the two DoF left are α_2 and α_3. (Passivity) Let $\boldsymbol{v}_h \in V_h$. Since $(M_0(\boldsymbol{n})\boldsymbol{v}_h, \boldsymbol{v}_h)_{\mathbb{R}^{d+1}} = (\check{M}_0\check{\boldsymbol{v}}_h, \check{\boldsymbol{v}}_h)_{\mathbb{R}^2}$ with $\check{\boldsymbol{v}}_h = [\ \boldsymbol{u}_h\cdot\boldsymbol{n}\quad \tilde{p}_h\ ]^\intercal$ and

$$\check{M}_0 \coloneqq \begin{bmatrix} \alpha_1 & \frac{\alpha_2+\alpha_3}{2} \\ \frac{\alpha_2+\alpha_3}{2} & \alpha_4 \end{bmatrix}, \tag{5.21}$$

condition (5.16) holds if and only if $\check{M}_0$ is positive semidefinite. The inequalities on α_2 and α_3 follows from the application of the following elementary lemma that is frequently used in the remainder of this paper.

Lemma 5.9. *A 2×2 symmetric matrix* $\begin{bmatrix} u & v \\ v & w \end{bmatrix}$ *is positive semidefinite if and only if $v^2 \leq uw$ and $u + w \geq 0$.*

Proof. A symmetric 2×2 matrix Σ is positive semidefinite if and only if $\det \Sigma \geq 0$ and $\operatorname{tr} \Sigma \geq 0$. (Product and sum of the two real eigenvalues.) □

□

Remark 5.10. In the case of a proportional impedance, the consistency (5.15) and passivity (5.16) conditions are the (DG1) and (DG2) properties stated in (Ern and Guermond 2006) and needed for the error analysis.

Therefore, after examination of the admissibility conditions there are two remaining DoF, α_2 and α_3, so that

$$\boldsymbol{v}^g \coloneqq \begin{bmatrix} \alpha_3 \boldsymbol{n}\otimes\boldsymbol{n} & \frac{1-\alpha_3}{a_0}\boldsymbol{n} \\ (1-\alpha_2)a_0\boldsymbol{n}^\intercal & \alpha_2 \end{bmatrix} \boldsymbol{v},\ M_0(\boldsymbol{n}) = c_0 \begin{bmatrix} (1-\alpha_2)a_0\boldsymbol{n}\otimes\boldsymbol{n} & \alpha_2\boldsymbol{n} \\ \alpha_3\boldsymbol{n}^\intercal & \frac{1-\alpha_3}{a_0} \end{bmatrix}. \tag{5.22}$$

Further constraints can be obtained by considering the continuity conditions (5.17) and (5.18):

$$\lim_{a_0\to 0}\alpha_2 = -1, \qquad \lim_{a_0\to 0}\alpha_3 = 1, \qquad \lim_{a_0\to\infty}\alpha_2 = 1, \qquad \lim_{a_0\to\infty}\alpha_3 = -1, \tag{5.23}$$

$$\lim_{a_0\to 0}(1-\alpha_2)a_0 = 0,\ \lim_{a_0\to 0}(1-\alpha_3)\frac{1}{a_0} \geq 0,\ \lim_{a_0\to\infty}(1-\alpha_2)a_0 \geq 0,\ \lim_{a_0\to\infty}(1-\alpha_3)\frac{1}{a_0} = 0. \tag{5.24}$$

The line (5.23) suggests defining $\alpha \coloneqq \alpha_2$ with $\alpha_3 = -\alpha$, which leads to the α-flux

$$\boldsymbol{v}^g \coloneqq \begin{bmatrix} -\alpha\boldsymbol{n}\otimes\boldsymbol{n} & \frac{(1+\alpha)}{a_0}\boldsymbol{n} \\ (1-\alpha)a_0\boldsymbol{n}^\intercal & \alpha \end{bmatrix} \boldsymbol{v},\ M_0(\boldsymbol{n}) = c_0 \begin{bmatrix} (1-\alpha)a_0\boldsymbol{n}\otimes\boldsymbol{n} & \alpha\boldsymbol{n} \\ -\alpha\boldsymbol{n}^\intercal & \frac{1+\alpha}{a_0} \end{bmatrix}. \tag{5.25}$$

Any flux of this form is admissible, as long as $\alpha \in [-1, 1]$. To respect the remaining continuity conditions (5.24), one can choose $\alpha = \beta_0 \coloneqq (a_0 - 1)/(a_0 + 1)$, which yields the β_0-flux

$$\boldsymbol{v}^g \coloneqq \begin{bmatrix} -\beta_0\boldsymbol{n}\otimes\boldsymbol{n} & (1-\beta_0)\boldsymbol{n} \\ (1+\beta_0)\boldsymbol{n}^\intercal & \beta_0 \end{bmatrix} \boldsymbol{v},\ M_0(\boldsymbol{n}) = c_0 \begin{bmatrix} (1+\beta_0)\boldsymbol{n}\otimes\boldsymbol{n} & \beta_0\boldsymbol{n} \\ -\beta_0\boldsymbol{n}^\intercal & 1-\beta_0 \end{bmatrix}, \tag{5.26}$$

an apparent computational interest of which is the boundedness of its components with respect to a_0. In summary, application of the admissibility and continuity conditions leads to (5.26), an expression that, to the best of the authors' knowledge, was first proposed by Ventribout (Ventribout 2006, § 1.3.2) with a view on application to optimal control. Further insights into the benefit of choosing $\alpha = \beta_0$ can be obtained by deriving a CFL stability condition.

CFL stability condition

For simplicity, let us consider the explicit Euler scheme

$$\boldsymbol{v}_h^{n+1} - \boldsymbol{v}_h^n + \Delta t\tilde{\mathcal{A}}_h\boldsymbol{v}_h^n + \Delta t\mathcal{A}_h^{\{0\}}\boldsymbol{v}_h^n = 0, \tag{5.27}$$

with constant time step Δt and CFL number defined as

$$\mathrm{CFL} \coloneqq \frac{\Delta t c_0}{h}. \tag{5.28}$$

To highlight the IBC contribution, the decomposition

$$\mathcal{A}_h \boldsymbol{v}_h = \tilde{\mathcal{A}}_h \boldsymbol{v}_h + \mathcal{A}_h^{\{0\}} \boldsymbol{v}_h$$

is used, where the operator

$$\mathcal{A}_h^{\{0\}} : V_h \to V_h$$

is the boundary term of $\mathcal{A}_h$ given by, assuming that the IBC is applied on the whole of Γ (i.e. $\Gamma_z = \partial\Omega$),

$$(\mathcal{A}_h^{\{0\}} \boldsymbol{v}_h, \boldsymbol{w}_h)_{L^2(\Omega)} \coloneqq \frac{1}{2}(M_0(\boldsymbol{n})\boldsymbol{v}_h - A(\boldsymbol{n})\boldsymbol{v}_h, \boldsymbol{w}_h)_{L^2(\partial\Omega)}, \tag{5.29}$$

so that

$$\begin{aligned}(\tilde{\mathcal{A}}_h \boldsymbol{v}_h, \boldsymbol{w}_h)_{L^2(\Omega)} \coloneqq & \sum_{T\in\mathcal{T}_h} (\mathcal{A}\boldsymbol{v}_h, \boldsymbol{w}_h)_{L^2(T)} - \sum_{F\in\mathcal{F}_h^i} (A(\boldsymbol{n}_F)[\![\boldsymbol{v}_h]\!], \{\boldsymbol{w}_h\})_{L^2(F)} \\ & + \frac{1}{2}\sum_{F\in\mathcal{F}_h^i} (|A(\boldsymbol{n}_F)|[\![\boldsymbol{v}_h]\!], [\![\boldsymbol{w}_h]\!])_{L^2(F)}.\end{aligned} \tag{5.30}$$

Using a discrete energy method (see 5.3.4), the following sufficient stability condition can be derived, the proof of which is postponed to Section 5.3.4.

Proposition 5.11. *Assume $\nabla \boldsymbol{u_0} = 0$ (uniform base flow) and $V_h = \mathbb{P}_d^0(\mathcal{T}_h)^{d+1}$ (finite volume discretization). A sufficient L^2 stability condition for (5.27) is*

$$\mathrm{CFL} \le \frac{1}{2C_{\mathrm{DG}}^2} \frac{1}{1 + \frac{|\boldsymbol{u_0}|}{c_0}}$$

and

$$\begin{cases} \alpha_1 + \alpha_4 \ge C_{\mathrm{tr}}^2 \mathrm{CFL}(\alpha_1^2 + (\alpha_3 - 1)^2 + \alpha_4^2 + (\alpha_2 - 1)^2) \\ (\alpha_2 + \alpha_3)^2 \le 4\left(\alpha_1 - C_{\mathrm{tr}}^2 \mathrm{CFL}(\alpha_1^2 + (\alpha_3 - 1)^2)\right)\left(\alpha_4 - C_{\mathrm{tr}}^2 \mathrm{CFL}(\alpha_4^2 + (\alpha_2 - 1)^2)\right), \end{cases} \tag{5.31}$$

where the positive constants C_{DG} and C_{tr}, defined in Lemmas 5.19 and 5.20, are non-dimensional and do not depend upon the initial data or the impedance.

Remark 5.12. Recall that, to be admissible, the matrix $M_0(\boldsymbol{n})$ given by (5.20) must obey Proposition 5.8. In particular, the passivity condition (5.16) requires the conditions

$$\begin{cases} \alpha_1 + \alpha_4 \ge 0 \\ (\alpha_2 + \alpha_3)^2 \le 4\alpha_1\alpha_4, \end{cases}$$

that are *less* stringent than (5.31).

The interest of Proposition 5.11 lies in condition (5.31) that gives the influence of the numerical flux on the CFL number. Let us highlight three particular cases of practical interest by considering the α-flux (5.14,5.25) with $\alpha \in [-1, 1]$, which has been derived above.

- (1-flux) If $\alpha = 1$ ($\alpha_1 = 0$), then $\tilde{p}^g = \tilde{p}$ and the flux does not control $\boldsymbol{u}_h \cdot \boldsymbol{n}$ at the impedance boundary since
$$(M_0(\boldsymbol{n})\boldsymbol{v}_h, \boldsymbol{v}_h)_{\mathbb{R}^{d+1}} = 2c_0 a_0^{-1} \tilde{p}_h^2.$$
A stability condition, namely
$$\mathrm{CFL} \le \frac{1}{C_{\mathrm{tr}}^2} \frac{\alpha_4}{1 + \alpha_4^2},$$
can be obtained from (5.31) if and only if $\alpha_2 = -1$ and $\alpha_3 = 1$. But since $\alpha_2 = \alpha = 1$, the scheme is not provably stable with the proposed energy analysis.

- (-1-flux) If $\alpha = -1$ ($\alpha_4 = 0$), then $\boldsymbol{u}^g = (\boldsymbol{u}\cdot\boldsymbol{n})\boldsymbol{n}$ and the numerical flux does not control $\tilde{p}_h$ since
$$(M_0(\boldsymbol{n})\boldsymbol{v}_h, \boldsymbol{v}_h)_{\mathbb{R}^{d+1}} = 2c_0a_0(\boldsymbol{u}_h\cdot\boldsymbol{n})^2.$$
Similarly, a stability condition cannot be obtained from Proposition 5.11 since that would require $\alpha_2 = 1$ and $\alpha_3 = -1$, values at odds with the definition of the α-flux with $\alpha = -1$.

- (β_0-flux) The α-flux satisfies
$$(M_0(\boldsymbol{n})\boldsymbol{v}_h, \boldsymbol{v}_h)_{\mathbb{R}^{d+1}} = c_0a_0(1-\alpha)(\boldsymbol{u}_h\cdot\boldsymbol{n})^2 + c_0a_0^{-1}(1+\alpha)\tilde{p}_h^2$$
and thus control both $\boldsymbol{u}_h\cdot\boldsymbol{n}$ and $\tilde{p}_h$ if $\alpha \in (-1,1)$. Under this assumption, the stability condition is given by (5.31) with $\alpha_1 = (1-\alpha)a_0$, $\alpha_4 = (1+\alpha)a_0^{-1}$, and $\alpha_2 = \alpha = -\alpha_3$. The β_0-flux (5.14,5.26) yields
$$\mathrm{CFL} \le \frac{1}{C_{\mathrm{tr}}^2}\min\left[\frac{1}{1+\beta_0^2}, \frac{1}{2(1+\beta_0)}, \frac{1}{2(1-\beta_0)}\right], \tag{5.32}$$
which shows that the CFL number has a positive upper bound with respect to a_0, namely $\mathrm{CFL} \le 4^{-1}C_{\mathrm{tr}}^{-2}$. By contrast, consider the 0-flux ($\alpha_2 = \alpha_3 = 0$) which yields
$$\mathrm{CFL} \le \frac{1}{C_{\mathrm{tr}}^2}\frac{a_0}{1+a_0^2},$$
so that the CFL number decreases to 0 as $a_0 \to \infty$ or $a_0 \to 0$. This recovers a result of Ventribout (Ventribout 2006, § 2.3).

In conclusion, among the admissible α-fluxes (5.14,5.25) with $\alpha \in [-1,1]$, the β_0-flux (5.14,5.26) is the optimal choice since its components are bounded with respect to $a_0 \in [0,\infty]$, it controls both $\tilde{p}_h$ and $\boldsymbol{u}_h\cdot\boldsymbol{n}$, and delivers the CFL stability condition (5.32). The extension of this result to nonlinear scattering operators $\mathcal{B}$ is done next in Section 5.3.3.

5.3.3 Weak enforcement of nonlinear impedance boundary conditions

Let us now consider the generic, possibly nonlinear, IBC under the three forms defined in Section 1.1
$$\begin{cases} \tilde{p} = a_0\boldsymbol{u}\cdot\boldsymbol{n} + a_{\mathcal{Q}}\mathcal{Q}(\boldsymbol{u}\cdot\boldsymbol{n}) & \text{(a)} \\ \boldsymbol{u}\cdot\boldsymbol{n} = a_0\tilde{p} + a_{\mathcal{Q}}\mathcal{Q}(\tilde{p}) & \text{(b)} \\ \tilde{p} - \boldsymbol{u}\cdot\boldsymbol{n} = \mathcal{B}(\tilde{p} + \boldsymbol{u}\cdot\boldsymbol{n}), & \text{(c)} \end{cases} \tag{5.33}$$
where
$$a_0 > 0,\ a_{\mathcal{Q}} \ge 0,$$
$\mathcal{Q}$ is an admissible impedance operator in the sense of Definition 1.1, and $\mathcal{B}$ is an admissible scattering operator in the sense of Definition 1.11. Following the methodology of Section 5.3.2, the admissible numerical flux is derived below for each form (5.33a,5.33b,5.33c), leading to the $\mathcal{Z}$-flux (5.14,5.35), the $\mathcal{Y}$-flux (5.14,5.37), and the $\mathcal{B}$-flux (5.14,5.39), and establish the superiority of the $\mathcal{B}$-flux.

Remark 5.13. As already emphasized, for the analysis presented below the IBCs (5.33) are only assumed to be admissible. In particular, they need not be given by one of the models covered in Section 2.4, so that this chapter is independent of Chapter 2. Note that $\mathcal{Q}$ may be a nonlinear operator.

Numerical flux based on the impedance or the admittance

To weakly enforce the IBC (5.33a) (impedance operator $z_0^{-1}\mathcal{Z}(\boldsymbol{u}\cdot\boldsymbol{n}) = a_0\boldsymbol{u}\cdot\boldsymbol{n} + a_{\mathcal{Q}}\mathcal{Q}(\boldsymbol{u}\cdot\boldsymbol{n})$), the ghost state is sought as

$$A(\boldsymbol{n})\boldsymbol{v}^g = M_0(\boldsymbol{n})\boldsymbol{v} + \boldsymbol{m}_{\mathcal{Q}}(\boldsymbol{n})\mathcal{Q}(\boldsymbol{u}\cdot\boldsymbol{n}), \tag{5.34}$$

where $M_0(\boldsymbol{n})$ is given by (5.20) and

$$\boldsymbol{m}_{\mathcal{Q}}(\boldsymbol{n}) = c_0 \begin{bmatrix} \gamma_1\boldsymbol{n} \\ \gamma_2 \end{bmatrix}.$$

Proposition 5.15 shows that the only admissible expression is

$$A(\boldsymbol{n})\boldsymbol{v}^g = c_0 \begin{bmatrix} 2a_0\boldsymbol{n}\otimes\boldsymbol{n} & -\boldsymbol{n} \\ \boldsymbol{n}^\intercal & 0 \end{bmatrix}\boldsymbol{v} + c_0 \begin{bmatrix} 2a_{\mathcal{Q}}\boldsymbol{n} \\ 0 \end{bmatrix}\mathcal{Q}(\boldsymbol{u}\cdot\boldsymbol{n}), \tag{5.35}$$

where there are no remaining DoF. The $\mathcal{Z}$-flux (5.14,5.35) fulfills the pressure-release continuity condition (5.18) but not the hard-wall one (5.17) since there is a singularity as $a_i \to \infty$. Moreover, note that

$$(M_0(\boldsymbol{n})\boldsymbol{v}_h, \boldsymbol{v}_h)_{\mathbb{R}^{d+1}} = 2c_0a_0(\boldsymbol{u}_h\cdot\boldsymbol{n})^2$$

so that there is no control of $\tilde{p}_h^2$ at the impedance boundary, a phenomenon already encountered in Section 5.3.2.

Example 5.14. One may think that the result of Proposition 5.15 is unnecessarily stringent, i.e. that the admissibility conditions proposed in Definition 5.6 are too constraining, but it can be verified numerically that it is not so. Let us consider the acoustical cavity $\Omega = (0,1)^2$ with $c_0 = 1$, $z_0 = 1$, and impedance

$$\mathcal{Z}(\boldsymbol{u}\cdot\boldsymbol{n}) = a_0\boldsymbol{u}\cdot\boldsymbol{n} + a_{\mathcal{Q}}\dot{\boldsymbol{u}}\cdot\boldsymbol{n}$$

applied to the whole of $\partial\Omega$. Two dispersion relations $\Delta_{1\mathrm{D}}(k_i, \hat{z}(\mathrm{j}\omega), \omega)$ can be derived for eigenfunctions with separated variables

$$\tilde{p}(\boldsymbol{x}) = \tilde{p}_1(x_1)\tilde{p}_2(x_2),\ \tilde{p}_i(x_i) = (A_ie^{\mathrm{j}k_ix_i} + B_ie^{-\mathrm{j}k_ix_i})$$

(note that it does not provide all the eigenvalues if $\hat{z}(s) \neq +\infty$). Figure 5.2 plots the eigenvalues computed with a sixth-order DG method, see Appendix F, and numerical flux

$$A(\boldsymbol{n})\boldsymbol{v}^g = c_0 \begin{bmatrix} (1-\alpha)a_0\boldsymbol{n}\otimes\boldsymbol{n} & \alpha\boldsymbol{n} \\ -\alpha\boldsymbol{n}^\intercal & \frac{1+\alpha}{a_0} \end{bmatrix}\boldsymbol{v} + c_0 \begin{bmatrix} (1-\alpha)a_{\mathcal{Q}}\boldsymbol{n} \\ -(1+\alpha)\frac{a_{\mathcal{Q}}}{a_0} \end{bmatrix}\mathcal{Q}(\boldsymbol{u}\cdot\boldsymbol{n}), \tag{5.36}$$

which reduces to the α-flux (5.14,5.25) if $a_{\mathcal{Q}} = 0$. The graph shows that the value $\alpha = -1$ yields stable eigenvalues that match the exact ones until a cut-off frequency. However, for $\alpha = \beta_0$, eigenfunctions have a less pronounced decay and can even be unstable. Hence *the impedance model $\mathcal{Z}$ is passive, but passivity is lost at the semi-discrete level.* This conforms with the fact that the flux (5.14,5.36) is consistent for any α but passive if and only if $\alpha = -1$ from Proposition 5.15.

Proposition 5.15. *The numerical flux function (5.14,5.34) is admissible if and only if the ghost state is given by (5.35).*

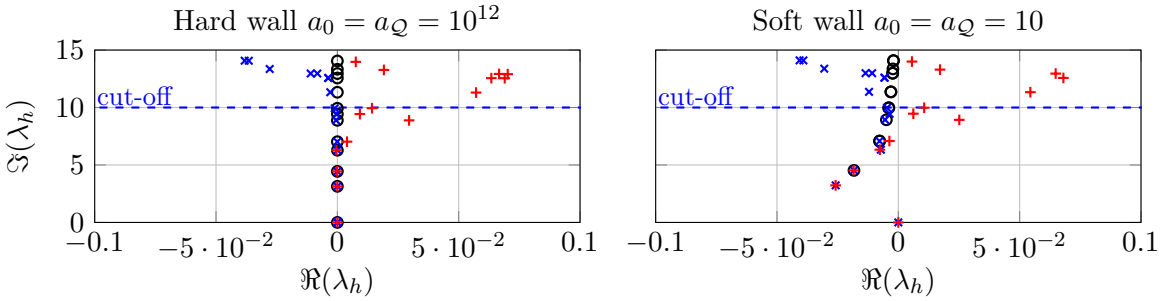

Figure 5.2. Eigenvalues $\lambda_h \in \sigma(-\mathcal{A}_h)$ for the acoustical cavity $\Omega = (0,1)^2$ with $c_0 = 1$, $z_0 = 1$, and impedance $\mathcal{Z}(\boldsymbol{u}\cdot\boldsymbol{n}) = a_0\boldsymbol{u}\cdot\boldsymbol{n} + a_{\mathcal{Q}}\dot{\boldsymbol{u}}\cdot\boldsymbol{n}$ on $\partial\Omega$. DG6 ($N_K = 8$ triangles, 504 DoF). (×): $\mathcal{Z}$-flux (5.14,5.35). (+): flux (5.14,5.36) with $\alpha = \beta_0$. (○): $\lambda = \mathrm{j}\omega = \pm\mathrm{j}c_0\sqrt{k_1^2+k_2^2}$ with two monodimensional dispersion relations $\Delta_{1\mathrm{D}}(k_i, \hat{z}(\mathrm{j}\omega), \omega) = 0$ (only covers eigenfunctions with separated variables).

Proof. Consistency and passivity conditions are checked. (Consistency) Condition (5.15) yields $\alpha_1 = (1-\alpha_2)a_0$, $\alpha_4 = (1-\alpha_3)/a_0$, $\gamma_1 = (1-\alpha_2)a_1$, and $\gamma_2 = -(1-\alpha_3)\frac{a_{\mathcal{Q}}}{a_0}$. (Passivity) Let $\boldsymbol{v}_h \in V_h$. We have

$$(A(\boldsymbol{n})\boldsymbol{v}_h^g, \boldsymbol{v}_h)_{\mathbb{R}^{d+1}} = (M_0(\boldsymbol{n})\boldsymbol{v}_h, \boldsymbol{v}_h)_{\mathbb{R}^{d+1}} + c_0(1-\alpha_2)a_{\mathcal{Q}}\mathcal{Q}(\boldsymbol{u}_h\cdot\boldsymbol{n})\boldsymbol{u}_h\cdot\boldsymbol{n} - c_0(1-\alpha_3)\frac{a_{\mathcal{Q}}}{a_0}\mathcal{Q}(\boldsymbol{u}_h\cdot\boldsymbol{n})\tilde{p}_h.$$

The passivity condition (5.16) holds true for any $\boldsymbol{v}_h$ and $\mathcal{Q}$ if and only if $(M_0(\boldsymbol{n})\boldsymbol{v}_h, \boldsymbol{v}_h)_{\mathbb{R}^{d+1}} \geq 0$, $(1-\alpha_2)a_{\mathcal{Q}} \geq 0$, and $\alpha_3 = 1$. Lemma 5.9 gives $\alpha_2 = -1$ and enables to conclude. □

The admittance case (5.33b) is identical, as an application of the admissibility conditions shows that the only admissible ghost state of the form

$$A(\boldsymbol{n})\boldsymbol{v}^g = M_0(\boldsymbol{n})\boldsymbol{v} + \boldsymbol{m}_{\mathcal{Q}}(\boldsymbol{n})\mathcal{Q}(\tilde{p})$$

is given by

$$A(\boldsymbol{n})\boldsymbol{v}^g = c_0\begin{bmatrix} 0_{d,d} & \boldsymbol{n} \\ -\boldsymbol{n}^\intercal & 2a_0 \end{bmatrix}\boldsymbol{v} + c_0\begin{bmatrix} \boldsymbol{0_d} \\ 2a_{\mathcal{Q}} \end{bmatrix}\mathcal{Q}(\tilde{p}), \tag{5.37}$$

which obeys the hard-wall continuity condition (5.17) but not the pressure-release one (5.18). Note that

$$(M_0(\boldsymbol{n})\boldsymbol{v}_h, \boldsymbol{v}_h)_{\mathbb{R}^{d+1}} = 2c_0a_0\tilde{p}_h^2$$

so that there is no control of $(\boldsymbol{u}_h\cdot\boldsymbol{n})^2$ at the impedance boundary. In view of the expressions (5.35) and (5.37), the fluxes based on impedance and admittance have symmetrical continuity properties such that the $\mathcal{Z}$ (resp. $\mathcal{Y}$)-flux should be preferred to the $\mathcal{Y}$ (resp. $\mathcal{Z}$)-flux when the impedance is close to a pressure-release wall (resp. hard wall). However, the next section shows these two fluxes are trumped by a flux based on the scattering operator $\mathcal{B}$.

Numerical flux based on the scattering operator

To weakly enforce the IBC under its scattering formulation (5.33c), the ghost state is sought as

$$A(\boldsymbol{n})\boldsymbol{v}^g = M_0(\boldsymbol{n})\boldsymbol{v} + \boldsymbol{m}_{\mathcal{B}}(\boldsymbol{n})\mathcal{B}(\tilde{p} + \boldsymbol{u}\cdot\boldsymbol{n}), \tag{5.38}$$

where $M_0(\boldsymbol{n})$ is given by (5.20) and

$$\boldsymbol{m}_{\mathcal{B}}(\boldsymbol{n}) = c_0 \begin{bmatrix} \gamma_1 \boldsymbol{n} \\ \gamma_2 \end{bmatrix}.$$

Proposition 5.17 below shows that the only admissible ghost state is given by

$$A(\boldsymbol{n})\boldsymbol{v}^g = c_0 \begin{bmatrix} \boldsymbol{n}\otimes\boldsymbol{n} & \mathbf{0}_d \\ \mathbf{0}_d^\intercal & 1 \end{bmatrix} \boldsymbol{v} + c_0 \begin{bmatrix} \boldsymbol{n} \\ -1 \end{bmatrix} \mathcal{B}(\tilde{p} + \boldsymbol{u}\cdot\boldsymbol{n}). \tag{5.39}$$

Note that with this flux there is control of both $\boldsymbol{u}_h\cdot\boldsymbol{n}$ and $\tilde{p}_h$ at the boundary, and the boundary dissipation term is

$$\begin{aligned} \frac{1}{2}\int_0^t (A(\boldsymbol{n})\boldsymbol{v}_h^g, \boldsymbol{v}_h)_{L^2(\Gamma_z)}\,\mathrm{d}\tau = \frac{c_0}{4}\int_0^t (\|\tilde{p}_h + \boldsymbol{u}_h\cdot\boldsymbol{n}\|^2_{L^2(\Gamma_z)} - \|\mathcal{B}(\tilde{p}_h + \boldsymbol{u}_h\cdot\boldsymbol{n})\|^2_{L^2(\Gamma_z)})\,\mathrm{d}\tau \\ + \frac{c_0}{4}\int_0^t \|\tilde{p}_h - \boldsymbol{u}_h\cdot\boldsymbol{n} - \mathcal{B}(\tilde{p}_h + \boldsymbol{u}_h\cdot\boldsymbol{n})\|^2_{L^2(\Gamma_z)}\,\mathrm{d}\tau, \end{aligned} \tag{5.40}$$

where the two terms on the right-hand side have a clear interpretation. The first one is the dissipation associated with the scattering operator $\mathcal{B}$, see the passivity condition (1.13), and the second one can be interpreted as a penalization term for the non-respect of the IBC.

Remark 5.16. The $\mathcal{B}$-flux (5.14,5.39) derived from the energy analysis carried out in the proof of Proposition 5.17 reads

$$(A(\boldsymbol{n})\boldsymbol{v})^* = \frac{c_0}{2}\begin{bmatrix} \boldsymbol{n} \\ 1 \end{bmatrix}(\tilde{p} + \boldsymbol{u}\cdot\boldsymbol{n}) + \frac{c_0}{2}\begin{bmatrix} \boldsymbol{n} \\ -1 \end{bmatrix}\mathcal{B}(\tilde{p} + \boldsymbol{u}\cdot\boldsymbol{n}).$$

It is interesting to note that this flux is exactly that derived using flux vector splitting (Toro 2009, Chap. 8), which for a linear hyperbolic PDE with constant coefficients amounts to exactly solving the monodimensional Riemann problem at the boundary. Indeed, given Assumption 5.1 we have at the impedance boundary Γ_z

$$\begin{aligned} A(\boldsymbol{n})\boldsymbol{v} = A(\boldsymbol{n})^{\oplus}\boldsymbol{v} - A(\boldsymbol{n})^{\ominus}\boldsymbol{v} &= \frac{c_0}{2}\begin{bmatrix} \boldsymbol{n}\otimes\boldsymbol{n} & \boldsymbol{n} \\ \boldsymbol{n}^\intercal & 1 \end{bmatrix}\boldsymbol{v} + \frac{c_0}{2}\begin{bmatrix} -\boldsymbol{n}\otimes\boldsymbol{n} & \boldsymbol{n} \\ \boldsymbol{n}^\intercal & -1 \end{bmatrix}\boldsymbol{v} \\ &= \frac{c_0}{2}\begin{bmatrix} \boldsymbol{n} \\ 1 \end{bmatrix}(\tilde{p} + \boldsymbol{u}\cdot\boldsymbol{n}) + \frac{c_0}{2}\begin{bmatrix} \boldsymbol{n} \\ -1 \end{bmatrix}(\tilde{p} - \boldsymbol{u}\cdot\boldsymbol{n}). \end{aligned}$$

Therefore, this flux has a direct interpretation based on characteristics, making it natural to use with a hyperbolic law.

Proposition 5.17. *The numerical flux (5.14,5.38) is admissible if and only if the ghost state is given by (5.39).*

Proof. (Consistency) Condition (5.15) leads to $\alpha_1 = \gamma_1 = 1 - \alpha_2$ and $\alpha_4 = -\gamma_2 = 1 - \alpha_3$ so that there are only two DoF left, α_2 and α_3. (Passivity) Let $\boldsymbol{v}_h \in V_h$. Recall that the passivity property of the scattering operator $\mathcal{B}$ reads (1.13), which makes the study of passivity more intricate than in the previous sections. The generic expressions of $M_0(\boldsymbol{n})$ and $\boldsymbol{m}_{\mathcal{B}}(\boldsymbol{n})$ give

$$\begin{aligned} \frac{1}{c_0}(A(\boldsymbol{n})\boldsymbol{v}_h^g, \boldsymbol{v}_h)_{\mathbb{R}^{d+1}} &= \frac{1}{c_0}(M_0(\boldsymbol{n})\boldsymbol{v}_h, \boldsymbol{v}_h)_{\mathbb{R}^{d+1}} + \frac{1}{c_0}(\boldsymbol{m}_{\mathcal{B}}(\boldsymbol{n})\mathcal{B}(\tilde{p}_h + \boldsymbol{u}_h\cdot\boldsymbol{n}), \boldsymbol{v}_h)_{\mathbb{R}^{d+1}} \\ &= (1-\alpha_2)(\boldsymbol{u}_h\cdot\boldsymbol{n})^2 + (1-\alpha_3)\tilde{p}_h^2 + (\alpha_2+\alpha_3)\tilde{p}_h\boldsymbol{u}_h\cdot\boldsymbol{n} \\ &\quad - \mathcal{B}(\tilde{p}_h + \boldsymbol{u}_h\cdot\boldsymbol{n})((1-\alpha_3)\tilde{p}_h - (1-\alpha_2)\boldsymbol{u}_h\cdot\boldsymbol{n}). \end{aligned}$$

Using the identity $ab = \frac{1}{2}a^2 + \frac{1}{2}b^2 - \frac{1}{2}(a-b)^2$ on $\mathcal{B}(\tilde{p}_h + \boldsymbol{u}_h\cdot\boldsymbol{n})\big((1-\alpha_3)\tilde{p}_h - (1-\alpha_2)\boldsymbol{u}_h\cdot\boldsymbol{n}\big)$ and collecting the terms yields

$$\begin{aligned}\frac{1}{c_0}(A(\boldsymbol{n})\boldsymbol{v}_h^g, \boldsymbol{v}_h)_{\mathbb{R}^{d+1}} &= \frac{1}{2}(\tilde{p}_h + \boldsymbol{u}_h\cdot\boldsymbol{n})^2 - \frac{1}{2}\mathcal{B}(\tilde{p}_h + \boldsymbol{u}_h\cdot\boldsymbol{n})^2 \\ &\quad + \frac{1}{2}\Big((1-\alpha_3)\tilde{p}_h - (1-\alpha_2)\boldsymbol{u}_h\cdot\boldsymbol{n} - \mathcal{B}(\tilde{p}_h + \boldsymbol{u}_h\cdot\boldsymbol{n})\Big)^2 \\ &\quad - \frac{1}{2}(\alpha_2\boldsymbol{u}_h\cdot\boldsymbol{n} - \alpha_3\tilde{p}_h)^2.\end{aligned}$$

Since this quantity must be non-negative for every admissible scattering operator $\mathcal{B}$ and every $\boldsymbol{v}_h \in V_h$, the passivity condition (5.16) is achieved if and only if $\alpha_2 = \alpha_3 = 0$. □

In summary, even for a generic nonlinear scattering operator $\mathcal{B}$, the $\mathcal{B}$-flux (5.14,5.39) keeps the properties mentioned when studying the proportional case, such as the control of both $\boldsymbol{u}_h\cdot\boldsymbol{n}$ and $\tilde{p}_h$ at the boundary. Note that this conclusion has been reached without considering *how* $\mathcal{B}$ is computed, i.e. the analysis is so far independent of Section 2.4. However, to conclude this section, it is insightful to derive a CFL stability condition, as in Section 5.3.2.

CFL stability condition

For this, let us consider the following reflection coefficient, inspired by the representation of physical models derived in Section 2.4,

$$\hat{\beta}(s) = \int_{\xi_{\min}}^{\xi_{\max}} \frac{1}{s+\xi}\mathrm{d}\mu(\xi), \tag{5.41}$$

where μ is a measure on $(\xi_{\min}, \xi_{\max})$ with $0 \le \xi_{\min} < \xi_{\max} < \infty$. A sufficient condition for $\hat{\beta}$ to be bounded-real is

$$\|\mu\|_{L^1}\Big\|\frac{\mu}{\xi^2}\Big\|_{L^1} \le 1,$$

see Appendix 5.3.4. The corresponding semi-discrete formulation results from a coupling between the additional variables φ_h, defined as (2.6), and the acoustic field $\boldsymbol{v}$ (space and time variables are explicitly stated to avoid ambiguity)

$$\begin{cases}\partial_t\varphi_h(t,\boldsymbol{x},\xi) = -\xi\varphi_h(t,\boldsymbol{x},\xi) + \tilde{p}_h(t,\boldsymbol{x}) + \boldsymbol{u}_h(t,\boldsymbol{x})\cdot\boldsymbol{n}(\boldsymbol{x}) \quad (x\in\partial\Omega,\ \xi\in[\xi_{\min},\xi_{\max}]) \\ \partial_t\boldsymbol{v}_h(t) = -\tilde{\mathcal{A}}_h\boldsymbol{v}_h(t) - \mathcal{A}_h^{\{0\}}\boldsymbol{v}_h(t) - \mathcal{A}_h^{\{\beta\}}\beta\star(\tilde{p}_h + \boldsymbol{u}_h\cdot\boldsymbol{n})(t).\end{cases} \tag{5.42}$$

The spatial discretization is given by (5.29,5.30) with an additional boundary contribution $\mathcal{A}_h^{\{\beta\}}$ in the decomposition of $\mathcal{A}_h$ compared to that of Section 5.3.2 given by, assuming that $\Gamma_z = \partial\Omega$,

$$(\mathcal{A}_h^{\{\beta\}}v_h, \boldsymbol{w}_h)_{L^2(\Omega)} \coloneqq \frac{1}{2}(\boldsymbol{m}_{\mathcal{B}}(\boldsymbol{n})v_h, \boldsymbol{w}_h)_{L^2(\partial\Omega)} = -\frac{c_0}{2}(v_h, (w_h^p - \boldsymbol{w}_h^u\cdot\boldsymbol{n}))_{L^2(\partial\Omega)}. \tag{5.43}$$

The result, stated in Proposition 5.18, is a natural extension of Proposition 5.11 and more specifically of (5.32). It shows that, with an explicit time integration, the maximum frequency $(2\pi)^{-1}\xi_{\max}$ of the scattering operator stiffens the system; in practice, $\xi_{\max}$ must be chosen consistently with the dissipation and dispersion properties of the spatial discretization, as advocated in Section 6.1.3. Numerical applications based on the scattering operator are considered in Chapter 6.

Proposition 5.18. *Assume $\nabla \boldsymbol{u_0} = 0$ (uniform base flow), $V_h = \mathbb{P}_d^0(\mathcal{T}_h)^{d+1}$ (finite volume discretization), and $\hat{\beta}$ bounded-real such that*

$$\|\mu\|_{L^1} \left\| \frac{\mu}{\xi^2} \right\| \leq 1.$$

A sufficient L^2 stability condition for (5.42) is

$$\mathrm{CFL} \leq \min \left(\frac{1}{2C_{\mathrm{DG}}^2} \frac{1}{1 + \frac{|\boldsymbol{u_0}|}{c_0}}, \frac{1}{2C_{\mathrm{tr}}^2}, \frac{c_0}{h\, \xi_{\max}} \right), \tag{5.44}$$

where the positive constants C_{DG} and C_{tr}, defined in Lemmas 5.22 and 5.20, are non-dimensional and do not depend upon the initial data or the impedance.

The proof is given in the next section, alongside the similar proof of Proposition 5.11.

5.3.4 Proofs of stability conditions

This section gathers the proofs of Propositions 5.11 and 5.18.

Proof of Proposition 5.11

Proof. (Proposition 5.11) The proof follows the energy method, in the spirit of the analysis carried out at the continuous and semi-discrete levels in Sections 5.1 and 5.3.2. A comprehensive analysis of the energy method to derive CFL-type stability condition for coercive problems can be found in (Levy and Tadmor 1998). Note that the stability conditions derived in (Levy and Tadmor 1998) cannot be directly applied herein since $\mathcal{A}_h$ is not coercive in the sense of (Levy and Tadmor 1998, Eq. 3.2), see (5.11). See also (Ern and Guermond 2004, Chap. 6), (Di Pietro and Ern 2012, § 7.5.2), and (Cohen and Pernet 2017, Chap. 7).

Given the expression of the continuous energy (5.3), we define the discrete energy as

$$\mathcal{E}_h^n \coloneqq \|\boldsymbol{v}_h^n\|_{L^2(\Omega)}^2.$$

By taking the scalar product of (5.27) with $\boldsymbol{v}_h^n$ and using the identity $ab = \frac{1}{2}a^2 + \frac{1}{2}b^2 - \frac{1}{2}(a-b)^2$, one obtains the standard discrete energy balance (Levy and Tadmor 1998, Eq. 3.4)

$$\frac{1}{2}\mathcal{E}_h^{n+1} = \frac{1}{2}\mathcal{E}_h^n + \frac{1}{2}\|\boldsymbol{v}_h^{n+1} - \boldsymbol{v}_h^n\|_{L^2(\Omega)}^2 - \Delta t(\mathcal{A}_h \boldsymbol{v}_h^n, \boldsymbol{v}_h^n).$$

The expression of $(\mathcal{A}_h \boldsymbol{v}_h, \boldsymbol{v}_h)_{L^2(\Omega)}$ given by (5.11) yields

$$\begin{aligned}\frac{1}{2}\mathcal{E}_h^{n+1} = \frac{1}{2}\mathcal{E}_h^n + \frac{1}{2}\|\boldsymbol{v}_h^{n+1} - \boldsymbol{v}_h^n\|_{L^2(\Omega)}^2 - \frac{\Delta t}{2}(C(\boldsymbol{u_0})\boldsymbol{v}_h^n, \boldsymbol{v}_h^n)_{L^2(\Omega)} \\ - \frac{\Delta t}{2}|\boldsymbol{v}_h^n|_{\mathrm{upw}}^2 - \frac{\Delta t}{2}(M_0(\boldsymbol{n})\boldsymbol{v}_h^n, \boldsymbol{v}_h^n)_{L^2(\partial\Omega)},\end{aligned}$$

where each term has a clear interpretation:

- $\frac{1}{2}\|\boldsymbol{v}_h^{n+1} - \boldsymbol{v}_h^n\|_{L^2(\Omega)}^2$ is the anti-dissipation due to the explicit nature of the time-marching scheme;
- $-(C(\boldsymbol{u_0})\boldsymbol{v}_h^n, \boldsymbol{v}_h^n)_{L^2(\Omega)}$ is the contribution of a non-constant base flow $\boldsymbol{u_0}$;
- $-|\boldsymbol{v}_h^n|_{\mathrm{upw}}^2$ is the dissipation due to the upwind flux (would be null with a centered flux);

- $-(M_0(\boldsymbol{n})\boldsymbol{v}_h^n, \boldsymbol{v}_h^n)_{L^2(\partial\Omega)}$ is the dissipation due to the IBC.

The key step of the proof is to estimate the anti-dissipation term $\frac{1}{2}\|\boldsymbol{v}_h^{n+1} - \boldsymbol{v}_h^n\|^2_{L^2(\Omega)}$. The decomposition of $\mathcal{A}_h$ readily yields the estimate

$$\frac{1}{2}\|\boldsymbol{v}_h^{n+1} - \boldsymbol{v}_h^n\|^2_{L^2(\Omega)} = \frac{\Delta t^2}{2}\|\mathcal{A}_h\boldsymbol{v}_h^n\|^2_{L^2(\Omega)} \leq \Delta t^2\|\tilde{\mathcal{A}}_h\boldsymbol{v}_h^n\|^2_{L^2(\Omega)} + \Delta t^2\|\mathcal{A}_h^{\{0\}}\boldsymbol{v}_h^n\|^2_{L^2(\Omega)},$$

where the energy production that occurs at the impedance boundary is bounded by $\|\mathcal{A}_h^{\{0\}}\boldsymbol{v}_h^n\|^2_{L^2(\Omega)}$. The estimate of this term is provided by Lemma 5.19, which does not require the finite volume hypothesis. Lemma 5.20 provides a bound for $\|\tilde{\mathcal{A}}_h\boldsymbol{v}_h^n\|_{L^2(\Omega)}$ that *does* need the finite volume hypothesis. Using both Lemmas 5.19 and 5.20, the discrete energy balance becomes

$$\begin{aligned}\frac{1}{2}\mathcal{E}_h^{n+1} \leq \frac{1}{2}(1 - \Delta t \min_{x\in\Omega}\lambda_{\min}(\boldsymbol{u_0}))\mathcal{E}_h^n - \frac{\Delta t}{2}(1 - 2C_{\mathrm{DG}}^2\Delta t(c_0 + |\boldsymbol{u_0}|)h^{-1})|\boldsymbol{v}_h|^2_{\mathrm{upw}} \\ - \frac{\Delta t}{2}(I(\boldsymbol{n})\boldsymbol{v}_h, \boldsymbol{v}_h)_{L^2(\partial\Omega)},\end{aligned}$$

where

$$I(\boldsymbol{n}) \coloneqq \frac{1}{2}(M_0(\boldsymbol{n}) + M_0(\boldsymbol{n})^\intercal) - \frac{C_{\mathrm{tr}}^2}{2}\mathrm{CFL}(N(\boldsymbol{n}) + N(\boldsymbol{n})^\intercal)$$

so that

$$(I(\boldsymbol{n})\boldsymbol{v}_h, \boldsymbol{v}_h)_{\mathbb{R}^{d+1}} = (\check{I}(\boldsymbol{n})\check{\boldsymbol{v}}_h, \check{\boldsymbol{v}}_h)_{\mathbb{R}^2}$$

with $\check{\boldsymbol{v}}_h \coloneqq (\boldsymbol{u}_h \cdot \boldsymbol{n}, \tilde{p}_h)^\intercal$ and

$$\check{I}(\boldsymbol{n}) \coloneqq c_0 \begin{bmatrix} (\alpha_1 - C_{\mathrm{tr}}^2\mathrm{CFL}(\alpha_1^2 + (\alpha_3 - 1)^2)) & \frac{\alpha_2+\alpha_3}{2} \\ \frac{\alpha_2+\alpha_3}{2} & \alpha_4 - C_{\mathrm{tr}}^2\mathrm{CFL}(\alpha_4^2 + (\alpha_2 - 1)^2) \end{bmatrix}.$$

The conclusion then follows from Lemma 5.9. □

The two lemmas referred to in the above proof are given below. Note that they imply a departure from the framework developed in (Ern and Guermond 2006), since the condition "(DG3a)" does not hold. The first one provides an estimate for the impedance boundary term (5.29).

Lemma 5.19. *For any* $\boldsymbol{v}_h \in \mathbb{P}_d^k(\mathcal{T}_h)^{d+1}$,

$$\|\mathcal{A}_h^{\{0\}}\boldsymbol{v}_h^n\|_{L^2(\Omega)} \leq \frac{C_{\mathrm{tr}}}{\sqrt{2}}c_0^{1/2}h^{-1/2}(N(\boldsymbol{n})\boldsymbol{v}_h, \boldsymbol{v}_h)^{1/2}_{L^2(\partial\Omega)},$$

where

$$N(\boldsymbol{n}) \coloneqq c_0 \begin{bmatrix} (\alpha_1^2 + (\alpha_3 - 1)^2)\boldsymbol{n}\otimes\boldsymbol{n} & \boldsymbol{0_d} \\ \boldsymbol{0_d}^\intercal & \alpha_4^2 + (\alpha_2 - 1)^2 \end{bmatrix}$$

and $C_{\mathrm{tr}} > 0$ *is defined in Lemma 5.4.*

Proof. Let $\boldsymbol{w}_h \coloneqq ((\boldsymbol{w}_h^u)^\intercal, w_h^{\tilde{p}})^\intercal \in \mathbb{P}_d^k(\mathcal{T}_h)^{d+1}$. The definition of $\mathcal{A}_h^{\{0\}}$ yields

$$\begin{aligned}(\mathcal{A}_h^{\{0\}}\boldsymbol{v}_h^n, \boldsymbol{w}_h)_{L^2(\Omega)} &\coloneqq \frac{1}{2}(M_0(\boldsymbol{n})\boldsymbol{v}_h - A(\boldsymbol{n})\boldsymbol{v}_h, \boldsymbol{w}_h)_{L^2(\partial\Omega)} \\ &= \frac{c_0}{2}\int_{\partial\Omega}\begin{pmatrix} \alpha_1\boldsymbol{u}_h\cdot\boldsymbol{n} \\ (\alpha_2 - 1)\tilde{p} \\ (\alpha_3 - 1)\boldsymbol{u}_h\cdot\boldsymbol{n} \\ \alpha_4\tilde{p}\end{pmatrix}\cdot\begin{pmatrix} \boldsymbol{w}_h^u\cdot\boldsymbol{n} \\ \boldsymbol{w}_h^u\cdot\boldsymbol{n} \\ w_h^{\tilde{p}} \\ w_h^{\tilde{p}}\end{pmatrix}\mathrm{d}\boldsymbol{x}.\end{aligned}$$

The Cauchy-Schwarz inequality then gives

$$(\mathcal{A}_h^{\{0\}}\boldsymbol{v}_h^n, \boldsymbol{w}_h)_{L^2(\Omega)} \le \frac{c_0^{1/2}}{\sqrt{2}}(N(\boldsymbol{n})\boldsymbol{v}_h, \boldsymbol{v}_h)_{L^2(\partial\Omega)}^{1/2}\|\boldsymbol{w}_h\|_{L^2(\partial\Omega)}$$

and the conclusion follows from Lemma 5.4. □

The second lemma provides an estimate for the non-boundary terms of $\mathcal{A}_h$, gathered in $\tilde{\mathcal{A}}_h$.

Lemma 5.20. *For any* $\boldsymbol{v}_h \in \mathbb{P}_d^k(\mathcal{T}_h)^{d+1}$,

$$\|\tilde{\mathcal{A}}_h\boldsymbol{v}_h\|_{L^2(\Omega)} \le C_{\mathrm{DG}}h^{-1/2}\||\boldsymbol{u_0}| + c_0\|_{L^\infty(\Omega)}^{1/2}|\boldsymbol{v}_h|_{\mathrm{upw}} + \|A(\nabla_h)\boldsymbol{v}_h + B\boldsymbol{v}_h\|_{L^2(\Omega)},$$

where

$$C_{\mathrm{DG}} \coloneqq \left(\sqrt{2} + \frac{1}{\sqrt{2}}\right)C_{\mathrm{tr}} > 0$$

with C_{tr} *defined in Lemma 5.4.*

Proof. This is a standard estimate that relies on the Cauchy-Schwarz and discrete trace inequalities, see (Di Pietro and Ern 2012, Chaps. 3 & 7) and (Ern and Guermond 2006). Let $\boldsymbol{w}_h \in \mathbb{P}_d^k(\mathcal{T}_h)^{d+1}$ with $k \in \mathbb{N}^*$. Each of the three terms in (5.30) is estimated separately. The first term readily yields

$$\sum_{T\in\mathcal{T}_h}(\mathcal{A}\boldsymbol{v}_h, \boldsymbol{w}_h)_{L^2(T)} = (A(\nabla_h)\boldsymbol{v}_h + B\boldsymbol{v}_h, \boldsymbol{w}_h)_{L^2(\Omega)} \le \|A(\nabla_h)\boldsymbol{v}_h + B\boldsymbol{v}_h\|_{L^2(\Omega)}\|\boldsymbol{w}_h\|_{L^2(\Omega)}.$$

For the last two terms, we use the inequality

$$(A(\boldsymbol{n}_F)\boldsymbol{v}_h, \boldsymbol{w}_h)_{L^2(F)} \le (|A(\boldsymbol{n}_F)|\boldsymbol{v}_h, \boldsymbol{v}_h)_{L^2(F)}^{1/2}(|A(\boldsymbol{n}_F)|\boldsymbol{w}_h, \boldsymbol{w}_h)_{L^2(F)}^{1/2}, \tag{5.45}$$

which follows from the fact that the real symmetric matrix A is diagonalizable with $A = P\Lambda P^\intercal$, where $\Lambda \coloneqq \mathrm{diag}(\boldsymbol{u_0}\cdot\boldsymbol{n} + c_0, \boldsymbol{u_0}\cdot\boldsymbol{n} - c_0, \boldsymbol{u_0}\cdot\boldsymbol{n}, \cdots, \boldsymbol{u_0}\cdot\boldsymbol{n})$ and P is an orthogonal matrix (recall that $|A| \coloneqq P|\Lambda|P^\intercal$). (This inequality yields the (DG8) condition in (Ern and Guermond 2006).) Using (5.45), the Cauchy-Schwarz inequality, and Lemma 5.4 give

$$\sum_{F\in\mathcal{F}_h^i}(A(\boldsymbol{n}_F)[\![\boldsymbol{v}_h]\!], \{\boldsymbol{w}_h\})_{L^2(F)} \le \sqrt{2}C_{\mathrm{tr}}h^{-1/2}\Big(\max_{F\in\mathcal{F}_h^i}\rho(|A(\boldsymbol{n}_F)|)\Big)^{1/2}|\boldsymbol{v}_h|_{\mathrm{upw}}\|\boldsymbol{w}_h\|_{L^2(\Omega)},$$

where $\rho(|A(\boldsymbol{n}_F)|)$ denotes the spectral radius. Similarly,

$$\frac{1}{2}\sum_{F\in\mathcal{F}_h^i}(|A(\boldsymbol{n}_F)|[\![\boldsymbol{v}_h]\!], [\![\boldsymbol{w}_h]\!])_{L^2(F)} \le \frac{1}{\sqrt{2}}C_{\mathrm{tr}}h^{-1/2}\Big(\max_{F\in\mathcal{F}_h^i}\rho(|A(\boldsymbol{n}_F)|)\Big)^{1/2}|\boldsymbol{v}_h|_{\mathrm{upw}}\|\boldsymbol{w}_h\|_{L^2(\Omega)}.$$

The final estimate follows from

$$\max_{F\in\mathcal{F}_h^i}\rho(|A(\boldsymbol{n}_F)|) \le \max_{F\in\mathcal{F}_h^i}(|\boldsymbol{u_0}| + c_0) \le \||\boldsymbol{u_0}| + c_0\|_{L^\infty(\Omega)}.$$

□

Remark 5.21. Assuming a uniform base flow ($\nabla\boldsymbol{u_0} \equiv 0$) and a finite volume discretization ($k = 0$), $\|A(\nabla_h)\boldsymbol{v}_h + B\boldsymbol{v}_h\|_{L^2(\Omega)} = 0$, and the estimate of Lemma 5.20 is reduced to

$$\|\tilde{\mathcal{A}}_h\boldsymbol{v}_h\|_{L^2(\Omega)} \le C_{\mathrm{DG}}h^{-1/2}(|\boldsymbol{u_0}| + c_0)^{1/2}|\boldsymbol{v}_h|_{\mathrm{upw}},$$

which is used in the above proof of Proposition 5.11 above to derive a sufficient stability condition using an energy method.

Proof of Proposition 5.18

The proof of Proposition 5.18 is similar to that of Proposition 5.11 but relies on an energy balance for the additional variables φ_h, given in Appendix E.

Proof. (Proposition 5.18) The proof relies on an energy analysis similar to that of Proposition 5.11 with one additional technicality: the energy is not reduced to $\|\boldsymbol{v}_h\|^2_{L^2(\Omega)}$ but must include a contribution $\mathcal{E}_\beta$ from the diffusive variable φ_h defined as (E.4). For the sake of clarity, we first write down the semi-discrete energy balance before considering its discretization.

(Semi-discrete energy balance) Using the energy balance associated with $\mathcal{E}_\beta$ (E.3), the semi-discrete energy balances reads

$$\begin{cases} \dfrac{1}{2}\dfrac{\mathrm{d}\mathcal{E}_\beta}{\mathrm{d}t} & \leq \dfrac{1}{2}((\tilde{p}_h + \boldsymbol{u}_h\cdot\boldsymbol{n})^2 - \beta(\tilde{p}_h+\boldsymbol{u}_h\cdot\boldsymbol{n})^2) \\ & \quad - \dfrac{\|\mu\|_{L^1}}{2}\displaystyle\int_{\xi^{\min}}^{\xi^{\max}} (-\xi\varphi_h + \tilde{p}_h + \boldsymbol{u}_h\cdot\boldsymbol{n})^2 \frac{\mathrm{d}\mu}{\xi^2} \\ \dfrac{1}{2}\dfrac{\mathrm{d}}{\mathrm{d}t}\|\boldsymbol{v}_h\|^2_{L^2(\Omega)} = & -\dfrac{1}{2}(C(\boldsymbol{u_0})\boldsymbol{v}_h,\boldsymbol{v}_h)_{L^2(\Omega)} - \dfrac{1}{2}|\boldsymbol{v}_h|^2_{\mathrm{upw}} - \dfrac{1}{2}(M_0(\boldsymbol{n})\boldsymbol{v}_h,\boldsymbol{v}_h)_{L^2(\partial\Omega)} \\ & - (\mathcal{A}_h^{\{\beta\}}\boldsymbol{v}_h,\boldsymbol{v}_h)_{L^2(\Omega)}. \end{cases}$$

The identity (5.40) enables to rewrite the second line to explicit the energy exchange between the diffusive variables φ_h and the perturbation field $\boldsymbol{v}$:

$$\begin{cases} \dfrac{1}{2}\dfrac{\mathrm{d}\mathcal{E}_\beta}{\mathrm{d}t} & \leq \dfrac{1}{2}((\tilde{p}_h + \boldsymbol{u}_h\cdot\boldsymbol{n})^2 - \beta(\tilde{p}_h+\boldsymbol{u}_h\cdot\boldsymbol{n})^2) \\ & \quad - \dfrac{\|\mu\|_{L^1}}{2}\displaystyle\int_{\xi^{\min}}^{\xi^{\max}} (-\xi\varphi_h + \tilde{p}_h + \boldsymbol{u}_h\cdot\boldsymbol{n})^2 \frac{\mathrm{d}\mu}{\xi^2} \\ \dfrac{1}{2}\dfrac{\mathrm{d}}{\mathrm{d}t}\|\boldsymbol{v}_h\|^2_{L^2(\Omega)} = & -\dfrac{1}{2}(C(\boldsymbol{u_0})\boldsymbol{v}_h,\boldsymbol{v}_h)_{L^2(\Omega)} - \dfrac{1}{2}|\boldsymbol{v}_h|^2_{\mathrm{upw}} \\ & - \dfrac{c_0}{4}\left[\|\tilde{p}_h + \boldsymbol{u}_h\cdot\boldsymbol{n}\|^2_{L^2(\partial\Omega)} - \|\beta(\tilde{p}_h+\boldsymbol{u}_h\cdot\boldsymbol{n})\|^2_{L^2(\partial\Omega)}\right] \\ & - \dfrac{c_0}{4}\|\tilde{p}_h - \boldsymbol{u}_h\cdot\boldsymbol{n} - \beta(\tilde{p}_h+\boldsymbol{u}_h\cdot\boldsymbol{n})\|^2_{L^2(\partial\Omega)}. \end{cases}$$

The semi-discrete energy balance is obtained by integrating the first inequality over $\partial\Omega$, multiplying it by $c_0/2$ and summing it with the second one

$$\begin{aligned} \frac{1}{2}\frac{\mathrm{d}\mathcal{E}_h}{\mathrm{d}t} \leq & -\frac{1}{2}(C(\boldsymbol{u_0})\boldsymbol{v}_h,\boldsymbol{v}_h)_{L^2(\Omega)} - \frac{1}{2}|\boldsymbol{v}_h|^2_{\mathrm{upw}} \\ & - \frac{c_0}{4}\|\mu\|_{L^1}\int_{\xi^{\min}}^{\xi^{\max}} \|-\xi\varphi_h + \tilde{p}_h + \boldsymbol{u}_h\cdot\boldsymbol{n}\|^2_{L^2(\partial\Omega)}\frac{\mathrm{d}\mu}{\xi^2} \\ & - \frac{c_0}{4}\|\tilde{p}_h - \boldsymbol{u}_h\cdot\boldsymbol{n} - \beta(\tilde{p}_h+\boldsymbol{u}_h\cdot\boldsymbol{n})\|^2_{L^2(\partial\Omega)}, \end{aligned} \tag{5.46}$$

where the extended energy is defined as

$$\mathcal{E}_h \coloneqq \|\boldsymbol{v}_h\|^2_{L^2(\Omega)} + \frac{c_0}{2}\mathcal{E}_\beta.$$

The third and fourth terms of the right-hand side express the dissipation that occurs at the impedance boundary (here, $\partial\Omega$).

(Discrete energy balance) The explicit Euler discretization of (5.42) leads to

$$\begin{aligned}(\boldsymbol{v}_h^{n+1}-\boldsymbol{v}_h^n,\boldsymbol{v}_h^n)_{L^2(\Omega)}+\frac{c_0}{2}\|\mu\|_{L^1}\int_{\xi^{\min}}^{\xi^{\max}}(\varphi_h^{n+1}-\varphi_h^n,\varphi_h^n)_{L^2(\partial\Omega)}\frac{\mathrm{d}\mu}{\xi}\\ \leq-\frac{\Delta t}{2}(C(\boldsymbol{u_0})\boldsymbol{v}_h^n,\boldsymbol{v}_h^n)_{L^2(\Omega)}-\frac{\Delta t}{2}|\boldsymbol{v}_h^n|_{\mathrm{upw}}^2\\ -\frac{c_0}{4}\Delta t\|\mu\|_{L^1}\int_{\xi^{\min}}^{\xi^{\max}}\|-\xi\varphi_h^n+\tilde{p}_h^n+\boldsymbol{u}_h^n\cdot\boldsymbol{n}\|_{L^2(\partial\Omega)}^2\frac{\mathrm{d}\mu}{\xi^2}\\ -\frac{c_0}{4}\Delta t\|\tilde{p}_h^n-\boldsymbol{u}_h^n\cdot\boldsymbol{n}-\beta(\tilde{p}_h^n+\boldsymbol{u}_h^n\cdot\boldsymbol{n})\|_{L^2(\partial\Omega)}^2,\end{aligned}$$

and the identity $(a-b)b=\frac{1}{2}a^2-\frac{1}{2}b^2-\frac{1}{2}(a-b)^2$ enables to rewrite this with the discrete extended energy

$$\mathcal{E}_h^n\coloneqq\|\boldsymbol{v}_h^n\|_{L^2(\Omega)}^2+\frac{c_0}{2}\|\mu\|_{L^1}\int_{\xi^{\min}}^{\xi^{\max}}\|\varphi_h^n\|_{L^2(\partial\Omega)}^2\frac{\mathrm{d}\mu}{\xi},$$

leading to

$$\begin{aligned}\frac{1}{2}\mathcal{E}_h^{n+1}\leq\frac{1}{2}\mathcal{E}_h^n-\frac{\Delta t}{2}(C(\boldsymbol{u_0})\boldsymbol{v}_h^n,\boldsymbol{v}_h^n)_{L^2(\Omega)}-\frac{\Delta t}{2}|\boldsymbol{v}_h^n|_{\mathrm{upw}}^2\\ -\frac{c_0}{4}\Delta t\|\mu\|_{L^1}\int_{\xi^{\min}}^{\xi^{\max}}\|-\xi\varphi_h^n+\tilde{p}_h^n+\boldsymbol{u}_h^n\cdot\boldsymbol{n}\|_{L^2(\partial\Omega)}^2\frac{\mathrm{d}\mu}{\xi^2}\\ -\frac{c_0}{4}\Delta t\|\tilde{p}_h^n-\boldsymbol{u}_h^n\cdot\boldsymbol{n}-\beta(\tilde{p}_h^n+\boldsymbol{u}_h^n\cdot\boldsymbol{n})\|_{L^2(\partial\Omega)}^2\\ +\frac{1}{2}\|\boldsymbol{v}_h^{n+1}-\boldsymbol{v}_h^n\|_{L^2(\Omega)}^2+\frac{c_0}{2}\|\mu\|_{L^1}\int_{\xi^{\min}}^{\xi^{\max}}\frac{1}{2}\|\varphi_h^{n+1}-\varphi_h^n\|_{L^2(\partial\Omega)}^2\frac{\mathrm{d}\mu}{\xi}.\end{aligned}$$

The task is now to estimate the two anti-dissipative terms so that they can be provably controlled by the three dissipative ones. Let us bound the anti-dissipation on $\boldsymbol{v}_h$ with Lemmas 5.22 and 5.20:

$$\begin{aligned}\frac{1}{2}\|\boldsymbol{v}_h^{n+1}-\boldsymbol{v}_h^n\|_{L^2(\Omega)}^2&=\frac{\Delta t^2}{2}\|\tilde{\mathcal{A}}_h\boldsymbol{v}_h+\mathcal{A}_h^{\{0\}}\boldsymbol{v}_h+\mathcal{A}_h^{\{\beta\}}\beta(\tilde{p}_h+\boldsymbol{u}_h\cdot\boldsymbol{n})\|_{L^2(\Omega)}^2\\ &\leq\Delta t^2\|\tilde{\mathcal{A}}_h\boldsymbol{v}_h\|_{L^2(\Omega)}^2+\Delta t^2\|\mathcal{A}_h^{\{0\}}\boldsymbol{v}_h+\mathcal{A}_h^{\{\beta\}}\beta(\tilde{p}_h+\boldsymbol{u}_h\cdot\boldsymbol{n})\|_{L^2(\Omega)}^2\\ &\leq C_{\mathrm{DG}}^2\Delta t^2(c_0+|\boldsymbol{u_0}|)h^{-1}|\boldsymbol{v}_h|_{\mathrm{upw}}^2\\ &\quad+\frac{C_{\mathrm{tr}}^2}{2}\Delta t^2c_0^2h^{-1}\|\tilde{p}_h-\boldsymbol{u}_h\cdot\boldsymbol{n}-\beta(\tilde{p}_h+\boldsymbol{u}_h\cdot\boldsymbol{n})\|_{L^2(\partial\Omega)}^2.\end{aligned}$$

Using Lemma 5.22 and the identity $\frac{1}{2}\|\varphi_h^{n+1}-\varphi_h^n\|_{L^2(\partial\Omega)}^2=\frac{\Delta t^2}{2}\|-\xi\varphi_h^n+\tilde{p}_h+\boldsymbol{u}_h\cdot\boldsymbol{n}\|_{L^2(\partial\Omega)}^2$, the energy balance becomes

$$\begin{aligned}\frac{1}{2}\mathcal{E}_h^{n+1}\leq\frac{1}{2}\mathcal{E}_h^n-\frac{\Delta t}{2}(C(\boldsymbol{u_0})\boldsymbol{v}_h^n,\boldsymbol{v}_h^n)_{L^2(\Omega)}\\ -\frac{\Delta t}{2}\left(1-2C_{\mathrm{DG}}^2\Delta t(c_0+|\boldsymbol{u_0}|)h^{-1}\right)|\boldsymbol{v}_h^n|_{\mathrm{upw}}^2\\ -\frac{c_0}{4}\Delta t\|\mu\|_{L^1}\int_{\xi^{\min}}^{\xi^{\max}}\|-\xi\varphi_h^n+\tilde{p}_h^n+\boldsymbol{u}_h^n\cdot\boldsymbol{n}\|_{L^2(\partial\Omega)}^2\left(\frac{1}{\xi}-\Delta t\right)\frac{\mathrm{d}\mu}{\xi}\\ -\left(\frac{c_0}{4}\Delta t-\frac{C_{\mathrm{tr}}^2}{2}\Delta t^2c_0^2h^{-1}\right)\|\tilde{p}_h^n-\boldsymbol{u}_h^n\cdot\boldsymbol{n}-\beta(\tilde{p}_h^n+\boldsymbol{u}_h^n\cdot\boldsymbol{n})\|_{L^2(\partial\Omega)}^2,\end{aligned}$$

which enables to conclude. □

The estimate used in the above proof is proven below.

Lemma 5.22. *For any* $\boldsymbol{v}_h \in \mathbb{P}_d^k(\mathcal{T}_h)^{d+1}$,

$$\|\mathcal{A}_h^{\{0\}}\boldsymbol{v}_h + \mathcal{A}_h^{\{\beta\}}\beta(\tilde{p}_h + \boldsymbol{u}_h\cdot\boldsymbol{n})\|_{L^2(\Omega)} \leq \frac{C_{\mathrm{tr}}}{\sqrt{2}}c_0 h^{-1/2}\|\tilde{p}_h - \boldsymbol{u}_h\cdot\boldsymbol{n} - \beta(\tilde{p}_h + \boldsymbol{u}_h\cdot\boldsymbol{n})\|_{L^2(\partial\Omega)},$$

where $C_{\mathrm{tr}} > 0$ *is defined in Lemma 5.4.*

Proof. Let $\boldsymbol{w}_h \coloneqq ((\boldsymbol{w}_h^u)^\intercal, w_h^{\tilde{p}})^\intercal \in \mathbb{P}_d^k(\mathcal{T}_h)^{d+1}$. The definition of $\mathcal{A}_h^{\{0\}} + \mathcal{A}_h^{\{\beta\}}$ and the Cauchy-Schwarz inequality yield

$$\begin{aligned}
&(\mathcal{A}_h^{\{0\}}\boldsymbol{v}_h, \boldsymbol{w}_h)_{L^2(\Omega)} + (\mathcal{A}_h^{\{\beta\}}\beta(\tilde{p}_h + \boldsymbol{u}_h\cdot\boldsymbol{n}), \boldsymbol{w}_h)_{L^2(\Omega)} \\
&\qquad \coloneqq \frac{1}{2}(M_0(\boldsymbol{n})\boldsymbol{v}_h - A(\boldsymbol{n})\boldsymbol{v}_h, \boldsymbol{w}_h)_{L^2(\partial\Omega)} + \frac{1}{2}(\boldsymbol{m}_{\mathcal{B}}(\boldsymbol{n})\beta(\tilde{p}_h + \boldsymbol{u}_h\cdot\boldsymbol{n}), \boldsymbol{w}_h)_{L^2(\partial\Omega)} \\
&\qquad = \frac{c_0}{2}(\tilde{p}_h - \boldsymbol{u}_h\cdot\boldsymbol{n} - \beta(\tilde{p}_h + \boldsymbol{u}_h\cdot\boldsymbol{n}), w_h^{\tilde{p}} - \boldsymbol{w}_h^u\cdot\boldsymbol{n})_{L^2(\partial\Omega)} \\
&\qquad \leq \frac{c_0}{\sqrt{2}}\|\tilde{p}_h - \boldsymbol{u}_h\cdot\boldsymbol{n} - \beta(\tilde{p}_h + \boldsymbol{u}_h\cdot\boldsymbol{n})\|_{L^2(\partial\Omega)}\|\boldsymbol{w}_h\|_{L^2(\partial\Omega)},
\end{aligned}$$

and the conclusion follows from Lemma 5.4. □

Chapter 6

Numerical validation and application to duct aeroacoustics

Contents

This chapter, drawn from (Monteghetti et al. 2018b), gathers numerical applications of TDIBCs in aeroacoustics, with a focus on acoustical liners. Section 6.1 contains reminders from Section 2.4. It recalls the derivation of discrete models from the analysis of physical impedance models of liners, leading to a time-local formulation that consists in composing a set of ODEs with a transport equation. The OD representation is discretized using an adaptation of the optimization method presented in Section 2.2 while the transport equation is discretized with a high order DG method. Applications are then shown in the last two sections. Section 6.2 deals with the impedance tube whose analytical solution is known even for nonlinear impedance. In particular, it validates the analysis of Chapter 5 by investigating the computational properties of a nonlinear algebraic scattering operator. Section 6.3 presents an application to two flow ducts documented in the literature.

6.1 Physical reflection coefficient models in the time domain

Following the terminology introduced in Section 1.3, a discrete TDIBC consists of three components: a discrete time-domain impedance model, an algorithm to compute said discrete model, and a coupling method with the considered PDE. This section tackles the first two components, while the last one has been covered *independently* in Chapter 5. Most of the content of this section has been covered in Chapters 1 and 2.

Section 6.1.1 recalls the models suitable for acoustical liners, including an example of nonlinear scattering operator. Section 6.1.2 recalls the OD representation of physical reflection

coefficients, which yields a formulation with an infinite number of *delayed* ODEs whose discretization is tackled in Section 6.1.3. The discretization methodology presented in Section 2.2 is adapted to deal with practical cases where experimental data are involved and the time delay is recast using a transport equation.

6.1.1 Physical models for acoustical liners

The numerical applications presented in this chapter involve two liners:

- A CT liner, depicted in Figure 1.4, made from a ceramic tubular core (channel of length l_c, diameter d_c, and porosity $\sigma_c \in (0, 1]$) and a rigid backplate.
- A micro-perforated (MP) liner, which is a SDOF liner made from a honeycomb core (cell of length l_c, diameter d_c, and porosity $\sigma_c \in (0, 1]$) sandwiched between a perforated facesheet (thickness l_p, hole diameter d_p, and porosity $\sigma_p \in (0, 1]$) and a rigid backplate, see Figure 1.6.

CT liners are mostly used in academic and benchmark experiments, while MP liners are widely used in industrial applications. Following Section 1.2, the standard linear impedance model for these liners reads

$$\hat{z}_{\text{phys}}(s) = \frac{1}{\sigma_p}\hat{z}_p(s) + \frac{1}{\sigma_c}\hat{z}_c(s) \quad (\Re(s) > 0)\,, \tag{6.1}$$

where $\hat{z}_p$ (resp. $\hat{z}_c$) is the impedance of a perforation (resp. cavity). The CT liner model $\hat{z}_{\text{CT}}$ is obtained with $\hat{z}_p = 0$, while $\sigma_c = 1$ yields the MP liner model $\hat{z}_{\text{MP}}$. The expression (6.1) separates the contribution of the perforated plate from that of the cavity, a feature that assumes the conservation of $\boldsymbol{u} \cdot \boldsymbol{n}$ across the perforation, which is satisfied as long as the perforation thickness l_p is much shorter than the considered wavelengths.

The chosen perforation model is given by a fractional polynomial

$$\frac{\hat{z}_p}{z_0}(s) = a_0 + a_{1/2}\sqrt{s} + a_1 s, \tag{6.2}$$

where each of the non-negative coefficients has a physical interpretation: a_0 models frequency-independent losses, $a_{1/2}$ frequency-dependent losses coming from visco-thermal dissipation, and a_1 is known as the mass reactance and does not incur any loss. The square root $\sqrt{s}$ is the principal branch defined in Example 2.14, which is analytic in $\mathbb{C}\backslash(-\infty, 0]$ and coincides with the real-valued square root on $(0, \infty)$. Values for the three coefficients can be obtained through various theoretical or empirical models; the high-frequency approximation of a model derived by Crandall, namely (1.20), yields

$$a_0 = \frac{3l_p\nu}{c_0\left(d_p/2\right)^2},\ a_{1/2} = \frac{2l_p\sqrt{\nu}}{c_0 d_p/2},\ a_1 = \frac{l_p}{c_0}, \tag{6.3}$$

where ν denotes the kinematic viscosity and c_0 the speed of sound.

For the cavity, the adopted model is a monodimensional wave equation with a fractional wavenumber $k_c(s)$

$$\frac{\hat{z}_c}{z_0}(s) = \coth(\mathrm{j}k_c(s)l_c),\ \mathrm{j}k_c(s)l_c = b_0 + b_{1/2}\sqrt{s} + b_1 s. \tag{6.4}$$

The non-negative coefficients b have a physical interpretation similar to those of (6.2): b_0 models frequency-independent losses, $b_{1/2}$ frequency-dependent losses, and b_1 is half the back-and-forth

traveling time in the cavity. The high-frequency approximation of a wavenumber derived by Bruneau, namely (1.26), gives

$$b_0 = 0,\ b_{1/2} = \frac{\sqrt{\nu}}{c_0 {}^{d_c}\!/_2}\left(\frac{\gamma-1}{\sqrt{\mathrm{Pr}}}+1\right) l_c,\ b_1 = \frac{l_c}{c_0}, \tag{6.5}$$

where Pr is the Prandtl number and γ the ratio of specific heat. From Proposition 1.8, the admissibility of this linear model follows from the fact that $\hat{z}$ is a positive-real function.

By contrast with the CT liner, the MP liner is sensitive to the incident sound pressure level (SPL): above a given threshold, nonlinear effects occur in the perforation. The prevailing nonlinear term for a perforated plate is given by (1.32); the computation of the corresponding nonlinear admittance and scattering operators has been discussed in Section 2.4.2.

6.1.2 Oscillatory-diffusive representation of physical models

The analysis of Section 2.4 gives a time-local realization of the impedance model covered in Section 6.1.1. We recall here the result for the reflection coefficient only, since Chapter 5 has shown its computational advantage.

To obtain the desired realization, the first step is to derive the so-called oscillatory-diffusive representation of the physical model z_{phys} using complex calculus. The starting point of the analysis is the identity (2.57) that enables to rewrite the reflection coefficient (1.15,6.1) as

$$\hat{\beta}_{\mathrm{phys}}(s) = 1 + \hat{h}_1(s) + e^{-s\tau}\hat{h}_2(s), \tag{6.6}$$

where the time delay $\tau \coloneqq 2b_1 > 0$ is the cavity back-and-forth traveling time and the functions $\hat{h}_1$ and $\hat{h}_2$, which induce deviations from the rigid wall $\hat{\beta}_{\mathrm{phys}}(s) = 1$, are given by

$$\hat{h}_1(s) = -\frac{2}{R(s)},\ \hat{h}_2(s) = -e^{-2b_0}\hat{h}_1(s)e^{-2b_{1/2}\sqrt{s}},$$

with common denominator

$$R(s) = 1 + \frac{1}{\sigma_c} + \frac{\hat{z}_p(s)}{\sigma_p} + \left(\frac{1}{\sigma_c} - 1 - \frac{\hat{z}_p(s)}{\sigma_p}\right) e^{-2\mathrm{j}k_c(s)l_c}.$$

The interest of the apparently gratuitous expression (6.6) is that both $\hat{h}_1$ and $\hat{h}_2$ admit an oscillatory-diffusive representation (6.7,6.8). The analytical expression of these two functions is used in the discretization methodology presented in Section 6.1.3. The representations of $\hat{h}_1$ and $\hat{h}_2$ are derived by inverting the Laplace transform using the residue theorem on a "keyhole-shaped" Bromwich contour, see Section 2.1.2 for the theory. Among the sufficient hypotheses needed to carry out the computations, $\hat{h}_i$ must decay uniformly on $\{|s| = R\}$ as $R \to \infty$ and admit finite residues at every poles and branch points (the only possible branch point of $\hat{h}_i$ is 0). The results of the analysis are as follows.

If $a_{1/2}$ or a_1 are positive, which is the case for an MP liner, the oscillatory-diffusive representation of $\hat{h}_i$ is given by Theorem 2.16 and reads

$$\hat{h}_i(s) = \sum_{n\in I}\frac{r_{i,n}}{s-s_n} + \int_0^\infty \frac{\mu_i(\xi)}{s+\xi}\mathrm{d}\xi \quad (i \in \{1,2\}), \tag{6.7}$$

where the sequence $(s_n)_n$ solves

$$R(s_n) = 0 \quad (n \in I \subset \mathbb{Z}),$$

$r_{i,n}$ is the associated residue

$$r_{i,n} \coloneqq \mathrm{Res}(\hat{h}_i, s_n)$$

with Res defined by (2.15), and μ_i is the so-called diffusive weight, linked to the jump of $\hat{h}_i$ across its cut $(-\infty, 0]$ by

$$\mu_i(\xi) \coloneqq \frac{1}{2\mathrm{j}\pi}\left[\hat{h}_i(\xi e^{-\mathrm{j}\pi}) - \hat{h}_i(\xi e^{+\mathrm{j}\pi})\right].$$

Remark 6.1. The sequence $(s_n)_n$ may include 0, which is a branch point of $\hat{h}_i$ when $a_{1/2} > 0$ hence not a pole since a pole is by definition an isolated singularity. However, since the focus of this chapter is the numerical applications, we will use a slight abuse of terminology and call s_n the sequence of poles even when it contains a branch point.

As highlighted in Remark 2.19 these quantities can be readily computed numerically, which enables to verify (6.7). The first (resp. second) term on the right-hand side of (6.7) is the oscillatory (resp. diffusive) part of $\hat{h}_i$. The oscillatory part is associated with the resonances, by contrast with the diffusive part that stems from visco-thermal losses. Indeed, without the multivalued fractional term $\sqrt{s}$ (physically, if $\nu = 0$, see (6.3)) the diffusive part vanishes, i.e. $\mu_i = 0$. The admissibility conditions given by Proposition 1.14 imply that $\mu(\xi) \in \mathbb{R}$ and that if s_n is a pole of $\hat{h}_i$ with residue $r_{i,n}$, then $\overline{s_n}$ is a pole of $\hat{h}_i$ with residue $\overline{r_{i,n}}$ (hermitian symmetry). The desired representation of $\hat{\beta}_{\mathrm{MP}}$ is then obtained by combining (6.6) and (6.7).

Although the physical model of the CT liner is similar to that of the MP liner, it does not admit the same OD representation. This is due to the fact that for the CT liner $\hat{z}_p(s) = 0$ so that $\hat{h}_1$ (and $\hat{h}_2$ if $b_{1/2} = 0$ but this case is not considered here) fails the decay condition (2.16). By considering instead $\hat{h}_1(s)/s$, the following representation can be derived, assuming $\sigma_c \neq 1$,

$$\hat{h}_1(s) = C + \sum_{n\in I} \frac{r_{1,n}}{s - s_n} + \int_0^\infty \frac{\mu_1(\xi)}{s + \xi}\mathrm{d}\xi, \tag{6.8}$$

which differs from (6.7) by a real constant C whose full expression follows from Lemma 2.40 and can be approximated as

$$C \simeq -\frac{1}{1 + \sigma_c^{-1}}.$$

The representation of $\hat{\beta}_{\mathrm{CT}}$ is then obtained by combining (6.6), (6.7) with $i = 2$, and (6.8).

Overall, for both liners, the physical reflection coefficient has the causal representation

$$\begin{aligned}\beta_{\mathrm{phys}}(t) = \beta_1\,\delta(t) + \sum_{n\in I} r_{1,n} e^{s_n t_+} + \int_0^\infty \mu_1(\xi) e^{-\xi t_+}\mathrm{d}\xi + \sum_{n\in I} r_{2,n} e^{s_n (t-\tau)_+} \\ + \int_0^\infty \mu_2(\xi) e^{-\xi (t-\tau)_+}\mathrm{d}\xi,\end{aligned} \tag{6.9}$$

where

$$e^{st_+} \coloneqq e^{st} H(t)$$

denotes the causal exponential function and $\beta_1 \in \mathbb{R}$. The importance of (6.9) lies in the fact that it provides a structural information on β_{phys}, namely that it "reduces" to an infinite number of first-order systems with delay

$$\begin{aligned}\beta_{\mathrm{phys}} \star v(t) = \beta_1 v(t) + \sum_{n\in I} r_{1,n}\varphi(t, -s_n) + \int_0^\infty \mu_1(\xi)\varphi(t,\xi)\mathrm{d}\xi + \sum_{n\in I} r_{2,n}\varphi(t-\tau, -s_n) \\ + \int_0^\infty \mu_2(\xi)\varphi(t-\tau,\xi)\mathrm{d}\xi,\end{aligned} \tag{6.10}$$

where φ is defined as (2.6) and v is a shorthand for "$\tilde{p} + \boldsymbol{u} \cdot \boldsymbol{n}$". The computational interest of (6.10) stems from the ability to compute φ through the first-order ODE (2.7). As a result, (6.10) is a time-local (but infinite-dimensional) representation of the hereditary convolution operator $v \mapsto \beta_{\text{phys}} \star v$. The above analysis informs the discrete model proposed in the next section.

6.1.3 Discrete reflection coefficient model

The identity (6.10) naturally suggests to define the discrete reflection coefficient model $\tilde{\beta}$ as

$$\hat{\tilde{\beta}}(s) = \tilde{\beta}_\infty + \sum_{n=1}^{N_s} \frac{\tilde{r}_{1,n}}{s - \tilde{s}_n} + \sum_{k=1}^{N_\xi} \frac{\tilde{\mu}_{1,k}}{s + \tilde{\xi}_k} + e^{-s\tilde{\tau}} \left(\sum_{n=1}^{N_s} \frac{\tilde{r}_{2,n}}{s - \tilde{s}_n} + \sum_{k=1}^{N_\xi} \frac{\tilde{\mu}_{2,k}}{s + \tilde{\xi}_k} \right) \tag{6.11}$$

$$\begin{aligned} \tilde{\beta} \star v(t) = \tilde{\beta}_\infty v(t) &+ \sum_{n=1}^{N_s} \tilde{r}_{1,n} \varphi(t, -\tilde{s}_n) + \sum_{k=1}^{N_\xi} \tilde{\mu}_{1,k} \varphi(t, \tilde{\xi}_k) + \sum_{n=1}^{N_s} \tilde{r}_{2,n} \varphi(t - \tilde{\tau}, -\tilde{s}_n) \\ &+ \sum_{k=1}^{N_\xi} \tilde{\mu}_{2,k} \varphi(t - \tilde{\tau}, \tilde{\xi}_k), \end{aligned}$$

where φ follows the first-order ODE (2.7). It involves

$$N_\varphi \coloneqq N_s + N_\xi$$

additional variables, where N_ξ (resp. N_s) variables come from the diffusive (resp. oscillatory) part of β_{phys}. Note that, from Proposition 1.14,

$$\tilde{\beta}_\infty = \hat{\tilde{\beta}}(+\infty) \in [-1, 1].$$

In summary, the analysis of the physical model (6.1) has led to the discrete model (6.11), which requires the computation and delay of N_φ ODEs. Without the delay $\tilde{\tau} = 0$, the derived model $\tilde{\beta}$ can be interpreted as a so-called multipole model, postulated in (Fung and Ju 2004) for instance. In preparation for the application of (6.11) presented in Sections 6.2 and 6.3, the computation of the poles $(\tilde{s}_n, \tilde{\xi}_k)_{n,k}$ and weights $(\tilde{r}_{i,n}, \tilde{\mu}_{i,k})_{n,k}$ as well as the discretization of the time delay are discussed below.

Poles and weights computation

The discrete model $\tilde{\beta}$ is fully determined by the constant $\tilde{\beta}_\infty$, N_φ poles $(\tilde{s}_n, \tilde{\xi}_k)_{n,k}$, $2N_\varphi$ weights $(\tilde{r}_{i,n}, \tilde{\mu}_{i,k})_{n,k}$, and time delay $\tilde{\tau}$. These parameters should be such that $\tilde{\beta}$ is a satisfactory representation of the considered sound absorbing material, typically known by its physical characteristics and possibly some experimental data $(\hat{\beta}_{\text{exp}}(\mathrm{j}2\pi f_m))_m$. Criteria for a satisfactory approximation include:

- $\hat{\tilde{\beta}}$ is a bounded real function (see Proposition 1.14);
- N_φ is as low as possible;
- $\omega \mapsto \hat{\tilde{\beta}}(\mathrm{j}\omega)$ has a physical behavior at frequencies not covered by the experimental data (usually low and high frequencies);
- the maximum frequency
$$(2\pi)^{-1} \max_{n,k} (|\tilde{s}_n|, \tilde{\xi}_k)_{n,k}$$
is consistent with the stability region of the time discretization scheme (otherwise the IBC could reduce the timestep of an explicit integration).

In Section 6.3, the three-step methodology given below is followed. The principle of the approach is to use as much as possible the information obtained on the physical model in Section 6.1.2 to ease the optimization process. The second step is a summary of the optimization method presented in full details in Section 2.2.1: the reader is referred to this section for background and possible variants.

1. (Physical model) Compute the coefficients a and b from the liner dimensions using the models (6.3,6.5). In particular, this provides a value for the constant β_1 and the time delay τ. These coefficients can then serve as an initial point for a nonlinear least squares minimization of
$$\omega \mapsto \|\hat{z}_{\text{phys}}(\mathrm{j}\omega) - \hat{z}_{\exp}(\mathrm{j}\omega)\|_2.$$
Physically, this optimization can be interpreted as computing the various physical impedance corrections (Cummings 1986; Melling 1973).
Inputs: material characteristics (l_p, d_p, σ_c, etc.), experimental data $(\hat{z}_{\exp}(\mathrm{j}2\pi f_m))_m$.
Outputs: coefficients $(\sigma_p^{-1}a_0, \sigma_p^{-1}a_{1/2}, \sigma_p^{-1}a_1, \sigma_c, b_0, b_{1/2}, b_1)$, time delay $\tau = 2b_1$, constant $\beta_1 = 1 - (1+\sigma_c^{-1})^{-1}$.

2. (Discrete model – Linear least squares) *Choose* N_ξ diffusive poles along the cut $(-\infty, 0]$ (typically, a logarithmic repartition is satisfactory). *Compute* N_s oscillatory poles $\tilde{s}_n$ by solving $R(\tilde{s}_n) = 0$. Compute the weights $(\tilde{r}_{n,i})_n$ and $(\tilde{\mu}_{k,i})_k$ by minimizing
$$\omega \mapsto \left\| \sum_{k=1}^{N_\xi} \frac{\tilde{\mu}_{k,i}}{\mathrm{j}\omega + \tilde{\xi}_k} + \sum_{n=1}^{N_s} \frac{\tilde{r}_{n,i}}{\mathrm{j}\omega - \tilde{s}_n} - \hat{h}_i(\mathrm{j}\omega) \right\|_2 \tag{6.12}$$
if the representation (6.7) holds (if the representation of h_i is instead given by (6.8), then add the constant term C in the cost function). This is an overdetermined *linear* least squares optimization that is solved instantaneously by pseudo-inverse. Note that the time delay $\tilde{\tau}$ has no role whatsoever during this step.
Inputs: $\hat{h}_i$ (from output of step 1), number of poles N_s, diffusive poles $(\xi_k)_{k\in[\![1,N_\xi]\!]}$.
Outputs: oscillatory poles $(\tilde{s}_n)_{n\in[\![1,N_s]\!]}$, weights $(\tilde{r}_{n,i})_{n\in[\![1,N_s]\!]}$ and $(\tilde{\mu}_{k,i})_{k\in[\![1,N_\xi]\!]}$ $(i \in \{1,2\})$.

3. (Discrete model – Nonlinear least squares) Compute new poles and weights with a nonlinear least squares optimization on
$$\omega \mapsto \|\hat{\tilde{\beta}}(\mathrm{j}\omega) - \hat{\beta}_{\exp}(\mathrm{j}\omega)\|_2$$
with initial poles and weights given by step 2, $\tilde{\beta}_\infty = \beta_1$ and $\tilde{\tau} = \tau$ from step 1. The constant $\tilde{\beta}_\infty$ and delay $\tilde{\tau}$ can also be optimized along the poles and weights, but this may lead to overfitting. Note that the expression of $\hat{\tilde{\beta}}(\mathrm{j}\omega)$ contains the term "$e^{-\mathrm{j}\omega\tilde{\tau}}$", although in practice the actual computation of the convolution $\tilde{\beta} \star v$ will involve a discretization (hence, an approximation) of the time delay; in other words, during this optimization step, the time delay is assumed to be perfectly approximated.
Inputs: $(\tilde{s}_n, \tilde{\xi}_k)_{n,k}$, $(\tilde{r}_{n,i}, \tilde{\mu}_{k,i})_{n,k}$, $\tilde{\tau} = \tau$, $\tilde{\beta}_\infty = \beta_1$, $(\hat{\beta}_{\exp}(\mathrm{j}2\pi f_m))_m$.
Outputs: $(\tilde{s}_n, \tilde{\xi}_k)_{n,k}$, $(\tilde{r}_{n,i}, \tilde{\mu}_{k,i})_{n,k}$, (optional) $\tilde{\tau}$, (optional) $\tilde{\beta}_\infty$.

As mentioned above, variants for step 2 are presented in Section 2.2.1. However, let us highlight here one that can yield interesting results for the problem at hand. Following Remark 2.41, it is also possible to compute the oscillatory weight $\tilde{r}_{n,i}$ by computing the residue
$$\tilde{r}_{n,i} \coloneqq \mathrm{Res}(\hat{h}_i, \tilde{s}_n)$$

using a quadrature rule to discretize the line integral (2.15). For the models considered herein, this computation can be done with a satisfactory accuracy. One advantage of computing the weights $(\tilde{r}_{n,i})_{n,i}$ in this way is that the only variables left in the minimization of (6.12) are the diffusive weights $(\tilde{\mu}_{k,i})_k$. For instance, the discrete models presented in Figure 2.11 have been obtained using this method. The only drawback of this method is that it may not yield parsimonious approximations when the residue $\mathrm{Res}(\hat{h}_i, \tilde{s}_n)$ has a slow decay as $n \to \infty$, which occurs when the fractional term in the expression of $\hat{h}_i$ is negligible (physically, when there is a lack of diffusion in the impedance model). The numerical results presented in this chapter always rely on optimizing both the oscillatory and diffusive weights.

When the physical model is satisfactory, as is the case for the MP and CT liners considered herein, the first two steps deliver a discrete model $\tilde{\beta}$ that may be sufficient for some engineering applications. If step 3 is used, its role is to adjust the poles and weights to improve the fit against experimental data. The first two steps can then be interpreted as using a physical model to help finding an initial guess for the poles and weights. When faced with a mismatch between the physical model and experimental data, tuning the former may be required, but this is not a computationally intensive task since there are few parameters and they have a physical interpretation. The third stage can be performed using any nonlinear least squares method: in Section 6, we simply relied on the trust region optimization method (Coleman and Y. Li 1996) implemented in MATLAB® `lsqnonlin`, whose execution takes a few seconds on a contemporary computer, but the more tailored vector fitting algorithm (Gustavsen and Semlyen 1999) can also be used, as in (Troian et al. 2017).

However, note that step 3 comes with the following caveat. There is a trade-off between the fit quality against the experimental data, which is usually narrowband, and the broadband behavior of $\hat{\tilde{\beta}}$. This trade-off is especially acute when using impedance identified with base flow, as these can be associated with significant uncertainties that ideally should be accounted for in the optimization process. This is exemplified by the question of whether to optimize the time delay $\tilde{\tau}$. Physically, it is linked to the anti-resonant frequencies f_n given by $f_n = {}^{n}/_{\tilde{\tau}}$ for (6.1) with a lossless cavity $b_0 = b_{1/2} = 0$ (i.e. a canonical Helmholtz resonator), see also Remark 1.23. Therefore, although $\tilde{\tau} \neq \tau$ may enable a better fit, it may not be worth altering the broadband behavior. Eventually, knowledge about both the model and experimental data is helpful to inform the optimization process.

Time delay discretization

The discretization of the time delay is done independently of the choice of weights and poles described above. Theoretically, the delay can be recast into

$$\varphi(t - \tilde{\tau}, s) = \psi(t, s, -l_{\tilde{\tau}})$$

where the additional function $\psi(\cdot, s, \cdot)$ obeys the following transport equation on $(-l_{\tilde{\tau}}, 0)$ with $l_{\tilde{\tau}} = c_{\tilde{\tau}}\tilde{\tau} > 0$

$$\begin{cases} \partial_t \psi(t, s, \theta) = c_{\tilde{\tau}} \partial_\theta \psi(t, s, \theta) \quad (t \in (0, \infty),\ \theta \in (-l_{\tilde{\tau}}, 0)) \\ \psi(t, s, 0) = \varphi(t, s),\ \psi(0, s, \theta) = 0. \end{cases} \tag{6.13}$$

This device is commonly used in theoretical and numerical studies of delay differential equations, see (Curtain and Zwart 1995, § 2.4), (Engel and Nagel 2000, § VI.6), (Michiels and Niculescu 2014), and the survey paper (Richard 2003). Although not needed herein, several delays $\tilde{\tau}_i$ can also be tackled by defining $\tilde{\tau} \coloneqq \max_i \tilde{\tau}_i$.

The monodimensional PDE (6.13) is discretized using a DG method with N_K elements and $N_p \geq 2$ nodes per element (order N_p). The discretization accuracy is measured by the number

of points per wavelength

$$\mathrm{PPW}_{\tilde{\tau}}(f_{\max}) \coloneqq \frac{N_\psi}{\tilde{\tau} f_{\max}}, \tag{6.14}$$

where

$$N_\psi \coloneqq N_K N_p$$

is the total number of nodes and $f_{\max}$ is the maximum frequency of interest. Target values for $\mathrm{PPW}_{\tilde{\tau}}$ as a function of N_p can be found in (Hu et al. 1999, Tab. 1), which shows that it is advantageous to choose $N_K = 1$ so that N_p is the sole discretization parameter. The impact of $\mathrm{PPW}_{\tilde{\tau}}$ is illustrated in Section 6.3. Herein, the main argument in favor of delaying through a transport equation, compared to continuous Runge-Kutta methods (Bellen and Zennaro 2003; Zennaro 1986), is the meaningfulness of (6.14) for wave propagation problems, which makes the discretization straightforward to set up a priori.

In summary, the discrete impedance model (6.11) is computed through

$$\begin{aligned}\tilde{\beta} \star v(t) = \tilde{\beta}_\infty v(t) &+ \sum_{n=1}^{N_s} \tilde{r}_{1,n} \varphi(t, -\tilde{s}_n) + \sum_{k=1}^{N_\xi} \tilde{\mu}_{1,k} \varphi(t, \tilde{\xi}_k) + \sum_{n=1}^{N_s} \tilde{r}_{2,n} \psi(t, -\tilde{s}_n, -l_{\tilde{\tau}}) \\ &+ \sum_{k=1}^{N_\xi} \tilde{\mu}_{2,k} \psi(t, \tilde{\xi}_k, -l_{\tilde{\tau}}),\end{aligned} \tag{6.15}$$

which implies the use of $(N_\psi + 1)N_\varphi$ additional variables. The two parameters to control are

- $\max_{k,n}(\xi_k, |s_n|)$, which is to be chosen in accordance with the spatial discretization scheme;
- $\mathrm{PPW}_{\tilde{\tau}}(f_{\max})$, for which values are given in (Hu et al. 1999, Tab. 1).

This covers the first two components of the TDIBC. The next sections deal with the numerical applications.

Remark 6.2. The discrete model (6.15) has been derived from a mathematical analysis that emphasizes the distinct components of the model (6.6): an oscillatory-diffusive part that models both oscillatory and diffusion phenomena (the latter of parabolic nature), and a hyperbolic part associated with the time delay that models a wave reflection phenomenon. See Table 2.1 for a summary.

Remark 6.3. An alternative discretization strategy is to perform a rational approximation of the time delay, see (Richard 2003) and references therein. For a pure time delay, i.e. $\hat{\beta}(s) \propto e^{-\tau s}$, a multipole approximation method is presented in (Douasbin et al. 2018): this amounts to discretizing the delay as if it was an OD kernel.

6.2 Numerical validation on nonlinear impedance tube

The purpose of this section is to validate the numerical flux functions proposed in Chapter 5, namely the $\mathcal{Z}$-flux (5.14,5.35) and the $\mathcal{B}$-flux (5.14,5.39), as well as to illustrate the computational advantage of the latter. Since, by definition, the IBC (1.1) is locally reactive, it is enough to consider a monodimensional impedance tube, depicted in Figure 6.1, whose analytical solution is known even for a nonlinear impedance boundary condition. This test case is the most convenient way of validating a TDIBC.

Let us briefly recall the impedance tube exact solution, expressed using the notations of Figure 6.1. At $x = 0$ the incoming characteristic is given by

$$(\tilde{p} + u)(t, 0) = \phi_s(t) \quad (t > 0),$$

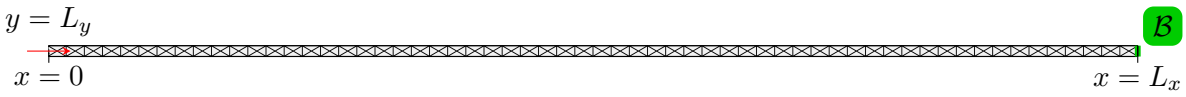

Figure 6.1. Impedance tube used in Section 6.2: $L_x = 1\,\mathrm{m}$, $L_y = {}^{L_x}/_{100}$, and mesh with 240 triangles.

where the source ϕ_s is causal (i.e. $\phi_s(t) = 0$ for $t < 0$). At $x = L_x$, the nonlinear IBC (1.12) is enforced. Assuming null initial conditions

$$\tilde{p}(0,x) = u(0,x) = 0 \quad (x \in (0, L_x))\,,$$

the exact solution is given by

$$\begin{cases} \tilde{p}(t,x) = \dfrac{1}{2}\phi_s\left(t - \dfrac{x}{c_0}\right) + \dfrac{1}{2}\mathcal{B}(\phi_s)\left(t - \dfrac{2L_x - x}{c_0}\right) \\ u(t,x) = \dfrac{1}{2}\phi_s\left(t - \dfrac{x}{c_0}\right) - \dfrac{1}{2}\mathcal{B}(\phi_s)\left(t - \dfrac{2L_x - x}{c_0}\right). \end{cases} \tag{6.16}$$

Note that this solution, which can be derived with an elementary application of the method of characteristics, is naturally expressed with the nonlinear scattering operator $\mathcal{B}$, not the impedance operator $\mathcal{Z}$. If the IBC is linear, then $\mathcal{B}(v) = \beta \star v$ and this solution can also be derived using the Laplace transform. The computation of the exact solution (6.16) only requires the computation of $\mathcal{B}(\phi_s)$. As detailed in Section 6.1, for the models considered herein the computation of $\mathcal{B}(\phi_s)$ may involve delayed ODEs.

In the computations presented below, the LEEs (5.1) are discretized using a fourth-order DG method, see Appendix F for the implementation details, and the RKF84 eight-stage fourth-order $2N$-storage Runge-Kutta method (Toulorge and Desmet 2012, Tab. A.9). The mesh of 240 triangles (2400 nodes) is shown in Figure 6.1. The source $\boldsymbol{v}_s$ at $x = 0$ is imposed using the upwind numerical flux

$$(A(\boldsymbol{n}_F)\boldsymbol{v})^*_s \coloneqq A(\boldsymbol{n}_F)^{\oplus}\boldsymbol{v}_{|T_1} - A(\boldsymbol{n}_F)^{\ominus}\boldsymbol{v}_s, \tag{6.17}$$

where the notation of Figure 5.1 is used. and the IBC is weakly enforced with either the $\mathcal{Z}$-flux (5.14,5.35) or the $\mathcal{B}$-flux (5.14,5.39), as discussed in Chapter 5.

Figure 6.2 shows the the exact and computed solutions at the inlet $x = 0$ for four impedance models and a Gaussian source centered at 2 kHz of amplitude

$$A_s = \sqrt{2}\frac{p_{\mathrm{ref}}}{z_0}10^{\frac{\mathrm{SPL}}{20}},$$

where the pressure of reference is

$$p_{\mathrm{ref}} = 2 \times 10^{-5}\,\mathrm{Pa}$$

and the incident SPL is expressed in dB. For the sake of clarity, the impedance tube is chosen long enough to avoid overlapping between the incident and reflected waves. For each of the four models the exact solution matches the computed one, which validates the proposed numerical flux functions. Let us now comment each graph individually.

The top right graph covers the linear TDIBC $\tilde{\beta}_A$ given in Table 6.2 and plotted in Figure 6.2 that models the MP liner studied in Section 6.3. The computation of $\tilde{\beta}_A \star v$ through (6.15) involves a transport equation whose N_ψ-point discretization is characterized by its number of points per wavelength (6.14): here, $N_\psi = 4$ is sufficient. The contrast with the hard wall shown in the top left graph illustrates the effect of $\tilde{\beta}_A$ on the incident wave.

The bottom left graph covers the *non-passive* scattering operator $\mathcal{B} = 3\mathcal{I}$, outside of the scope of the analysis presented in Chapter 5. However, the $\mathcal{B}$-flux does enable to compute this

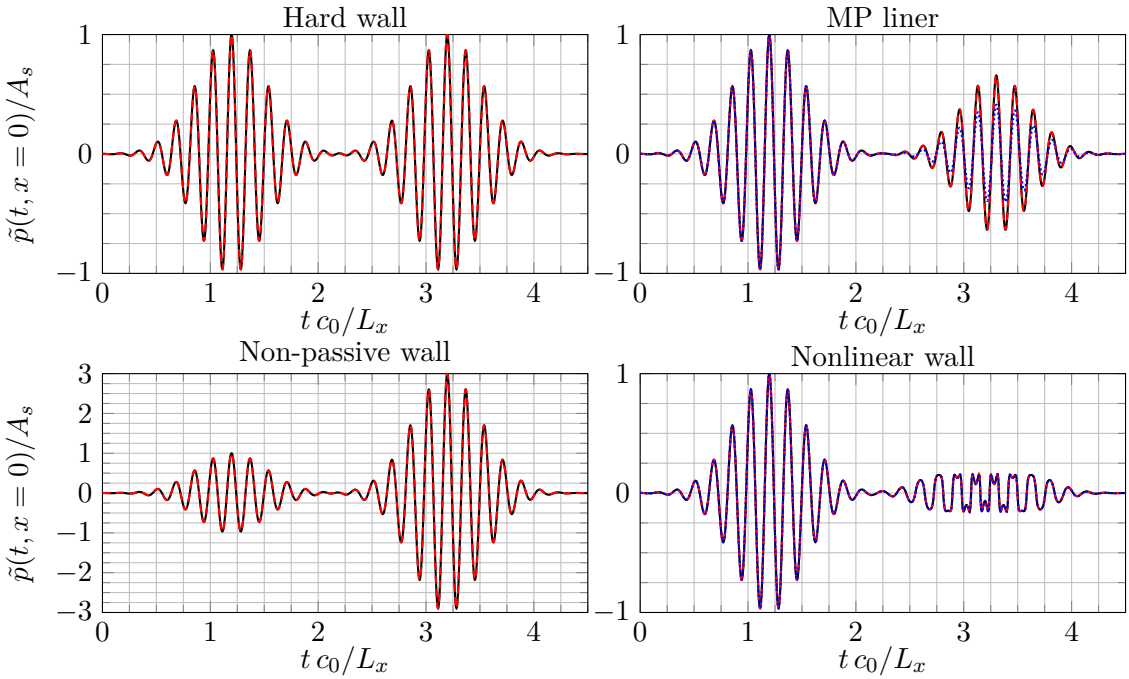

Figure 6.2. Acoustic pressure $\tilde{p}$ at $x = 0$ (see Figure 6.1). Gaussian-modulated sinusoidal source centered at 2 kHz of amplitude $A_s = \sqrt{2}\frac{p_{\text{ref}}}{z_0} 10^{\frac{\text{SPL}}{20}}$ ($L_x = 1\,\text{m}$, $L_y = {}^{L_x}/_{100}$, $c_0 = 344.32\,\text{m} \cdot \text{s}^{-1}$, $z_0 = 405.26\,\text{kg} \cdot \text{m}^{-2} \cdot \text{s}^{-1}$, $p_{\text{ref}} = 2 \times 10^{-5}\,\text{Pa}$, and SPL = 192.15 dB). (——) Exact solution (6.16). (- - - -) DG4-RKF84-$\mathcal{B}$-flux (5.14,5.39) and CFL = 0.85. [Top left] Hard wall $\mathcal{B} = \mathcal{I}$. [Bottom left] Non-passive wall $\mathcal{B} = 3\mathcal{I}$. [Bottom right] Nonlinear model (2.73) with $(a_0, C_{\text{nl}}) = (0, 1)$. (·····) DG4-RKF84-$\mathcal{Z}$-flux (5.14,5.35). [Top right] Linear TDIBC $\tilde{\beta}_A$, see Figure 6.5 and Table 6.2. (- - - -) DG4-RKF84-$\mathcal{B}$-flux, $N_\psi = 4$, and $\text{PPW}_{\tilde{\tau}}(2\,\text{kHz}) = 9.64$. (·····) DG4-RKF84-$\mathcal{B}$-flux, $N_\psi = 2$, and $\text{PPW}_{\tilde{\tau}}(2\,\text{kHz}) = 4.82$.

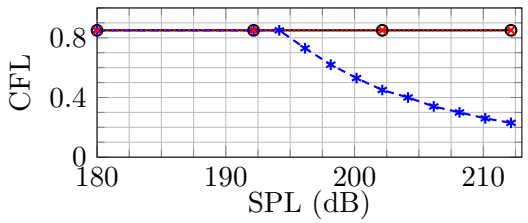

Figure 6.3. Maximum CFL number against incident SPL for the impedance tube of Figure 6.2. (—o—) Hard wall $\mathcal{B} = I$ and DG4-RKF84-$\mathcal{B}$-flux. (- - * - -) Nonlinear model (2.73) with $(a_0, C_{\text{nl}}) = (0, 1)$ and DG4-RKF84-$\mathcal{Z}$-flux. (·····×·····) Same nonlinear model (2.75) with DG4-RKF84-$\mathcal{B}$-flux.

case, by contrast to the $\mathcal{Z}$-flux with which no stable computations could be obtained, even with a reduced CFL number and different meshes. Therefore, although we do not prove this, the $\mathcal{B}$-flux seems to be advantageous to compute non-passive material.

Finally, the bottom right plot considers the algebraic nonlinear model (2.73) with $C_{\mathrm{nl}} = 1$, whose scattering operator is given by (2.75). As expected, both the $\mathcal{Z}$ and $\mathcal{B}$ fluxes lead to the same solution, which validates the derived expressions. The graph shows harmonic distortion, a genuinely nonlinear feature.

In all the computations of Figure 6.2, the CFL number has been kept at 0.85, its maximum value with a hard wall, for all cases. However, the analysis of Chapter 5 has shown that the $\mathcal{B}$-flux is to be favored over the $\mathcal{Z}$-flux. Figure 6.3 illustrates this point with the nonlinear model used in Figure 6.2. With the $\mathcal{Z}$-flux, the maximum CFL number that leads to a stable computation decreases as the incident SPL increases, since the resistance increases. By contrast, the $\mathcal{B}$-flux enables to keep the same CFL number, which can be understood from the passivity condition (1.13) that manifests itself in Lemma 2.51. The value $C_{\mathrm{nl}} = 1$ has been chosen arbitrarily, to highlight the nonlinear effect; as the nonlinear coefficient C_{nl} (resp. contraction coefficient C_c) goes to infinity (resp. zero), the SPL value above which the CFL drops with the $\mathcal{Z}$-flux goes to zero. Although this example is elementary, it illustrates the advantage of the nonlinear scattering formulation. A more advanced but linear application is presented in the next section.

Remark 6.4 (Value of C_{nl}). The value $C_{\mathrm{nl}} = 1$ has been chosen for simplicity, as the purpose of this section is merely to highlight a numerical effect. In Figure 6.3, the timestep reduction when using the $\mathcal{Z}$-flux occurs for incident SPLs above

$$\mathrm{SPL}_{\max} \simeq 194.15\,\mathrm{dB}.$$

Physically, at this pressure level, the LEEs should not be used as the propagation itself becomes nonlinear. A full numerical characterization of the nonlinear impedance tube considered in this figure would consist in plotting $\mathrm{SPL}_{\max}$ against C_{nl} so that, given a value of C_{nl}, one can estimate the range of incident SPLs for which the $\mathcal{Z}$-flux yields the same timestep as the $\mathcal{B}$-flux.

6.3 Aeroacoustical duct

In this section, numerical simulations to two flow ducts are compared with experimental data, a summary of which is given in Section 6.3.1. Section 6.3.2 describes the employed numerical methodology. Comparison with experimental data is done in the last two sections, Sections 6.3.3 and 6.3.4.

6.3.1 Experimental methodology and data

The study focuses on two ducts designed by the National Aeronautics and Space Administration (NASA), namely the Grazing Incidence Tube (GIT) and Grazing Flow Impedance Tube (GFIT). A short summary of the experiments reported in (Jones et al. 2005) and (Primus et al. 2013) is provided below.

Experimental setup The GIT and GFIT share a similar geometry, described in Figure 6.4 and Table 6.1. The acoustical source is placed upstream of the entry plane $x = 0$, where a reference microphone is positioned on the lower wall. The source is monochromatic, with a frequency chosen below the lowest cut-off frequency so that only plane waves propagate in the duct. A near-anechoic termination is placed at the exit plane $x = L$. The sound absorbing material sample is mounted on the top wall between L_{x1} and L_{x_2}, while microphones are located

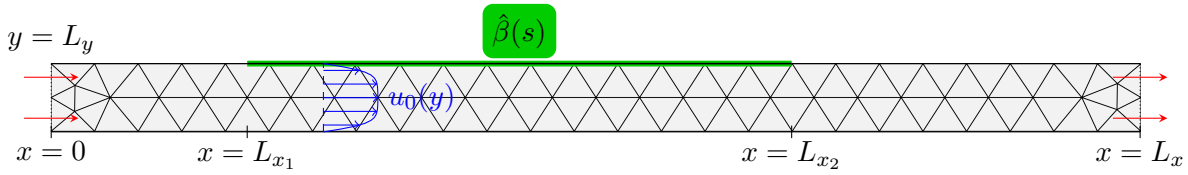

Figure 6.4. Flow duct considered in Section 6.3 (aspect ratio of the GIT). Mesh of 106 triangles used in Figure 6.12. Pressure measurements are taken on the lower wall $y = 0$. See Table 6.1 for geometrical dimensions corresponding to the GIT and GFIT.

	L_{x_1} (mm)	L_{x_2} (mm)	L_x (mm)	L_y (mm)	$f_{\text{cut-off}}$ (kHz)
GIT (Jones et al. 2005)	203	609	812.8	51	3.38
GFIT (Primus et al. 2013)	203.2	812.8	1016	63.5	2.71

Table 6.1. Geometrical dimensions of the GIT and GFIT. The acoustical cut-off frequency is computed through $f_{\text{cut-off}} = c_0(2L_y)^{-1}$, with $c_0 = \sqrt{\gamma r T} \simeq 344.32\,\text{m}\cdot\text{s}^{-1}$ ($T = 295\,\text{K}$, $\gamma = 1.4$, and $r = 287.058\,\text{J}\cdot\text{kg}^{-1}\cdot\text{K}^{-1}$).

on the lower wall. A Pitot probe system enables to measure the base flow u_0 at given cross-sections. See (Jones et al. 2005, Fig. 2) and (Primus et al. 2013, Fig. 5) for visualizations of the ducts.

Impedance identification methodology At each source frequency f_s, pressure measurements are taken on the lower wall $y = 0$ and used to identify the impedance value $\hat{z}_{\text{id}}(\text{j}2\pi f_s)$. The inverse problem relies on the 2D convected Helmholtz equation

$$(\partial_t + u_0\partial_x)^2 p - c_0^2 \Delta p = 0$$

derived from the LEEs (5.1) by taking a uniform base flow

$$\boldsymbol{u_0} = c_0 M_{\text{avg}} \boldsymbol{e_x},$$

where M_{avg} is the measured average Mach number. Since the base flow is assumed uniform, the IBC used for the identification is *not* (1.3), as considered in this dissertation, but the standard Ingard-Myers boundary condition with uniform impedance and straight boundary: (Jones et al. 2005, Eq. 2)

$$-\hat{z}_{\text{id}}(s)\partial_n \hat{p} = \frac{s}{c_0}\hat{p} + 2M_{\text{avg}}\partial_x \hat{p} + \frac{c_0 M_{\text{avg}}^2}{s}\partial_x^2 \hat{p}.$$

Although in principle more accurate results could be obtained by using corrected versions of the Ingard-Myers boundary condition (see Remark 5.2), the identified impedance $\hat{z}_{\text{id}}$ has proven satisfactory. Note that in addition to $\hat{z}_{\text{id}}$ another impedance is identified, namely the exit impedance enforced at the outlet $x = L$: this impedance is close to 1 since the exit is nearly anechoic in the experiments.

Experimental data The material considered in the GFIT experiment is a MP liner made from a honeycomb core (thickness $l_c = 38.1\,\text{mm}$, cell diameter $d_c = 9.5\,\text{mm}$) sandwiched between a perforated facesheet (thickness $l_p = 0.8\,\text{mm}$, hole diameter $d_p = 0.3\,\text{mm}$, and porosity $\sigma_p = 5\,\%$) and a rigid backplate. Impedance identifications have been done at an incident SPL of 120 dB (chosen to minimize nonlinear effects), average Mach numbers in {0,0.180,0.271}, and frequencies ranging from 0.4 kHz to 2.6 kHz by steps of 0.2 kHz. The GIT experiment focused on a ceramic tubular liner (CT57) made from a ceramic tubular core ($l_c = 85.6\,\text{mm}$, $d_c = 0.6\,\text{mm}$, $\sigma_c = 57\,\%$)

and a rigid backplate. The experimental data, partially reported in (Jones et al. 2005, Tabs. 1–9), covers an incident SPL of 130 dB, average Mach numbers in {0,0.079,0.172,0.255,0.335,0.400}, and frequencies ranging from 0.5 kHz to 3 kHz by steps of 0.1 kHz. The 0.5 kHz data is excluded since it is less reliable (Jones et al. 2005).

6.3.2 Numerical methodology

Discretization The discretization of the LEEs (5.1) is identical to that of Section 6.2. In all of the computations, the CFL number is kept at 0.85, its maximum value with a hard wall (i.e. the TDIBC does not reduce the time step). At the entry plane $x = 0$, a plane wave source is imposed using the flux $(A(\boldsymbol{n}_F)\boldsymbol{v})^*_s$ defined by (6.17), while a non-reflecting boundary condition, exact only for plane waves, is imposed at $x = L_x$ using

$$(A(\boldsymbol{n}_F)\boldsymbol{v})^*_{\text{out}} \coloneqq A(\boldsymbol{n}_F)^{\oplus}\boldsymbol{v}_{|T_1}, \tag{6.18}$$

where the notation of Figure 5.1 is used. Note that no exit impedance is considered, by contrast with the impedance identification methodology used in (Jones et al. 2005; Primus et al. 2013). The TDIBC is given by (6.15) and is weakly enforced with the $\mathcal{B}$-flux (5.14,5.39) derived in Section 5.3.3.

Base flow The chosen base flow is given by

$$\boldsymbol{u_0} = c_0 M_0(y)\boldsymbol{e}_x,$$

where $y \mapsto M_0(y)$ is the hyperbolic velocity profile, proposed in (Rienstra and Vilenski 2008, Eq. 4) and used in e.g. (Khamis and Brambley 2017, Eq. 2.4a),

$$M_0(r) = M_c \tanh\left(\frac{1-|r|}{\delta}\right) + M_c\left[1-\tanh\left(\frac{1}{\delta}\right)\right]\left[\frac{1+\tanh\left(\frac{1}{\delta}\right)}{\delta} + 1 + |r|\right](1-|r|) \tag{6.19}$$

with $r \in [-1, 1]$ and centerline Mach number given by

$$M_c = \frac{M_{\text{avg}}}{\delta \ln\left(\cosh\left(\frac{1}{\delta}\right)\right) + \left[1-\tanh\left(\frac{1}{\delta}\right)\right]\left[\frac{1+\tanh\left(\frac{1}{\delta}\right)}{6\delta} + \frac{2}{3}\right]}.$$

This velocity profile, depicted in Figure 6.4, has two parameters: the average Mach number M_{avg} and the nondimensional boundary layer thickness $\delta \in (0, 1]$. For $\delta = 1$, the velocity profile is almost identical to the Poiseuille profile

$$M_0(r) = \frac{3}{2}M_{\text{avg}}(1-r^2) \quad (r \in [-1, 1]).$$

More accurate alternatives to this velocity profile include using a turbulent eddy viscosity model where M_0' is known analytically (Marx and Aurégan 2013, Eqs. 3-4), or, when possible, an interpolation of the experimental flow. Using these other velocity profiles does not significantly alter the presented results, but imply the use of a more refined mesh, hence why (6.19) is chosen herein.

In both experiments, the identified impedance values exhibit a dependency on the grazing base flow. In Sections 6.3.3 and 6.3.4, to account for this dependency, we follow a simple approach inspired by the experimental study (Kirby and Cummings 1998), recalled in Section 1.2.3. The grazing flow is considered as an additional parameter, so that the physical quantities found in the acoustical model (6.1), such as l_p or l_c for instance, are tweaked when a base flow is present. This empirical approach has been found to be sufficient to match the experimental results.

Remark 6.5 (Base flow discretization). A characteristic of the employed DG implementation that is relevant to highlight here relates to the discretization of the base flow, more specifically the computation of the surface and line integrals involving the base flow $\boldsymbol{u_0}$. Our implementation, described in Appendix F, exhibits an error when the base flow is not constant, known as a polynomial aliasing error: the stronger the shear $|M_0'|$, the larger the aliasing error. In principle, the instability associated with this aliasing error can be reduced by decreasing the mesh size or increasing the polynomial order, see (Hesthaven and Warburton 2008, § 5.3) and references therein.

However, it is known that the LEEs with $\boldsymbol{u_0} \neq \boldsymbol{0}$ and an IBC can be unstable at certain frequencies; herein, for example, such instability is encountered in the GIT around 1 kHz. At such an unstable frequency, increasing the resolution of the spatial discretization reduces the numerical dissipation, which destabilizes the numerical solution. Hence, in the presented results, the mesh size and the value of δ result from an empirical trade-off between damping the physical instability (if any) and damping the polynomial aliasing instability.

Post-processing A polychromatic source

$$p_s(t) = \sum_{f_s \in I} \sin(2\pi f_s t)$$

is used, and each frequency is then separated at the post-processing stage using a sixth-order recursive band-pass filter designed and applied using the MATLAB® Signal Processing Toolbox™ (functions `designfilt` and `filter`). The filtered pressure signals are then used to compute root-mean-square (RMS) values p_{RMS} at each frequency and microphone locations along the bottom wall. The decibel (dB) values are computed with

$$p_{\mathrm{dB}} = 20 \log_{10}(p_{\mathrm{RMS}}) + C,$$

where the constant C is chosen so that $p_{\mathrm{dB}}(x = 0)$ matches the experimental value at the reference microphone. (Since the numerical scheme is linear, decibel values are indeed defined up to an additive constant.) The simulation is performed over 80 periods of the lowest frequency and convergence of the RMS value is checked.

6.3.3 Grazing Flow Impedance Tube (GFIT)

Following the three-step methodology described in Section 6.1.3 discrete models $\tilde{\beta}$ are built to match the values identified in the GFIT at $M_{\mathrm{avg}} = 0$ and $M_{\mathrm{avg}} = 0.271$, see Table 6.2.

$M_{\mathbf{avg}} = 0$ case The physical model (6.1) with coefficients given by (6.3,6.5) provides a fair initial point for the nonlinear least-squares optimization of step 1, the output of which is plotted in Figure 6.5. The optimized model accounts for the resistance increase at 0.4 kHz and exhibits a high frequency behavior close to that of the non-optimized model (not plotted), with anti-resonances located around the approximate values

$$f_n = \frac{nc_0}{2l_c}.$$

The output of step 2, i.e. the discrete oscillatory-diffusive representation of the physical model obtained using a linear least-squares optimization, is therefore satisfactory. In step 3, it is used as an initial guess to build the final discrete model $\tilde{\beta}_A$ (the time delay $\tilde{\tau}$ is not optimized) shown in Figure 6.5. A large number of poles, namely three pairs of oscillatory poles s_n and two high frequency diffusive poles ξ_k, have been chosen to build a broadband approximation.

The corresponding SPLs along the lower wall are given in Figure 6.6 for two choices of N_ψ to illustrate the impact of the delay discretization: a value of $N_\psi = 4$ is sufficient here. The agreement with experimental pressure measurements is satisfactory, the largest error occurring at 1.4 kHz. However, based on the plot of $|\hat{\beta}_{\rm id}|$ given at the bottom left of Figure 6.5, this point appears to be an outlier. To confirm this, the SPLs obtained with the identified impedance values are also given. They are computed using *six* proportional-integral-derivative (PID) impedance models

$$\hat{z}_{{\rm PID},i}(s) = d_{0,i}s^{-1} + d_{1,i} + d_{2,i}s$$
$$z_{{\rm PID},i}(t) = d_{0,i}\,H(t) + d_{1,i}\,\delta(t) + d_{2,i}\,\delta' \quad (i \in [\![1,6]\!])\,,$$

each chosen so that

$$\hat{z}_{{\rm PID},i}({\rm j}2\pi f_i) = \hat{z}_{\rm id}({\rm j}2\pi f_i).$$

The plot shows that at 1.4 kHz the tuned PID model also exhibit a significant error.

Remark 6.6 (Time-domain computation of PID models). The time-domain computation of the first two terms of the convolution $z_{{\rm PID},i} \star u$, namely

$$(d_{0,i}\,H + d_{1,i}\,\delta) \star u$$

is done using one additional variable exactly as in (6.15) with $\tilde{\tau} = 0$, i.e.

$$(d_{0,i}\,H + d_{1,i}\,\delta) \star u(t) = d_{0,i}\varphi(t,0) + d_{1,i}\,u(t).$$

The remaining derivative term is interpreted as a strong derivative, i.e.

$$\delta' \star u(t) = \frac{{\rm d}u}{{\rm d}t}(t), \tag{6.20}$$

which is already computed by the employed time-integration scheme so that only a modification of the global mass matrix "M" is required, see Appendix F. Note that, mathematically, $\delta' \star u$ is the weak derivative of u so that the identity (6.20) requires $u(0) = 0$, see (A.4).

$M_{\mathbf{avg}} = 0.271$ **case** The identified values exhibit a strong resistance increase compared to the no flow case. Here, step 1 requires some care: the optimization of the physical model coefficients (6.1) is strongly dependent on the initial point, in stark contrast to the other three cases considered in this paper. A contributing factor to this sensitivity is the lack of anti-resonance in the experimental data, which stops at 2.6 kHz. Figure 6.7 plots an optimized model that exhibits two anti-resonances, obtained by doubling l_c in the initial guess (6.1,6.3,6.5). Additional experimental data would be needed to validate this model above 2.6 kHz. This sensitivity is also exhibited by step 3. If the time delay $\tilde{\tau}$ is optimized, it is greatly reduced (i.e. $\tilde{\tau} \ll \tau$) thus modifying the high frequency behavior. To illustrate this point, Figure 6.7 shows two discrete models. The model $\tilde{\beta}_C$ is obtained by keeping l_c to its physical value in the initial guess of step 1, choosing only one pair of oscillatory poles s_n in step 2, and optimizing on $\tilde{\tau}$ in step 3. It provides an adequate approximation of the experimental data but a poor high frequency behavior, linked to its negligible delay $\tilde{\tau} \simeq \tau/54$. The model $\tilde{\beta}_B$ is obtained by using the physical model shown in Figure 6.7 during step 1, choosing three pairs of oscillatory poles s_n and one high frequency diffusive pole ξ_k in step 2, and keeping $\tilde{\tau}$ constant in step 3.

Figure 6.8 plots the computed SPL distributions. The dotted curves enable to check the relevance of the identified impedance values. The strongest disparities are obtained below 1 kHz where the measurements suggest the presence of a longitudinal resonance not modeled with our non-reflecting outlet, also noticeable in the no flow case, see Figure 6.6. At these low frequencies, the fidelity of the SPLs obtained with $\tilde{\beta}_B$ and $\tilde{\beta}_C$ is therefore bound to be limited. Although the TDIBC B is significantly more expensive than C, both lead to similar SPLs with no significant discrepancies. The time delay of $\tilde{\beta}_C$ is negligible on the considered frequency range so that the minimal value $N_\psi = 2$ is already too large, as shown by the value of $\mathrm{PPW}_{\tilde{\tau}}$.

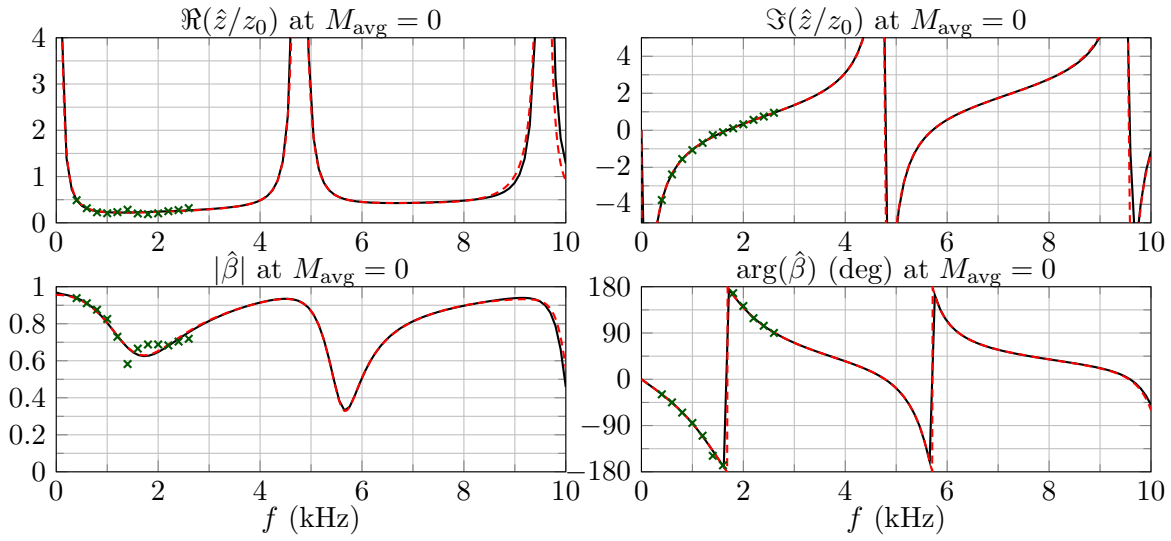

Figure 6.5. Impedance $\hat{z}$ and reflection coefficient $\hat{\beta}$. (×) $\hat{z}_{\text{id}}/z_0$ identified with the methodology described in Section 6.3.1. MP liner in the GFIT at $M_{\text{avg}} = 0$ and 120 dB. (Primus et al. 2013, Fig. 12) (——) $\hat{z}_{\text{MP}}/z_0$ (6.1) with optimized coefficients $\sigma_p^{-1}a_0 = 2.221 \times 10^{-14}$, $\sigma_p^{-1}a_{1/2} = 2.518 \times 10^{-3}\,\text{s}^{1/2}$, $\sigma_p^{-1}a_1 = 3.408 \times 10^{-5}\,\text{s}$, $\sigma_c^{-1} = 1.107$, $b_0 = 1.750 \times 10^{-2}$, $b_{1/2} = 2.321 \times 10^{-4}\,\text{s}^{1/2}$, and $b_1 = 1.037 \times 10^{-4}\,\text{s}$; time delay $\tau = 2b_1 = 2.075 \times 10^{-4}\,\text{s}$. (----) TDIBC $\hat{\tilde{\beta}}_A$: $N_\varphi = 8$ poles ($N_\xi = 2$, $N_s = 6$), $(2\pi)^{-1}\max(\xi_k, |s_n|) = 1.008 \times 10^1\,\text{kHz}$, and $\tilde{\tau} = 2.075 \times 10^{-4}\,\text{s}$. (This curve assumes that the time delay term $e^{-2\pi\text{j}f\tilde{\tau}}$ is perfectly approximated, see Remark 2.46.)

6.3.4 Grazing Incidence Tube (GIT)

$M_{\text{avg}} = 0$ case Step 1 delivers an adequate set of coefficients for the physical model (6.1), see Figure 6.9. The model $\tilde{\beta}_D$ is obtained by choosing the first two pairs of oscillatory poles s_n in step 2 and optimizing the time delay $\tilde{\tau}$ in step 3 (although it can be kept constant as well). The slight decay of the physical model at high frequency is linked to a small but non-null diffusive part that can be captured by adding diffusive poles ξ_k to $\tilde{\beta}_D$. However, this is not needed here in view of the computed SPLs shown in Figure 6.10. Compared to the MP liner considered in Section 6.3.3, both a higher delay and a higher maximum frequency lead to a sensible increase in N_ψ.

$M_{\text{avg}} = 0.4$ case The identified impedance values display a very low resistance within $[0.7, 1.1]$ kHz and the shape of $|\hat{\beta}_{\text{id}}|$ suggests the presence of noise in the data, see the bottom left of Figure 6.11, as one may expect due to the high value of M_{avg}. The output of step 1 is sensitive to the chosen experimental points since the physical model (6.1) cannot fit both the low and high resistance regions, namely $[0.7, 1.1]$ kHz and $[2.3, 3]$ kHz. However, step 1 is not sensitive to the initial guess provided that the chosen data points cover the anti-resonance. Additionally, the 1 kHz value is best removed since it leads to an instability with the LEEs as shown in the dotted curve at the top right of Figure 6.12, and investigated in (Burak et al. 2009, § VI.B.2). (Including the 1 kHz point in the optimization process has been found to systematically lead to an unstable pole, i.e. $\Re(s_n) > 0$ or $\xi_k < 0$.) Due to the shortcomings of the physical model, step 3 has a tendency to overfit the experimental data, so that we do not optimize on the delay $\tilde{\tau}$ during step 3.

The discrete model $\tilde{\beta}_E$, plotted in Figure 6.11, is obtained by using only 2 oscillatory poles s_n and excluding the data points in/at $[0.7, 0.8]$, $[1, 1.4]$, 1.8, and $[2.1, 2.3]$ kHz. Figure 6.12 shows that $\tilde{\beta}_E$ compares favorably to the experimental pressure measurements. The increased

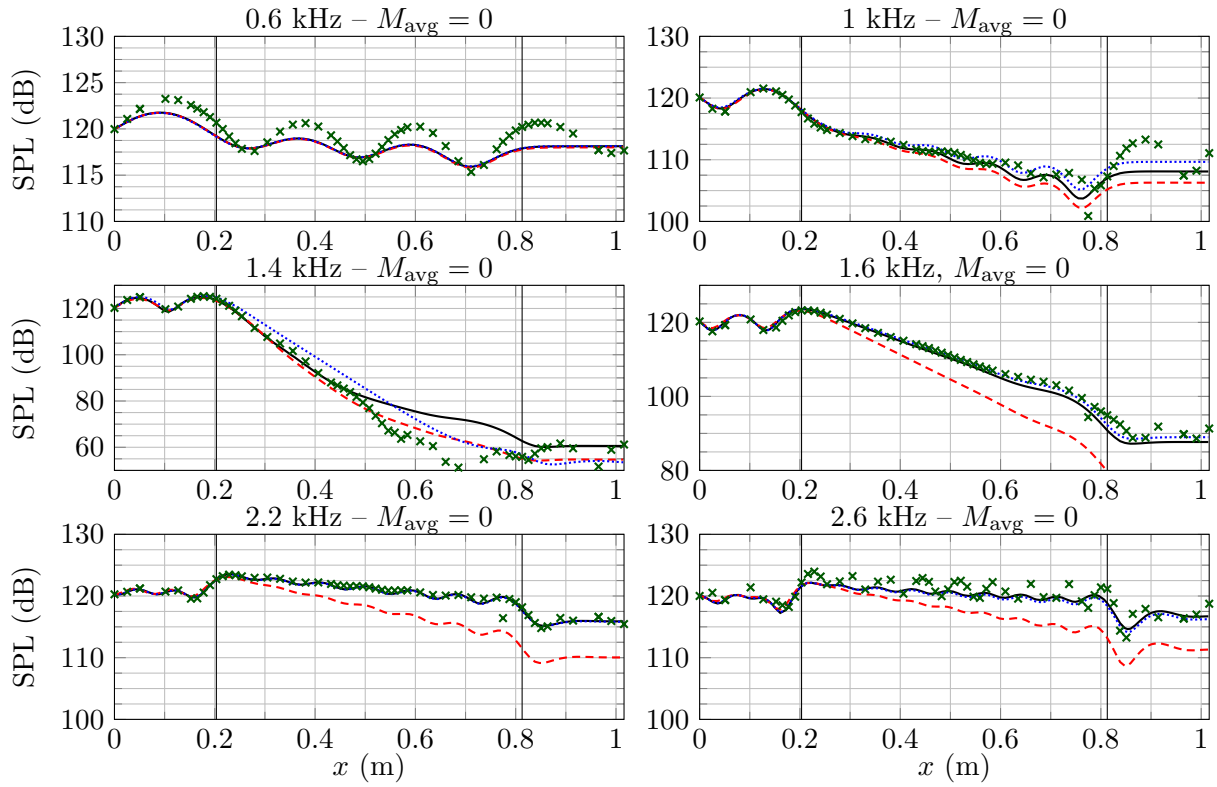

Figure 6.6. RMS values of acoustic pressure p_{RMS} on the lower wall $y = 0$ (see Figure 6.4). DG4-RKF84-$\mathcal{B}$-flux on 110 triangles (1100 nodes), CFL = 0.85. (——) TDIBC $\tilde{\beta}_A$ with $N_\psi = 4$ so that $\text{PPW}_{\tilde{\tau}}(2.6\,\text{kHz}) = 7.42$. (- - - -) TDIBC $\tilde{\beta}_A$ with $N_\psi = 2$ so that $\text{PPW}_{\tilde{\tau}}(2.6\,\text{kHz}) = 3.71$. (·····) Six proportional–integral–derivative TDIBCs $\tilde{\beta}_{\text{PID}}$, each matching the identified impedance at one frequency only. (×) MP liner in the GFIT at $M_{\text{avg}} = 0$ and 120 dB. (Primus et al. 2013)

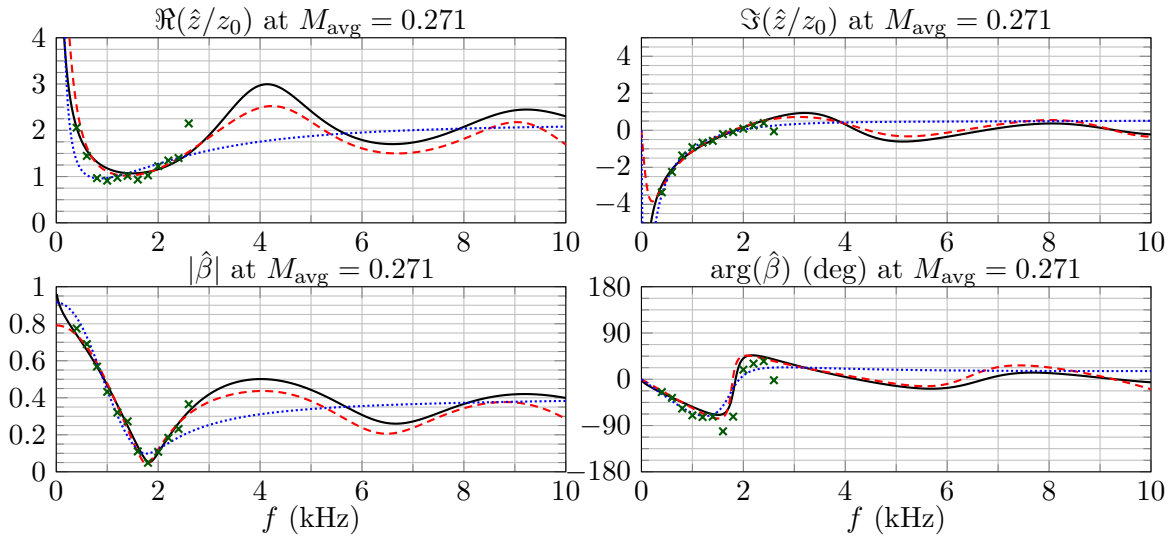

Figure 6.7. Impedance $\hat{z}$ and reflection coefficient $\hat{\beta}$. (×) $\hat{z}_{\text{id}}/z_0$. MP liner in the GFIT at $M_{\text{avg}} = 0.271$ and 120 dB. (Primus et al. 2013) (——) $\hat{z}_{\text{MP}}/z_0$ (6.1) with optimized coefficients $\sigma_p^{-1}a_0 = 2.220 \times 10^{-14}$, $\sigma_p^{-1}a_{1/2} = 2.220 \times 10^{-14}\,\text{s}^{1/2}$, $\sigma_p^{-1}a_1 = 2.220 \times 10^{-14}\,\text{s}$, $\sigma_c^{-1} = 2.116$, $b_0 = 2.220 \times 10^{-14}$, $b_{1/2} = 7.67 \times 10^{-3}\,\text{s}^{1/2}$, and $b_1 = 8.494 \times 10^{-5}\,\text{s}$; $\tau = 1.699 \times 10^{-4}\,\text{s}$. (- - - -) TDIBC $\hat{\tilde{\beta}}_B$: $N_\varphi = 7$ poles ($N_\xi = 1$, $N_s = 6$), $(2\pi)^{-1}\max(\xi_k, |s_n|) = 1.203 \times 10^1$ kHz, and $\tilde{\tau} = 1.699 \times 10^{-4}\,\text{s}$. (·····) TDIBC $\hat{\tilde{\beta}}_C$: $N_\varphi = 2$ poles ($N_\xi = 0$, $N_s = 2$), $(2\pi)^{-1}\max(\xi_k, |s_n|) = 1.136$ kHz, and $\tilde{\tau} = 3.101 \times 10^{-6}\,\text{s}$. (The last two curves assume that the time delay term $e^{-2\pi\mathrm{j}f\tilde{\tau}}$ is perfectly approximated, see Remark 2.46.)

resistance at 1 kHz compared with the identified value reduces the instability, although not enough to fit the experiment. The discrepancy at 3 kHz, since it is also obtained with the identified value, could be explained by the presence of higher-order modes in the experiment, which can be assessed using the cut-off frequency of a hard walled duct with uniform flow, given by

$$c_0(2L_y)^{-1}\sqrt{1 - M_{\text{avg}}^2} = 3.01\,\text{kHz}.$$

The discrete model $\tilde{\beta}_F$ is obtained by excluding the data points in/at $[0.7, 1.2]$, 1.8, and $[2.1, 2.3]$ kHz. Compared to $\tilde{\beta}_E$, the addition of one pair of oscillatory poles s_n and two high frequency diffusive poles ξ_k leads to an overfit that significantly alter the high frequency behavior, see Figure 6.11. However, the corresponding SPLs are satisfactory, especially at 3 kHz. Since the delay of both models is close, they share a common value of N_ψ.

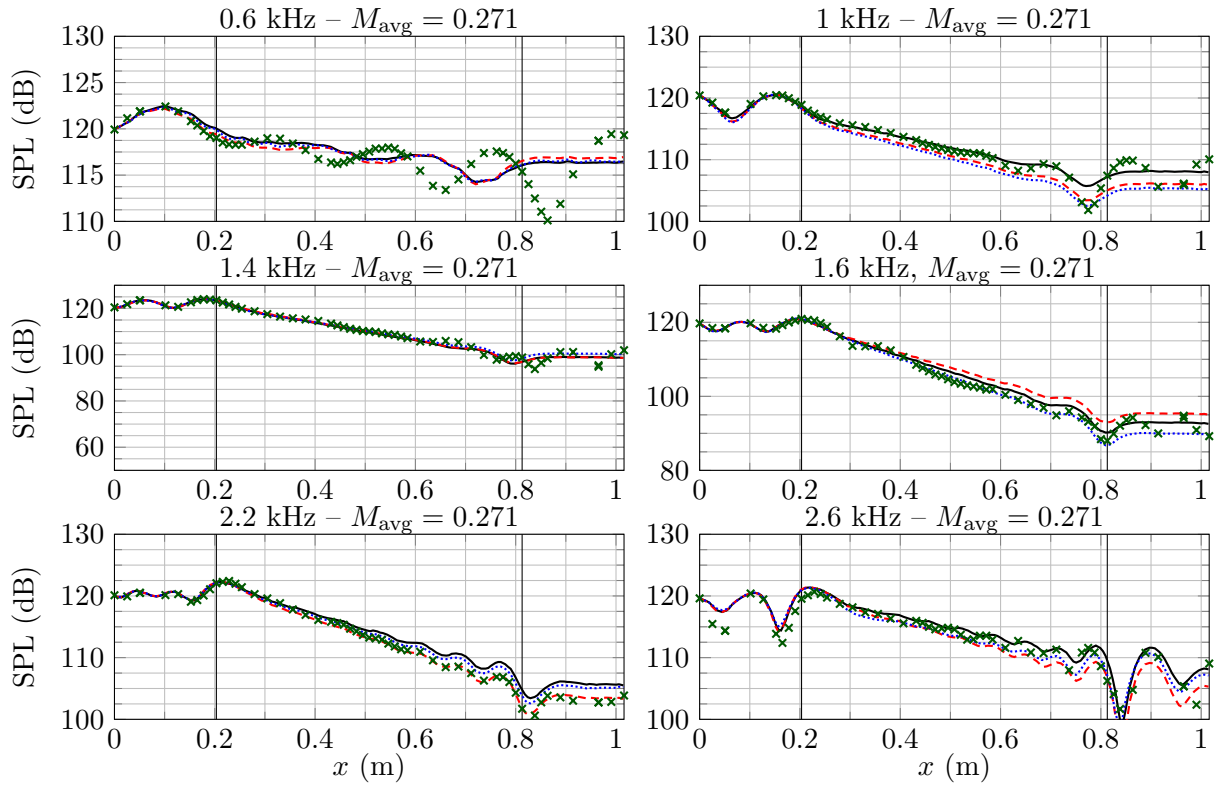

Figure 6.8. RMS values of acoustic pressure p_{RMS} on the lower wall $y = 0$. DG4-RKF84-$\mathcal{B}$-flux on 326 triangles (3260 nodes), CFL = 0.85. Base flow (6.19) with $M_{\text{avg}} = 0.271$ and $\delta = 0.2$. (——) TDIBC $\tilde{\beta}_B$ with $N_\psi = 3$ so that $\text{PPW}_{\tilde{\tau}}(2.6\,\text{kHz}) = 6.79$. (- - - -) TDIBC $\tilde{\beta}_C$ with $N_\psi = 2$ so that $\text{PPW}_{\tilde{\tau}}(2.6\,\text{kHz}) = 248$. (·····) Six TDIBCs $\tilde{\beta}_{\text{PID}}$ with $\delta = 0.25$. (×) MP liner in the GFIT at $M_{\text{avg}} = 0.271$ and 120 dB. (Primus et al. 2013)

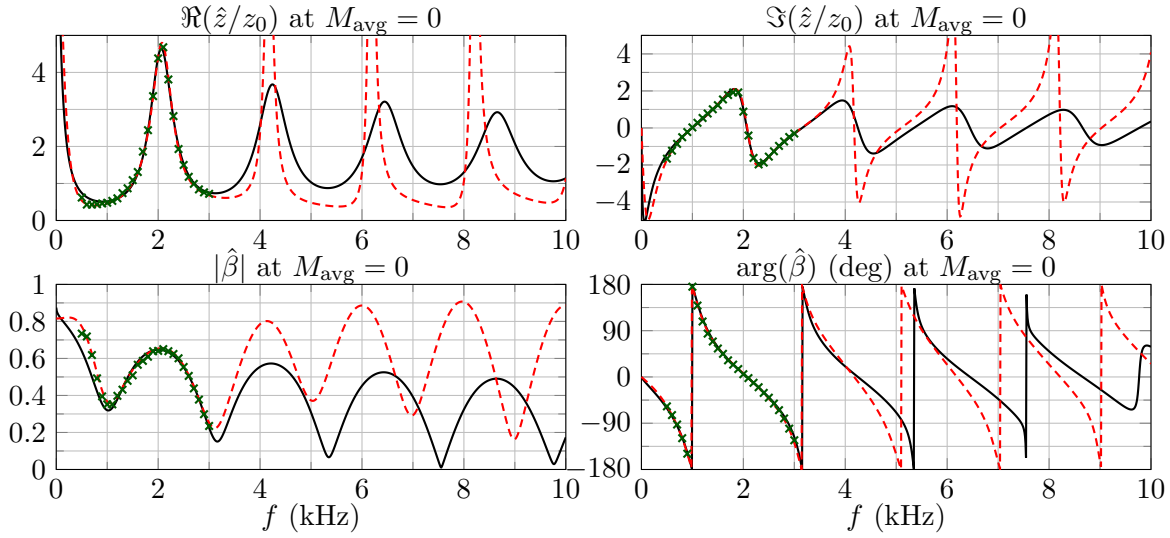

Figure 6.9. Impedance $\hat{z}$ and reflection coefficient $\hat{\beta}$. (×) $\hat{z}_{\text{id}}/z_0$. CT57 liner in the GIT at $M_{\text{avg}} = 0$ and 130 dB. (Jones et al. 2005) (——) $\hat{z}_{\text{CT}}/z_0$ (6.1) with optimized coefficients $\sigma_c^{-1} = 1.728$, $b_0 = 1.161 \times 10^{-1}$, $b_{1/2} = 3.413 \times 10^{-3}\,\text{s}^{1/2}$, and $b_1 = 2.207 \times 10^{-4}\,\text{s}$; $\tau = 4.412 \times 10^{-4}\,\text{s}$. (----) TDIBC $\hat{\tilde{\beta}}_D$: $N_\varphi = 4$ poles ($N_\xi = 0$, $N_s = 4$), $(2\pi)^{-1}\max(\xi_k, |s_n|) = 5.432\,\text{kHz}$, and $\tilde{\tau} = 4.799 \times 10^{-4}\,\text{s}$. (This curve assumes that the time delay term $e^{-2\pi \text{j} f\tilde{\tau}}$ is perfectly approximated, see Remark 2.46.)

$(\tilde{s}_n, -\tilde{\xi}_k)_{n,k}$ $(\text{rad}.s^{-1})$	$\tilde{r}_{1,n}, \tilde{\mu}_{1,k}$	$\tilde{r}_{2,n}, \tilde{\mu}_{2,k}$
$\tilde{\beta}_A$	$\tilde{\beta}_\infty$ =1	$\tilde{\tau}$ =2.074709e-04 s
-9.425004e+04	4.399745e+05	-3.301477e+05
-1.005288e+05	-4.844596e+05	3.648366e+05
-6.590198e+03+8.091231e+03i	-3.316669e+03+1.245272e+03i	3.034471e+03-1.360501e+03i
-3.313575e+03+3.441899e+04i	-2.597563e+03+2.012662e+03i	2.246072e+03-1.972699e+03i
-2.074806e+03+6.332235e+04i	-2.161554e+03+1.610479e+03i	1.750988e+03-1.684290e+03i
$\tilde{\beta}_B$	$\tilde{\beta}_\infty$ =1	$\tilde{\tau}$ =1.698885e-04 s
-4.397915e+04	-3.896423e+04	9.305033e+03
-9.339632e+03+8.499373e+03i	-2.058287e+03-2.722431e+03i	-1.203382e+03-2.923788e+03i
-1.645826e+04+3.974646e+04i	-7.781838e+03-3.535171e+03i	-8.796038e+02+3.204374e+02i
-2.106499e+04+7.256816e+04i	-1.507929e+04-1.588215e+04i	-1.536644e+03+7.662377e+02i
$\tilde{\beta}_C$	$\tilde{\beta}_\infty$ =1	$\tilde{\tau}$ =3.100751e-06 s
-5.748740e+03+4.228554e+03i	-1.010084e+05+2.101821e+05i	1.005155e+05-2.103401e+05i
$\tilde{\beta}_D$	$\tilde{\beta}_\infty$ =0.5	$\tilde{\tau}$ =4.799390e-04 s
-3.816516e+03+4.734560e+03i	-7.194232e+02-5.447907e+02i	1.625807e+03+9.996580e+01i
-2.765741e+04+2.000290e+04i	-7.179701e+03-7.336684e+03i	1.614688e+04+1.930627e+04i
$\tilde{\beta}_E$	$\tilde{\beta}_\infty$ =0.7	$\tilde{\tau}$ =5.099183e-04 s
-9.424902e+04+3.641784e+04i	-7.932877e+04-1.495889e+05i	5.737738e+04+8.853810e+04i
$\tilde{\beta}_F$	$\tilde{\beta}_\infty$ =5.888134e-01	$\tilde{\tau}$ =5.217335e-04 s
-6.414157e	9.506538e+04	-1.096633e+04
-2.051627e+04	-1.320127e+05	1.486746e+04
-4.849574e+03+6.072352e+03i	-1.457643e+03+3.397179e+04i	5.526842e+02+7.586494e+02i
-6.618336e+03+1.885015e+04i	3.599154e+03+3.495625e+03i	-4.862369e+02+5.032293e+02i

Table 6.2. TDIBCs (6.11) obtained in Section 6.3. Only poles in the upper half-plane $\{s \,|\, \Im(s) \geq 0\}$ are given (the full set is obtained by complex conjugation).

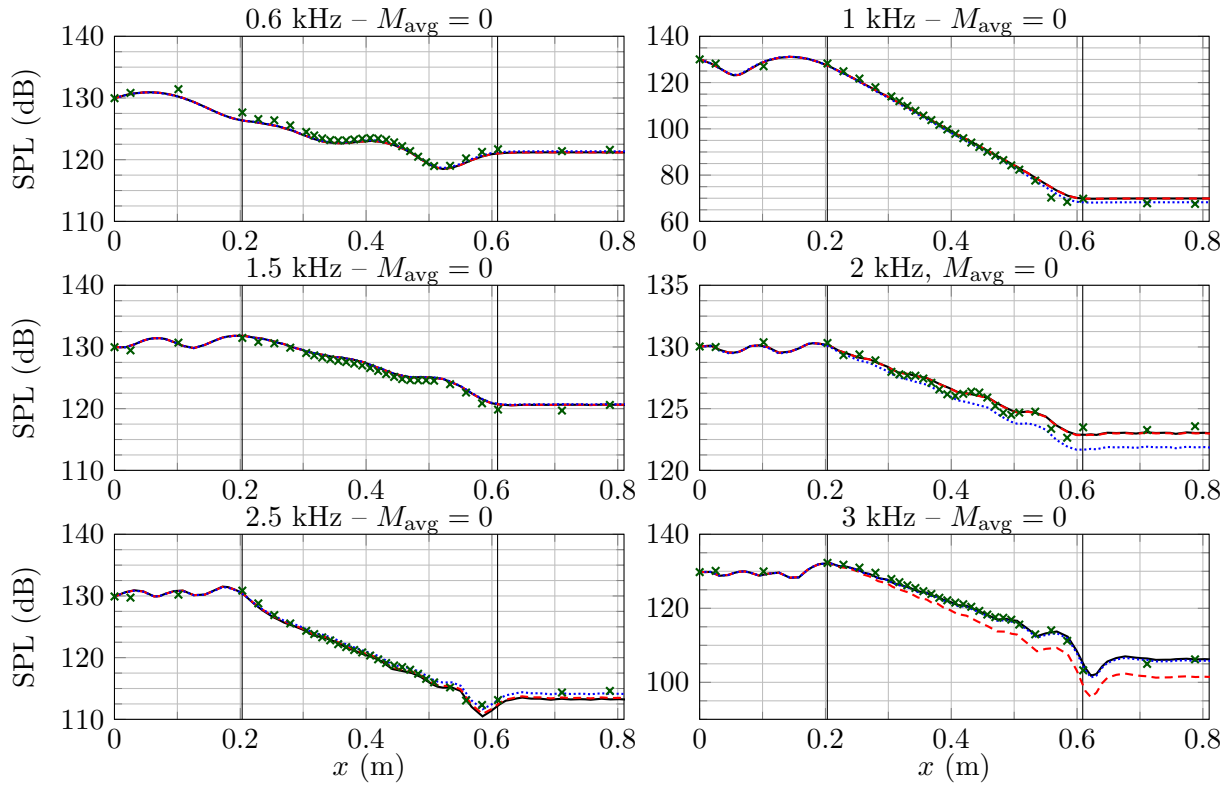

Figure 6.10. RMS values of acoustic pressure p_{RMS} on the lower wall $y = 0$. DG4-RKF84-$\mathcal{B}$-flux on 52 triangles (520 nodes), CFL = 0.85. (——) TDIBC $\tilde{\beta}_D$ with $N_\psi = 8$ so that $\text{PPW}_{\tilde{\tau}}(3\,\text{kHz}) = 5.56$. (----) TDIBC $\tilde{\beta}_D$ with $N_\psi = 6$ so that $\text{PPW}_{\tilde{\tau}}(3\,\text{kHz}) = 4.17$. (·····) Six TDIBCs $\tilde{\beta}_{\text{PID}}$ with CFL = 0.84. (×) CT57 liner in the GIT at $M_{\text{avg}} = 0$ and 130 dB. (Jones et al. 2005, Tab. 3)

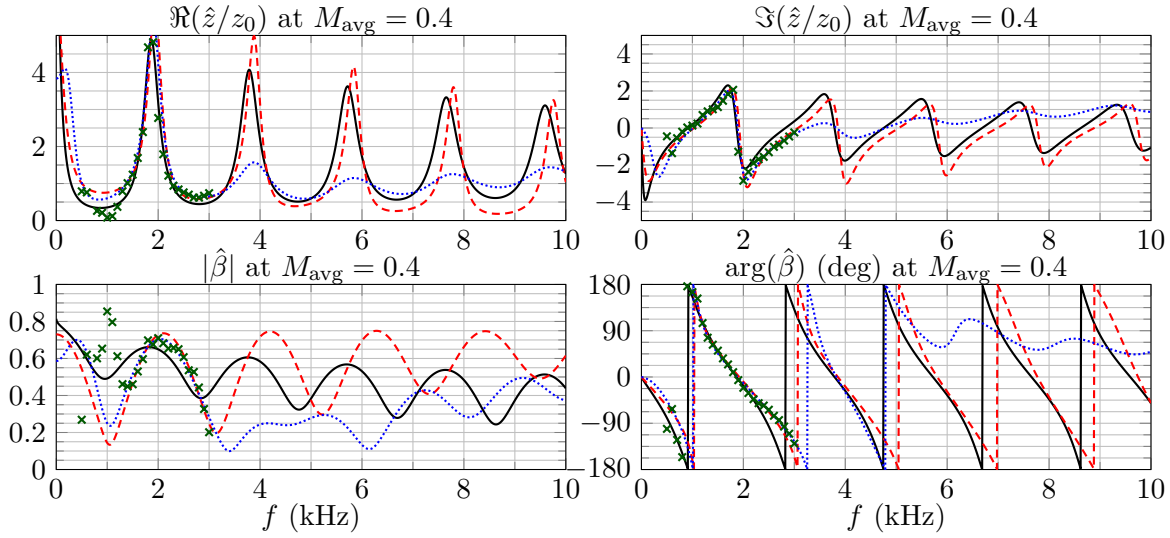

Figure 6.11. Impedance $\hat{z}$ and reflection coefficient $\hat{\beta}$. (×) $\hat{z}_{\text{id}}/z_0$. CT57 liner in the GIT at $M_{\text{avg}} = 0.4$ and 130 dB. (Jones et al. 2005) (——) $\hat{z}_{\text{CT}}/z_0$ (6.1) with optimized coefficients $\sigma_c^{-1} = 1.398$, $b_0 = 1.442 \times 10^{-1}$, $b_{1/2} = 1.956 \times 10^{-3}\,\text{s}^{1/2}$, and $b_1 = 2.550 \times 10^{-4}\,\text{s}$; $\tau = 5.099 \times 10^{-4}\,\text{s}$. (----) TDIBC $\hat{\tilde{\beta}}_E$: $N_\varphi = 2$ poles ($N_\xi = 0$, $N_s = 2$), $(2\pi)^{-1}\max(\xi_k, |s_n|) = 1.608 \times 10^1\,\text{kHz}$, and $\tilde{\tau} = 5.099 \times 10^{-4}\,\text{s}$. (·····) TDIBC $\hat{\tilde{\beta}}_F$: $N_\varphi = 6$ poles ($N_\xi = 2$, $N_s = 4$), $(2\pi)^{-1}\max(\xi_k, |s_n|) = 3.180\,\text{kHz}$, and $\tilde{\tau} = 5.217 \times 10^{-4}\,\text{s}$. (The last two curves assume that the time delay term $e^{-2\pi\text{j}f\tilde{\tau}}$ is perfectly approximated, see Remark 2.46.)

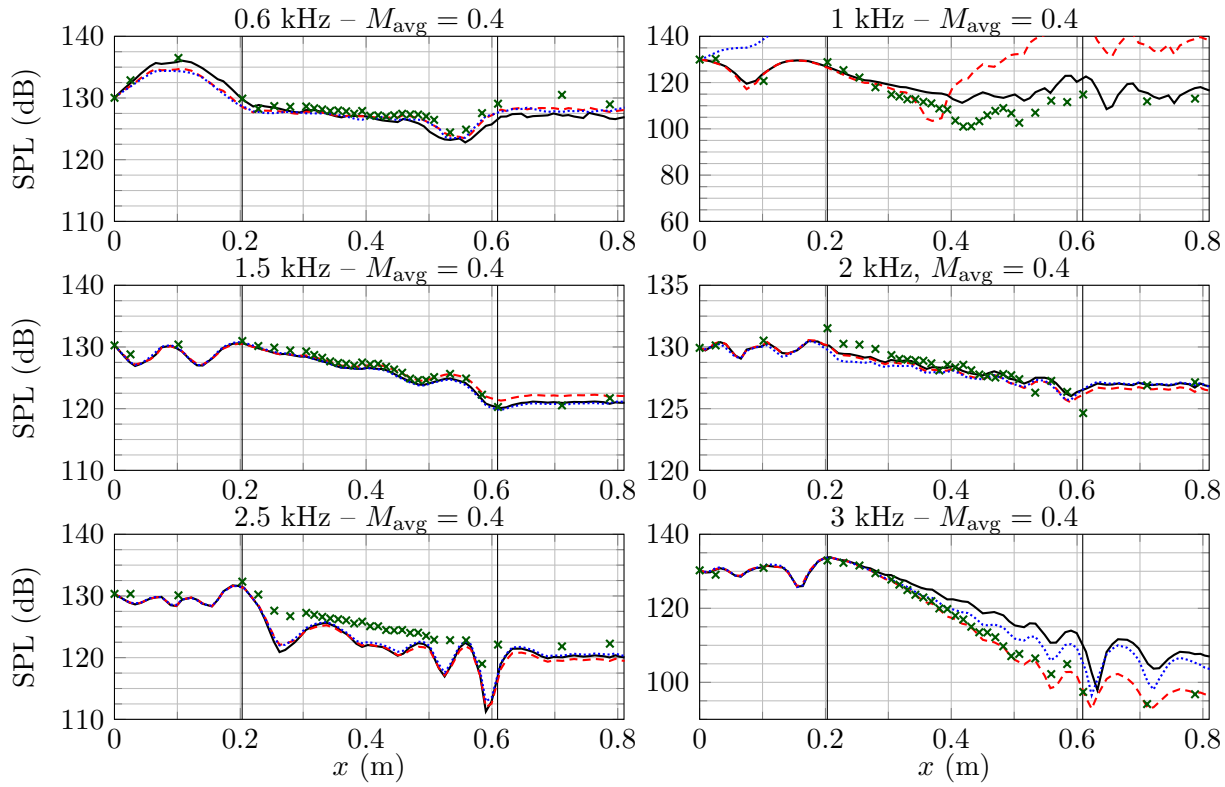

Figure 6.12. RMS values of acoustic pressure p_{RMS} on the lower wall $y = 0$. DG4-RKF84-$\mathcal{B}$-flux on 106 triangles (1060 nodes), CFL = 0.85. Base flow (6.19) with $M_{\text{avg}} = 0.4$ and $\delta = 0.2$. (——) TDIBC $\tilde{\beta}_E$ with $N_\psi = 8$ so that $\text{PPW}_{\tilde{\tau}}(3\,\text{kHz}) = 5.23$. (----) TDIBC $\tilde{\beta}_F$ with $N_\psi = 8$ so that $\text{PPW}_{\tilde{\tau}}(3\,\text{kHz}) = 5.11$. (·····) Six TDIBCs $\tilde{\beta}_{\text{PID}}$ with $\delta = 0.26$. (×) CT57 liner in the GIT at $M_{\text{avg}} = 0.4$ and 130 dB. (Jones et al. 2005, Tab. 8)

Conclusion

Summary

The summary of this dissertation is provided below as answers to the questions formulated in the introduction.

(a) What is the mathematical structure of physical impedance models?

This question has been answered in two steps, each one corresponding to a chapter in Part I.

Section 1.1 defined admissibility conditions for both linear and nonlinear IBCs using system theory, where many strong results are available, such as Proposition 1.8 and 1.14. These two propositions mean that the admissibility of a linear IBC is fully characterized by its Laplace transform, which must be either positive-real (impedance $\hat{z}$ and admittance $\hat{y}$) or bounded-real (reflection coefficient $\hat{\beta}$).

Linear physical models for acoustical liners, recalled in Section 1.2, turn out to have irrational Laplace transforms as they exhibit terms such as $\sqrt{s}$ or $\coth\sqrt{s}$, linked to visco-thermal dissipation, see e.g. (1.19) and (1.25). The derivation of time-local realizations of these models has been carried out in Section 2.4, by relying on the representation theorems derived in Section 2.1.2 whose application has been illustrated in Section 2.1.4 on basic examples. The derived realizations, see e.g. (2.62) for the CT liner model, consists in the composition of two components:

- a realization of the oscillatory-diffusive parts of the model through an ODE on an infinite dimensional state φ, see Section 2.1.3;
- a realization of the time delay through a monodimensional transport equation on ψ, recalled in Section 2.3.

An intuitive physical interpretation of each component has been provided in Table 2.1.

(b) How does the IBC (1) affect well-posedness and stability?

The discussion of well-posedness and stability has been done in Part II using energy methods.

The definition of classes of boundary conditions suitable for the LEEs has been discussed in Chapter 3 using the theory of Friedrichs system. IBCs that are admissible in the sense of Section 1.1 naturally yield a priori energy estimates in spacetime, which gives uniqueness. The literature review carried out in Section 3.2 has shown that although these estimates are indeed a crucial part of existing proofs of well-posedness, they are theoretically not sufficient since additional technical conditions are required. Section 3.4 has highlighted that these conditions exclude non-smooth geometries such as the flow duct considered in the applications of Chapter 6, even with an elementary proportional IBC. However, these technical difficulties stem from the

presence of a base flow, i.e. from the current state of the theory of Friedrichs systems, not from the proposed definition of admissible IBC.

Chapter 4 has dealt with the no flow case, i.e. the wave equation, where the focus is on the IBC. The asymptotic stability of the multidimensional wave equation coupled with the IBC (4.4), which consists in the addition of distinct physically-motivated positive-real components, has been proven. The method of proof consists in formulating an abstract Cauchy problem on an extended state space using a realization of the impedance, be it finite or infinite-dimensional. The asymptotic stability of the corresponding strongly continuous semigroup of contractions is then obtained by verifying the sufficient spectral conditions of the ABLV theorem.

(c) How to discretize an IBC?

Our answer to this question is spread out over Parts I and III. Let us first recall that, following the terminology introduced in Section 1.3, a discrete TDIBC consists of three components:

1. a discrete impedance model;

2. a numerical algorithm used to evaluate the said discrete model;

3. a coupling method with the considered PDE.

Our answer for each component is as follows.

1. In Section 2.4, discrete models have been *derived from* the representation of physical models of acoustical liners. For example, the representation (2.61) of the CT liner model has led to the discrete model (2.63), which can be interpreted as a delayed multipole model. This derivation has led us to formulating the following remarks.

   - The presented analysis sheds a light on the meaning and applicability of existing multipole models, which so far were only postulated in the literature. The physical interpretation of each component of the discrete model, namely the time delay and the oscillatory-diffusive part, has been given in Table 2.1.
   - Practically, the presented analysis suggests an elementary way of computing the poles and the weights of a derived multipole model, using the methods given in Section 2.2.
   - As a rule, a different physical model is likely to lead to a different discrete model. This contrasts with a one-size-fits-all approach, where one numerical model is postulated and applied regardless of the material considered.

2. The time-domain computation of the discrete model is done by composing a set of ODEs with a transport equation, which respects the mathematical structure of the model, discussed above in (a). For the discretization of the time delay a criterion based on the PPW (6.14) has proven to be relevant.

3. The analysis given in Section 5.3 has shown the computational interest of a numerical flux based on the scattering operator $\mathcal{B}$ (1.14), namely the so-called $\mathcal{B}$-flux (5.14,5.39), over fluxes based on the impedance and admittance, namely the $\mathcal{Z}$-flux (5.14,5.35) and the $\mathcal{Y}$-flux (5.14,5.37). This has been illustrated in Chapter 6 with Figure 6.3 that shows the impact of the incident SPL on the maximum CFL number for an algebraic nonlinear IBC.

(d) What about nonlinear absorption mechanisms?

In Section 1.1, nonlinear definitions of the impedance, admittance, and scattering operator have been given. The standard nonlinear perforation impedance model has been recalled in Section 1.2.3 and the computation of the associated admittance and scattering operators has been discussed in Section 2.4.2. In the algebraic case (2.73), the corresponding admittance and scattering operators are given by (2.74) and (2.75). These expressions have been used used in a numerical impedance tube in Section 6.2, thus showing the relevance of the proposed definitions.

Outlook

We list below some topics for future research that arise from this dissertation.

Physical modeling

The present work shows that TDIBCs benefit from physical knowledge about the impedance. This calls for additional investigations into the suitability of available models in the presence of grazing flow and broadband sources, as well as the inclusion of uncertainties during both identification and simulation.

Additionally, the physical relevance of using a nonlinear impedance model with the LEEs could be investigated, by comparison with experimental data gathered in an impedance tube at high SPL.

Representation of acoustical models

The analysis of Section 2.4.1 has focused on the models (2.58,2.70), which can be interpreted as high or low frequency approximations of (1.19,1.25), see e.g. (1.20,1.26). These approximations are accurate enough in practice, see Figure 1.5. However, whether the complete models (2.58,2.70) admit a computationally relevant time-domain representation remains unanswered.

TDIBC for DDOF liners

Appendix B has provided the OD representation of an impedance model for DDOF liners, following the methodology laid out in Section 2.4. However, none of the derived representations have been used in the numerical applications of this dissertation. These representations could serve as a basis to build a TDIBC suited to DDOF liners.

TDIBCs using Convolution Quadrature

In this dissertation, we have derived multipole models, possibly delayed, from the OD representation of physical models. When such a representation is not available, the convolution can still be computed with the sole knowledge of the Laplace transform using the Convolution Quadrature algorithm (Lubich and Ostermann 1993), see (Hiptmair et al. 2014; Sauter and Schanz 2017). This could constitutes an alternative to multipole models.

Quadrature-based discretization of diffusive representations

The main drawback of the quadrature method proposed in Definition 2.44, as well as any other existing quadrature-based discretization method, is that it does not apply to OD kernels whose diffusive weight μ is less well-behaved, for instance with sharp variations or oscillations, as encountered in e.g. Lemma 2.28 for $a_1 \gg a_{\frac{1}{2}}$, Lemma 2.30, and Lemma 2.37. In these cases, any

method that solely relies on change of variables and quadrature rules breaks down. In principle, circumventing this issue would require to use an adaptative strategy or a method suited to oscillatory integrals. Since MATLAB® `integral` (Shampine 2008) is able to accurately compute $\int e^{-\xi t}\mu(\xi)\mathrm{d}\xi$ for most of the cases encountered in this chapter, an adaptive quadrature algorithm possibly combined with splitting the integration domain may provide a satisfactory answer.

Computation of an integro-differential scattering operator

The nonlinear numerical applications presented in Section 6.2 are restricted to the algebraic scattering operator (2.75), which corresponds to the impedance operator (2.73). For the general case (2.76), formulas (2.78) and (2.79) have been proposed but not considered. The numerical application of these formulas constitutes a perspective of this work.

IBCs with other PDEs

The last two parts of this dissertation have focused on the LEEs.

In the flow duct application presented in Section 6.3, there would be a computational benefit in considering the linearized Navier-Stokes equations instead, since this would mitigate the instabilities encountered at some frequencies. Doing so requires to deal with the diffusion term at the boundary, which is well-known.

The full Navier-Stokes equations should be considered for applications where hydrodynamic phenomena cannot be neglected, such as close to a supersonic fan tip where shocks occur (Astley et al. 2011, § 5.3) or for flow control. For example, the interaction between an impedance wall and a turbulent boundary layer has received scrutiny in recent works such as (Scalo et al. 2015) and (Olivetti et al. 2015). A challenge when dealing with the Navier-Stokes equations is the filtering of the perturbation at the boundary: the impedance models recalled in Section 1.2 apply a priori only to acoustic waves, so that in practice one may desire to separate the "turbulent part" of the perturbation from its "acoustic part". If this filtering is done with a linear time-domain filter Ψ, it can be interpreted as modifying the impedance through

$$z \to \Psi \star z,$$

so that the IBC (1.3) stays locally reacting and it is admissible if and only if $\hat{\Psi}\hat{z}$ is a positive-real function. However, if the filter Ψ has a spatial dependency (e.g. a dependency on a spatial wave number k), then it breaks the locally reacting nature of the IBC.

Asymptotic stability of wave equation with an IBC

Chapter 4 has focused on the asymptotic stability of the wave equation coupled with admissible IBCs drawn from physical models, namely rational impedance in Section 4.3, time-delayed impedance in Section 4.4, standard diffusive impedance (e.g. fractional integral) in Section 4.5, and extended diffusive impedance (e.g. fractional derivative) in Section 4.6. Finally, the invariance of the derived asymptotic stability results under the addition of a derivative term in the impedance has been discussed in Section 4.7. The proofs crucially hinge upon the knowledge of a dissipative realization of the IBC, since it employs the ABLV theorem. By combining these results, asymptotic stability has been obtained for the impedance $\hat{z}$ introduced in Section 4.1 and given by (4.4). This suggests the following perspective of this work, formulated as a conjecture.

Conjecture 6.7. *Assume $\hat{z}$ is positive-real, without isolated singularities on $\mathrm{j}\mathbb{R}$. Then the Cauchy problem (4.2,4.3) is asymptotically stable in a suitable energy space.*

The substitution of "rational positive-real" for "positive-real" yields the result of Section 4.3. Establishing this conjecture using the method of proof used in Chapter 4 entails building a dissipative realization of the impedance operator $u \mapsto z \star u$, i.e. using a suitable infinite-dimensional variant of the positive-real lemma recalled in Theorem 4.22, for instance (Staffans 2002, Thm. 5.3). This result would be sharp, in the sense that is known that exponential stability is not achieved in general (consider for instance $\hat{z}(s) = 1/\sqrt{s}$ that induces an essential spectrum with accumulation point at 0, see Remark 4.49). If this conjecture proves true, then the rate of decay of the solution could also be studied and linked to properties of the impedance $\hat{z}$.

To illustrate this conjecture, let us give two examples of positive-real impedance kernels that are *not* covered by the results of Chapter 4. Both examples arise in physical models and have been used in the numerical applications. The first example is a kernel similar to (4.4), namely

$$\hat{z}(s) = z_0 + z_\tau e^{-\tau s} + z_1 s + \hat{Z}(s) + \int_0^\infty \frac{\mu(\xi)}{s+\xi}\,\mathrm{d}\xi \quad (\Re(s) > 0)\,,$$

where $\tau > 0$, $z_\tau \in \mathbb{R}$, $z_0 \geq |z_\tau|$, $z_1 > 0$, $\hat{Z}$ is a positive-real and proper rational function, and the weight $\mu \in \mathcal{C}^\infty((0,\infty))$ satisfies the condition

$$\int_0^\infty \frac{|\mu(\xi)|}{1+\xi}\mathrm{d}\xi < \infty$$

and is such that $\hat{z}$ is positive-real. When the sign of μ is indefinite the passivity condition (4.65) does not hold, so that this impedance is not covered by the presented results despite the fact that, overall, $\hat{z}$ is positive-real with a realization formally identical to that of the impedance (4.4) defined in Section 4.1.

The second and last example is

$$\hat{z}(s) = z_0 + z_\tau \frac{e^{-\tau s}}{\sqrt{s}},$$

with $z_\tau \geq 0$, $\tau > 0$, and $z_0 \geq 0$ sufficiently large for $\hat{z}$ to be positive-real, specifically

$$z_0 \geq -z_\tau \cos(\tilde{x} + \frac{\pi}{4})\sqrt{\tau/\tilde{x}}$$

where $\tilde{x} \simeq 2.13$ is the smallest positive root of

$$x \mapsto \tan(x + \frac{\pi}{4}) + \frac{1}{2x}.$$

A simple realization can be obtained by combining Sections 4.4 and 4.5, i.e. by delaying the diffusive representation using a transport equation: the convolution then reads, for a causal input u,

$$z \star u = z_0 u + z_\tau \int_0^\infty \chi(t, -\tau, \xi)\,\mathrm{d}\mu(\xi),$$

where φ and μ are defined as in Section 4.5, and for a.e. $\xi \in (0,\infty)$ the function $\chi(\cdot,\cdot,\xi)$ obeys the transport equation (4.41ab) but with $\chi(t,0,\xi) = \varphi(t,\xi)$. So far, the author has not been able to find a suitable Lyapunov functional (i.e. a suitable definition of $\|\cdot\|_H$) for this realization.

Part IV

Appendices

Appendix A

Convolution, Fourier and Laplace transforms

Contents

The purpose of this appendix is to justify why in this dissertation the Laplace transform is used instead of the Fourier transform, often encountered in acoustical works. The first two sections gather key definitions and properties from distribution theory: Section A.1 recalls the common spaces of distributions and the basic properties of the convolution while Section A.2 covers the Fourier and Laplace transforms. The next two sections illustrate the differences between the Fourier and Laplace transforms on examples of interest in acoustics: the expression of physical models in Section A.3 and the formulation of admissibility conditions in Section A.4. Lastly, Section A.5 proves a convergence result used in the representation theorems of Chapter A.

A.1 Distribution theory

Introductions to distribution theory can be found in the following references.

- The translated book (Schwartz 1966) is aimed at physicists and cover, among other topics, distribution theory including the definitions and properties of the Fourier and Laplace transforms.

- The book (Dupraz 1977), only available in French, is similar and also covers both the Fourier and Laplace transforms, with an interest in signal processing.

- The references (Zemanian 1965) and (Beltrami and Wohlers 1966) cover distribution theory with applications to the theory of passive linear systems. (As such, they have been cited many times in Section 1.1.)

- (Gasquet and Witomski 2000) and its translation (Gasquet and Witomski 1999) cover distribution theory including the Fourier transform, with a focus on applications to filtering and signal processing.
- The untranslated book (Bony 2001) covers distribution theory including the Fourier transform, with applications to multidimensional PDEs.

These references cover the elements of distribution theory needed in this dissertation. More in-depth treatments are available in (Hörmander 1990; Schwartz 1978). The purpose of this section is to introduce the notations and spaces used in this dissertation; we refer to the references above for proofs and details.

Definition

The space of distributions of a real variable is denoted $\mathcal{D}'(\mathbb{R})$ and is defined as the topological dual of $\mathcal{C}_0^\infty(\mathbb{R})$ (the notation comes from the fact that $\mathcal{C}_0^\infty(\mathbb{R})$ is also denoted $\mathcal{D}(\mathbb{R})$). The topology on $\mathcal{C}_0^\infty(\mathbb{R})$ relies on the theory of locally convex spaces, but in practice the following sequential characterization of continuity often suffices:

$$u_n \xrightarrow[n\to\infty]{\mathcal{D}'(\mathbb{R})} u \;\Leftrightarrow\; \forall \varphi \in \mathcal{C}_0^\infty(\mathbb{R}),\; u_n(\varphi) \xrightarrow[n\to\infty]{\mathbb{C}} u(\varphi).$$

The quantity $u_n(\varphi)$ is commonly denoted using the duality bracket

$$u_n(\varphi) = \langle u_n, \varphi \rangle_{\mathcal{D}'(\mathbb{R}),\mathcal{C}_0^\infty(\mathbb{R})},$$

which is useful to indicate in which spaces both quantities belongs. The simplest, and historical, example of distribution is the Dirac distribution δ defined as

$$\langle \delta, \varphi \rangle_{\mathcal{D}'(\mathbb{R}),\mathcal{C}_0^\infty(\mathbb{R})} \coloneqq \varphi(0), \tag{A.1}$$

whose shifted variant is

$$\langle \delta(\cdot - \tau), \varphi \rangle_{\mathcal{D}'(\mathbb{R}),\mathcal{C}_0^\infty(\mathbb{R})} = \varphi(\tau).$$

These identities can also be understood by viewing δ as a discrete measure. Any locally integrable function $u \in L^1_{\text{loc}}(\mathbb{R})$ defines a distribution, also denoted u with a slight abuse of notation, such that

$$\langle u, \varphi \rangle_{\mathcal{D}'(\mathbb{R}),\mathcal{C}_0^\infty(\mathbb{R})} = \int_{\mathbb{R}} u(t)\varphi(t)\,\mathrm{d}t.$$

This implies that non locally integrable functions such as $x \mapsto \frac{1}{x}$ do not define distributions directly, which leads to the definitions of the Cauchy principal value and Hadamard finite part.

Spaces

The three following subspaces of $\mathcal{D}'(\mathbb{R})$ are encountered in this dissertation.

- $\mathcal{E}'(\mathbb{R})$, topological dual of $\mathcal{C}^\infty(\mathbb{R})$, is the space of compactly supported distributions. It contains for example δ and any locally integrable function with compact support. (The notation comes from the fact that $\mathcal{C}^\infty(\mathbb{R})$ is also denoted $\mathcal{E}(\mathbb{R})$.)
- The second subspace of interest is $\mathcal{S}'(\mathbb{R})$, the space of tempered distributions. Intuitively, it contains distributions that grows at most like a polynomial at infinity. For example, any polynomial is tempered, $t \mapsto e^{-t}H(t)$ is tempered, but $t \mapsto e^{-t}$ is not tempered. The notation comes from the fact that the space of tempered distributions is the topological dual of $\mathcal{S}(\mathbb{R})$, a subspace of $\mathcal{C}^\infty(\mathbb{R})$ known as the Schwartz space.

- The third space is $\mathcal{D}'_+(\mathbb{R})$, the space of causal distributions, i.e. of distributions whose support in included in $[0,\infty)$. Any locally integrable function such that $u(t)=0$ for a.e. $t<0$ is a causal distribution.

Differentiation

A differentiation can be defined on $\mathcal{D}'(\mathbb{R})$ using the usual differentiation on $\mathcal{C}_0^\infty(\mathbb{R})$ through

$$\left\langle u^{(n)},\varphi\right\rangle_{\mathcal{D}'(\mathbb{R}),\mathcal{C}_0^\infty(\mathbb{R})} \coloneqq (-1)^n \left\langle u,\varphi^{(n)}\right\rangle_{\mathcal{D}'(\mathbb{R}),\mathcal{C}_0^\infty(\mathbb{R})} \quad (n\in\mathbb{N})\,. \tag{A.2}$$

Therefore, since functions in $\mathcal{C}_0^\infty(\mathbb{R})$ are infinitely differentiable, every distribution is infinitely differentiable. The simplest of example is the Dirac distribution, whose successive derivatives are given by

$$\left\langle \delta^{(n)},\varphi\right\rangle_{\mathcal{D}'(\mathbb{R}),\mathcal{C}_0^\infty(\mathbb{R})} = (-1)^n\,\varphi^{(n)}(0),$$

and which is the derivative of the Heaviside function H, i.e.

$$\left\langle H',\varphi\right\rangle_{\mathcal{D}'(\mathbb{R}),\mathcal{C}_0^\infty(\mathbb{R})} = -\left\langle H,\varphi'\right\rangle_{\mathcal{D}'(\mathbb{R}),\mathcal{C}_0^\infty(\mathbb{R})} = \varphi(0) = \langle\delta,\varphi\rangle_{\mathcal{D}'(\mathbb{R}),\mathcal{C}_0^\infty(\mathbb{R})}\,.$$

The differentiation defined by (A.2), known as the *weak differentiation*, is a generalization of the usual, *strong differentiation* in the following sense: if a locally integrable function f has a strong derivative (i.e. a derivative in the usual sense), then it admits a weak derivative and both coincides.

A locally integrable function always admits an infinite number of weak derivatives, even though it may not be differentiable in the strong sense. This is the case for causal functions, which are encountered throughout the dissertation. Let $u\in L^1_{\mathrm{loc}}([0,\infty))$ be a causal function that is $\mathcal{C}^1$ on $[0,\infty)$. We can write u as

$$u(t)=\phi_u(t)H(t)\quad(t\in\mathbb{R})\,,$$

where $\phi_u\in\mathcal{C}^1([0,\infty))$. The strong derivative of u is not defined on $\mathbb{R}$ but only on $\mathbb{R}^*$ and is given by

$$\frac{\mathrm{d}u}{\mathrm{d}t}(t)=\left[\frac{\mathrm{d}\phi_u}{\mathrm{d}t}(t)\right]H(t)\quad(t\in\mathbb{R}^*)\,. \tag{A.3}$$

By contrast, the weak derivative is well-defined in $\mathcal{D}'(\mathbb{R})$ and is given by

$$u' = \left[\frac{\mathrm{d}\phi_u}{\mathrm{d}t}\right]H+\phi_u(0^+)\delta.$$

For convenience, we write this identity with a slight abuse of notation, namely

$$u'(t)=\frac{\mathrm{d}u}{\mathrm{d}t}(t)+u(0^+)\delta(t)\quad(t\in\mathbb{R})\,, \tag{A.4}$$

which emphasizes the difference between the strong and weak derivatives for a causal function u. If $u(0^+)=0$ then the weak derivative u' is a function that coincides with the strong derivative $\frac{\mathrm{d}u}{\mathrm{d}t}$. If $u(0^+)\neq 0$, then u' is not a function anymore: the differentiation of u incurs a loss of regularity. The difference between these two derivatives has practical implications, particularly when using properties of the convolution product. In this case, we will see that ignoring the Dirac term in the right-hand side of (A.4) can lead to mistakes.

Example A.1 (First-order kernel)**.** To illustrate formula (A.4), let us take the example of the causal kernel e_ξ defined by (2.3) and that is used repeatedly in this dissertation. Since e_ξ is not continuous at 0, its strong derivative is only defined on $\mathbb{R}^*$ as

$$\frac{\mathrm{d}e_\xi}{\mathrm{d}t}(t) = -\xi e_\xi(t) = \begin{cases} -\xi e^{-\xi t} & (t > 0) \\ 0 & (t < 0) \end{cases} \quad (t \in \mathbb{R}^*)\,. \tag{A.5}$$

However, since e_ξ is locally integrable on $\mathbb{R}$, it belongs to $\mathcal{D}'(\mathbb{R})$ and is thus infinitely differentiable in $\mathcal{D}'(\mathbb{R})$ with first and second weak derivatives given by

$$\begin{aligned} e_\xi'(t) &= \left(e^{-\xi t}H(t)\right)' = \left(e^{-\xi t}\right)' H(t) + \left(e^{-\xi t}\right) H'(t) = -\xi e_\xi(t) + \delta(t) \\ e_\xi^{(2)}(t) &= -\xi e_\xi'(t) + \delta'(t) = \xi^2 e_\xi(t) - \xi\delta(t) + \delta'(t). \end{aligned} \tag{A.6}$$

Note that each differentiation induces a loss of regularity on the kernel, due to the Dirac terms: starting from a locally integrable function e_ξ, $e_\xi^{(n)}$ is a distribution of order n.

Convolution

If z and u both belong to $L^1(\mathbb{R})$, their convolution product is defined as (Gasquet and Witomski 1999, Chap. 20)

$$z \star u(t) = \int_{\mathbb{R}} z(t-\tau)u(\tau)\,\mathrm{d}\tau \quad (t \in \mathbb{R})\,, \tag{A.7}$$

and is a $L^1(\mathbb{R})$ function such that

$$\|z \star u\|_1 \leq \|z\|_1 \|u\|_1.$$

If additionally both z and u are causal then (A.7) reduces to

$$z \star u(t) = \int_0^t z(t-\tau)u(\tau)\,\mathrm{d}\tau \quad (t \in \mathbb{R})\,, \tag{A.8}$$

so that $z \star u$ is also causal. The identity (A.8) also holds for z and u causal and locally integrable on $[0, \infty)$, in which case $z \star u$ is also causal and locally integrable on $[0, \infty)$.

The convolution product defined above can be extended to the space of distributions either by using the multiplication of distributions $\otimes$ or by density: the definition can be found in the references given above. In this dissertation, we will exclusively use the convolution product in $\mathcal{D}'_+(\mathbb{R})$, which enjoys the following elementary properties:[1]

- if $z, u \in \mathcal{D}'_+(\mathbb{R})$, then $z \star u$ exists and lies in $\mathcal{D}'_+(\mathbb{R})$,
- the convolution in $\mathcal{D}'_+(\mathbb{R})$ is commutative, associative, with identity element δ, i.e.

$$\delta \star u = u.$$

A fundamental property of the convolution is its behavior under weak differentiation, namely

$$(z \star u)^{(n)} = z^{(n)} \star u = z \star u^{(n)}, \tag{A.9}$$

[1] The space $\left(\mathcal{D}'_+(\mathbb{R}), +, \star\right)$ is a commutative ring. However, it is not a field since, for $z \in \mathcal{D}'_+(\mathbb{R})$ given, the convolution equation $z \star u = \delta$ may not have a causal solution u. Consider e.g. $\delta(\cdot - \tau) \star \delta(\cdot + \tau) = \delta$.

which implies another expression of the n-th weak derivative:

$$\delta^{(n)} \star u = u^{(n)}. \tag{A.10}$$

It is crucially important to note that in general (A.9) holds true only for the *weak* derivative. If $u \in L^1_{\mathrm{loc}}([0,\infty))$ is a causal function, we have using (A.4) that

$$(z \star u)' = z \star u' = z \star \left[\frac{\mathrm{d}u}{\mathrm{d}t} + u(0^+)\delta\right] = z \star \frac{\mathrm{d}u}{\mathrm{d}t} + u(0^+)z. \tag{A.11}$$

Example A.2 (First-order kernel)**.** Let us illustrate the practical significance of (A.9) by considering the first-order kernel. For a causal distribution $u \in \mathcal{D}'_+(\mathbb{R})$, the combination of (2.8) and (A.9) yields

$$(e_\xi \star u)' = e'_\xi \star u = -\xi e_\xi \star u + u,$$

so that we recover the ODE followed by φ as defined in Section 2.1.1. However, note that applying (A.9) with the strong derivative instead of the weak one leads to the wrong identity

$$\frac{\mathrm{d}}{\mathrm{d}t}(e_\xi \star u) = \frac{\mathrm{d}}{\mathrm{d}t} e_\xi \star u = -\xi e_\xi \star u.$$

Remark A.3 (Regularization). If we replace z by g, the identity (A.11) is exactly the identity (2.36) encountered in Remark 2.25. Hence, using the notation of this remark, we deduce another expression for the regularization of the convolution operator $u \mapsto h \star u = g \star u'$, namely $\langle T, u\rangle = g \star \frac{\mathrm{d}u}{\mathrm{d}t}$. This regularization therefore consists in replacing the weak derivative u' of a causal input $u \in L^1_{\mathrm{loc}}([0,\infty))$ by the corresponding strong derivative. The typical example of this is encountered in fractional calculus, where, for $\alpha \in (0,1)$,

$$D^{\mathrm{RL}}_\alpha u \coloneqq Y_{1-\alpha} \star u' = (Y_{1-\alpha} \star u)' = \frac{\mathrm{d}}{\mathrm{d}t}(Y_{1-\alpha} \star u) \tag{A.12}$$

is the Riemann-Liouville fractional derivative, while

$$D^{\mathrm{C}}_\alpha u \coloneqq Y_{1-\alpha} \star \frac{\mathrm{d}u}{\mathrm{d}t} \tag{A.13}$$

is the Caputo fractional derivative, see (Matignon 2009). From (A.4), both operations are identical when $u(0^+) = 0$.

Let us close this section of reminders of distribution theory with the following fundamental result that states that linear, continuous, time-invariant operators are convolution operators, and vice-versa. This is a mathematical justification for the role that convolution plays in physical modeling.

Proposition A.4. *Let $\mathcal{Z} : \mathcal{E}'(\mathbb{R}) \to \mathcal{D}'(\mathbb{R})$ be a linear, continuous, time-invariant operator. It can be expressed as $u \mapsto z \star u$, where $z = \mathcal{Z}(\delta) \in \mathcal{D}'(\mathbb{R})$. Conversely, $u \mapsto z \star u$ with $z \in \mathcal{D}'(\mathbb{R})$ defines a linear, continuous, time-invariant operator that maps $\mathcal{E}'(\mathbb{R})$ to $\mathcal{D}'(\mathbb{R})$.*

Proof. First, note that the convolution $z \star u$ is well-defined and belongs to $\mathcal{D}'(\mathbb{R})$ since $h \in \mathcal{D}'(\mathbb{R})$ and $u \in \mathcal{E}'(\mathbb{R})$. The result can be found in (Schwartz 1978, Thm. VI.X) (if $\mathcal{Z}$ commutes with translations, it commutes with differentiation, see the cited proof) and (Beltrami and Wohlers 1966, Thm. 1.18). A lighter version, aimed at physicists, can be found in (Schwartz 1966, § III.3). □

The same results hold true for causal distributions (Beltrami and Wohlers 1966, p. 28): If $\mathcal{Z} : \mathcal{D}'_+(\mathbb{R}) \to \mathcal{D}'_+(\mathbb{R})$ is a linear, continuous, and time-invariant, then it can be expressed as $u \mapsto z \star u$, where $z = \mathcal{Z}(\delta) \in \mathcal{D}'_+(\mathbb{R})$.

A.2 Fourier and Laplace transforms

This section gives the definitions of the Fourier and Laplace transforms used in this dissertation and recalls some properties of the latter.

A.2.1 Fourier transform

If $u \in L^1(\mathbb{R})$, its Fourier transform is defined as (Gasquet and Witomski 1999, § 17.1)

$$\mathcal{F}[u](\omega) = \int_{\mathbb{R}} u(t) e^{-\mathrm{j}\omega t} \,\mathrm{d}t \quad (\omega \in \mathbb{R})$$

and is a continuous and bounded function such that

$$\lim_{|\omega| \to \infty} \mathcal{F}[u](\omega) = 0.$$

When both u and $\mathcal{F}[u]$ lie in $L^1(\mathbb{R})$, then $\mathcal{F}^{-1} = (2\pi)^{-1}\,\overline{\mathcal{F}}$, i.e.

$$u(t) = \frac{1}{2\pi} \int_{\mathbb{R}} \mathcal{F}[u](\omega) e^{+\mathrm{j}\omega t} \,\mathrm{d}\omega \quad (t \in \mathbb{R}).$$

More generally, the Fourier transform can be defined over the set of tempered distributions $\mathcal{S}'(\mathbb{R})$ as follows (Schwartz 1966, Chap. V) (Zemanian 1965, Chap. 7) (Beltrami and Wohlers 1966, § 1.8) (Bony 2001, Def. 9.4.1).

Definition A.5 (Fourier transform)**.** Let $u \in \mathcal{S}'(\mathbb{R})$. Its Fourier transform is defined as

$$\forall \varphi \in \mathcal{S}(\mathbb{R}),\ \langle \mathcal{F}[u], \varphi \rangle_{\mathcal{S}'(\mathbb{R}),\mathcal{S}(\mathbb{R})} = \langle u, \mathcal{F}[\varphi] \rangle_{\mathcal{S}'(\mathbb{R}),\mathcal{S}(\mathbb{R})}\,.$$

The quantity $\mathcal{F}[\varphi]$ is well-defined since $\mathcal{S}(\mathbb{R}) \subset L^1(\mathbb{R})$. Defined as above, the Fourier transform is a bijection in $\mathcal{S}'(\mathbb{R})$ with inverse

$$\mathcal{F}^{-1} = \frac{1}{2\pi}\overline{\mathcal{F}}.$$

Note that a direct consequence of the above definition is that the Fourier transform does not apply to exponentially growing functions like $t \mapsto e^{-\xi t}H(t)$ with $\xi < 0$ and $t \mapsto e^{-t}$.

A.2.2 Laplace transform

The Laplace transform of functions is defined below (Schwartz 1966, § VI.1) (Zemanian 1965, § 8.2).

Definition A.6 (Laplace transform)**.** Let $u \in L^1_{\mathrm{loc}}([0,\infty))$ be a locally integrable function. If there are $c > 0$ and $M > 0$ such that

$$\forall t > 0,\ e^{-ct}\,|u(t)| \leq M,$$

then u has a Laplace transform given by

$$\hat{u}(s) \coloneqq \int_0^\infty u(t) e^{-st} \,\mathrm{d}t \quad (\Re(s) > c)\,. \tag{A.14}$$

The most elementary example is

$$\widehat{e_\xi}(s) = \frac{1}{s+\xi} \quad (\Re(s) > -\xi)\,.$$

Note that, for $\xi < 0$, e_ξ does not have a Fourier transform since it is exponentially growing at infinity. More generally, the Laplace transform is defined over the set of causal distributions $\mathcal{D}'_+(\mathbb{R})$ with at most finite exponential growth at infinity (Schwartz 1966, Chap. VI) (Zemanian 1965, Chap. 8) (Beltrami and Wohlers 1966, Chap. II), see the definition below.

Definition A.7 (Laplace transform)**.** Let $u \in \mathcal{D}'_+(\mathbb{R})$. If there is $c > 0$ such that

$$\forall \sigma > c,\ t \mapsto e^{-\sigma t} u(t) \in \mathcal{S}'(\mathbb{R}),$$

then u admits a Laplace transform defined as

$$\hat{u}(\sigma + \mathrm{j}\omega) \coloneqq \mathcal{F}\left[e^{-\sigma t} u(t)\right](\omega) \quad (\sigma > c,\ \omega \in \mathbb{R}),$$

which can be more compactly written as

$$\hat{u}(s) = \left\langle u, e^{-st} \right\rangle \quad (\Re(s) > c)\,.$$

A practical consequence of these definitions is that the Laplace transform is always an analytic *function* of an open right half-plane $\mathbb{C}_c^+$ while the Fourier transform may only be a tempered *distribution*. This fact will be illustrated in Section A.3.

Inversion of the Laplace transform

The proposition below answers the following question: given an analytic function f on $\mathbb{C}_c^+$ with $c \geq 0$, does it define the Laplace transform of a causal distribution? It can be understood as a causality condition. See (Schwartz 1978, Prop. VIII.6) and (Beltrami and Wohlers 1966, Thm. 2.5) for a proof.

Theorem A.8. *Let $u \in \mathcal{D}'_+(\mathbb{R})$ and $c \geq 0$ be such that $e^{-\sigma t} u \in \mathcal{S}'(\mathbb{R})$ for $\sigma > c$. Then its Laplace transform $\hat{u}$ has the following properties:*

(i) *$\hat{u}$ is analytic in $\mathbb{C}_c^+$,*

(ii) *for every compact $K \subset (c, \infty)$, there is a polynomial $P_K(s)$ such that*

$$\forall s \in \mathbb{C} :\ \Re(s) \in K,\ |\hat{u}(s)| \leq |P_K(s)|.$$

Conversely, if a function $s \mapsto f(s)$ is analytic in $\mathbb{C}_c^+$ and satisfies the above boundedness condition, it is the Laplace transform of a causal distribution u such that $e^{-\sigma t} u \in \mathcal{S}'(\mathbb{R})$ for $\sigma > c$.

If $\hat{u}$ satisfies the condition of the theorem, the inversion formula is

$$u(t) = \frac{1}{2\pi} e^{+\sigma t} \overline{\mathcal{F}}[\hat{u}(\sigma + \mathrm{j}\cdot)](t) \quad (\sigma > c),$$

which reduces to

$$u(t) = \frac{1}{2\mathrm{j}\pi} \int_{\sigma - \mathrm{j}\infty}^{\sigma + \mathrm{j}\infty} \hat{u}(s) e^{+st}\, \mathrm{d}s \quad (\sigma > c) \tag{A.15}$$

when the right-hand side of (A.15) is defined.

It is a basic fact of harmonic analysis that the faster the decay of $\hat{u}$ at infinity, the stronger the regularity of u. Consider for example

$$\widehat{\delta^{(n)}}(s) = s^n \quad (n \in \mathbb{N})\,. \tag{A.16}$$

This is further illustrated by the following proposition, proven in (Schwartz 1966, § VI.4).

Proposition A.9. *Let $f : \mathbb{C}_c^+ \to \mathbb{C}$ be an analytic function with $c \geq 0$. If there is $M > 0$ such that*

$$|f(s)| \leq \frac{M}{|s|^2} \quad (\Re(s) > c),$$

then $f = \hat{u}$ with u causal and continuous on $\mathbb{R}$ given by the Bromwich integral (A.15).

Laplace transform and convolution

A basic property of the Laplace transform is that, for z and u in $\mathcal{D}'_+(\mathbb{R})$, we have

$$\widehat{z \star u}(s) = \hat{z}(s)\hat{u}(s) \quad (\Re(s) > c)$$

for some $c \geq 0$. By combining with (A.10) and (A.16) we obtain

$$\widehat{u^{(n)}}(s) = s^n \hat{u}(s).$$

Note that in general the above formula holds true only for the weak derivative. For a causal function $u \in L^1_{\mathrm{loc}}([0,\infty))$, we deduce from (A.4) that

$$\mathcal{L}\left[\frac{\mathrm{d}u}{\mathrm{d}t}\right](s) = s\hat{u}(s) - u(0^+), \tag{A.17}$$

which can also be directly derived from (A.14) with an integration by parts. Equation (A.17) is another illustration of the difference between the weak and strong derivative for a causal function.

Remark A.10 (Fractional derivatives). For a causal function $u \in L^1_{\mathrm{loc}}([0,\infty))$, the Laplace transform of (A.12) reads

$$\mathcal{L}\left[D_\alpha^{\mathrm{RL}} u\right](s) = s^{\alpha-1} s\hat{u}(s) = s^\alpha \hat{u}(s),$$

while that of (A.13) reads

$$\mathcal{L}\left[D_\alpha^{\mathrm{C}} u\right](s) = s^{\alpha-1}\left(s\hat{u}(s) - u(0^+)\right) = s^\alpha \hat{u}(s) - u(0^+)s^{\alpha-1}.$$

This illustrates the difference between $D_\alpha^{\mathrm{RL}} u$ and $D_\alpha^{\mathrm{C}} u$ in the Laplace domain.

A.3 Expression of physical impedance models

The purpose of this section is to illustrate the differences between the Fourier and Laplace transforms by considering two physical models encountered in Section 1.2.2.

As recalled in Section A.2, the Laplace transform $\hat{z}$ of a physical impedance model is an analytic function of the open right half-plane. Since, from Proposition 1.8, it is a positive-real function, the Fourier transform $\mathcal{F}(z)$ exists and belongs to $\mathcal{S}'(\mathbb{R})$ (Beltrami and Wohlers 1966, § 3.5). However, note that the mere substitution of $\mathrm{j}\omega$ for s in the expression of $\hat{z}(s)$ does *not* yield the Fourier transform in general, i.e.

$$\mathcal{F}[z](\omega) \neq \hat{z}(\mathrm{j}\omega) \quad (\omega \in \mathbb{R})\,.$$

This is due to the fact that the limit

$$\lim_{\sigma \to 0} \hat{z}(\sigma + \mathrm{j}\omega) \quad (\omega \in \mathbb{R})$$

may only exist in the space of tempered distributions $\mathcal{S}'(\mathbb{R})$. In this section, we will illustrate this on two examples. The first result covers the impedance model $\hat{z}(s) = 1/s$ and is a textbook example of this phenomenon.

Lemma A.11. *Let $z = H \in \mathcal{D}'_+(\mathbb{R})$, with Laplace transform*

$$\hat{z}(s) = \frac{1}{s} \quad (\Re(s) > 0)\,. \tag{A.18}$$

The kernel z is tempered, i.e. $z \in \mathcal{S}'(\mathbb{R})$, and its Fourier transform is given by

$$\mathcal{F}[z](\omega) = \mathrm{pv}\left(\frac{1}{\mathrm{j}\omega}\right) + \pi\delta, \tag{A.19}$$

where pv *denotes the Cauchy principal value.*

Proof. Let

$$\hat{f}_\sigma(\omega) \coloneqq \hat{z}(\sigma + \mathrm{j}\omega) \quad (\sigma > 0,\ \omega \in \mathbb{R}).$$

By definition, when $\sigma > 0$, $\hat{f}_\sigma \in \mathcal{S}'(\mathbb{R}) \cap L^1_{\mathrm{loc}}(\mathbb{R})$. However, $\hat{f}_0 \notin L^1_{\mathrm{loc}}(\mathbb{R})$ since

$$\omega \mapsto \frac{1}{\omega}$$

exhibits a non-integrable singularity at $\omega = 0$: as a result it is not a distribution and thus cannot be a Fourier transform. Hence, we know that $\mathcal{F}[z](\omega) \neq \frac{1}{\mathrm{j}\omega}$. To compute the limit

$$\lim_{\sigma \to 0} \hat{f}_\sigma$$

in $\mathcal{S}'(\mathbb{R})$, the following standard trick can be used. Consider a primitive of $\hat{f}_\sigma$, given for instance by the principal branch of the logarithm

$$\hat{F}_\sigma(\omega) \coloneqq \frac{1}{\mathrm{j}}\left[\ln|\sigma + \mathrm{j}\omega| + \mathrm{j}\,\mathrm{Arg}\,(\sigma + \mathrm{j}\omega)\right] \quad (\omega \in \mathbb{R}).$$

It is smooth enough to admit a limit in $\mathcal{S}'(\mathbb{R}) \cap L^1_{\mathrm{loc}}(\mathbb{R})$ given by

$$\hat{F}_\sigma(\omega) \xrightarrow[\sigma \to 0]{\omega \in \mathbb{R}} \frac{1}{\mathrm{j}} \ln|\omega| + \mathrm{Arg}\,(\mathrm{j}\omega)\,.$$

By continuity of the *weak* derivative in $\mathcal{S}'(\mathbb{R})$ we deduce the desired limit

$$\hat{f}_\sigma(\omega) \xrightarrow[\sigma \to 0]{\mathcal{S}'(\mathbb{R})} \frac{1}{\mathrm{j}}\left(\ln|\omega|\right)' + \left(\mathrm{Arg}\,(\mathrm{j}\omega)\right)' = \frac{1}{\mathrm{j}}\,\mathrm{pv}\left(\frac{1}{\omega}\right) + \left(\frac{\pi}{2} - \left(-\frac{\pi}{2}\right)\right)\delta(\omega).$$

Since

$$\hat{f}_\sigma(\omega) = \mathcal{F}\left[H(t)e^{-\sigma t}\right](\omega) \quad (\sigma > 0,\ \omega \in \mathbb{R}),$$

the result is deduced from the continuity of $\mathcal{F}$ in $\mathcal{S}'(\mathbb{R})$. □

Remark A.12 (Causality). The causality of (A.19) is not obvious, by contrast with that of (A.18). By using (Gasquet and Witomski 1999, § 31.6)

$$\mathcal{F}^{-1}\left[\mathrm{pv}\left(\frac{1}{\omega}\right)\right](t) = \frac{\mathrm{j}}{2}\mathrm{sign}(t),\ \mathcal{F}^{-1}[\delta] = \frac{1}{2\pi},$$

we recover

$$\mathcal{F}^{-1}\left[\mathcal{F}[z]\right](t) = \frac{1}{\mathrm{j}}\left[\frac{\mathrm{j}}{2}\mathrm{sign}(t)\right] + \frac{1}{2} = H(t).$$

Notice how in (A.19) the term "$\pi\delta$" is needed for causality.

The second lemma considers the lossless cavity model.

Lemma A.13. *Let $z \in \mathcal{D}'_+(\mathbb{R})$ be given by its Laplace transform*

$$\hat{z}(s) = \coth(b_1 s) \quad (\Re(s) > 0), \tag{A.20}$$

with $b_1 > 0$. The kernel z is tempered, i.e. $z \in \mathcal{S}'(\mathbb{R})$, and its Fourier transform is given by

$$\mathcal{F}[z](\omega) = \mathrm{pv}\left(\coth(\mathrm{j}b_1\omega)\right) + \frac{\pi}{b_1}\sum_{n\in\mathbb{Z}}\delta\left(\omega - \frac{n\pi}{b_1}\right), \tag{A.21}$$

where the series converges in $\mathcal{S}'(\mathbb{R})$.

Proof. The proof follows the same methodology than that of Lemma A.11, with the added subtlety that $\hat{z}$ is periodic. Let

$$\hat{f}_\sigma(\omega) \coloneqq \coth(b_1(\sigma + \mathrm{j}\omega)) \quad (\sigma > 0,\ \omega \in \mathbb{R}).$$

By definition, when $\sigma > 0$, $\hat{f}_\sigma \in \mathcal{S}'(\mathbb{R}) \cap L^1_{\mathrm{loc}}(\mathbb{R})$ and is a π/b_1 periodic function. However, $\hat{f}_0 \notin L^1_{\mathrm{loc}}(\mathbb{R})$ since it admits singularities at the anti-resonant angular frequencies $\omega_n = n\pi/b_1$ and therefore cannot be a Fourier transform, so that

$$\mathcal{F}[z](\omega) \neq \coth(\mathrm{j}b_1\omega).$$

The limit $\sigma \to 0$ must be taken in the sense of periodic distributions. To that end, we first define

$$\hat{f}^{\mathrm{per}}_\sigma(\omega) \coloneqq \hat{f}_\sigma(\omega) \quad \left(\sigma > 0,\ \omega \in \left[-\frac{\pi}{2b_1}, \frac{\pi}{2b_1}\right)\right),$$

whose sole singularity is at 0, and a primitive

$$\hat{F}^{\mathrm{per}}_\sigma(\omega) \coloneqq \frac{1}{\mathrm{j}b_1}\ln\left(\sinh(b_1(\sigma + \mathrm{j}\omega))\right) \quad \left(\sigma > 0,\ \omega \in \left[-\frac{\pi}{2b_1}, \frac{\pi}{2b_1}\right)\right),$$

where ln is the principal branch of the logarithm. The function $\hat{F}^{\mathrm{per}}_\sigma$ admits a limit in L^1_{loc} given by

$$\hat{F}^{\mathrm{per}}_0(\omega) = \frac{1}{\mathrm{j}b_1}\ln|\sin(b_1\omega)| + \frac{1}{b_1}\mathrm{Arg}\left(\mathrm{j}\sin(b_1\omega)\right) \quad \left(\omega \in \left[-\frac{\pi}{2b_1}, \frac{\pi}{2b_1}\right)\right).$$

By using the identity (Schwartz 1966, Ex. IV.7)

$$\left(\ln|\sin(b_1\omega)|\right)' = b_1\,\mathrm{pv}\left(\cot(b_1\omega)\right)$$

and the continuity of the weak differentiation in the space of π/b_1 periodic distributions we get

$$\lim_{\sigma\to 0}\hat{f}^{\mathrm{per}}_\sigma(\omega) = \frac{1}{\mathrm{j}}\,\mathrm{pv}\left(\cot(b_1\omega)\right) + \frac{1}{b_1}\left(\frac{\pi}{2} - \left(-\frac{\pi}{2}\right)\right)\delta(\omega) = \frac{1}{\mathrm{j}}\,\mathrm{pv}\left(\cot(b_1\omega)\right) + \frac{\pi}{b_1}\delta(\omega).$$

The corresponding π/b_1 periodic distribution in $\mathcal{S}'(\mathbb{R})$ is

$$\lim_{\sigma\to 0}\hat{f}_\sigma(\omega)=\frac{1}{\mathrm{j}}\,\mathrm{pv}\left(\cot\left(b_1\omega\right)\right)+\frac{\pi}{b_1}\sum_{n\in\mathbb{Z}}\delta\left(\omega-\frac{n\pi}{b_1}\right),$$

and the claimed result follows by continuity of the Fourier transform in $\mathcal{S}'(\mathbb{R})$. □

Remark A.14 (Causality). By contrast with the Laplace transform (A.20), the causality of the Fourier transform (A.21) is not obvious. Causality can be shown by using the Fourier series expansion of both terms in the right-hand side of (A.21), namely (Dupraz 1977, Ex. III-1)

$$\mathrm{pv}\left(\cot(b_1\omega)\right)=-\sum_{n\geq 1}\mathrm{j}e^{\mathrm{j}2nb_1\omega}+\sum_{n\leq -1}\mathrm{j}e^{\mathrm{j}2nb_1\omega},$$

and

$$\frac{\pi}{b_1}\sum_{n\in\mathbb{Z}}\delta\left(\omega-\frac{n\pi}{b_1}\right)=\sum_{n\in\mathbb{Z}}e^{\mathrm{j}2nb_1\omega}$$

so that

$$\begin{aligned}\mathcal{F}\left[z\right](\omega)&=-\mathrm{j}\left[-\sum_{n\geq 1}\mathrm{j}e^{\mathrm{j}2nb_1\omega}+\sum_{n\leq -1}\mathrm{j}e^{\mathrm{j}2nb_1\omega}\right]+\sum_{n\in\mathbb{Z}}e^{\mathrm{j}2nb_1\omega}\\&=\left[-\sum_{n\geq 1}e^{\mathrm{j}2nb_1\omega}+\sum_{n\leq -1}e^{\mathrm{j}2nb_1\omega}\right]+\sum_{n\in\mathbb{Z}}e^{\mathrm{j}2nb_1\omega}\\&=1+2\sum_{n\leq -1}e^{\mathrm{j}2nb_1\omega}\end{aligned}\tag{A.22}$$

and

$$z(t)=\delta(t)+2\sum_{n\geq 1}\delta(t-2nb_1).$$

In the above computations, the series $\sum_{n\in\mathbb{Z}}\delta\left(\omega-\frac{n\pi}{b_1}\right)$ is needed to obtain causality, since $\mathcal{F}^{-1}\left[\mathrm{pv}\left(\coth(\mathrm{j}b_1\omega)\right)\right]$ is not causal.

To conclude this remark, let us note that the identity (A.22) can be obtained in a much simpler manner using (2.57) and the sum of the geometric series. Using the notation of the proof of Lemma A.13, we have for $\sigma>0$

$$\hat{f}_\sigma(\omega)=1+2\frac{e^{-2b_1(\sigma+\mathrm{j}\omega)}}{1-e^{-2b_1(\sigma+\mathrm{j}\omega)}}=1+2e^{-2b_1(\sigma+\mathrm{j}\omega)}\sum_{n\geq 0}e^{-2nb_1(\sigma+\mathrm{j}\omega)},$$

and (A.22) follows by taking the limit in $\mathcal{S}'(\mathbb{R})$, which is defined from (Gasquet and Witomski 1999, Prop. 31.1.9) since a constant sequence is a slowly increasing sequence.

A.4 Admissibility conditions

In Section 1.1, admissibility conditions have been formulated using the Laplace transforms $\hat{z}$, $\hat{y}$, and $\hat{\beta}$, see Propositions 1.8 and 1.14. These conditions are straightforward to verify in practice using the expressions of physical models. However, formulating the same admissibility conditions using the Fourier transform is more involved. Let us illustrate this point by considering the causality condition for a tempered distribution $z\in\mathcal{S}'(\mathbb{R})$. The distribution z is causal if and only if its Fourier transform $\mathcal{F}\left[z\right]$ satisfies a so-called dispersion relation (Beltrami and Wohlers

1966, Thm. 3.10), which links its real and imaginary parts. By contrast, the causality condition on the Laplace transform consists in checking its growth at infinity, see Theorem A.8.

In the particular case of a rational function, admissibility conditions can be formulated using the Fourier transform in a simple manner, see the two propositions below, reproduced from (Lozano et al. 2000, Thms. 2.8 & 2.10).

Proposition A.15. *A rational function f is positive-real if and only if it satisfies the following conditions.*

(i) *f is analytic in $\mathbb{C}_0^+$.*

(ii) *$\overline{f(\mathrm{j}\omega)} = f(-\mathrm{j}\omega)$ for any $\omega \in \mathbb{R}$ such that $\mathrm{j}\omega$ is not a pole.*

(iii) *$\Re[f(\mathrm{j}\omega)] \geq 0$ for any $\omega \in \mathbb{R}$ such that $\mathrm{j}\omega$ is not a pole.*

(iv) *If $\mathrm{j}\omega_0$ is a pole of f, then it is a simple pole whose residue is positive.*

(v) *If $\lim_{\omega\to\pm\infty} |f(\mathrm{j}\omega)| = \infty$, then $\lim_{\omega\to\pm\infty} \frac{f(\mathrm{j}\omega)}{\mathrm{j}\omega} > 0$.*

Proposition A.16. *A rational function f is bounded real if and only if it satisfies the following conditions.*

(i) *f is analytic in $\overline{\mathbb{C}_0^+}$.*

(ii) *$\overline{f(\mathrm{j}\omega)} = f(-\mathrm{j}\omega)$ for any $\omega \in \mathbb{R}$.*

(iii) *$|f(\mathrm{j}\omega)| \leq 1$ for any $\omega \in \mathbb{R}$.*

To conclude this section, let us consider an example that illustrates how a formal use of the Fourier transform can lead to mistakes. Let us consider the kernel given by

$$z(t) = \delta(t) + \delta(t+\tau) \quad (t \in \mathbb{R}),$$

with $\tau > 0$. Since $\tau > 0$, z is not causal. A simple examination shows that its Laplace transform

$$\hat{z}(s) = 1 + e^{+s\tau} \quad (\Re(s) > 0)$$

is not positive-real since

$$\Re\left(1 + e^{+s\tau}\right) < 0$$

for some $s \in \mathbb{C}_0^+$ with a sufficiently large real part. This is consistent with the fact, recalled in Section 1.1, that a real (continuous) LTI system cannot be both anticausal and passive. However, note that although the Laplace transform satisfies

$$\hat{z}(\mathrm{j}\omega) = \overline{\hat{z}(-\mathrm{j}\omega)},\ \Re(\hat{z}(\mathrm{j}\omega)) \geq 0 \quad (\omega \in \mathbb{R}),$$

the operator $u \mapsto z \star u$ is not passive. The link between "$\Re[\hat{z}(\mathrm{j}\omega)] \geq 0$" and passivity requires causality, as illustrated by the proposition below.

Proposition A.17 (Passivity condition)**.** *Let $z \in L^1(\mathbb{R})$ be a causal kernel. The operator $u \mapsto z \star u$ is passive if and only if*

$$\forall \omega \in \mathbb{R},\ \Re[\hat{z}(\mathrm{j}\omega)] \geq 0.$$

Proof. The proof is inspired from (Lozano et al. 2000, Chap. 2); we detail it here as it is instructive. Let $T > 0$. Let $u \in \mathcal{C}_0^\infty(\mathbb{R})$ be a real-valued input. Since z is causal, we can without loss of generality take u causal. Since z is real-valued, we can without loss of generality take u real-valued (see (Zemanian 1965, p. 302)). We define the truncated input

$$u_{|(0,T)}(t) \coloneqq u(t)\mathbb{1}_{(0,T)}(t) \quad (t \in \mathbb{R}).$$

The energy supplied to the system is

$$\begin{aligned}
\int_{-\infty}^{T} (z \star u)(t)u(t)\,\mathrm{d}t &= \int_{0}^{T} (z \star u)(t)u(t)\,\mathrm{d}t && \text{(Causality)}\\
&= \int_{\mathbb{R}} (z \star u_{|(0,T)})(t)u_{|(0,T)}(t)\,\mathrm{d}t\\
&= (2\pi)^{-1} \int_{\mathbb{R}} \overline{\mathcal{F}(z \star u_{|(0,T)})(\omega)}(\mathrm{j}\omega)\mathcal{F}(u_{|(0,T)})(\omega)\,\mathrm{d}\omega && \text{(Parseval in } L^2(\mathbb{R}))\\
&= (2\pi)^{-1} \int_{\mathbb{R}} \overline{\hat{z}(\mathrm{j}\omega)\mathcal{F}(u_{|(0,T)})(\omega)}\mathcal{F}(u_{|(0,T)})(\omega)\,\mathrm{d}\omega\\
&= (2\pi)^{-1} \int_{\mathbb{R}} \overline{\hat{z}(\mathrm{j}\omega)}|\mathcal{F}(u_{|(0,T)})(\omega)|^2\,\mathrm{d}\omega\\
&= (2\pi)^{-1} \int_{\mathbb{R}} \Re\left[\left(\overline{\hat{z}(\mathrm{j}\omega)}\right)\right]|\mathcal{F}(u_{|(0,T)})(\omega)|^2\,\mathrm{d}\omega,
\end{aligned}$$

where for the last line we have used the fact that the right-hand side is real-valued. □

Note that the proof of Proposition A.17 crucially relies on the causality of h, otherwise we do not get the nonnegative term "$|\mathcal{F}(u_{|(0,T)})(\omega)|^2$" and no conclusion can be reached. Unfortunately, the applicability of this result is rather limited since physical impedance models are usually not integrable; consider for instance the proportional-derivative impedance

$$\hat{z}(s) = a_0 + a_1 s \quad (\Re(s) > 0)\,,\ z(t) = a_0\delta(t) + a_1\delta'(t) \quad (t \in \mathbb{R})$$

or the fractional impedance

$$\hat{z}(s) = \frac{1}{\sqrt{s}} \quad (\Re(s) > 0)\,,\ z(t) = \frac{H(t)}{\sqrt{\pi t}} \quad (t \in \mathbb{R})\,.$$

A.5 A convergence result

Proposition A.18. *Let $(x_n)_{n\in\mathbb{Z}}$ and $(y_n)_{n\in\mathbb{Z}}$ be two complex-valued sequences. If*

(i) *y_n has only a finite number of null elements.*

(ii) *$\Re(y_n) \leq 0$.*

(iii) *There are $C > 0$ such that*

$$\forall n \in \mathbb{Z}, \quad |x_n| \leq C\frac{|y_n|^2}{1+n^2}. \tag{A.23}$$

(iv) *The quantity $\sum_{|n|\leq N} \frac{x_n}{y_n}$ has a limit in $\mathbb{C}$ for $N \to \infty$.*

Then,

$$S \coloneqq t \mapsto \sum_{n\in\mathbb{Z}} x_n e^{y_n t}H(t) \in \mathcal{S}'(\mathbb{R}) \cap \mathcal{D}'_+(\mathbb{R}).$$

Proof. We will prove that S belongs to $\mathcal{S}'(\mathbb{R})$ by using the continuity of the differentiation in $\mathcal{S}'(\mathbb{R})$. Without loss of generality we assume that $y_n \neq 0$ for all $n \in \mathbb{Z}$. Let C be as in (A.23) and define for $t \in \mathbb{R}$

$$F_N(t) \coloneqq \sum_{n=-N}^{N} \frac{x_n}{y_n^2} e^{y_n t} H(t), \quad S_N(t) \coloneqq \sum_{n=-N}^{N} x_n e^{y_n t} H(t).$$

Let us first focus on $F_N \in \mathcal{C}(\mathbb{R})$. For any $t \in \mathbb{R}$, $F_N(t)$ has a limit as $N \to \infty$ since

$$|F_N(t)| \leq \sum_{n=-N}^{N} \frac{C}{1+n^2} e^{\Re(y_n)t} H(t) \leq \sum_{n=-\infty}^{\infty} \frac{C}{1+n^2},$$

from which we deduce that $F_N \to F$ in $\mathcal{D}'(\mathbb{R})$ (Gasquet and Witomski 1999, Prop. 29.3.3). Let us now show that $F \in \mathcal{S}'(\mathbb{R})$. It suffices to show that for any $\varphi_p \in \mathcal{D}(\mathbb{R})$ such that $\varphi_p \to 0$ in $\mathcal{S}(\mathbb{R})$ we have $\langle F, \varphi_p \rangle \to 0$ (Gasquet and Witomski 1999, Prop. 31.1.3), which follows from

$$|\langle F_N, \varphi_p \rangle| \leq \sum_{n=-N}^{N} \frac{C}{1+n^2} \|\varphi_p\|_{L^\infty(\mathbb{R})}.$$

Using $\left(e^{y_n t} H(t)\right)' = y_n e^{y_n t} H(t) + \delta$, we deduce

$$S_N(t) = F_N''(t) - \left(\sum_{n=-N}^{N} \frac{x_n}{y_n^2} \right) \delta'(t) - \left(\sum_{n=-N}^{N} \frac{x_n}{y_n} \right) \delta(t),$$

since both series are convergent by assumption and $F_N'' \to F''$ in $\mathcal{S}'(\mathbb{R})$, we deduce that $S_N \to S$ in $\mathcal{S}'(\mathbb{R})$. The causality of S follows directly from its definition. □

Remark A.19. Condition (iv) of Theorem A.18 can be intuitively understood by considering the Laplace transform of S, namely

$$\hat{S}(s) = \sum_{n \in \mathbb{Z}} \frac{x_n}{s - s_n},$$

which is defined in $s \in \mathbb{C}_0^+$.

Appendix B

Representation of a DDOF liner impedance model

This appendix provides the OD representation of an impedance model for DDOF liners, following the methodology laid out in Section 2.4. Note that none of the formulas given below have been used in the numerical applications of Chapter 6, which focused exclusively on a model for SDOF liners.

In Section 1.2.2, the following physical model for DDOF liners has been given:

$$\hat{z}_{\mathrm{DDOF}} = \frac{1}{\sigma_{p_1}}\hat{z}_{p_1} + \frac{1}{\sigma_{c_1}}\hat{z}_{\mathrm{tube}}(k_1, z_{c_1}, \hat{z}_{2|S_{c_1}}), \tag{B.1}$$

with $\hat{z}_{\mathrm{tube}}$ defined as (1.16),

$$\hat{z}_{2|S_{c_1}} = \frac{\sigma_{c_1}}{\sigma_{p_2}}\left[\hat{z}_{p_2} + z_{c_2}\frac{\sigma_{p_2}}{\sigma_{c_2}}\coth(\mathrm{j}k_2)\right],$$

and, for the sake of concision,

$$\hat{z}_{p_i} \coloneqq \hat{z}_{\mathrm{perf}}(l_{p_i}, d_{p_i}),\ k_i \coloneqq k_{c_i} l_{c_i} \quad (i \in \{1, 2\})\,.$$

In this appendix, we consider a fractional polynomial model for both the perforation impedance and the cavity wavenumber, namely

$$\begin{aligned}\mathrm{j}k_i(s) &= b_{i,0} + b_{i,1/2}\sqrt{s} + b_{i,1}s\\ \hat{z}_{p_i}(s) &= a_{i,0} + a_{i,1/2}\sqrt{s} + a_{i,1}s,\end{aligned}$$

where $b_{i,1} > 0$ and the other coefficients are nonnegative. We define the time delays associated with each cavity as

$$\tau_i \coloneqq 2b_{i,1} > 0.$$

Below, the OD representation is given for the impedance, admittance, and scattering formulations.

Impedance

The OD representation of $\hat{z}_{p_1}$ has already been given in Section 1.2.2 so that there are no differences between the SDOF and DDOF model on that respect. The difficulty specific to (B.1)

is the representation of $\hat{z}_{\text{tube}}$. To avoid computations that are too lengthy, it is best to rewrite $\hat{z}_{\text{tube}}$ using only cosh and sinh, and avoid coth and tanh, as follows.

$$\begin{aligned}
&\frac{1}{\sigma_{c_1}}\hat{z}_{\text{tube}}(k_1, z_{c_1}, \hat{z}_{2|S_{c_1}}) \\
&\qquad = \frac{z_{c_1}}{\sigma_{c_1}} \frac{\hat{z}_{2|S_{c_1}} \cosh(\mathrm{j}k_1) + z_{c_1} \sinh(\mathrm{j}k_1)}{z_{c_1} \cosh(\mathrm{j}k_1) + \hat{z}_{2|S_{c_1}} \sinh(\mathrm{j}k_1)} \\
&\qquad = \frac{z_{c_1}}{\sigma_{c_1}} \frac{\frac{\sigma_{c_1}}{\sigma_{p_2}}\left[\hat{z}_{p_2} + z_{c_2}\frac{\sigma_{p_2}}{\sigma_{c_2}} \coth(\mathrm{j}k_2)\right] \cosh(\mathrm{j}k_1) + z_{c_1} \sinh(\mathrm{j}k_1)}{z_{c_1} \cosh(\mathrm{j}k_1) + \frac{\sigma_{c_1}}{\sigma_{p_2}}\left[\hat{z}_{p_2} + z_{c_2}\frac{\sigma_{p_2}}{\sigma_{c_2}} \coth(\mathrm{j}k_2)\right] \sinh(\mathrm{j}k_1)} \\
&\qquad = \frac{z_{c_1}}{\sigma_{c_1}} \frac{\frac{\sigma_{c_1}}{\sigma_{p_2}}\left[\hat{z}_{p_2} \sinh(\mathrm{j}k_2) + z_{c_2}\frac{\sigma_{p_2}}{\sigma_{c_2}} \cosh(\mathrm{j}k_2)\right] \cosh(\mathrm{j}k_1) + z_{c_1} \sinh(\mathrm{j}k_2)\sinh(\mathrm{j}k_1)}{z_{c_1} \sinh(\mathrm{j}k_2)\cosh(\mathrm{j}k_1) + \frac{\sigma_{c_1}}{\sigma_{p_2}}\left[\hat{z}_{p_2} \sinh(\mathrm{j}k_2) + z_{c_2}\frac{\sigma_{p_2}}{\sigma_{c_2}} \cosh(\mathrm{j}k_2)\right] \sinh(\mathrm{j}k_1)}.
\end{aligned}$$

Then, we use the identities

$$\cosh \mathrm{j}k_i = \frac{1 + e^{-2\mathrm{j}k_i}}{2e^{-\mathrm{j}k_i}},\ \sinh \mathrm{j}k_i = \frac{1 - e^{-2\mathrm{j}k_i}}{2e^{-\mathrm{j}k_i}}$$

to get

$$\begin{aligned}
&\frac{1}{\sigma_{c_1}}\hat{z}_{\text{tube}}(k_1, z_{c_1}, \hat{z}_{2|S_{c_1}}) \\
&\quad = \frac{z_{c_1}}{\sigma_{c_1}} \frac{\frac{\sigma_{c_1}}{\sigma_{p_2}}\left[\hat{z}_{p_2}\left[1 - e^{-2\mathrm{j}k_2}\right] + z_{c_2}\frac{\sigma_{p_2}}{\sigma_{c_2}}\left[1 + e^{-2\mathrm{j}k_2}\right]\right]\left[1 + e^{-2\mathrm{j}k_1}\right] + z_{c_1}\left[1 - e^{-2\mathrm{j}k_2}\right]\left[1 - e^{-2\mathrm{j}k_1}\right]}{z_{c_1}\left[1 - e^{-2\mathrm{j}k_2}\right]\left[1 + e^{-2\mathrm{j}k_1}\right] + \frac{\sigma_{c_1}}{\sigma_{p_2}}\left[\hat{z}_{p_2}\left[1 - e^{-2\mathrm{j}k_2}\right] + z_{c_2}\frac{\sigma_{p_2}}{\sigma_{c_2}}\left[1 + e^{-2\mathrm{j}k_2}\right]\right]\left[1 - e^{-2\mathrm{j}k_1}\right]} \\
&\quad = \frac{z_{c_1}}{\sigma_{c_1}} \frac{\frac{\sigma_{c_1}}{\sigma_{p_2}}\left[\hat{z}_{p_2} + z_{c_2}\frac{\sigma_{p_2}}{\sigma_{c_2}} + \left[z_{c_2}\frac{\sigma_{p_2}}{\sigma_{c_2}} - \hat{z}_{p_2}\right]e^{-2\mathrm{j}k_2}\right]\left[1 + e^{-2\mathrm{j}k_1}\right] + z_{c_1}\left[1 - e^{-2\mathrm{j}k_2}\right]\left[1 - e^{-2\mathrm{j}k_1}\right]}{z_{c_1}\left[1 - e^{-2\mathrm{j}k_2}\right]\left[1 + e^{-2\mathrm{j}k_1}\right] + \frac{\sigma_{c_1}}{\sigma_{p_2}}\left[\hat{z}_{p_2} + z_{c_2}\frac{\sigma_{p_2}}{\sigma_{c_2}} + \left[z_{c_2}\frac{\sigma_{p_2}}{\sigma_{c_2}} - \hat{z}_{p_2}\right]e^{-2\mathrm{j}k_2}\right]\left[1 - e^{-2\mathrm{j}k_1}\right]} \qquad \text{(B.2)} \\
&\quad = \hat{h}_1(s) + \hat{h}_2(s)e^{-\tau_1 s} + \hat{h}_3(s)e^{-\tau_2 s} + \hat{h}_4(s)e^{-(\tau_1+\tau_2)},
\end{aligned}$$

where

$$\begin{aligned}
\hat{h}_1(s) &= \frac{z_{c_1}}{\sigma_{c_1}} \frac{\frac{\sigma_{c_1}}{\sigma_{p_2}}\left[\hat{z}_{p_2} + z_{c_2}\frac{\sigma_{p_2}}{\sigma_{c_2}}\right] + z_{c_1}}{R(s)} \\
\hat{h}_2(s) &= \frac{z_{c_1}}{\sigma_{c_1}} e^{-2b_{1,0}} \frac{\frac{\sigma_{c_1}}{\sigma_{p_2}}\left[\hat{z}_{p_2} + z_{c_2}\frac{\sigma_{p_2}}{\sigma_{c_2}}\right] - z_{c_1}}{R(s)} e^{-2b_{1,1/2}\sqrt{s}} \\
\hat{h}_3(s) &= \frac{z_{c_1}}{\sigma_{c_1}} e^{-2b_{2,0}} \frac{\frac{\sigma_{c_1}}{\sigma_{p_2}}\left[z_{c_2}\frac{\sigma_{p_2}}{\sigma_{c_2}} - \hat{z}_{p_2}\right] - z_{c_1}}{R(s)} e^{-2b_{2,1/2}\sqrt{s}} \\
\hat{h}_4(s) &= \frac{z_{c_1}}{\sigma_{c_1}} e^{-2(b_{1,0}+b_{2,0})} \frac{\frac{\sigma_{c_1}}{\sigma_{p_2}}\left[z_{c_2}\frac{\sigma_{p_2}}{\sigma_{c_2}} - \hat{z}_{p_2}\right] + z_{c_1}}{R(s)} e^{-2\left(b_{1,1/2}+b_{2,1/2}\right)\sqrt{s}}
\end{aligned}$$

with common denominator

$$R(s) = z_{c_1}\left[1 - e^{-2\mathrm{j}k_2}\right]\left[1 + e^{-2\mathrm{j}k_1}\right] + \frac{\sigma_{c_1}}{\sigma_{p_2}}\left[\hat{z}_{p_2} + z_{c_2}\frac{\sigma_{p_2}}{\sigma_{c_2}} + \left[z_{c_2}\frac{\sigma_{p_2}}{\sigma_{c_2}} - \hat{z}_{p_2}\right]e^{-2\mathrm{j}k_2}\right]\left[1 - e^{-2\mathrm{j}k_1}\right].$$

The representation is similar to that of SDOF liner models, apart from the fact that there are now three delays. The time-local realization of $\hat{z}_{\text{tube}}$ requires a transport equation on

$$(-\tau_1 - \tau_2, 0)$$

and reads (assuming for simplicity that $R(\infty) = \infty$, i.e. that $a_{2,1/2}$ or $a_{2,1}$ are non-null)

$$\begin{aligned} z_{\text{tube}} \star u(t) = &\sum_{k\in\mathbb{Z}} \text{Res}(\hat{h}_1, s_k)\psi(t, -s_k, 0) + \int_0^\infty \psi(t, \xi, 0)\, \mu_{\hat{h}_1}(\xi)\, \mathrm{d}\xi \\ &+ \sum_{k\in\mathbb{Z}} \text{Res}(\hat{h}_2, s_k)\psi(t, -s_k, -\tau_1) + \int_0^\infty \psi(t, \xi, -\tau_1)\, \mu_{\hat{h}_2}(\xi)\, \mathrm{d}\xi \\ &+ \sum_{k\in\mathbb{Z}} \text{Res}(\hat{h}_3, s_k)\psi(t, -s_k, -\tau_2) + \int_0^\infty \psi(t, \xi, -\tau_2)\, \mu_{\hat{h}_3}(\xi)\, \mathrm{d}\xi \\ &+ \sum_{k\in\mathbb{Z}} \text{Res}(\hat{h}_4, s_k)\psi(t, -s_k, -\tau_1 - \tau_2) + \int_0^\infty \psi(t, \xi, -\tau_1 - \tau_2)\, \mu_{\hat{h}_4}(\xi)\, \mathrm{d}\xi. \end{aligned}$$

Admittance

The admittance is given by

$$\hat{y}_{\text{DDOF}} = \frac{1}{\frac{1}{\sigma_{p_1}}\hat{z}_{p_1} + \frac{1}{\sigma_{c_1}}\hat{z}_{\text{tube}}(k_1, z_{c_1}, \hat{z}_{2|S_{c_1}})}.$$

We can directly use the expression (B.2) obtained above to write

$$\begin{aligned} \hat{y}_{\text{DDOF}}(s) &= \frac{1}{\frac{1}{\sigma_{p_1}}\hat{z}_{p_1} + \frac{z_{c_1}}{\sigma_{c_1}} \frac{\frac{\sigma_{c_1}}{\sigma_{p_2}}\left[\hat{z}_{p_2} + z_{c_2}\frac{\sigma_{p_2}}{\sigma_{c_2}} + \left[z_{c_2}\frac{\sigma_{p_2}}{\sigma_{c_2}} - \hat{z}_{p_2}\right]e^{-2\mathrm{j}k_2}\right]\left[1+e^{-2\mathrm{j}k_1}\right] + z_{c_1}\left[1-e^{-2\mathrm{j}k_2}\right]\left[1-e^{-2\mathrm{j}k_1}\right]}{z_{c_1}\left[1-e^{-2\mathrm{j}k_2}\right]\left[1+e^{-2\mathrm{j}k_1}\right] + \frac{\sigma_{c_1}}{\sigma_{p_2}}\left[\hat{z}_{p_2} + z_{c_2}\frac{\sigma_{p_2}}{\sigma_{c_2}} + \left[z_{c_2}\frac{\sigma_{p_2}}{\sigma_{c_2}} - \hat{z}_{p_2}\right]e^{-2\mathrm{j}k_2}\right]\left[1-e^{-2\mathrm{j}k_1}\right]}} \\ &= \hat{h}_1(s) + \hat{h}_2(s)e^{-\tau_1 s} + \hat{h}_3(s)e^{-\tau_2 s} + \hat{h}_4(s)e^{-(\tau_1+\tau_2)}, \end{aligned}$$

where

$$\begin{aligned} \hat{h}_1(s) &= \frac{z_{c1} + \frac{\sigma_{c_1}}{\sigma_{p_2}}\left[\hat{z}_{p_2} + z_{c_2}\frac{\sigma_{p_2}}{\sigma_{c_2}}\right]}{R(s)} \\ \hat{h}_2(s) &= e^{-2b_{1,0}} \frac{z_{c_1} - \frac{\sigma_{c_1}}{\sigma_{p_2}}\left[\hat{z}_{p_2} + z_{c_2}\frac{\sigma_{p_2}}{\sigma_{c_2}}\right]}{R(s)} e^{-2b_{1,1/2}\sqrt{s}} \\ \hat{h}_3(s) &= e^{-2b_{2,0}} \frac{-z_{c_1} + \frac{\sigma_{c_1}}{\sigma_{p_2}}\left[z_{c_2}\frac{\sigma_{p_2}}{\sigma_{c_2}} - \hat{z}_{p_2}\right]}{R(s)} e^{-2b_{2,1/2}\sqrt{s}} \\ \hat{h}_4(s) &= e^{-2(b_{1,0}+b_{2,0})} \frac{-z_{c_1} - \frac{\sigma_{c_1}}{\sigma_{p_2}}\left[z_{c_2}\frac{\sigma_{p_2}}{\sigma_{c_2}} - \hat{z}_{p_2}\right]}{R(s)} e^{-2\left(b_{1,1/2}+b_{2,1/2}\right)\sqrt{s}} \end{aligned}$$

with common denominator

$$\begin{aligned} R(s) = \frac{1}{\sigma_{p_1}} \Bigg[&z_{c_1}\left[1 - e^{-2\mathrm{j}k_2}\right]\left[1 + e^{-2\mathrm{j}k_1}\right] \\ &+ \frac{\sigma_{c_1}}{\sigma_{p_2}}\left[\hat{z}_{p_2} + z_{c_2}\frac{\sigma_{p_2}}{\sigma_{c_2}} + \left[z_{c_2}\frac{\sigma_{p_2}}{\sigma_{c_2}} - \hat{z}_{p_2}\right]e^{-2\mathrm{j}k_2}\right]\left[1 - e^{-2\mathrm{j}k_1}\right]\Bigg]\hat{z}_{p_1} \\ &+ \frac{z_{c_1}}{\sigma_{c_1}}\Bigg[\frac{\sigma_{c_1}}{\sigma_{p_2}}\left[\hat{z}_{p_2} + z_{c_2}\frac{\sigma_{p_2}}{\sigma_{c_2}} + \left[z_{c_2}\frac{\sigma_{p_2}}{\sigma_{c_2}} - \hat{z}_{p_2}\right]e^{-2\mathrm{j}k_2}\right]\left[1 + e^{-2\mathrm{j}k_1}\right] \\ &+ z_{c_1}\left[1 - e^{-2\mathrm{j}k_2}\right]\left[1 - e^{-2\mathrm{j}k_1}\right]\Bigg]. \end{aligned}$$

Reflection coefficient

The reflection coefficient is given by

$$\begin{aligned}\hat{\beta}_{\mathrm{DDOF}} &= 1 - \frac{2}{1+\hat{z}_{\mathrm{DDOF}}} \\ &= 1 - \frac{2}{1+\frac{1}{\sigma_{p_1}}\hat{z}_{p_1} + \frac{1}{\sigma_{c_1}}\hat{z}_{\mathrm{tube}}(k_1, z_{c_1}, \hat{z}_{2|S_{c_1}})},\end{aligned}$$

so that using the expression (B.2) obtained above yields

$$\begin{aligned}\hat{\beta}_{\mathrm{DDOF}} &= 1 - \frac{2}{1+\hat{z}_{\mathrm{DDOF}}} \\ &= 1 - \frac{2}{1+\frac{1}{\sigma_{p_1}}\hat{z}_{p_1} + \frac{z_{c_1}}{\sigma_{c_1}}\frac{\frac{\sigma_{c_1}}{\sigma_{p_2}}\left[\hat{z}_{p_2}+z_{c_2}\frac{\sigma_{p_2}}{\sigma_{c_2}}+\left[z_{c_2}\frac{\sigma_{p_2}}{\sigma_{c_2}}-\hat{z}_{p_2}\right]e^{-2\mathrm{j}k_2}\right]\left[1+e^{-2\mathrm{j}k_1}\right]+z_{c_1}\left[1-e^{-2\mathrm{j}k_2}\right]\left[1-e^{-2\mathrm{j}k_1}\right]}{z_{c_1}\left[1-e^{-2\mathrm{j}k_2}\right]\left[1+e^{-2\mathrm{j}k_1}\right]+\frac{\sigma_{c_1}}{\sigma_{p_2}}\left[\hat{z}_{p_2}+z_{c_2}\frac{\sigma_{p_2}}{\sigma_{c_2}}+\left[z_{c_2}\frac{\sigma_{p_2}}{\sigma_{c_2}}-\hat{z}_{p_2}\right]e^{-2\mathrm{j}k_2}\right]\left[1-e^{-2\mathrm{j}k_1}\right]}} \\ &= 1 + \hat{h}_1(s) + \hat{h}_2(s)e^{-\tau_1 s} + \hat{h}_3(s)e^{-\tau_2 s} + \hat{h}_4(s)e^{-(\tau_1+\tau_2)},\end{aligned}$$

where

$$\begin{aligned}\hat{h}_1(s) &= -2\frac{z_{c_1} + \frac{\sigma_{c_1}}{\sigma_{p_2}}\left[\hat{z}_{p_2} + z_{c_2}\frac{\sigma_{p_2}}{\sigma_{c_2}}\right]}{R(s)} \\ \hat{h}_2(s) &= -2e^{-2b_{1,0}}\frac{z_{c_1} - \frac{\sigma_{c_1}}{\sigma_{p_2}}\left[\hat{z}_{p_2} + z_{c_2}\frac{\sigma_{p_2}}{\sigma_{c_2}}\right]}{R(s)}e^{-2b_{1,1/2}\sqrt{s}} \\ \hat{h}_3(s) &= -2e^{-2b_{2,0}}\frac{-z_{c_1} + \frac{\sigma_{c_1}}{\sigma_{p_2}}\left[z_{c_2}\frac{\sigma_{p_2}}{\sigma_{c_2}} - \hat{z}_{p_2}\right]}{R(s)}e^{-2b_{2,1/2}\sqrt{s}} \\ \hat{h}_4(s) &= -2e^{-2(b_{1,0}+b_{2,0})}\frac{-z_{c_1} - \frac{\sigma_{c_1}}{\sigma_{p_2}}\left[z_{c_2}\frac{\sigma_{p_2}}{\sigma_{c_2}} - \hat{z}_{p_2}\right]}{R(s)}e^{-2\left(b_{1,1/2}+b_{2,1/2}\right)\sqrt{s}}\end{aligned}$$

with common denominator

$$\begin{aligned}R(s) = \quad & \left[1 + \frac{1}{\sigma_{p_1}}\hat{z}_{p_1}\right]\left[z_{c_1}\left[1 - e^{-2\mathrm{j}k_2}\right]\left[1 + e^{-2\mathrm{j}k_1}\right]\right. \\ & + \frac{\sigma_{c_1}}{\sigma_{p_2}}\left[\hat{z}_{p_2} + z_{c_2}\frac{\sigma_{p_2}}{\sigma_{c_2}} + \left[z_{c_2}\frac{\sigma_{p_2}}{\sigma_{c_2}} - \hat{z}_{p_2}\right]e^{-2\mathrm{j}k_2}\right]\left[1 - e^{-2\mathrm{j}k_1}\right] \\ & + \frac{z_{c_1}}{\sigma_{c_1}}\left[\frac{\sigma_{c_1}}{\sigma_{p_2}}\left[\hat{z}_{p_2} + z_{c_2}\frac{\sigma_{p_2}}{\sigma_{c_2}} + \left[z_{c_2}\frac{\sigma_{p_2}}{\sigma_{c_2}} - \hat{z}_{p_2}\right]e^{-2\mathrm{j}k_2}\right]\left[1 + e^{-2\mathrm{j}k_1}\right]\right. \\ & \left. + z_{c_1}\left[1 - e^{-2\mathrm{j}k_2}\right]\left[1 - e^{-2\mathrm{j}k_1}\right]\right].\end{aligned}$$

Appendix C

Miscellaneous results of functional analysis

Contents

This appendix gathers some results of functional analysis used in Chapter 4.

C.1 Compact embedding and trace operator

Let $\Omega \subset \mathbb{R}^d$, $d \in [\![1, \infty[\![$, be a bounded open set with a Lipschitz boundary.

The embedding $H^1(\Omega) \subset H^s(\Omega)$ with $s \in [0, 1)$ is compact (Grisvard 2011, Thm. 1.4.3.2). (See (Lions and Magenes 1972, Thm. 16.17) for smooth domains.)

The trace operator $H^s(\Omega) \to H^{s-1/2}(\partial\Omega)$ with $s \in (1/2, 1]$ is continuous and surjective (Grisvard 2011, Thm. 1.5.1.2). (See (Ding 1996, Thm. 1) if Ω is also simply connected and (Lions and Magenes 1972, Thm. 9.4) for smooth domains.)

The trace operator $H_{\mathrm{div}}(\Omega) \to H^{-\frac{1}{2}}(\partial\Omega)$, $\boldsymbol{u} \mapsto \boldsymbol{u} \cdot \boldsymbol{n}$ is continuous (Girault and Raviart 1986, Thm. 2.5), and the following Green's formula holds for $\psi \in H^1(\Omega)$ (Girault and Raviart 1986, Eq. 2.17)

$$(\boldsymbol{u}, \nabla\psi) + (\operatorname{div} \boldsymbol{u}, \psi) = \langle \boldsymbol{u} \cdot \boldsymbol{n}, \overline{\psi} \rangle_{H^{-\frac{1}{2}}(\partial\Omega), H^{\frac{1}{2}}(\partial\Omega)}. \tag{C.1}$$

C.2 Hodge decomposition

Let $\Omega \subset \mathbb{R}^d$, $d \in [\![1, \infty[\![$, be a connected open set with a Lipschitz boundary. The following orthogonal decomposition holds (Dautray and Lions 1990, Prop. IX.1)

$$(L^2(\Omega))^d = \nabla H^1(\Omega) \oplus H_{\mathrm{div}\,0,0}(\Omega), \tag{C.2}$$

where

$$\nabla H^1(\Omega) \coloneqq \left\{ \boldsymbol{f} \in (L^2(\Omega))^d \mid \exists g \in H^1(\Omega) : \ \boldsymbol{f} = \nabla g \right\}$$

is a closed subspace of $(L^2(\Omega))^d$ and

$$H_{\mathrm{div}\,0,0}(\Omega) \coloneqq \left\{ \boldsymbol{f} \in H_{\mathrm{div}}(\Omega) \mid \operatorname{div} \boldsymbol{f} = 0, \ \boldsymbol{f} \cdot \boldsymbol{n} = 0 \text{ in } H^{-\frac{1}{2}}(\partial\Omega) \right\}.$$

Remark C.1. The space $H_{\operatorname{div} 0,0}(\Omega)$ is studied in (Dautray and Lions 1990, Chap. IX) for $n = 2$ or 3. For instance,

$$\mathbb{H}_1 \coloneqq H_{\operatorname{div} 0,0}(\Omega) \cap \left\{ \boldsymbol{f} \in (L^2(\Omega))^d \mid \nabla \times \boldsymbol{f} = \boldsymbol{0} \right\}$$

has a finite dimension under suitable assumptions on the set Ω (Dautray and Lions 1990, Prop. IX.2).

C.3 Asymptotic stability of semigroups

Theorem C.2 (Lumer-Phillips)**.** *Let H be a complex Hilbert space and $\mathcal{A} : \mathcal{D}(\mathcal{A}) \subset H \to H$ an unbounded operator. If $\Re(\mathcal{A}X, X)_H \leq 0$ for every $X \in \mathcal{D}(\mathcal{A})$ and $\mathcal{I} - \mathcal{A}$ is surjective, then $\mathcal{A}$ is the infinitesimal generator of a strongly continuous semigroup of contractions $\mathcal{T}(t) \in \mathcal{L}(H)$.*

Proof. The result follows from (Pazy 1983, Thms. 4.3 & 4.6) since Hilbert spaces are reflexive (Lax 2002, Thm. 8.9). □

Theorem C.3 (Asymptotic stability (Arendt and Batty 1988; Lyubich and Vũ 1988))**.** *Let H be a complex Hilbert space and $\mathcal{A} : \mathcal{D}(\mathcal{A}) \subset H \to H$ be the infinitesimal generator of a strongly continuous semigroup $\mathcal{T}(t) \in \mathcal{L}(H)$ of contractions. If $\sigma_p(\mathcal{A}) \cap i\mathbb{R} = \varnothing$ and $\sigma(\mathcal{A}) \cap i\mathbb{R}$ is countable, then $\mathcal{T}$ is asymptotically stable, i.e. $\mathcal{T}(t)X_0 \to 0$ in H as $t \to \infty$ for any $X_0 \in H$.*

Appendix D

Aeroacoustic energy

Contents

The energy analysis carried out in Chapter 5 relies on the standard L^2 norm, i.e. the acoustic energy. This appendix shows that using an aeroacoustic energy instead would not change the results.

D.1 Physical considerations

The LEEs, derived by perturbing a conservation law, do not enjoy an energy conservation law of the form

$$\partial_t e + \nabla \cdot \boldsymbol{I} = 0, \tag{D.1}$$

where e in $\mathrm{J} \cdot \mathrm{m}^{-3}$ is an energy density and $\boldsymbol{I}$ in $\mathrm{W} \cdot \mathrm{m}^{-2}$ is an energy flux. Due to the benefit that (D.1) brings to physical analyses, many works have been dedicated to finding under which conditions an energy conservation law can be recovered. The standard acoustic energy density ($\mathrm{J} \cdot \mathrm{m}^{-3}$) is defined as (Kinsler and Frey 1962; Morse and Ingard 1968)

$$e_a(t) = \frac{1}{2}\frac{1}{\rho_0 c_0^2}|p|^2 + \frac{1}{2}\rho_0|\boldsymbol{u}|^2,$$

where c_0 is the speed of sound and ρ_0 the medium density. With this definition, an energy conservation law (D.1) can only be obtained under the acoustical assumption $\boldsymbol{u_0} = \boldsymbol{0}$ that yields the standard acoustic energy flux

$$\boldsymbol{I_a} \coloneqq p\boldsymbol{u}.$$

This breaks down when $\boldsymbol{u_0} \neq \boldsymbol{0}$, since there are energy exchanges between the perturbation $(p, \boldsymbol{u})$ and the base flow $\boldsymbol{u_0}$. To include these interactions extended energies have been proposed; they write

$$e = e_a + e_c, \ \boldsymbol{I} = \boldsymbol{I_a} + \boldsymbol{I_c},$$

where e_c and $\boldsymbol{I_c}$ are correction terms that vanish when $\boldsymbol{u_0} = \boldsymbol{0}$.

A naive correction can be obtained by simply changing the energy flux with

$$e_{c,1} = 0, \ \boldsymbol{I_{c,1}} = e_a\boldsymbol{u_0},$$

see (5.4). This correction is rather limited since an energy conservation law can only be obtained with a uniform flow (to cancel $(C(\boldsymbol{u_0})\boldsymbol{v},\boldsymbol{v})_{\mathbb{R}^{d+1}}$).

The difficulty lies in finding correction terms for inhomogeneous base flow. To the best of the author's knowledge, the relevant correction term for the homentropic LEEs, and the one we investigated, is that commonly attributed to Cantrell and Hart (Cantrell and Hart 1964, Eq. 16) (Morfey 1971, Eq. 23)

$$e_{c,\mathrm{CH}} = \frac{1}{c_0^2}p(\boldsymbol{u_0}\cdot\boldsymbol{u}),\ \boldsymbol{I_c},_{\mathrm{CH}} = \rho_0(\boldsymbol{u_0}\cdot\boldsymbol{u})\boldsymbol{u} + \left(\frac{1}{\rho_0 c_0^2}p^2 + \frac{1}{c_0^2}(\boldsymbol{u_0}\cdot\boldsymbol{u})p\right)\boldsymbol{u_0}. \tag{D.2}$$

Computing $\partial_t e_{c,\mathrm{CH}} + \nabla\cdot\boldsymbol{I_c},_{\mathrm{CH}}$ and canceling the source terms show that an energy conservation law can be obtained under rather strong assumptions on the base flow: at least irrotational (Morfey 1971, § 3.3). The definition of $e_{c,\mathrm{CH}}$ served as a basis for additional considerations in (Myers 1986, 1991). See also (Brazier 2011) for related considerations on the Galbrun equation as well as numerical illustrations of the differences between various correction terms.

From now on, we focus on the correction terms (D.2).

D.2 Mathematical considerations

In order to use the correction terms (D.2), we must first check that it defines a norm. The Cantrell-Hart energy reads

$$e_{\mathrm{CH}} = \frac{1}{2}\frac{1}{\rho_0 c_0^2}|p|^2 + \frac{1}{2}\rho_0|\boldsymbol{u}|^2 + \frac{1}{c_0^2}p(\boldsymbol{u_0}\cdot\boldsymbol{u}),$$

which yields the following energy definition

$$\left\|\begin{pmatrix}\boldsymbol{u}\\ \tilde{p}\end{pmatrix}\right\|_{\mathrm{CH}}^2 := |\tilde{p}|^2 + |\boldsymbol{u}|^2 + 2\tilde{p}(\boldsymbol{M}_0\cdot\boldsymbol{u}). \tag{D.3}$$

Elementary calculus shows that this can be written

$$\left\|\begin{pmatrix}\boldsymbol{u}\\ \tilde{p}\end{pmatrix}\right\|_{\mathrm{CH}}^2 := |\boldsymbol{u}+\tilde{p}\boldsymbol{M}_0|^2 + \left(1-|\boldsymbol{M}_0|^2\right)|\tilde{p}|^2,$$

which directly gives that this defines a norm only for a subsonic base flow.

Proposition D.1. *The Cantrell-Hart energy $\|\cdot\|_{CH}$ given by (D.3) defines a norm if and only if $|\boldsymbol{u_0}| < c_0$.*

D.3 Impact of the norm choice on the presented analysis

Let us assume that the base flow is subsonic so that $\|\cdot\|_{\mathrm{CH}}$ is a norm. What would be the impact of using $\|\cdot\|_{\mathrm{CH}}$ on the analysis presented in Chapter 5? Let us examine both the volume and surface terms of (5.4).

Impact on the volume term In (5.4), the expression of $(C(\boldsymbol{u_0})\boldsymbol{v},\boldsymbol{v})_{L^2(\Omega)}$ would change, such that one may achieve $(C(\boldsymbol{u_0})\boldsymbol{v},\boldsymbol{v})_{L^2(\Omega)} = 0$ for a wider range of base flow, which include potential and incompressible base flows such that $\boldsymbol{u_0}\cdot\nabla\boldsymbol{u_0} = \boldsymbol{0}$. Base flows encountered in practice do not obey these conditions, so that it seems of little relevance to our study.

Impact on the surface term In (5.4), the surface term $(A(\boldsymbol{n})\boldsymbol{v},\boldsymbol{v})_{\mathbb{R}^{d+1}}$ would be replaced by

$$(A_{\mathrm{CH}}(\boldsymbol{n})\boldsymbol{v},\boldsymbol{v})_{\mathbb{R}^{d+1}} \coloneqq (\boldsymbol{u_0}\cdot\boldsymbol{n})\left[3\tilde{p}^2+|\boldsymbol{u}|^2+4\tilde{p}\boldsymbol{M}_0\cdot\boldsymbol{u}\right]+2c_0\left[\tilde{p}+\boldsymbol{M}_0\cdot\boldsymbol{u}\right](\boldsymbol{u}\cdot\boldsymbol{n}).$$

For a boundary condition to be dissipative, this quantity must be nonnegative. Note the peculiarity of the situation: the incoming and outgoing characteristics of the LEEs have *not* changed, so that the possible class of boundary conditions has *not* changed. However, the dissipative nature of these boundary conditions is now judged using $(A_{\mathrm{CH}}(\boldsymbol{n})\boldsymbol{v},\boldsymbol{v})_{\mathbb{R}^{d+1}}$ instead of the natural boundary term $(A(\boldsymbol{n})\boldsymbol{v},\boldsymbol{v})_{\mathbb{R}^{d+1}}$ as in the dissertation. (The matrix $A(\boldsymbol{n})$, known as the characteristic matrix, is of fundamental importance to study the properties of the LEEs, see Chapter 3.)

Following Assumption 5.1, let us assume that $\boldsymbol{M}_0\cdot\boldsymbol{n}=0$ at the impedance wall. The dissipation term now reads

$$(A_{\mathrm{CH}}(\boldsymbol{n})\boldsymbol{v},\boldsymbol{v})_{\mathbb{R}^{d+1}} \coloneqq 2c_0\left(\tilde{p}+(\boldsymbol{M}_{0,\parallel}\cdot\boldsymbol{u}_{\parallel})\right)\boldsymbol{u}\cdot\boldsymbol{n}, \tag{D.4}$$

where the subscript "$\parallel$" denotes the tangential component. We want to control the sign of (D.4) using an IBC that, intuitively, provides an equilibrium between $\tilde{p}$ and $\boldsymbol{u}\cdot\boldsymbol{n}$. The following points justify why this is not carried out in the dissertation.

(a) Since $\boldsymbol{M}_0\cdot\boldsymbol{n}=0$, the impedance wall is a characteristic boundary with only one incoming characteristic so that only one scalar boundary condition can be imposed. Therefore, we cannot impose $\boldsymbol{u}_{\parallel}=\boldsymbol{0}$ for instance. Controlling the sign of (D.4) must therefore have to be done, not with an IBC, but with a scalar condition of the form $\Phi(\tilde{p},(\boldsymbol{M}_{0,\parallel}\cdot\boldsymbol{u}_{\parallel}),\boldsymbol{u}\cdot\boldsymbol{n})=0$. Apart from $\boldsymbol{u}\cdot\boldsymbol{n}=0$, the only viable possibility we can see is $\tilde{p}=\mathcal{Z}(\boldsymbol{u}\cdot\boldsymbol{n})-\boldsymbol{M}_{0,\parallel}\cdot\boldsymbol{u}_{\parallel}$ where $\mathcal{Z}$ is an admissible impedance operator, which does not seem physically meaningful, at least not in the modeling of locally reacting sound absorbing material.

(b) The choice of using (D.4) would be grounded in physical considerations. However, physically, as recalled in Remark 5.2, we need to impose $\boldsymbol{M_0}=\boldsymbol{0}$ at the impedance wall, so that

$$(A_{\mathrm{CH}}(\boldsymbol{n})\boldsymbol{v},\boldsymbol{v})_{\mathbb{R}^{d+1}}=(A(\boldsymbol{n})\boldsymbol{v},\boldsymbol{v})_{\mathbb{R}^{d+1}}.$$

In view of these remarks, using the Cantrell-Hart energy (D.3) would lead to peculiar considerations and not change the results of the presented analysis.

Appendix E

Energy balance of diffusive representations

Contents

This appendix gathers energy balances associated with diffusive realizations. Sections E.1 and E.2 recall energy balances for standard and extended diffusive kernels, which are well-known in the literature. The last section, namely Section E.3, is original and gives the energy balance for a diffusive kernel in the scattering formulation, which is used in a stability proof of Chapter 5.

E.1 Standard

Let h be a diffusive kernel given by

$$\hat{h}(s) = \int_0^\infty \frac{1}{s+\xi}\mu(\xi)\,\mathrm{d}\xi \quad (\Re(s) > 0)\,,$$

where $\mu \in \mathcal{C}((0,\infty))$ satisfies the integrability condition (2.18) and is real-valued. As recalled in Section 2.1.3, the realization of h reads

$$\begin{cases} \partial_t\varphi(t,\xi) = -\xi\varphi(t,\xi) + u(t) \quad (t>0,\ \xi\in(0,\infty))\,,\ \varphi(0,\xi) = 0 \\ h\star u(t) = \int_0^\infty \varphi(t,\xi)\mu(\xi)\,\mathrm{d}\xi. \end{cases}$$

This realization defines a well-posed linear system, see (Matignon and Zwart 2004). For a smooth real-valued input u, the associated energy balance is obtained as follows.

$$\begin{aligned} (h\star u)(t)u(t) &= \int_0^\infty \varphi(t,\xi)u(t)\mu(\xi)\,\mathrm{d}\xi \\ &= \int_0^\infty \varphi(t,\xi)\left(\partial_t\varphi(t,\xi) + \xi\varphi(t,\xi)\right)\mu(\xi)\,\mathrm{d}\xi \\ &= \frac{1}{2}\frac{\mathrm{d}}{\mathrm{d}t}\int_0^\infty \varphi(t,\xi)^2\mu(\xi)\,\mathrm{d}\xi + \int_0^\infty \xi\varphi(t,\xi)^2\mu(\xi)\,\mathrm{d}\xi, \end{aligned}$$

so that when μ is nonnegative,

$$(h \star u)(t)u(t) \geq \frac{1}{2}\frac{\mathrm{d}}{\mathrm{d}t}\int_0^\infty \varphi(t,\xi)^2\mu(\xi)\,\mathrm{d}\xi.$$

Remark E.1. If μ is nonnegative, then $\hat{h}$ is positive-real.

E.2 Extended

Let h be a diffusive kernel extended by differentiation, i.e.

$$\hat{h}(s) = \int_0^\infty \frac{s}{s+\xi}\mu(\xi)\,\mathrm{d}\xi,$$

where $\mu \in \mathcal{C}((0,\infty))$ satisfies the integrability condition (2.18) and is real-valued. It formally admits the realization

$$\begin{cases} \partial_t\varphi(t,\xi) = -\xi\varphi(t,\xi) + u(t) \quad (t>0,\ \xi\in(0,\infty))\,,\ \varphi(0,\xi)=0 \\ h\star u(t == \int_0^\infty \left(-\xi\varphi(t,\xi)+u(t)\right)\mu(\xi)\,\mathrm{d}\xi. \end{cases}$$

When $\int \mu(\xi)\,\mathrm{d}\xi = \infty$, the definition of the functional spaces for this realization is more intricate, see Section 4.6. The energy balance is obtained as in the standard case.

$$\begin{aligned}(h\star u)(t)u(t) &= \int_0^\infty \left(-\xi\varphi(t,\xi)+u(t)\right)u(t)\mu(\xi)\,\mathrm{d}\xi \\ &= \int_0^\infty \left(-\xi\varphi(t,\xi)+u(t)\right)\left(-\xi\varphi(t,\xi)+u(t)+\xi\varphi(t,\xi)\right)\mu(\xi)\,\mathrm{d}\xi \\ &= \int_0^\infty \partial_t\varphi(t,\xi)\xi\varphi(t,\xi)\mu(\xi)\,\mathrm{d}\xi + \int_0^\infty \left(-\xi\varphi(t,\xi)+u(t)\right)^2\mu(\xi)\,\mathrm{d}\xi \\ &= \frac{1}{2}\frac{\mathrm{d}}{\mathrm{d}t}\int_0^\infty \varphi(t,\xi)^2\xi\mu(\xi)\,\mathrm{d}\xi + \int_0^\infty \left(-\xi\varphi(t,\xi)+u(t)\right)^2\mu(\xi)\,\mathrm{d}\xi,\end{aligned}$$

so that when μ is nonnegative

$$(h\star u)(t)u(t) \geq \frac{1}{2}\frac{\mathrm{d}}{\mathrm{d}t}\int_0^\infty \varphi(t,\xi)^2\xi\mu(\xi)\,\mathrm{d}\xi.$$

E.3 Bounded real

Let β be a diffusive kernel given by

$$\hat{\beta}(s) = \int_{\xi_{\min}}^{\xi_{\max}} \frac{1}{s+\xi}\mu(\xi)\,\mathrm{d}\xi,$$

where $\mu \in \mathcal{C}((\xi_{\min},\xi_{\max}))$ satisfies the integrability condition (2.18) on $(\xi_{\min},\xi_{\max})$ and is real-valued. Its realization is

$$\begin{cases} \partial_t\varphi(t,\xi) &= -\xi\varphi(t,\xi)+a(t),\ \varphi(0,\xi)=0 \\ b(t) &= \int_{\xi_{\min}}^{\xi_{\max}}\varphi(t,\xi)\mu(\xi)\,\mathrm{d}\xi. \end{cases} \tag{E.1}$$

The difference with Section E.1 is that, here, we are interested in the passivity of the associated scattering operator $u \mapsto \beta\star u$, see (1.13).

Proposition E.2. *A sufficient condition for $\hat{\beta}$ to be bounded-real is*

$$\|\mu\|_1 \left\| \frac{\mu}{\xi^2} \right\|_1 \leq 1. \tag{E.2}$$

Then, the corresponding energy balance is

$$\frac{1}{2} b(t)^2 + \frac{1}{2} \frac{\mathrm{d}}{\mathrm{d}t} \mathcal{E}_\beta(t) \leq \frac{1}{2} a(t)^2 - \frac{\|\mu\|_{L^1}}{2} \int_{\xi_{\min}}^{\xi_{\max}} (-\xi\varphi(t,\xi) + a(t))^2 \frac{|\mu(\xi)|}{\xi^2} \mathrm{d}\xi, \tag{E.3}$$

where the energy is defined as

$$\mathcal{E}_\beta(t) \coloneqq \|\mu\|_{L^1} \int_{\xi_{\min}}^{\xi_{\max}} |\varphi(t,\xi)|^2 \frac{|\mu(\xi)|}{\xi} \mathrm{d}\xi, \tag{E.4}$$

Proof. Let a be a smooth real-valued input and let $b = \beta \star a$ be the output. Using Jensen's inequality and the realization (E.1) of β, we get

$$b(t)^2 = \left(\int \varphi(t,\xi) \mu(\xi) \, \mathrm{d}\xi \right)^2 \leq \|\mu\|_1 \int \varphi^2 |\mu(\xi)| \mathrm{d}\xi, \tag{E.5}$$

where

$$\|\mu\|_1 = \int_{\xi_{\min}}^{\xi_{\max}} |\mu(\xi)| \, \mathrm{d}\xi.$$

The result will be obtained by rewriting the right-hand side of (E.5). First, we have

$$\begin{aligned} \|\mu\|_1 \int \varphi^2 |\mu(\xi)| \mathrm{d}\xi &= \|\mu\|_1 \int (\partial_t \varphi - a)^2 \frac{|\mu(\xi)|}{\xi^2} \mathrm{d}\xi = \|\mu\|_1 \int \left(a^2 + (\partial_t \varphi)^2 - 2a \partial_t \varphi \right) \frac{|\mu(\xi)|}{\xi^2} \mathrm{d}\xi \\ &= \|\mu\|_1 \left\| \frac{\mu}{\xi^2} \right\|_1 a(t)^2 + \|\mu\|_1 \int \partial_t \varphi \left(\partial_t \varphi - a \right) \frac{|\mu(\xi)|}{\xi^2} \mathrm{d}\xi \\ &\quad - \|\mu\|_1 \int a \partial_t \varphi \frac{|\mu(\xi)|}{\xi^2} \mathrm{d}\xi. \end{aligned}$$

The identities

$$\partial_t \varphi \left(\partial_t \varphi - a \right) = \partial_t \varphi \left(-\xi \varphi \right) = -\frac{\xi}{2} \partial_t \left(\varphi^2 \right)$$

and

$$a \partial_t \varphi \frac{1}{\xi^2} = a \left(-\xi\varphi + a \right) \frac{1}{\xi^2} = -\frac{\varphi a}{\xi} + \frac{a^2}{\xi^2} = -\frac{1}{2} \varphi^2 + \frac{1}{2} \frac{a^2}{\xi^2} + \frac{1}{2\xi^2} \left(-\xi\varphi + a \right)^2$$

yield

$$\begin{aligned} \|\mu\|_1 \int \varphi^2 |\mu(\xi)| \mathrm{d}\xi = \frac{\|\mu\|_1}{2} \left\| \frac{\mu}{\xi^2} \right\|_1 a(t)^2 - \frac{\|\mu\|_1}{2} \frac{\mathrm{d}}{\mathrm{d}t} \int \varphi^2 \frac{|\mu(\xi)|}{\xi} \mathrm{d}\xi - \frac{\|\mu\|_1}{2} \int \left(-\xi\varphi + a \right)^2 \frac{|\mu(\xi)|}{\xi^2} \mathrm{d}\xi \\ + \frac{\|\mu\|_1}{2} \int \varphi^2 |\mu(\xi)| \mathrm{d}\xi, \end{aligned}$$

hence half the right-hand side of (E.5) is

$$\frac{1}{2} \|\mu\|_1 \int \varphi^2 |\mu(\xi)| \mathrm{d}\xi = \frac{\|\mu\|_1}{2} \left\| \frac{\mu}{\xi^2} \right\|_1 a(t)^2 - \frac{\|\mu\|_1}{2} \frac{\mathrm{d}}{\mathrm{d}t} \int \varphi^2 \frac{|\mu(\xi)|}{\xi} \mathrm{d}\xi - \frac{\|\mu\|_1}{2} \int \left(-\xi\varphi + a \right)^2 \frac{|\mu(\xi)|}{\xi^2} \mathrm{d}\xi.$$

By using this identity in (E.5), we obtain the desired energy balance

$$\frac{1}{2} b(t)^2 \leq \frac{\|\mu\|_1}{2} \left\| \frac{\mu}{\xi^2} \right\|_1 a(t)^2 - \frac{\|\mu\|_1}{2} \frac{\mathrm{d}}{\mathrm{d}t} \int \varphi^2 \frac{|\mu(\xi)|}{\xi} \mathrm{d}\xi - \frac{\|\mu\|_1}{2} \int \left(-\xi\varphi + a \right)^2 \frac{|\mu(\xi)|}{\xi^2} \mathrm{d}\xi,$$

from which we deduce that the scattering operator $a \mapsto \beta \star a$ is passive when (E.2) holds. However, from Proposition 1.14, $\hat{\beta}$ must then be a bounded-real function. □

Appendix F

Implementation details

The purpose of this appendix is to provide some implementation details for the numerical application presented in Chapter 6. Section F.1 presents the spatial discretization scheme, while Section F.2 focuses on the IBC.

F.1 Discontinuous Galerkin method

PDE

The bidimensional hyperbolic PDE of interest is written as

$$\partial_t \boldsymbol{v}(t,\boldsymbol{x}) + \sum_{m=1}^{2} \partial_m \left[A_m \boldsymbol{v}\right](t,\boldsymbol{x}) + B\boldsymbol{v}(t,\boldsymbol{x}) = 0 \quad (t>0,\ \boldsymbol{x}\in\Omega), \tag{F.1}$$

where $\boldsymbol{v}(t,\boldsymbol{x}) \in \mathbb{R}^{N_v}$ and A_m, $B : \Omega \to \mathbb{R}^{N_v \times N_v}$ ($N_v = 3$ for the LEEs). To derive the numerical flux functions, we assume that the matrix fields A_m are at least continuous on $\overline{\Omega}$. Formally, the weak formulation of (F.1) is given by

$$\forall \Phi \in \mathcal{C}^\infty(\overline{\Omega}),\ (\partial_t \boldsymbol{v}, \Phi)_{L^2(\Omega)} + (\partial_m \left[A_m \boldsymbol{v}\right], \Phi)_{L^2(\Omega)} + (B\boldsymbol{v}, \Phi)_{L^2(\Omega)} = 0,$$

which reads using Green's theorem

$$\forall \Phi \in \mathcal{C}^\infty(\overline{\Omega}),\ (\partial_t \boldsymbol{v}, \Phi)_{L^2(\Omega)} - (A_m \boldsymbol{v}, \partial_m \Phi)_{L^2(\Omega)} + (B\boldsymbol{v}, \Phi)_{L^2(\Omega)} = -(A(\boldsymbol{n})\boldsymbol{v}, \Phi)_{L^2(\partial\Omega)}, \tag{F.2}$$

where the characteristic matrix $A(\boldsymbol{n})$ is given by

$$A(\boldsymbol{n}) = \sum_{m=1}^{2} n_m A_m.$$

Nodal approximation

The domain Ω is discretized using N_K disjoint triangles:

$$\Omega = \bigcup_{k\in[\![1,N_K]\!]} \Omega_k.$$

The implemented space discretization is a standard DG method. The discrete solution $\boldsymbol{v}_h$ is assumed to be a polynomial of degree N over each element Ω_k:

$$\boldsymbol{v}_h(t,\boldsymbol{x}) \coloneqq \sum_{j\in[\![1,N_p]\!]} \boldsymbol{v}_j^k(t)\, l_j(\boldsymbol{x}) \quad (k\in[\![1,N_K]\!],\ \boldsymbol{x}\in\Omega_k), \tag{F.3}$$

where the N_p polynomials l_j are the Lagrange polynomials[1] associated with N_p nodes $\boldsymbol{x}_j^k$, distributed on Ω_k, described in (Hesthaven and Warburton 2008, § 6.1). For a polynomial of degree N (DG of order $N+1$), the number of points is given by

$$N_p = \frac{(N+1)(N+2)}{2}.$$

Hence, by definition of the discrete solution $\boldsymbol{v}_h$, we have the identity

$$\boldsymbol{v}_j^k(t) = \boldsymbol{v}_h(t, \boldsymbol{x}_j^k),$$

which justifies the terminology "nodal approximation" to designate (F.3).

Semi-discrete formulation

To derive the semi-discrete formulation, we first write the weak formulation (F.2) on each of the N_K triangles Ω_k, using the Lagrange polynomials $(l_i)_i$ as test functions

$$\begin{aligned}&\forall (i,k) \in [\![1, N_p]\!] \times [\![1, N_K]\!]\,,\\ &\qquad (\partial_t \boldsymbol{v}, l_i)_{L^2(\Omega_k)} - (A_m \boldsymbol{v}, \partial_m l_i)_{L^2(\Omega_k)} + (B\boldsymbol{v}, l_i)_{L^2(\Omega_k)} = -(A(\boldsymbol{n})\boldsymbol{v}, l_i)_{L^2(\partial\Omega_k)}.\end{aligned}$$

We do not enforce continuity of the discrete solution $\boldsymbol{v}_h$ on $\partial\Omega_k$, so that the number of DoF on an edge shared by two triangles is twice that of a continuous approximation. Instead, the coupling between each formulation is achieved through a numerical flux function, denoted $(n_m A_m \boldsymbol{v})^*$, whose purpose is to approximate the boundary integral

$$\text{“}(A(\boldsymbol{n})\boldsymbol{v}, l_i)_{L^2(\partial\Omega_k)} \simeq \left((A(\boldsymbol{n})\boldsymbol{v})^*, l_i\right)_{L^2(\partial\Omega_k)}\text{”}.$$

This leads to the semi-discrete formulation

$$\begin{aligned}&\forall (i,k) \in [\![1, N_p]\!] \times [\![1, N_K]\!]\,,\\ &\qquad (\partial_t \boldsymbol{v}_h, l_i)_{L^2(\Omega_k)} - (A_m \boldsymbol{v}_h, \partial_m l_i)_{L^2(\Omega_k)} + (B\boldsymbol{v}_h, l_i)_{L^2(\Omega_k)} = -\left((A(\boldsymbol{n})\boldsymbol{v})^*, l_i\right)_{L^2(\partial\Omega_k)}.\end{aligned}$$

By using (F.3), we get the final formulation

$$\begin{aligned}&\forall (i,k) \in [\![1, N_p]\!] \times [\![1, N_K]\!]\,,\\ &\sum_{j \in [\![1, N_p]\!]} (l_j, l_i)_{L^2(\Omega_k)}\, \dot{\boldsymbol{v}}_j^k - (A_m l_j, \partial_m l_i)_{L^2(\Omega_k)} \boldsymbol{v}_j^k + (B\, l_j, l_i)_{L^2(\Omega_k)} \boldsymbol{v}_j^k = -\left((A(\boldsymbol{n})\boldsymbol{v})^*, l_i\right)_{L^2(\partial\Omega_k)},\end{aligned} \tag{F.4}$$

which is, once the numerical flux functions are known, a finite-dimensional ODE whose unknown is the nodal vector

$$(\boldsymbol{v}_h(\boldsymbol{x}_i^k))_{i,k} \in \mathbb{R}^{N_v N_K N_p}.$$

Numerical flux functions

At an edge shared by two triangles, we use the upwind flux defined in Section 5.2, namely (5.7) using the notations of Figure 5.1. In the presented numerical application, we use three kinds of boundary conditions: inflow, outflow, and IBC. As described in Section 6.3.2, inflow and outflow boundary conditions are weakly imposed using this upwind flux, leading to (6.17) and (6.18), respectively. As for the IBC, the numerical flux is given by (5.14) using the desired expression for the ghost state $\boldsymbol{v}^g$. For a generic IBC (5.33), we have considered the $\mathcal{Z}$-flux (5.14,5.35), the $\mathcal{Y}$-flux (5.14,5.37), and the $\mathcal{B}$-flux (5.14,5.39).

[1] Note that we should write l_j^k, but there will be little risk of confusion, since l_j will always be manipulated over Ω_k.

Numerical quadrature

To compute the solution of the finite-dimensional ODE (F.4), we first need to evaluate the integrals that arise from the weak formulation; to do so, two strategies can be considered.

1. The first consists in using quadrature rules of sufficient accuracy, so as to reduce aliasing error as much as practically possible (Hesthaven and Warburton 2008, § 6.6.1). Each DG triangle Ω_k then uses two sets of nodes: the interpolation nodes $(\boldsymbol{x}_i^k)_{i\in[\![1,N_p]\!]}$ already introduced (at which the solution is computed) and the quadrature nodes. (If these are distinct, then an additional interpolation from the solution nodes to the quadrature nodes must be carried out.)

2. A cheaper alternative consists in approximating each integral so as to reduce it to the simpler integrals $(l_i, l_j)_{L^2(\Omega_k)}$, $(l_i, \partial_m l_j)_{L^2(\Omega_k)}$, or $(l_i, l_j)_{L^2(\partial\Omega_k)}$, which only involve the nodal basis functions and can be computed both accurately and cheaply.

Let us detail the cheaper strategy, which is systematically employed in our implementation. We cover each of the integral in (F.4).

- The surface integral $(A_m l_j, \partial_m l_i)_{L^2(\Omega_k)}$ is computed as

$$(A_m l_j, \partial_m l_i)_{L^2(\Omega_k)} \simeq A_m(\boldsymbol{x}_j^k)(l_j, \partial_m l_i)_{L^2(\Omega_k)}. \tag{F.5}$$

  This crude approximation can be interpreted as making the following polynomial approximation

$$A_m(\boldsymbol{x})\boldsymbol{v}_h(t,\boldsymbol{x}) \simeq \sum_{j\in[\![1,N_p]\!]} A_m(\boldsymbol{x}_j^k)\boldsymbol{v}_h(t,\boldsymbol{x}_j^k)l_j(\boldsymbol{x}) \quad (\boldsymbol{x}\in\Omega_k)\,. \tag{F.6}$$

  In other words, the approximation (F.5) means that the function $\boldsymbol{x}\mapsto A_m(\boldsymbol{x})\boldsymbol{v}_h(t,\boldsymbol{x})$ is considered to be a polynomial of degree N on Ω_k.

- The second surface integral $(B\, l_j, l_i)_{L^2(\Omega_k)}$ is approximated similarly as

$$(B\, l_j, l_i)_{L^2(\Omega_k)} \simeq B(\boldsymbol{x}_j^k)(l_j, l_i)_{L^2(\Omega_k)},$$

  which assumes that

$$B(\boldsymbol{x})\boldsymbol{v}_h(t,\boldsymbol{x}) \simeq \sum_{j\in[\![1,N_p]\!]} B(\boldsymbol{x}_j^k)\boldsymbol{v}_h(t,\boldsymbol{x}_j^k)l_j(\boldsymbol{x}) \quad (\boldsymbol{x}\in\Omega_k)\,.$$

- Let $\partial\Omega_{k,n}$ denotes the n-th edge of the triangle Ω_k. On each edge $\partial\Omega_{k,n}$, the line integral in (F.4) is approximated as

$$((A(\boldsymbol{n})\boldsymbol{v})^*, l_i)_{L^2(\partial\Omega_{k,n})} \simeq \sum_{j\in[\![1,N_p]\!]} (A(\boldsymbol{n})\boldsymbol{v})^*(\boldsymbol{x}_j^k)\,(l_j, l_i)_{L^2(\partial\Omega_{k,n})},$$

  where the sum is actually restricted to the nodes that belongs to the edge $\partial\Omega_{k,n}$, since the nodal basis function l_j is non-null on $\partial\Omega_{k,n}$ if and only if $\boldsymbol{x}_j^k \in \partial\Omega_{k,n}$ (this is a computationally convenient property of the nodal basis). This assumes the polynomial approximation

$$(A(\boldsymbol{n})\boldsymbol{v})^*(\boldsymbol{x}) \simeq \sum_{j\in[\![1,N_p]\!]} (A(\boldsymbol{n})\boldsymbol{v})^*(\boldsymbol{x}_j^k)\, l_j(\boldsymbol{x}) \quad (\boldsymbol{x}\in\partial\Omega_{k,n})\,.$$

Note that this cheap strategy comes with a drawback. A polynomial interpolation like (F.6) can induce a large aliasing error if A_m has sharp variations, which can create numerical instabilities. If the exact solution $\boldsymbol{v}$ is smooth enough, instabilities caused by aliasing errors can be reduced by reducing the mesh size or increasing the polynomial order N, see (Hesthaven and Warburton 2008, § 5.3) and references therein.

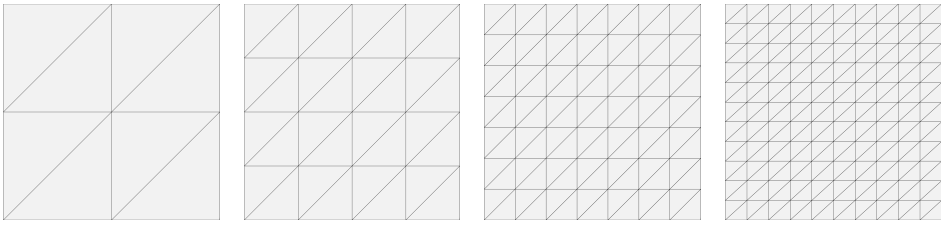

(a) $N_K = 8$. **(b)** $N_K = 32$. **(c)** $N_K = 98$. **(d)** $N_K = 220$.

Figure F.1. Example of meshes used for the order validation.

Implementation and validation

The DG scheme described above has been implemented in object-oriented MATLAB®; some of the core methods are the ones described in (Hesthaven and Warburton 2008). To validate our implementation we rely on the impedance tube exact solution given in Section 6.2. To isolate the error due to the spatial discretization (and avoid that due to time discretization), it is convenient to consider the time-harmonic formulation

$$\mathrm{j}\omega p(\omega, \boldsymbol{x}) + \nabla \cdot \boldsymbol{u}(\omega, \boldsymbol{x}) = 0,\ \mathrm{j}\omega \boldsymbol{u}(\omega, \boldsymbol{x}) + \nabla p(\omega, \boldsymbol{x}) = 0 \quad (\omega \in \mathbb{R},\ x \in \Omega)$$

with $\Omega = (0,1) \times (0,1)$. On $\{x_1 = 0\}$, a monochromatic source boundary condition is (weakly) imposed using the numerical flux (6.17) with

$$\boldsymbol{v}_s = \begin{bmatrix} 1 \\ 1 \\ 1 \end{bmatrix}.$$

On both $\{x_2 = 0\}$ and $\{x_2 = 1\}$ a hard-wall condition is (weakly) imposed using the $\mathcal{B}$-flux (5.14,5.39) with $\mathcal{B}(v) = v$. Finally, on $\{x_1 = 1\}$ the linear IBC

$$p(\omega, \boldsymbol{x}) - \boldsymbol{u}(\omega, \boldsymbol{x}) \cdot \boldsymbol{n} = \hat{\beta}(\mathrm{j}\omega)\,(p(\omega, \boldsymbol{x}) - \boldsymbol{u}(\omega, \boldsymbol{x}) \cdot \boldsymbol{n})$$

is (weakly) imposed using the $\mathcal{B}$-flux (5.14,5.39) with $\mathcal{B}(v) = \hat{\beta}(\mathrm{j}\omega)\, v$. For the validation, we use meshes with 8, 18, 32, 50, 98, and 220 triangles; four of them are shown in Figure F.1. The meshes are built with Gmsh (Geuzaine and Remacle 2009). The results are shown in Figure F.2, where the chosen characteristic length is

$$r \coloneqq \frac{1}{N_K} \sum_{k \in [\![1, N_K]\!]} r_k,$$

with r_k denoting the radius of the inscribed circle of the triangle Ω_k (Hesthaven and Warburton 2008, § 6.4) and the L^2 error is

$$\epsilon_{L^2} \coloneqq \left[\frac{1}{3 N_K N_p} \sum_{(j,k) \in [\![1, N_p]\!] \times [\![1, N_K]\!]} \left| \boldsymbol{v}_h\left(\boldsymbol{x}_j^k\right) - \boldsymbol{v}_{\text{exact}}\left(\boldsymbol{x}_j^k\right) \right|^2 \right]^{1/2}.$$

F.2 Impedance boundary condition

Let us now assume that the linear TDIBC is given by

$$\tilde{\mathcal{B}}(w)(t) = \tilde{\beta}_\infty w(t) + \mathcal{Q}_1(w)(t) + \mathcal{Q}_2(w)(t - \tilde{\tau}),$$

which corresponds to the TDIBC (6.11), where w is a shorthand for "$\tilde{p}_h + \boldsymbol{u}_h \cdot \boldsymbol{n}$". The global assembly is performed in three steps. We consider the LEEs, so $N_v = 3$.

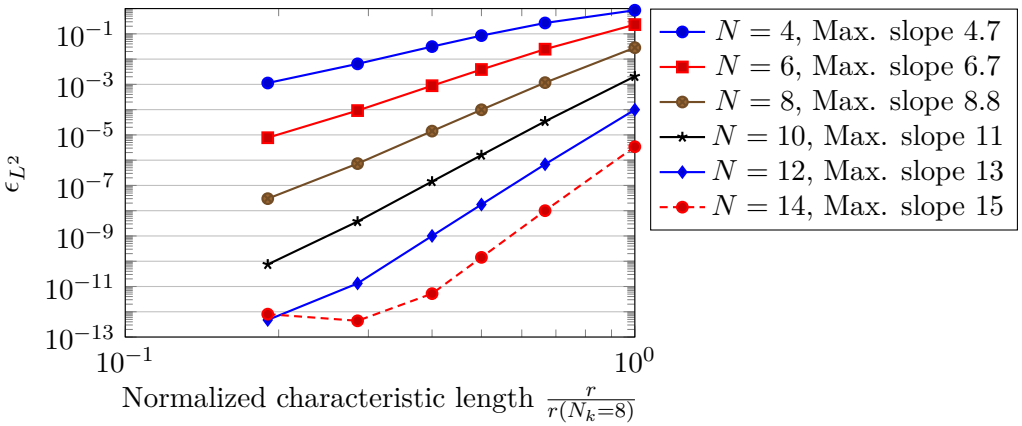

Figure F.2. Validation of the spatial order of the implemented DG discretization. Time-harmonic impedance tube with $\omega = 20$, $\mathcal{B}$-flux (5.14,5.39), and $\hat{\beta}(\mathrm{j}\omega) = 0.5$. The legend gives N, the polynomial degree on each cell Ω_k, and the maximum slope.

(1) Spatial discretization

The global DG formulation of (F.4) reads

$$M\dot{\boldsymbol{v}} + K\boldsymbol{v} = F_s\boldsymbol{v}_s + F_{\mathcal{Q}_1}\mathcal{Q}_1(C_{\Gamma_z}\boldsymbol{v}) + F_{\mathcal{Q}_2}\mathcal{Q}_2(C_{\Gamma_z}\boldsymbol{v})(t-\tilde{\tau}), \tag{F.7}$$

where

$$\boldsymbol{v} \coloneqq (\boldsymbol{v}_h(\boldsymbol{x}_i^k))_{i,k}$$

is the discrete acoustic field ($3N_KN_p$ elements), and M, K, and F are the standard mass, stiffness, and flux DG matrices. The IBC manifests itself through the (rectangular) observation matrix C_{Γ_z} that are associated with the DoF that belong to the impedance boundary Γ_z. The operators $\mathcal{Q}_i$ are applied to each component of the vector $C_{\Gamma_z}\boldsymbol{v}$ of length N_{Γ_z}. Note that, at this stage, the actual definition of the operators $\mathcal{Q}_i$ does not matter; hence, a modification of the IBC does not require a modification of the implementation of the spatial discretization.

(2) State-space realization

By construction, the operators $\mathcal{Q}_i$ have a state-space realization with state vector

$$\boldsymbol{\varphi} \coloneqq (\varphi_i)_{i\in[\![1,N_\varphi]\!]}$$

of length N_φ that reads

$$\begin{aligned}\dot{\boldsymbol{\varphi}}(t) &= A\boldsymbol{\varphi}(t) + Bw(t)\\ \mathcal{Q}_i(w)(t) &= C_{\mathcal{Q}_i}\boldsymbol{\varphi}(t) + D_{\mathcal{Q}_i}w(t),\end{aligned} \tag{F.8}$$

where

$$A = \mathrm{diag}(s_n, -\xi_k)_{n,k}$$

is a diagonal $N_\varphi \times N_\varphi$ matrix,

$$B = (1)_{i\in[\![1,N_\varphi]\!]},\ C_{\mathcal{Q}_i} = (\tilde{r}_{n,i}, \tilde{\mu}_{k,i})_{n,k},\ D_{\mathcal{Q}_i} = 0.$$

Then, injecting (F.8) into (F.7) leads to the following formulation

$$M\dot{\boldsymbol{v}}(t) + K\boldsymbol{v}(t) = F_s\boldsymbol{v}_s(t) + B_\tau(C_\tau\boldsymbol{v})(t-\tilde{\tau}), \tag{F.9}$$

where $\boldsymbol{v}$ now denotes the extended state

$$\boldsymbol{v} \coloneqq ((\boldsymbol{v}_h(\boldsymbol{x}_i^k))_{i,k}, (\boldsymbol{\varphi}^k)_k)$$

of length $3N_K N_p + N_\varphi N_{\Gamma_z}$ and the matrices are obtained by concatenation (the same notations M, K, and F_s are used for the sake of concision). For instance,

$$C_\tau \boldsymbol{v} = (\boldsymbol{\varphi}^k)_k = (\varphi_j^k)_{k,j}$$

is of length $N_\varphi N_{\Gamma_z}$. This is a finite-dimensional delay differential equation that can be advanced in time with a variety of methods.

(3) Time delay computation

Following Section 6.1.3, each of the $N_\varphi N_{\Gamma_z}$ variables φ_j^k are delayed through a monodimensional DG on $(-l_{\tilde{\tau}}, 0)$ that reads

$$\begin{aligned} &M_{\mathrm{DG1D}} \dot{\boldsymbol{\psi}}_j^k + K_{\mathrm{DG1D}} \boldsymbol{\psi}_j^k = F_{\mathrm{DG1D}} \varphi_j^k \\ &\varphi_j^k(t - \tilde{\tau}) = C_{\mathrm{DG1D}} \boldsymbol{\psi}_j^k(t), \end{aligned} \tag{F.10}$$

where $\boldsymbol{\psi}_j^k$ is vector of length N_ψ. Note that (F.10) can be written as (F.8), i.e. it is a state-space realization of the time delay. Combining (F.9) with (F.10) leads to the final global formulation

$$M \dot{\boldsymbol{v}} + K \boldsymbol{v} = F_s \boldsymbol{v}_s,$$

where the vector $\boldsymbol{v}$, of length $3N_K N_p + (N_\psi + 1) N_\varphi N_{\Gamma_z}$, now includes the acoustic field $[\boldsymbol{v}_h(\boldsymbol{x}_i^k)]_{i,k}$ as well as the additional variables $(\varphi_j^k)_{k,j}$ and $(\boldsymbol{\psi}_j^k)_{k,j}$.

The addition of a nonlinear term $\mathcal{Q}_{\mathrm{nl}}$ to the discrete model $\tilde{\mathcal{B}}$ does not change the assembly process described above, which yields

$$M \dot{\boldsymbol{v}} + K \boldsymbol{v} = F_s \boldsymbol{v}_s + F_{\mathcal{Q}_{\mathrm{nl}}} \mathcal{Q}_{\mathrm{nl}}(C_{\mathcal{Q}_{\mathrm{nl}}} \boldsymbol{v}).$$

In the case of (2.75), $\mathcal{Q}_{\mathrm{nl}}(w)$ can be directly computed. If it exists, $\mathcal{Q}_{\mathrm{nl}}(w)$ can be replaced by its nonlinear state-space realization.

Bibliography

Abbas, Z. and S. Nicaise (2013). "Polynomial decay rate for a wave equation with general acoustic boundary feedback laws". In: *SeMA Journal* 61.1, pp. 19–47. DOI: 10.1007/s40324-013-0002-5 (cit. on pp. 88, 100).

— (2015). "The Multidimensional Wave Equation with Generalized Acoustic Boundary Conditions I: Strong Stability". In: *SIAM Journal on Control and Optimization* 53.4, pp. 2558–2581. DOI: 10.1137/140971336 (cit. on pp. xviii, 88, 100).

Abramowitz, M. and I. A. Stegun (1970). *Handbook of Mathematical Functions with Formulas, Graphs, and Mathematical Tables*. 9th ed. Washington DC: National Bureau of Standards (cit. on p. xi).

Alabau-Boussouira, F., J. Prüss, and R. Zacher (2009). "Exponential and polynomial stability of a wave equation for boundary memory damping with singular kernels". In: *Comptes Rendus Mathematique* 347.5, pp. 277–282. DOI: doi.org/10.1016/j.crma.2009.01.005 (cit. on p. 88).

Alinhac, S. (2009). *Hyperbolic Partial Differential Equations*. New York: Springer. DOI: 10.1007/978-0-387-87823-2 (cit. on p. 73).

Allard, J. and N. Atalla (2009). *Propagation of Sound in Porous Media: Modelling Sound Absorbing Materials*. 2nd ed. Chichester, United Kingdom: Wiley. ISBN: 978-0-470-74661-5 (cit. on pp. 12, 14).

Anderson, B. D. O. (1967). "A System Theory Criterion for Positive Real Matrices". In: *SIAM Journal on Control* 5.2, pp. 171–182. DOI: 10.1137/0305011 (cit. on p. 100).

Antonić, N. and K. Burazin (2009). "Graph spaces of first-order linear partial differential operators". In: *Mathematical communications* 14.1, pp. 135–155 (cit. on pp. 71, 77).

— (2010). "Intrinsic boundary conditions for Friedrichs systems". In: *Communications in partial differential equations* 35.9, pp. 1690–1715. DOI: 10.1080/03605300903540927 (cit. on pp. 70, 78, 79).

— (2011). "Boundary operator from matrix field formulation of boundary conditions for Friedrichs systems". In: *Journal of differential equations* 250.9, pp. 3630–3651. DOI: 10.1016/j.jde.2011.02.004 (cit. on p. 79).

Antonić, N., K. Burazin, and M. Vrdoljak (2013). "Heat equation as a Friedrichs system". In: *Journal of Mathematical Analysis and Applications* 404.2, pp. 537–553. DOI: 10.1016/j.jmaa.2013.03.023 (cit. on pp. 71, 79, 83).

— (2014). "Second-order equations as Friedrichs systems". In: *Nonlinear analysis: real world applications* 15, pp. 290–305. DOI: 10.1016/j.nonrwa.2011.08.031 (cit. on p. 83).

Arendt, W. and C. J. Batty (1988). "Tauberian theorems and stability of one-parameter semigroups". In: *Transactions of the American Mathematical Society* 306.2, pp. 837–852. DOI: 10.1090/S0002-9947-1988-0933321-3 (cit. on pp. 120, 196).

Astley, R., R. Sugimoto, and P. Mustafi (2011). "Computational aero-acoustics for fan duct propagation and radiation. Current status and application to turbofan liner optimisation". In:

Journal of Sound and Vibration 330.16, pp. 3832–3845. DOI: 10.1016/j.jsv.2011.03.022 (cit. on pp. xvii, 172).

Atkinson, K. (1989). *An introduction to numerical analysis*. 2nd ed. New York: John Wiley & Sons (cit. on pp. 53, 54).

Baranowski, J. (2017). "Quadrature Based Approximations of Non-integer Order Integrator on Finite Integration Interval". In: *Theory and Applications of Non-integer Order Systems*. Ed. by A. Babiarz, A. Czornik, J. Klamka, and M. Niezabitowski. Cham: Springer International Publishing, pp. 11–20 (cit. on p. 53).

Beggs, J. H., R. Luebbers, K. S. Yee, and K. S. Kunz (1992). "Finite-difference time-domain implementation of surface impedance boundary conditions". In: *IEEE Transactions on Antennas and Propagation* 40.1, pp. 49–56. DOI: 10.1109/8.123352 (cit. on p. xvii).

Bellen, A. and M. Zennaro (2003). *Numerical Methods for Delay Differential Equations*. Oxford: Oxford University Press. ISBN: 0-198-50654-6 (cit. on p. 152).

Beltrami, E. J. and M. R. Wohlers (1966). *Distributions and the boundary values of analytic functions*. New York: Academic Press (cit. on pp. 4–6, 9, 88, 91, 177, 181–184, 187).

Benzoni-Gavage, S. and D. Serre (2007). *Multi-dimensional hyperbolic partial differential equations: First-order Systems and Applications*. Oxford: Oxford University Press. ISBN: 978-0-19-921123-4 (cit. on pp. 71, 73, 74, 76–79).

Bin, J., M. Hussaini, and S. Lee (2009). "Broadband impedance boundary conditions for the simulation of sound propagation in the time domain". In: *The Journal of the Acoustical Society of America* 125.2, pp. 664–675. DOI: 10.1121/1.2999339 (cit. on pp. xvi, 22, 123).

Birk, C. and C. Song (2010). "An improved non-classical method for the solution of fractional differential equations". In: *Computational Mechanics* 46.5, pp. 721–734. DOI: 10.1007/s00466-010-0510-4 (cit. on pp. 26, 53).

Bony, J.-M. (2001). *Cours d'analyse. Théorie des distributions et analyse de Fourier*. Éditions de l'École Polytechnique. ISBN: 978-2-73-020775-1 (cit. on pp. 27, 178, 182).

Botteldooren, D. (1995). "Finite-difference time-domain simulation of low-frequency room acoustic problems". In: *The Journal of the Acoustical Society of America* 98.6, pp. 3302–3308. DOI: 10.1121/1.413817 (cit. on p. xvi).

Brambley, E. J. (2009). "Fundamental problems with the model of uniform flow over acoustic linings". In: *Journal of Sound and Vibration* 322.4, pp. 1026–1037. DOI: 10.1016/j.jsv.2008.11.021 (cit. on pp. 20, 74, 79, 126).

— (2011). "Well-posed boundary condition for acoustic liners in straight ducts with flow". In: *AIAA journal* 49.6, pp. 1272–1282. DOI: 10.2514/1.J050723 (cit. on p. 20).

Brazier, J.-P. (2011). "Derivation of an exact energy balance for Galbrun equation in linear acoustics". In: *Journal of Sound and Vibration* 330.12, pp. 2848–2868. DOI: 10.1016/j.jsv.2011.01.009 (cit. on p. 198).

Brezis, H. (2011). *Functional Analysis, Sobolev Spaces and Partial Differential Equations*. New York: Springer. DOI: 10.1007/978-0-387-70914-7 (cit. on pp. 93, 127).

Brockett, R. (1970). *Finite Dimensional Linear Systems*. New York: John Wiley and Sons (cit. on pp. 20, 25).

Bruneau, M. (2006). *Fundamentals of acoustics*. London: ISTE Ltd. ISBN: 978-1-90-520925-5 (cit. on p. 15).

Burak, M. O., M. Billson, L.-E. Eriksson, and S. Baralon (2009). "Validation of a time-and frequency-domain grazing flow acoustic liner model". In: *AIAA journal* 47.8, pp. 1841–1848. DOI: 10.2514/1.40870 (cit. on p. 160).

Burazin, K. and M. Erceg (2016). "Non-stationary abstract Friedrichs systems". In: *Mediterranean journal of mathematics* 13.6, pp. 3777–3796. DOI: 10.1007/s00009-016-0714-8 (cit. on pp. 72, 79, 83).

Cantrell, R. H. and R. W. Hart (1964). "Interaction between Sound and Flow in Acoustic Cavities: Mass, Momentum, and Energy Considerations". In: *The Journal of the Acoustical Society of America* 36.4, pp. 697–706. DOI: 10.1121/1.1919047 (cit. on p. 198).

Caputo, M. (1976). "Vibrations of an infinite plate with a frequency independent Q". In: *The Journal of the Acoustical Society of America* 60.3, pp. 634–639. DOI: 10.1121/1.381126 (cit. on p. 40).

Casenave, C. and G. Montseny (2010). "Introduction to diffusive representation". In: *4th IFAC symposium on system, structure and control*. Ancona, Italy. DOI: 10.3182/20100915-3-IT-2017.00064 (cit. on pp. 28, 34, 42).

Cazenave, T. and A. Haraux (1998). *An introduction to semilinear evolution equations*. Oxford: Oxford University Press. ISBN: 0-198-50277-X (cit. on p. 98).

Chen, G. (1981). "A note on the boundary stabilization of the wave equation". In: *SIAM Journal on Control and Optimization* 19.1, pp. 106–113. DOI: doi.org/10.1137/0319008 (cit. on pp. 88, 96).

Chevaugeon, N., J.-F. Remacle, and X. Gallez (2006). "Discontinuous Galerkin implementation of the extended Helmholtz resonator model in time domain". In: *12th AIAA/CEAS Aeroacoustics Conference (27th AIAA Aeroacoustics Conference)*. AIAA Paper 2006-2569. Cambridge, MA, USA. DOI: 10.2514/6.2006-2569 (cit. on p. 22).

Cohen, G. and S. Pernet (2017). *Finite Element and Discontinuous Galerkin Methods for Transient Wave Equations*. Dordrecht: Springer. DOI: 10.1007/978-94-017-7761-2 (cit. on p. 138).

Coleman, T. and Y. Li (1996). "An Interior Trust Region Approach for Nonlinear Minimization Subject to Bounds". In: *SIAM Journal on Optimization* 6.2, pp. 418–445. DOI: 10.1137/0806023 (cit. on p. 151).

Cornilleau, P. and S. Nicaise (2009). "Energy decay for solutions of the wave equation with general memory boundary conditions". In: *Differential and Integral Equations* 22.11/12, pp. 1173–1192 (cit. on p. 88).

Costabel, M. (1990). "A remark on the regularity of solutions of Maxwell's equations on Lipschitz domains". In: *Mathematical Methods in the Applied Sciences* 12.4, pp. 365–368. DOI: 10.1002/mma.1670120406 (cit. on p. 99).

Cotté, B. and P. Blanc-Benon (2009). "Time-domain simulations of sound propagation in a stratified atmosphere over an impedance ground". In: *The Journal of the Acoustical Society of America* 125.5, EL202–EL207. DOI: 10.1121/1.3104633 (cit. on pp. xvi, 22).

Crandall, I. B. (1926). *Theory of vibrating systems and sound*. D. Van Nostrand Company (cit. on p. 13).

Cremer, L. (1953). "Theory regarding the attenuation of sound transmitted by air in a rectangular duct with an absorbing wall, and the maximum attenuation constant produced during this process". In: *Acustica* 3. In German, pp. 249–263 (cit. on pp. xvi, 11).

Cummings, A. (1986). "Transient and multiple frequency sound transmission through perforated plates at high amplitude". In: *The Journal of the Acoustical Society of America* 79.4, pp. 942–951. DOI: 10.1121/1.393691 (cit. on pp. 19, 150).

Cummings, A. and W. Eversman (1983). "High amplitude acoustic transmission through duct terminations: Theory". In: *Journal of Sound and Vibration* 91.4, pp. 503–518. DOI: 10.1016/0022-460X(83)90829-5 (cit. on p. 18).

Curtain, R. F. and H. Zwart (1995). *An Introduction to Infinite-Dimensional Linear Systems Theory*. New York: Springer. DOI: 10.1007/978-1-4612-4224-6 (cit. on pp. 20, 25, 56, 88, 103, 151).

Dafermos, C. and M. Slemrod (1973). "Asymptotic behavior of nonlinear contraction semigroups". In: *Journal of Functional Analysis* 13.1, pp. 97–106. DOI: 10.1016/0022-1236(73)90069-4 (cit. on p. 98).

Dautray, R. and J.-L. Lions (1990). *Mathematical Analysis and Numerical Methods for Science and Technology*. Vol. 3. Berlin: Springer-Verlag. DOI: 10.1007/978-3-642-61529-0 (cit. on pp. 195, 196).

Davis, P. and P. Rabinowitz (1984). *Methods of Numerical Integration*. 2nd ed. San Diego: Academic Press (cit. on pp. 53, 54).

Davis, S. (1991). "Low-dispersion finite difference methods for acoustic waves in a pipe". In: *The Journal of the Acoustical Society of America* 90.5, pp. 2775–2781. DOI: 10.1121/1.401874 (cit. on p. 21).

Delorme, P., P. Mazet, C. Peyret, and Y. Ventribout (2005). "Computational aeroacoustics applications based on a discontinuous Galerkin method". In: *Comptes Rendus Mécanique* 333.9, pp. 676–682. DOI: 10.1016/j.crme.2005.07.007 (cit. on p. 124).

Desch, W., E. Fašangová, J. Milota, and G. Propst (2010). "Stabilization through viscoelastic boundary damping: a semigroup approach". In: *Semigroup Forum*. Vol. 80. 3. Springer, pp. 405–415. DOI: 10.1007/s00233-009-9197-2 (cit. on p. 88).

Desch, W. and R. K. Miller (1988). "Exponential stabilization of Volterra integral equations with singular kernels". In: *The Journal of Integral Equations and Applications* 1.3, pp. 397–433. DOI: 10.1216/JIE-1988-1-3-397 (cit. on pp. 25, 90, 107).

Di Pietro, D. A. and A. Ern (2012). *Mathematical aspects of discontinuous Galerkin methods*. Berlin Heidelberg: Springer-Verlag. DOI: 10.1007/978-3-642-22980-0 (cit. on pp. 126–128, 130, 138, 140).

Diethelm, K. (2008). "An investigation of some nonclassical methods for the numerical approximation of Caputo-type fractional derivatives". In: *Numerical Algorithms* 47.4, pp. 361–390. DOI: 10.1007/s11075-008-9193-8 (cit. on pp. 26, 53).

Ding, Z. (1996). "A proof of the trace theorem of Sobolev spaces on Lipschitz domains". In: *Proceedings of the American Mathematical Society* 124.2, pp. 591–600. DOI: 10.1090/S0002-9939-96-03132-2 (cit. on p. 195).

Douasbin, Q., C. Scalo, L. Selle, and T. Poinsot (2018). "Delayed-time domain impedance boundary conditions (D-TDIBC)". In: *Journal of Computational Physics* 371, pp. 50–66. DOI: doi.org/10.1016/j.jcp.2018.05.003 (cit. on pp. xvii, 124, 152).

Dragna, D., P. Pineau, and P. Blanc-Benon (2015). "A generalized recursive convolution method for time-domain propagation in porous media". In: *The Journal of the Acoustical Society of America* 138.2, pp. 1030–1042. DOI: 10.1121/1.4927553 (cit. on p. 22).

Dragna, D. and P. Blanc-Benon (2014). "Physically Admissible Impedance Models for Time-Domain Computations of Outdoor Sound Propagation". In: *Acta Acustica united with Acustica* 100.3, pp. 401–410. DOI: 10.3813/AAA.918719 (cit. on p. 42).

Duffy, D. G. (2004). *Transform methods for solving partial differential equations*. 2nd ed. Boca Raton: CRC press. ISBN: 1-584-88451-7 (cit. on pp. 28, 32, 107).

Dupraz, J. (1977). *La théorie des distributions et ses applications*. Toulouse: Éditions Cépaduès. ISBN: 2-854-28024-5 (cit. on pp. 177, 187).

Engel, K.-J. and R. Nagel (2000). *One-parameter semigroups for linear evolution equations*. New York: Springer-Verlag. ISBN: 0-387-98463-1 (cit. on pp. 56, 88, 103, 113, 151).

Ern, A. and J.-L. Guermond (2004). *Theory and Practice of Finite Elements*. New York: Springer-Verlag. DOI: 978-1-4419-1918-2 (cit. on pp. 126, 128, 138).

— (2006). "Discontinuous Galerkin Methods for Friedrichs' Systems. I. General theory". In: *SIAM Journal on Numerical Analysis* 44.2, pp. 753–778. DOI: 10.1137/050624133 (cit. on pp. 127, 128, 130, 131, 139, 140).

Ern, A., J.-L. Guermond, and G. Caplain (2007). "An Intrinsic Criterion for the Bijectivity of Hilbert Operators Related to Friedrichs' Systems". In: *Communications in partial differential equations* 32.2, pp. 317–341. DOI: 10.1080/03605300600718545 (cit. on pp. 70, 77–79, 83).

Escouflaire, M. (2014). "Theoretical and Numerical Investigation of Time-Domain Impedance Models for Computational aero acoustics". PhD thesis. Université du Maine (cit. on p. 21).

Eversman, W. and R. J. Beckemeyer (1972). "Transmission of Sound in Ducts with Thin Shear Layers—Convergence to the Uniform Flow Case". In: *The Journal of the Acoustical Society of America* 52.1B, pp. 216–220. DOI: 10.1121/1.1913082 (cit. on p. 20).

Folland, G. B. (1999). *Real analysis. Modern Techniques and Their Applications*. 2nd ed. New York: John Wiley & Sons (cit. on p. 27).

Friedrichs, K. O. (1954). "Symmetric hyperbolic linear differential equations". In: *Communications on Pure and Applied Mathematics* 7.2, pp. 345–392. DOI: 10.1002/cpa.3160070206 (cit. on p. 71).

— (1958). "Symmetric positive linear differential equations". In: *Communications on Pure and Applied Mathematics* 11.3, pp. 333–418. DOI: 10.1002/cpa.3160110306 (cit. on pp. 70, 71, 78).

Fung, K.-Y. and H. Ju (2001). "Broadband Time-Domain Impedance Models". In: *AIAA journal* 39.8, pp. 1449–1454. DOI: 10.2514/2.1495 (cit. on p. 22).

— (2004). "Time-domain impedance boundary conditions for computational acoustics and aeroacoustics". In: *International Journal of Computational Fluid Dynamics* 18.6, pp. 503–511. DOI: 10.1080/10618560410001673515 (cit. on pp. 123, 149).

Gabard, G. and E. J. Brambley (2014). "A full discrete dispersion analysis of time-domain simulations of acoustic liners with flow". In: *Journal of Computational Physics* 273.Supplement C, pp. 310–326. DOI: 10.1016/j.jcp.2014.05.004 (cit. on pp. xvi, 123, 126).

Gamelin, T. W. (2001). *Complex Analysis*. New York: Springer-Verlag. ISBN: 0-387-95093-1 (cit. on pp. 8, 10, 28–30, 32, 33).

Garcia, G. and J. Bernussou (1998). "Identification of the dynamics of a lead acid battery by a diffusive model". In: *ESAIM: Proceedings*. Vol. 5. EDP Sciences, pp. 87–98. DOI: 10.1051/proc:1998015 (cit. on p. 49).

Garrappa, R., F. Mainardi, and M. Guido (2016). "Models of dielectric relaxation based on completely monotone functions". In: *Fractional Calculus and Applied Analysis* 19.5, pp. 1105–1160. DOI: 10.1515/fca-2016-0060 (cit. on pp. 25, 90, 107).

Gasquet, C. and P. Witomski (1999). *Fourier Analysis and Applications*. New York: Springer. DOI: 10.1007/978-1-4612-1598-1 (cit. on pp. 25, 178, 180, 182, 186, 187, 190).

— (2000). *Analyse de Fourier et applications*. Paris: Dunod. ISBN: 978-2-10-005018-5 (cit. on p. 178).

Geuzaine, C. and J.-F. Remacle (2009). "Gmsh: A 3-D finite element mesh generator with built-in pre- and post-processing facilities". In: *International Journal for Numerical Methods in Engineering* 79.11, pp. 1309–1331. DOI: 10.1002/nme.2579 (cit. on p. 208).

Gilbarg, D. and N. S. Trudinger (2001). *Elliptic Partial Differential Equations of Second Order*. 2nd ed. Berlin: Springer-Verlag. ISBN: 3-540-41160-7 (cit. on p. 94).

Girault, V. and P.-A. Raviart (1986). *Finite Element Methods for Navier-Stokes Equations*. Berlin: Springer-Verlag. ISBN: 0-387-15796-4 (cit. on pp. 99, 195).

Grabowski, P. (2013). "Stabilization of Wave Equation Using Standard/Fractional Derivative in Boundary Damping". In: *Advances in the Theory and Applications of Non-integer Order Systems: 5th Conference on Non-integer Order Calculus and Its Applications, Cracow, Poland*. Ed. by W. Mitkowski, J. Kacprzyk, and J. Baranowski. Cham: Springer, pp. 101–121 (cit. on pp. xviii, 89).

Gripenberg, G., S.-O. Londen, and O. J. Staffans (1990). *Volterra integral and functional equations*. Cambridge: Cambridge University Press. ISBN: 0-521-37289-5 (cit. on pp. 26–28, 107).

Grisvard, P. (2011). *Elliptic problems in nonsmooth domains*. Philadelphia: SIAM. ISBN: 0-273-08647-2 (cit. on p. 195).

Guess, A. (1975). "Calculation of perforated plate liner parameters from specified acoustic resistance and reactance". In: *Journal of Sound and Vibration* 40.1, pp. 119–137. DOI: 10.1016/S0022-460X(75)80234-3 (cit. on p. 14).

Gustavsen, B. and A. Semlyen (1999). "Rational approximation of frequency domain responses by vector fitting". In: *IEEE Transactions on Power Delivery* 14.3, pp. 1052–1061. DOI: 10.1109/61.772353 (cit. on pp. 51, 151).

Haddar, H., J.-R. Li, and D. Matignon (2010). "Efficient solution of a wave equation with fractional-order dissipative terms". In: *Journal of Computational and Applied Mathematics* 234.6, pp. 2003–2010. DOI: 10.1016/j.cam.2009.08.051 (cit. on p. 53).

Haddar, H. and D. Matignon (2008). *Theoretical and numerical analysis of the Webster Lokshin model*. Tech. rep. RR-6558. INRIA (cit. on pp. 108, 114).

Hale, J. K. (1969). "Dynamical systems and stability". In: *Journal of Mathematical Analysis and Applications* 26.1, pp. 39–59. DOI: 10.1016/0022-247X(69)90175-9 (cit. on p. 98).

Héleschewitz, D. (2000). "Analyse et simulation de systemes différentiels fractionnaires et pseudo-différentiels sous representation diffusive". PhD thesis. ENST Paris (cit. on pp. 28, 42, 47).

Hélie, T. and D. Matignon (2006a). "Diffusive representations for the analysis and simulation of flared acoustic pipes with visco-thermal losses". In: *Mathematical Models and Methods in Applied Sciences* 16.04, pp. 503–536. DOI: 10.1142/S0218202506001248 (cit. on pp. 25, 28, 32, 37, 90, 107).

— (2006b). "Representations with poles and cuts for the time-domain simulation of fractional systems and irrational transfer functions". In: *Signal Processing* 86.10, pp. 2516–2528. DOI: 10.1016/j.sigpro.2006.02.017 (cit. on pp. 23, 26, 28, 32, 37, 41, 49, 51).

Hersh, A., B. Walker, and J. Celano (2003). "Helmholtz resonator impedance model, part 1: Nonlinear behavior". In: *AIAA journal* 41.5, pp. 795–808. DOI: 10.2514/2.2041 (cit. on p. 19).

Hesthaven, J. S. and T. Warburton (2008). *Nodal discontinuous Galerkin methods: algorithms, analysis, and applications*. New York: Springer. DOI: 10.1007/978-0-387-72067-8 (cit. on pp. 130, 158, 206–208).

Hiptmair, R., M. López-Fernández, and A. Paganini (2014). "Fast convolution quadrature based impedance boundary conditions". In: *Journal of Computational and Applied Mathematics* 263, pp. 500–517. DOI: 10.1016/j.cam.2013.12.025 (cit. on pp. 88, 171).

Hörmander, L. (1990). *The analysis of linear partial differential operators I*. 2nd ed. Berlin: Springer-Verlag. ISBN: 3-540-52345-6 (cit. on pp. 90, 178).

Hu, F. Q., M. Hussaini, and P. Rasetarinera (1999). "An analysis of the discontinuous Galerkin method for wave propagation problems". In: *Journal of Computational Physics* 151.2, pp. 921–946. DOI: 10.1006/jcph.1999.6227 (cit. on p. 152).

Hubbard, H. H., ed. (1991). *Aeroacoustics of Flight Vehicles: Theory and Practice. Volume 2: Noise Control*. WRDC 90-3052. NASA (cit. on p. xvi).

Ingard, K. U. (1953). "On the Theory and Design of Acoustic Resonators". In: *The Journal of the Acoustical Society of America* 25.6, pp. 1037–1061. DOI: 10.1121/1.1907235 (cit. on p. 14).

— (1959). "Influence of fluid motion past a plane boundary on sound reflection, absorption, and transmission". In: *The Journal of the Acoustical Society of America* 31.7, pp. 1035–1036. DOI: 10.1121/1.1907805 (cit. on p. 20).

Ioannou, P. and G. Tao (1987). "Frequency domain conditions for strictly positive real functions". In: *IEEE Transactions on Automatic Control* 32.1, pp. 53–54. DOI: 10.1109/TAC.1987.1104447 (cit. on p. 8).

Jaensch, S., C. Sovardi, and W. Polifke (2016). "On the robust, flexible and consistent implementation of time domain impedance boundary conditions for compressible flow simulations". In: *Journal of Computational Physics* 314.Supplement C, pp. 145–159. DOI: 10.1016/j.jcp.2016.03.010 (cit. on pp. xvii, 22, 123, 124).

Jensen, M. (2005). "Discontinuous Galerkin methods for Friedrichs systems with irregular solutions". PhD thesis. University of Oxford (cit. on pp. 71, 77, 78).

Jones, M. G., W. R. Watson, and T. L. Parrott (2005). "Benchmark Data for Evaluation of Aeroacoustic Propagation Codes with Grazing Flow". In: *11th AIAA/CEAS Aeroacoustics Conference*. AIAA Paper 2005-2853. Monterey, CA, USA. DOI: 10.2514/6.2005-2853 (cit. on pp. xvi, 15, 16, 19, 20, 59, 155–157, 164–167).

Joubert, L. (2010). "Approche asymptotique pour l'étude mathématique et la simulation numérique de la propagation du son en présence d'un écoulement fortement cisaillé". PhD thesis. France: École Polytechnique (cit. on pp. 20, 74, 79).

Kato, T. (1995). *Perturbation Theory for Linear Operators*. 2nd ed. Berlin: Springer-Verlag. ISBN: 3-540-58661-X (cit. on pp. 108, 110).

Khamis, D. and E. J. Brambley (2016). "Acoustic boundary conditions at an impedance lining in inviscid shear flow". In: *Journal of Fluid Mechanics* 796, pp. 386–416. DOI: 10.1017/jfm.2016.273 (cit. on p. 20).

— (2017). "Viscous effects on the acoustics and stability of a shear layer over an impedance wall". In: *Journal of Fluid Mechanics* 810, pp. 489–534. DOI: 10.1017/jfm.2016.737 (cit. on pp. xvi, 126, 157).

Kinsler, L. E. and A. R. Frey (1962). *Fundamentals of acoustics*. 2nd ed. New York: John Wiley & Sons (cit. on pp. xvi, 10–12, 125, 197).

Kirby, R. and A. Cummings (1998). "The impedance of perforated plates subjected to grazing gas flow and backed by porous media". In: *Journal of Sound and Vibration* 217.4, pp. 619–636. DOI: 10.1006/jsvi.1998.1811 (cit. on pp. 19, 20, 157).

Komornik, V. and E. Zuazua (1990). "A direct method for the boundary stabilization of the wave equation". In: *Journal de Mathématiques Pures et Appliquées* 69.1, pp. 33–55 (cit. on pp. 88, 96).

Kuttruff, H. (2007). *Acoustics: An Introduction*. Abingdon, UK: Taylor & Francis. ISBN: 0-203-97089-6 (cit. on p. 12).

Lagnese, J. (1983). "Decay of solutions of wave equations in a bounded region with boundary dissipation". In: *Journal of Differential equations* 50.2, pp. 163–182. DOI: 10.1016/0022-0396(83)90073-6 (cit. on pp. 88, 96).

Laurens, S., E. Piot, A. Bendali, M. Fares, and S. Tordeux (2014). "Effective conditions for the reflection of an acoustic wave by low-porosity perforated plates". In: *Journal of Fluid Mechanics* 743, pp. 448–480. DOI: 10.1017/jfm.2014.46 (cit. on pp. xv, 10).

Lawson, C. and R. Hanson (1974). *Solving Least Squares Problems*. Englewood Cliffs, New Jersey: Prentice-Hall (cit. on p. 51).

Lax, P. D. (2002). *Functional Analysis*. New York: John Wiley & Sons (cit. on pp. 92, 93, 196).

Levy, D. and E. Tadmor (1998). "From Semidiscrete to Fully Discrete: Stability of Runge-Kutta Schemes by The Energy Method". In: *SIAM review* 40.1, pp. 40–73. DOI: 10.1137/S0036144597316255 (cit. on p. 138).

Li, C., J. Liang, and T.-J. Xiao (2018). "Polynomial stability for wave equations with acoustic boundary conditions and boundary memory damping". In: *Applied Mathematics and Computation* 321, pp. 593–601. DOI: 10.1016/j.amc.2017.11.019 (cit. on p. 88).

Li, J.-R. (2010). "A fast time stepping method for evaluating fractional integrals". In: *SIAM Journal on Scientific Computing* 31.6, pp. 4696–4714. DOI: 10.1137/080736533 (cit. on p. 53).

Li, X. Y., X. D. Li, and C. Tam (2012). "Improved Multipole Broadband Time-Domain Impedance Boundary Condition". In: *AIAA journal* 50.4, pp. 980–984. DOI: 10.2514/1.J051361 (cit. on p. 22).

Lighthill, M. J. (1952). "On Sound Generated Aerodynamically. I. General Theory". In: *Proceedings of the Royal Society of London A: Mathematical, Physical and Engineering Sciences* 211.1107, pp. 564–587. DOI: 10.1098/rspa.1952.0060 (cit. on p. xv).

Lions, J.-L. and E. Magenes (1972). *Non-Homogeneous Boundary Value Problems and Applications*. Vol. I. Berlin: Springer-Verlag. DOI: 10.1007/978-3-642-65161-8 (cit. on p. 195).

Liu, X., X. Huang, and X. Zhang (2014). "Stability analysis and design of time-domain acoustic impedance boundary conditions for lined duct with mean flow". In: *The Journal of the Acoustical Society of America* 136.5, pp. 2441–2452. DOI: 10.1121/1.4896746 (cit. on pp. xvi, 22, 123).

Lombard, B. and D. Matignon (2016). "Diffusive approximation of a time-fractional Burger's equation in nonlinear acoustics". In: *SIAM Journal on Applied Mathematics* 76.5, pp. 1765–1791. DOI: 10.1137/16M1062491 (cit. on pp. 40, 49, 51, 90, 107, 114).

Lozano, R., B. Brogliato, O. Egeland, and B. Maschke (2000). *Dissipative systems analysis and control: theory and applications*. London: Springer-Verlag. DOI: 10.1007/978-1-4471-3668-2 (cit. on pp. 4, 8, 10, 91, 188, 189).

Lubich, C. (1986). "Discretized fractional calculus". In: *SIAM Journal on Mathematical Analysis* 17.3, pp. 704–719. DOI: 10.1137/0517050 (cit. on p. 26).

Lubich, C. and A. Ostermann (1993). "Runge-Kutta methods for parabolic equations and convolution quadrature". In: *Mathematics of Computation* 60.201, pp. 105–131. DOI: 10.1090/S0025-5718-1993-1153166-7 (cit. on p. 171).

Luebbers, R., F. P. Hunsberger, K. S. Kunz, R. B. Standler, and M. Schneider (1990). "A frequency-dependent finite-difference time-domain formulation for dispersive materials". In: *IEEE Transactions on Electromagnetic Compatibility* 32.3, pp. 222–227. DOI: 10.1109/15.57116 (cit. on p. 22).

Luo, Z.-H., B.-Z. Guo, and Ö. Morgül (2012). *Stability and stabilization of infinite dimensional systems with applications*. London: Springer-Verlag. DOI: 10.1007/978-1-4471-0419-3 (cit. on p. 98).

Lyubich, Y. and P. Vũ (1988). "Asymptotic stability of linear differential equations in Banach spaces". In: *Studia Mathematica* 88.1, pp. 37–42 (cit. on pp. 120, 196).

Mainardi, F. (1997). "Fractional calculus: some basic problems in continuum and statistical mechanics". In: *Fractals and fractional calculus in continuum mechanics*. Ed. by A. Carpinteri and F. Mainardi. Springer Verlag. DOI: 10.1007/978-3-7091-2664-6 (cit. on pp. 25, 90, 107).

Malmary, C. (2000). "Etude théorique et expérimentale de l'impédance acoustique de matériaux en présence d'un écoulement d'air tangentiel". PhD thesis. Université du Maine (cit. on p. 14).

Marx, D. and Y. Aurégan (2013). "Effect of turbulent eddy viscosity on the unstable surface mode above an acoustic liner". In: *Journal of Sound and Vibration* 332.15, pp. 3803–3820. DOI: 10.1016/j.jsv.2013.02.005 (cit. on p. 157).

Matignon, D. and H. Zwart (2004). "Standard diffusive systems are well-posed linear systems". In: *16th International Symposium on Mathematical Theory of Networks and Systems*. Leuven, Belgium: Katholieke Universiteit Leuven (cit. on p. 201).

— (in revision). "Standard diffusive systems as well-posed linear systems". In: *International Journal of Control* (cit. on pp. 25, 32, 107, 108, 113).

Matignon, D. (1994). "Représentations en variables d'état de modèles de guides d'ondes avec dérivation fractionnaire". PhD thesis. Université Paris XI Orsay (cit. on pp. 43, 46, 47).
— (1998). "Stability properties for generalized fractional differential systems". In: *ESAIM: Proceedings*. Vol. 5. EDP Sciences, pp. 145–158. DOI: 10.1051/proc:1998004 (cit. on p. 37).
— (2006). "Asymptotic stability of the Webster-Lokshin model". In: *17th International Symposium on Mathematical Theory of Networks and Systems*. Kyoto, Japan (cit. on p. 102).
— (2009). "An introduction to fractional calculus". In: *Scaling, Fractals and Wavelets*. Ed. by P. Abry, P. Gonçalvès, and J. Levy-Vehel. London–Hoboken: ISTE–Wiley, pp. 237–277. ISBN: 978-1-84-821072-1. DOI: 10.1002/9780470611562.ch7 (cit. on pp. 26, 40, 107, 114, 181).
Matignon, D. and C. Prieur (2005). "Asymptotic stability of linear conservative systems when coupled with diffusive systems". In: *ESAIM: Control, Optimisation and Calculus of Variations* 11.03, pp. 487–507. DOI: 10.1051/cocv:2005016 (cit. on p. 89).
— (2014). "Asymptotic stability of Webster-Lokshin equation". In: *Mathematical Control and Related Fields* 4.4, pp. 481–500. DOI: 10.3934/mcrf.2014.4.481 (cit. on pp. xx, 89, 100, 108, 113, 114).
Mechel, F. (2008). *Formulas of Acoustics*. 2nd ed. Berlin: Springer-Verlag. ISBN: 978-3-54-076834-0 (cit. on p. 12).
Meissner, M. (1999). "The influence of acoustic nonlinearity on absorption properties of Helmholtz resonators. Part I. Theory". In: *Archives of Acoustics* 24.2, pp. 179–190 (cit. on p. 19).
— (2000). "The influence of acoustic nonlinearity on absorption properties of Helmholtz resonators. Part II. Experiment". In: *Archives of Acoustics* 25.2 (cit. on p. 19).
Melling, T. H. (1973). "The acoustic impedance of perforates at medium and high sound pressure levels". In: *Journal of Sound and Vibration* 29.1, pp. 1–65. DOI: 10.1016/S0022-460X(73)80125-7 (cit. on pp. 14, 18, 150).
Michiels, W. and S.-I. Niculescu (2014). *Stability, Control, and Computation for Time-Delay Systems*. 2nd ed. Philadelphia: SIAM. ISBN: 978-0-898716-32-0 (cit. on pp. 56, 151).
Mignot, R., T. Hélie, and D. Matignon (2009). "On the singularities of fractional differential systems, using a mathematical limiting process based on physical grounds". In: *Physica Scripta* T136.014023. DOI: 10.1088/0031-8949/2009/T136/014023 (cit. on p. 37).
Monteghetti, F. (2015). "Time-Domain Simulation of an Acoustic Liner Impedance Model using the Diffusive Representation of Fractional Operators". MA thesis. Toulouse, France: ISAE-SUPAERO, Université de Toulouse (cit. on pp. xviii, xix, 13, 14).
Monteghetti, F., G. Haine, and D. Matignon (2017a). "Stability of linear fractional differential equations with delays: a coupled parabolic-hyperbolic PDEs formulation". In: *20th World Congress of the International Federation of Automatic Control (IFAC)*. (Toulouse, France). DOI: 10.1016/j.ifacol.2017.08.1966 (cit. on pp. xix, 40, 104, 114).
— (2018a). "Asymptotic stability of the multidimensional wave equation coupled with classes of positive real impedance boundary conditions". (Submitted.) (cit. on pp. xx, 87).
Monteghetti, F., D. Matignon, and E. Piot (2018b). "Energy analysis and discretization of nonlinear impedance boundary conditions for the time-domain linearized Euler equations". In: *Journal of Computational Physics* 375, pp. 393–426. DOI: 10.1016/j.jcp.2018.08.037 (cit. on pp. xix–xxi, 88, 99, 123, 145).
— (2018c). "Quadrature-based diffusive representation of the fractional derivative with applications in aeroacoustics and eigenvalue methods for stability". In: *10th Workshop Structural Dynamical Systems: Computational Aspects (SDS2018)*. (Capitolo (Monopoli), Italy) (cit. on p. xix).
— (2018d). "Time-local discretization of fractional and related diffusive operators using Gaussian quadrature with applications". (In revision.) (cit. on pp. xix, 49, 53, 55).

Monteghetti, F., D. Matignon, E. Piot, and L. Pascal (2016a). "Design of broadband time-domain impedance boundary conditions using the oscillatory-diffusive representation of acoustical models". In: *The Journal of the Acoustical Society of America* 140.3, pp. 1663–1674. DOI: 10.1121/1.4962277 (cit. on pp. xix, 57, 61, 90, 103, 107).

— (2016b). "High-order time-domain simulation of acoustic impedance models using diffusive representation". In: *Poster session of the XVII Spanish-French School Jacques-Louis Lions about Numerical Simulation in Physics and Engineering*. (Gijón, Spain) (cit. on p. xix).

— (2016c). "Simulation temporelle d'un modèle d'impédance de liner en utilisant la représentation diffusive d'opérateurs". In: *13e Congrès Français d'Acoustique*. (Le Mans, France). 000130, pp. 2549–2555 (cit. on p. xix).

— (2017b). "Asymptotic stability of the linearised Euler equations with long-memory impedance boundary condition". In: *13th International Conference on Mathematical and Numerical Aspects of Wave Propagation (WAVES 2017)*. (Minneapolis, MN, USA) (cit. on p. xx).

Montseny, G. (1998). "Diffusive representation of pseudo-differential time-operators". In: *ESAIM: Proceedings*. Vol. 5. EDP Sciences, pp. 159–175. DOI: 10.1051/proc:1998005 (cit. on pp. 24–26, 38, 106).

— (2005). *Représentation diffusive*. Paris: Éditions Lavoisier. ISBN: 2-74-621146-7 (cit. on pp. 24, 42).

Morfey, C. (1971). "Acoustic energy in non-uniform flows". In: *Journal of Sound and Vibration* 14.2, pp. 159–170. DOI: 10.1016/0022-460X(71)90381-6 (cit. on p. 198).

Morse, P. M. and K. U. Ingard (1968). *Theoretical acoustics*. Princeton: Princeton University Press. ISBN: 0-691-08425-4 (cit. on pp. xvi, 125, 197).

Myers, M. K. (1980). "On the acoustic boundary condition in the presence of flow". In: *Journal of Sound and Vibration* 71.3, pp. 429–434. DOI: 10.1016/0022-460X(80)90424-1 (cit. on p. 20).

— (1986). "An exact energy corollary for homentropic flow". In: *Journal of Sound and Vibration* 109.2, pp. 277–284. DOI: 10.1016/S0022-460X(86)80008-6 (cit. on p. 198).

— (1991). "Transport of energy by disturbances in arbitrary steady flows". In: *Journal of Fluid Mechanics* 226, pp. 383–400. DOI: 10.1017/S0022112091002434 (cit. on p. 198).

Nicaise, S. and C. Pignotti (2006). "Stability and instability results of the wave equation with a delay term in the boundary or internal feedbacks". In: *SIAM Journal on Control and Optimization* 45.5, pp. 1561–1585. DOI: 10.1137/060648891 (cit. on pp. 88, 103).

Olivetti, S., R. D. Sandberg, and B. J. Tester (2015). "Direct numerical simulation of turbulent flow with an impedance condition". In: *Journal of Sound and Vibration* 344.Supplement C, pp. 28–37. DOI: 10.1016/j.jsv.2015.01.039 (cit. on pp. xvii, 123, 172).

Ostashev, V. E., S. L. Collier, D. K. Wilson, D. F. Aldridge, N. P. Symons, and D. Marlin (2007). "Padé approximation in time-domain boundary conditions of porous surfaces". In: *The Journal of the Acoustical Society of America* 122.1, pp. 107–112. DOI: 10.1121/1.2743153 (cit. on p. 22).

Özyörük, Y., L. N. Long, and M. G. Jones (1998). "Time-Domain Numerical Simulation of a Flow-Impedance Tube". In: *Journal of Computational Physics* 146.1, pp. 29–57. DOI: 10.1006/jcph.1998.5919 (cit. on pp. xvi, 21, 123).

Pascal, L., E. Piot, and G. Casalis (2015). "A New Implementation of the Extended Helmholtz Resonator Acoustic Liner Impedance Model in Time Domain CAA". In: *Journal of Computational Acoustics*. DOI: 10.1142/S0218396X15500150 (cit. on p. 22).

Pazy, A. (1983). *Semigroups of Linear Operators and Applications to Partial Differential Equations*. 2nd ed. New York: Springer-Verlag. ISBN: 978-1-4612-5563-5 (cit. on pp. 95, 108, 196).

Peralta, G. R. (2016). "Stabilization of viscoelastic wave equations with distributed or boundary delay". In: *Zeitschrift für Analysis und ihre Anwendungen* 35.3, pp. 359–381. DOI: 10.4171/ZAA/1569 (cit. on p. 88).

— (2018). "Stabilization of the wave equation with acoustic and delay boundary conditions". In: *Semigroup Forum* 96.2, pp. 357–376. DOI: 10.1007/s00233-018-9930-9 (cit. on p. 88).

Podlubny, I. (1999). *Fractional Differential Equations*. San Diego: Academic Press (cit. on pp. 40, 114).

Popie, V. (2016). "Modélisation asymptotique de la réponse acoustique de plaques perforées dans un cadre linéaire avec étude des effets visqueux". PhD thesis. ISAE-SUPAERO, Université de Toulouse (cit. on p. 10).

Pridmore-Brown, D. C. (1958). "Sound propagation in a fluid flowing through an attenuating duct". In: *Journal of Fluid Mechanics* 4.4, pp. 393–406. DOI: 10.1017/S0022112058000537 (cit. on pp. xvi, 126).

Primus, J. (2012). "Détermination de l'impédance acoustique de matériaux absorbants en écoulement par méthode inverse et mesures LDV". PhD thesis. INSA Toulouse, Université de Toulouse (cit. on p. 11).

Primus, J., E. Piot, F. Simon, M. G. Jones, and W. R. Watson (2013). "ONERA-NASA Cooperative Effort on Liner Impedance Eduction". In: *19th AIAA/CEAS Aeroacoustics Conference*. 2013-2273. Berlin, Germany. DOI: 10.2514/6.2013-2273 (cit. on pp. 20, 155–157, 160–163).

Rauch, J. (1985). "Symmetric positive systems with boundary characteristic of constant multiplicity". In: *Transactions of the American Mathematical Society* 291.1, pp. 167–187. DOI: 10.1090/S0002-9947-1985-0797053-4 (cit. on pp. 70, 77).

— (1994). "Boundary value problems with nonuniformal characteristic boundary". In: *Journal de mathématiques pures et appliquées* 73.4, pp. 347–353 (cit. on pp. 77, 78, 82).

Rellich, F. (1940). "Darstellung der eigenwerte von $\Delta u + \lambda u = 0$ durch ein randintegral". In: *Mathematische Zeitschrift* 46.1, pp. 635–636 (cit. on p. 94).

Reymen, Y., M. Baelmans, and W. Desmet (2006). "Time-Domain Impedance Formulation Based on Recursive Convolution". In: *12th AIAA/CEAS Aeroacoustics Conference (27th AIAA Aeroacoustics Conference)*. AIAA Paper 2006-2685. Cambridge, MA, USA. DOI: 10.2514/6.2006-2685 (cit. on p. 22).

Richard, J.-P. (2003). "Time-delay systems: an overview of some recent advances and open problems". In: *Automatica* 39.10, pp. 1667–1694. DOI: 10.1016/S0005-1098(03)00167-5 (cit. on pp. 56, 151, 152).

Richter, C. (2010). "Liner impedance modeling in the time domain with flow". PhD thesis. Technische Universität Berlin (cit. on pp. xvi, 11, 70).

Richter, C., J. A. Hay, Ł. Panek, N. Schönwald, S. Busse, and F. Thiele (2011). "A review of time-domain impedance modelling and applications". In: *Journal of Sound and Vibration* 330.16, pp. 3859–3873. DOI: 10.1016/j.jsv.2011.04.013 (cit. on pp. xvi, 22).

Rienstra, S. W. (2006). "Impedance Models in Time Domain, Including the Extended Helmholtz Resonator Model". In: *12th AIAA/CEAS Aeroacoustics Conference (27th AIAA Aeroacoustics Conference)*. AIAA Paper 2006-2686. Cambridge, MA, USA. DOI: 10.2514/6.2006-2686 (cit. on pp. 4, 5, 22, 123).

Rienstra, S. W. and A. Hirschberg (2016). *An introduction to acoustics*. Tech. rep. Extended and revised edition of Report IWDE 92-06. Eindhoven University of Technology (cit. on pp. xv, 12).

Rienstra, S. W. and D. K. Singh (2018). "Nonlinear Asymptotic Impedance Model for a Helmholtz Resonator of Finite Depth". In: *AIAA Journal* 56.5, pp. 1792–1802. DOI: 10.2514/1.J055882 (cit. on p. 19).

Rienstra, S. W. and G. G. Vilenski (2008). "Spatial Instability of Boundary Layer Along Impedance Wall". In: *14th AIAA/CEAS Aeroacoustics Conference*. AIAA Paper 2008-2932. Vancouver, BC, Canada. DOI: 10.2514/6.2008-2932 (cit. on p. 157).

Roche, J.-M. (2011). "Simulation numérique de l'absorption acoustique de matériaux résonants en présence d'écoulement". PhD thesis. Université du Maine (cit. on p. 18).

Rolls-Royce plc (1996). *The Jet Engine*. 5th ed. Derby (cit. on pp. xvi, 17).

Samko, S. G., A. A. Kilbas, and O. I. Marichev (1993). *Fractional Integrals and Derivatives*. Yverdon, Switzerland: Gordon and Breach (cit. on pp. 26, 40, 107).

Sauter, S. and M. Schanz (2017). "Convolution quadrature for the wave equation with impedance boundary conditions". In: *Journal of Computational Physics* 334.Supplement C, pp. 442–459. DOI: 10.1016/j.jcp.2017.01.013 (cit. on pp. xviii, 88, 171).

Sbardella, L., B. J. Tester, and M. Imregun (2001). "A time-domain method for the prediction of sound attenuation in lined ducts". In: *Journal of Sound and Vibration* 239.3, pp. 379–396. DOI: 10.1006/jsvi.2000.3173 (cit. on p. 22).

Scalo, C., J. Bodart, and S. K. Lele (2015). "Compressible turbulent channel flow with impedance boundary conditions". In: *Physics of Fluids* 27.3. DOI: 10.1063/1.4914099 (cit. on pp. xvii, 123, 124, 172).

Scherer, R., S. L. Kalla, Y. Tang, and J. Huang (2011). "The Grünwald-Letnikov method for fractional differential equations". In: *Computers & Mathematics with Applications* 62.3, pp. 902–917. DOI: 10.1016/j.camwa.2011.03.054 (cit. on p. 26).

Schwartz, L. (1966). *Mathematics for the Physical Sciences*. Paris: Hermann (cit. on pp. xii, 32, 35, 43, 90, 91, 177, 181–184, 186).

— (1978). *Théorie des distributions*. Paris: Hermann. ISBN: 2-7056-551-4 (cit. on pp. 178, 181, 183).

Shampine, L. (2008). "Vectorized adaptive quadrature in MATLAB". In: *Journal of Computational and Applied Mathematics* 211.2, pp. 131–140. DOI: 10.1016/j.cam.2006.11.021 (cit. on pp. 53, 172).

Staffans, O. J. (1994). "Well-posedness and stabilizability of a viscoelastic equation in energy space". In: *Transactions of the American Mathematical Society* 345.2, pp. 527–575. DOI: 10.1090/S0002-9947-1994-1264153-X (cit. on pp. 25, 107).

— (2002). "Passive and conservative continuous-time impedance and scattering systems. Part I: Well-posed systems". In: *Mathematics of Control, Signals and Systems* 15.4, pp. 291–315 (cit. on pp. 8, 173).

— (2005). *Well-posed linear systems*. Cambridge: Cambridge University Press. ISBN: 978-0-521-82584-9 (cit. on p. 107).

Tam, C. (2012). *Computational aeroacoustics: A wave number approach*. Cambridge: Cambridge University Press, pp. 181–182. ISBN: 978-0-521-80678-7 (cit. on pp. xv, xvi, 21).

Tam, C. and L. Auriault (1996). "Time-domain impedance boundary conditions for computational aeroacoustics". In: *AIAA journal* 34.5, pp. 917–923. DOI: 10.2514/3.13168 (cit. on p. 21).

Tester, B. J. (1973a). "Some aspects of "sound" attenuation in lined ducts containing inviscid mean flows with boundary layers". In: *Journal of Sound and Vibration* 28.2, pp. 217–245. DOI: 10.1016/S0022-460X(73)80104-X (cit. on p. 20).

— (1973b). "The optimization of modal sound attenuation in ducts, in the absence of mean flow". In: *Journal of Sound and Vibration* 27.4, pp. 477–513. DOI: 10.1016/S0022-460X(73)80358-X (cit. on p. 11).

— (1973c). "The propagation and attenuation of sound in lined ducts containing uniform or 'plug' flow". In: *Journal of Sound and Vibration* 28.2, pp. 151–203. DOI: 10.1016/S0022-460X(73)80102-6 (cit. on p. xvi).

Toro, E. F. (2009). *Riemann Solvers and Numerical Methods for Fluid Dynamics*. 3rd ed. Springer-Verlag. DOI: 10.1007/978-3-540-49834-6 (cit. on p. 136).

Toulorge, T. and W. Desmet (2012). "Optimal Runge-Kutta schemes for discontinuous Galerkin space discretizations applied to wave propagation problems". In: *Journal of Computational Physics* 231.4, pp. 2067–2091. DOI: 10.1016/j.jcp.2011.11.024 (cit. on p. 153).

Troian, R., D. Dragna, C. Bailly, and M.-A. Galland (2017). "Broadband liner impedance eduction for multimodal acoustic propagation in the presence of a mean flow". In: *Journal of Sound and Vibration* 392, pp. 200–216. DOI: doi.org/10.1016/j.jsv.2016.10.014 (cit. on pp. xvi, 151).

Tucsnak, M. and G. Weiss (2014). "Well-posed systems – The LTI case and beyond". In: *Automatica* 50.7, pp. 1757–1779. DOI: 10.1016/j.automatica.2014.04.016 (cit. on p. 107).

Tudisco, P., R. Ranjan, S. Menon, S. Jaensch, and W. Polifke (2017). "Application of the Time-Domain Impedance Boundary Condition to Large-Eddy Simulation of Combustion Instability in a Shear-Coaxial High Pressure Combustor". In: *Flow, Turbulence and Combustion* 99.1, pp. 185–207. DOI: 10.1007/s10494-017-9804-3 (cit. on pp. xvii, 19, 124).

Ventribout, Y. (2006). "Contrôle des perturbations aéroacoustiques par impédances de parois: application à un modèle de matériaux poreux". PhD thesis. Toulouse: Ecole nationale superieure de l'aéronautique et de l'espace (cit. on pp. 81, 82, 124, 131, 133).

Wang, J.-M., B.-Z. Guo, and M. Krstic (2011). "Wave Equation Stabilization by Delays Equal to Even Multiples of the Wave Propagation Time". In: *SIAM Journal on Control and Optimization* 49.2, pp. 517–554. DOI: 10.1137/100796261 (cit. on pp. xviii, 88).

Weiss, G., O. J. Staffans, and M. Tucsnak (2001). "Well-posed linear systems–a survey with emphasis on conservative systems". In: *International Journal of Applied Mathematics and Computer Science* 11, pp. 7–33 (cit. on p. 107).

Widder, D. V. (1946). *The Laplace transform*. Princeton: Princeton University Press (cit. on pp. 26, 27).

Willms, N. B. and G. M. L. Gladwell (1994). "Saddle points and overdetermined problems for the Helmholtz equation". In: *Zeitschrift für angewandte Mathematik und Physik* 45.1, pp. 1–26 (cit. on p. 94).

Yosida, K. (1980). *Functional Analysis*. 6th ed. New York: Springer-Verlag. ISBN: 0-387-10210-8 (cit. on pp. xi, 93, 95, 104).

Yuan, L. and O. Agrawal (2002). "A numerical scheme for dynamic systems containing fractional derivatives". In: *ASME Journal of Vibration and Acoustics* 124.2, pp. 321–324. DOI: 10.1115/1.1448322 (cit. on p. 53).

Yuferev, S. V. and N. Ida (2010). *Surface Impedance Boundary Conditions: A Comprehensive Approach*. Boca Raton: CRC Press (cit. on pp. xvii, 88).

Zemanian, A. (1965). *Distribution Theory and Transform Analysis*. McGraw-Hill (cit. on pp. xii, 4–7, 35, 177, 182, 183, 189).

Zennaro, M. (1986). "Natural Continuous Extensions of Runge-Kutta Methods". In: *Mathematics of Computation* 46.173, pp. 119–133. DOI: 10.1090/S0025-5718-1986-0815835-1 (cit. on p. 152).

Zhang, Q. and D. J. Bodony (2016). "Numerical investigation of a honeycomb liner grazed by laminar and turbulent boundary layers". In: *Journal of Fluid Mechanics* 792, pp. 936–980. DOI: 10.1017/jfm.2016.79 (cit. on pp. xv, 19, 20).

Zhong, S., X. Zhang, and X. Huang (2016). "A controllable canonical form implementation of time domain impedance boundary conditions for broadband aeroacoustic computation". In: *Journal of Computational Physics* 313.Supplement C, pp. 713–725. DOI: 10.1016/j.jcp.2016.03.002 (cit. on pp. xvi, 22, 123).

Zhou, K., J. C. Doyle, and K. Glover (1996). *Robust and optimal control*. Englewood Cliffs, New Jersey: Prentice Hall (cit. on p. 99).